APPLICATION OF GIS AND REMOTE SENSING FOR WATER RESOURCE MANAGEMENT IN ARID AREA – WADI DAHAB BASIN – SOUTH EASTERN SINAI-EGYPT (CASE-STUDY)

Dissertation

der Mathematisch-Naturwissenschaftlichen Fakultät

der Eberhard Karls Universität Tübingen

zur Erlangung des Grades eines

Doktors der Naturwissenschaften

(Dr. rer. nat.)

vorgelegt von

M.Sc. Adel Fouad Abdou Omran

aus Giza, Ägypten

Tübingen

2013

Tag der mündlichen Qualifikation:	28.10.2013
Dekan:	Prof. Dr. Wolfgang Rosenstiel
1. Berichterstatter:	Prof. Dr. Klaus-Dieter Balke
2. Berichterstatter:	Prof. Dr.-Ing. Dietrich Schröder
3. Berichterstatter:	Prof. Dr. Mohammed Helmi Geriesh

Acknowledgments

First, thanks to "ALLAH" for the continuous and persistent supply with patience and effort to produce this work.

I would like to express my deep thank for Prof. Dr. Klaus-Dieter Balke, Prof. Dr. Peter Grathwohl (University Tübingen-Germany), Prof. Dr.-Ing. Dietrich Schröder (Hochschule für Technik-Germany) and Prof. Dr. Mohammed Helmi Geriesh (Suez Canal University-Egypt) for their supervision, discussion, supplying me with required facilities, materials for the success of my research work and their valuable comments and advices provided to me where necessary throughout this work.

I wish to express my deepest appreciation to Prof. Dr. Michael Hahn (Hochschule für Technik- Germany) and Prof. Dr. Volker Hochschild (University Tübingen-Germany) for their help and unlimited support. Especial appreciation and great indebted to Dr. Ahmed El-Rayes, (Suez Canal University - Egypt) for his valuable guidance, direct supervision, field work, critical revision of the manuscript and encouragement.

I wish to express my gratitude and sincere appreciation to Mr. Matthias Flegr, for his help, kindness, provided necessary assistance and co-operation to complete this work.

I would like to extent my sincere thanks also to the DAAD for the financial assistance which made this research possible. I would like also to thank my Egyptian university "Suez University" to give great support to continue my PhD study in Germany. Great appreciation is expressed to Dr. Abdelaal Attia (Egyptian Geological survey Authority) and Water Resource Research Institute for their valuable support with data about Sinai and guidance to available field data. All thank are extended to all staff member of the Institute of Geosciences, Tuebingen University for their kind assistance and co-operation.

Actually no words can express my deep and great appreciation to my sincere lovely wife "Hanaa" for her help and continuous encouragement.

I would like to express my deep thanks and gratitude to my family, especially my parent for their help and support. This work would have never been done without their encouragement.

Finally this work for my lovely son "Amr" and my lovely daughter "Nada"

ADEL FOUAD OMRAN

Kurzfassung

In dieser Arbeit werden geologische, hydrogeologische, geomorphologische, hydrogeochemische, klimatologische sowie hydrologische Aspekte beschrieben, mit denen diverse wasserbezogene Probleme auf der südlichen Sinai-Halbinsel in Ägypten untersucht wurden. Das Land liegt zwar innerhalb der ariden Zone, wird aber immer wieder von sintflutartigen Starkregen heimgesucht, die extreme Hochwasserereignisse auslösen können, gerade auch auf dem südlichen Sinai. Die Untersuchungen erfolgten im Einzugsgebiet des Wadi Dahab, das sich im südöstlichen Teil der Sinai-Halbinsel befindet und in fünf Teileinzugsgebiete gegliedert werden kann. Gelegentlich fallen enorme Niederschlagsmengen, die in den tiefer gelegenen Teilen der Wadis zu starken Überschwemmungen führen und zudem auch die dort lebende Bevölkerung und ihre landwirtschaftlichen Aktivitäten gefährden.

Diese Arbeit erfolgte auch, um das Hochwasserrisiko im Einzugsgebiet des Wadi Dahab besser abschätzen zu können und den Aufbau eines geeigneten Managementsystems zu entwerfen, wie die sehr großen Abflussmengen kontrolliert abgeleitet werden könnten. Hydrogeologische und -geochemische Untersuchungen dienten der Bestimmung desaktuellen Standes der Grundwasserverunreini-gungenund einem künftig verbesserten Umgang mit den beschränkten (Grund)Wasservorkommen in den Wadis, wobei auch entsprechende Vorschläge für die betroffene Bevölkerung und Behörden entwickelt wurden.

Aus geologischer Sicht wird das Einzugsgebiet des Wadi Dahab hauptsächlich von präkambrischen bis kreidezeitlichen Gesteinen aufgebaut. Jüngere Lockersedimente bilden vor allem die Talfüllun-gen der Wadis. Die Ergebnisse des AdvancedSpaceborne Thermal Emission Radiometers (ASTER) wurden bei der lithologischen Kartierung des Gebietes ausgewertet, aus der eine neue geologische Karte hervorging, wobei auch mehrere Gesteinstypen neu hinzugefügt werden konnten. Das Einzugsgebiet des Wadi Dahab wird von mehreren großen Störungszonen durchzogen, die in den tektonischen Hauptrichtungen N-S, NE-SW und NNE-SSE verlaufen. Insbesondere im östlichen und südlichen Teil des Einzugsgebietes Dahab ist eine hohe Dichte der Lineamente festzustellen.

Das Untersuchungsgebiet kann geomorphologisch in insgesamt fünf Teilgebiete gegliedert werden. Mit Hilfe des ASTER Digital Elevation Models (DEM) wurde das Entwässerungssystem der Teileinzugsgebiete beschrieben und diese hinsichtlich ihrer natürlichen Anfälligkeit für Hochwasserereignisse analysiert. Daraus ergibt sich, dass auf ca. 35% der Fläche ein sehr hohes und auf 60% ein mittleres Hochwasserrisiko besteht. In diesen Gebieten sind weitere Untersuchungsschritte erforderlich, um letztlich konkrete, vor allem auch praktische Schutzmaßnahmen empfehlen zu können.

Die alluvialen Talablagerungen sowie die geklüfteten Festgesteine bilden die beiden wichtigsten Grundwasserleiter im Gebiet. In den höher gelegenen Regionen der Teileinzugsgebiete befinden sich die Grundwasserspiegel in einer Tiefe zwischen 6 m und 35 m unter der Geländeoberfläche, im Be-

reich der Unterläufe dagegen in Tiefen zwischen 35 m und 60 m. Derdurchschnittliche hydraulische Durchlässigkeitsbeiwert kf der Talfüllungen liegt dabei zwischen Werten von 1,83 x 10-6 m/s und 4,17 x 10-5 m/s. Das Kluftsystem in den Festgesteinen spielt die entscheidende Rolle für die Ergiebigkeit der vorhandenen Trinkwasserbrunnen in den tiefer gelegenen Gebieten. Auch die hydraulische Durchlässigkeit des geklüftetenFestgesteinsaquifers wurde daher an einigen Orten im Einzugsgebiet des Wadi Dahab ermittelt, wobei auch Methoden des Remote Sensing eingesetzt wurden. Die entsprechenden Untersuchungen ergaben einen Mittelwert von 4,0 x 10-7 m/s.

Die in verschiedenen Bereichen des Einzugsgebietes des Wadi Dahab entnommenen Grundwasserproben können hydrochemisch in vier Gruppen unterteilt werden. Bezogen auf ihren Salzgehalt können die Grundwässer mit Ausnahme von zwei Proben als Trinkwasser genutzt werden. Die chemischen Analysen zeigen, dass die meisten der im Wasser gelösten Ionen der Verwitterung der gesteinsbildenden Minerale entstammen und auf die sowohl in den Talablagerungen als auch Festgesteinen weit verbreiteten Silikate zurückzuführen sind. Die Analysen erbrachten aber auch, dass die Konzentrationen einiger Wasserinhaltsstoffe wie vor allem Nitrat, Flour, Bor, Arsen und Uran zumindest in einigen Proben über den derzeitigen Grenzwerten der WHO liegen und daher bedenklich hinsichtlich des längerfristigen menschlichen Gebrauchs dieser Wässer sind. Vor allem die Brunnen am Unterlauf des Wadi Dahab sowie die meisten Brunnen im Bereich des Wadi Saal sind für den Einsatz zur Trinkwasserversorgung der hier lebenden Bevölkerung eigentlich nicht geeignet.

Die gelegentlichen Starkregenereignisse können teilweise gefährliche Überschwemmungen in den Wadis verursachen. Im Bereich des Wadi Dahab fällt normalerweise ein Niederschlagsvolumen von etwa 66 Mio. m3 pro Jahr. Bei einem einzelnen Starkregenereignis können jedoch auch bis zu (gemessenen) 76 mm Regen pro Tag fallen, was einem Volumen von 150 Mio. m3 Wasser entspricht! Die Untersuchungen ergaben, dass innerhalb des Einzugsgebietes des Wadi Dahab vor allem das Wadi Zaghraa sehr stark hochwassergefährdet ist: Bezogen auf das Beispiel des oben genannten Starkregenereignisses wurde hier ein Abflußvolumen von 64 Mio. m3 ermittelt, wobei der Spitzenabfluss einen Wert von 556 m3/s erreichte und die Zeitdifferenz bis zur Hochwasserspitze nur etwa 27 Stunden betrug. Ganz allgemein scheint der mittlere und südwestliche Teil des Einzugsgebietes des Wadi Dahab besonders hochwassergefährdet zu sein, nicht jedoch der nördliche Teil.

Um das Überflutungsrisiko in den gefährdeten Teilbereichen zu reduzieren und die ankommenden Abflußmengen kontrolliert ableiten zu können, wird ein ganzes System von Hilfsmaßnahmen vorgeschlagen, angefangen beim verstärkten Bau von Zisternen in den höher gelegenen Gebieten bis hin zum Bau von Rückhaltedämmen und Entlastungskanälen in den Wadis. Der Bau von Dämmen bewirkt zudem, dass in den überstauten Bereichen eine verstärkte Grundwasserneubildung infolge einer großflächigen Versickerung in die alluvialen Talablagerungen hinein stattfinden kann. Der Bau solcher Dämme wird vor allem in den besonders hochwassergefährdeten Wadis Rimthy, Nasab, Saal und Abu Khshieb empfohlen. Mit einem Speichervolumen von rund 7 Mio. m3 wäre hierbei insbe-

sondere ein Damm im Wadi Nasab sehr effektiv, mit demetwa 43% des gesamten, von dem oben genannten Starkregenereignis verursachten Abflußvolumens kurzzeitig gespeichert werden könnten.
Schließlich wurde mit Hilfe von GIS und Remote Sensing auch noch untersucht, welche Bereiche des Einzugsgebietes des Wadi Dahab sich für eine künftige Grundwasserexploration besonders gut eignen. Hierbei wurden sechs Parameter betrachtet, die für eine potentielle Grundwasserneubildung mitentscheidend sind: Jahresniederschlagsmenge, Lithologie, Dichte der Lineamente, Topographie, Hangneigungen und Dichte des Entwässerungsnetzes. Es zeigt sich, dass ungefähr 19,5% der Gebietsfläche ein hohes Potential für die Gewinnung von Grundwasser aufweisen, vor allem der nördliche Teil des Untersuchungsgebietes mit den Wadis ElGenah, Saal und Rimthy sowie einige Bereiche im Wadi Nasab. Umgekehrt werden etwa 40% der Fläche als nur wenig ergiebig bewertet. Dabei handelt es sich insbesondere um die südlichen und östlichen Teile des Einzugsgebietes des Wadi Dahab, in dem die Festgesteine die Geländeoberfläche bilden.

Abstract

This research comprises geological, geomorphological, hydrogeological, hydrogeochemical, climatological, and hydrological studies to investigate the water problems in Southern Sinai-Egypt. Egypt is located within an arid area. It experiences some torrential rainfall, especially in Southern Sinai which causes dangerous flash floods. The Wadi Dahab as an area of investigation is located in the south eastern part of the Sinai Peninsula. Dahab basin comprises five main subbasins, namely W. Zaghraa, W. Abu Khshieb and W. El Ghaieb. W. Dahab frequently receives a huge amount of rainwater. These quantities produce flash floods at the outlets of this wadi. Additionally, farming activities may cause some contaminations of shallow groundwater.

The present work is conducted to estimate the flood risks areas in W. Dahab and to design a suitable management system to control its huge runoff quantities. Hydrogeological and -chemical investigations are necessary in order to define the water pollution and manage the available water resources in the study area. Moreover, Maps indicating the natural water resources should be drawn to show the future review of these resources and setting of the suggested tools to manage water resources in the study area. Many of investigations have been done for reaching the aim of this work.

Geologically, Wadi Dahab catchments are covered mainly from Precambrian to Cretaceous rocks and Wadi deposits cover the valley floors of the main streams. The Advanced Spaceborne Thermal Emission and Reflection Radiometer (ASTER) has been used for lithological mapping in the study area. Band ratio and supervised classification were employed for the classification and discrimination of different rock types. An achievement of this study is a lithological map which extends the Egyptian Geological Survey Mining Authority (EGSMA) map by adding some rock units such as ring-dykes at W. Ferani and metasediment, acidic metavolcanics and basic metavolcanics in W. Saal and W. Rimthy. Dahab basin is affected by many faults which are grouped into three main sets trending NS, NE-SW and NNE-SSW. The density lineament map shows that the high density area is recorded at the basement area especially in the eastern and southern parts of Dahab basin, while the low density area is located in the northern part of study area.

Geomorphologically, the study area is subdivided into five geomorphic units. Based on the Aster Digital Elevation Model, the drainage patterns of the Wadi's sub-basins are delineated, the sub-basins are morphometrically analyzed to assess flash flood susceptibility. The parameters were computed using ESRI's ArcGIS 9.3, enriched by some Visual Basic (VB) code to compute stream numbers according to Strahler Theory. The results of the study show that more than 35% of the sub-basins have high susceptibility of flooding and about 60% have medium susceptibility. Basins of high and moderate flood risk require detailed studies in order to implement actions to protect these areas against flood hazard. The high risk zones are concentrated in three main zones: W. Zaghraa-Nasab which has two main subbasins (W. Nasab and W. Rimthy), headwater parts of W. Abu Khshieb and

of W. El Ghaieb. W. Saal and W. El Genah are ranked as moderate to low levels of flooding risk respectively.

The unconfined aquifers in the study area could be differentiated into alluvial aquifer and fractured basement aquifer. The levels of the groundwater tables are situated from 6 to 35m below the ground surface at wells in the upstream area of Dahab basin while they range from 35 to 60m depth in the downstream area. The hydraulic conductivities of alluvial deposits vary between 0.011 cm/ min to 0.25 cm/min. These values increase in the upstream areas of W. Rimthy and W. El-Ghaieb while they decrease in the upstream area of W. Nasab and the downstream areas of Dahab basin. Fractures play a vital role as conduits-fractures from the recharge zone to feed the production wells in the low-laying fault zones of the basement aquifer. Due to their wide spatial distribution, the hydraulic conductivities of fractured basement rocks have been estimated at some locations in W. Dahab using the remote sensing techniques and deterministic district fractured network (DFN). The results show that the hydraulic conductivities range between 2.3×10^{-7} to 6.1×10^{-7} m/s with an average of about 4×10^{-7} m/s (2 mm/hr).

Hydrochemically, the groundwater is divided into four facies groups. According to their salinity, the groundwater ranges from potable water (the majority of samples) to saline water in only two samples. The chemical analyses show that most of the dissolved ions in groundwater originate mainly by weathering of rocks forming minerals. The distribution of silicate minerals in the basement rocks or in alluvial deposits as weathered material are considered the main sources of cations dissolved in the groundwater. The analysis shows that some substances such as NO_3, F, U, B and As affect human health directly and have concentrations above the limiting values of WHO. Those wells bearing groundwater of acceptable quality are specified in the study. Most of wells in W. Nasab, two wells in W. Saal and one well (G2) at W. El Genah are suitable for drinking purposes, while wells in the downstream of Dahab basin, most wells in W. Saal and one well (R1) in W. Rimthy are unsuitable for drinking purposes.

The study area has an arid to desertic climate with high rainfall intensity during storm events, high temperature and high evaporation rate. Occasional heavy rainfall storms cause dangerous flash floods. W.Dahab basin receives 66 Mm^3 annually. During a maximum storm event, the rainfall enters at up to 76mm/day (150 Mm^3/storm). Approximately 48% of the maximum rainfall contributes to dangerous runoff events. The results show that W. Zaghraa has the highest flooding risk in W. Dahab because it has the highest runoff volume of 64 Mm^3, the highest peak discharge of 556 m^3/s and the time to peak of 27 hr. W. El Ghaieb subbasin is considered as a low risk subbasin due to its moderate peak discharge of 119 m^3/s, its relative long duration to peak of 20 hr with a low volume of about 12 Mm^3. W. Rimthy, part of the W. Zaghraa system, is considered the highest risk because it has an average peak discharge of 200 m^3/s, a short time to peak of 18 hr and a moderate runoff volume in maximum storm of 16 Mm^3. W. Genah, in the W. Zaghraa system, is considered as low risk because it has a low value of average peak discharge of 64 m^3/s, a relative long time to peak of 22 hr and a low

runoff volume storm of about 11 Mm^3 at maximum storm. It can be seen that the wadi path W. Rimthy-W. Zaghraa Nasab – W. Zaghraa in the middle and southwestern part of Dahab basin is the most risky route for runoff which directly affects the downstream area of Dahab basin, while the northern part of Dahab basin is considered a low risk area for runoff especially in W. El Genah, W. Saal and northern part of W. El Ghaieb.

A system of cisterns, detention and reservoir dams in addition to mitigation canals is proposed to control floods in risky basins. This system is very important to enhance recharging the existing aquifers in the wadis. This system is suggested at the risky subbasins such as W. Rimthy, W. Nasab, W. Saal and W. Abu Khshieb. The total storage capacity of the proposed design at W. Rimthy may store a maximum of 1.6 Mm^3 of flood water with an efficiency of about 10.6% of the total runoff at maximum rainstorm. It is estimated that the proposed system for protection in W. Nasab can store as a maximum 7 Mm^3 of runoff water with an efficiency of about 43% of the maximum rainstorm. In W. Abu Khshieb, the proposed protection plan may store a maximum volume of 0.4 Mm^3 of surface runoff with an efficiency of 12.6 % at maximum storm while in W. Saal, the proposed system can store 2.2 Mm^3 with an efficiency of about 24 % at maximum storm. Finally, an integrated approach using GIS and remote sensing was adopted to find new potential sites for groundwater exploration in the Dahab basin. Six different effective weighted parameters were included such as annual rainfall, lithology, lineament density, topography, slope and drainage density. The final map of groundwater potential shows that about 19.5% in W. Dahab is classified as high potential areas for groundwater exploration, concentrated in the northern part of study area at W. El Genah, W. Saal and W. Rimthy and in some parts along the main stream of W. Nasab and W. Zaghraa. Up to 40% of the study area falls within the class of low potential for groundwater exploration, concentrated in the southern and eastern part of W. Dahab, where the basement rocks are outcropping.

LIST OF CONTENTS

Page

Acknowledgments i
Kurzfassung ii
Abstract v
List of Contents viii
List of Figures xiv
List of Table xxv

INTRODUCTION 1

1. Preface……... 1
2. Area of Study…… 2
3. The main features of W. Dahab……... 3
4. The Problems……. 4
5. Aim of this study……..……. 5
6. Objective and methodology…….……. 6
7. Structure of Thesis……..…….…….…. 7

Chapter I GEOLOGICAL SETTING 10

1.1 Lithology in W. Dahab……... 10
1.1.1 Precambrian Rocks…….……..... 10
1.1.1.1 Geology of W. Saal and Wadi Zaghraa…….…….. 11
1.1.1.1.A Sheared meta-volcanics rocks……..... 12
1.1.1.1.B Metamorphosed Tuffs……... 12
1.1.1.1.C Metamorphosed Sediment……..…. 12
1.1.1.1.D Granites ...…….…….. 12
1.1.1.2 Geology of W. Nasab, W. El Ghaieb and W. Ferani…..…….. 13
1.1.1.2.A Older Granitoids …..……..…... 13
1.1.1.2.B Ruting Volcanics …..……..……. 14
1.1.1.2.C Ferani Volcanics …...……..……..... 14
1.1.1.2.D Younger Granitoids …..……..……... 14
1.1.1.2.D.1 Quartez monzogranites …..……..…… 15
1.1.1.2.D.2 Alkali Feldspar Granites..……. 15
1.1.1.2.E Dykes……. 15
1.1.2 Phanerozoic Rocks…….……...…… 17
1.1.2.1 Cambrian Rocks…….…….... 18
1.1.2.2 Cretaceous Rocks…… 18
1.1.2.2.A Lower Cretaceous……..……... 18
1.1.2.2.B Upper Cretaceous……. 19
1.1.2.2.B.1 Raha Formation……. 19
1.1.2.2.B.2 Abu Qada Formation....……..... 19
1.1.2.2.B.3 Wata Formation…….. 19
1.1.3 Wadi Deposits……..……. 20
1.2 Lithological Map in Dahab Basin……..…… 20

1.2.1 Introduction…… 20
1.2.2 Aster Data …… 21
1.2.3 Methodology..... 22
1.2.3.1 Band Ratio…… 22
1.2.3.2 Supervised Classification…… 23
1.2.3.3 Accuracy Assessment……..... 24
1.2.4 Analysis and Results……. 26
1.2.4.1 Central and Southern Part of Dahab basin: Igneous Rocks…… 26
1.2.4.1.A Band Ratio 4/8…….……. 26
1.2.4.1.B Band Ratio 8/5…… 26
1.2.4.1.C Band Ratio 11/14…… 27
1.2.4.2 Central and Southern Part of Dahab basin:Metamorphic Rocks…… 30
1.2.4.3 Northern Part of Dahab basin: Sedimentary Rocks…… 32
1.3 Structure Setting Map in Dahab Basin……..…….. 36
1.3.1 Introduction…….. 36
1.3.2 Method of Lineament Extraction.....……..…….. 37
1.3.2.1 Manual Extraction for Major Faults……..…… 38
1.3.2.2 Automatic Extraction for Lineaments…..…….. 39
1.3.3 The results and Discussion…..……..…… 40

Chapter II GEOMORPHOLOGY 45

2.1 Stream and Basin Delineation……. 45
2.1.1 Drainage Pattern Extraction…… 46
2.1.2 Basin Delineation……..……. 47
2.2. Qualitative Geomorphology…..……..... 51
2.2.1 Mountainous Basement Terrain……... 52
2.2.2 Flat-Topped limestone plateau……. 53
2.2.3 Alluvial Fan…….…… 53
2.2.4 Coastal Plain…… 54
2.2.5 Drainage Network.....……..... 54
2.2.5.1 Rectangular Drainage…….. 55
2.2.5.2 Dendritic Drainage……..…… 56
2.2.5.3 Trellis Drainage…… 56
2.2.5.4 Parallel Drainage……..……. 56
2.3 Quantitative Geomorphology…… 57
2.3.1 Morphometric Analysis of Drainage Network……. 58
2.3.1.1 Stream Order (U)……..…….. 60
2.3.1.2 Bifurcation Ratio (R_b)……. 60
2.3.1.3 Stream Length (L_u)……..…… 63
2.3.1.4 Drainage Frequency (F)…….. 65
2.3.1.5 Drainage Density (D)…… 66
2.3.1.6 Overland Flow (OLF)……. 67
2.3.2 Morphometric Analysis of Basins…….…….. 68
2.3.2.1 Basins Area (A_u)……. 68
2.3.2.2 Basins Dimensions……. 70
2.3.2.2.A Basin Length……..…… 70
2.3.2.2.B Basin Width……..…….. 70
2.3.2.2.C Basin Perimeters…… 71
2.3.2.3 Basins Shape…… 71

2.3.2.3.A Circularity Ratio…… 71
2.3.2.3.B Elongation Ratio…… 72
2.3.2.4 Basins Surface…… 73
2.3.2.4.A Slope Surface……..... 74
2.3.2.4.B Gradient……..…..... 75
2.4 Flood Hazard Risk Map……..…… 77

Chapter III HYDROGEOLOGICAL AND HYDROGEOCHEMICAL INVESTIGATIONS 82

3.1 Hydrogeological Conditions……..... 83
3.1.1 Factors Affecting Groundwater Occurrence……..…….. 83
3.1.1.1 Climatic Factors……..…….…. 83
3.1.1.2 Topographic Factors……..…….…. 83
3.1.1.3 Structural Factors……..…… 84
3.1.2 Aquifer Types…… 84
3.1.2.1 Alluvial Aquifer……..…… 84
3.1.2.2 Basement Aquifer……..…… 85
3.1.3 Hydrological Boundary Conditions…….. 85
3.1.2.1 Wadi Nasab……..……..…. 86
3.1.2.2 Wadi Saal……..…… 89
3.1.2.3 Downstream of W. Dahab……..…… 91
3.2 Hydraulic Properties……..…….. 93
3.2.1 Hydraulic Conductivity of Alluvial Deposits……. 93
3.2.2 Hydraulic Conductivity of Fractured basement Rocks…… 97
3.2.2.1 The Method of investigation……..……..…. 99
3.2.2.2 The Result and Evaluation……..……..…. 101
3.3 Hydrogeochemical Properties and Environmental Impacts…….. 106
3.3.1 Introduction…… 106
3.3.2 Physical and Chemical parameters……..…. 107
3.3.2.1 Electrical Conductivity (Ec)……..……..…. 107
3.3.2.2 Total Dissolved Salts (TDS)……..…… 109
3.3.2.3 pH……..……..…… 111
3.3.2.4 Accuracy of Samples Analyses……..... 112
3.3.2.5 Major Elements……..…… 113
3.3.2.5.A Chloride (Cl^-)……..…… 113
3.3.2.5.B Sulphate (SO_4^{2-})……..……..…. 115
3.3.2.5.C Bicarbonate (HCO_3^-)……..……..…… 116
3.3.2.5.D Sodium (Na^+)……..……..…… 117
3.3.2.5.E Potassium (K^+)……..……..……. 118
3.3.2.5.F Calcium (Ca^{2+})……..…… 119
3.3.2.5.G Magnesium (Mg^{2+})……..……..…….. 121
3.3.2.5.H Silica (SO_2)……..……..…….. 122
3.3.2.5.I Bromide (Br)……..……..……..…… 123
3.3.2.6 Heavy Metals……..……..…….. 124
3.3.2.6.A Zinc (Zn) & Cadmium (Cd)……..……. 126
3.3.2.6.B Chromium (Cr) & Nickel (Ni)……..…..... 127
3.3.2.6.C Manganese (Mn) & Iron (Fe)……..... 129
3.3.3 Hydrogeochemical Groups…… 130
3.3.3.1 Group (A)……..…… 131
3.3.3.2 Group (B)……..…… 132
3.3.3.3 Group (C)……..…… 133
3.3.3.4 Group (D)……..…… 135

3.3.4 Hydrogeochemical Ratio…….. 140
3.3.4.1 rMg/rCl ratio…….. 141
3.3.4.2 rNa/rCl ratio…….. 142
3.3.4.3 $rCl/rHCO_3$ ratio…….. 143
3.3.4.4 rSO_4/rCl ratio…….. 144
3.3.4.5 rBr/rCl ratio…….. 144
3.3.5 Hydrogeochemical Processes…….. 145
3.3.5.1 Origin of dissolved ions…….. 146
3.3.5.2 Origin of Groundwater Salinity…….. 149
3.3.5.2.A Rock Type…….. 150
3.3.5.2.B Groundwater Movement..…….. 150
3.3.5.2.C Water Table Position..…….. 150
3.3.5.2.D Agricultural Uses..…….. 151
3.3.6 Health and Environmental Impacts…… 151
3.3.6.1 Total Dissolved Solids Distributions as a Contamination Indicator…… 151
3.3.6.2 Nitrate (NO_3-)…….. 152
3.3.6.3 Flouride (F)…….. 154
3.3.6.4 Uranium (U)…….. 157
3.3.6.5 Boron (B)…….. 159
3.3.6.6 Arsenic (As)…….. 161
3.3.7 Water uses in Drinking Purposes…… 163

Chapter IV CLIMATE AND RUNOFF ANALYSIS 166

4.1 Climate Analysis……..... 166
4.1.1 Temperature…….. 167
4.1.2 Humidity…….. 169
4.1.3 Wind…….. 170
4.1.4 Precipitation……..... 171
4.1.4.1 Annually and Monthly Distribution....……..... 173
4.1.4.2 Average Rainfall over the Study Area....……..... 173
4.1.4.3 The Highest Amounts of Rainfall and Their Dates……..... 175
4.1.4.4 High Storm Analysis..……..... 176
4.1.5 Evaporation……..... 178
4.2 Runoff Analysis……..... 182
4.2.1 Hydrograph ……..... 183
4.2.2 Synthetic Hydrograph……..... 184
4.2.2.1 Geomorphic Unit Hydrograph .....…… 185
4.2.2.1.A The Concept of Geomorphic Unit Hydrograph based on Nash Model…….. 186
4.2.2.1.B Determination of Horton's Ratio…….. 188
4.2.2.2 Spatially Distributed Unit Hydrograph……..... 190
4.2.3 Models Development……..... 193
4.2.3.1 Topographic Data .....……..... 193
4.2.3.1.A Digital Elevation Model (DEM)……..... 193
4.2.3.1.B Slope……..... 194
4.2.3.2 Land Cover .....……..... 194
4.2.3.3 Climate Data .....……. 196
4.2.3.4 Velocity of Flow .....…… 197
4.2.4 The Results……..... 198
4.2.5 Data Comparison with Other Location …….…..... 201

4.2.6 Integrated Hydrologic Parameter ……..... 203

Chapter V WATER MANAGEMENT 207

5.1 Surface Water Management…….……. 207
5.1.1 Evaluation of Existing Dams……..... 207
5.1.2 Specifications of Existing Major Protective Dams..…….. 211
5.1.2.1 Dam (1)....……..……..... 211
5.1.2.2 Dam (2)....……..……..... 212
5.1.2.3 Dam (3)....……..……..... 212
5.1.2.4 Dam (4)....……..……..... 213
5.1.2.5 Dam (5)....……..……..... 214
5.1.2.6 Dam (6)....……..……..... 214
5.1.3 Factors affecting Surface Water Management..…… 214
5.1.3.1 Climatic Condition and Rainfall Analysis..……..…..... 214
5.1.3.2 Runoff Volume..…….. 215
5.1.3.3 Mean Groundwater Recharge..……..……... 216
5.1.4 Delineating Areas of possibly High Flooding Risk..…..……...…. 216
5.1.4.1 Wetness Index (WI)..……..….. 217
5.1.4.2 Relative Stream Power Index (SP)..…….……..... 219
5.1.5 Runoff Management..……..……. 221
5.1.5.1 Cisterns..…….…..….... 221
5.1.5.2 Storage and Detention Dams..…….….. 221
5.1.5.3 Storage and Recharge Pit..……..……... 222
5.1.5.4 Retardation System..……... 224
5.1.5.4.A Sand and Rock Barriers……... 224
5.1.5.4.B Terracing…….....…. 224
5.1.5.4.C Rainwater Collectors……....……... 225
5.1.6 Proposed Design and Flood Control Efficiency…….…… 226
5.1.6.1 Flood Control in W. Nasab and its Efficiency……. 226
5.1.6.2 Flood Control in W. Rimthy and its Efficiency……..... 228
5.1.6.3 Flood Control in W. Saal and its Efficiency……..... 230
5.1.6.4 Flood Control in W. Abu Khshieb and its Efficiency……..…. 238
5.2 Potential Map For Groundwater Exploration…… 234
5.2.1 Introduction..... 234
5.2.2 The Model…….……..…. 235
5.2.2.1 Annual Rainfall Factor…….. 236
5.2.2.2 Lithology Factor…….…….. 236
5.2.2.3 Lineament Density…… 238
5.2.2.4 Drainage Density……..…… 238
5.2.2.5 Topography Factor (Elevation and Slope)…….. 240
5.2.2.6 Method of Weighting Factors……...…… 241
5.2.3 Results and Discussion……..…… 243

Chapter VI SUMMARY, CONCLUSIONS AND RECOMMENDATION 247

6.1 Summary and Conclusions…… 247
6.2 Recommendations……..…… 253

REFERENCES **255**

APPENDIX **265**

LIST OF FIGURES

INTRODUCTION

Figure 1 Location Map of W. Dahab Basin…… 2

Figure 2 The Main features of W. Dahab Basin……. 4

Figure 3 Some of Destructive Effects of Runoff on Infrastructure in W. Dahab 5

Figure 4 Structure of Dissertation……. 9

Chapter I GEOLOGICAL SETTING

Figure 5 Geologic Map of the W. Saal Area (Hegazi; 2006)……. 11

Figure 6 Geological map of the W. Ferani Area and the Downstream area of Dahab Basin (Modified after El Masry; 2003)…… 13

Figure 7 Monzogranite in W. Nasab Basin …… 15

Figure 8 Alkali Granites Rocks and Dissected by Basin Dykes W. Nasab…… 16

Figure 9 Post Granitic Dykes (Basic Dykes)…… 16

Figure 10 Cambrian Rocks in W. El Ghaieb…….. 18

Figure 11 Lower Cretaceous (Malha Fm) and Upper Cretaceous Rocks outcropping at W. El Ghaieb…… 19

Figure 12 Aster Scene Characteristics……...…….. 21

Figure 13 Process Flow Diagram For Lithological Mapping of the Dahab Basin Area…….. 23

Figure 14 A) Band Combination 7-3-1 of Dahab Basin Area
B) Map of the Wadi Deposits……..……. 26

Figure 15 A) Band Ratio 4/8 Image

	B&C) Spectral Signature of Biotite and Chlorite (Clark et al. 2007)…….....	27
Figure 16	A) Band Ratio 8/5 Image B) Spectral Signature of Kaolinite (Clark et al. 2007)……	27
Figure 17	Band Ratio 11/14 Image…….……..……	28
Figure 18A	Stacked Band Ratio Image (8/5 R, 4/8 G, 11/14B)……	29
Figure 18B	ML Classification Using The Stacked Band Ratio Image (8/5 R, 4/8 G, 11/14B)…….	29
Figure 19	A) Stacked Band Ratio 4/6, 4/7, 4/10 Image of W. Rimthy Area……..…… B) Stacked Band Ratio 4/6, 4/7, 4/10 Image of W. Saal Area……..……	31
Figure 20	A) ML Classification of Stacking Band Ratio 4/7 R, 4/6 G and 4/10B Images for W. Saal…… B) ML Classification of Stacking Band Ratio 4/7 R, 4/6 G and 4/10B Images for W. Rimthy……	31
Figure 21	A) Band Ratio 7/6 Image of the Northern Part of Dahab Basin Area B) Spectral Signature of Calcite (Clark et al. 2007)…….	33
Figure 22	Band Ratio 6/4 Image of the Northern Part of the Dahab Basin……	33
Figure 23	Supervised Classification of Band Ratio 7/6 Image of the Northern Part of Dahab Basin Area……..	34
Figure 24	Final Lithological Map of Dahab Basin Area……	35
Figure 25	Gulf of Aqaba Formation which Results From Dead Sea Rift (Mechie and El Isa, 1988)……	36
Figure 26	Work Flow of the Lineament Extraction…….	38
Figure 27	Edge Enhancement Results of W. Dahab…….……	39
Figure 28	Major Fault Map of W. Dahab……	41
Figure 29	Major Fault Map of Western Side of Gulf of Aqaba (Modified after Eyal et al.1981)……..…	42
		43

Figure 30 Minor Lineament Map of W. Dahab & its Rose Diagram……

Figure 31 Lineament Density Map of W. Dahab (km/km^2)…… 43

Figure 32 Field Measurements Locations for Lineament Features in W. Dahab Basin…… 44

Chapter II GEOMORPHOLOGY

Figure 33 Model Builder Diagram Showing the Workflow to Extract the Drainage Pattern From Digital Elevation Model (DEM)…… 47

Figure 34
A) Digital Elevation Model…….
B) Raster Fill of Digital Elevation Model……
C) Raster Data of Flow Direction…… 48
D) Raster Layer of Flow Accumulation…….
E) Raster Layer of Streamline…….
F) Drainage Network of Dahab Basin……

Figure 35 Main Basins and Sub-basins in W. Dahab…… 50

Figure 36 Geomorphic Units in W. Dahab Basin……. 51

Figure 37 Mountains in W. Dahab Basin…….. 52

Figure 38 Spot Scene of Delta W. Dahab Basin…… 55

Figure 39 The Drainage Patterns in Some Subbasins Within Dahab Basin… 57

Figure 40 Strahler Ordering System…… 58

Figure 41 Relationship Between Basin Order and Stream Order Number…… 61

Figure 42 Bifurcation Ratio of Different Subbasin in Dahab Basin…… 62

Figure 43 Relationship Between Basin Length and Stream Order Number in Dahab Basin…… 64

Figure 44 Stream Frequency Map in Dahab Basin…… 65

Figure 45 Stream Density Map in Dahab Basin…… 66

Figure 46 Overland Flow Map in Dahab Basin……. 68

Figure 47 Relationship Between Basin Area and Stream Order Number in Representative Subbasins at Dahab Basin…… 69

Figure 48 Circulatory Ratio Map of W. Dahab Basin…….. 72

Figure 49 Elongation Ratio Map of W. Dahab Basin…… 73

Figure 50 Neighborhood Algorithm Estimates Percent Slope in cell 5 by Comparing the Elevations of Neighboring Grid Cells…… 74

Figure 51 Slope Degrees For The Surface of Dahab Basin…… 75

Figure 52 (A-F) Gradient of Different Subbasins in Dahab Basin…… 76

Figure 53 Flood Hazard Risk Map Based on Morphometric Parameter for Dahab Basin……..... 80

Chapter III HYDROGELOGICAL AND HYDROCHEMICAL INVESTIGATIONS

Figure 54 Well Location Distribution in W. Dahab…… 82

Figure 55 A) Effect of Basic Dykes at Upper Stream in W. Nasab……
B) Spring Along Fault Zones at Upper Stream in W. Nasab…… 86

Figure 56 Boreholes Distribution at W. Nasab…… 87

Figure 57 Hydrogeological Cross Section of W. Nasab……..… 88

Figure 58 Boreholes (5N) at W. Nasab……. 88

Figure 59 Distribution Boreholes Locations in W. Saal…… 89

Figure 60 Hydrogeological Cross in W. Saal…… 90

Figure 61 A) Borehole S11 (Safra well) at W. Saal…….. 90

B) The Effect of Structure on Groundwater Occurrence……

Figure 62 Well Locations in Downstream of W. Dahab…… 92

Figure 63 Hydrogeological Cross Section in Downstream of W. Dahab…… 93

Figure 64 Location Sites For Infiltration Tests…… 94

Figure 65 Estimated Infiltration Capacity of Alluvial Deposits in each Subbasins in W. Dahab…… 96

Figure 66 Schematic Hydrogeological Cross section at Upstream Part of W. Dahab (Modified afte El Rayes, 2004)…… 97

Figure 67 Location of Investigation Sites…… 98

Figure 68 Flow Chart of the Used Data Layer For Lineament Extraction…… 99

Figure 69 Results of Truncation Effect Result From Length Data of the Extracted Lineament in Area (1) and Area (3)…… 100

Figure 70 Orientation Rose Diagram of Fractures at Area around Well 6 & Well 7…….. 101

Figure 71 Trend Diagram of Minor Fracture Measurements at W. Nasab Area…… 101

Figure 72 Field Measurements of Lineaments at W. Nasab Area…… 102

Figure 73 Lineament Intersections Density of Basement Rocks of W. Nasab Area Basin……. 102

Figure 74 The DFN for Investigation Areas (A1-A4)…….. 103

Figure 75 Hydraulic Conductivity Tensors for the Studied Discrete Fracture Networks (DFN) at Four Investigation Area at W. Nasab…….. 104

Figure 76 The Linear Relation Between TDS and Electric Conductivity…… 109

Figure 77 TDS Distribution in Dahab Basin , (A) W. Nasab and (B) W. Saal….. 110

Figure 78 Comparison of TDS Values of Groundwater in W. Dahab Basin…… 110

Figure 79 pH Distribution in Groundwater of Dahab Basin…… 112

Figure 80 Distribution of Chlorine Ion in Groundwater of W. Dahab Basin… 114

Figure 81	**Distribution of Chlorine Ion in Groundwater of W. Nasab……**	**114**
Figure 82	**Sulphate Distribution in Groundwater of Dahab Basin……**	**115**
Figure 83	**Bicarbonate Distribution in Groundwater of W. Nasab Basin……**	**117**
Figure 84	**Sodium Distribution in Groundwater of W. Nasab……**	**118**
Figure 85	**Calcium Distribution in Groundwater of W. Dahab Basin……**	**120**
Figure 86	**Outcrops of Upper Cretaceous Rocks Near W. S11 in W. Saal……**	**121**
Figure 87	**Relation Between Ca & Mg Concentrations in Groundwater of Dahab Basin……..**	**122**
Figure 88	**Bromide Distribution in Groundwater of W. Dahab Basin……**	**124**
Figure 89	**Zinc Distribution in Groundwater of W. Dahab Basin During Rainy and Dry seasons……**	**126**
Figure 90	**The Relationship Between Nickel and Sulphate Contents in Groundwater of Dahab Basin……..**	**128**
Figure 91	**Comparison Chromium and Nickel Concentrations in Dry and Rainy Seasons in Groundwater of Dahab Basin……**	**128**
Figure 92	**Availabilities of Iron and Manganese During Dry and Rainy Seasons in Groundwater of W. Dahab Basin……**	**129**
Figure 93	**Dug waterhole in Basement Rocks at the Upstream of W. Nasab……**	**131**
Figure 94	**Scheoller Diagram of Hydrochemical Group (A)……**	**132**
Figure 95	**Scheoller Diagram Representing Group (B) Groundwater of Dahab Basin……**	**133**
Figure 96	**Scheoller Diagram of Group (C) Facies of Groundwater at Dahab Basin……**	**134**
Figure 97	**Scheoller Diagram of Hydrochemical Group (D)-Subgroup(1)at W. Dahab Basin Area……**	**135**
Figure 98	**A) Well N11 at Downstream of W. Nasab …… B) Well (S1) at the Upstream of W. Saal……**	**137**
Figure 99	**Scheoller Diagram of Hydrochemical Group (D), Sub-group(2) of Groundwater at Dahab Basin……**	**138**
Figure 100	**Relation Between Sodium Concentration and TDS of Groundwater at W. Saal……**	**139**

Figure 101	**A) Hydrochemical Facies in W. Nasab…… B) Hydrochemical Facies in W. Saal……**	**139**
Figure 102	**A) Hydrochemical Facies in W. Rimthy ……. B) Hydrochemical Facies in Downstream of Dahab …….**	**140**
Figure 103	**A) rMg/rCl Distribution along W. Nasab …… B) rMg/rCl Distribution along W. Saal……..**	**142**
Figure 104	**Relation Between rCl/rHCO$_3$ Ratio and TDS in Groundwater of W. Saal……**	**143**
Figure 105	**Relation Between rBr/rCl ratio and Cl Concentration in Groundwater of W.Dahab……**	**145**
Figure 106	**Gibbs Diagram of Groundwater of W. Dahab……**	**147**
Figure 107	**Relation Between Total Cation (meq/l) and K+Na (meq/l) in Groundwater of Dahab Basin……**	**147**
Figure 108	**Relation Between Cl (meq/l) and K+Na (meq/l) in Groundwater of Dahab Basin……**	**148**
Figure 109	**Relation Between Ca+Mg (meq/l) and SO$_4$+HCO$_3$ (meq/l) in Groundwater of Dahab Basin……..**	**149**
Figure 110	**TDS Distribution in Groundwater of Dahab Basin……**	**152**
Figure 111	**Relationship Between Cl and TDS in Groundwater of Dahab Basin…….**	**153**
Figure 112	**Relationship Between NO$_3$ and TDS in Groundwater of Dahab Basin……**	**154**
Figure 113	**NO$_3$ Distribution in Groundwater of Dahab Basin……**	**155**
Figure 114	**Relationship Between Flouride and TDS in Groundwater of Dahab Basin……**	**155**
Figure 115	**Flouride Distribution in Groundwater of Dahab Basin……**	**156**
Figure 116	**Uranium Concentration in Groundwater of W. Nasab During Dry and Rainy Seasons……**	**157**
Figure 117	**Uranium Concentration in Groundwater of W. Rimthy During Dry and Rainy Seasons……**	**158**
Figure 118	**Uranium Concentration in Groundwater of W. Saal During Dry and**	

Rainy Seasons…… 159

Figure 119 Boron Distribution in Groundwater of Dahab Basin…… 160

Figure 120 Relation Between Calcium and Boron Concentrations in Groundwaters of Dahab Basin…… 160

Figure 121 Relation Between TDS and Boron Concentration in Groundwater of Dahab Basin…….. 161

Figure 122 Arsenic Distribution in Groundwater of Dahab Basin…… 162

Figure 123 Potential Risk Map For Drinking Water at W. Dahab Basin……..… 165

Chapter IV CILMATE AND RUNOFF ANALYSIS

Figure 124 Meteorological Stations Surrounds W. Dahab Basin ……. 167

Figure 125 Average Maximum and Minimum Temperature in Stations Surrounding W. Dahab…… 168

Figure 126 Average Humidity in Stations Surrounding W. Dahab …… 169

Figure 127 Rose Diagram of Wind Direction at The Station Surrounding Dahab Basin…….. 170

Figure 128 Weighted Annual Rainfall in Dahab Basin…….. 174

Figure 129 Maximum Daily Storm Recorded at Saint Catherine Station from (1934-2004)…… 176

Figure 130 A) The Probability Curve For the Maximum Rainfall Event in Saint Catherine Station ……. B) Recurrence Time Curve For the Maximum Rainfall Event in Saint Catherine Station……. 178

Figure 131 A-C) Water Surplus Period of the Studied Records of Different Meteorological Station Surrounding W. Dahab …… 179

Figure 132 Average Evaporation loss According to Calculated Evaporation and Measured values at Dahab Basin in Storm Months…….. 182

Figure 133 Schematic Diagram of Geomorphic Unit Hydrograph Model…….... 186

Figure 134 Schematic Diagram of Spatially Distributed Unit Hydrograph Model……. 190

Figure 135 The Main Concept of Spatially Distributed Unit Hydrograph Model (after Maidment;1993)…… 191

Figure 136 Digital Elevation Model of Subbasins in W. Nasab…… 193

Figure 137 Decimal Slope of Subbasins in W. Nasab…… 194

Figure 138 Manning Value "n" of Subbasins in W. Nasab…… 195

Figure 139 Measured Hyetograph of Maximum Storm (76.2mm) in Saint Catherine Station (WRRI, 2006)…….. 196

Figure 140 Variation of Time of Concentration With Rainfall Excess……. 200

Figure 141 Maximum Observed Discharges Versus Watershed Area After (Ben Zvi & Shentsis, 2000)…… 202

Figure 142 Maximum Observed Volumes Versus Watershed Area After (Ben Zvi & Shentsis, 2000)…… 202

Figure 143 Integrated Runoff Risk Map Depending on Hydrologic Parameters……. 205

Chapter V WATER MANAGEMENT

Figure 144 Dam Locations in W. Dahab Basin ……..... 208

Figure 145 Retention Dam of Dam No. 4…….. 209

Figure 146 Retention Dam of Dam No. 3…….. 209

Figure 147 Storage Reservoir at W. El Ghaieb…… 209

Figure 148 Storage Reservoir at W. Saal…… 209

Figure 149 Chart of Methodology for Measuring Storage Capacity of Dams using GIS……..…… 210

Figure 150 The Main concept for Cut and Fill Tool Working for Calculating Storage Capacity of Dams using GIS…… 211

Figure 151 Protective Dam (1) at W. El Ghaieb ……..... 212

Figure 152 Protective Dam (2) at W. El Ghaieb ……. 212

Figure 153 Protective Dam (3) at W. El Ghaieb..... 213

Figure 154 Protective Dam (4) at W. El Genah……..……. ……..... 213

Figure 155 Protective Dam (6) at W. El Saal ……..... 214

Figure 156 Wetness Index Distribution in Subbasins of W. Dahab…… 218

Figure 157 Stream Power Index of Subbasins at W. Dahab Basin……... 220

Figure 158 Proposed Design of Cistern (after Geriesh, 1998)…… 222

Figure 159 Dimensions of the Proposed Mitigation Canal……. 223

Figure 160 Proposed Zigzag Rock Barriers……. 224

Figure 161 Proposed Terracing Method at Wide Area Within Basin…….. 225

Figure 162 Proposed Rainfall Storage (Collector) Method in W. Zaghraa…….. 225

Figure 163 Proposed Water Management Plan in W. Nasab…….. 226

Figure 164 Efficiency of Proposed Design at Different Storms in W. Nasab Basin…… 228

Figure 165 Proposed Water Management Plan in W. Rimthy…… 229

Figure 166 Proposed Water Management Plan of W.Saal……..... 231

Figure 167 Efficiency of Proposed Design at Different Storms in W. Saal Basin. 232

Figure 168 **Proposed Water Management plan at W. Abu Khshieb……** **233**

Figure 169 **Flow Chart for Groundwater Potential Model……** **235**

Figure 170 **A, B) Average rainfall and Lithology Classification Classes of Dahab Basin**
C.,D) Lineament Density and Drainage Density Classification Classes of Dahab Basin
E, F) Slope (Degree) and Elevation Classification Classes of Dahab Basin **241**

Figure 171 **Groundwater Potentiality Map of W.Dahab……** **244**

Figure 172 **Ratios of Groundwater Potentiality Rank Areas in W. Dahab……** **245**

Figure 173 **Comparison Between Model Results and Productive wells in Dahab Basin……** **245**

LIST OF TABLES

INTRODUCTION

Table 1 Statistics of population in Southern Sinai (after reports of South Sinai and Environmental Action Plan, 2003)…… 3

Chapter I GEOLOGICAL SETTING

Table 2 Granitic Rocks Types in Dahab Basin Area…… 17

Table 3 Accuracy Evaluation of The Classification Map for Igneous Rocks Types……... 30

Table 4 Accuracy Evaluation of The Classification Map for Metamorphic Rocks Types……... 32

Table 5 Accuracy Evaluation of The Classification Map for Sedimentary Rocks Types…….. 34

Table 6 Sobel Filter Kernels in Four Principal Directions……..… 39

Chapter II GEOMORPHOLOGY

Table 7 Comparison Between Order Number in Topographic Map 1:50000 and DEM 30m Resolution. …….. 60

Table 8 Length Stream Order of Different Subbasin in Dahab Basin …….. 64

Table 9 Basin Area of Different Basin Order in Each Subbasins at Dahab Basin ……..……. 69

Table 10 Score Assigned of Morphometric Parameters in Dahab Basin ……..… 78

Table 11 Flood Risk Results for Each Subbasins in Dahab Basin ……. 80

Chapter III HYDROGELOGICAL AND HYDROCHEMICAL INVESTIGATIONS

Table 12 Boreholes Data in W. Nasab……... 87

Table 13	**Boreholes Data in W. Saal……**	**91**
Table 14	**The Result of Infiltration rate (I) in the field and Hydraulic Conductivity (K) in the Lab of Alluvial Deposits……..**	**95**
Table 15	**Results of the Trace Line Map Analysis……..…..**	**100**
Table 16	**Result of hydraulic conductivity of fractures basement rocks at selected areas in W. Nasab…….……**	**105**
Table 17	**Results of Chemical Analysis Studied Groundwater Samples in Dahab Basin…….**	**108**
Table 18	**Groundwater Classification of Dahab Basin Based on Chebotarev's Classification…….**	**111**
Table 19	**Results of Heavy Metals Analysis within Groundwater Samples in Dahab Basin……..…**	**125**
Table 20	**Hydrogeochemical Groups of The Examined Groundwater of Dahab Basin……..**	**130**
Table 21	**Hydrogeochemical Ratios For Groundwater Samples in Dahab Basin……..……**	**141**
Table 22	**Chemical parameters affecting drinking water at Dahab Basin…….**	**164**

Chapter IV CLIMATE AND RUNOFF ANALYSIS

Table 23	**Location of Meteorological Stations Surrounds Dahab Basin……..**	**167**
Table 24	**Average Wind Velocity at Meteorological Stations (Knot/hr) (Source-General Egyptian Meteorological Authority)……...**	**171**
Table 25	**Average Monthly of rainfall (Source -General Egyptian Meteorological Authority)……**	**173**
Table 26	**Average Annually of rainfall (Source GMA and WRRI)……..**	**173**
Table 27	**Isohyetal Method for Calculation Weighted Rainfall in Dahab Basin……**	**174**

Table 28	**Maximum Rainfall in (mm/day) Data in Dahab Basin (Source General Meteorological Authority)…….**	**175**
Table 29	**Mean Daily Evaporation (mm/day) from period (1934 to 2004) (Source – GMA)……..…**	**179**
Table 30	**Calculated Evaporation at the Study Area……..…..**	**181**
Table 31	**Results of Hydrographs Paramters for the Main subbasins in Dahab Basin…….…..**	**195**
Table 32	**Comparison Between Calculated Runoff Volume and Calculated Runoff Volume by Equation's Meirovich et al., 1988……**	**203**
Table 33	**Hydrological Paramters for The Design Runoff Risk Map in Dahab Basin……..**	**204**

Chapter V WATER MANAGEMENT

Table 34	**Dams Specifications of Dahab Basin….…….…….…….**	**209**
Table 35	**Specification of Constructed Dams in Dahab basin……..…**	**212**
Table 36	**Storage Capacities and Efficiency of the Proposed Management Design at W. Nasab basin……....**	**227**
Table 37	**Storage Capacities and Efficiency of the Proposed Management Design in W. Rimthy basin……..…**	**230**
Table 38	**Storage Capacities and Efficiency of the Proposed Management Design in W. Saal basin……...**	**232**
Table 39	**Storage Capacities and Efficiency of the Proposed Management Design at W. Abu Khshieb basin……..**	**234**
Table 40	**Different Permeabilties, Weighted Values for Lithological Units in Dahab Basin…….**	**237**
Table 41	**Weight Values and Rank of Drainage Density of Dahab Basin …….**	**239**
Table 42	**Weight Values and Rank of Slope (Degree) of Dahab Basin……**	**240**
Table 43	**Ranks and Weights for Factors and Their Influencing Classes Used for Groundwater Potentiality Mapping in Dahab Basin……**	**242**

INTRODUCTION

Introduction

1. Preface

Worldwide more than 1.1 billion people have no access to clean water and about 2.4 billion people no access to basic sanitation (UNEP, 2007). One reason for this situation is the extremely unbalanced water distribution in the world determined by on regional climates. Especially, Arid zones mainly located in Africa and Asia, are characterized by a chronic shortness of water. In those areas groundwater is often the only reliable source of fresh water due to sporadic rainfalls. Nowadays, water problems in arid regions are rising primarily from the rapidly increasing water demands due to the growing population as well as pollution, on the one hand and natural water shortage on the other hand.

In the future, arid regions may profit from global climatic changes and an increasing number of thunder storms which may produce huge quantities of rain water. But, there is a big danger that the immersion runoff may have catastrophic effects on the new communities and their surrounding environment. Additionally, a lot of (rain) water is lost due to evaporation or draining to the sea without any use for development as in many areas in arid zones. A suitable management system to control those runoff quantities is of great importance.

Groundwater is a very important component in the water policy of any government but especially those in arid zones and is evaluated as a safe source of potable water in these areas. The alluvial deposits within the wadi systems of the arid regions are the main aquifer, so the management plan should aim at a sustainable use of those water resources as well as of the natural environment.

Egypt is located within arid areas and faces catastrophic problems related to water shortage, for especially people living in desert areas. Water availability in Egypt is less than 1000 m^3 per capita and year (UNEP, 2007). In Egypt groundwater is considered an important source of fresh water. Currently, it is exploited from two main sources: The first one is the deep aquifer systems with non-renewable fossil groundwater in sedimentary rocks in the Western desert, the Nile delta and some locations in the Northern part of the Sinai Peninsula. The second source is represented by the shallow alluvial aquifers and fractured basement rocks in the mountainous regions such as in the Eastern desert and Southern Sinai.

The Egyptian government has made big efforts to develop the desert areas and new productive land forced by a distinct increase in population as well as agricultural and industrial production. Water availability is the main factor for any development and creating new settlements. At the very beginning of any development, the quantity and quality of local and regional water resources have to be investigated. So, the aim of this work is the assessment of possibilities of protection against flood hazard risks at effective areas in W. Dahab basin, Southern Sinai, which is considered as an important spot in the development concept in Egypt.

2. Area of study

W. Dahab is evaluated as one of the most important areas on the Sinai peninsula because many tourist projects are located there which are the biggest source of Egypt`s national income. The area of W. Dahab basin is located at the South Eastern part of the Sinai peninsula and is bounded by latitude 28^{O} 22\ 43.4\\ and 28^{O} 52\ 18.5\\ N and longitude 33^{O} 55\ 46.9\\ and 34^{O} 31\ 28.8\\ E. It covers an area of about 2080 km^2 (Fig. 1.A). It is bordered by the Gulf of Aqaba in the East, G. Gidid, G. Sheikh El-Arab and G. Ferani in the South,G. Catherine, G. Um Alawi, G. Um Loz, G. Hamami in the West and G. El Genah and G. Ghalium in the North (fig.1B).

The catchment area of W. Dahab is part of the mountainous regions of Southern Sinai exceeding heights of 2000 m a.s.l. W. Dahab collects a huge amount of flood flow from main tributaries such as W. Zaghra, W. Nasab and W. Saal. All these Wadis start from steep granitic heights and run eastwards to join with W. Dahab which is the stream that finally flows into the Gulf of Aqaba.

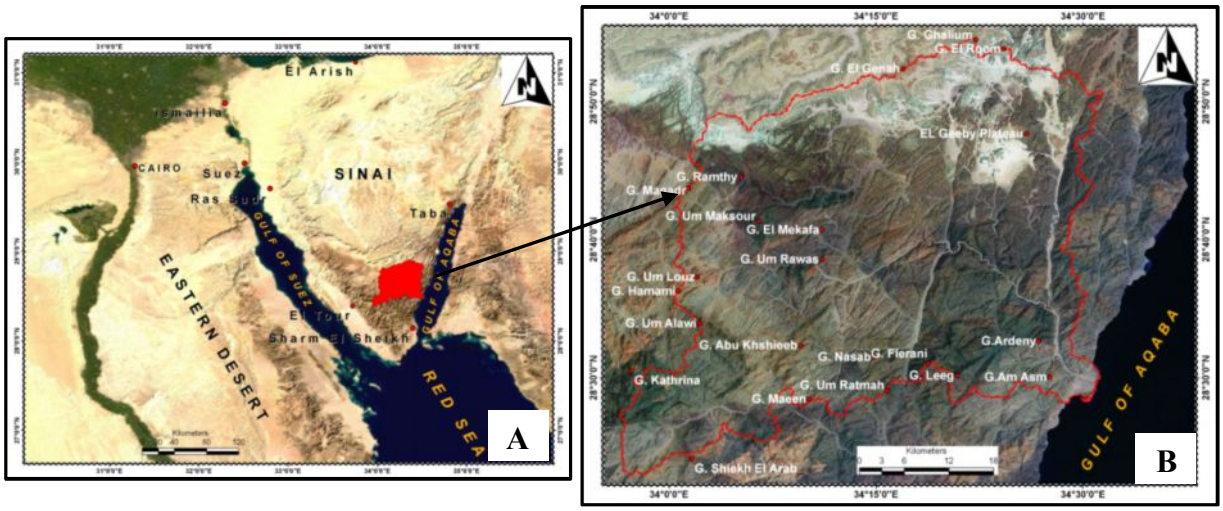

Figures1A + B: Location Map of W. Dahab Basin

The Water Resources Research Institute –Cairo (WRRI, 2006) was the only institution which made a plan for protection against flood damages in the study area during 2005. It suggested some local sites of dams along W. Dahab to protect Dahab City, in particular, which is located on its lower course.

Similar to other arid areas all over the world, the environmental and weather conditions of the W. Dahab basin include extreme aridity, long hot and rainless summer months and mild winters. The only source of fresh water is the rainfalls in winter, spring and autumn. During these months the area experiences short, but very intensive rainfalls which bring the Wadi close to overflow. Sometimes they cause severe flash floods endangering and damaging the infrastructure and even affecting human lives.

In the past years, several floods took place along W. Dahab, the last one in 1994. According to field investigations and discussions with local people, the water level at the wadi exit raised up to

more than 2,5 m. As a result, there were big damages to buildings and roads. Based on an analysis of historical rainfall data, it has to be mentioned that the 1994 flood was probably not the maximum possible flood. The probability of risky flood events is between one and two times in 100 years, with the occurrence of higher floods, much higher damages have to be expected (WRRI, 2006).

Groundwater is one of the most important water resources in the study area supporting life of the local inhabitants, most of them bedouins. The daily production of groundwater reaches up to 1300 m^3 (Report of South Sinai and Environmental Action Plan, 2003). But, compared with the amount of water needed by the population and its activities, it`s not enough. So, we should think about ways to enhance these resources to make them sufficient for all the people living in W. Dahab area. Desalination of seawater is the second main water resource in Dahab basin. This water is used available for touristic purposes especially and provided to resorts and hotels. Private plants produce about 1000 m^3daily, while governmental desalination plant produces daily about 5000 m^3. Besides the high costs of the desalination process, these amounts are not sufficient for development of the study area

3. The main features of W. Dahab

The City of Dahab is located on the mouth of W. Dahab and the Gulf of Aqaba. It is connected by two main roads with Sharm El-Sheikh in the South (100 km distance) and Nuweiba City in the North (60 km distance). The latter also leads to Saint Catherine in the very West of the study area (fig. 2).

In 1960 the official Census of Egypt recorded only 4,355 inhabitants living in Southern Sinai; almost all of them indigenous bedouins. By 1986 the number of inhabitants increased to 28,576, and by 1996 to 54,826, representing an annual increase of 6.7% (South Sinai Environmental Action Plan, 2003). In 2003 it was estimated that around 7,628 inhabitants lived in the Dahab area. Projections up to 2017 indicate the population might increase to some 30,000 persons on a conservative forecast, representing about 11% of the total population of Southern Sinai as shown in Table 1.

In 2010 the population in the W. Dahab area reached 12,000 people. They are mainly concentrated in W. Nasab, W. Saal, W.Zaghraa and along the lower course of W. Dahab. The development of population until 2013 has been estimated based on a number of assumptions related to the increase of operating hotels, indirect tourism employment multipliers and the settlement of workers in the tourism industry and their families. Due to the recent political and economic situation in Egypt in general and its influence on tourism, the predicted numbers of inhabitants in the Dahab area and Southern Sinai for 2013 and 2017 won`t be reached.

	2003	2008	2013	2017
Dahab area	7,628	10,919	20,382	31,744
South Sinai total	111,226	157,482	219,599	289,718

Table 1: Statistics of population in Southern Sinai (after reports of South Sinai and Environmental Action Plan, 2003)

4. Problems

Arid regions are affected by major, sometimes catastrophic rainfalls (Baker, 1977). Such events are rare, they tend to be scattered in space, and their scientific documentation is mostly inadequate. Although most of Egypt is located within the desert belt, it experiences some torrential rainfalls, which causes flash floods all over the Sinai Peninsula. Flash floods in hot deserts are characterized by high flow velocity and short duration with sharp discharge peak (Ashour, 2002). High sediment loads are carried by floods threatening settlements in the wadis and the people living there.

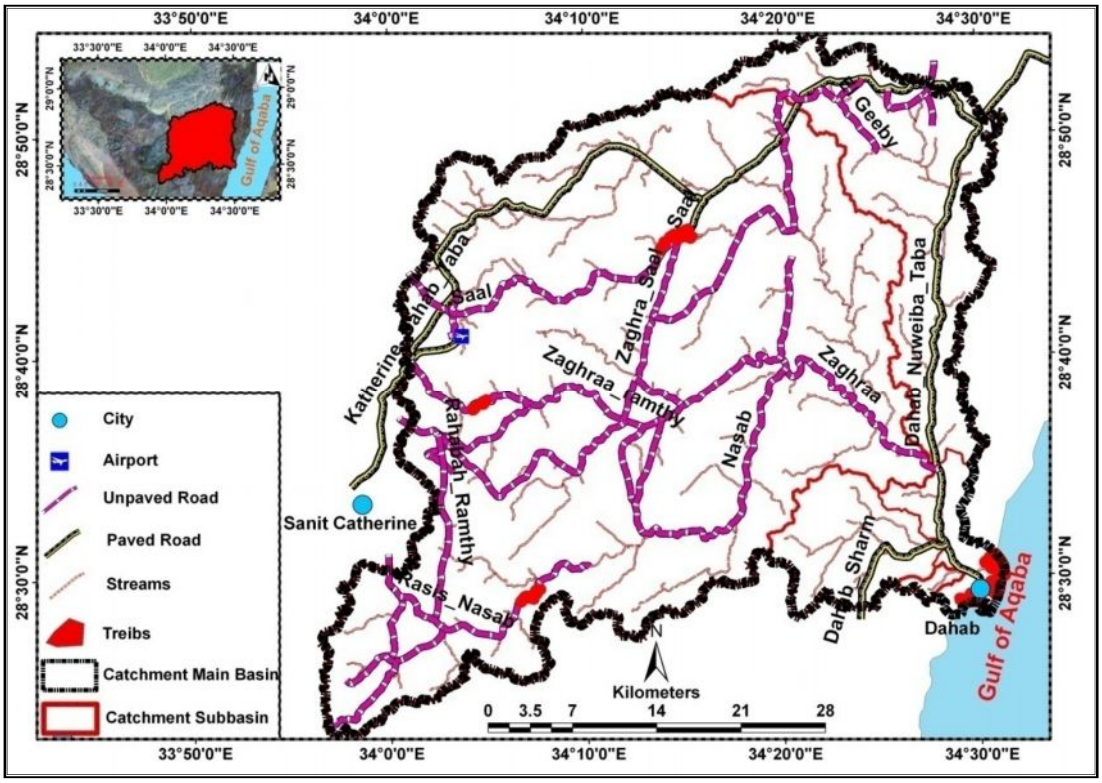

Figure 2: The Main features of W. Dahab Basin

The extreme spottiness of rare heavy rainfalls precludes any efficient forecasting. Thus, although the limited amount of data still is reflected, chances of developing a warning system for floods in the desert are low. The relatively short flood-to-peak time interval, a characteristic of those floods, presents an additional impediment to any efficient use of warning systems.

Generally, the study of runoff calculation is very difficult especially in Sinai because of the lack of direct runoff data. Many researchers have faced this problem, and it will remain unsolved until long-term runoff data will become available (JICA and WRRI, 1999). Thus, it may be helpful to use other methods to estimate runoff in the study area such as morphometric analyses combined with the evaluation of climatic data. Severe floods along W. Dahab could cause significant damages to properties and loss of lives within Dahab City (fig. 3). Due to the meteorological conditions of South Sinai, flood events are not frequent, but severe. After several dry years, creating a false impression of

safety, an extreme flood event may occur. The affected areas include tourist locations as well as dwellings of local people.

Flash floods happen every few years transporting variable amounts of sand, gravel and boulders from the mountainous areas to the coastal zone. Weathering products of igneous, metamorphic and sedimentary rocks are transported to the coast by flood waters, accumulating it along as detritus sediments. We can summarize the major problems in the W.Dahab basin as follows:

Figure 3: Some of Destructive Effects of Runoff on Infrastructure in W. Dahab

1- Many of the hydrographic basins in W. Dahab are subjected to unexpected thunder storm rainfall causing flash floods.

2- There are losses of great amount of water without any beneficial usage such as the recharge of shallow aquifers.

3- The maximum expected rainfall quantities could run floods to the outlet of the wadis (valleys) in arid regions causing catastrophic effects on the infrastructure, the surrounding environment and the local inhabitants.

4- Groundwater of shallow aquifers at the wadi (valley) outlets is subjected to pollution. This water resource is considered as the main water resource in the arid region, and need to be protected.

5- The shortage of fresh water resources in relation to the increase of population in the future will be a severe problem in the study area.

5. Aim of this study

The thesis aims to study the water resources of the Wadi Dahab area mainly from the view of hydrogeology and -chemistry on the one hand. The results obtained should lead to a water management plan to protect the area against flood risks and to save the existing groundwater resources for the future, on the other hand. Combined with these aspects, it is necessary to consider

the sources of the pollution of the groundwater and possibilities of groundwater recharge in alluvial deposits along the wadis. In detail, the different steps and aims of this study are as follows:

1- Estimation of the flood risks of an arid hydrographic basin to design a suitable management system for protection. Huge runoff quantities have to be controlled and considered as possible source of water under the aspect of development strategies for the W. Dahab area.

2- Geological and hydrogeological maps have to be drawn to evaluate the occurrence of water resources.

3- Hydrogeological and -chemical investigations have to be carried out in order to design and manage the available water resources in the study area as well as designing a suitable protection system depending on the seasonal amount of both flooded water and infiltrated water through the flood channels.

4- Maps indicating the natural water resources should be drawn to show the future review of these resources and setting of the suggested tools to manage water resources in arid areas (W. Dahab basins as case study)

6. Objectives and methodology

1- Geological maps have been established by means of satellite data as ETM+ 7 band and ASTER image 15 bands to show the lithological, structural and hydrogeological situation in the study area. Using suitable ASTER band ratios, it is possible to differentiate various rock units in order to enhance the already existing geologic map of the area and facilitate the geological mapping of similar areas. Further, it is intended as a step forward for updating the geological maps of all the Southern Sinai Peninsula and hydrogeological investigations of the Wadi Dahab basin.

2- A map of the drainage network has been developed using the Digital Elevation Model (DEM-ASTER data, 30 m resolution) as well as a topographical map for carrying out a topographical analysis. Different morphometric parameters have been investigated to estimate the level of flood risk of several sub-watersheds within the catchment area of Wadi Dahab. Due to the topographical situation, different sites of high flood risk have been specified. GIS techniques have been used to extract parameters of the wadi network and to produce a flood hazard risk map based on the results of the morphometric analysis.

3- The hydraulic properties "infiltration rate" and "hydraulic conductivity" have been calculated for the alluvial deposits by making infiltration tests at different sites of the study area representing the different hydrological situations along upper and lower course sections of the wadis. The hydraulic properties of fractured basement rocks as major units within the study area have been determined by using a new method: The hydraulic conductivity of this rock type has been estimated by using remote sensing techniques. The extracted lineaments from satellite images have been used to develop a method to qualify and quantify fluid flow through Discrete Fracture

Networks (DFN). Based on the DFN analysis, it is possible to determine the hydraulic conductivity tensor of the fracture system.

4- Hydrogeological cross sections have been drawn according to collected data of groundwater wells to investigate the updated situation of groundwater conditions in the area. Hydro-chemical analyses of groundwater samples (major and trace elements) have been studied to determine the chemical characteristics of the groundwater drained from the aquifer and collected in wells. Besides, the recent pollution of the groundwater has been another aspect which results from an interaction with rocks, domestic use and effects of agricultural land use. It is important, too, as it may affect the health of the people who live in the wadis and are dependent on this groundwater produced by shallow wells.

5- Meteorological data have been collected to study the climate conditions of the study area. Effective storm events on Wadi Dahab had been defined to perform calculations of the probably of maximum storm events. Unmeasured meteorological parameters have been calculated such as evaporation. Precipitation data has been studied to investigate the volume of water input and water losses. These results are used for estimating the mean maximum runoff volume which may affect the wadi system.

6- A hydrological model has been established to calculate hydrological parameters as maximum discharge, time to peak, time of concentration and volume of runoff caused by high storm events. As the estimation of hydrographs in areas without any gauge stations depends on synthetic hydrograph techniques, GIS has been used as an important tool to construct this model.

7- Finally, a suitable managing design for surface water is suggested which can be used for protecting the area against floods on the one hand and offering a possibility for groundwater recharge within the shallow aquifer of alluvial deposits, on the other hand. Using GIS and remote sensing techniques, the future development of the water resources in this area is estimated for the case the suggested management design is realized.

7. Structure of Thesis

The present thesis consists of the introduction and five chapters as shown in figure (4):-

Chapter 1:- Description of the geological settings of the study area. For that purpose, lithological maps based on satellite data have been created. The geological background is important for understanding the function of the main aquifers. Besides, the tectonic structures dominate both the interior morphology of aquifers as well as the drainage system of the wadi network.

Chapter 2:- This chapter introduces to the geomorphological characteristics of the study area. The analysis is divided into qualitative and quantitative studies. The qualitative aspects for studying the main geomorphic features have been extracted from satellite data. Quantitative geomorphology shows the morphometric analysis of the main subbasins and their drainage network in the study area. It is divided into three parts: The first one describes the geomorphic units in the Wadi Dahab area, the

second part concerns the morphometric analysis of the drainage networks which has been extracted mainly from topographic maps and DEM images. The third part of this chapter is related to the morphometric analysis of the basins, indicating hazard map based on morphometric analysis and the most important flood risk zones in the Wadi Dahab area.

Chapter 3:- The description of hydrogeological and -geochemical investigations of groundwater aquifers in the study area and their results is divided into two parts: The first part provides a discussion on the aquifer types in Dahab basin, the recent situation of groundwater levels and some hydrogeological cross sections; additionally the hydraulic conductivities of different rock forming aquifer types are defined. The second part is related to groundwater hydrogeochemistry and its characteristics from different views. Finally, a potential risk map for drinking water is established for the complete Dahab basin to define zones where suitable groundwater for drinking purposes can be found.

Chapter 4:- This chapter describes the climate conditions in the study area such as temperature, humidity, wind and evaporation. The main part is dedicated to rainfall data to study its distribution over the entire area. The other part concerns the estimation of runoff by various methods of synthetic hydrographs to calculate different runoff parameters. Finally, risk areas for flash floods are determined.

Chapter 5:- The chapter concerns flash flood hazard mitigation. Its first part gives an evaluation of already existing dams in the study area. The next part discusses the best methods which can help to mitigate flood hazards in arid zones as well. The last part presents a groundwater exploration map based on previous data to define promising locations for groundwater wells.

Chapter 6:- The last chapter deals with the most important results of the study. Additionally, the chapter offers important recommendations, based on the results and which should be implemented and completed by future studies to improve the management of water resources in the study area.

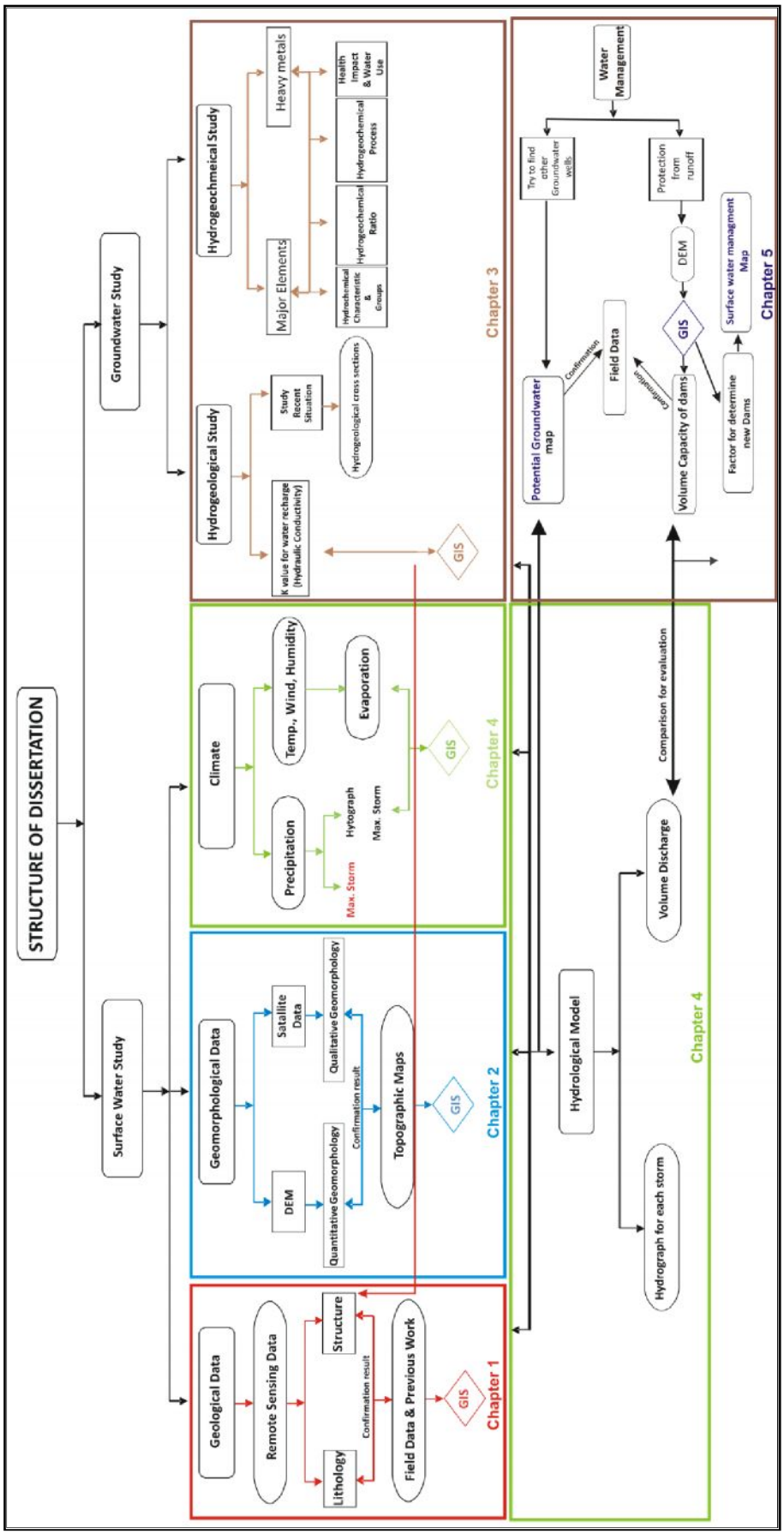

Figure 4: Structure of Dissertation

CHAPTER I

GEOLOGICAL SETTING

Chapter I

Geological Setting

W. Dahab basin is located in the old Archean Triangle that belongs to Arbo-Nubian Shield. The basin is composed of different rock types which includes igneous, metamorphic and sedimentary rocks. The igneous rocks cover nearly 1319 km² (about 63.2 %) of the study area, while the metamorphic rocks cover about 135 km² (6%) of total area, and the sedimentary rocks expand on the surface for 276, 8 km² (13.2%). The recent deposits cover 356 km² (nearly 17%); they are distributed as deltas, alluvial fans, terraces and wadis fillings.

The following is a brief description of the geologic setting of Dahab Basin;

1.1 Lithology in W. Dahab

The lithology of W. Dahab basin is discussed by many authors; among them are: "Hume (1906), Said (1962), Soliman (1986), El Shafei et.al. (1992), Kora and Genedi (1995), Zalata et.al (1997), El Masry et.al (2003), Hegazi (2006), and Hassen et.al (2007). They subdivided the lithologic cover of the area into two types of rocks:

1- Precambrian igneous rocks which cover more than 63% of the study area and metamorphic rocks which cover small parts of the study area, especially in W. Feirani, W. Saal and W. Zaghraa.
2- Sedimentary rocks which cover the northern part of the study area including Cambrian to Upper Cretaceous rocks.

1.1.1 Precambrian Rocks

The Precambrian complex of the Arabian Nubian Shield is dominated by rocks that have evolved and cratonised during the pan-African tectono-thermal event. Its initial stages are widely governed by a compressional tectonic system. The major crusts have been found between 900 and 600 Ma ago and give rising to voluminous Calc alkaline granitoids (Bentor, 1985). The final stage (600-540 Ma) of cratonization is dominated by NW –trending strike slip faults, strong extension which is accompanied by magmatic activity, and the deposition of molasses sediments (Stern, 1985; Jarrar et al. 1992).

The crustal structures of Southern Sinai as a part of the Arabian-Nubian Shield result from complex events of subduction, accretion and extension during Pan African times. Shimron (1984) classified the basement rocks of Sinai into three principal units: a high metamorphic rank basal complex, lower grade calc alkaline volcano-sedimentary associations and late kinematic to post-kinamatic (Pan –African) calc alkaline and alkaline volcanic and plutonic masses.

Many researchers studied the geological settings in different parts within W. Dahab basin. These studies can be summarized according to their location within Dahab basin:

1.1.1.1 Geology of W. Saal and W. Zaghraa

Geological and geochemical studies in W. Saal area have been carried out by Hume (1935), Shimron et.al. (1993), Soliman, 1986, Bentor, (1985), El Shafei et al. 1992, Hassen et al. 2004, and Hegazi, 2006). W. Saal area belongs to one of two main metamorphic belts in southern Sinai. The first group, Fieran-Solaf belt and Taba metamorphic belt, is composed of medium to high grade metasediments, ortho-gneisses and magmatities. The second group comprises volcano-sedimentary rocks of Kid and Saal belts metamorphosed to greenschist facies.

The Saal–Zaghraa Belt is a Late Precambrian assemblage of metavolcanics and metasediments. The metasediments are originally sediments derived most probably from a rapidly rising volcanic chain (Soliman 1986). On the other hand, Hassen et al. (2004) mentioned that the widespread occurrence of andesite, dacite and rhyolite tuffs, as well as epiclastic rocks such as litharenite and conglomerate, are consistent with a volcanic-arc setting.

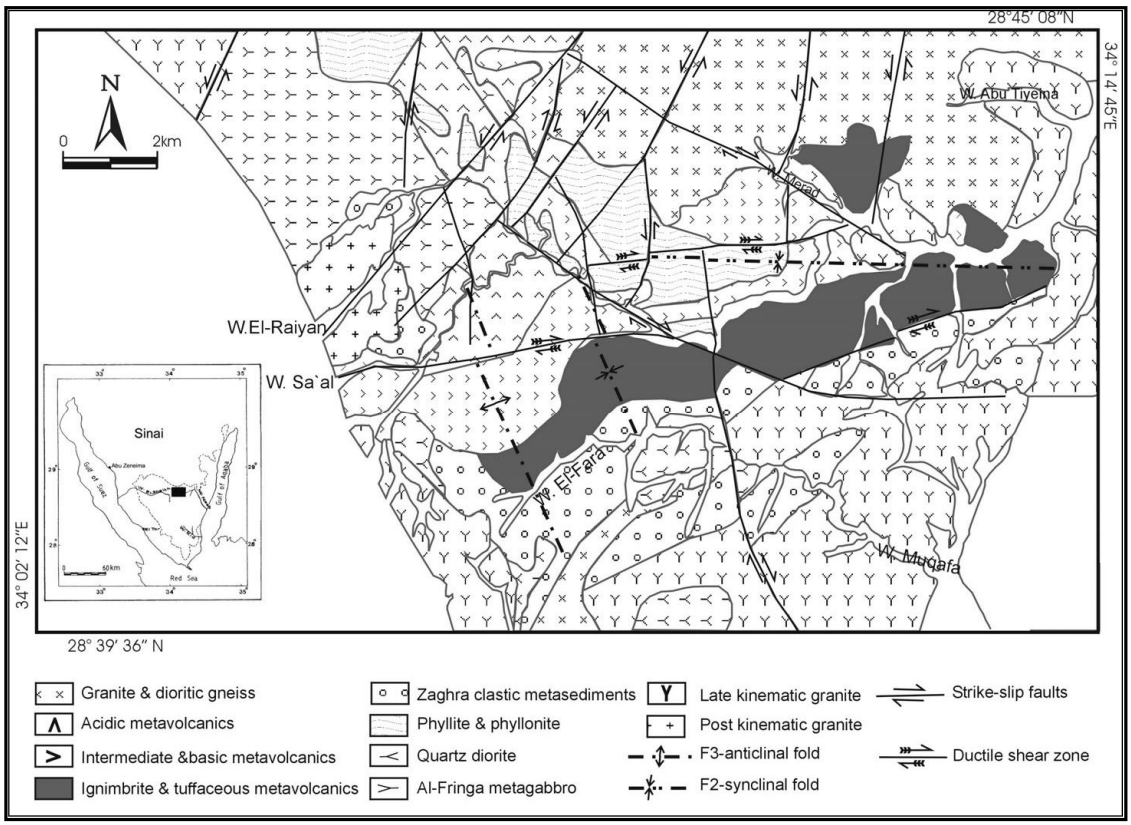

Figure 5: Geologic Map of the W. Saal Area (Hegazi; 2006)

Soliman (1986) stated that Saal belt is a complex of metamorphosed volcanic-arc volcano-sedimentary succession intruded by gabbros and calc alkaline and alkaline granotoids. The area experienced polyphase deformation (Soliman, 1986; El-Shafei et al. 1992). The major unit rocks are distinguished in W. Saal according to Hegazi. (2006), namely sheared metamorphosed volcanices,

sheared metamorphosed sediments, gabbroic rocks, calc alkaline rocks (Qz diorite and granodiorites) and alkali feldspar granites (fig.5).

1.1.1.1.A Sheared metavolcanics Rocks

They are considered to be the most rock cover of W. Saal and they are present in the central part of the basin. The metavolcanic rocks are comprised of a variety from metaryholite to metabasalts, including intermediate types. The acidic metavolcanic rocks are mainly metarhyolites and rhyodacites with intercalated metasediment. The intermediate and basic metavolcanics consist mainly of metaandesite and metabasalt. Metaandesite comprised lava flows and tuffs that are moderately foliated. It is typically porphyritic with phenocrysts of plagioclase.

Main minerals are biotite and amphiboles with accessory sericite, chlorite, and epidote. The metabasalt has a phenocryst assemblage which includes plagioclase and pyroxene. Secondary minerals are comprised of epidote, chlorite, and hematite.

1.1.1.1.B Metmorphosed tuffs

They comprise sheared and massive varieties which are closely associated with metamorphosed volcanics. Ignimbrite and tuffaceous metarhyolites are widely distributed in the study area, well-foliated, and are tectonically bounded by other meta-volcanic bodies. They are characterized by fine-grained sanidine phenocrysts and strongly oriented, fine-grained sanidine, muscovite, and quartz. The epidote and sphene are the most conspicuous indicators of metamorphism up to greenschist facies.

1.1.1.1.C Metamorphosed Sediment

The metavolcanics are interbedded with volcanogenic arenites and metasedimentary rocks. They occur as small outcrops in W. Saal El-Rayan and W. Saal. The rocks are fine-grained, dark in color and schistose, and are highly fractured with conspicuous foliation.

Hassan et.al. 2004, 2007 differentiated the metamorphosed sediments into chlorite phyllite, calcareous metapelites, metasiltstone, metaconglomerate; dolomite marbles, volcanogenic lith-arenites and arkosic and quartizite. The metamorphic mineral assemblage includes mainly albite and chlorite, whereas cordierite, sericite, epidote and carbonate are less abundant.

1.1.1.1.D Meta-Gabbro

Soliman, 1986 recognized a large body in the north of W. Saal El Rayan in the Fringa area with several exposures occuring along W. Saal and W. Saal El Rayan. The same researcher points out that this unit includes an alteration of epidote and chlorite. Hassan et. al. (2004) referred to this unit as metamorphosed and that it also occurs as intrusive bodies including xenoliths of metasediments and metavolcanics.

1.1.1.1.E Granites

It considers the most abundant intrusive rocks. They are commonly coarse- to medium-grained usually with xenoliths of mafic rocks fragments. Hassan et. al. (2004) differentiated two types:

- Late kinematic granites which are more distributed in W. Saal and comprised of Qz diorite and granodiorite. Both contain xenoliths from meta-volcanic and metasediments.
- Post kinematic granites which are considered orthoclase- rich granites (Alkali granites). They are comprised of Qz syenite, Qz monazites, monazites, and syenites.

1.1.1.2 Geology of W.Nasab and W. El Ghaieb and W. Fierani

The Geology of Nasab area and the surrounding part of Saint Catherine and Gebel Fierani are investigated by many authors such as Hume (1906), Bentor and Eyal (1979), Mohana (1989), Khalil (1990), Abu El Lail et al. (1990); El Masry (1998) and El Masry et al. (2003). The rock types in W. Nasab basin can be distinguished by six categories as shown in figure (6):

1- Older Granitoids, 2- Ruting Volcanics , 3- Fierani Volcanics, 4- Younger Granitoids, 5- Dykes and 6- Wadi Deposits

1.1.1.2.A Older Granitoids

This type of rock that occupies a vast area in South Sinai basement has been classified either according to their color as grey granites (Akaad and El Ramly, 1960) or as syn to late tectonic granitoids (El Ramly, 1972) or relative to age the rock, has been classified as older granitoids (Akaad and Noweir, 1980). The older granitic rocks are entirely devoid of any internal structure, except porphyritic textures. They consist of plagioclase, Hornblendee, biotite, quartz and orthoclase. These granitoids rocks are traversed by acidic, intermediate and basic dykes with a general trend of NE-SW and N-S.

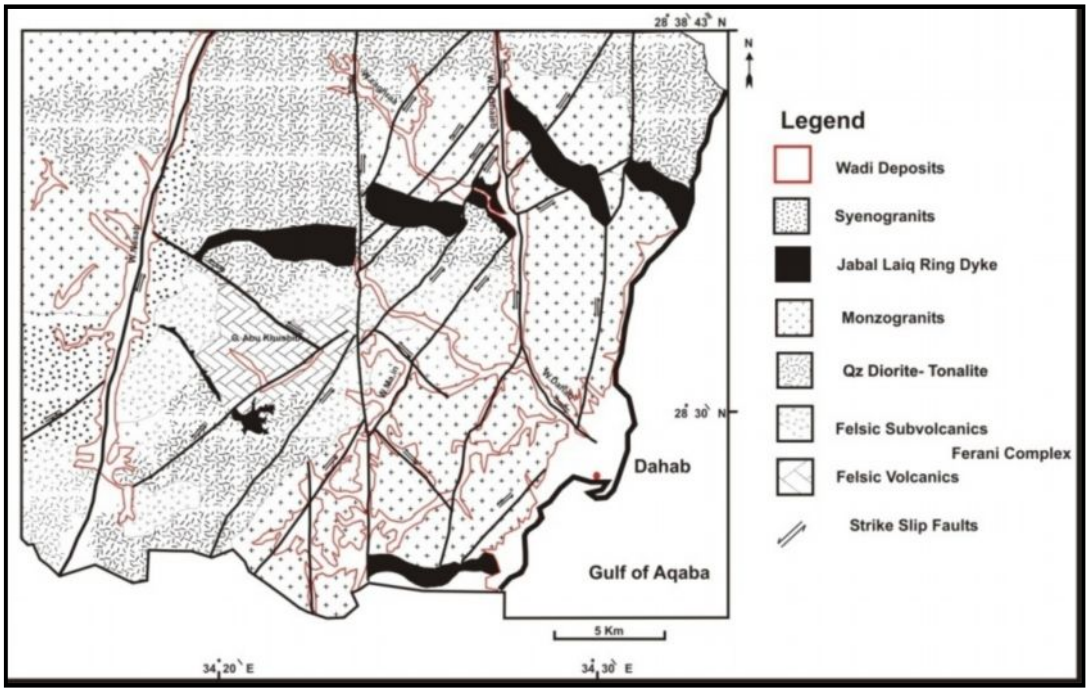

Figure 6: Geological map of the W. Ferani area and the Downstream area of Dahab Basin (Modified after El Masry; 2003)

Older granitoids are distributed in different parts in Dahab basin and represent more than 60% of the rock occurrence in the study area. They outcrop in most parts of W. Nasab basin. Oada (1995) stated that older granitoids are distributed in El Rahabah plain, W. El Shallal and Gebel Nasab, in W. El Ghaieb and in the surrounding Gebel Ferani. Older granitoids can be differentiated into many types of rocks as Qz diorite and Tonalite in addition to granodiorite.

1.1.1.2.B Ruting Volcanics

Rutig Volcanics are a slightly metamorphosed, gently dipping thick volcano-clastic succession of alternating pyroclastics with intermediate to acid lava flows. According to Khaliel, (1990) they are equivalent to Dokhan volcanics which spread out in the eastern desert of Egypt. Ruting and Catherine volcanics are defined in W. Nasab, especially in W. El Ruting and W. Rasis (El Morsey, 1988). They consist mainly of andesites, rhyodacites and rhyolites. Rutig Volcanics are characterized by their relatively low joint density. They are cut by dykes of different compositions: acidic, intermediate and basic.

1.1.1.2.C Ferani Volcanics

Ferani volcanics can be found in the southern part of Dahab Basin, especially west of the town of Dahab. Ferani volcanics are studied by Hume (1906), Bentor (1985), Bentor and Eyal (1987), Abu El Leil et al. (1990), El Masry (1998) and Moussa (2003).

Ferani volcanics are defined as a volcano-sedimentary succession (El Masry, 1998) and are distinguished into two groups of rocks. The first composes interbedded volcaniclastics and epiclastics, while the second is represented by subvolcanic intrusion consisting of porphyry rhyodacite. Epiclastic rocks consist of laminated coarse to medium sandstone and conglomerate interbedded with mudstone. Volcanics include pyroclastics which are dominated in the Ferani area. Pyroclastics are distinguished into laminated or massive tuff and lapilli-tuff (El Masry, 1991). Mineralogically, pyroclastics are composed of muscovite, biotite and andalusite; on the other hand, lava flow consists mainly of grey aphanitic rhyodacite and rhyolite.

1.1.1.2.D Younger Granitoids

Younger granitic rocks constitute a major part of southern Sinai rocks. According to Hume (1935), younger granitics have been previously mapped as Gattarian granites, also (Akaad and El Ramly, 1960) as pink and red granites, (El Shazly, 1964) as younger granites relative to the older granitoids, and (El Gaby, 1975) as late to post orogenic pink and red granites.

Younger granitoids outcrop in many parts in the Nasab basin. They are exposed at W. El Rasis, W. Nasab and G. Kharban. They form mountains of moderate to high relief relative to adjacent land forms. They vary in color from reddish brown to pinkish white and coarse- to medium-grained in texture. Khaliel (1990), Abu EL Leil et. al (1990) and El Masry (1991) mapped younger granitoids in W. Nasab basin. Younger granitoids can be differentiated into monzogranites and Alkali granites. The following is a brief description of these units:

1.1.1.2.D.1 Quartz monzogranites

Quartz monzogranites cover an extensive terrain around W. Abu Khusheib and Maaen and at the downstream of W. Nasab (fig.7). It forms mountains of moderate to high relief that are cut by several dykes swarms directed NE. The quartz monzonites are intruded by alkali feldspar granites and Ring Dyke rocks and crossed by numerous basic dykes and pegmatitic veins (El Rayes, 1992). Qz monzogranites are composed of K-Feldspar, plagioclase feldspar, Hornblende, and biotite with accessory minerals includes Fe-Ti oxides, sphene, zircon, apatite, chalcopyrite and pyrite (Mohana, 1989). They are highly fractured and weathered.

Figure 7: Monzogranite in W. Nasab Basin

1.1.1.2.D.2 Alkali Feldspar Granites

The alkali feldspar granites are pink colored, medium- to coarse-grained homogeneous rocks (fig.8). They are exposed at W. Nasab and W. Rasis. The medium-grained variety occupies the high peaks and is characterized by high joint density, where the coarse-grained type occurs. Mineralogically, the alkali feldspar granites are composed mainly of quartz, potash feldspar and plagioclase with a variable amount of mafic minerals. Iron oxides, sphene, zircon and apatite are accessory minerals. The granitic rocks intrude into the older quartz monzonites with sharp, steeply dipping outward intrusive contacts. Field investigation showed that the alkali feldspar granites belong to the youngest rock unit encountered in the study area.

1.1.1.2.E Dykes

The area of study is intruded by many dykes varying in composition from acidic to intermediate to basic rocks. The dykes are investigated by many authors like Eyal et al. (1981), Mahana (1989) and

El Masry et al. (2003). Eyal et al. (1981) and Mahana (1989) stated that dykes originated in southern Sinai in three phases. The first is associated with the volcanic process, the second follows the intrusion of younger granites, and the third is younger than Late Neogene age dykes. The position of dykes are espeically NE-SW, E-W, N-S and NW-SW.

Figure 8: Alkali Granites Rocks and Dissected by Basin Dykes W. Nasab

Figure 9: Post Granitic Dykes (Basic Dykes)

The dykes and dykes swarms have different dimensions and sizes and are controlled by many joint and fracture systems and zones. El Masry et al. (2003) mapped ring dykes in Gebel. El Laiq and stated that the" jabal Laiq Ring Dyke" intrusion is made of two geomorphic elements, namely the upper and outer parts. The geometry of ring dykes intrusion is elongated with its axies of E-W direction and is approximately 24 Kilometers long. The dykes cut the rocks at W. Zaghraa, W. El Ghaieb, W. Maan, W. Um Shauki and W. Nasab; they are composed of medium granular to porphyritic Qz syenite, hornblende-biotite syenogranite and microgranite. Mineralogically, they consist of K-Feldspar microperthite, Qz, plagioclase feldspar, Hornblende, biotite, zircon, apatite and Fe-Ti oxides.

It can be concluded that granitic rocks are the most abundant rock type in the study area. They extend at W. Nasab, W. Rimthy, W. dahab and W. El Ghaieb. The granitic rocks in the study area are divided into late kinematic and past kinematic rocks (Hassen et al. 2004 and El Masry et al. 2003). Egyptian Geological Survey and Mining Authority (EGSMA,1994) divides the granitic rocks into monzogranite, syanogranite, granodiorite and quartez diorite. Based on mineral composition, the granitic rocks have been distingushed into two main groups in the investigation area, older granitoid and younger granitoid rocks (Table 2).

Types of Granites	Forming Rocks	Forming Minerals
Older Granitoid	Granodiorite, Qz Diorite, Diorite	Qz, Plagioclase, Hornblende, Pyroxene
Younger Granitoid	Alkali granite, Monzogranite	Qz, K-Feldspare, Plagioclase, Biotite,

Table 2: Granitic Rocks Types in Dahab Basin Area

The mineral composition of Younger Granites consists of quartz and k-feldspar, plagioclase, hornblende and biotite, zircon, apatite, sercite (Kaolinite) and opaques (El Masry et al. 2003). The Older Granitoids are composed mainly of plagioclase feldspar, k-feldspar microperthite, hornblende, biotite, quartz, zircon, sphene, apatite and opaques are among the accessory components. Weathering of hornblende, biotite and plagioclase leads to the forming of clay minerals.

Metamorphic rocks of the study area are distributed along W. Saal, W. Rimthy and W. Zaghraa. Soliman (1986) and Hassen et al. (2004 & 2007) mapped the metamorphic rocks at W. Saal and W. Zaghraa-Rimthy. They differentiate these rocks into metasediment, basic metavolcanic, acidic metavolcanic and metagabbro. The metamorphic belts were intruded by Syn and Late Granitoids and gabbroic rocks. Metasedimentary rocks consist mainly of Phyllite, metasiltstone, meta-conglomerate and volcanogenic sediment, while the metavolcanics included a wide variety of rock types such as andesite, dacite and rhyolite associated with minor basaltic bodies.

1.1.2 Phanerozoic Rocks

The northern part of Dahab basin has a geological setting different from its southern part. Phanerozoic rocks are the most prevalent rocks that cover this part of the study area. They are

distributed in the northern part of W. Saal, W. El Genah and the northern part of W. El Ghaieb. The describtion of the rocks is summerzied according to previous studies and EGSMA map as follows:

1.1.2.1 Cambrian Rocks

The rocks are well distributed in the northern part of W. Dahab, especially at W. Genah and W. El Ghaieb. Paleozoic exposures of Sinai are those of Hassan (1967), Soliman and El Fetouh (1970), Omara (1972). These rocks are concentrated at the nothern part of study area and occur especially at the north of W. El Genah and W. El Ghaieb (fig.10). They consist of laminated sandstone with intercalation of clay and ferruginous bands. They overlay unconformable basement rocks. The upper parts of the sequences consist of white, massive sandstones. They are coarse- to medium-grained, weakly indurate to friable and include kaolin matrix.

Figure 10: Cambrian Rocks in W. El Ghaieb

1.1.2.2 Cretaceous Rocks

1.1.2.2.A Lower Cretaceous

This formation represents Lower Cretaceous rocks (Abdallah and Adindani 1963). They appear in different parts of the northern Dahab Basin, especially along the Taba-Nuwayba'highway and in southwestern Sinai. They also extended along the Gunnah scarp. They consist of grey and violet colored pebbly and granular sandstone intercalated by Kaolin in upper part and impregnated with iron oxides in the top of the sequences. Malha Formation is well exposed also at G. El Dhalal in El Tih escarp in the northern part of study area which consists of pebbly sandstone intercalated with thin carbonaceous shales (Said, 1971).

1.1.2.2.B Upper Cretaceous

The Upper Cretaceous rocks of the Eastern central Sinai are partly described by Bartov and Steinitz (1977), Kora and Hamama (1988) and Ziko et al. (1993). The authors describe the different stratigraphic units in eastern Sinai and southern Negev with subsidiary sedimentological interpretation.

1.1.2.2.B.1 Raha Formation

It overlays, without visible unconformity, the pebbly sandstones of Malha Formation of Early Cretaceous age and underlies, conformably, the Abu Qada Frmation. It begins with alternating beds of yellow fossiliferous sandstones, dolostones, limestones, marls and glauconitic shales with pelecypod moulds, echinoids and trace fossils of horizontal burrowings. The upper part of this formation is represented by fossiliferous dolomitic limestone beds with gastropods, echinoids, and many oyster shells. It is well developed in the northern part of Dahab, especially at W. El Ghaieb (fig.11).

1.1.2.2.B.2 Abu Qada Formation

It is represented by green glauconitic and red fossiliferous shales and marls with yellow limestone intercalations overcrowded with large-sized oysters and ammonites. It outcrops in the area at W. El-Ghaieb and the southern Scarp of Gabal Genah.

1.1.2.2.B.3 Wata Formation

It consists of a thick carbonate sequence of limestone, marl and dolomitic limestone with thin inter-beds of silty claystone and yellowish-orange, fine-grained sandstone. It outcrops well in the study area, especially in W. El Ghaieb and Scarp of El Genah scarp. The thickness of the rock units in W. El Ghaieb amounts to 12 m whereas at Gebel El Genah it amounts to 70m. The present thicknesss of this formation may be a result most likely from erosion after the Neogene and Quaternary tectonic movements (Grarfunkel and Bartov, 1977).

Figure 11: Lower Cretaceous (Malha Fm) and Upper Cretaceous Rocks outcropping at W. El Ghaieb

1.1.3 Wadi deposits

Alluvial deposits are composed mainly of gravels, sands, silts and clays admixed with variable ratios of rock fragments of cobble and boulder sizes. The alluvial deposits form the most important aquifer in the study area due to their good hydraulic properties. The alluvial deposits cover the floors of the stream channels with variable thickness and texture. The thickness ranges from about one meter in the upper stream to more than 50 m at the downstream of Dahab basin.

To Summarize, sedimentary rocks are concentrated in the northern part of the study area. These rocks are Cambrian, Lower Cretaceous and Upper Creataceous in age. Mineralogically, the lower cretaceous rocks are mainly composed of quartz and kaolinite with a minor amount of calcite. This helps to distinguish them from Upper Cretaceous rocks in which the amount of calcite is high. A high degree of similarity exists in the mineral composition of Cambrian rocks and the clastic part of Lower Cretaceous rocks, especially with respect to quartz and kaolinite minerals. But the Cambrian rocks are more ferriginated than lower cretaceous rocks, which allows differentiation between them.

1.2 Lithological map in Dahab basin

1.2.1 Introduction

A main purpose of the Advanced Spaceborne Thermal Emission and Radiometer (ASTER) mission is to extend the understanding of local and regional phenomena of the earth's surface and its atmosphere. Goals of geologic research using ASTER are summarized by Gomez et al. (2005). They put the focus on "studying the geologic phenomena of tectonic surfaces and geologic history through detailed mapping of the Earth topography and geological formation".

ASTER data has been successfully used in geological mapping since early 2000. In comparison to Landsat TM data, ASTER data has the advantage of combining wide spectral coverage and high spatial resolution in the visible and infrared regions which makes it attractive for geological mapping (e.g. Hewson et al. 2001, Bedell, 2001). Yamaguchi and Naito (2003) studied spectral index images for lithological mapping. Index images are found by a linear transformation of reflectance values of the five ASTER short wave infrared (SWIR) bands. The idea of this transformation is to direct the transformation axes to the spectral pattern of the target minerals. The calculated indices are named according to the minerals: alunite, kaolinite, calcite and montmorillonite. An advantage of this approach is that the transformation coeffcients are not scene dependent. A simulated ASTER dataset is used to prove the usefulness of the spectral index images.

Rowan and Mars (2003) have used in situ measurements of spectral reflectance curves for calibrating the visible and near infrared radiometer (VNIR) bands of ASTER. Lithological mapping is carried out by selecting and introducing image spectra of various lithological groups into classification processes. Hewson et al. (2001) studied a regolith and alteration area in Australia and showed how to improve an existing 1:100,000 geological map with ASTER data. For their

investigations they rely on previous surveys using airborne Hyperspectral Mapper (HyMap) recordings of visible, shortwave and thermal IR bands and spectral measurements collected in field campaigns. They have concluded that their experimental results indicated "that ASTER could discriminate mineral groups not achievable from Landsat TM, though more precise mineral species mapping is not possible".

Dahab basin is located within an arid climatic belt. Rocks dominate the appearance of the landscape which is sparsely covered by desert vegetation. One of the aims of this study is to work out details of a classification approach for improving the existing geologic map of the Dahab basin. It further intends to point a way forward for updating the geological maps of the southern Sinai Peninsula. A second reason for generating a lithological map in this study is to provide an updated basis for hydrological investigations of the Dahab basin.

1.2.2 Aster Data

ASTER is an advanced multispectral image that was launched on board the Terra spacecraft in December 1999. ASTER image covers a wide spectral region with 14 bands from visible to thermal infrared with high spatial, spectral and radiometric resolution. This wide spectral region is covered by three telescopes, three VNIR bands with a spatial resolution of 15 m, six SWIR bands with a spatial resolution of 30 m and five TIR (Thermal Infrared Radiometer) bands with a spatial resolution of 90 m. The spectral passed bands are shown in (fig.12).

ASTER Bands

Band	Label	Wavelength	Resolution
B1	VNIR_Band1	0.52 - 0.60	15m
B2	VNIR_Band2	0.63 - 0.69	15m
B3	VNIR_Band3N	0.76 - 0.86	15m - Nadir view
B4	VNIR_Band3B	0.76 - 0.86	15m - Backward scan (used to create high resolution DEM)
B5	SWIR_Band4	1.60 - 1.70	30m
B6	SWIR_Band5	2.145 - 2.185	30m
B7	SWIR_Band6	2.185 - 2.225	30m
B8	SWIR_Band7	2.235 - 2.285	30m
B9	SWIR_Band8	2.295 - 2.365	30m
B10	SWIR_Band9	2.36 - 2.43	30m
B11	TIR_Band10	8.125 - 8.475	90m
B12	TIR_Band11	8.475 - 8.825	90m
B13	TIR_Band12	8.925 - 9.275	90m
B14	TIR_Band13	10.25 - 10.95	90m
B15	TIR_Band14	10.95 - 11.65	90m

Figure 12: Aster Scene Characteristics

ASTER data is offered at various processing levels such as levels 1A or 1B. Level-1A data is reconstructed, unprocessed instrument data at full resolution which consist of the image data, radiometric and geometric coefficients and other auxiliary data without applying calibration processes to the image data to maintain the original data values. The Level-1B data is generated by applying radiometric and geometric coefficients for radiometric calibration and geometric resampling. ASTER

scene used in this research is AST3A1 – 15 bands – 2006 which is a Level 3A data product. This so-called Terrain Correction Image included Level-1B image data projected in universal transverse mercator (UTM) zone 36 (WGS 84) which is orthorectified using a DEM. The scene covers an area of 60 by 60 km^2 which encloses the study area.

1.2.3 Methodology

The study area includes many rock types which could be subdivided into basement rocks and phanerozoic rocks. To differentiate classes of different rock types of the Dahab basin using ASTER data, a process based on band ratio images and supervised classification was developed. The reflectance spectra of minerals are well known and catalogued, e.g. in the USGS Digital Spectral Library (Clark et al., 2007). The fact that rocks are a complex mixture of minerals and the direct utilization of those spectra may be limited for rock differentiation and investigation. The use of the spectra is further lowered by the fairly broad bandwidth and the small number of spectral bands of ASTER. The challenge for the remote sensing approach is to analyse the reflectance of the mineral mix recorded by the ASTER bands. The proposed overall process flow for creating a lithological map of the Dahab basin is shown in figure 13.

1.2.3.1 Band Ratio

The technique of band ratio has been used for many years in remote sensing to effectively display spectral variations. The technique is implemented by dividing the digital number (DN) in one band by the corresponding DN in another band for each pixel (Drury, 1987). The majority of these fractional values are between zero and three. Thus, for visibility reasons the ratios are often rescaled to produce ratio images with higher contrast. Band rationing has been widely used for lithological maps due to its proven ability to display spectral variations effectively. Another well-known effect of rationing is the reduction of the impact of shadows in the ratio images. Band ratio is particularly suitable for enhancing a certain rock type or mineral depending on the dominance of the mineral in the reflected data. Spectral signatures give useful hints to make decisions about the bands used for rationing. Combinations of three band ratio images can be visualized as color composites.

Many researches used this technique for differentiation of rock types. Gad and Kusky (2007) have recommended the use of band ratios (4/7, 4/6, 4/10) for mapping the granite and metamorphic belt of the W. Kid area of Sinai and for mapping metamorphic rocks in the Arabian Nubian Shield and other arid areas. Reda et al. (2010) used band ratios (2+4)/3, (5+7)/6, (7+9)/8 to discriminate between different ophiolitic and granitic rocks in the central eastern desert of Egypt. Madani and Emam (2009) have investigated the band ratio composite (8/5, 5/4, 7/8) to differentiate between alkali granites (younger granitoids), granodiorites and quartz diorite (old granitoids) in the W. El-Hudi area, which is located in the southeastern desert of Egypt. Qari et al. (2008) utilized the (6/8, 4/8, and 11/14) band

ratio image to discriminate the basement rocks in the Arafat area of the Western Arabian Shield, Saudi Arabia, and created a 1:100,000 geological map.

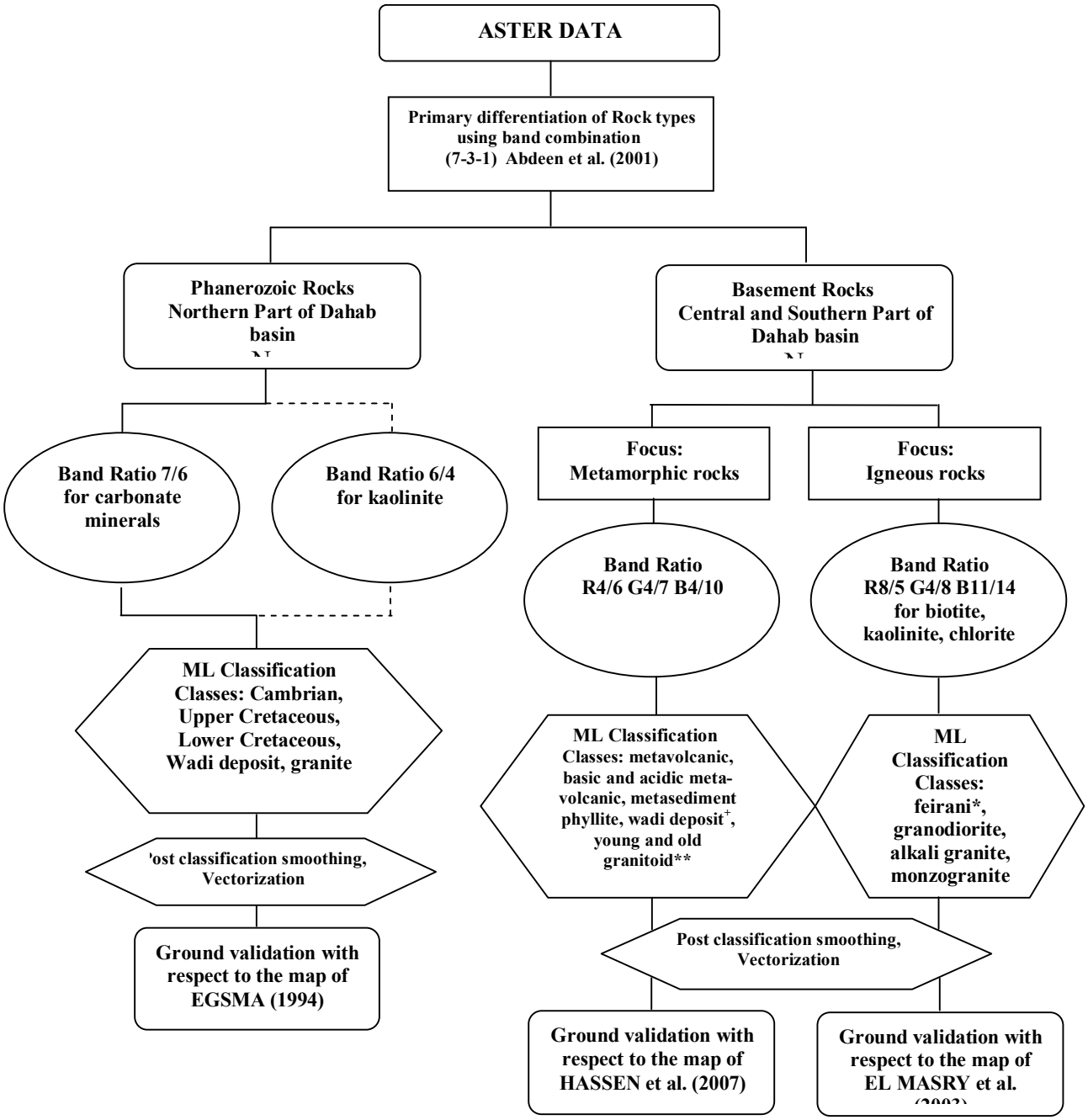

Figure 13: Process Flow diagram For Lithological Mapping of the Dahab Basin Area (* a metamorphic rock, ** an igneous rock, + not introduced into ML classification)

1.2.3.2 Supervised Classification

Multispectral classification is the process of sorting pixels into a finite number of individual classes or categories of data based on their data file value. If a pixel satisfies a certain set of criteria,

the pixel will be assigned to the class that corresponds to those criteria (Erdas Field Guide, 2001). The image processing software (Erdas) system is then used to develop a statistical characterization of the reflectance for each information class. Once a statistical characteristization has been achieved for each class, the image is then classified by the examination of the reflectance for each pixel and by making a decision about which signature it resembles most (Eastman, 1995). Maximum likelihood classification is used to make classifications of various classes. It is a statistical criterion to assist in the classification of overlapping signatures; pixels are assigned to the class of highest probability.

Lithological mapping may be carried out on the computer screen by human interpretation of the images. This is a promising way, in particular if the human operator is very experienced. To increase the degree of automation within the mapping process, the tools of image classification can be employed. The human operator is still a key factor for the mapping success as he will be involved in selecting proper training areas for supervised classification by taking advantage of existing maps or field visits.

The training areas for the maximum likelihood classification are selected on the basis of existing geologic maps together with supporting field visits. As a part of this study, field visits at 23 locations of the study area have been undertaken. However, the use of field visit data as a reference is not suffecient because of the small number of the sample size. Therefore, the areas of rock types for geologic maps are further used as references for evaluating the accuracy of the classification result.

Maximum likelihood classification of the entire study area in a one step process is not optimal. The mineral compositions of sedimentary rocks (sandstone), cambrian rocks and lower cretaceous age are similar to the mineral compositions of granite rocks. Therefore, the analysis of the northern part of study area, which included sedimentary rocks, is separated from the analysis of the southern part where the basement rocks form the main rock component.

1.2.3.3 Accuracy Assessments

Accuracy assessment is one of the most important steps in any classification and without this step the results would be of low relevance. A quantitative assessment method is used to undergo a comparison between pixel locations on a classified map against the results of field investigation information (geologic map) for the same location. The error matrix is the standard concept in the classification of remote sensing data (see. Congalton, 1991).

The accuracy investigations of the classification results are carried out with respect to the geological reference maps published by Hassen et al. (2004), El Masry et al. (2003) and EGSMA (1994). GIS tools are used to make an accuracy assessment. A tabulated area tool was used to compare selected sites (classes) in a supervised classification map (raster layer) with the evaluation lithological field map (vector layer). The result occurs as a matrix comparison between both layers. The accuracy of the classified map can be divided into:

- **User accuracy** is expressed by the number of correctly classified pixels in a given class divided by the number of classified pixels in the class. The user may want to know how many pixels on the classified map should not be included within the field map.
- **Producer accuracy** is expressed by the number of correctly classified pixels in a given class divided by the number of reference pixels in the class. This accuracy aims to know how many of the pixels on the classified map are classified correctly.

The basic idea of this process is to use the prior knowledge of the existing EGSMA map to guide the classification of the rocks. With this knowledge, supervised classification will be specifically applied to the input image data for a certain area. According to the EGSMA map, phanerozoic rocks mainly cover the northern part of the study area and basement rocks dominate in the central and southern part of the Dahab basin. For the primary differentiation of phanerozoic rocks and basement rocks, our process follows the proposal of Abdeen et al. (2001). Spatial separation between the northern and central parts is done by manual digitization using ASTER band combination 7-3-1.In each of the two regions, band ratio images are used as input for supervised classification of different rock types. For this purpose, some band ratios which have been successfully used by other researcher are used. In addition, a new ASTER band ratio stacking (8/5, 4/8, 11/14) is introduced which is inspired by the work of Madani and Emam (2009), as well as Qari et al. (2008) .

The processing flow (fig.13) points out the different band ratio images used for maximum likelihood classification. In the northern part of the basin the mapped classes are Cambrian rocks, Upper Cretaceous and Lower cretaceous rocks, granodiorite and Wadi deposits. In the central and southern part of the basin there are the metamorphic rocks with metavolcanic, basic metavolcanic, acidic metavolcanic, metasediment, phyllite and metagabbro. Wadi deposits are also taken into account, in particular, for comparisons in the reference map. For the igneous rocks, the other major group in the central and southern part of the study area, the rock types granodiorite, alkali granite, monzogranite are mapped by image classification. Ring dykes are visually recognizable in the image. Supported by field visits, they have been digitized interactively. In classifying this group of igneous rocks, the metamorphic Feirani metavolcaniclastic rocks are added for comparison reasons in the reference map.

A post classification smoothing of the classification results is carried out by majority filtering and by the suppression of very small areas. The results of the lithological mapping process are the data found by vectorisation of the post processed classification maps. The classification accuracy assessment is the last step in the overall processing flow (fig.13). Ideally, representative field mapped ground field data is used as reference data. Due to the lack of sufficient field data, the existing geologic maps are used. The EGSMA map is used as a reference in the northern part of the basin. The more detailed map of Hassen et al. (2007) is used as a reference in the areas of W. Saal, Wadis Zaghraa and Rimthy. The map of El Masry (2003) was used as a reference in the areas of W. Nasab,

W. El Ghaieb und W. Feirani. The limitations of this accuracy analysis are obvious; the error matrix provides information about how well the classification map and the existing maps coincide.

1.2.4 Analysis and Results

The usefulness of Landsat ETM band combination 7-4-2 for geological mapping in arid regions and the far-reaching consistency of this band combination to ASTER band combination 7-3-1 is pointed out by Abdeen et al. (2001). Figure 14(A) shows ASTER band combination 7-3-1 in which the metamorphic rocks appear as greenish and reddish colors, the granitic rocks as light yellow to light brown, the sedimentary rocks as white, and the Wadi deposits as light grey. A manual mapping of the Wadi deposits is shown in figure 14(B). This layer of the Wadi deposits is used as overlay in other figures to simplify visual orientation.

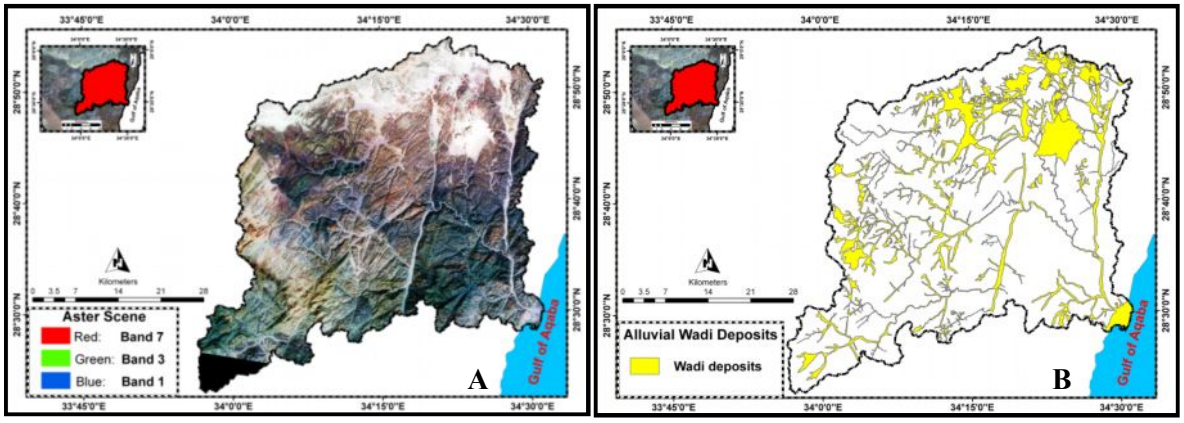

Figure 14-A: Band Combination 7-3-1 of Dahab Basin Area – B: Map of the Wadi Deposits

1.2.4.1 Central and Southern Part of the Dahab Basin: Igneous Rocks

A new band ratio stacking with the ratio images (8/5, 4/8, 11/14) is used for differentiation between younger granitoids and older granitoids in the central and southern part of the study area.

1.2.4.1.A Band ratio 4/8

Alkali granites appear as dark, monzogranite grey while older granitoids show light grey to bright color (fig. 15A). The light color of older granitoids is due to alteration products of hornblende and plagioclase into chlorite and clay minerals, whereas the presence of biotite and K-feldspar minerals in alkali granites (El Masry et al. 2003) produces a dark color in band ratio 4/8. The dark color is a consequence of the lower reflectance in band 4 (figs. 15 B and C).

1.2.4.1.B Band ratio 8/5

Younger granitoids appear as light grey and older granitoids as grey in color (Fig. 16A). In band ratio image 8/5, Feirani metavolcaniclastic rocks show a dark grey color. This is due to the presence of biotite and K-feldspar in addition to the alteration products of hornblende and plagioclase into clay minerals. Rocks rich in feldspar commonly weather to kaolinite. Fig. 16B shows an absorption feature

of kaolinite near band 5, thus, the high 8/5 band ratio values (fig. 16) indicates younger granitoids. On the other hand, the dark grey and grey colors of old granitoids and metamorphic rocks are due to the absorption property of chlorite (fig. 15C), which leads to low 8/5 band ratio values.

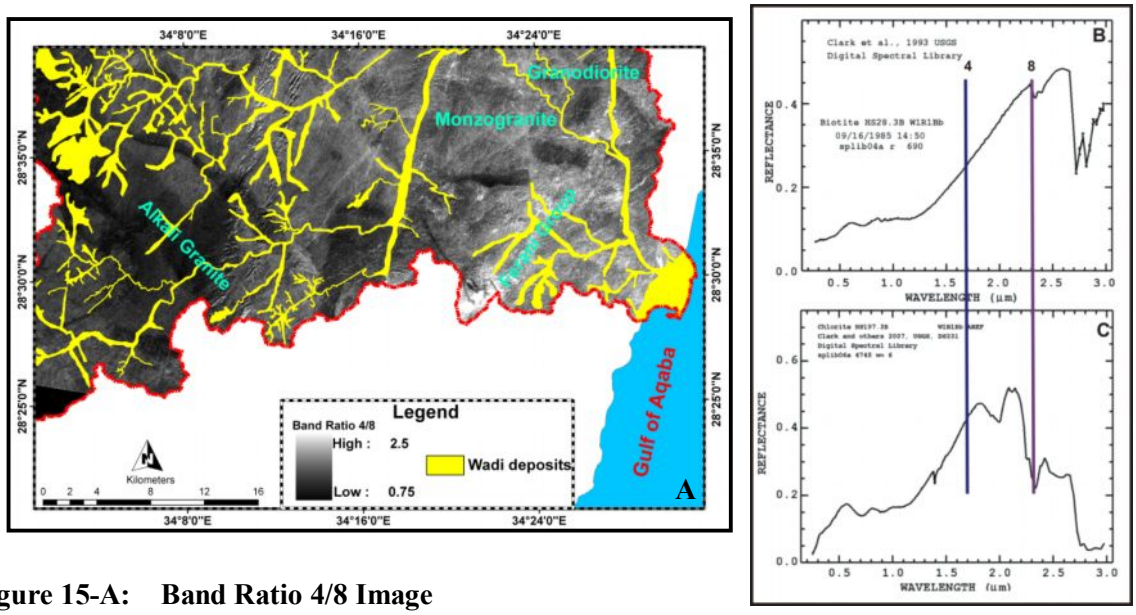

Figure 15-A: Band Ratio 4/8 Image

Figure 15-(B&C): Spectral Signature of Biotite and Chlorite (Clark et al. 2007)

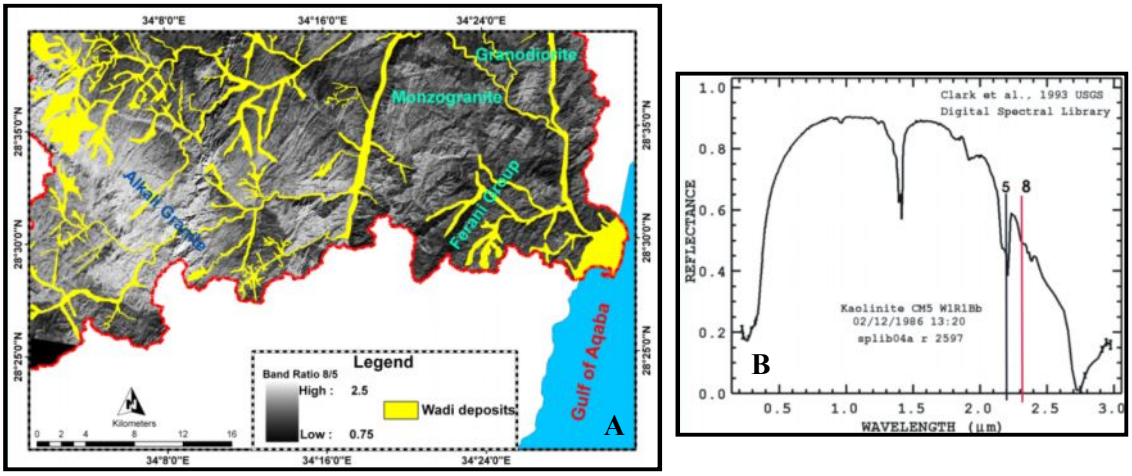

Figure 16-A: Band ratio 8/5 image
Figure 16-B: Spectral signature of Kaolinite (Clark et al.2007)

1.2.4.1.C Band ratio 11/14

Younger granitoids appear as a dark color while older granitoids show a light grey to bright color (fig. 17). The dark color of younger granitoids may be interpreted by their high ability to reflect the sun radiation on their light colored surfaces; hence, they represent cooler surfaces which appear dark in the band image. In contrast, older granitoids absorb more sun radiation and get warmer than other rock types; hence, they appear brighter in the band image.

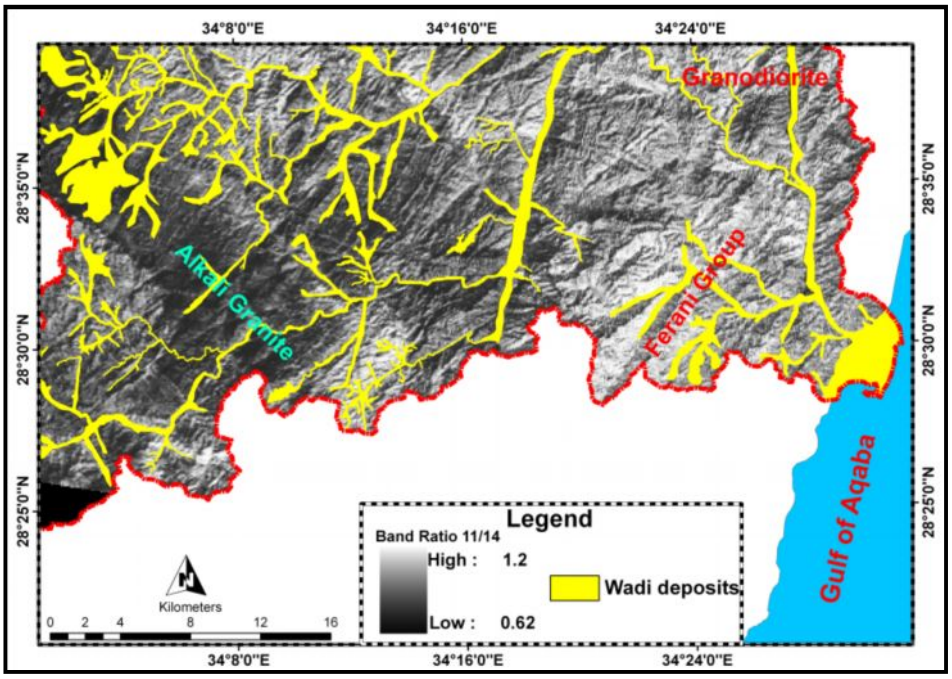

Figure 17: Band Ratio 11/14 Image

In experiments with different band ratio stackings, it is found that the color composite (8/5, 4/8, 11/14) reveals subtle differences between the younger and older granitoids. Figure 18A shows alkali granites that appear in red color and monzogranites and acidic volcanic that appear pink in color. The Feirani group appears as light green whereas older granitoids appear green and purple. The visual comparison of this new stacking with the ratio stack image (8/5, 5/4, 7/8) is used by Medani and Emam (2009) in the El Hudi area of southeastern desert in Egypt and shows its strength with respect to the discrimination of younger granitoids. Alkali granite and monzogranite rocks are much better distinguished in the new stacking. But with respect to older granitoids (granodiorite and Qz diorite), the Medani and Emam (2009) stacking seems to be a bit more favorable.

The color composite of the single band ratios is used for defining the training areas of the four rock classes: alkali granites, monzogranites, Ferani metavolcaniclastic, and old granitoids. For each class, several (at least 4) training areas are selected to get representative samples. In figure 18B the maximum likelihood classification result of the four rock classes is shown together with the wadi deposit layer. Alkali granites are colorized in red, monzogranites in pink, Ferani metavolcaniclastic in light green, old granitoids in dark green and wadi deposits in yellow.

The investigation of the accuracy of the classification result of the geologic map of El Masry et al. (2003) is used as reference. This local map is generated on detailed field work and covers the Gebel Feirani area. Figure 6 shows the location of the Gebel Feirani area at the downstream part of the Dahab basin. In addition to alkali granites, monzogranites, and Feirani metavolcaniclastic, the El Masry map includes granodiorite, Qz diorite, and tonalite. The latter two cannot be distinguished from granodiorite by image classification. Therefore, the prevalent granodiorite is introduced as a class on its own. Ring-dyke is interactively mapped because it is visually recognizable by its dyke-like body

(fig. 18B). It has the same composition as alkali granites and thus, belongs to this class in the classification map.

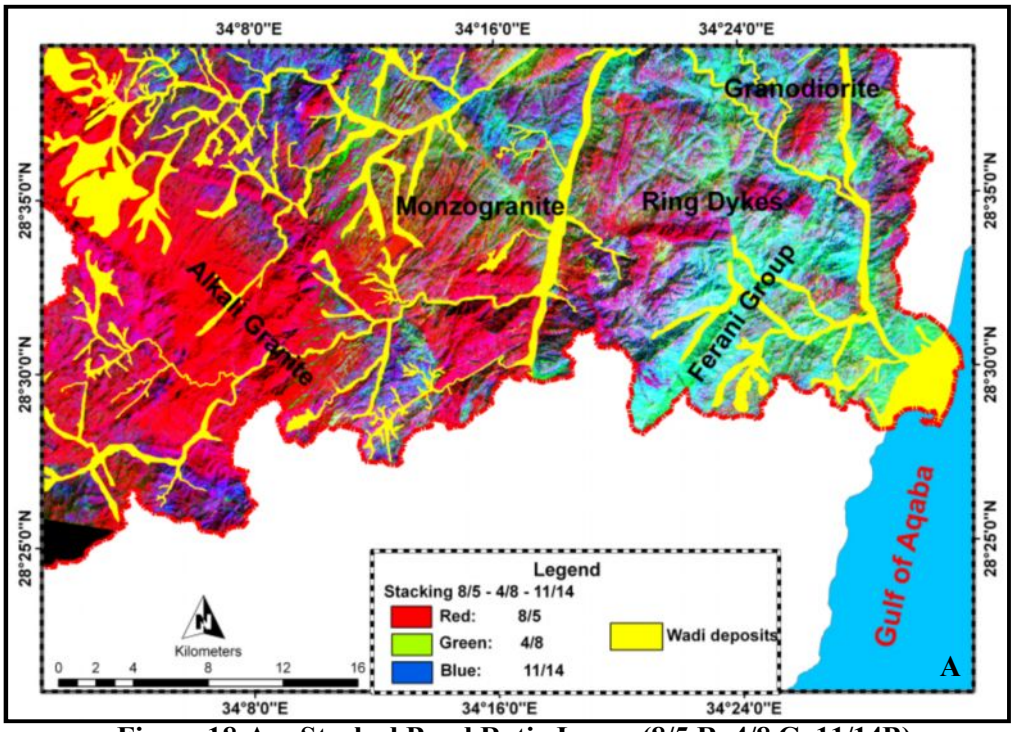

Figure 18-A: Stacked Band Ratio Image (8/5 R, 4/8 G, 11/14B)

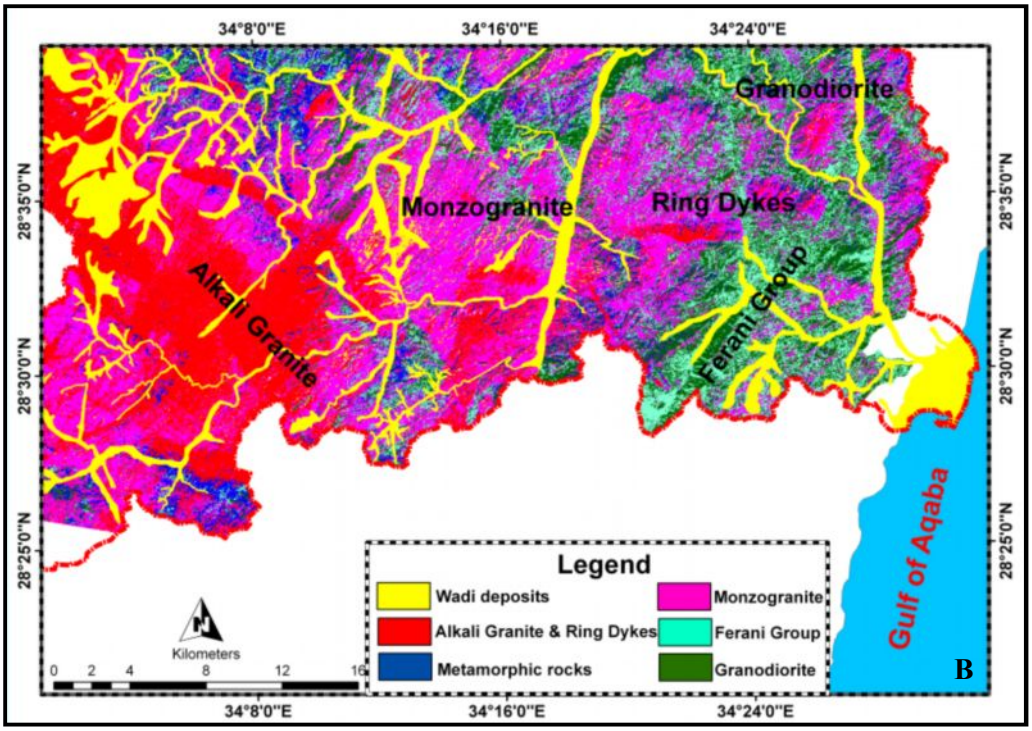

Figure 18-B: ML Classification Using the Stacked Band Ratio Image (8/5 R, 4/8 G, 11/14B)

The quantitative comparison between the results of the classification map and the reference map is summarized by the error matrix in Tab. 3. Reference data is selected from the reference map for the raster locations defined by the classification map. The procedure for selecting samples in each

category follows the stratified random sampling strategy. For each class in the classification map, 4 to 5 samples were taken as reference data. The results indicate an overall accuracy of 85%. Apart from the user's accuracy of 68% for monzogranite, the user's and producer's accuracies of the other classes are all above 80%. The interfering contacts between monzogranite and alkali granite lead to a fairly high misclassification of monzogranite with the consequence of a low user's accuracy for this class. Similar is the situation for the Ferani metavolcanics and the granodiorite but with less significant consequences for the user's accuracy.

		Class types from the geological map (El Masry et al. 2003)					
Class types of the classification map	Pixels	**Ferani**	**Grano**	**Alkali**	**Monzo**	***Total***	**User's Accuracy**
	Feirani	393	47	0	5	445	88%
	Granodiorite	81	392	8	3	484	81%
	Alkali Granite	0	5	775	18	798	97%
	Monzogranite	1	13	177	413	604	68%
	Total	475	457	960	439	2330	
Producer's Accuracy		83%	86%	81%	94%		**85%**

Table 3: Accuracy Evaluation of the Classification Map for Igneous Rock Types

1.2.4.2 Central and Southern part of the Dahab basin: Metamorphic Rocks

For the discrimination of different metamorphic rock types the procedure follows the proposal of Gad and Kusky (2007) by applying the band ratio stacking (4/6R, 4/7G and4/10B). The main reason for using this band ratio is because the volcano-sedimentary belt of W. Saal is similar to the area of W. Kid in the southern part of Dahab basin (El Shafei and Kusky, 2003). Additionally, Gad and Kusky (2007) recommended the use of this stacking for mapping metamorphic rocks in Arabian Nubian Shield and other arid regions.

The staking shows the metavolcanic (metatuffa) rocks in greenish yellow and the basic metavolcanic rocks in reddish brown color. The acidic metavolcanic rocks shows up as light violet colors, the metasediment phyllite rocks in light green, the younger granitoidrocks have dark blue color and the light blue color refers to old granitoid rocks (fig. 19 A&B).

Training areas have been defined in the color composite (4/6, 4/7, 4/10) by following the same procedure described in section 5.1. The classification is carried out for seven classes of rock units. Figure 20 shows the classification results for W. Saal (fig. 20A) and W. Rimthy (fig. 20B). Metavolcanics are colored in blue, basic metavolcanics in purple, acidic metavolcanics in light green, metasediments (phyillite) in dark green, younger granitoids in red, older granitoids in pink and metasedimentary rocks (in W. Rimthy only) in dark green.Wadi deposits have also been introduced into the classification and show up in yellow in the classification map.

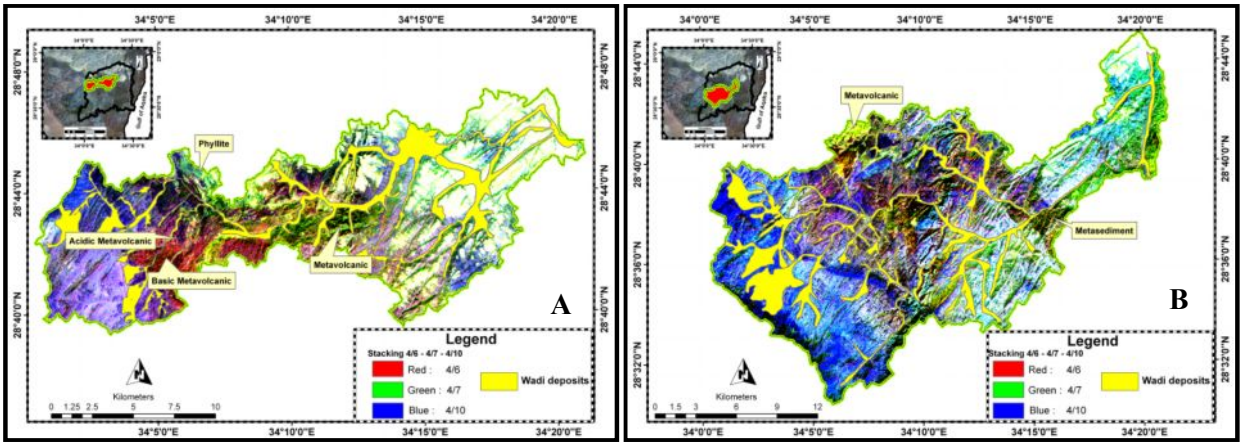

Figure 19-A: Stacked Band Ratio 4/6, 4/7, 4/10 Image of W. Rimthy Area
Figure 19-B: Stacked Band Ratio 4/6, 4/7, 4/10 Image of W. Saal Area

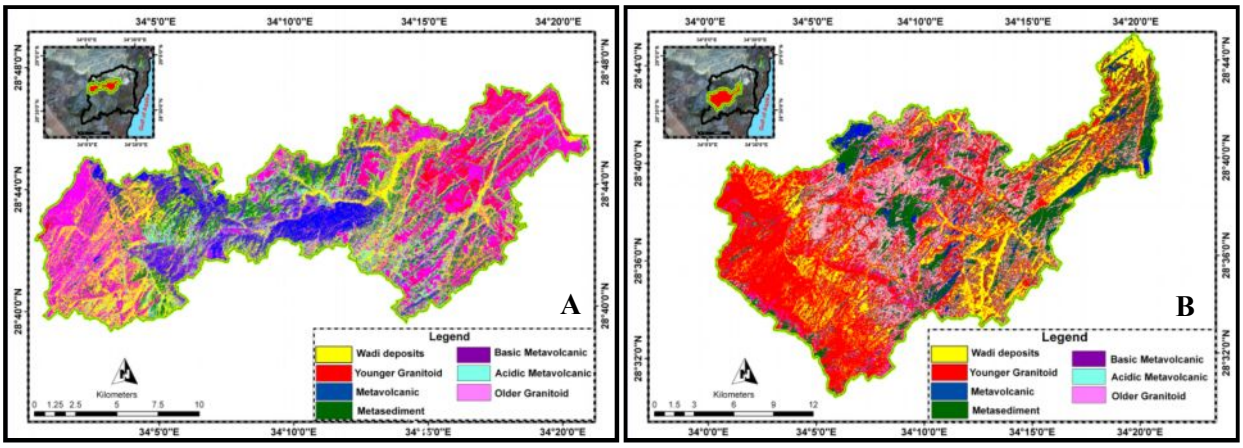

Figure 20-A: ML Classification of Stacking Band Ratio 4/7 R, 4/6 G and 4/10B Images for W. Saal
Figure 20-B: ML Classification of Stacking Band Ratio 4/7 R, 4/6 G and 4/10B Images for W. Rimthy

For the accuracy investigation, the classification maps are compared to the geologic map created by Hassen et al. (2007) based on field observations. This geologic map covers the areas of the Wadis Saal, Zaghraa and Rimthy. The error matrix was found by stratified random sampling and is listed in Table 4. The overall accuracy of 83% confirms the good matching between the classification map and Hassen's reference map for both wadis. The error matrix (Table 4) has quite some similarity to the error matrix found for the classification of the igneous rocks. The producer's accuracy is fairly high between 79% and 96% for all classes. The user's accuracy of 66% for metasedimentary rocks suffers from misclassification of metavolcanics and basic metavolcanics rocks. The small outcrops of acidic metavolcanics, metasediments, Wadi deposits and older granitoids produces a lot of uncertainly with respect to the other classes which results in user's accuracies between 66% and 76% for these classes.

		Class types from the Geological Map (Hassen et al. 2007)								
Class types of the classification map	Pixels	met_vol	met_ba	met_ac	met_sed	wd	young	old	Total	User's Accuracy
	Metavolcanic	281	23	1	0	0	0	1	306	92%
	Basic Metavolcanic	49	181	0	2	3	0	0	235	77%
	Acidic Metavolcanic	3	11	56	0	1	3	0	74	76%
	Metasediment	8	11	1	41	1	0	0	62	66%
	Wadi deposits	5	2	1	3	28	1	0	40	70%
	younger granitoid	0	0	4	0	0	73	0	77	95%
	older granitoid	0	0	2	0	0	5	22	29	76%
	Total	346	228	65	46	33	82	23	823	
Producer's Accuracy		81%	79%	86%	89%	85%	89%	96%		83%

Table 4: Accuracy Evaluation of the Classification Map for Metamorphic Rock Types

1.2.4.3 Northern part of the Dahab basin: Sedimentary Rocks

Band ratio 7/6 can be used to differentiate sedimentary rocks with respect to carbonate minerals, in particular, calcite and aragonite which are the main components of limestone (upper cretaceous) rocks. The absorption features of calcite near band 7 (fig. 21B), together with its high reflectance in band 7, produces the dark appearance of the cretaceous rocks in figure 21A. The cambrian rocks appear as a bright color, whereas the granites appear as a darker grey tone. Alternatively, band ratio 6/4 can be used to discriminate between different classes of sedimentary rocks. Quartz and kaolin (altered to clay), together with iron oxide, are the main minerals of cambrian rocks which lead to dark colors in this band ratio due to the absorption feature of kaolinite near band 6 and the high reflectance in band 4. Upper cretaceous rocks appear in grey and granites appear in bright tones in band ratio 6/4 (fig. 22).

A visual comparison of the 7/6 versus the 6/4 band ratio indicates that the discriminative efficiency of 7/6 ratio is higher than that of the 6/4 ratio. Therefore, the analysis focuses in analysing band ratio 7/6. A joint use of both bands would have been possible but is not pursued in this analysis. Supervised classification including post classification smoothing and vectorization is carried out by using band ratio 7/6 as input image. In the classification map, upper cretaceous rocks are colorized in red and lower cretaceous rocks in light green. For granites, violet is used and for cambrian rocks, blue is used. Wadi deposits appeared yellow in the classification map (fig. 23).

The final geological map of the Dahab basin comprises of 19 classes of phanerozoic, metamorphic and igneous rocks according to the proposed process flow as shown in figure 24. Apart from the ring dykes, all other classes have been created by supervised image classification followed by post classification smoothing and vectorization of the raster data. The same especial rock units are

found in the lithological map are added to the general geological map of EGSMA. Added are ring-dykes at W. El Ghaieb, acidic metavolcanics, basic metavolcanics and metasediments at the Wadis Saal, Zaghraa and Rimthy and metasediments at W. Rimthy. Alluvial wadi deposits are also included in the final lithological map.

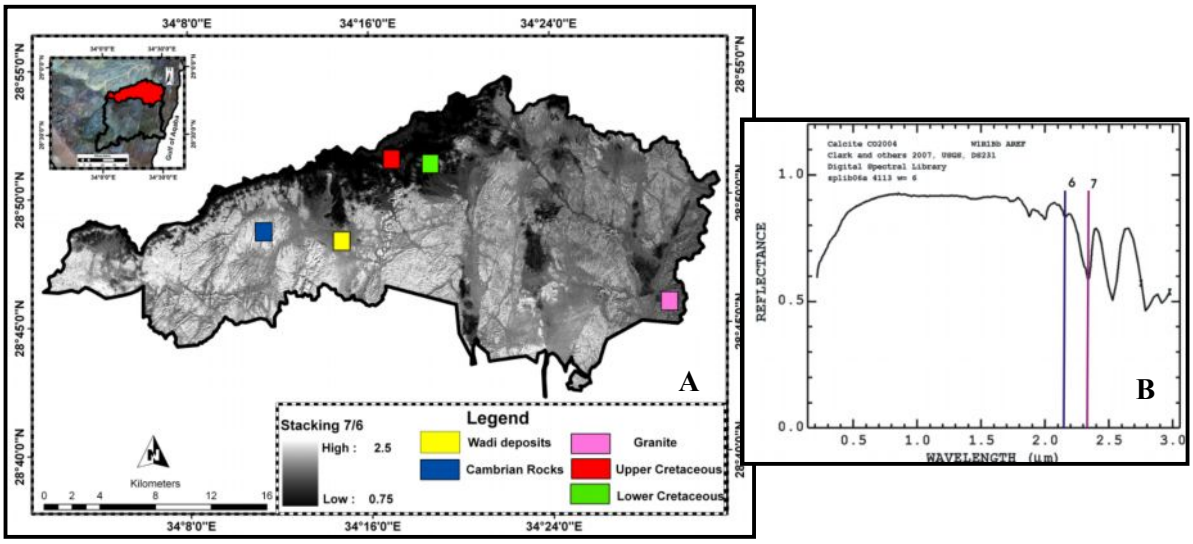

Figure 21: (A) Band Ratio 7/6 Image of the Northern Part of Dahab Basin Area
Figure 21: (B) Spectral Signature of Calcite (Clark et al. 2007)

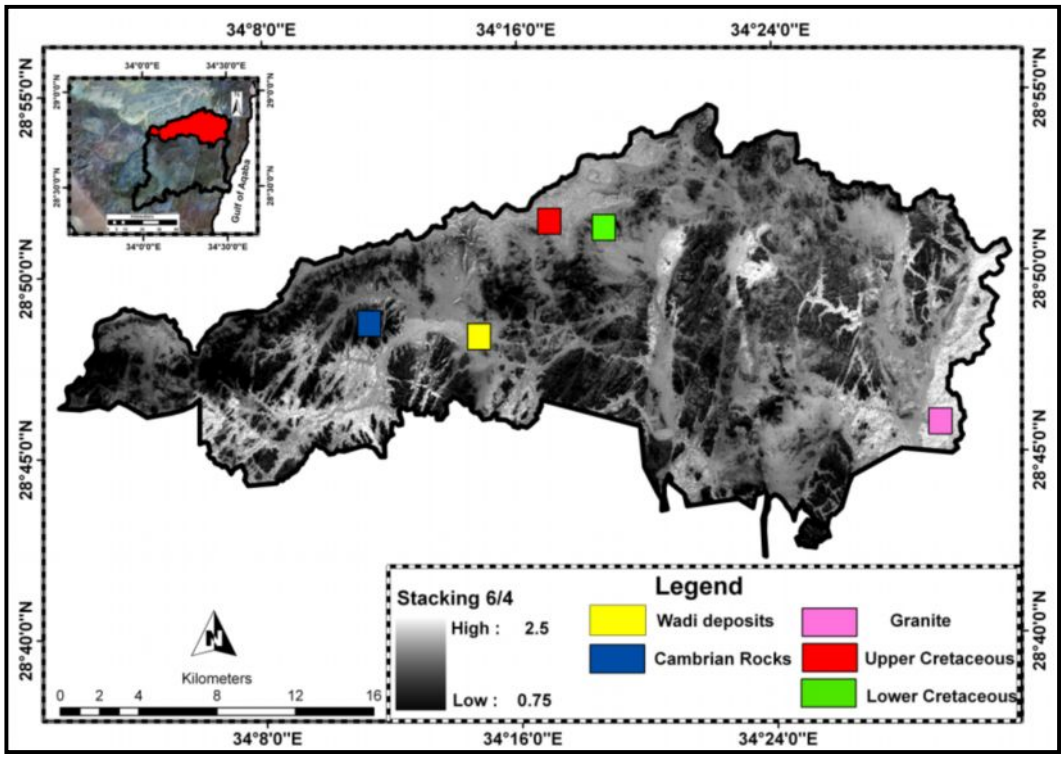

Figure 22: Band Ratio 6/4 Image of the Northern Part of the Dahab Basin

For the accuracy investigation the geological map provided by EGSMA (1994) is used as a reference. The overall accuracy was quite high (94%, Table 5). User's and producer's accuracies of 89% to 99% indicate a high agreement of the classification map and the reference. The only exception is the granitic rocks with a user's and a producer's accuracy of 74%. Granitic rocks and alluvial wadi deposits were in contact with each other; this was probably the main reason for this lower accuracy.

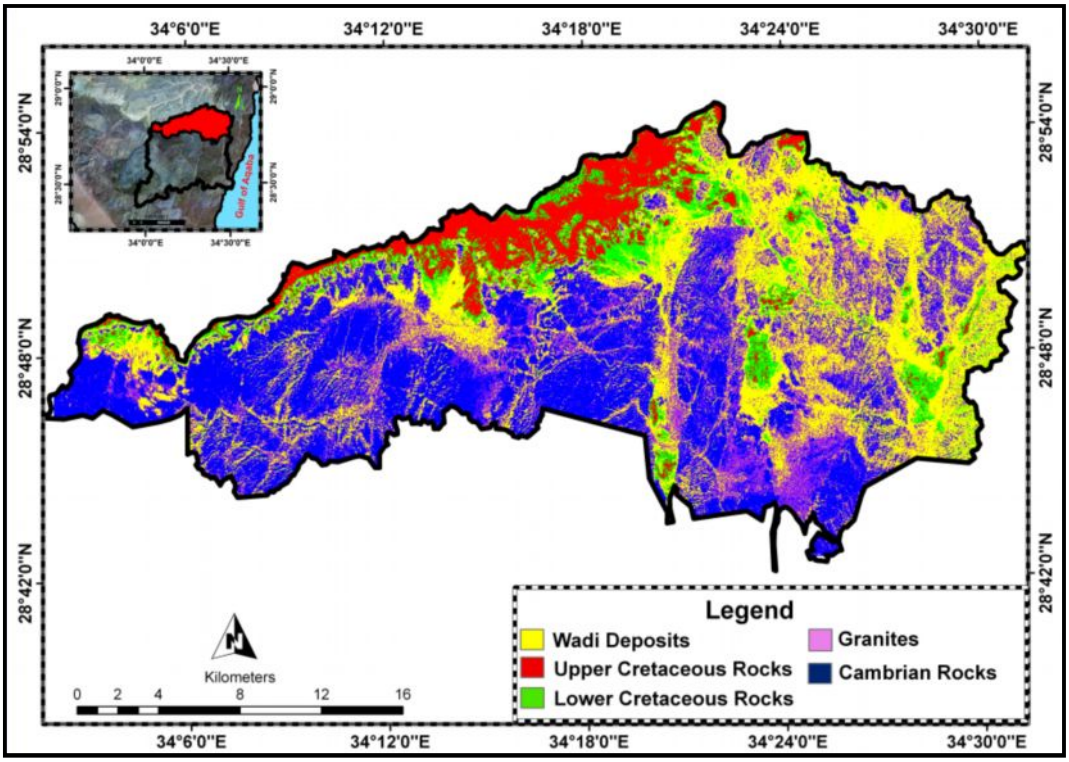

Figure 23: Supervised Classification of Band Ratio 7/6 Image of the Northern Part of Dahab Basin Area

		Class types from geological map (EGSMA, 1994)						
Class types of the classification map	Pixels	Camb.	Up. Cret.	Wd	Low. Cret.	Gran.	Total	User's Accuracy
	Cambrian Rocks	191	0	0	0	23	214	89%
	Upper Cretaceous	0	97	0	6	0	103	94%
	Wadi deposits	0	0	994	2	13	1009	99%
	Lower Cretaceous	0	12	1	131	3	147	89%
	Granites	1	0	36	2	111	150	74%
	Total	192	109	1031	141	150	1623	
Producer's Accuracy		99%	89%	96%	93%	74%		94%

Table 5: Accuracy Evaluation of the Classification Map for Sedimentary Rock Types

The final geological map of the Dahab basin comprises of 19 classes of phanerozoic, metamorphic and igneous rocks according to the proposed process flow as shown in figure 24. Apart from the ring dykes, all other classes have been created by supervised image classification followed by post classification smoothing and vectorization of the raster data. The same especial rock units are found in the lithological map are added to the general geological map of EGSMA. Added are ring-dykes at W. El Ghaieb, acidic metavolcanics, basic metavolcanics and metasediments at the Wadis Saal, Zaghraa and Rimthy and metasediments at W. Rimthy. Alluvial wadi deposits are also included in the final lithological map.

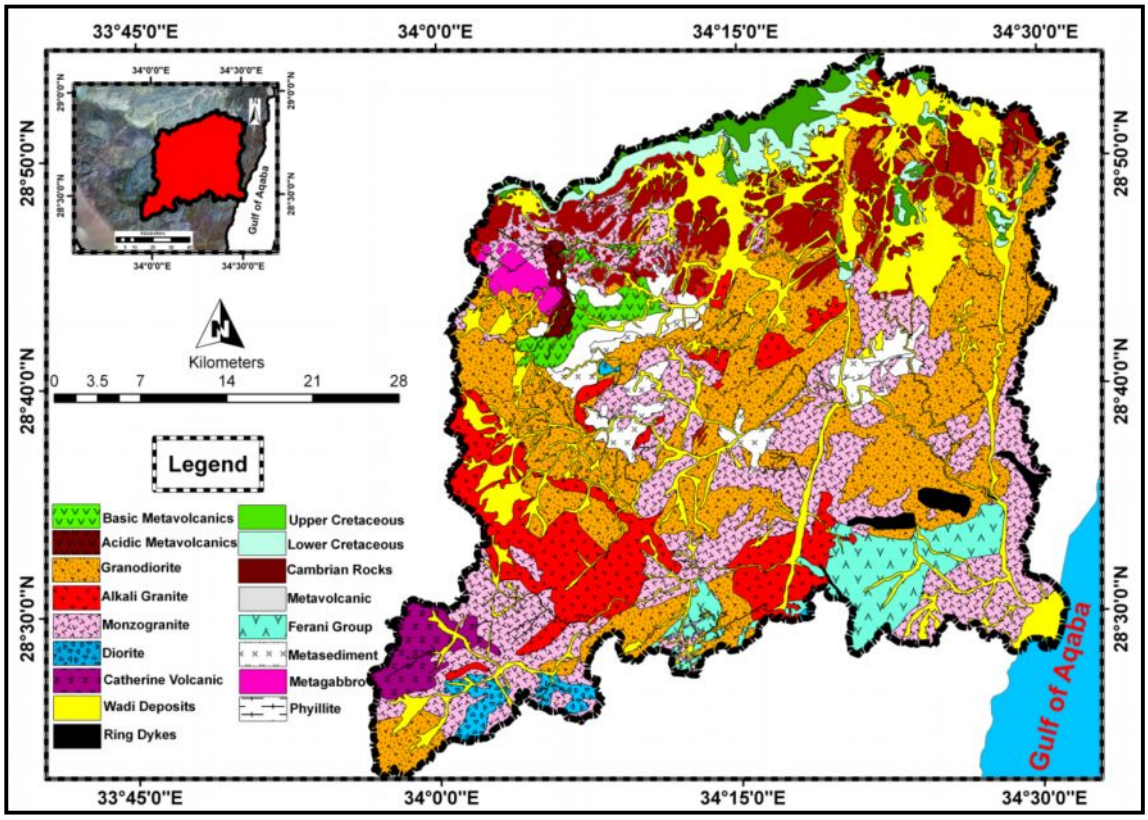

Figure 24: Final Lithological Map of Dahab Basin Area

The goal to develop a classification based approach in which only minor interactive digitization was included was fully achieved. Interactive digitization was used to separate the northern, central, and southern parts of the basin, as well as for the mapping of the ring dykes. Through classification, different types of granitoid rocks (monzogranites, alkali granites, granodiorites), metamorphic rocks (metasediments and metavolcanics) and phanerozoic rocks (cambrian, lower cretaceous, upper cretaceous rocks and loose wadi deposits) have been differentiated. For checking the quality of the classification map, an accuracy assessment was carried out. For this purpose, an error matrix was determined which compares the classification map with respect to existing geologic maps. The calculated error matrices indicate overall accuracies between 83% and 94%.

1.3 Structure setting in the Dahab basin

1.3.1 Introduction

The geology of Southern Sinai is strongly influenced by the Red Sea rifting, Gulf of Suez (NW-SE trend) and Gulf of Aqaba (NNE-SSW trend) when many faults are formed during their developments. Tectonically, the Gulf of Aqaba originates at the southern part of the Dead Sea rift (fig.25). The Dead Sea transform faults are related to the boundaries of the Arabian and African plates, as well as to the Sinai Peninsula sub-plate. On a larger scale, divergence in the Red Sea is accommodated by plate convergence in Iraq-Iran (Zagros Mountains) as the Arabian plate is moved north relative to the African plate (Mechie and El-Isa, 1988).

Bayer et al. (1988) concluded that the kinematics of the Red Sea area changed from passive rifting with a WSW -ENE extension to strike slip movement sinistral shear slipping along a NNE direction (Aqaba-Levant transform, Fig.) in the Late Miocene age. Freund et al. (1970) suggested that the strike-slip movement occurred in two phases, i.e., one of 60 km, during post-Cretaceous ages and another of 45 km, from the Pliocene onwards. Eyal et al. (1981) stated that the tectonic development of the western margin of the Gulf of Aqaba Rift was the main objective. They described a 30 km wide shear belt of sub parallel faults trending N-S to NE-SW that developed along the western coast of the Gulf of Aqaba. This shear belt was observed mainly within the Precambrian basement terrain.

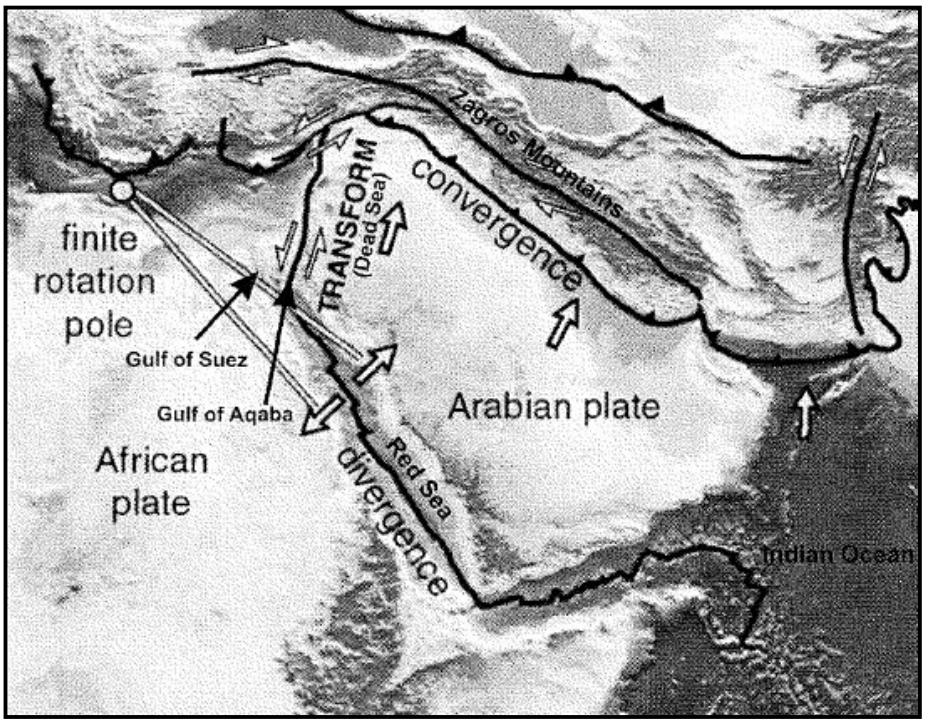

Figure 25: Gulf of Aqaba Formation which Results From Dead Sea Rift (Mechie and El Isa, 1988)

Said (1962) listed the faults in the region: W. Dahab, W. El Ghaib (Ghaib), W. Nasb and W. Taba faults which were thought to be contemporaneous with the faults of the Gulf of Suez. Northeast-

trending faults that determine the location of the Gulf of Aqaba were attributed to be younger, presumably of Pleistocene age. Freund et al. (1970) showed that these faults are left-lateral shears with displacement ranging from several meters to a few kilometers.

Eyal et al. (1981) described faults in the study area and indicated the existence of theGhaib fault which is characterized by an acute straight shape. The faults east of W. Ghaieb are characterized by an arcuate shape; all branches off the gulf on the south and the Wadi Ghaieb fault terminate at the gulf on the north. The faults system to the west of the Wadi Ghaieb fault are essentially straight, having no connection with the gulf, and lateral displacements on them are smaller.

The structure elements in W. Dahab including faults and joints, have an important role for the hydrogeological situation in this area. Hence, they act as a major pass for groundwater and form a substantial part of the reservoir in the study area. Major fractures patterns are often clearly visible in topography and satellite images. The major fractures are dissected with numerous dykes and viens that their altitudes are mostly controlled by prevailing major faults.

Linear features appear to be tremendous on hard rock bodies and negligible on soft terrain. Linear features on satellite images have attracted the attention of hydrogeologists who believe that lineaments perceived in remotely sensed images are attributed to geologic structures. Hence, identification of these features is important in hydrogeological assessment, since they reflect fracture traces and thus may represent zones of higher infilteration and groundwater potential.

1.3.2 Method of lineament detection

The combination of techniques including remote sensing and GIS have been used with the available published geological data and our own field measurements such as regional fractures and structural analysis to identify lineaments features and to analyze their directions and densities. The various steps of processing which have been followed in the study are shown on the flow chart (fig. 26). The processing work was done using remote sensing (Erdas 8.5 and PCI Geomatics) software. According to structure elements in study area, the lineaments extractions are divided into two steps: the first one is extraction of the major structure elements (major faults) which can be easily seen within the image manually. ETM+ 7 bands (1, 2, 3, 4, 5 and 7) have been used in this first step. Band 6 is not used due to its low resolution. The second step is the extraction of small lineaments which needed high image resolution as in Band 8 panchromatic (15m). The automatic extraction is used to get enough data for the analysis of the structure setting in Dahab basin and for hydrogeological application (see chapter 3). The extracted results from processed satellite images are compared to geoscientific field data in addition to available digital data which is prepared by digitizing the structural lineaments from Egyptian Geological Survey maps (1:250000) and other previous published maps.

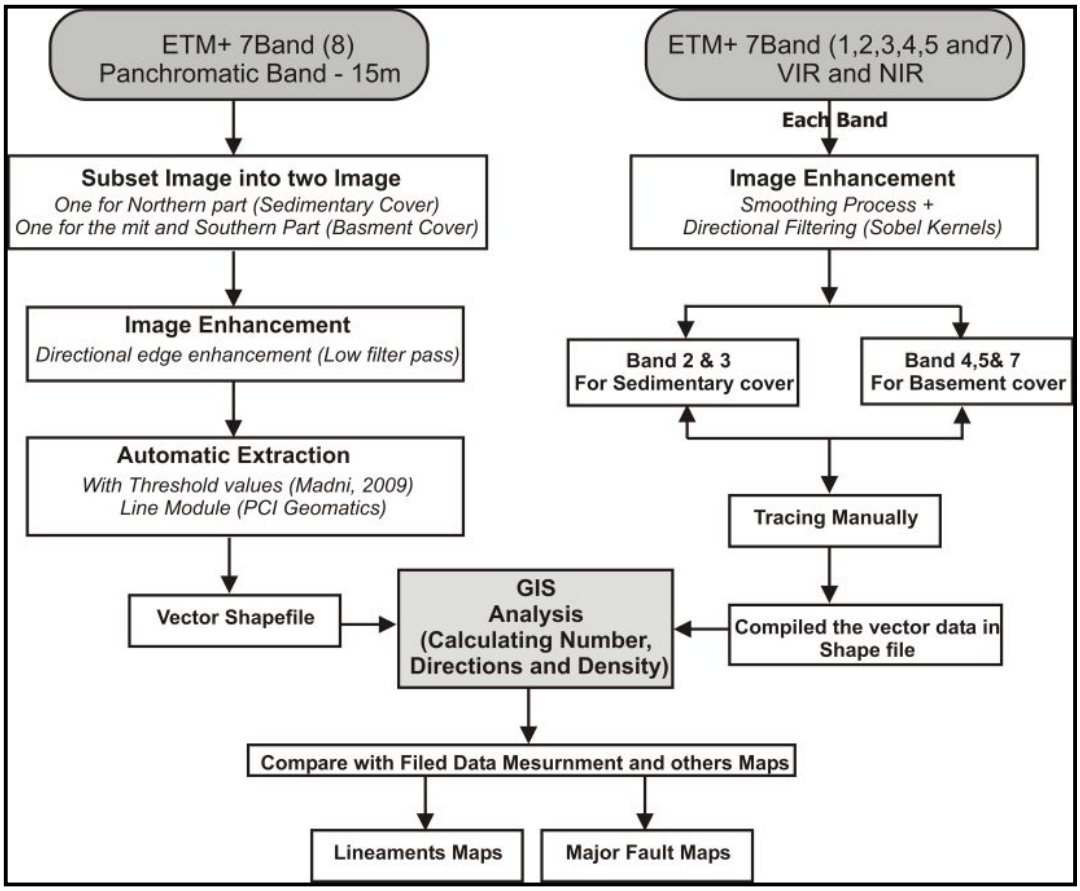

Figure 26: Work Flow of the Lineament Extraction

The proposed overall process flow for extraction of lineaments from satellite images can be summarized as the following:

1.3.2.1 Manual extraction for major faults

For manual lineament extraction, each band is smoothed with an average low pass filter in order to eliminate the noise. Then, the directional filtering methods are selected to enhance the lineament features. The common filters which are used for edge detection filters are Gradient-Sobel; the directional nature of Sobel kernels generates an effective and faster way to evaluate lineaments in four principal directions (Süzen and Toprak, 1998). The image directional Sobel filter kernels are presented in four directions (Table 6). A Sobel kernel of 3x3 pixel size is selected and employed along directions N (0°), NW (45°), NE (45°) and EW (90°) to highlight linear features in their respective directions as in (fig.27).

The main advantage of manual extraction is that the human eye can easily separate the non-geological lineaments such as roads, fences, and field boundaries from geological structures. It is found that band 1 and 2 are best for the northern part of the study area (Sedimentary cover) and band 3, 4, 5 and 7 for basement covers in the southern part of the study area.

E-W	NE-SW	N-S	NW-SE
-1 -2 1	-2 -1 0	-1 0 1	0 1 2
0 0 0	-1 0 1	-2 0 2	-1 0 1
-1 2 1	0 1 2	-1 0 1	-2 -1 0

Table 6: Sobel Filter Kernels in Four Principal Directions

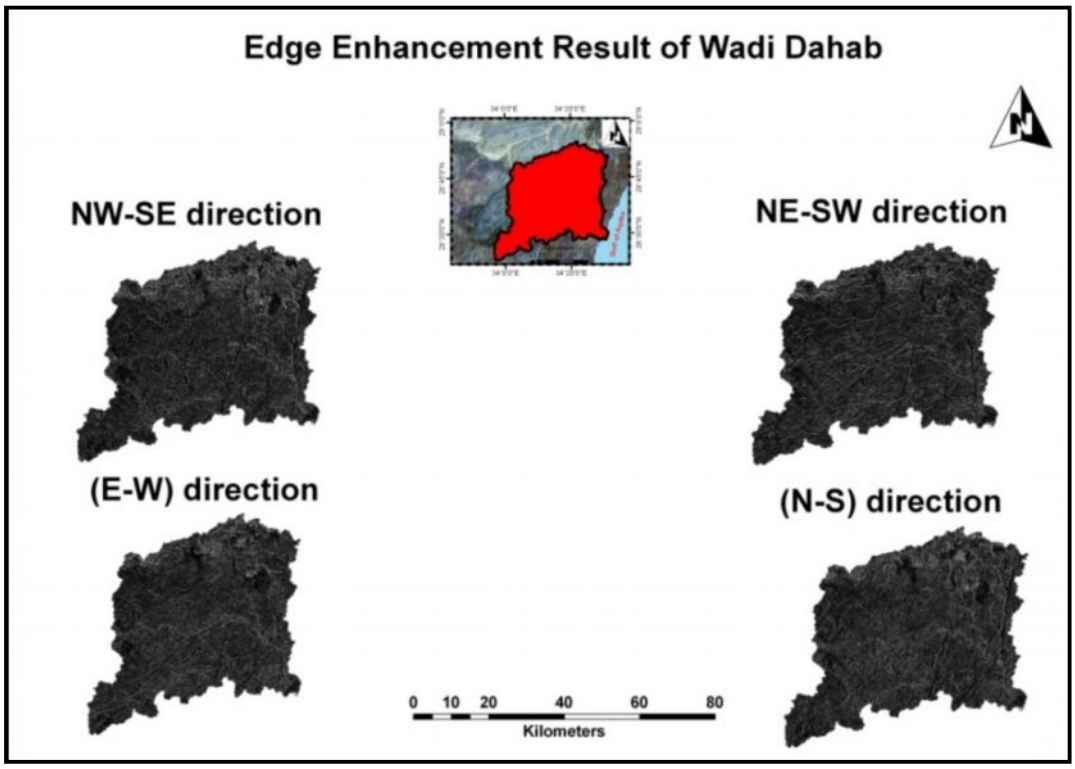

Figure 27: Edge Enhancement Results of W. Dahab

1.3.2.2 Automatic extraction for lineaments

Automatic lineament extraction from remote sensing data is an important approach for regional structural studies and hydrogeological studies in basement rock. The extracted lineament trends are mostly compatible with the main structure of Dahab basin. The lineaments analysis aims to understand the relationship between the lineament trends and zones of high recharge to aquifers. Percolated water through recognized recharge zones will continue to flow through fractures (identified lineaments).

Landsat panchromatic image (15m) is prepared to conduct this analysis using user defined parameters of LINE module of PCI software. Automatic lineaments extraction from Landsat panchromatic image is run with three major steps: edge detection, threshold and lineament extraction. Kocal et al. (2004) illustrated the LINE module to extract lineaments from image channels as input. If the image is 16-bit or 32-bit, the image is scaled to 8 bit using a nonlinear scaling routine. The output of the program is a vector segment which contains linear features extracted from the image.

The lineaments usually appear as straight lines or edges on satellite images (Wang et al., 1990). In order to detect (enhance) these edges in Band 8, the following steps are applied:

1- Subsetting of raw image into two images: one represents areas which are covered with sedimentary rocks and the other represents zones outcropping with basements rocks. Separation is necessary because of difficulties which may be encountered in detecting lineaments within sedimentary terrain due to their lithological nature and the effect of the high tone of basement rocks onto sedimentary rocks.
2- Applying of edge enhancement to generate a convolved image: a significant Kernels including directional low pass filters with size 3 ×3 (Süzen and Toprak, 1998).
3- The enhanced image is used in PCI Geomatics LINE module using the same threshold value as Madani (2009) to extract the lineament.
4- GIS is used to calculate the number and the length of the segments and to prepare a map of lineaments length density per unit area (1 km × 1 km).

Many researches (Madani, (2009), Qari et al. (2008), and Al Saud, (2008)) have discussed automatic lineament extraction from basement terrains. They have used the same software and threshold values according to the available data and nature of the study area. Madani, (2009) has applied threshold parameter values on ETM+7 (Band 8) at exposed basement cover in Baharah area on the western side of Saudi Arabia. Because the lithological and structural conditions at Baharah area similar to Dahab basin, it is favorable to use the same threshold value in the investigated area to extract the lineament.

1.3.3 Results and discussion

Most of the fault traces in Dahab basin are depicted as straight lines representing steeply dipping planar faults. More than 350 faults are extracted manually from different bands. The lengths range between 0.6 and 36 km. Generally, the prominent faults set in the study area are parallel to the well-known Gulf of Aqaba fault trend NE-SW strike (54%) and NW-SE direction (33%) as shown in (fig. 28). The trend and the length of the faults are measured and plotted on a rose diagram (fig.28). The longest fault is 35 km long in W. Ghaieb fault while the fault of W. Nasab has a length of 22 km with direction NS to NE-SW and NNE-SSW. It can be concluded that the main directions of the major faults in study area were NE-SW, NW-SW and N-S. It is observed from the analysis of lineaments that most drainage streams are structurally controlled and that they are created according to tectonic effects of the Gulf of Aqaba.

The comparison between the extracted results and previous works should give a confirmation about the general structure setting of the study area and preliminary reassurance for the lineament extraction method. Eyal et al. (1981) described that Dahab basins are located in Bir Zreir zone which extends to about 70 Km long from shahira pass in the south to W. Watir in the north along Gulf of

Aqaba (fig. 29). This zone is structurally active and has a large amount of strike slip movement. It includes faults such as W. Nasab fault, W. El Ghaieb fault and shahira fault. W. Ghaieb and downstream of Dahab basin are affected by tectonics of the Gulf of Aqaba where the main directions are NW-SE, NE-SW and N-S with steeply dipping strike slip faults (El Masry et al. 2003). At W. Saal and W. Zaghraa, due to the compression stress, two conjugate shear planes are affected in Saal belt. The first one is a left lateral strike-slip fault set trending NE to NNE, and the second a right-lateral strike-slip fault set trending NW (Hegazi et.al., 2006). Oada (1995) mentioned at W. Nasab that the major faults at W. Rahab, W. Nasab, W. El Shethan and W. El Shellal are directed NE- NNE to SW-SSW. On the other hand, there are other faults at W. El Rasis and W. El Waraa that are mainly directed NW-SE to the Gulf of Suez trend.

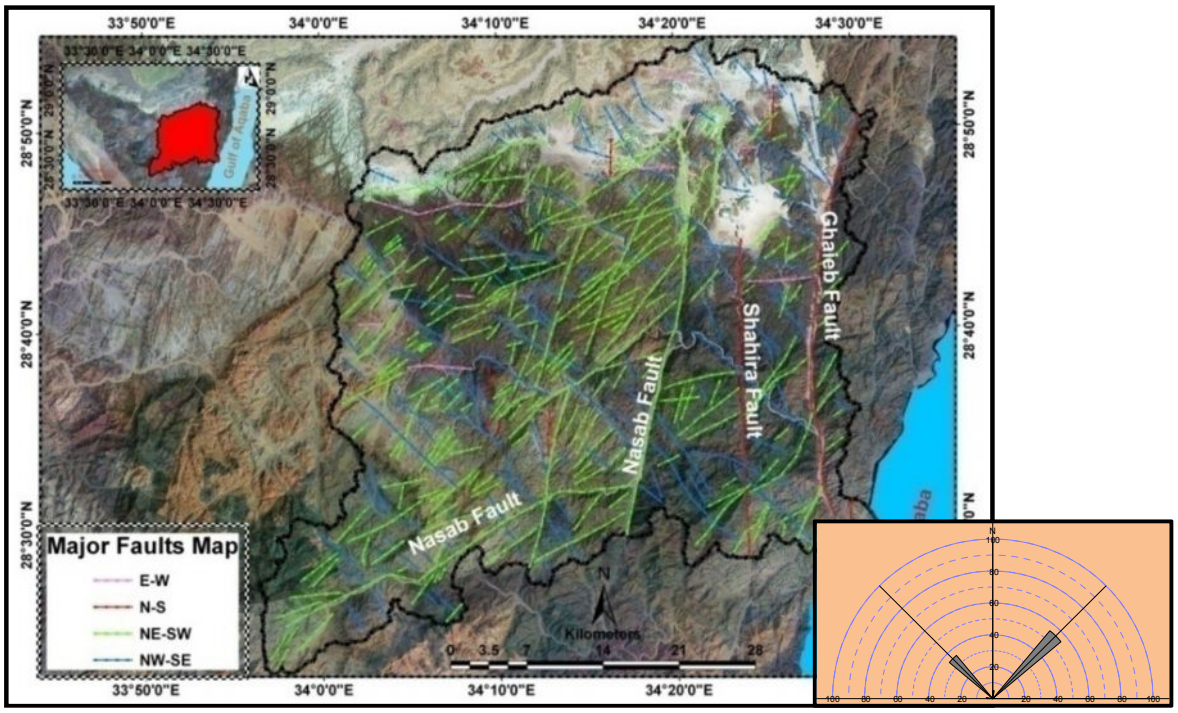

Figure 28: Major Fault Map of W. Dahab

The resulting map of minor lineament shows that there are eight main directions dominated in the study area which are NNE-SSW, NE-SW, NW-SE, ENE-WSE, NNW-SSE and N-S respectively. The main trends are NNE-SSW (26%), NE-SW (21%), ENE-WSW (19%), NNW-SSE (10%) and N-S (5%) (fig. 30). The prominent directions of these lineaments coincide with major structure trends in the study area. The field data shows that the most of the dykes are directed NNE-SSW and NW-SE in direction.

The average density of the lineament is high on the basement outcrops (5.5 to 7 km/km^2), especially at the eastern and southern parts of Dahab basin, as in W. Nasab, W. Rimthy, W. Saal and W. Abu Khshieb, which are highly affected by the shear tectonics of the Gulf of Aqaba (fig.31). The

northern and western parts of Dahab basin have a low lineament density (0.2 to 1.5 km/km^2) due to sedimentary covers in the northern and western parts of the study area and along the main stream. Groundwater is known to be accumulated in fracture zones which can be found in different rock types. The areas of higher density of lineaments should deliver higher quantities of groundwater recharge and additionally, the locations of the lineament intersections should also be good zones for groundwater recharge.

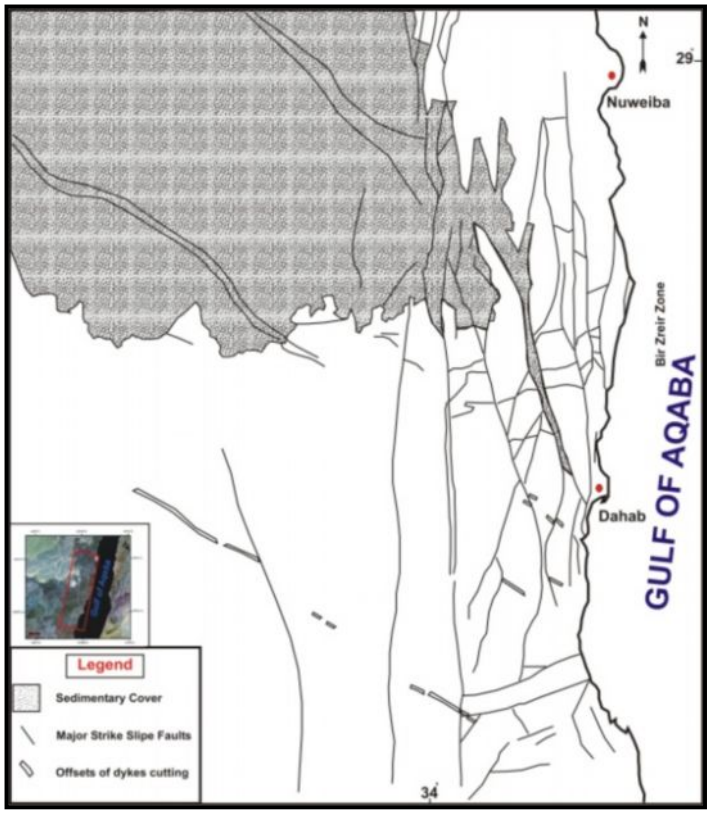

Figure 29: Major Fault Map of Western Side of Gulf of Aqaba (Modified after Eyal et al.1981)

Measurements at 13 field stations in different locations within Dahab basin are used to evaluate the extracted data. This data is statistically investigated and rose diagrams are used to reveal the orientations of steeply dipping linear features. These diagrams show that the main orientations are NE to NNE which is mainly parallel to effect the Gulf of Aqaba tectonic structure as shown in (fig.32). NW-SE trend represents the second main direction, but a N-S direction also occurs in the study area. Dahab basin is characterized by the abundance of joints as lineament features of different directions and amounts of dip.

The main directions are NNE-SSW, NE-SW and NW-SE respectively according to abundance. The amount of dip varies from 0 for horizontal joints to 90 for vertical joints. The high density area is accompanied with fault zones and shear belts. These shear belts result from tectonic processes in the Gulf of Aqaba. These shear zones are distributed mainly in W. Nasab, W. Saal and W. Rimthy which have trends mainly NE-SW, NNE-SSW, NW-SE and N-S respectively. It is importantly to mention

here, that these structural elements could play an essential role for controlling groundwater recharge and flow condition in the study area. This will be discussed in the following Chapters.

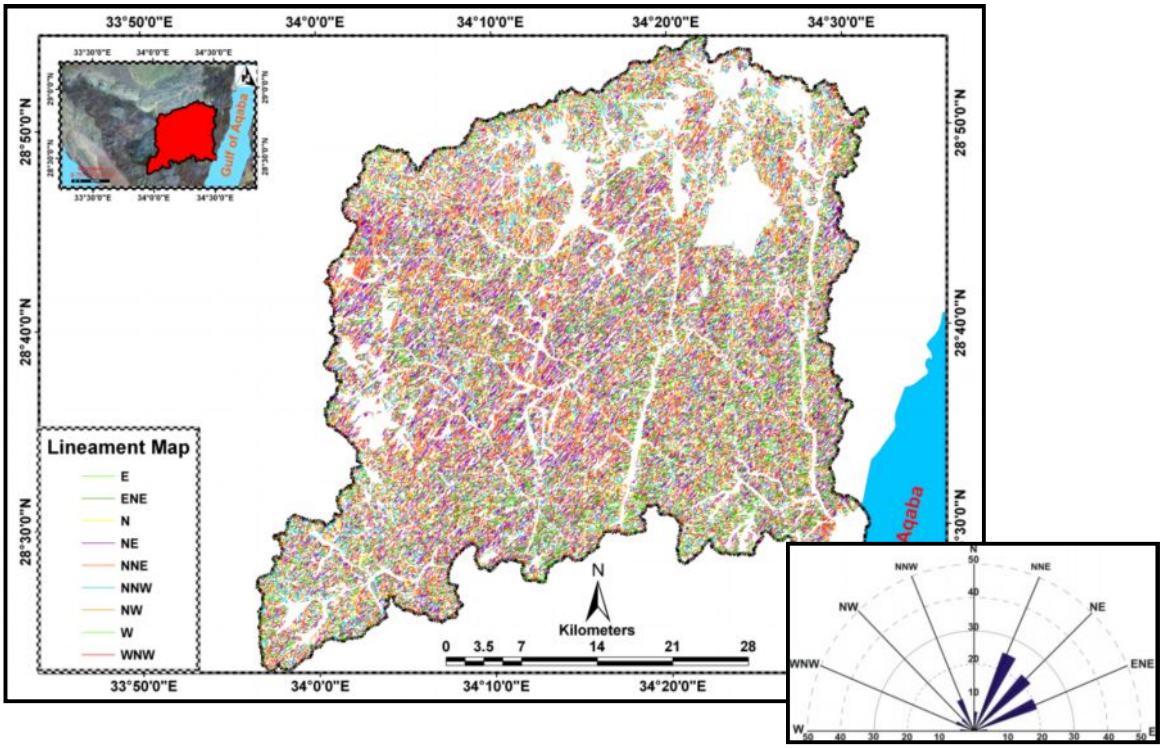

Figure 30: Minor Lineament Map of W. Dahab and its Rose Diagram

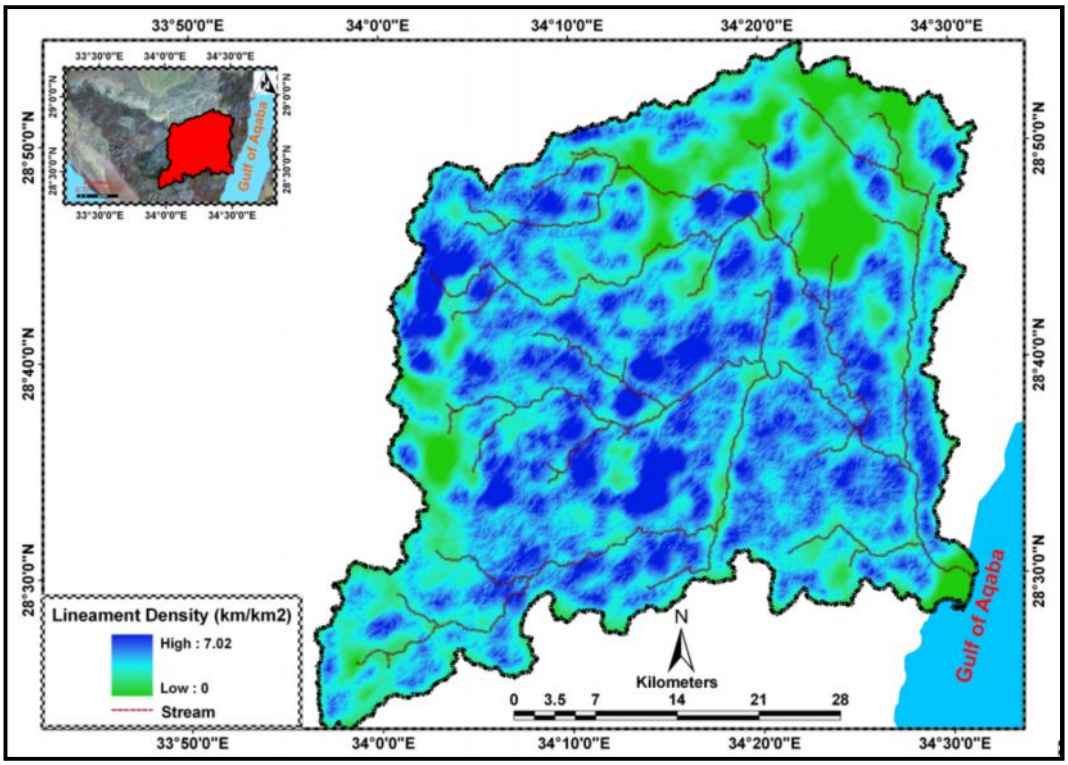

Figure 31: Lineament Density Map of W. Dahab (km/km^2)

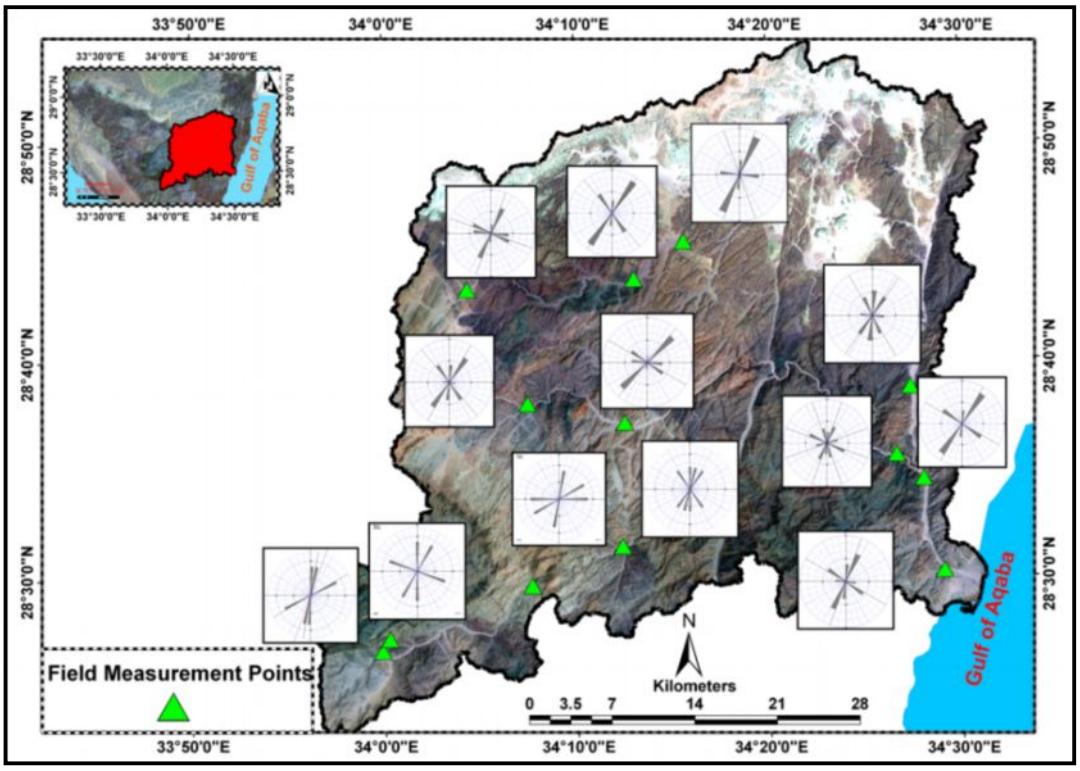

Figure 32: Field Measurements Locations for Lineament Features in W. Dahab Basin

CHAPTER II

GEOMORPHOLOGY

Chapter II

Geomorphology

Geomorphic processes are influenced by tectonics, climate, ecology, and human activity. In addition, some of those factors can be affected by the ongoing evolution of the Earth's surface, for example, isostasy. Many geomorphologists are particularly interested in the potential for feedback between climate and tectonics mediated by geomorphic processes. Therefore, geomorphology is an important factor in hazard assessments such as landslide prediction and mitigation, Runoff control and restoration, and coastal protection studies.

The landform terms are used by geoscientific modelers to denote a portion of the earth that unites the qualities of homogeneous and continuous relief due to the action of common geological and geomorphological processes. Geomorphometry, a subdiscipline of geomorphology, is the quantitative and qualitative description and measurement of landforms (Pike, 2002) and is based mainly on the analysis of variations in elevation as a function of distance.

A basic principal underlying geomorphometrics is the existence of a relationship between relief form and the numerical parameters used to describe it, as well as to the processes related to its genesis and evolution. Clarke (1966) stated that morphometry is the measurement and mathematical analysis of configuration of the earth surface, shape and dimensions of its landforms. Therefore, morphometric analysis of landforms is considered as one of the important fundamentals in geomorphological studies. Morphometric analyses have been used to estimate the flash flood risk levels of sub-watersheds within the main watershed. Both the drainage network and drainage watershed characteristics are captured by a set of network and basin parameters that are relevant to the flash flood risk.

Dahab basin has many togographic features which affect the hydrogeological and hydrological situation. It includes many wadis like W. Zaghraa, W. Nasab, W. Rimthy-Zaghra, W. Saal, W. El Genah and W. El Ghaieb. Those wadis separate different mounds and mountains that are composed of basement rocks. The coastal areas along the Gulf of Aqaba are composed of sediments that are washed out by wadi runoff from the western high land and are debouched into the eastern low lands.

The main objective of this chapter is to investigate the geomorphic units of the basin and its impact on both surface runoff and groundwater accumulation. Therefore, the chapter will discuss the geomorphology of the study area from a qualitative and quantitative point of view. Finally, the potential areas with endangered flood hazards will be determined in Dahab basin based on geomorphmetric parameters.

2.1 Stream and basin delineation

To achieve reasonable qualitative and quantitative geomorphological results, the drainage network and watershed divide should be extracted and delineated. The analysis of drainage networks

is manually conducted via tracing the stream network and basin delineation from the topographic maps. For this task, it is better to use digital elevation models (DEM) within a GIS environment and then compare the results with topographic maps (Omran et al. 2011).

GIS and digital elevation models (DEM) can be used to perform watershed delineation to a point, or an area of interest, which is usually one of the important steps in such studies. This part presents the methodology to process a DEM in order to facilitate interactive watershed delineation and stream network extraction. As a result, watersheds can be delineated quickly and with consistent time response. The extraction of the drainage network and basin delineation is carried out using an ASTER DEM (2006) with a 30m×30m grid cell size.

2.1.1 Drainage pattern extraction

The application of geomorphic principles to determine flood potential or flood risk have led to a noteworthy amount of research attempting to identify the relationships between basin morphometry and flooding impact (Patton, 1988). Identification of drainage networks within basins or sub-basins can be achieved using traditional methods such as field observations and topographic maps, or alternatively, with advanced methods using remote sensing and DEM (Macka, 2001, Maidment, 2002). Many authors have pointed out that it is difficult to examine all drainage networks from field observations due to their extent throughout rough terrain and over vast areas.

Morphometric studies include the evaluation of streams through measurement of stream network properties. The proposed work automatically extracts segments from a drainage pattern associated with their order and also estimated various attributes related to the same segment order. It relies on the concept of Strahler's ordering technique for performing a qualitative and quantitative assessment of the drainage system. The automated method for delineating streams follows a series of steps (fig.33).

A common problem with drainage network delineation using DEM is the presence of sinks: in fact, the main problems are the positioning of the ends of drainage networks and the assignment of flow directions to individual cells, particularly in flat areas and depressions. Therefore, the sinks are commonly removed prior to DEM processing for drainage identification. For this reason, a fill process should be used before starting the drainage extraction which involves filling each depression in DEM with an appropriate limit. A filled DEM process should be iterated until filling all sinks and the elevation raster void of depressions should be created (fig.34-B). A depression is a cell or cells in an elevation raster that are surrounded by higher elevation values, and thus represented an area of internal drainage. Therefore, sinks have to be removed from a DEM through the filled process. A common method for removing a sink is to increase its cell value to the lowest overflow point out of the sink.

In the next step, the flow direction raster will be created. A flow direction raster shows the direction water will flow out of each cell of a filled DEM. A widely used method for deriving flow direction is the D8 method. This method is used by ArcGIS and assigns a cell's flow direction to the

one of its eight surrounding cells that has the steepest distance as weighted gradient. The D8 method produces good results in high gradient slopes but tends to result in parallel flow lines along less steep areas.

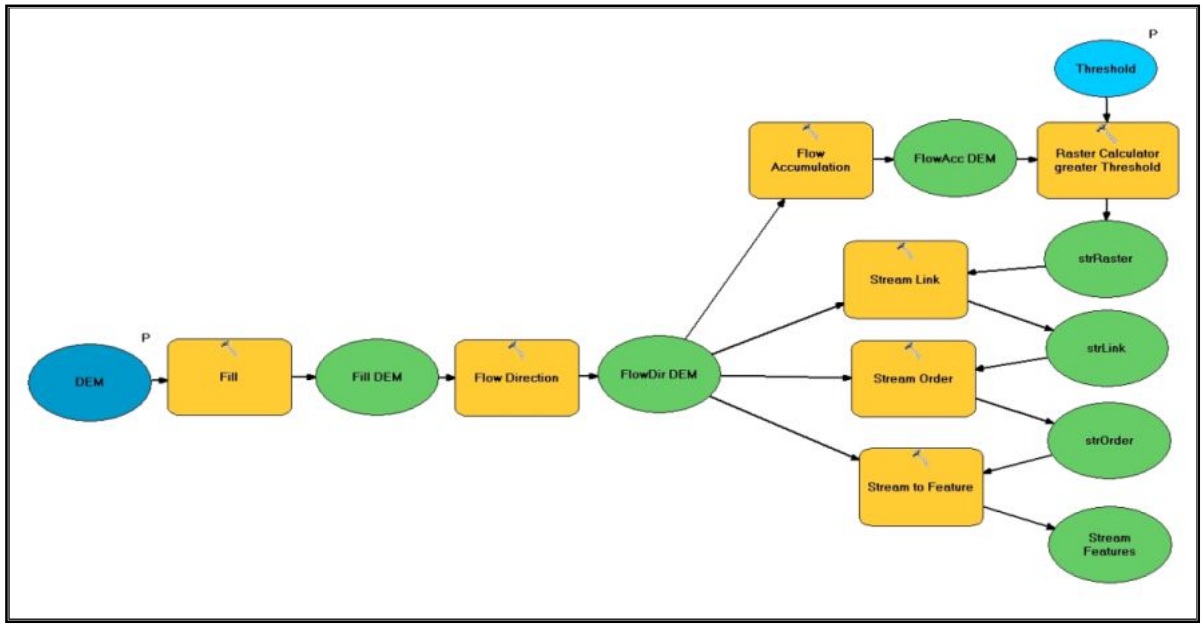

Figure 33: Model Builder Diagram Showing the Workflow to Extract the Drainage Pattern From Digital Elevation Model (DEM)

Next, the flow accumulation will be used: this tool aims to extract a flow accumulation raster which tabulates the number of cells from which surface water will flow to it for each cell. Thus, it records how many upstream cells are contributed to the drainage of each cell (fig.34-D). Stream network and stream link delineation are performed in the next steps. A stream network raster is derived from the accumulation raster. This step is based on a threshold accumulation value (fig.34-E). Here, several drainage network maps have been extracted by defining different threshold values. After the stream network is derived from the flow accumulation raster, each section of the stream raster line is assigned a unique value and is associated with flow direction. As threshold value 100 related to the area of basin was used, the results of stream network with this value match the area of the basin. This means that the stream link raster resembles the vector stream layer. As the last stage, the drainage streams are ordered by the Strahler method and transformed into a vector layer for further analysis.

The final result of this step is the stream network map of Dahab basin (fig. 34-F). Referred to the ordering system of Strahler, Dahab basin is of eighth order (See app. 3). The obtained results are confirmed and evaluated by comparing the extracted parameters with a georeferenced topographic map (1:50,000).

2.1.2 Basin delineation

A drainage basin is an area where water from rain or snow melts drains downhill into a body of water, such as the Gulf of Aqaba. The drainage basin acts like a funnel, collecting all the water within

the basin area and channeling it into a waterway. The drainage basin includes both the streams that convey the water as well as the land surfaces from which water drains into those channels. Each drainage basin is separated topographically from adjacent basins by a ridge, hill or mountain, known as a water divide.

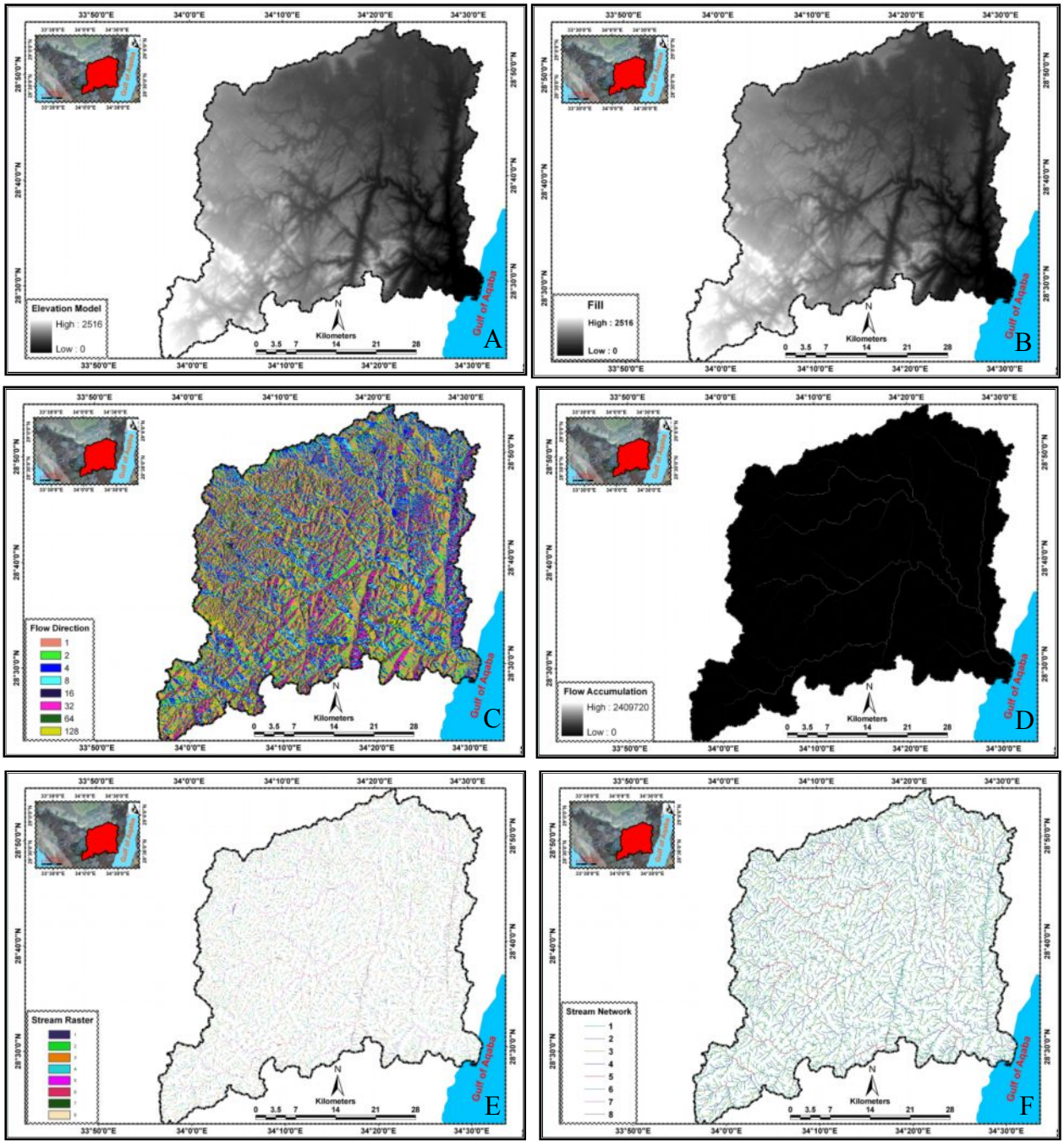

Figure 34-A: Digital Elevation Model **Figure 34-B: Raster Fill of Digital Elevation Model**
Figure 34-C: Raster Data of Flow Direction **Figure 34-D: Raster Layer of Flow Accumulation**
Figure 34-E: Raster Layer of Streamline **Figure 34-F: Drainage Network of Dahab Basin**

Watersheds, or basins draining into one another, are found in the form of a nested hierarchy. The topography helps to determine where and how water flows from one area to the next. However, each

large drainage basin can be broken into smaller drainage basins with their own topographic and hydrologic characteristics; these are called sub-watersheds, or subbasins for short. Delineation of a watershed meant determining the boundary of the watershed, i.e. the ridgeline. Ridgeline is the line that joins the highest elevation points and thus become the boundary of the watershed. The most important aspect for defining and delineating a watershed is to fix the outlet of the drainage course. Basically, location of the outlet defines the area of the watershed.

The delineation of drainage basins can be done manually using topographic information. On the other hand, the widespread availability of elevation data in digital format has bolstered the development of automated tools that can be used to delineate drainage basins and their associated stream networks. Most of the hydrologic modeling tools work with elevation data in raster format (DEMs). A watershed of any size can be delineated by using the following procedures.

The Basin delineation starts with pour point digitization. Pour points are indicated by the location where water would flow out of the cell. Thus, a pour point should be located within an area of high flow accumulation because it is used to calculate the total contributing water flow to that given point. By calibrating the results of the stream network (see following paragraphs) with the topographic map, pour points have been identified and digitized. The snap pour point tool is used to ensure that the digitzied points are dragged to the high accumulated flow. Then, the final step is the watershed tool: a flow direction (raster layer) and pour point (vector layer) are required to delineate watershed sub-basins. As in the extraction of a stream network, it is important not to use the simplification option while converting the raster map to vector features. Otherwise, the delineated stream networks and basins will not match exactly, which is a prerequisite of the following steps for automating counting and joining of the drainage network.

The result of these steps is the delineation of 174 sub-basins in W. Dahab. These sub-basins are created based on their nested hierarchy up to the main stream represented by the downstream of Dahab basin (fig.35). W. Dahab is subdivided into five main sub-basins which are W.Abu Khshieb, W.Um Assam, W.South Zaghraa, W. Zaghraa Ghaieb. W. Zaghraa is considered the largest sub-basin in the study area. All previous sub-basins drained directly into the downstream of Dahab basin.

W. Zaghraa is subdivided into two main sub-basins: W. Zaghraa saal and W. Zaghraa Nasab, while W. El Ghaieb is divided into seven sub-basins: W. El Geeby and W. Abu Gerdan as the largest sub-basins. W. Abu Khshieb is subdivided into W. Um Shawky, W. South Abu Khshieb and W. Maaen. Both W. Zaghraa and W. El Ghaieb are considered the largest main sub-basins in the study area. W. Zaghraa Nasab is divided into three subbasins. W. Korna, W. Nasab and W. Rimthy are important sub-basins, while W. Zaghraa Saal is divided into nine sub-basins where sub-basins W. Saal and W. Genah are the largest sub-basins. On the other hand, W. El Geeby is subdivided into four sub-basins: W. South Small El Geeby, W. South El Geeby, W. El Marwah and W. Abu Haiethat.

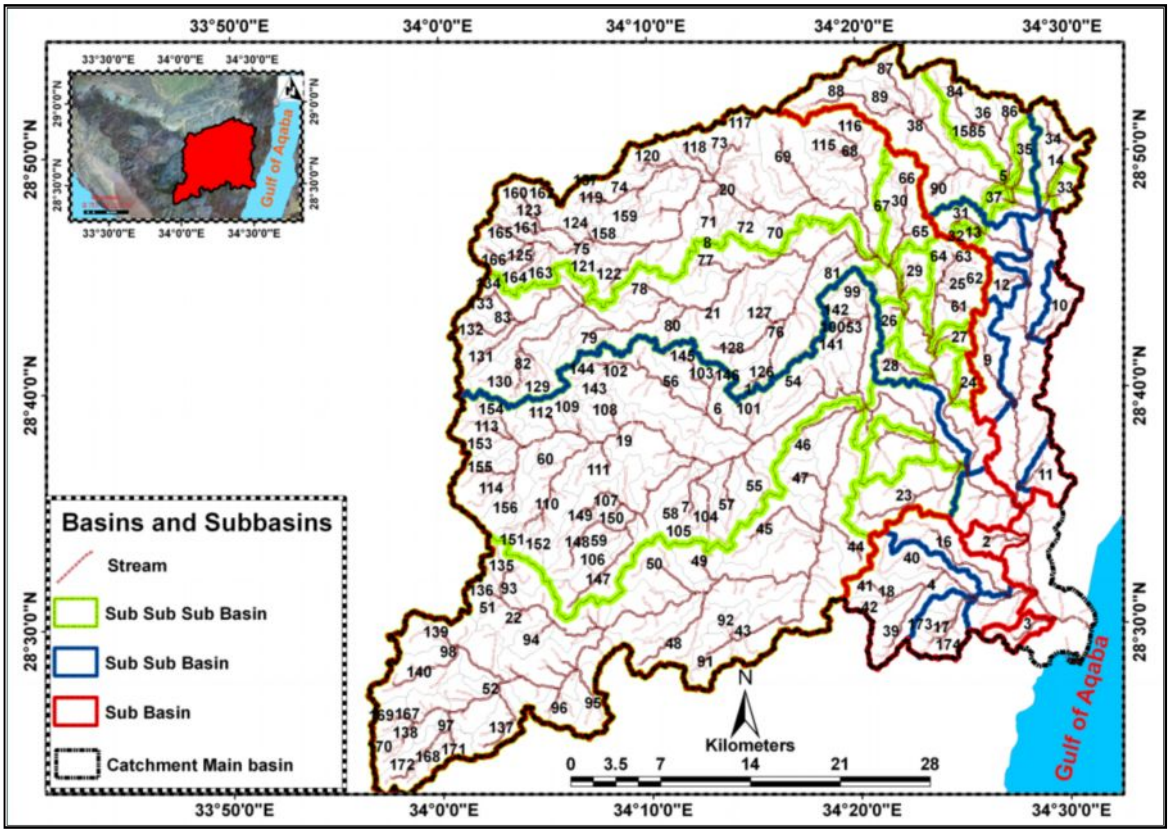

NAME	Basin No.	NAME	Basin No.	NAME	Basin No.	NAME	Basin No.	NAME	Basin No.
Wadi Mega Dahab	1	Wadi Fieran	44	Wadi Ghalium	87	Wadi Small Mywilha	130	Wadi West Maeen	173
Wadi South Zaghraa	2	Wadi Meer	45	Wadi Bathier	88	Wadi Small Saal	131	Wadi East Maeen	174
Wadi Um Asaam	3	Wadi Tieeba	46	Wadi North Bathier	89	Wadi Saal El Atshan	132		
Wadi Abu Khshieeb	4	Wadi Hamam	47	Wadi Mezirah	90	Wadi Manader	133		
Wadi El Ghaieb	5	Wadi Agnid	48	Wadi Um Shietan	91	Wadi Small Saal El Rayan	134		
Wadi Zaghraa	6	Wadi Sudud	49	Wadi Masharaah	92	Wadi Small Abu Khashab	135		
Wadi Zaghraa Nasab	7	Wadi Nabaa	50	Wadi Main Abu Khshab	93	Wadi Hassa	136		
Wadi Zaghraa Saal	8	Wadi Abu Khshab	51	Wadi Haziema	94	Wadi El Waraa	137		
Wadi Abu Rwies	9	Wadi Nasab Main	52	Wadi Wedah	95	Wadi Nasab Small	138		
Wadi Kharza	10	Wadi Merkh	53	Wadi Um Ariefat	96	Wadi Myenat	139		
Wadi Hamarah Ghai	11	Wadi El Faraa	54	Wadi Small Nasab	97	Wadi Roting	140		
Wadi South Um Marha	12	Wadi Meer Zaghraa	55	Wadi Rasies	98	Wadi Haialah	141		
Wadi Hodbah	13	Wadi Mekaffa	56	Wadi Baryiga	99	Wadi Small Haialah	142		
Wadi Abu Gerdan	14	Wadi Um Retm	57	Wadi Small Merkh	100	Wadi Um Harhal	143		
Wadi El Geeby	15	Wadi Um Saial	58	Wadi Naieema	101	Wadi Small El Faraa	144		
Wadi Um Shawky	16	Wadi Sanad	59	Wadi Main Mekaffa	102	Wadi Homrah	145		
Wadi Maeen	17	Wadi Zaghraa Main	60	Wadi Small Mekaffa	103	Wadi Small Homrah	146		
Wadi Small Abu Khshieb	18	Wadi Um Athan	61	Wadi El Kasied	104	Wadi Goo	147		
Wadi Zaghraa Ramthy	19	Wadi North Um Athan	62	Wadi Small Um Saial	105	Wadi Abu Tabak	148		
Wadi El Genah	20	Wadi Small Barka1	63	Wadi Gabr	106	Wadi Abu Sahsieh	149		
Wadi Mega Saal	21	Wadi Small Barka 2	64	Wadi Small Sanad	107	Wadi Khadrah	150		
Wadi Mega Nasab	22	Wadi Small North Akry	65	Wadi El Maha El Olia	108	Wadi Small Maraan	151		
Wadi Korna	23	Wadi Maryowat	66	Wadi Dakek	109	Wadi East Small Maraan	152		
Wadi Small El Hamam	24	Wadi El Kurry	67	Wadi Maaran	110	Wadi Small Ramthy	153		
Wadi Mega Barka	25	Wadi El Matamier	68	Wadi Mokhzenah	111	Wadi Small Zaghraa	154		
Wadi Naghmishy	26	Wadi Ghradah	69	Wadi El Mokhtar	112	Wadi Hamami	155		
Wadi South Um Athan	27	Wadi Habibah	70	Wadi S. Ramthy	113	Wadi El Aranyia	156		
Wadi Remty	28	Wadi Mabad	71	Wadi Rakieta	114	Wadi Abu Tehimah	157		
Wadi South Akry	29	Wadi El Hoo	72	Wadi Aska	115	Wadi South Abu Tehimah	158		
Wadi Mega North Akry	30	Wadi Naqab Um Rdeem	73	Wadi Small Matamier	116	Wadi El Saraah	159		
Wadi Small Hodbah	31	Wadi Sorah	74	Wadi Defdeef	117	Wadi Small Tabieh	160		
Wadi South Small Hodbah	32	Wadi Big Morah	75	Wadi West Deef	118	Wadi South Small Tabaieh	161		
Wadi Khalal	33	Wadi Mytorah	76	Wadi Big Sorah	119	Wadi North Small Tabaieh	162		
Wadi Geb Um Reglah	34	Wadi Tyniah	77	Wadi Samll Sorah	120	Wadi Retem	163		
Wadi El Marwah	35	Wadi Murad	78	Wadi West Borady	121	Wadi North Retem	164		
Wadi Abu Haiethat	36	Wadi Um Maksour	79	Wadi Borady	122	Wadi Small Tabaiek	165		
Wadi South Small El Geeb	37	Wadi El Thmilah	80	Wadi El Tabieh	123	Wadi South Small Tabaiek	166		
Wadi Small El Geeby	38	Wadi El Halall	81	Wadi Meksan	124	Wadi Zaraa	167		
Wadi Um Ataqa	39	Wadi Mwyilha	82	Wadi Tabaiek	125	Wadi Rahabah	168		
Wadi S. Abu Khshieeb	40	Wadi Saal El Rayan	83	Wadi Um Asaam	126	Wadi North Zaraa	169		
Wadi Um Harq	41	Wadi Hagag	84	Wadi Thmilah	127	Wadi South Zaraa	170		
Wadi South Um Harq	42	Wadi South Hagag	85	Wadi Small Mytorah	128	Wadi Nasab Upstream	171		
Wadi El Shalal	43	Wadi Abu Arshy	86	Wadi Abu Dalal	129	Wadi Small Rahabah	172		

Figure 35: Main Basins and Sub-basins in W. Dahab

2.2 Qualitative geomorphology

The topography of the study area is controlled by the lithologic composition of the exposed rock units and the existing structural elements. The main landforms in the coastal zone of the Gulf of Aqaba are reflected by endogenic tectonic- structural forces and types of lithology, as related to their plate tectonic suite. The topographic highs are mostly structurally controlled and are made up of basement rocks. The topographic lows are also structurally controlled and are filled with loose sediment that resulted from being washed out by wadi runoff and weathering effects from the western high land. They drain into the eastern low lands of the coastal area.

Topographic features are studied depending on eight topographical maps with the scale (1:50,000), DEM- Aster version, 30 meter resolution, ETM+7 satellite data and the ancillary geologic data to identify geomorphic units of the study area. Many researchers have described geomorphological units along the Gulf of Aqaba. (Issawi et al. 1998, Ashmaway et al. 2000, Hassan et al. 2005). From a geomorphological point of view, the study area can be classified into (fig.36):

1- Mountainous Basement terrain.
2- Flat-Topped Limestone plateau.
3- Alluvial Fans
4- Coastal plain
5- Drainage network geomorphological units.

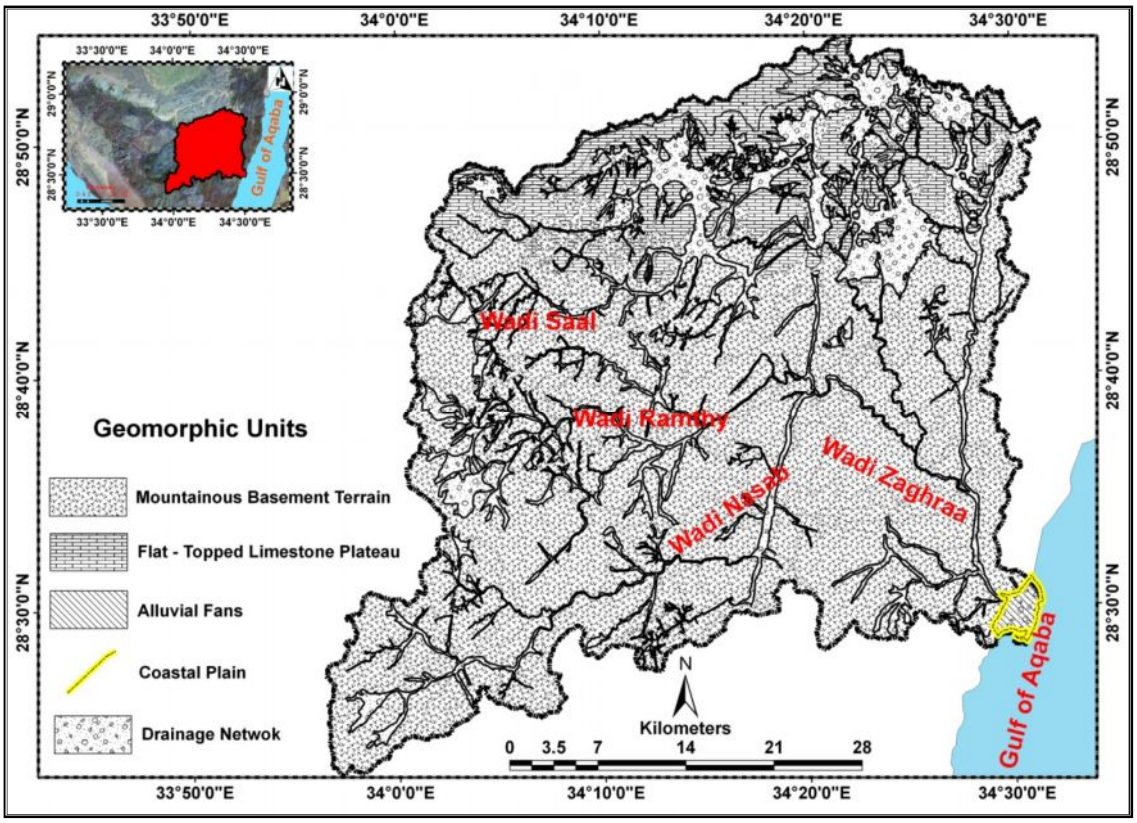

Figure 36: Geomorphic Units in W. Dahab Basin

2.2.1 Mountainous basement terrain

The mountainous terrain is composed by the basement of the Arabian-Nubian Shield. This Massif includes various types of rocks of igneous and metamorphic origin, mainly old and young granites, gneisses, migmatites, gabbros and metasediments. The metamorphic basement is intruded by gabbro-diorite to granite batholiths. These rocks are dissected by many dykes. Dyke ridges originate due to the intrusion of magma into joints and faults that affected ancient mountain blocks.

This mountainous terrain occupies most of the western, south western and southern parts in W. Dahab basin. They represent mainly a huge catchment area of precipitation receivers in the study area. Average height of the mountains reaches in the western side of Dahab basin between levels 1500 to 2000 m as in G. Hamami, G. Um Louz and G. Um Alwai, while average peaks in south western part reach between levels 2000 to 2700m as in G. Catherine, G. Shiekh El Arab and G. Abu Masud (fig.37).

This mountainous terrain is intensively cut by a large number of wadis and drainage lines which developed during the pluvial periods of the Oligocene, Miocene, Pliocene and Pleistocene ages. At present, water flow occurs in these wadis occasionally during rainstorms of high intensity. Although the cross section of these wadis exhibits the characteristics of fluvial action, all wadi floors are covered with fluvial sediments of gravel, sand and silt either as wadi fill or as fans when tributaries meet the main wadi.

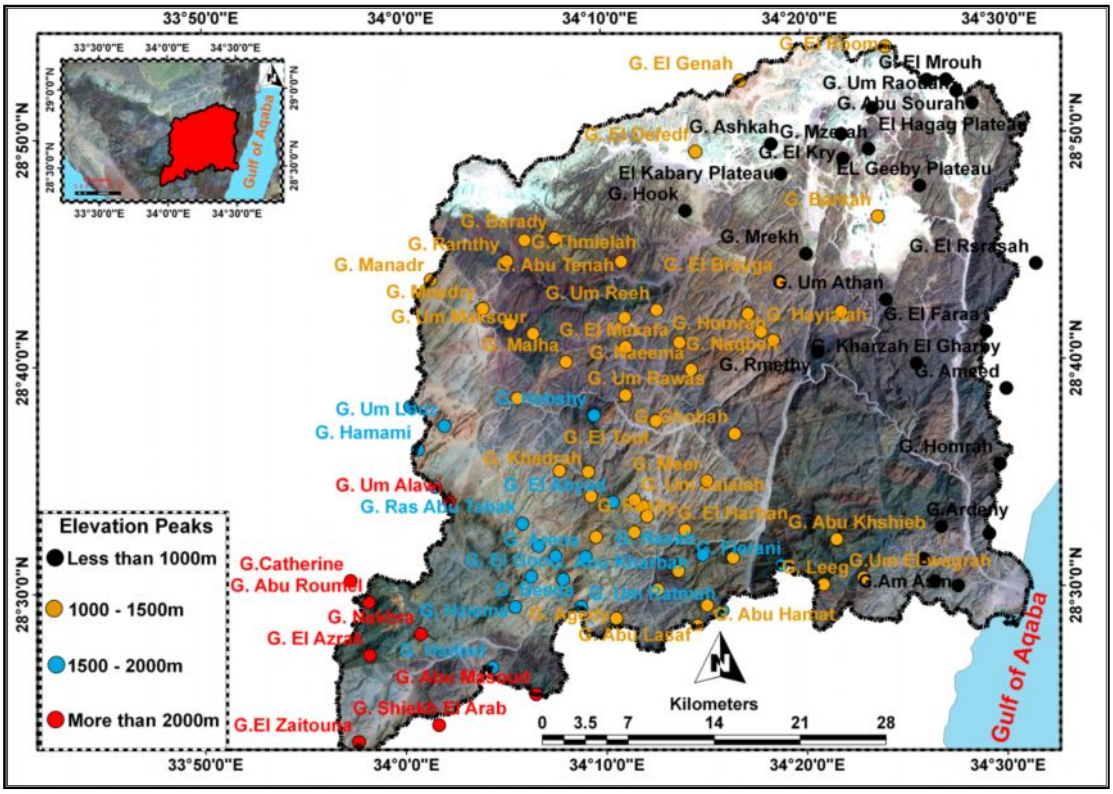

Figure 37: Mountains in W. Dahab Basin

This terrain has structural forms which include wadis, inter-mountain basins which depend on fault zones, and dyke ridges. Faults control, wholly or partially, the development of straight wadis occupied by straight and narrow grabens, which took the form of canyons. These canyons extend for several tens of kilometers such as for W. El-Ghaieb and W. Nasab. Subsidence of some blocks due to faulting results in the development of inter-mountain local basins. These basins represent depositional sites for wadis that drained towards them. Due to sediment accumulation, the level of the basins becomes higher in time; therefore, their present level does not represent the original one. Most likely, the accumulated fluvial sediments represent ground water aquifers.

2.2.2 Flat-Topped Limestone plateau

Flat-topped limestone plateau occupies the northern part of Dahab basin where it is immediately flanked by a stretch of the flat–topped limestone plateau of El Tih. This plateau is controlled by the gently dipping structure of this region. The plateau made of a sequence of alternating clastic and non clastic beds capped by hard limestone beds of Cretaceous age.

This plateau takes the form of cuesta with two major slopes: steep cuesta escarpments, which face southward to Dahab basin and a dipping slope with a gentle gradient towards the north out of the study area (Awad, 1952). This plateau is bounded by some steep fault scarps and detached blocks with elevations of up to 1000 m higher than the surrounding terrain. El-Gunah Plateau represents the northern part of the study area. The average height of the escarpment decreases eastwards where the average height is 700 m in the west and 300 m in the east. It is intensively dissected by drainage lines descending easterly towards the Gulf of Aqaba.

2.2.3 Alluvial fan

The primary landforms of the Gulf of Aqaba are shaped by tectonic movements that are modified and degraded by mass destruction, erosion and sedimentation. Consequently, W. Dahab fan is developed in the coastal plain of the Gulf of Aqaba. The dominance of runoff on the mountainous slopes leads to high rates of sediments transport and delivery in depositional sites. The alluvial fans have a conical surface form with slopes radiating away from the apex at the point where a stream issues from the mountain catchments.

The area of the delta of W. Dahab has an area of about 11 km^2 and is separated by the main channel of the wadi. It has a length of about 2.25 km (fig. 36). The main channel of the wadi separates the city into a northern and a southern part. The area of the northern part is 3 km^2, while the southern part is 8 km^2. The main channel is used to discharge major flood waters and sediments into the Gulf of Aqaba. However, increasing encroachment of urbanization has narrowed the exit of the main channel width from several hundred meters to merely 30 meters approximately.

The main fan area is represented by the southeastern part of the delta close to the Gulf of Aqaba; it has a maximum elevation of about 29m at the apex and decreases gradually in a radial pattern until it reaches the sea shore. Two parts are distinguished in the main fan area, separated by the main trunk stream. The northern part is of a triangular shape, while the southern part is of a square-like shape.

2.2.4 Coastal plain

The coastline originates by faulting; it can be classified as a tectonic coastline. Therefore, the coastline is generally straight with steep slopes towards the floor of the Gulf. The coastline has a limited extent and appears in the form of disconnected deltas downstream from the main channel. It includes some patches and small low relief hillocks of a few meters in height scattered at or very near to the shore.

The coastal plain at W. Dahab has a significant form of small deltas, submerged wadis (estuaries), and coral reef terraces along this tectonic coast. This delta extends into the Gulf below sea level as can be inferred from bathymetric maps and from the development of fringing coral reefs at their submerged cones. Space images and aerial photographs show that these deltas developed during several cycles of deposition due to the change in climatic conditions (El Asmar, 1997). Sand beaches are flat areas along the shore and consist, at least partially, of unconsolidated materials of sand, cobble, boulder and shingle. These beaches are witnesses to some human and natural activitie,s for example, the urban and residential build up in Dahab city.

The evolution of the coast is influenced by the coral reef which, in the areas with coastal transport, is isolated from the coast or completely absent (fig. 38). Sites A and B show a bay most likely generated by sea actions coming from the south that set the deposits of the alluvial fan delta in motion, creating a cove and leaving a discovered coralline barrier on the side towards the land. These sites need to maintain a significant solid transport towards the littoral zone so as to limit the erosion caused by the wave motion, particularly in the zones which are not protected by the coralline barrier.

2.2.5 Drainage network

The drainage pattern reflects the nature of the bed rock, the attitude of stratification and the arrangement of weak surfaces (Zernitz, 1932). The margin of the coastal area is characterized by numerous lines of weakness that appear in the form of faults and joints. The heterogeneity of geological structure and paleoclimatic and lithological conditions prevails over the area during the late Tertiary and Quaternary age. Therefore, many drainage networks have been developed and cut their way through the rock surface with high drainage density values and lead to the formation of steep slopes.

The drainage networks are classified on the basis of their form and texture. Their shape or patterns have been developed in response to the local topography and subsurface geology. Drainage channels are evolved due to the effect of surface runoff and structure. Then, the weathered rock

materials provide the least resistance to erosion. The texture is governed by soil infiltration and the volume of water available in a given period of time to enter the surface. The drainage system and its effects on the terrain demand classification of the system into identifiable orders.

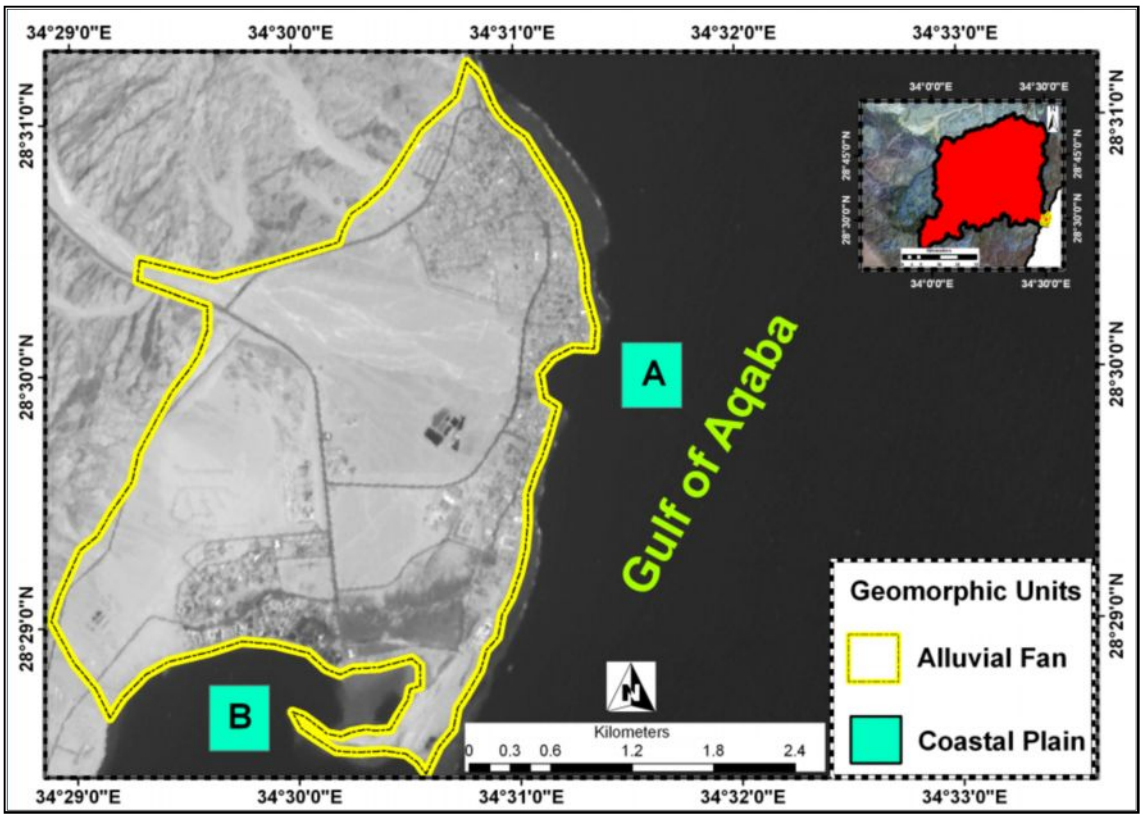

Figure 38: Spot Scene of Delta W. Dahab Basin

A drainage pattern pertaining to a terrain is a mesh of interconnected streams. This pattern may be of different types such as Dendritic, Trellied or Lattice, Radial or Concentric, Parallel, and Rectangular. Different patterns have occurred in W. Dahab basin, which reflect different rock types and the effect of erosion power on these rocks. It can be summarized as follows:

2.2.5.1 Rectangular drainage

The rectangular pattern is characterized by right-angled bends in both the main stream and its tributaries. The pattern is characterized by non perfect parallelism and greater irregularity in shape. This pattern is prominently structurally controlled, as the pattern is directly conditioned by the right-angled jointing or faulting of rocks. They typically develop in areas where streams flow along zones of weakened rocks adjacent to intersecting faults. Because of fault control, streams generally meet at right angles and have similarly shaped bends.

A rectangle pattern is distributed in different sub-basins within Dahab Basin. It appears in W. Saal sub-basin where it is considered as a structurally controlled basin, as well as in W. El Halal and in

tributaries of W. Saal and W. Nasab (fig. 39 -A). Both of them are considered to be a good example of a fault zone mainly in igneous rocks.

2.2.5.2 Dendritic drainage

It is the most common form and looks like the branching pattern of tree roots. It develops in regions underlain by homogeneous material. In this case, the subsurface geology has a similar resistance to weathering so there is no apparent control over the direction the tributaries take. Tributaries join larger streams at acute angles (less than 90 degrees). Rocks differing in composition, but of equal resistance, may occur in regions which have suffered intense metamorphism. The dentritic drainage pattern has been found in most basins, especially in the northern part of the study area at W. Genah, especially at W. El Matamier sub-basin (fig. 39-B). Dentritic patterns can also be found in W. Rahaba at the tributaries of W. Nasab basin.

2.2.5.3 Trellis drainage

This drainage system represents regular and parallel side tributaries when it enters the main river at approximately 90 degree angles, causing a trellis-like appearance of the drainage system. The term trellis should not be applied where only one set of tributaries joins a main stream at right angles, but the stream may represent the beginning of dendritic or rectangular drainage. By contrast, the trellis pattern implies a lattice effect which is originated by the elongated parallel secondary tributaries (Zernitz, 1932).

Trellis drainage develops in W. Nasab especially at W. Meer sub-basin (fig 39 -C) and appears in the upstream part of W. Rimthy and W. Saal. The appearance of a trellis patter reflects the homogeneity of rock types where most of the previous locations have granitic rocks as the main rock type. The effect of structure gives evidence clearly for formation of this pattern on the surface where these areas are fractured with joints and minor faults.

2.2.5.4 Parallel drainage

This pattern form occurs where there is a pronounced steep slope of the surface with some relief. A parallel pattern develops in regions of parallel, elongated landforms like outcropping resistant rock bands. A parallel pattern sometimes indicates the presence of a major fault system that cuts across an area of steeply folded bedrock. A parallel drainage occurs mainly in W. Rimthy basin which drains into W. Zaghraa. W. El Faraa is one of the tributaries in Rimthy Basin (fig. 39–D). The parallel drainage pattern occurs in the northern part of W. El Ghaieb where it is influenced tectonically by the Gulf of Aqaba as a fault zone.

It can be concluded that there are many drainage patterns in the study area due to the variation of lithology and structure, i.e., faults and joints which are detected as rectangular drainage systems that contribute to a parallel drainage. The geomorphological stages have played a significant role in the

occurrence of some consequent drainage patterns such as dendritic parallel patterns, whereas, the dendritic (first stage) drainage pattern is considered a preamble surface as in the northern part of Dahab basin and in the upstream part of W. Rimthy. Then, the parallel drainage pattern is formed as the second stage with prescription in the central part of W. Rimthy and W. Saal. This means that the development of a land form has played a main role in changing types of drainage patterns.

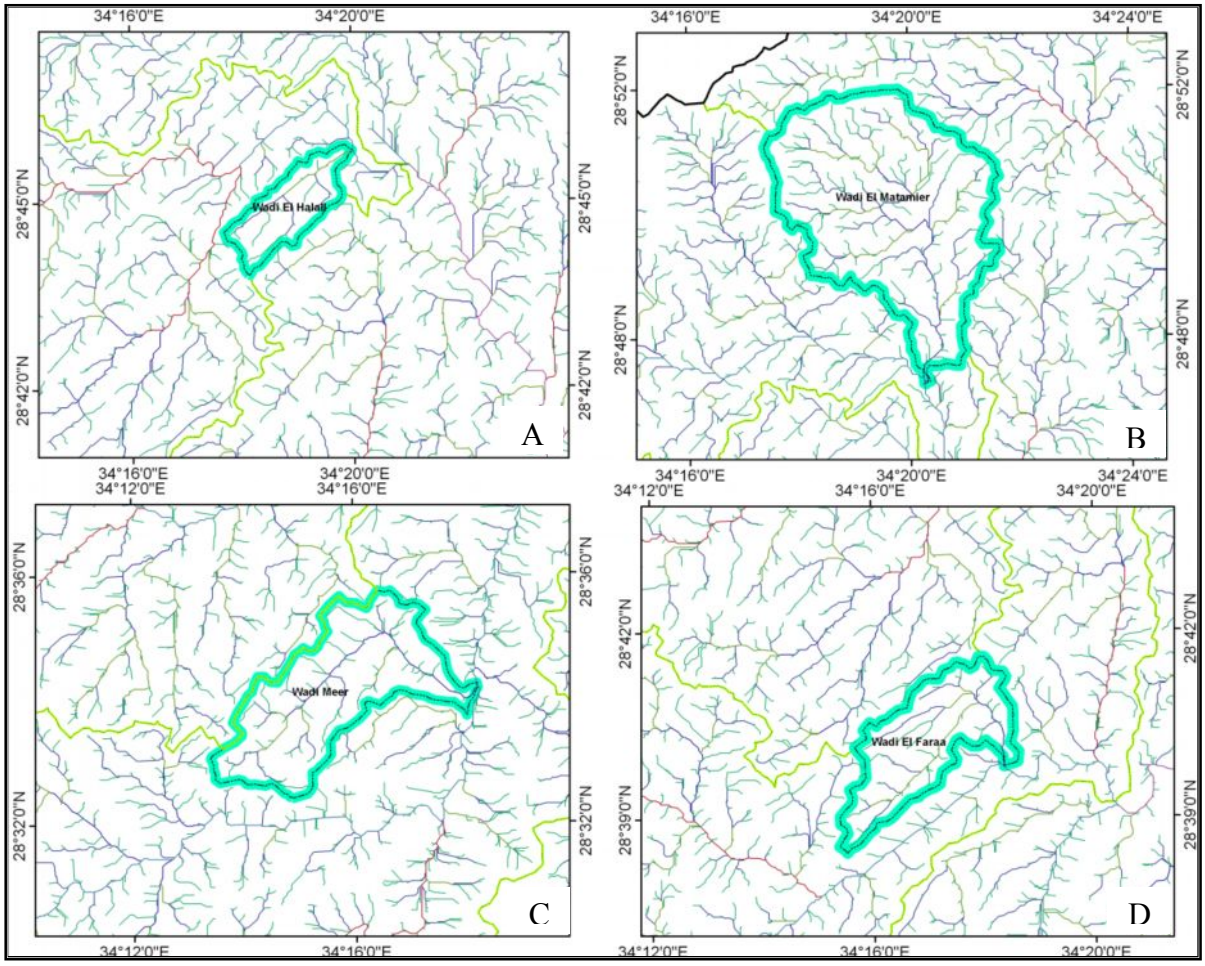

Figure 39: The Drainage Patterns in Some Subbasins within Dahab Basin

2.3 Quantitative geomorphology

Quantitative geomorphology deals with quantifying the main drainage basins that dissects the plains, central plateau and elevating high mass region. The resulting numerical parameters, which are called morphometric parameters, are used to assess the hydrologic situation of this basin.

Morphometric analysis of landforms is considered to be one of the important fundamentals in geomorphological studies. The analysis is performed as an attempt to elucidate the possible surface water potentialities of this basin and its bearings on flash flood behavior.

A systematic description of the geometry of a drainage basin and its network-channel system requires measurements of two main elements: morphometric analysis of the drainage network and morphometric analysis of the basins.

2.3.1 Morphometric analysis of drainage network

The quantification of any hydrographic basin can be achieved through measuring several geomorphic parameters of the drainage system. These parameters include stream order (U), bifurcation ratio (R_b), stream frequency (F), drainage density (D), drainage length (L_u) and overland flow (OLF). These parameters are determined according to the definitions given by Horton (1945), Strahler (1964), and Melton (1958b).

GIS techniques have proven to be effective tools in the extraction of stream networks. It is well known that the extraction of stream networks using GIS can be done easily, while it is still difficult to count stream segments and measure their lengths of different order with the provided generic tools (Omran et al. 2011). Moreover, the workflow to extract the information needed for larger areas, in particular, is still time consuming as many manual procedures are involved. An automated workflow GIS technique is used to both extract stream network parameters, with emphasis on ordering, and measuring the length and number of each stream segment in each sub-basin.

The drainage network map (vector layer) was created using an automated workflow (fig. 33). The attribute table for the drainage map includes the order number and number of segments for each order. To count the correct number of stream segments, the stream lines previously extracted have to be similar to the definition of stream segments of Strahler, which didn't match the definition of segments in ArcGIS (fig. 40). A stream segment in ArcGIS is defined from a source or confluence of a tributary to the next confluence, while according to Strahler, a tributary of lower order would not split a stream segment of higher order. For instance, as shown in figure 40, there would be only two segments of order two according to Strahler's definition, whereas ArcGIS would define five different segments of this order.

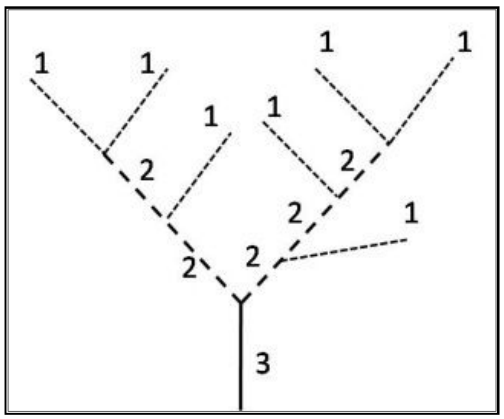

Figure 40: Strahler Ordering System

As the attribute table of the stream order contains all the information needed, i.e. the order number and the topology in the correct downstream order in form of the two attributes "from node" and "to node", by a simple algorithm, a dissolve attribute can be added to the segments attribute table, so that in a second step, the polylines can be dissolved according to Strahler's definition. The algorithm is given in a simplified form of pseudo code implemented in Visual Basic (VB) (see app. 1). Next, the number of streams in each sub-basin has to be calculated. Here, a spatial join of the sub-basins with the dissolved stream networks using the spatial operator contains has to be performed.

Due to the independent vectorization of the stream network and the sub-basins, there might be a shift of the point of confluence by one pixel of the raster layer resulting in order confluence of different tributaries (for example, tributaries of order n may be sited in a sub-basin of order n+1). Thus, before applying the spatial join, the stream network has to be pre-processed again. After intersecting the stream network with the sub-basins, all small segments with a length of less than one pixel would be deleted. As the calculation has to be done for each stream order, a Python-modified GIS model is used. In particular, a loop over all the orders has been added (see app.2) (Omran et. al, 2011). Finally, by repeating the spatial join, the total length for all stream orders of each sub-basin can be added. In this process, the final attribute table contains the total length in each sub-basin in addition to the total number for each order.

The extracted stream number and its order from raster data (DEM) should be evaluated. The evaluation is done using a topographic map scale (1:50,000) which covers the study area with eight topographic sheets. The topographic map is represented by truth data which is prepared for survey measurements in the field. Therefore, the numbers of extracted streams for each order from DEM are compared with those from the topographic map (Table 7).

The comparison showed that there are excellent matches in high order from stream order eight to order five with a validation percent of 100%, while the evaluation percent begins to decrease from stream order four until order one. The results presented shows that the number of stream for orders four to one on the vector map is higher than the number of the same stream orders on topographic sheets. The differences result from the effect of the threshold value which is used for stream extraction from DEM without taking into account human errors for counting and drawing in maps. It can be concluded that the rise of the evaluation percent reflects the most appropriate choice for threshold value according to the condition of the study area. The morphometric parameters have been calculated and the results are represented in appendixes 3-10. The study of morphometric parameters are dependent on the analysis of various drainage parameters, such as ordering of the various streams and basin areas, drainage density, stream frequency and bifurcation ratio (Kumar et al., 2000). The analysis is performed as an attempt to elucidate the possible surface water potentialities of these basins and their bearings on flash flood behavior. Locating high risk spots in the study area is possible after the evaluation of data from all 174 sub-basins.

Stream order	Number in Vector Map	Number in Topographic Map	Evaluation Percent
First Order	8083	6010	75%
Second Order	1846	1440	78%
Third Order	427	377	88%
Fourth Order	94	90	97%
Fifth Order	24	24	100%
Sixth Order	6	6	100%
Seventh Order	2	2	100%
Eighth Order	1	1	100%

Table 7: Comparison Between Order Number in Topographic Map Scale 1:50000 and DEM 30m Resolution.

2.3.1.1 Stream order (U)

The first step in drainage-network analysis is the designation of stream orders, following a system introduced by Horton (1945) and slightly modified by Strahler (1952); Melton (1958b) explained the mathematical concept involved. The stream order is a dimensionless value and is directly proportional to the area of the contributing watershed, to the channel dimensions and to the stream discharge. The numbers of drainage-network elements are assigned to their order, and then the segments of each order are counted to yield the number of segments (N_u) of the given order (U) (Strahler, 1964).

Assuming the availability of a channel-network map, including all intermittent and permanent flow lines located in clearly defined valleys, the smallest finger tip tributaries are designated order 1. The trunk stream, through which all discharge of water and sediment passes, is therefore the stream segment of highest order. Horton (1945), Schumm (1956) and others discussed the relationship between stream order and factors composing a drainage basin.

The result shows that stream order increases as the area of drainage basin increases (app. 3-10). The shortest and steepest streams have the smallest drainage basins (Strahler, 1964). According to Strahler's classification and to the drainage network map of Dahab basin, the main Dahab hydrographic basin has eight orders and its length reaches 19.1 km, whereas W. Zaghraa has eight orders but with less length than in Dahab basin, i.e. 6 km (app. 3). Both W. Zaghraa nasab and W. Zaghraa Saal are ofseventh stream order; the length of the main trunk is respectively 25 km. W. Nasab, W.Rimthy, W. Genah, W. Saal, W. El Ghaieb and W. Big Morah are of sixth order.

2.3.1.2 Bifurcation ratio (R_b)

Schumm (1956) defined bifurcation ratio as the ratio between the number of the same streams of an order U (N_u) and the number of streams of the next order (N_{u+1}) as expressed by the following equation:

$$R_b = \frac{N_u}{N_{u+1}} \qquad \textbf{Equation (1)}$$

To get more representation of the bifurcation ratio for the whole basin, Strahler (1952) used a weighted mean bifurcation ratio (R_{bw}) by multiplying the bifurcation ratio for each successive pair of orders by the total numbers of streams involved in the ratio and taking the mean of the sum of these values.

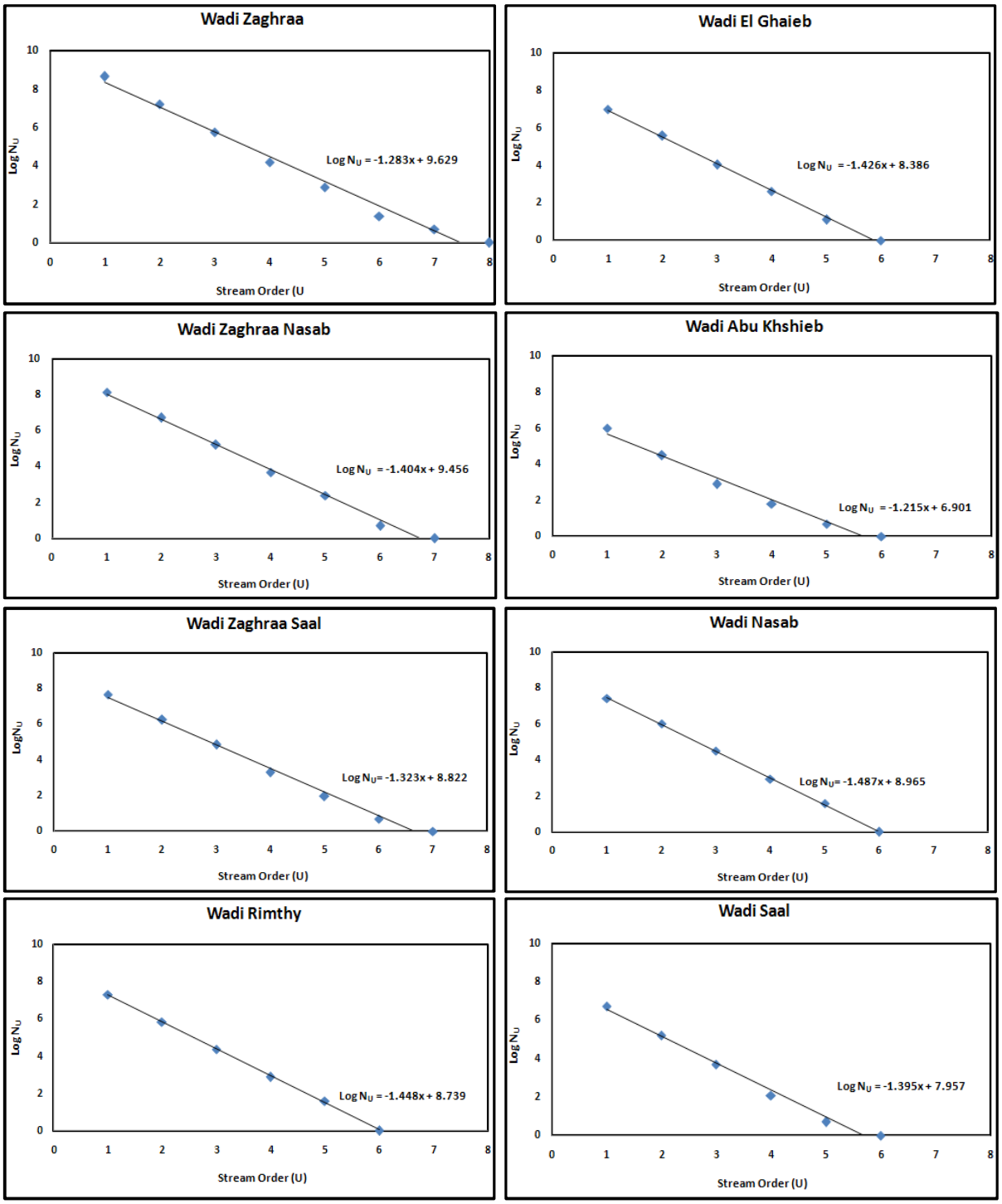

Figure 41: Relationship Between the Basin Order and the Number of Stream Order

The relationship between stream orders and stream numbers for different sub-basins of the study area are shown in figure 41. The inverse proportion relationship dominates in all basins which means that when the stream orders increase, the number of drainage streams decreases. Strahler (1954) stated that the theoretical minimum possible value of 2 is rarely approached under natural conditions, therefore, all the results of bifurcation ration in Dahab basin are more than 2 (app.7 - 10) . Basins of high bifurcation ratio are elongated in shape and permit the passage of runoff over an extended period of time, thus, having more chances to feed the ground water. Basins of low bifurcation ratio are circular in shape, allowing the runoff to pass in a short time, forming a sharp peak. The bifurcation ratio values of the hydrographic basins of the study area are estimated and listed in appendixes 7-10.

The weighted bifurcation ratios range between 2.1 and 6.86. High values ranging from 5 to 6.8 are located downstream of W. El Ghaieb, W. South Zaghraa, W. Zaghraa and some parts upstream of W. Zaghraa. This range should be considered as an exception of Strahler theory due to the special geological conditions (tectonics) in the study area. Most of the sub-basins have a moderate value ranging from 3.5 to 5. This range occurs at W. Abu Khshieb, W. Zaghraa Nasab, W. Zaghraa Saal, W. Saal, W. Nasab, W. Rimthy and Dahab mega-basin. The low values of bifurcation ratio range from 2.1 to 3.5 which are distributed in the northern part of the study area, especially upstream of W. Nasab as W.Zaraa, upstream of W. Abu Khshieb as W. East Maaen, W. Saal El Rayan, W. Manader at W. Saal and some sub-basins in W. Zaghraa Saal. The lower values reflect the slight elongation of the basin shapes and hence, may produce high runoff downstream (fig. 42).

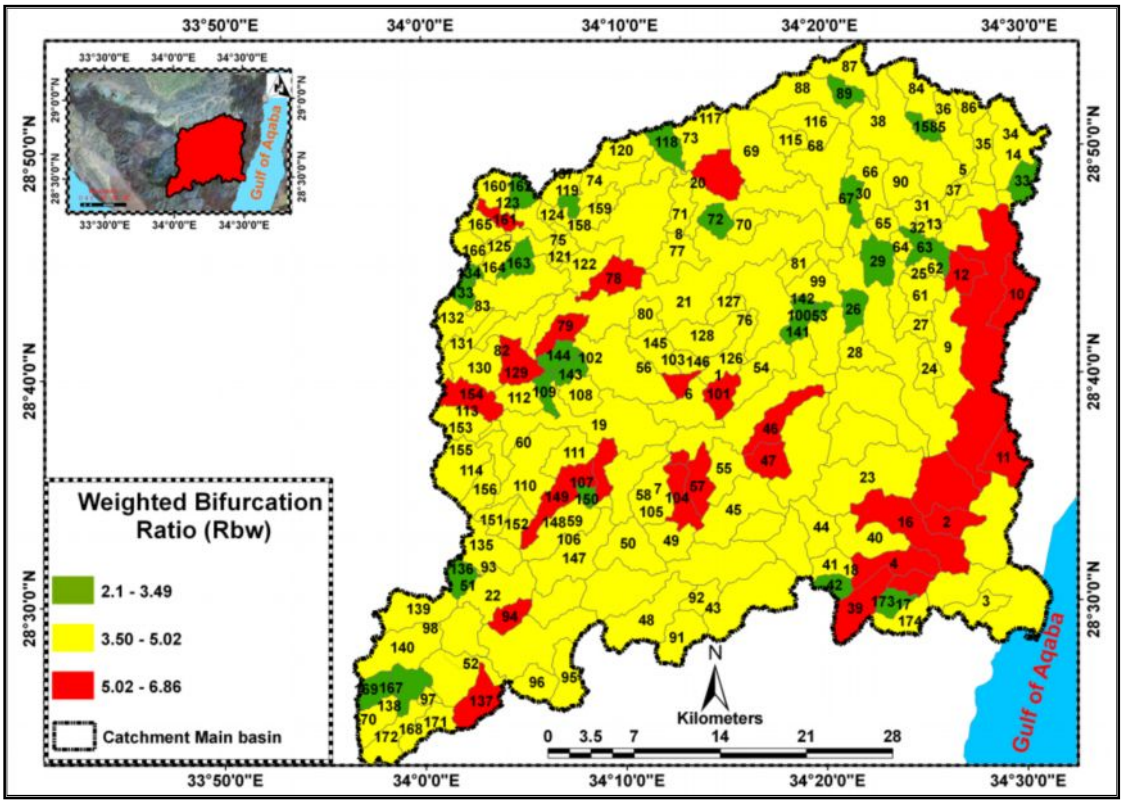

Figure 42: Bifurcation Ratio of Different Subbasin in Dahab Basin

2.3.1.3 Stream Length (L_u)

The stream length (L_u) of a stream-channel segment of order U has a dimensional property revealing the characteristic size of the drainage network and its contributing basin surface (Strahler, 1964). It is one of the most significant hydrorological features of a basin as it reveals the surface runoff characteristics. Streams of relatively smaller length are characterized for areas with larger slopes and finer texture. Longer lengths generally indicate flatter gradients of streams.

The first order stream channel with its contributing first-order drainage-basin surface area should be regarded as the smallest unit of any watershed. Actually, the streams of first order resemble the mountainous surface which is characterized by a steep slope. These streams are short, obstructive, fast flowing and join quickly to form the streams of the second order, whereas the streams of higher order always record a higher mean length. Generally, the total length of stream segments is maximum in first order and decreases as the stream order increases. The length of the main stream of W.Dahab reaches up to 19 km at the 8th order, while the same order at W. zaghraa is 25 km. The 6th order is considered the highest order at wadis Nasab, Rimthy, Saal, El Genah, Ghaieb and W.Abu Khshieb. The length of order six ranges from 6 to 54 km and W. Nasab has the highest length in this order of 54 km.

Mean stream length (L_m) is a characteristic property related to the drainage network components and their associated basin surfaces (Strahler, 1964). This has been calculated by dividing the total stream length of order (u) by the number of stream segments in this order. The relationship between the average length of a stream and the basin order is a strong positive relation as shown in figure 43 for sub-basins of the study area. This parameter helps to calculate stream-length ratio (R_L) which is used as a topographic factor (Horton's ratio parameter) to estimate the geomorphic unit hydrograph (see chapter four) for storm events and to calculate maximum runoff discharge.

The mean stream lengths are presented in Table 8. It can be seen that L_m values exhibit variations from 0.24 to 54.76. It can also be observed that there are deviations in the highest order as in the sixth stream order of W. Zaghraa. The mean length value is 27.25 at the sixth stream order, while at the fifth stream order, it is 8.4, but in seventh order is 19.24. The deviation might have resulted from the change in topographic elevation and the slope of the area where it is covered by basement rocks.

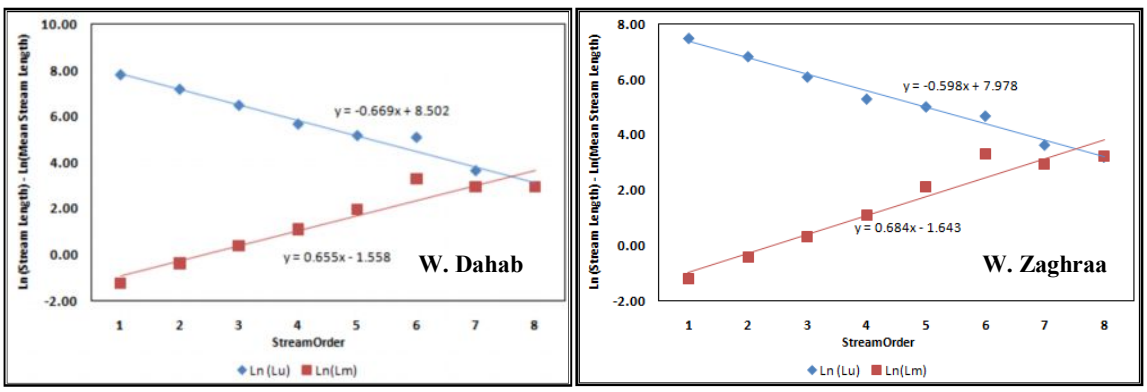

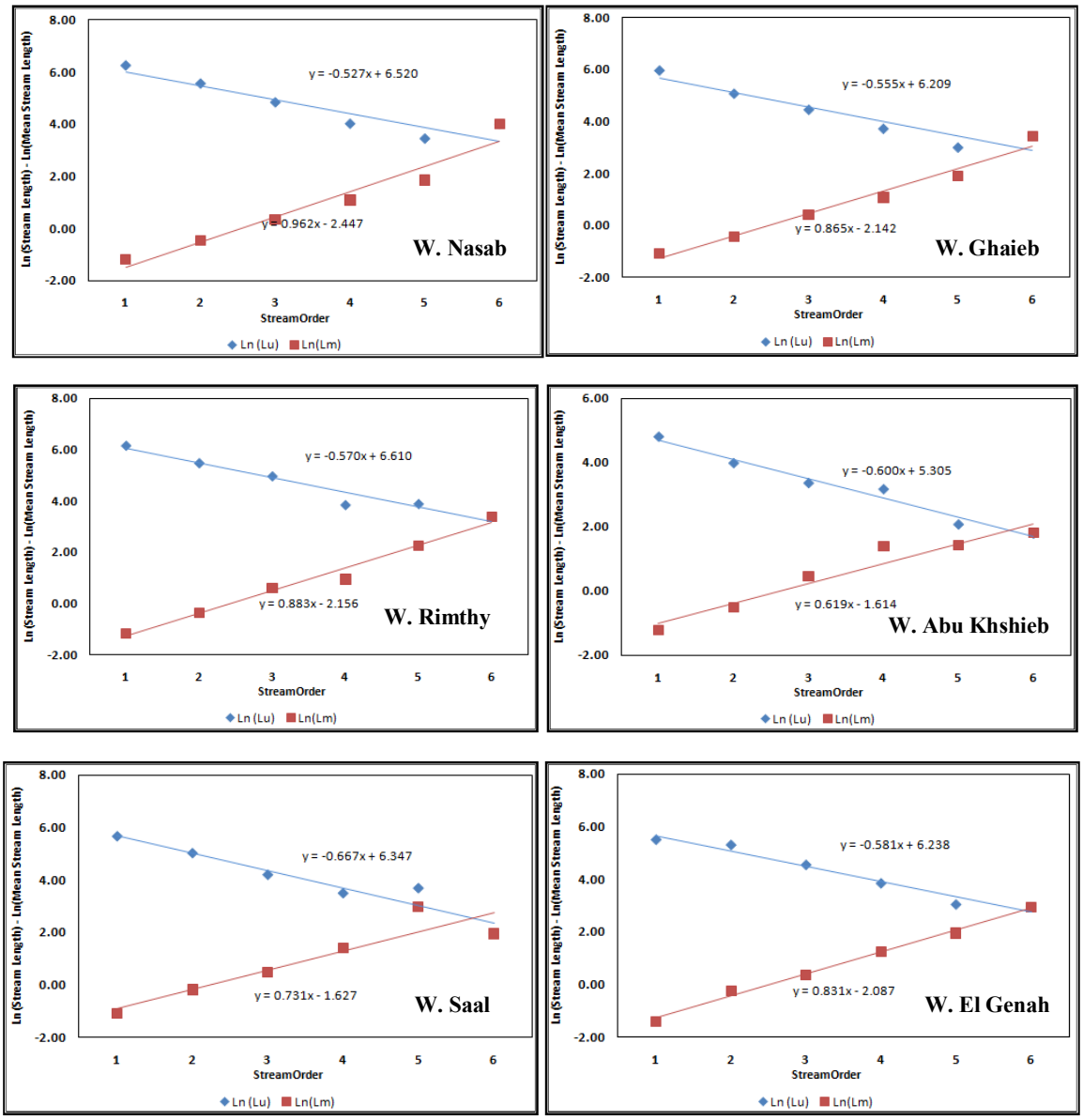

Figure 43: Relationship Between Basin Length and Stream Order Number in Dahab Basin

	First		Second		Third		Fourth		Fifth		Sixth		Seventh		Eighth	
	L_u (km)	L_m	L_u (km)	L_m	L_u (km)	L_m	L_u (km)	L_m	L_u (km)	L_m	L_u (km)	L_m	L_u (km)	L_m	L_u (km)	L_m
Wadi Mega Dahab	2429	0.30	1295	0.70	645	1.51	286	3.04	174	7.25	161	26.83	38	19.00	19	19.00
Wadi Zaghraa	1779	0.31	923	0.67	444	1.40	201	3.00	152	8.44	109	27.25	38	19.24	25	25.00
Wadi Zaghraa Nasab	1071	0.31	549	0.66	97	0.53	112	2.80	84	7.67	83	41.39	13	13.00	0	0.00
Wadi Zaghraa Saal	650	0.30	426	0.83	198	1.56	89	3.30	86	12.29	30	15.00	25	25.00	0	0.00
Wadi Abu Khshieeb	123	0.30	54	0.60	29	1.57	24	3.97	8	4.12	6	6.00	0	0.00	0	0.00
Wadi El Ghaieb	381	0.34	157	0.65	85	1.49	41	2.94	20	6.80	31	31.00	0	0.00	0	0.00
Wadi Nasab	516	0.30	257	0.61	125	1.40	55	2.90	31	6.30	54	54.00	0	0.00	0	0.00
Wadi Rimthy	478	0.31	240	0.69	143	1.81	46	2.56	48	9.54	29	29.00	0	0.00	0	0.00
Wadi El Genah	248	0.25	203	0.80	95	1.45	47	3.57	21	7.10	19	19.00	0	0.00	0	0.00
Wadi Mega Saal	294	0.34	154	0.84	67	1.63	33	4.10	40	19.70	7.12	7.12	0	0.00	0	0.00
Wadi Korna	34	0.27	19	0.61	8	1.30	5	2.72	5	5.00	0	0.00	0	0.00	0	0.00
Wadi Barka	37	0.34	26	1.06	12	1.99	2	1.12	4	4.00	0	0.00	0	0.00	0	0.00
W. South Zaghraa	18	0.48	4	0.71	2	1.08	3	3.00	0	0.00	0	0.00	0	0.00	0	0.00
W.Assam	8	0.24	5	0.66	2	0.85	3	3.00	0	0.00	0	0.00	0	0.00	0	0.00

Table 8: Length Stream Order of Different Subbasin in Dahab Basin.

2.3.1.4 Drainage frequency (F)

Stream frequency has been defined as the ratio of the total number of stream segments of all orders within a given basin to the total area of the basin (Horton, l945) and is expressed by the following equation:

$$F = \frac{N}{A} \qquad \textbf{Equation (2)}$$

Where N is the total number of streams of all orders and A is the area of that basin.

Basins of high stream frequency and density value may tend to have more possibilities for flood initiation. A high value of stream frequency tends tohave more possibilities for collection of runoff water. Quantitatively, stream frequency doesn't give direct indication to the quantity of runoff. However, it could be used in determining the drainage density which could not be estimated directly from available data (Saad et al. 1980), but it could give good indication with other paramters, such as drainage density, about the potenial runoff risk zones.

Stream frequency is calculated for W. Dahab basin. The stream frequency (F) has a range from 3.6 to 9.6. The high frequency values range from 6 to 9.6. This range occurs along W. El Ghaieb, Zaghraa and along the upstream area of W. Abu Khshieb, W. Nasab, W.Rimthy and W. El Genah. Most of the sub-basins in the study area have a moderate range between 4.5 to 5.9. The middle range is located along W. Rimthy, W.Saal, W. Nasab, W. El Genah and some locations in W. Ghaieb and W. Dahab mega-basin (fig. 44).

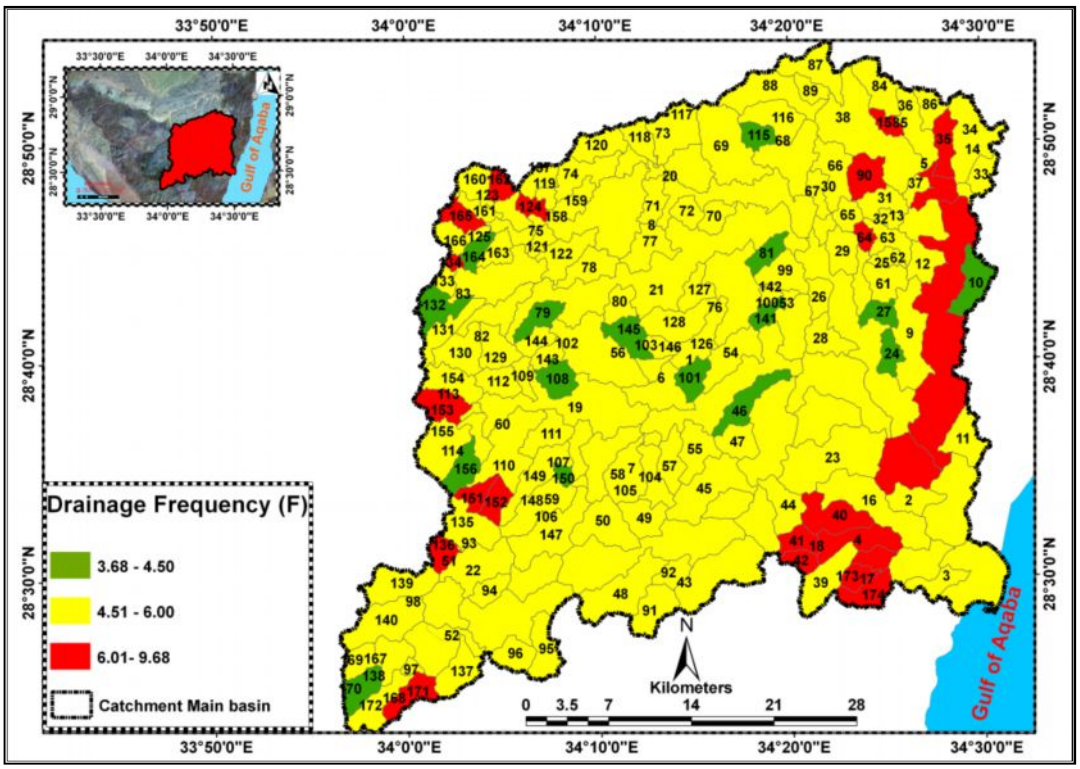

Figure 44: Stream Frequency Map in Dahab Basin

The frequency map of W. Dahab shows that the high frequency values are at the eastern and southern catchment with small parts at the western catchment. These values reflect the possibilities of increasing runoff percentage, especially at W. Abu Khshieb, W. Ghaieb, W. Zaghraa and its catchment at W. Nasab and W.Rimthy. The low values distribute mainly in the middle part of W. Zaghraa Saal along its main stream where the possibility of collection runoff might decrease.

2.3.1.5 Drainage density (D)

It is probably the parameter which most globally represents the interaction between climate and geomorphology in the development of the drainage network (Ignoacio and Luis, 1982). It is a measure for the degree of fluvial dissection and is influenced by numerous factors, among which resistance to erosion of rocks, infiltration capacity of the land and climatic conditions rank high (Verstappen, 1983). According to Horton (1945), the drainage density (D) is defined as the total length of streams (L) divided by the area of drainage basin (A). It is expressed as:

$$\mathbf{D = \frac{L}{A}} \qquad \textbf{Equation (3)}$$

Drainage density expresses the closeness of tributaries in the basin and reflects the type of the surface layer, its permeability and roughness. So a basin having a low value of drainage density due to its little number and length of segments may reflect highly permeable sub soil and or flat area. High drainage density is the result of weak or impermeable sub-surface material, sparce vegetation and mountainous relief.

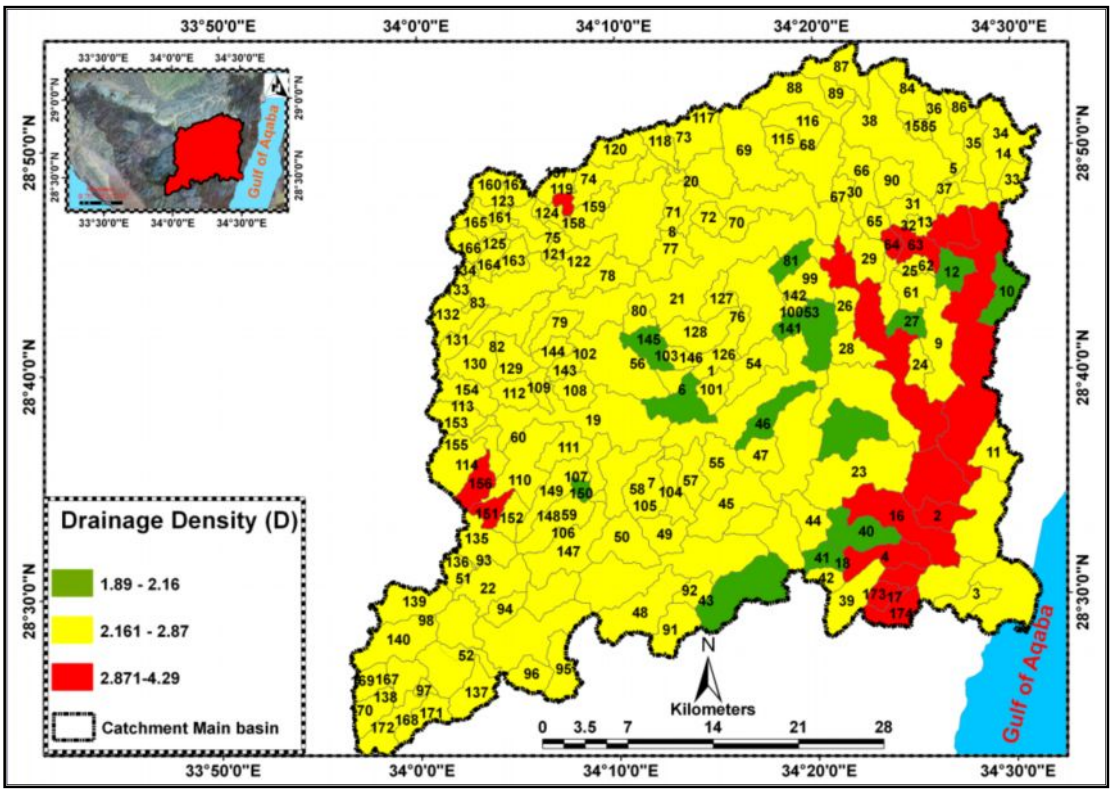

Figure 45: Stream Density Map in Dahab Basin

The drainage density values in the study area range from 1.89 to 4.29. The value of drainage density increases in the downstream areas of W.Zaghraa, W. El Ghaieb and W. Abu Khshieb where it ranges from 2.8 to 4.2, indicating an impermeable surface which gives considerable chance to surface runoff occurrence (app. 7-10). The high density zones are covered with basement rocks that have low conductivity and the chance for runoff generation is high. The low values of drainage density located at the course of W. Nasab and W. Rimthy range between 1.8 to 2.1, indicating permeable soil and the chance of low runoff formation. The drainage density map shows that there is a matching of high density zones with high frequency zones. The highest zone for both parameters is located at eastern and southern catchments. It indicates that the chance of runoff gerneration is high . Overall, the drainage density value of W. Dahab basin is 2.4 which is considered as moderate to high, indicating areas of moderate to high flooding possibility (fig. 45).

2.3.1.6 Overland Flow (OLF)

Overland flow across the ground surface to the nearest channel is defined as surface runoff (Linsley et al., 1982). Basins of long overland flow induce high infiltration and have low risk of flash flooding. On the other hand, basins of short overland flow have high flooding possibility with high risk of flash flooding. The average length of overland flow is expressed by the following equation:

$$\mathbf{OLF} = \frac{\mathbf{1}}{\mathbf{2D}} \qquad \textbf{Equation (4)}$$

Where: D = Drainage density

The calculated values of overland flow range between 0.11 and 0.26 (app. 7-10). The high values between 0.22 to 0.26 are located along the main stream of W. Nasab, W.El Shalal and W. Nabaa where they are drained directly to W.Nasab. The value increases at sub-basins of W. Rimthy as in W. Mekaffa, W. Merkh and W. Sanad. These zones indicate flow of runoff taking a long pass inducing high infilteration.

Low values of overland flow range from 0.11 to 0.16. This range occurs at W. Zaghraa, W. Abu Khshieb, W. El Ghaieb and small sub-basins in W.Zaghraa saal. The low parameter refers to short overland flow with high chance for flash flooding. It can be observed that the same zones of high density and high frequency have short overland flow (fig. 45).

The OLF values decrease to moderate levels, ranging between 0.17 to 0.22 at most parts of W. Dahab basin (fig. 46). The probability of flood initiation might occur during the rain storm. W. Dahab basin has a moderate overland flow value of 0.21, reflecting the equal probabilities of water infiltration and flood initiation during the periods of a rainstorm.

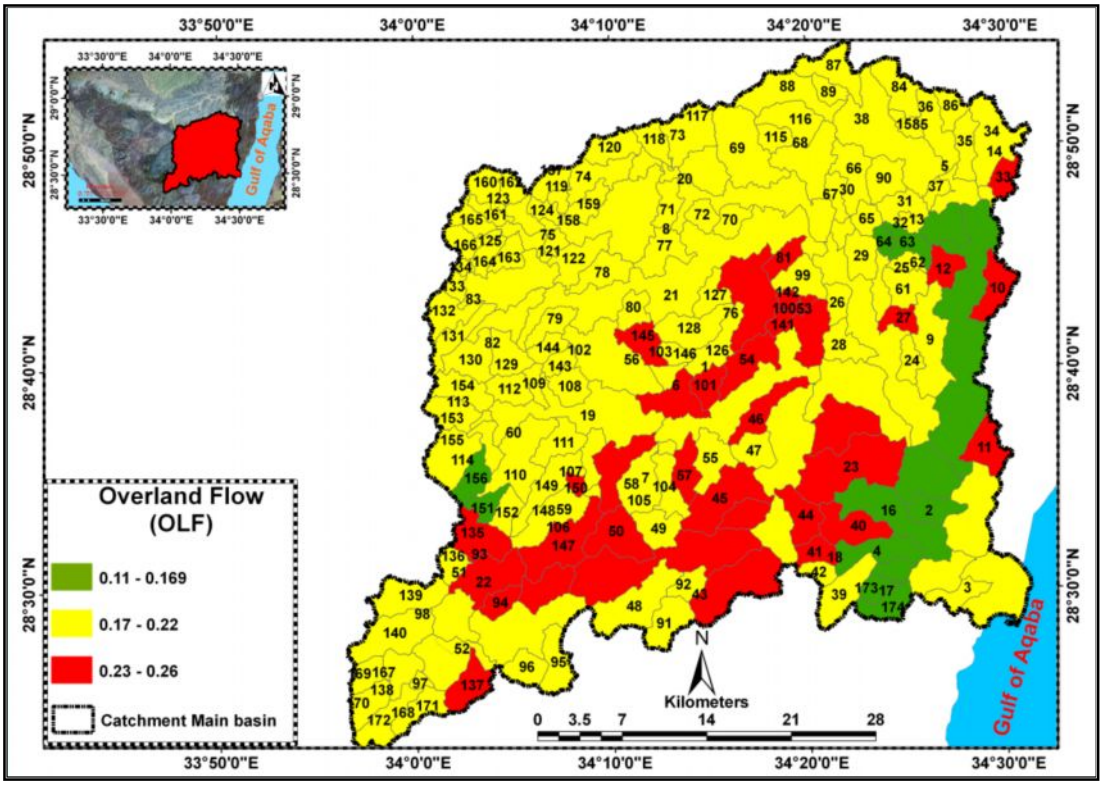

Figure 46: Overland Flow Map in Dahab Basin

2.3.2 Morphometric analysis of basins

A drainage basin is a system which is morphologically governed and geometrically characterized by some functional relationships. These relationships were determined by measuring the different elements described as follows:

2.3.2.1 Basins area
2.3.2.2 Basins dimensions (Length, width, and perimeters)
2.3.2.3 Basins shape
2.3.2.4 Basins surface

2.3.2.1 Basins area (A_u)

Basin area is considered as one of the most important elements in the basin analysis. Strahler (1952) said that basins which have similar characteristics in area and form were also similar in their geomorphological characteristics. Therefore, it is no doubt that basin area has a great influence on the drainage network and the topographic characteristics of the basin (Akl, 1994). The basin size is the most important factor affecting runoff. Determining the basin area that contributes to the flow at the sites of drainage structure is a basic step in hydrologic analysis regardless of the method used to evaluate runoff.

The total area of the main basins in the study area is 2085 km^2 which has been separated to five main sub-basins regarding every basin is as a geomophological unit. W. Zaghraa basin is considered the biggest sub-basin in W. Dahab with 1617km^2, following W. El Ghaieb subbasin (299 km^2) and W.

Abu Khshieb basin (107 km^2), while the smallest sub-basins are W. Um Assam (7 km^2) and W. South Zaghraa (8.2 km^2). W. Zaghraa includes fourteen sub-basins where the largest one is W.Nasab (445 km^2) followed by W. Rimthy (413 km^2), W. El Genah (285 km^2) W.Saal (246 km^2) and the smallest sub-basin, W. Naghmishy (5.6 km^2).

	First		Second		Third		Fourth		Fifth		Sixth		Seventh		Eighth		Total Basin
	A_u (km^2)	A_m	A_u (km^2)	A_m	A_u (km^2)	A_m	A_u (km^2)	A_m	A_u (km^2)	A_m	A_u (km^2)	A_m	A_u (km^2)	A_m	A_u (km^2)	A_m	A (km^2)
W.Dahab	1143	0,15	1155	0,33	1194	0,69	1053	11,57	1149	52,23	1793	298,8	1591	795,5	2088	2088	2088
W.Zaghraa	888	0,15	890	0,64	948,6	2,98	802	11,97	937,8	52,1	1387	346,8	1591	795,5	1617	1617	1617
W. Zaghraa Nasab	490	0,14	502	0,6	512	2,8	445	11,13	494	44,91	856,3	428,2	936	936			936
W. Zaghraa Saal	450	0,21	410	0,79	393	3,09	305	11,3	444	63,4	530,4	265,20	663	663			663
W. El Ghaieb	170	0,34	183,3	0,65	170,1	1,49	155,3	2,94	141,8	6,8	298,8	298,8					298,8
W. Nasab	255	0,15	201	0,48	235,2	2,56	206,3	10,86	184	36,8	444	444					444
W.Rimthy	205	0,13	240	0,7	260	3,29	206	11,44	277	55,4	412,3	412,3					412,3
W. Saal	139,3	0,34	150,9	0,84	142,1	1,63	103,1	4,1	225,6	19,7	245,8	245,8					245,8
W. El Genah	170,3	0,17	182,09	0,72	179,3	2,76	193,6	14,89	163,3	54,44	284,6	284,6					284,6
W.Aub Khshieb	61	0,15	54,22	0,6	54,67	3,04	80,15	13,36	69,22	34,61	107	107					107
W. Um Assam	4,3	0,14	4,15	0,59	4,04	2,02	7,04	7,04									7,04

Au: Area of Basin order **Am:- Average of Basin order area**

Table 9: Basin Area of Different Basin Order in Each Subbasins at Dahab basin.

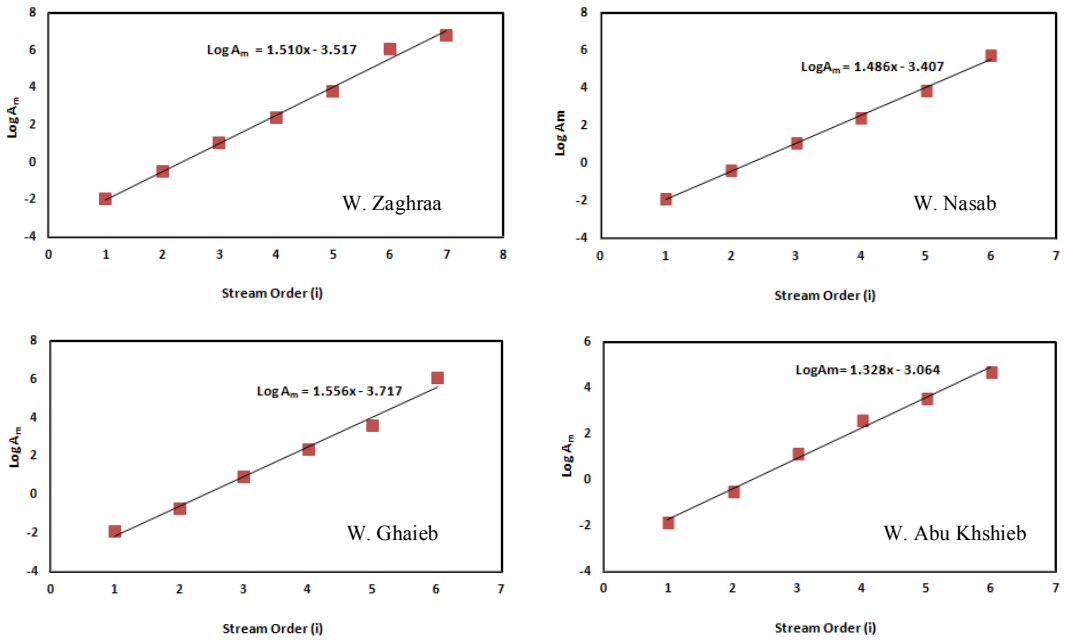

Figure 47: Relationship Between Basin Area and Stream Order Number in Representative Subbasins at Dahab Basin

A drainage basin reflects the volume of water that can be generated from rainfall. Thus, basin area is required as input data to calculate the amount of volume runoff and its discharge. Schumm (1956) proposed a Law of Stream Areas to relate the average areas (A_m) drained by streams of successive order due to the effect of basin size as the topographical factor on hydrological condition of the basin. The average basin area increases with increase of the stream order. It is quite logical because the geomorphological processes of the first order streams focus on vertical erosion, saving the lateral erosion and erosion processes in small areas are mainly inactive. The ratio of the average area of

stream order to the average area of the next order is used as a topographic factor to estimate the geomorphic unit hydrograph (see chapter three) and then to calculate expected discharge for the high storm event.

The average areas of the basin range from 0.13 to 2088 in Table 9. It ranges for the first order between 0.13 in W. Rimthy sub-basin to 0.34 at W. Saal and W. El Ghaieb. In the second order, the average area ranges from 0.48 in W. Nasab to 0.84 in W. Saal, while in the third order it ranges from 1.5 at W. El Ghaieb to 3.2 at W. Rimthy. The average for fifth order ranges between 6.8 at W. El Ghaieb to 63 W. Zaghraa Saal. It shows that there is a direct relationship between the average area of the basin and basin order (fig. 47).

2.3.2.2 Basins dimensions

2.3.2.2.A Basin length

It estimates a straight distance between the mouth of basin and the highest point on the drainage divide (Schumm, 1963). Conceptually, this is the distance traveled by the surface drainage and is sometimes more appropriately labeled as hydrologic length. This length is used in computing a time parameter, which is a measure of the travel time of water flow through a watershed. The basin length is measured along the principal flow path from the watershed outlet to the basin boundary.

The length of the major subbasins is different from one basin to another in the study area due to the differences of the area: slopes, lithology and structure. W. Zaghraa is the longest sub-basin within the study area with a length of 47 km, while the shortest sub-basin is W.South Zaghraa basin with a length of 5 km (app. 7-10). W. Nasab is the longest sub-basin in W. Zaghraa at 48 km long, whereas the shortest one is W. Small Saal El Rayan at the upstream part of W. Saal at about 1.9 km long.

2.3.2.2.B Basin width

The main limitation of the width of a basin is the surface slope. If the surface has steep slope, the basin will be narrow; otherwise too much sediment movement would be needed to obtain the base of the basin floor. There are three methods used to measure the width of a basin; the first is the result of the division of the basin area with the basin length, the second is to compare the maximum width of the basin with the maximum length in the basin, whereas the third is the average of several measurements of width along the basin stream course. The third one in this study is applied to get the average width in the upstream and downstream areas of the basin.

W. Rimthy basin is the widest basin in W.Zaghraa at 18.7 km while the narrowest basin is 1.09 km in W. El Kurry. On the other hand, W. Um Asaam sub-basin and W. El-Ghaieb are considered the narrowest basins in Dahab basin, whereas the width reaches only 1.2 and 10.5 km respectively (app.7-10).

2.3.2.2.C Basin perimeters

The basin perimeter is the total length of the drainage basin boundary which reflects the geomorphological stage of basins. It is considered as the main element of basin dimensions because it could be used to compute some morphometric parameters such as basin shape (Circulatory ratio). The basin perimeters are measured along the water divide of basins which were delineated previously using a digital elevation model with GIS tools.

W. Nasab sub-basin has the highest perimeter in W. Zaghraa basin at 169.8 km, followed by W. El Ghaieb basin at 140 km. W. Abu Khsieeb and Um Asaam sub-basins have the smaller lengths of the perimeter at 53.7 and 15.6 km respectively (app.7-10). It is observed that the perimeter of the W. Dahab basin has a lot of zigzags due to the effect of structure where its perimeter is 288 km.

2.3.2.3 Basins shape

The shape, or outline form of a drainage basin, as projected upon the horizontal plane of a map, is another factor affecting the stream discharging characteristics. Circular basins produce larger floods than longitudinal watersheds if they are of similar sizes because circular basins can accumulate the floods within a short time. The basin shape has a relation with the stream network; it states that long, narrow basins with high bifurcation ratios are expected to have attenuated flood- discharge periods, whereas round basins of low bifurcation ratio would be expected to have sharply peaked flood discharge (Strahler, 1964). Generally, the shape of a basin is related with hydrological parameters such as amount of discharge, flow velocity, peak of runoff and lag time. Basin shape is expressed by two parameters: circularity ratio and elongation ratio.

2.3.2.3.A Circularity ratio (R_c)

The circularity ratio (R_c) is a dimensionless parameter which is defined as the ratio of basin area (A_u) to the area of a circle (A_c) having the same perimeter as the basin (Miller, 1953). The circularity ratio might be expressed by the following equation:

$$\mathbf{R_c = \frac{4*\pi*A}{P^2}} \qquad \textbf{Equation (5)}$$

Where :-

R_c = Circularity ratio A = Basin area (Km^2) P = Basin perimeter (Km)

The results of the ratio calculation are shown in appendixes 7-10.Circulatory ratios vary in the study area from one basin to another. The ratio values range between 0.16 and 0.72. The value increases mainly at the sub-basin in the catchment boundary as shown in figure (48). The high values occur in 37 sub-basins in W.Dahab, ranging from 0.55 to 0.72. Thirty sub-basins have high range values of circularity ratio in W. Zaghraa, especially upstream of W. Nasab, W. Rimthy and W. Saal as in W. South zaraa, W. Hassa, W.Small nasab, W. Um shietan, W. Rakita, W. Alranyia and W. El mokhtar, W. Small saal El rayan and W. Manader. The other seven sub-basins occur at W. Abu

Khshieb and W. El Ghaieb as W. Maaen, W. Um harqa and W.Mezriha. All previous basins had a circular shape which reflected that the possibility of runoff velocity would be increased.

The ratio decreases downstream of most sub-basins. The law value ranges between 0.18 and 0.34. Low circulatory values concentrate at the sub-basins of W. Saal, W. El Ghaieb and W. El Genah, while moderate values range from 0.35 to 0.55 at W. Zaghraa, especially at W. Nasab, W. Rimthy and W. Abu Khshieb (fig 48).

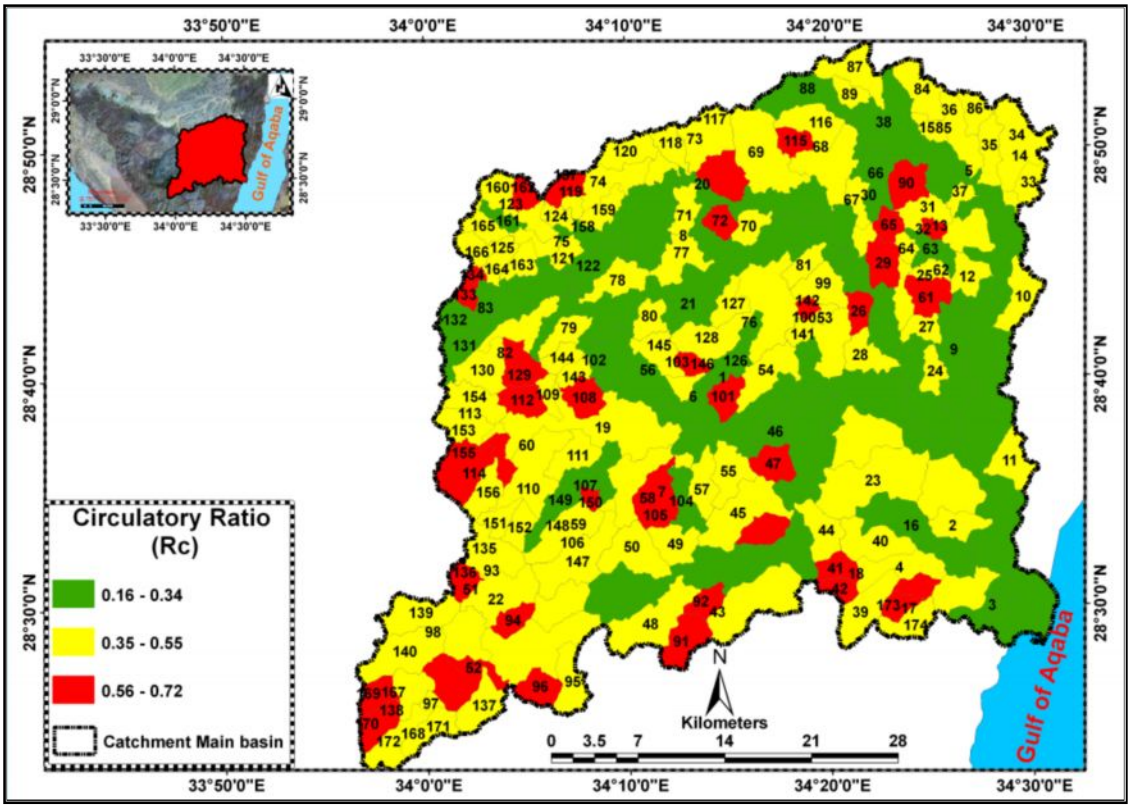

Figure 48: Circulatory Ratio Map of W. Dahab Basin

2.3.2.3.B Elongation ratio (R_e)

The elongation ratio is determined according to Schumm (1956). It is defined as the ratio of the diameter of a circle of the same area as the basin to the maximum basin length. It is expressed by the following equation:

$$\mathbf{R_e = \frac{\sqrt{4 * A}}{\frac{\pi}{L}}} \qquad \textbf{Equation (6)}$$

Where:-

R_e = Elongation ratio A = Basin area (Km^2) L= Basin length (Km)

The calculation of the elongation ratio for all sub-basins in Dahab is shown in appendixes 7-10 .The (R_e) ratio runs between 0.26 and 0.8 over basins at W. Dahab. The high values range from 0.53 to 0.8: they are generally associated with strong relief, steep ground slope and the basins are not more

or less elongated. High ranges occur upstream of the sub-basins of Dahab basin, especially at W. Nasab, W. Rimthy, W. Saal and W. Zaghraa (fig. 49). The low values range from 0.26 to 0.32 and occur at the sub-basin which drains directly downstream of W. Dahab as in W. Asaam, and which drains to W.Zaghraa as W. Nasab,W. Saal and W. El Genah. Those basins are more elongated than circular in shape.Most of the sub-basins have a moderate elongation ratio that ranges from 0.33 to 0.52 as shown in figure 49. These values occur mainly at W. Rimthy (0.53), W. El Ghaieb (0.4) and W. Abu Khshieeb (0.43). These values reflect their slightly elongated shapes; thus, these basins have chances for flooding and/or aquifer recharging by infiltration.

In conclusion, the value of the circularity ratio (Rc) is close to 1; it indicates a nearly circular basin, while the decrease in value indicates an increase in the elongation of the basin. Basins of circular shapes have short drainage lines which yield strong floods, while those with elongated shape posses longer drainage lines which have good chances for downward infiltration and hence, augmentation of existing groundwater.

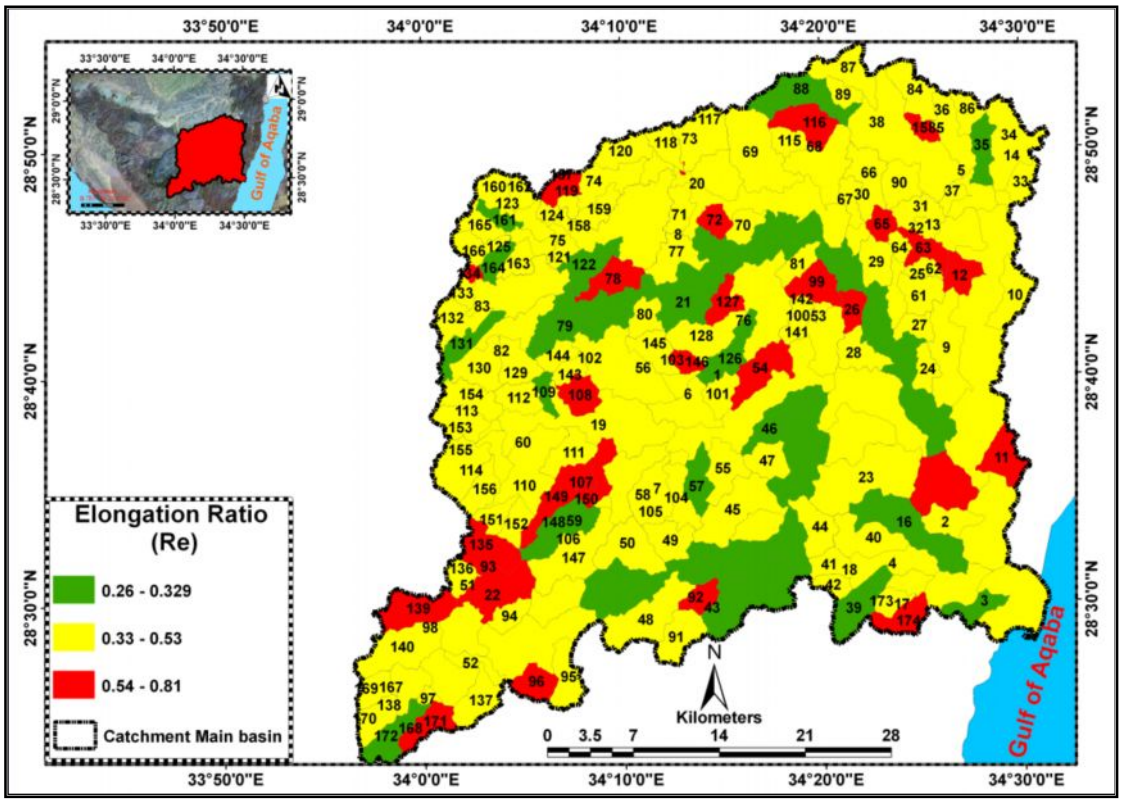

Figure 49: Elongation Ratio Map of W. Dahab Basin

2.3.2.4 Basins surface

These analyses include the description of the surfaces of basin which are basin slope and gradient. Slope is a measurement that gives the steepness of the ground surface and is measured by calculating the tangent of the surface. The tangent is calculated by dividing the vertical change in elevation by the

horizontal distance of pixels. The gradient is estimated by dividing the difference in elevation between the upstream and the mouth of the basin by the length of the stream (Taylor and Schwarz, 1952).

2.3.2.4.A Slope surface

The slope is measured using the DEM (Raster layer) slope tool in GIS. Several algorithms have been developed to calculate percent or degree of slope. The simplest one is called the neighborhood method. The neighborhood method calculates the slope at one grid point by comparing the elevations of the eight grid points that surround it. Conceptually, the slope function fits a plane to the z-values of a 3 x 3 cell neighborhood around the processing or center cell (fig. 50).

Z_1	Z_2	Z_3
Z_4	Z_5	Z_6
Z_7	Z_8	Z_9

$$S_5 = \left(\sqrt{[S_{e-w}^2 + S_{n-s}^2]} \times 100\right) \qquad \textbf{Equation (7)}$$

Figure 50: Neighborhood Algorithm Estimates Percent Slope in cell 5 by Comparing the Elevations of Neighboring Grid Cells

The neighborhood algorithm estimates slope at grid cell 5 (Z5) as the sum of the absolute values of the east-west slope and north-south slope. The diagram below illustrates how the east-west slope and north-south slope are calculated. Essentially, the east-west slope is estimated as the difference between the sums of the elevations in the first and third columns of the 3 x 3 matrix. Similarly, the north-south slope is the difference between the sums of elevations in the first and third rows (note that in each case the middle value is weighted by a factor of two). Every cell in the output raster has a slope value. The lower slope value is the flatter terrain and the higher slope value is the steeper terrain. The output slope raster is calculated as the percent or degree of slope (fig. 50).

$$S_{e-w} = \frac{(z_3+2z_6+z_9-z_1-2z_4-z_7)}{8D} \qquad \textbf{Equation (8)}$$

$$S_{n-s} = \frac{(z_1+2z_2+z_3-z_7-2z_8-z_9)}{8D} \qquad \textbf{Equation (9)}$$

D:- is the raster resolution (30 m)

The slope at W. Dahab ranges between 0º and 68º (fig. 51), where very low values, less than 2° represent plain topography. This zone covers about 111 km^2 with 5 % of the total study area. Plain topography is located in the northern part of study area, especially at W. El Genah, in the northern part of W. El Ghaieb, at the western side at the upstream parts of W. Saal, W. Rimthy, and at the downstream of W. Dahab. The gentle slope values range from 2º to 8º. This range occupies the main

stream of W. Dahab, Zaghraa, Nasab, Rimthy and Saal; the gentle slope zone covers 617 km^2 with 29 % of the total area of Dahab basin.

The moderate slope value ranges between 8º and 15º; this slope zone covers about 540 km^2 (25%) of the total Dahab basin. This zone represents a weathered surface at high topographic level which refers to till blanket over bed rocks. The high values (15º - 30º) are found in the belt of igneous and metamorphic rocks which have many escarpments. Examples are the upper parts of basins such as W. Nasab, W.Rimthy, W.Abu Khshieb, W.El Ghaieb, and W. Zaghraa. This slope range covers a large area in Dahab basin, representing about 31% of the total study area. The high slope zones occur at the southern part of the study area, especially at W.Nasab, W. Rimthy, W. Abu Khshieb and downstream of W. Zaghraa. This zone ranges from 30 º to 67 º and it covers about 178 km^2, about 8.5% of the total area.

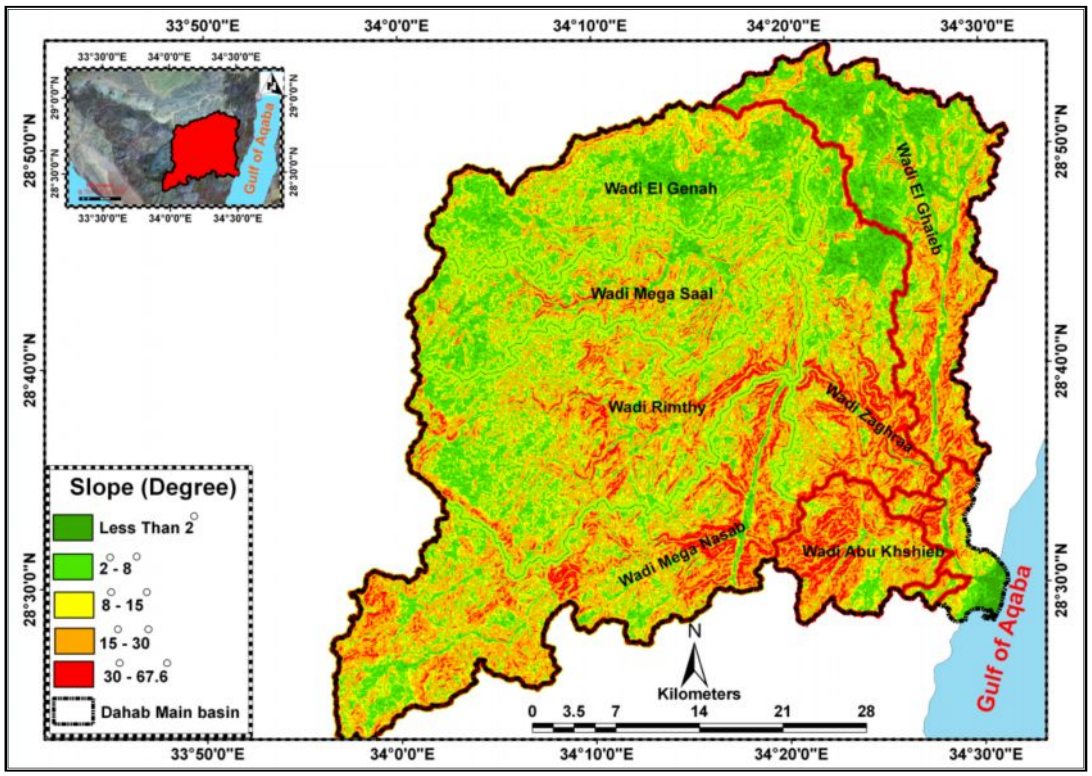

Figure 51: Slope Degrees For The Surface of Dahab Basin

2.3.2.4.B Gradient

The gradient of streams under a wide range of climatic and geological conditions might reflect the probability of floods and water infiltration. Basins with steeper slopes have a high probability of flood generation. In contrast, gentle slope basins have the chance that surface water could flow for a long time above ground giving a high probability of aquifer recharging. Gradient values represent the slope of the main stream of the drainage basin. This factor proves to be a significant drainage basin characteristic influencing the hydrological parameters such as the peak flow discharge.

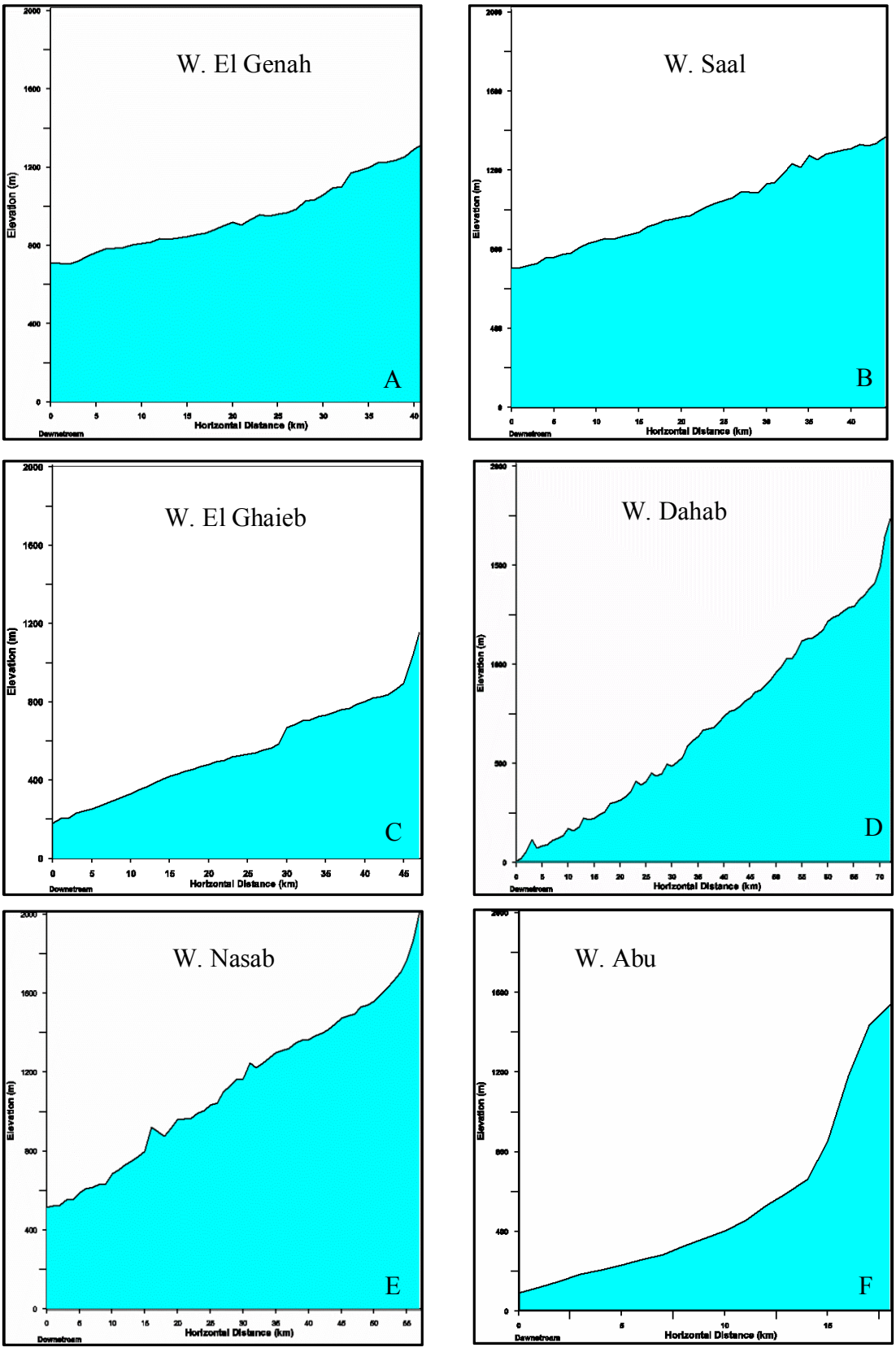

Figure 52 A-F: Gradient of Different Subbasins in Dahab Basin

The obtained data shows that W. Genah and W. Saal basins have a low drainage gradient of 14.7 and 15m/km respectively. Figure 52-A shows the gradient along the main stream of W.Genah. The covers of sedimentary rocks and loose sediments of the different streams affect the gradient of the main stream. The low gradient at W. Genah and W. Saal basins reflects the high probability of water infiltration recharging the existing aquifer and enhancing the augmenting of water within the basin.

W. El Ghaieb basin has a moderate gradient of 19.8m/km along the main stream as shown in Figure 52-C. The value of gradient increases in the upstream area of W. El Ghaieb basin at W. Hagag, W. Mezirah and W. Ghalium. On the other hand, low drainage gradients are recorded at some other parts of W. El Ghaieb where it would be favorable to recharge the existing aquifer as in W. Khalal and W. El Marwah. The Dahab basin area has a moderate value of 24.3 m/km. The value reflects that some parts of study area have good sites for aquifer recharge but on the other hand, there are also sites for flood generation (fig.52-D).

W. Nasab, W. Rimthy and W. Abu Khshieb basins have a moderate to high drainage gradient along the main streams. They have gradient values ranging from 26 to 27 m/km. The drainage gradient is not regular along the main stream (fig. 52E). The value increases at some parts of these sub-basins as in W. Rasies, W. El Waraa in W. Nasab, W. Sanad, W. Remty, and W.Rekita in W.Rimthy. The gradient reaches a maximum at W. Abu Khshieb with 80m/km (fig. 53-F). The cover of basement rocks and the tectonic setting of these basins are the main reasons for the high gradient of these basins. Generally, the gradient of these basins indicate a high probability of flood generation.

2.4 Flood hazard risk map

Flash floods are among the catastrophic natural hazards in the world causing the largest amount of deaths and property damage (CEOS, 2003). Floods could have an impact on many aspects of human life due to their destructive effect, and could create significant expenses through mitigation efforts.

There are many studies on flood hazard and risk mapping using remote sensing data and GIS tools. Radar remote sensing data has been extensively used for flood monitoring across the globe (Hess et. al., 1995, Le Toan et al., 1997), and many of these studies have applied probabilistic methods (Horritt and Bates, 2002, Pradhan, 2010b). Hydrological and stochastic rainfall methods for flood susceptibility mapping have been employed in other areas (Haeng et. al,. 2001, Cunderlik and Burn, 2002). Flood susceptibility mapping using GIS and network methods have been applied in various case studies (Sanyal and Lu 2005, Zerger, 2002).

The aim of this part of the chapter is to use analyzed morphometric parameters to estimate the flash flood risk levels of sub-watersheds within the watershed. Both the drainage network and drainage watershed are analyzed. Each characteristic is captured by a set of network and basin parameters that are relevant to the flash flood risk.

A total of 5 variables are considered as layers introduced into a model. It is assumed that all these variables are presented throughout the study area and are of equal importance. A general model has been established on the basis of causative factors including basin surface and its drainage characteristics. These factors are listed below:

1) Bifurcation ratio 2) Stream Frequency 3) Stream Density

3) Circularity Ratio 4) Elongation Ratio

The integration of this data could give the location of high risk spots in the study area. The quantitative values associated with each type of data should have a different score on a scale according to its importance in flood or risk. An overlay operation would then evaluate the intersected regions by a sum of the scores, so each region is characterized by a score measuring its potential for flood probability.

Based upon the relationship between the parameter values and the risk of flash flood, the analysis of each parameter is calculated using a simple statistical method (Youssef et al., 2010, Pradhan, 2010b). Each parameter is classified into three classes based on the morphometric characteristics and their relations to their potential degree of risk. The equation used is (Max–Min)/3. Then, the values for each parameter are classified into three intervals as shown in table 10.

Parameter	Flood Probability	Attribute	Raw Score	Normalized Score
Frequency	Low	□ 4.5	1	0
	Medium	4.6-6	2	0.5
	High	> 6	3	1
Density	Low	□ 2.2	1	0
	Medium	2.3-3	2	0.5
	High	> 3	3	1
Weighted Bifurcation Ratio	Low	□ 3.5	1	0
	Medium	3.6- 5.1	2	0.5
	High	> 5.1	3	1
Circularity Ratio	Low	□ 0.35	1	0
	Medium	0.36-0.55	2	0.5
	High	> 0.55	3	1
Elongation Ratio	Low	□ 0.33	1	0
	Medium	0.33-0.53	2	0.5
	High	> 0.53	3	1

Table 10: Score Assigned of Morphometric Parameters in Dahab Basin.

To come up with a final assessment of flood hazards, different scores on a scale according to their importance to flood risk are assigned. An overlay operation will evaluate the intersected regions by a

summation of scores, so that each region is characterized by a score measure. To present a readable final map, the result is divided into three categories (low, medium and high risk) using equal intervals. The results are scored on a 1 to 3 scale, in ascending order of hazard significance. The raw score for each feature is normalized using equation 10, taking into account the different signs of parameters as well. The normalized scores are ranged from 0 to 1 to minimize the value of total flood risk after summation of all the parameters (equation 11).

Basins of high frequency and high density values tend to collect more runoff water, which increases the rate of flow discharge out of a basin, resulting in a high risk value. In such basins, the rate of downward infiltration is expected to be low, while the basin bifurcation ratio will be low as well, reflecting a high flooding risk. Basins with higher circularity and elongation ratios (R_c and R_e) tend to have higher flash flood potentiality. Circular basins are also more susceptible to flash floods. The weight ratings assigned to each attribute layer and their respective classes are presented in table 11.

$$X_j = \frac{(R_j - R_{min})}{(R_{max} - R_{min})} \qquad \textbf{Equation 10}$$

Where:

Xj= normalized score Rj= raw score

R_{min}= minimum score R_{max}= maximum score

The final flooding risk of the study area according to morphometric parameters of the Dahab basin is estimated as:

Flooding risk = ***Normalized Average Bifurcation Ratio (R_b) + Normalized Frequency (F) + Normalized Density (D) + Normalized Circularity (Rc) + Normalized Elongation (Re)***

Equation 11

According to this equation, the study area could be divided into three classes of flood hazard susceptibility, as shown in the final map (fig.53).

The flood hazard risk map of Dahab Mega-basin (Fig. 53) shows that 34% of the total sub-basins in the Dahab basin have a high flooding risk. Most of these sub-basins are draining into basins of higher order as W. Nasab, W. Rimthy and W. Ghaieb. 60% of all sub-basins have medium flooding risk. Only a few percent, about 6%, of the sub-basins have a low risk flooding susceptibility.

More than 50% of high potential risk basins are concentrated in W. Zaghraa Nasab at W. Zaghraa, in others parts in W. Abu Khashieb and in small parts at W. El Ghaieb. High risk zones occur at the catchment part of W. Abu Khashieb as in W. Um Harq, W. Maaen, W. south Harq and W. Small Abu Khshieb. At W. El Ghaieb, the high risks are located in W. Mezirah, W. North Bathier and W. Hagag (Table 11).

The catchment of W. Nasab has a high potential risk for floods as in W. Hassa, W. Zaraa, W. Rahabah, W. El Roting and W. Myenat. Also, high risk occurs in W. Um Shietan, W. Masharaah and W. Nabaa. In W. Rimthy; the catchment of this basin has a high risk as shown in W. Rekita, W. El

Mokhtar, W. Hamami, W. Faraa and W. Merkh. W. El Genah and W. Saal are considered to have moderate to low flood risk; on other hand, there are some sub-basins that have a high risk as in W. Manader and W. Saal El Rayan in Saal basin, W. Retem, W. Meskan, W. Abu Tehimah and W. El Hoo in Genah sub-basins (Table 16). It can be summarized that the high flooding risk zones are located mainly in three zones. The first zone is W. Zaghraa where it appears in two main sub-basins (W. Nasab and W. Rimthy). The second is at W. Abu Khshieb and the last zone is at W. El Ghaieb (fig. 53).

Class	Risk	N.S	Percent	Basins
1	Low	<2	6%	**8,50,81,162**
2	Medium	2 – 3.49	60%	**1,2,3,4,6,7,10,11,12,13,14,15,17,18,21,27,28,29,30,31,33,34,36,37,38,39, 42,43,44,45,45,46,47,48,51,53,54,56,57,58,59,60,61,63,67,69,70,71,72,73 ,76,77,78,79,80,82,83,84,85,86,88,89,90,95,96,98,99,102,103,104,105,10 7,108,110,110,111,112,114,116,118,120,121,122,123,124,126,127,129,13 0,131,132,133,138,141,142,143,146,148,149,150,155,157,160,161,165,16 7,169,172,176,178**
3	Large	>3.5	34%	**5,9,16,19,20,22,23,24,25,26,32,35,40,41,49,52,55,62,64,65,66,68,74,75,8 7,91,92,93,94,97,100,101,106,109,113,115,117,119,125,128,134,135,136, 137,139,140,144,145,147,151,152,153,154,156,158,159,163,164,166,168, 170,171,173,174,175,177**

Table 11: Flood Risk Results for Each Subbasin in Dahab Basin.

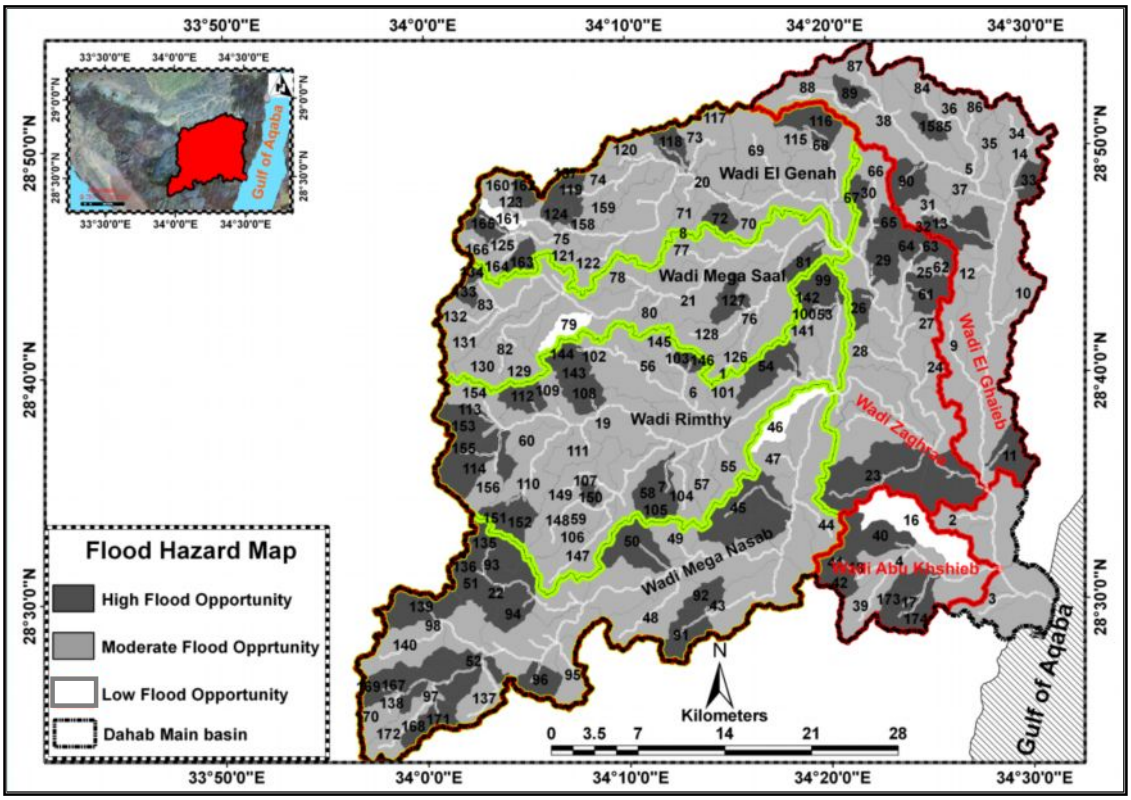

Figure 53: Flood Hazard Risk Map Based on Morphometric Parameter for Dahab Basin

Flood risk maps that depend on the analysis of morphometric parameters might be considered as a first step to evaluate the flooding risk of hydrographic basins. The preliminary results reflect the need

to conduct a more detailed study in the next chapters which will take other factors into consideration, such as the amount of surface discharge, rainfall statistics, infiltration and evaporation at locations of high risk in W. Dahab basin.

The GIS technique has been proven as a useful tool for creating flood risk maps. In particular, it is useful for drawing and measuring linear objects, such as stream length, in order to build up the stream network, which is the main morphometric element needed for the creation of such maps. The GIS models helps to enhance the automatic measuring process of stream network parameters, such as ordering and length estimation, without manual coding, editing, or any time consuming processes.

CHAPTER III

HYDROGEOLOGICAL AND HYDROCHEMICAL INVESTIGATIONS

Chapter III

Hydrogeological and Hydrochemical Investigations

Development of arid and semi-arid areas depends upon the availability of groundwater and surface water resources and their proper utilization. Wadi Dahab basin is one of these areas in which considerable inhabitants and different activities were sporadically distributed. The groundwater is the only source for all purposes.

During the last few decades, groundwater exploitation in the Sinai Peninsula increased dramatically, mainly due to an increase in population and agricultural, tourism and industrial activities. To meet the needs of drinking water for future generations, sustainable watershed management is an essential target that requires more detailed knowledge about water resource availabilities and recharge processes.

The carried out hydrogeological investigation depends on detailed surveying of thirty boreholes distributed in Dahab basin. Most of these borehole locations were concentrated in W. Nasab, W. Rimthy in the south western part of the basin, W. Saal in the western part of the Dahab basin and at the downstream of Dahab basin (fig. 54). Hydrogeological surveying and water monitoring were carried out during two different seasons. On the other hand, tentative reviewing of the previous investigation and literatures has been considered in order to recognize the hydrogeologic setting of the study area.

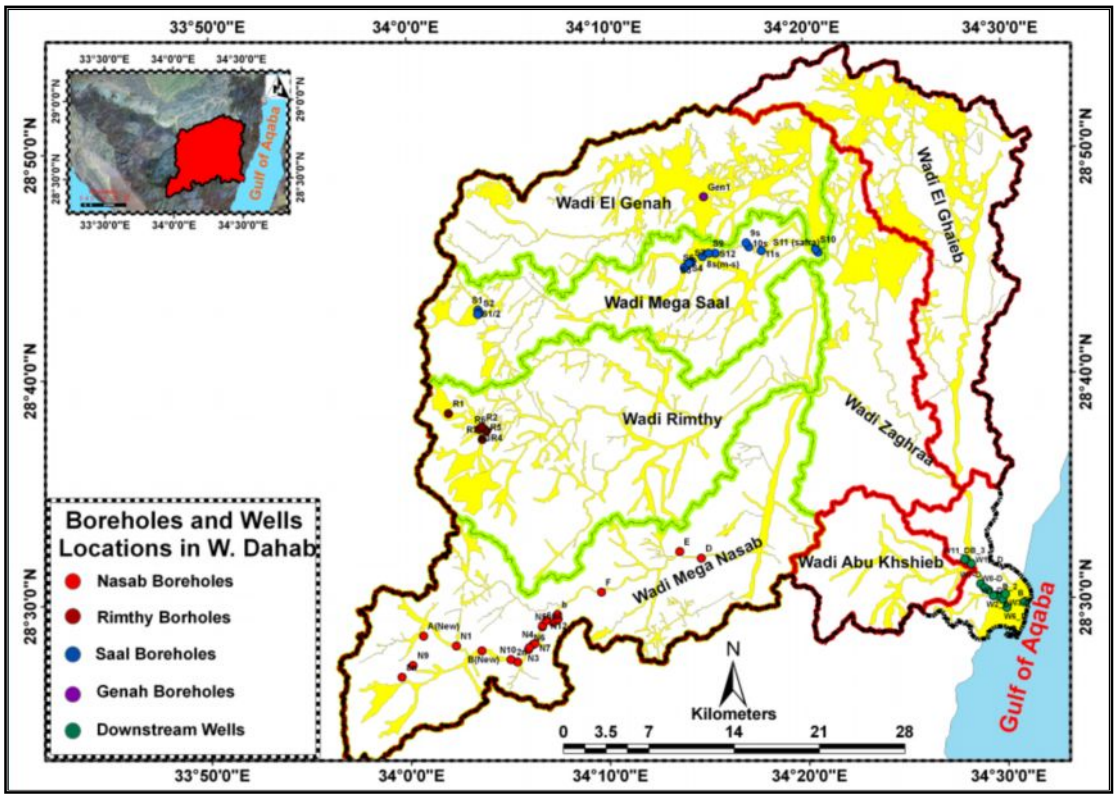

Figure 54: Well Location distribution in W. Dahab

3.1 Hydrogeological conditions

Several hydrogeological studies have been carried out in the area of consideration, among them works of El Rayes (1992), Shendi and El Rayes (1992), El Kiki et.al (1992), Oada (1995), Shendi and Oada (1999), Shendi et. al. (1997). Most of these studies were carried out on a regional scale and deal with qualitative hydrology of the study area.

The hydrogeological condition of Dahab Basin was highly controlled by many factors such as geological, structural, and climatic conditions. In the study area, groundwater occurred in fractured crystalline rocks and in alluvial wadi fillings. The catchment area of Dahab basin received huge quantities of precipitation in the form of rainfall along its uppermost upstream area. A considerable amount of this rainfall ran as surface runoff along the main streams to the Gulf of Aqaba without benefits for the people.

Rainfall is the essential source of groundwater recharge in the basement rocks. Then, it moves through the fractures downward to recharge the alluvial aquifers. A huge amount of rainfall percolates of alluvial sediments and is stored in basement aquifers. The recharge of the groundwater takes place by direct infiltration from rainfall and by percolation through alluvial fillings within streams.

3.1.1 Factors affecting groundwater occurrence

Water occurrences are related to the interaction of some environmental factors such as climatic factors, topographic factors and structure factors.

3.1.1.1 Climatic factors

Rainfall is the essential source for groundwater recharge. Dahab basin is in an arid basin characterized by long, hot, rainless summers and mild winters. The rainfall prevailed as thunder storms during periods from January to March and October to December.

Flash floods frequently occurred as a result of heavy rainfall storms within a short period. Light rainfalls of long duration support infiltration and aquifer recharge (El Rayes, 1992). The maximum potential rainfall in Dahab basin was about 76. 4 mm (Dames and Moore, 1983), that exceeds the average annual rainfall amount (35mm/year). The average amount of evaporation during storm periods range between 1.5 and 10 mm/day. The average exceeds the light rainfall during rainy periods.

3.1.1.2 Topographic factors

The gradient of the basin measured the indication of potential energy of the drainage system, related to the level of the basin mouth. It measured the overall steepness of the drainage basin and it influences on the speed of water runoff in the wadi. The higher value of the slope causes high-speed runoff and minimal infiltration; in contrast, areas of low value can be anticipated to cause more infiltration.

El Rayes (1992) stated that geomorphical characteristics, as well as the existence of thick alluvial deposits with good hydraulic properties covering the wadi floor provide a suitable environment for the infiltration of running water and the formation of good aquifers. As described in chapter two, results of geomorphic analysis showed that in the W. Saal and W. El Genah there is a low risk for flooding and good possibility for the infiltration of water. The thickness of the alluvial aquifers changed along the main stream of different sub-basins in W. Dahab due to the effect of topography. On the other hand, there were many areas which were promising for groundwater recharge related to alluvial thickness as in W. Saal, the middle part of W. Nasab and the downstream of Dahab basin.

3.1.1.3 Structural factors

The structural elements such as deep seated shear, tension fractures and thrust faults act as conduits for groundwater. Within certain linear zones, the hydraulic conductivity could be higher in the compact basement rocks. The highly jointed rocks increased percolation and storage of rain water as in the catchment area of W. Nasab.

The gradual downward decrease of joint densities throughout the hydrogeological units influences the general flow system of the study area. Rainwater which is directly infiltrated in the highly jointed upper unit is gradually transmitted into fault zones and the alluvial aquifers through the weakly jointed lower unit. The intersections of fractures are good sites for construction of water wells.

3.1.2 Aquifer types

Based on the lithological conditions, the water bearing formations were classified into A) alluvial Aquifers and B) basement Aquifer. Groundwater moves downward and laterally through the open fractures to recharge the alluvial deposits of the main valleys (El Rayes, 1992). Thus, alluvial deposits of Dahab basin received large amounts of recharge water from the fractured basement rocks.

3.1.2.1 Alluvial aquifers

Alluvial deposits represented the main streams of W. Nasab, W. Saal and W. El Ghaieb. Alluvial aquifers have a heterogeneous composition. They vary from sand to gravel to boulders with intercalations of silt and clay. The dykes also play an important role in order to accumulate groundwater in aquifers which act as subsurface barriers for the groundwater flow. In this way, good groundwater reservoirs were developed. These aquifers have normally good hydraulic properties and the yield can reach to 1.9×10^{-3} m/s in the Nasab well (Oada, 1995). The recharge of the alluvial aquifer happens by surface runoff coming through the main streams from the catchment area during high storms and by base flow and lateral flow from the basement rocks surrounding the alluvial deposits.

The thickness of the alluvial aquifers varies within the study area due to structural and topographic effects. Geophysically, the thickness of the sediments was measured in W. Nasab using Geo-electric Sounding (VES) by Oada, (1995), Shendi et.al. (1997) in W. Saal, Morsy, et.al. (2007) along the downstream of Dahab basin, and by the Water Resources Research Institute (2006) along W. Zaghara.

The measured thickness of the alluvial deposits in W. Nasab ranged from 5 to 25 m at the upper stream and reaches up to 30 m at the downstream, while at W. Saal the alluvial deposit ranges from 5 to 30 m along the main stream and from 4 to 25m at W. Zaghraa- Rimthy and from 35 to 55m along the main fan of Dahab basin.

3.1.2.2 Basement aquifers

Basement aquifers are the most important aquifers in the study area, especially the fractured or weathered basement parts of them. This type of aquifer consists of older granitoids (granodirite, quartz diorites and monzogranites), younger granitoids (syanogranites), volcanic rocks and metamorphic rocks. El Rayes (1992) classified the basement aquifers in southern Sinai into three hydrogeological members.

A) The main aquifer unit

This group is highly jointed and reflects good hydraulic conductivity; it has a high capacity to store large amounts of rain water and snow melt as shown in borehole A at W. Nasab and S1 at W. Saal. It occupies the mountainous ridges and high peaks.

B) Leaky aquitard unit

This unit has low joint density and low hydraulic conductivity. It acts as a barrier which can restrict vertical flow of stored water from the main aquifers that occur along the main stream of W.Saal and the upstream of W. Rimthy.

C) Local aquifer unit

This unit represents fault zones, alluvial deposits and jointed rocks adjacent to basic dykes in the upstream area of W. Nasab (3n) (fig.55-A). It occurs also in discharge areas such as the spring areas of the upper stream of W. Nasab borehole No. 8n (fig. 55-B).Generally, the basement aquifers widely distributed in Dahab basin are highly weathered and characterized by low yield. The prevailing dyke systems (daming, improving through flow) play an important role to catch groundwater where they can conduit water because of having been fractured as in the acidic dykes; they act as a boundary or a sealing member where they are slightly fractured as basic dykes (Oada, 1995).

3.1.3 Hydrogeological boundary condition

The hydrogeological boundary conditions vary greatly in Dahab basin. The change of hydrogeological properties is caused by erosion and deposition of sediments due to structure and topography of the basement rocks. The 80 % of the study area that is covered by basement rocks represents the major aquifer in Dahab basin.

Figure 55-A: Effect of Basic Dykes at Upper Stream in W. Nasab
Figure 55-B: Spring along Fault Zones at Upper Stream in W. Nasab

3.1.3.1 W. Nasab

W. Nasab located in the south western part of Dahab basin and is one of the most important sub-basins in the study area. Many tribes and local inhabitants live in this wadi and depend mainly on water wells for their grazing and watering plants. More than 13 wells and 2 springs have been visited during the dry season (April/2009) and the rainy season (January/2010) as shown in Table 12 and fig 56.

W. Nasab was studied with electrical and magnetic tools and it was classified geophysically into three hydrogeological zones (Oada, 1995). The hydrogeological cross section was drawn according to field measurements and previous data (fig. 57). W. Nasab was subdivided into three zones:

- The first zone is represented by top layers of 9 to 11 m thickness and consists of fine sand and silts with the electrical resistivity ranging from 240 to 500 Ωm.
- The second zone consists of alluvial deposits of fractured basement rocks. According to geophysical measurements, this is the water bearing zone with electrical resistivity of about 650 Ωm. Its thickness ranges from 17 to 30 m. This zone includes the upper part of the basement rocks which was highly fractured. The lower part of this zone represents the productive layer for wells.

- The third zone represents less fractured basement rocks or massive rocks. The rocks of this zone are dry with high resistivity of more than 2000 Ωm (Oada, 1995). The surface of this zone is irregular according to the topography of basement rocks and the effect of tectonics in Southern Sinai. The top of the basement ranges from 1424 m above sea level (a.s.l) at well A.

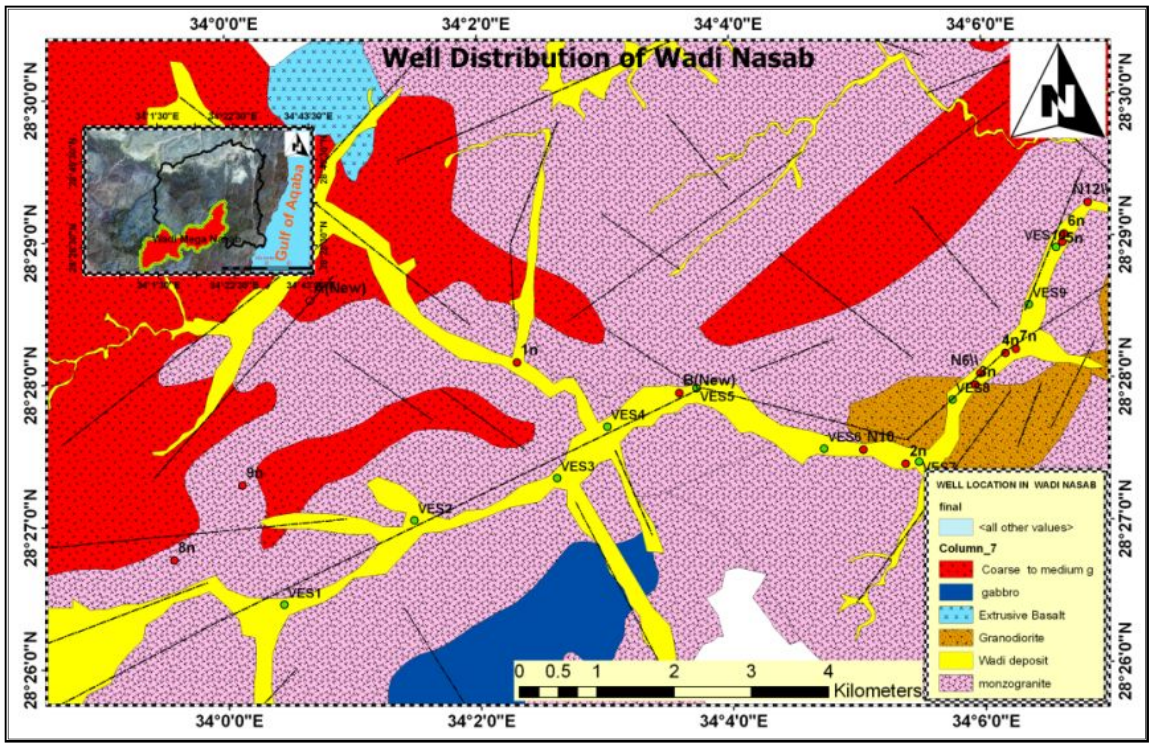

Figure 56: Boreholes Distribution at W. Nasab

Well No.	Symbol	Latitute	Longitute	Elevation (m)	DTW (4/2009) (m)	DTW (1/2011) (m)	TD (m)	EC (µs/m)	T	pH	Aquifer	Age_well	NAME
1	A	28 28 39.7	34 00 34.9	1695		6	7	540	14.9	8.14	Basement	New_Well	Nasab _Upstream
2	1n	28 28 16	34 02 21	1503	28.0	13.70	30	491	22.2	8.13	Alluvial	New_Well	at W.Rasis with W. El- Malz
3	B	28 27 54.8	34 03 35.4	1416		43.25	51	573	19.2	8.3		New_Well	Main W. Nasab
4	2n	28 27 24	34 05 22.2	1365	33.5		35				Alluvial	New_Well	Um Graf Well
5	3n	28 27 57.9	34 05 55.6	1344	35.0	33	37	592	19	8.3	Alluvial	New_Well	Main W. Nasab
6	4n	28 28 10.2	34 06 10.7	1335	28.5		30				Alluvial	New_Well	Main W. Nasab
7	5n	28 28 56.7	34 06 38.2	1322	28.0	22	30	606	16.7	8.4	Alluvial	New_Well	Nasab well
8	6n	28 29 0.15	34 06 39.17	1317	26.0		28				Alluvial	New_Well	Nasab well within village
9	6n/	28 28 02.7	34 05 58.5	1350		33.3	36	579	22.2	8.21	Alluvial	New_Well	Main W. Nasab
10	7n	28 28 11.9	34 06 15.4	1331	33.5	29.3	35	587	19.7	7.3	Alluvial	New_Well	Main W. Nasab
11	8n	28 26 45.7	33 59 35.4	1661	4.0		5				Basement	spring	W.Rahaba Well
12	9n	28 27 16.8	34 00 6.3	1660	6.5		8				Basement	spring	Well El Nakeb Omran
13	10n	28 27 30.5	34 05 02	1344		38.9	46	569	22.5	8.22	Alluvial	New_Well	Main W. Nasab
14	11n	28 29 17.5	34 07 26.14	1276	7.4	10.5	12.6	1281	18.1	8.2	Alluvial	Old_Well	a
15	12n	28 29 9.8	34 07 10.4	1292	10.3	21	23	1135	18	8.13	Alluvial	Old_Well	c
16	b	28 29 30.24	34 07 23.78	1262	7.8		0				Alluvial	Old_Well	b

Table 12: Boreholes Data in W. Nasab

The aquifer was considered an unconfined aquifer and its water level matches the configuration of the general topography of the area. Depth to water table (DTW) changed due to the topography and the effect of climate. It ranged from 13 to 30 m at the upstream area of W. Nasab. The groundwater level at well N5 is located at 22m and it decreased again in the middle of W. Nasab to 10m and 21m at well N11 and N12. The effect of precipitation and groundwater recharge was investigated during

the dry season (April/2009) and the rainy season (January/ 2011). The differences of groundwater levels after stormy rains amounted up to 5 m (Table12). The topographical and the structural factors affected fluctuation on groundwater table surface. Many boreholes are located at the contact zone between the dykes and basement as shown in figure 57. Some dykes in W. Nasb area are basic dykes which accumulate groundwater and act as subsurface dams forming many local isolated basins in the subsurface as shown in well 3N and well 5N (fig. 58).

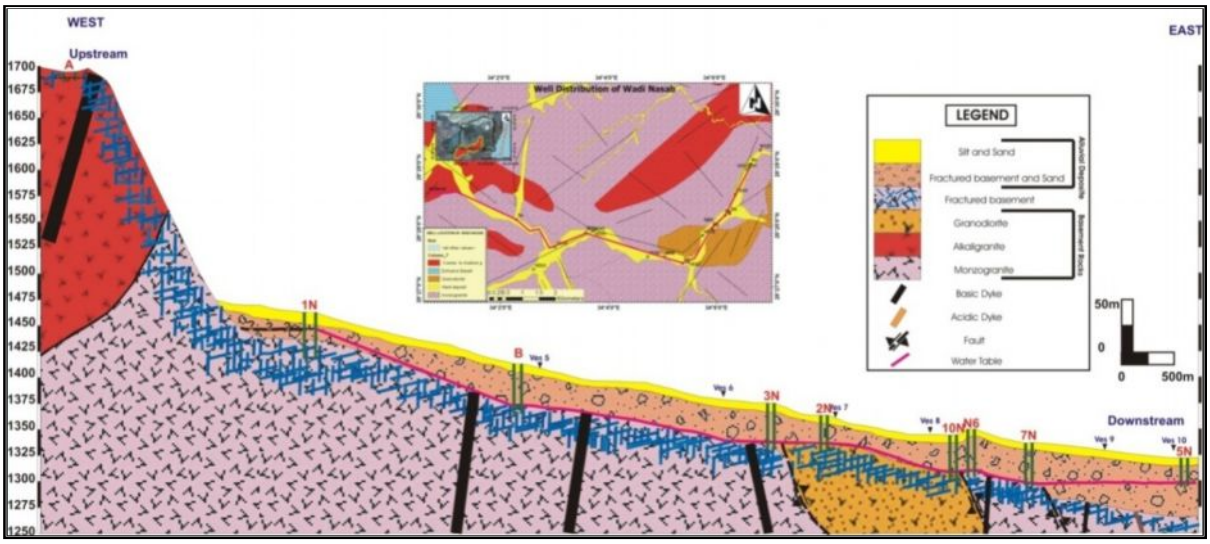

Figure 57: Hydrogeological Cross Section of W. Nasab

Figure 58: Boreholes (5N) at W. Nasab

3.1.3.2 W. Saal

W. Saal is located in the northern part of Dahab basin. Many Bedouins live in W. Saal and form large communities. They depend mainly on groundwater wells and additionally on clean water transported by tanks from Dahab city. Water is needed for grazing, agriculture and domestic use. Fourteen boreholes were visited in the dry season (April/2009) and the rainy season (January/2010) (fig. 59). The Hydrogeological conditions were studied by Shendi et al. (1997) as well.

The groundwater of W. Saal exists in three unconfined aquifers: weathered and fractured basement, alluvial aquifers and some local limestone aquifers. The hydrogeological cross section was drawn according to field measurements and previous data shown in figure 60. Geophysically, this area was studied by Shendi et al. (1997) who classified the aquifers of W. Saal into four zones:

- The first zone represents dry top layer sediment of 1 m in the upstream and 17 m thickness in the downstream areas. This zone consists of fine sand, clay and gravel of middle to high hydraulic conductivity.

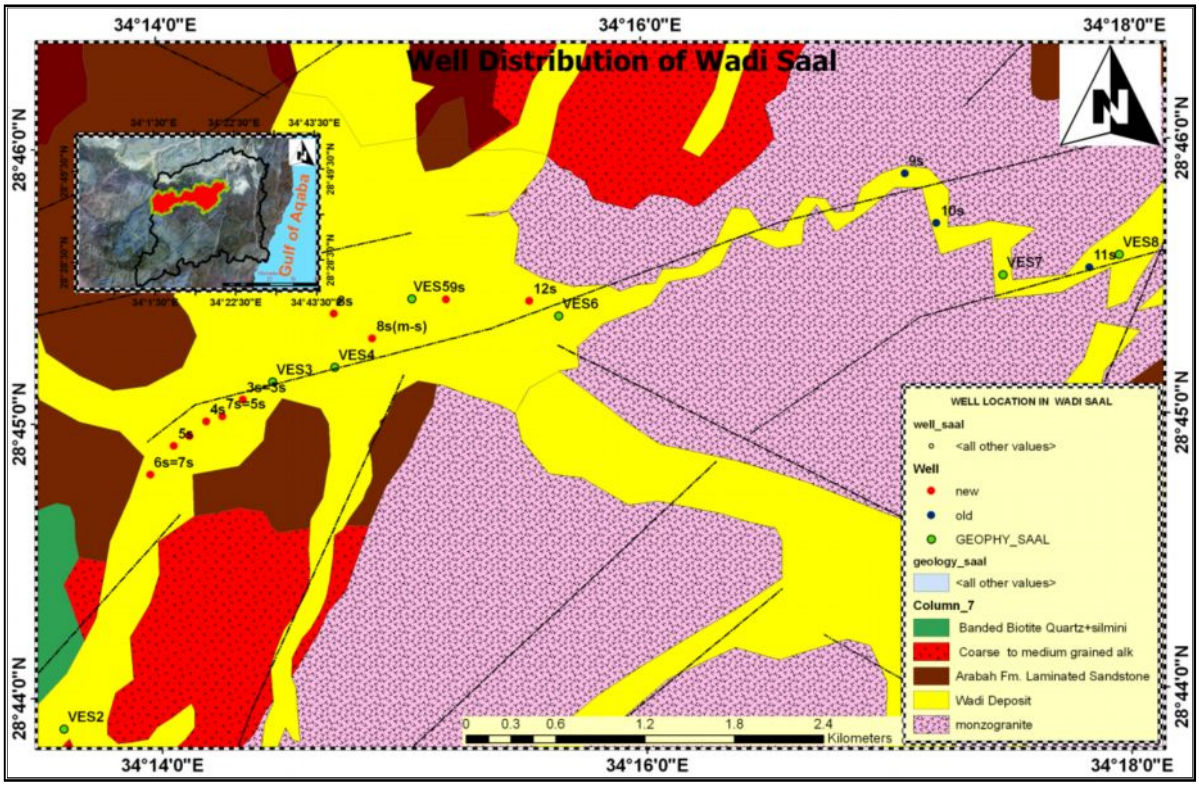

Figure 59: Distribution Borehole Locations in W. Saal

- The second zone layer consists mainly of sand and gravel with granitic boulders. The thickness of the zone ranges from 11 m at well 9s to 45 m at well 6s and 4s. This layer is obviously the water bearing zone. The resistivity of this zone ranges from 100 - 150 Ωm. Locally, this zone includes limestone (Cretaceous aquifer) which occurs in W. Saal at Well 11S (Safra well, fig 61-A). The occurrence of carbonate rocks is shown in figure 61-B. The high salinity (Chloride) of the

groundwater of this well (4.18ms/cm) indicates the occurrence of evaporates. This aquifer forms an alluvial fan and lacustrine deposits, especially downstream of the W. Saal basin (Shendi et al. 1997).

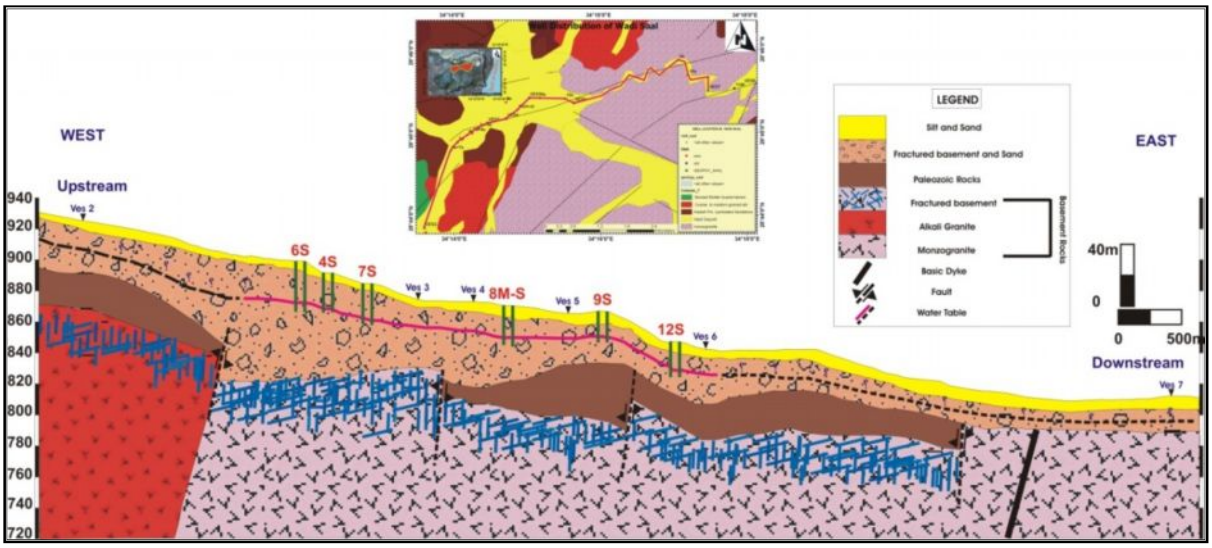

Figure 60: Hydrogeological Cross Section in W. Saal

- The third zone consists of fractured granitic and volcanic rock. Geophysically, It represents the top of basement in thicknesses from 5 to more than 20m. The reachargabilty of this zone depends mainly on direct precipitation in Well S1 (Fringa well) and S2 which could be shown the fluctuation of the water in this zone. The presence of dykes plays an essential role in the groundwater occurrence as it represents traps for groundwater accumulation.
- The fourth zone represents less permeable rocks that are formed mainly by the fractured basement cap and by water barriers. Their thickness cannot be determined and resistivity exceeds 1000 Ωm. The surface of this zone is irregular according to the topography of the underlying basement rock.

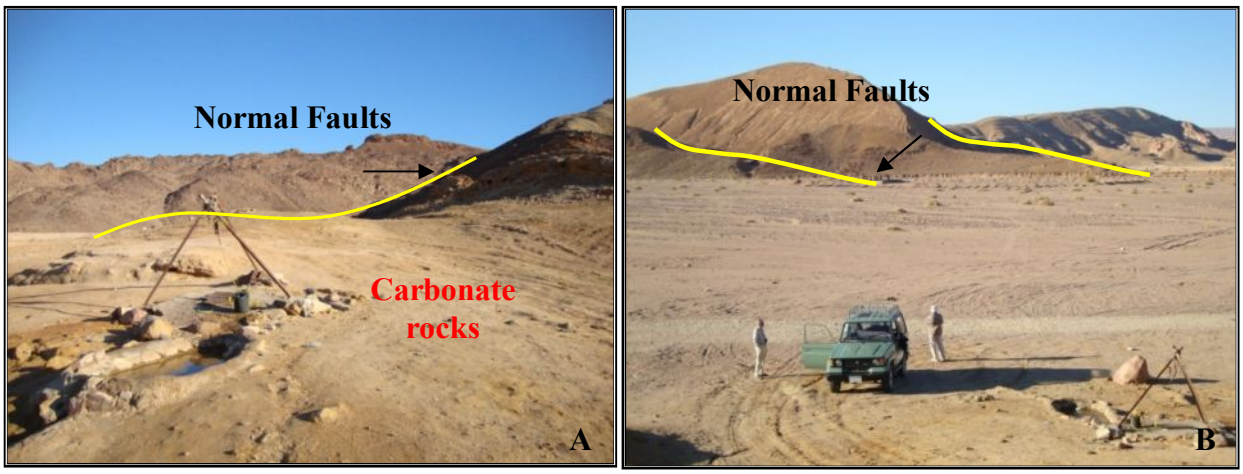

Figure 61-A: Borehole S11 (Safra well) at W. Saal
Figure 61-B : The Effect of Structure on Groundwater Occurrence

Generally, the groundwater table varies due to structural effects which formed small and separate sub-basins. The depth to water is considered as shallow in the upstream wells e.g Fringa wells (1S,2S and 2S/) with values 12 to 13 m below ground surface. It reaches down to 22 m below ground surface at well 6s in the downstream part of Saal sub-basin.

Well No.	Symbol	Latitute	Longitute	Elevation (m)	DTW (4/2009) (m)	DTW (1/2010) (m)	TD (m)	EC (µs/m)	T	pH	Aquifer	Age	NAME
1	1s	28 43 49	34 03 32	1316	18.0	13.8	20	2.67(ms/cm)	14.7	7.7	Basement	Old_Well	El Ferenga
2	2s	28 42 52.9	34 03 35.5			12.8	13.6	3.24 (ms/cm)	13.9	7.3	Alluvial	New_Well	
3	2s/	28 42 49.6	34 03 31.5			13.6	17	1547	17.1	7.3	Alluvial	New_Well	
4	3s	28 45 04	34 14 20	880	19.0		22	Yes			Alluvial	Old_Well	W. Saal
5	4s	28 44 57	34 14 00	892	25.0	20.4	27	917	23.7	7.7	Alluvial	Old_Well	W.Saal
6	5s	28 44 55	34 14 01	891	28.0		30	Yes			Alluvial	Old_Well	W.Saal
7	6s	28 44 48	34 13.57	899	23.0	21.3	24	904	22.8	7.7	Alluvial	Old_Well	W. Saal
8	7s	28 45 00	34 14 10	885	23.0	18.8	25	1130	18.9	7.6	Alluvial	Old_Well	W. Saal
9	8s	28 45 23	34 14 43	864	16.0		18	Yes			Alluvial	Old_Well	W. Saal
10	8s(m-s)	28 45 18	34 14 55	872	26.0	11.5	30	1119	22.6	7.8	Alluvial	Old_Well	Well Mai Saal
11	9s	28 45 26.4	34 15 11.03			11.3	14.5	1573	20.1	7.7	Alluvial	New_Well	W.Saal
12	10s	28 45 33.8	34 20 35.1			6	6.5	2.57(ms/cm)	12.8	7.8	Alluvial	New_Well	W.Saal
13	12s	28 45 25.9	34 15 31.8			13.6	14.3	3.16(ms/cm)	16.2	7.8	Alluvial	New_Well	W.Saal
14	11s	28 45 25.9	34 15 31.8			13.6	14.3	4.18(ms/cm)	21.6	7.6	carbonate	Old_Well	Safra
15	13s	28 45 00	34 14 11.4			17.5	18.5	1330	14.9	7.8		New_Well	
16	a	28 44 52.5	34 17 10	802				No			Alluvial	Old_Well	W.Saal
17	b	28 45 42.1	34 17 12.6	810				No			Alluvial	Old_Well	W. Saal
18	c	28 45 39.9	34 17 58.4	788				No			Alluvial	Old_Well	W.Saal

Table 13: Boreholes Data in W. Saal.

The water level fluctuates rapidly during the season of the year. The difference in level between the two seasons may range between 5 meters at the upstream and 2 to 4m at wells in the downstream area. The difference in water levels increases in the upstream area because of its high permeability and hydraulic gradient (Table 13). It is considered to receive area from direct precipitation where the rate of percolation is very high according to fluctuation towards wells at the downstream area located in a low permeable zone.

3.1.3.3 Downstream area of W. Dahab

The downstream of Dahab basin has a great groundwater occurrence in mainly the alluvial fan of Dahab basin. More than 8 wells were drilled during the period of 1982 to 1987. Most of these wells tap alluvial aquifers and one well produces water from basement rock. All these wells were cased wells except one and did not work during the investigation period except two, wells 4D and 9D (fig. 62).

Several geophysical methods were applied to define aquifer characteristics downstream of Dahab basin and to differentiate between water quality in the different hydrogeological zones at the aquifer domain. Three zones were distinguished from top to bottom of the drilled wells.

- The first zone represents dry heterogeneous alluvial sediment. The layer consists of sand, silt and gravel. The thickness increases toward the distal part of the alluvial fan; it ranges from 22 m to 40 m. This zone has a high electrical resistivity up to 500 Ωm.
- The second zone represents the upper most aquifer. It consists of sand, silt and weathered basement boulder with a clayey matrix. The thickness ranges from 30m at well 8D to 60 m at well 6D. The variation of the thickness points to an irregular topographic surface of basement rocks.

The lower part of this zone has a high content of clay and the electrical resistivity decreases gradual from 200 Ωm at its upper part to 10 Ωm reflecting high salinity /or high clay content (El –Kiki et.al, 1992).

- The third zone is the lower part of the second zone. It bears saline water indicated by a low electrical resistivity of 5 Ωm. This zone was not fully penetrated by a drilled well. The cross section based on geophysical measurement illustrated that the lower part of this zone was invaded with sea water and the salinity confirms sea water intrusion. This reason may cause the ceasing of work in most of wells at Dahab city as in wells 6D, 1D, 2D and 3D.

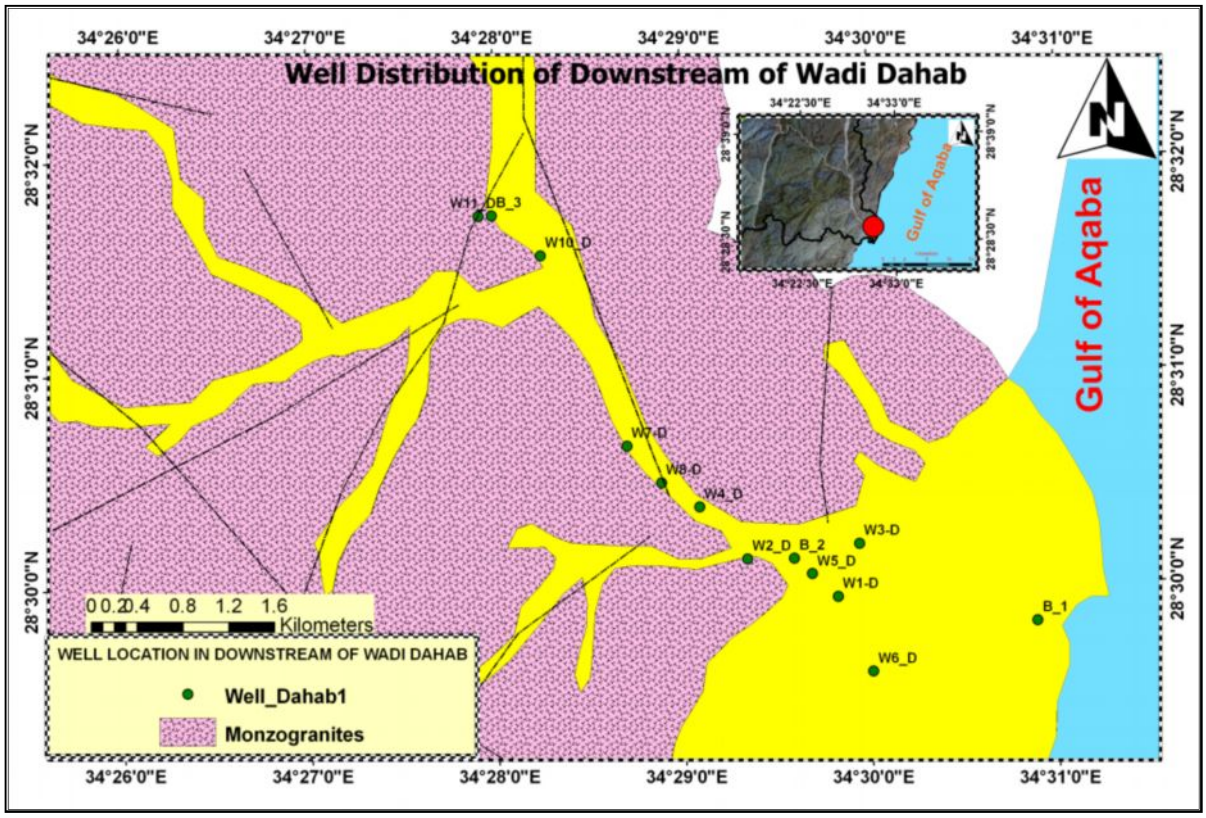

Figure 62: Well Locations in Downstream of W. Dahab

The salinity of groundwater in most of the wells was measured from 1986 to 2010. The measurements confirm that there were increases in the salinity as well (see fig. 63). The salinity ranged between 1188 and 3033 ppm in 1986 and increased from 2160 to 3155 ppm in 1988; it reached from 2900 to 3300 ppm in 1995. The water salinity raised in the wells during the period of investigation (2009-2010) to more than 4000 ppm (well 4D). The hydrogeological cross section showed that there was an increase of marine influences because the water table decreases more near seawater (fig. 63). The depth to water increased from well 4 to well 7 and became nearer to seawater level. The fluctuation of the salinity was dominated due to the low rate of recharge to groundwater at this zone and the increase of pumping rates and water demands.

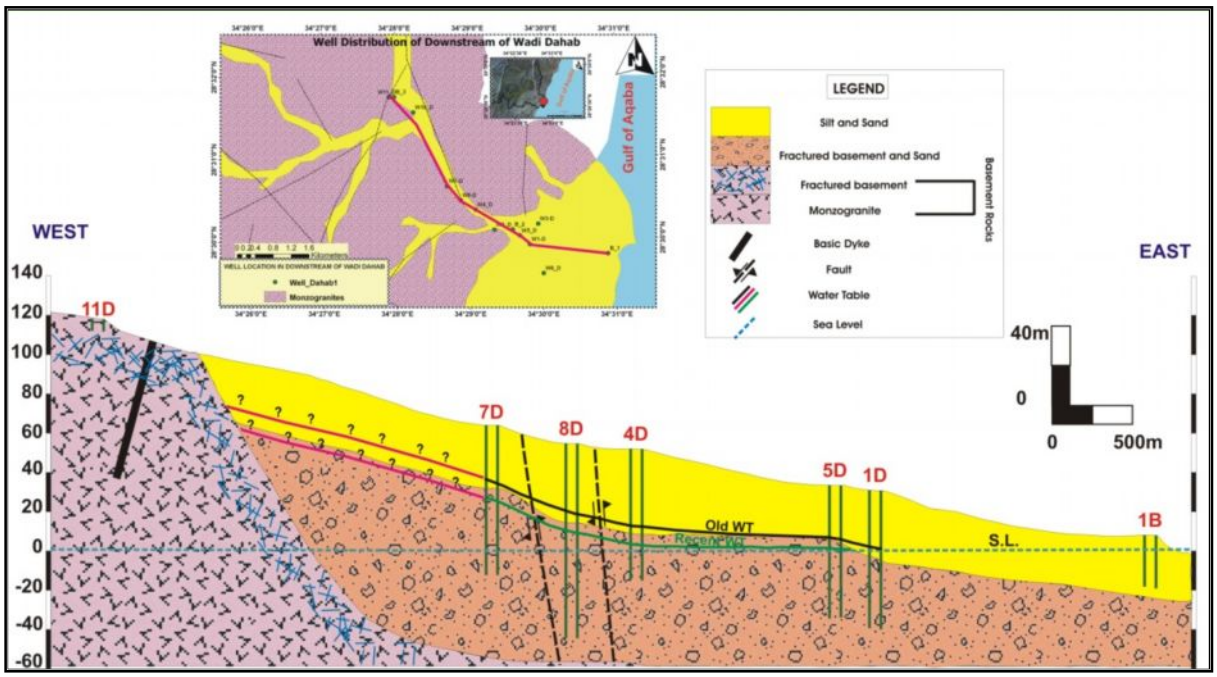

Figure 63: Hydrogeological Cross Section in Downstream of W. Dahab

From the carried out field observations, Dahab basin could be classified into two different provinces of groundwater bearing systems. The first one is the catchment province representing W. Nasab and W. Saal; the second province is represented by the downstream area of Dahab basin.The catchment province is represented mainly by an alluvial aquifer with a fractured basement at the upstream part, especially at W. Nasab and W. Saal. Both depend mainly on the recharge from direct precipitation. Due to relative low thickness of the alluvial layer at the upstream, most of the wells produce water mainly from the contact zone between fractured basement rocks and alluvial layers. The geological structure plays an important role in forming many subsurface basins which enable the construction of wells and springs along the wadi course in the prevailing basement outcrops. The rate of recharge increases in the upstream area of the province because of generally high hydraulic conductivity and high hydraulic gradient.

The downstream province depends mainly on alluvial aquifers producing groundwater, especially in the Dahab basin. Because of the large thickness of the alluvial aquifer, the water table is deeper than that in the catchment province. Water level ranges from 35 to 60m below ground surface. The low rate of recharge in this province and the increased water extraction cause a lowering of the water table and an increase in the salinity in all wells. The problem of the mixing and flushing of marine water can be shown in this province due to its close location to the Gulf.

3.2 Hydraulic properties

3.2.1 Hydraulic conductivity of Alluvial Deposits

In arid regions, surface water losses are usually high due to infiltration and evaporation. Infiltration rates vary widely, depending several factors such as the condition of the land surface

(eventually crust), the type, extent, and density of plant cover, the physical properties of the soil, including grain size and gradation, the storm character, i.e., intensity and duration, and the water temperature (Ponce,1989).

Previous infiltration experiments were applied in W. Saal and W. El Shiekh in Saint Catherine areas in the western part of Dahab basin in alluvial deposits at different locations along the main course of wadis by Geriesh (1998) and Shendi et al. (1997). The results show that average infiltration rate in W. Saal was 8 m/day while in W. El Sheikh it was around 1 m/day.

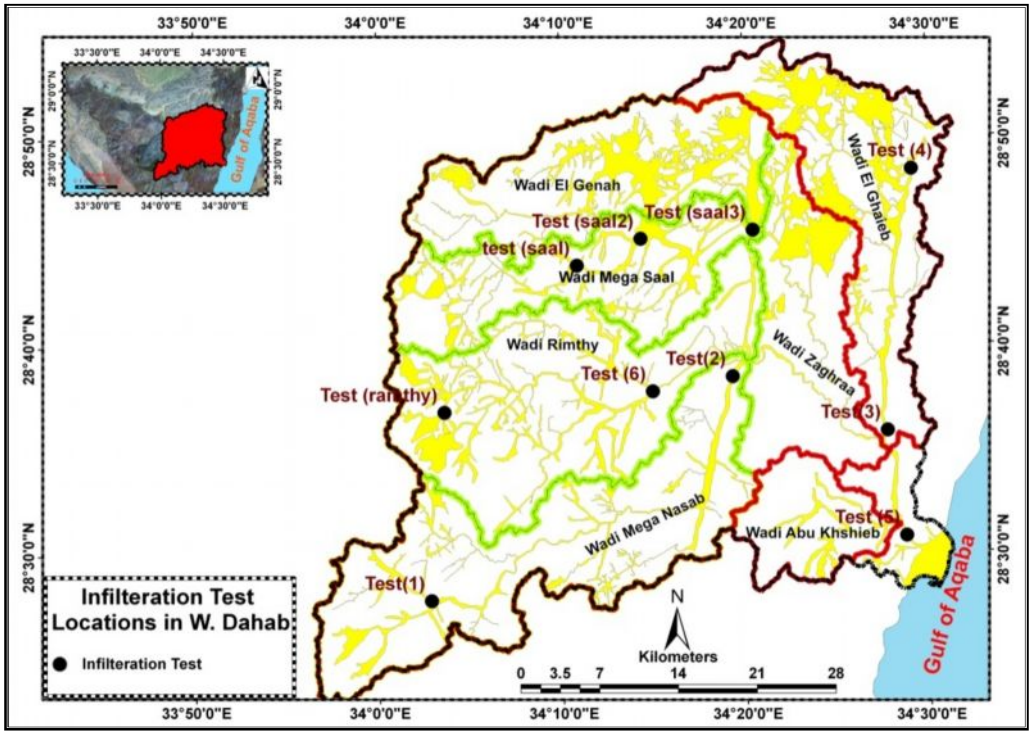

Figure 64: Location Sites For Infiltration Tests

In this study, the infiltration tests were completed at 7 different locations along the main stream course of W. Nasab, W. Rimthy, W. El Ghaieb and at the downstream of Dahab basin as shown in figure 64. The field tests were carried out by using the double ring infiltrometer and applying the Philip (1957a) method for measuring infiltration rate (I). Directly after finishing the test, a cross section of the tested area was drawn to the extension of the wet front in order to measure its depth. Core samples of the saturated soil were also collected to measure the hydraulic conductivity, saturated water content (θs) and initial water content (θ_0).

A constant head – permeameter method was used to measure saturated hydraulic conductivity (K) in the lab. It was based on direct application of Darcy's equation for a saturated soil column of uniform cross- section area. The disturbed core samples representing each layered profile were covered at one end with a piece of cloth held in place with the aid of rubber bands and allowed to stand overnight in water to ensure complete saturation. Saturated hydraulic conductivity (K) was calculated using Darcy's equation:

$$K = \frac{V * L}{A * t * H} \qquad \textbf{Equation (12)}$$

Where **K** = saturated hydraulic conductivity in cm/s, **V** = Volume of water in cm^3, **t** = Time in seconds, **A** = cross section of core samples in cm^2, **L** = Length of soil samples in cm and **H** = change in head in cm.

The obtained results from field tests showed that the infiltration rate of the examined sites vary between 0.013 cm /min (0.18 m/day) at the outlet of W. Nasab, 0.59 cm/min (8.4m/ day) at the upstream site of W. Saal and 0.38 cm/min (5 m/day) at the upstream site of W. Rimthy (fig. 65, Table 14). The examined soil section of each test indicated that grain size of sediment is the main factor controlling the infiltration capacity. Along the upstream parts, the soil is characterized by poorly sorted grains. It is composed of variable grain size ranging from coarse boulder to fine sand. While the soil of downstream large sections is characterized by successive sequences of gravel and sands along the main stream course, in the lower part of the section, grain size and circularity and massif silty sand decreased.

	Qvs	*Qvi*	*t* $min^{1/2}$	*x* *cm*	*Sp* $cm/min^{1/2}$	*K* *cm/min*	*I* *cm/min*
Ramthy (1)	0.310	0.075	10.4	85	1.92	0.25	0.38
Ramthy (Downstream)	0.380	0.050	23	65	0.9	0.01	0.02
Nasab (1)	0.380	0.030	13	95	2.5	0.022	0.12
Nasab (Downstream)	0.320	0.060	33	74	1.9	0.011	0.013
El Ghaieb (1)	0.380	0.080	9.2	80	2.5	0.18	0.32
El Ghaieb (Downstream)	0.330	0.020	32	70	0.62	0.012	0.0189
Saal	0.210	0.090	11.62	75	1.2	0.61	0.62
Saal (2)	0.310	0.064	9.64	46	1.17	0.42	0.48
Saal (3)	0.390	0.058	9.87	41	1.39	0.52	0.591
Dahab (Downstream)	0.260	0.075	15.49	65	0.77	0.041	0.065
					Avarage	**0.2076**	**0.2628**

Qvs: Volume of water content of saturated sample **Qvi**: Volume of water content of dry sample

t: Time of Test **Sp:** Sorpativity **x:** depth of wetted front

Table 14: The Result of Infiltration rate (I) in the field and Hydraulic Conductivity (K) in the Lab of Alluvial Deposits.

The figure 65 shows the estimated infiltration capacity in each of the sub-basins of W. Dahab. The examined infiltration capacity of 0.26 cm/min (2.4 m/day) at W. Dahab basin (356 km^2) means that the alluvial cover has an infiltration capability of 708 million m^3/day if the sediments are dry or

partially saturated. While the average infiltration rate capacity at W. Nasab (43 km^2) was 0.06 cm/min (0.8 m/day), this means that the alluvial cover has an infiltration capacity amount of about 34.3 million m^3/day. At the W. Rimthy (53.8 km^2), the average infiltration rate is about 0.2 cm/min (2.6 m/day), that means 140 million m^3/day. The average infiltration rate in W. El Ghaieb (40 km^2) is 0.14 cm/min (1.8 m/day) amounting to about72 million m^3/day while at W. Saal (37 km^2) the infiltration amounts to about 8 m/day, according to Shendi et al. (1997), meaning more than 300 million m^3 /day can be passing through alluvial covers (fig. 65).

Now, the lab results of hydraulic conductivity for examined soil will be discussed. The saturated core samples were examined in the lab to measure hydraulic conductivity. The results show that the hydraulic conductivity varies between 0.011 cm/ min and 0.25 cm/min. The investigations of core sample sediment shows that hydraulic conductivity increased at the upstream side of W. Rimthy and W. El-Ghaieb, where it ranges between 0.18 to 0.25 cm/min (2.5 to 3.6 m/day), while at W. Nasab the hydraulic conductivity decreased to 0.02 cm/min (0.2 m/day). The values of hydraulic conductivity decrease at the downstream of the wadis ranging from 0.4 to 0.011 cm/min (0.15 to 5 m/day).

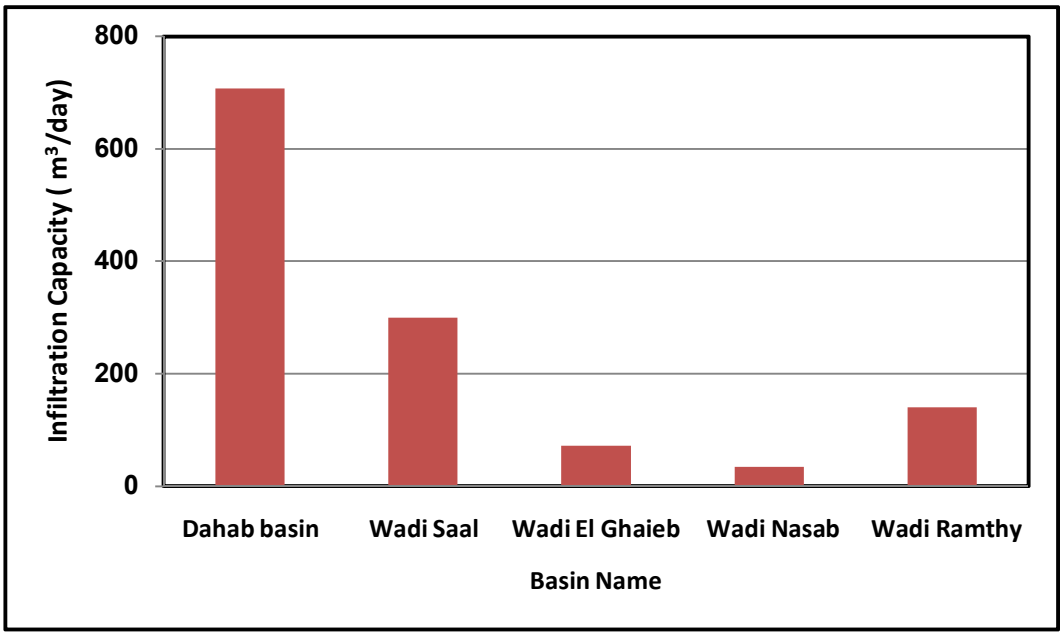

Figure 65: Estimated Infiltration Capacity of Alluvial Deposits in each Subbasins in W. Dahab

Accordingly to the results, the plain areas (low gradient) can be recommended for further groundwater exploitation. However, due to lack of information about the thickness of alluvial deposits in the basin, a detailed geophysical investigation is recommended to determine their geometric configuration and consequently, their capacity to restore groundwater, especially at W. Rimthy, W. El Ghaieb and W. El Genah. It should be mentioned that alluvial deposits represent about 17 % of the total area of the Dahab basin. These areas are characterized by increased groundwater recharge in comparison with basement rocks. It fills the wadis and some parts of the upstream areas in W. Dahab basin. While 70% of Dahab basin is covered by basement rocks, especially at the southern, western

and north eastern parts of the upstream areas. Therefore, the runoff from the upstream sites is high due to narrow, high slope drainage and low conductivity of basement rocks which cover the drainage system. It can be concluded that hydraulic conductivity of basement rocks is considered more representative for groundwater recharge, especially at the areas of highly flooding risk.

3.2.2 Hydraulic conductivity of fractured Basement Rocks

Hard rocks and their associated aquifers occur in many areas of Dahab basin. The importance of hard-rock aquifers for hydrogeological and water management issues differ from one place to another, depending on various factors, especially on the overall availability of water and the water demand. El-Rayes (2004) measured the yield of wells draining the basement rocks at Saint Catherine area relative to the dominating lineaments and joints. He obtained yield values that ranged from 5 to 12.3 m^3/day. The length and frequency of fractures have an important influence on the recharge and yield of the Basement aquifer (El-Rayes, 2004).

Fractures play a vital role as conduits from the recharge zone into the alluvial aquifer that feed production wells in the low-laying fault zones of the basement aquifer (El-Rayes, 1992). The presence of water conduits reaching the recharge zone may enhance the productivity of the adjacent wells (El Rayes, 2004). The rainwater is directly infiltrated and stored in highly fractured basement rocks, especially in the upper unit, gradually transmitted into both the fault zones and the alluvial aquifers through the low density fractured unit as shown in fig.66.

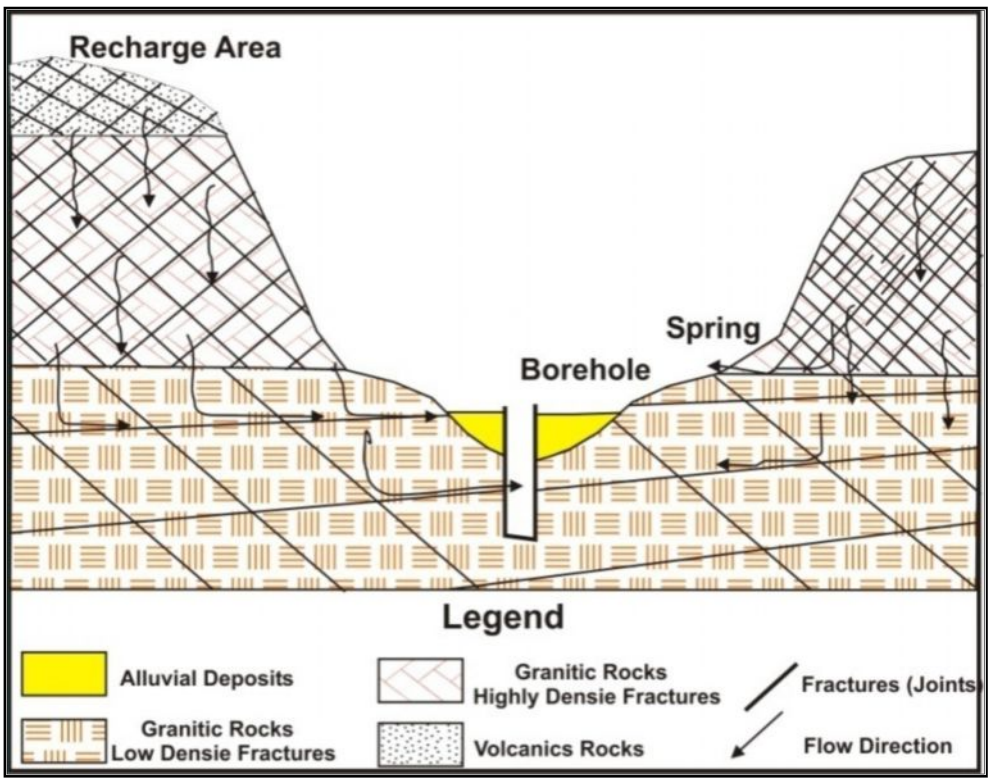

Figure 66: Schematic Hydrogeological Cross section of the Upstream Part of W. Dahab (Modified after El Rayes, 2004)

The lengths and frequency of the fractures have a great influence on the groundwater recharge, its storage and yield. The fracture densities were defined by measuring different length of the fractures and by calculating the average value for that site. Consequently, structurally deformed rocks which were extensively jointed are likely to contain larger amounts of groundwater.

Zeeb et al. (2010) developed a method to qualify and quantify fluid flow through deterministic discrete fracture network (DFN) based mainly on satellite images and to estimate in situ hydraulic apertures for the upper Waji sandstone aquifer in Saudi Arabia. Blum et al. (2005) developed the code (Frac Frac) to generate DFN based on power-law fracture length distribution using a density constant and a fractal dimension which is based on fractured length. For visualization, Blum et al. (2007) developed fractures connected to the Visual basic code in order to find out how to cut out the area from fracture trace lines. This method is related to an area of 100 m×100 m. The code can scan each fracture for the intersection nodes with other fractures.

The main objective is to estimate the hydraulic conductivity of fractured basement rocks. The extracted lineaments from Satellite images were used to develop an additional method to quantify fluid flow through DFN. Based on DFN simulation (Zeeb et al., 2010), it was possible to determine the hydraulic conductivity tensor of the fracture system. The obtained results were compared with the previous published data (Yair and Lavee, 1976) to define the relative hydraulic conductivity of the basement rocks in our study area.

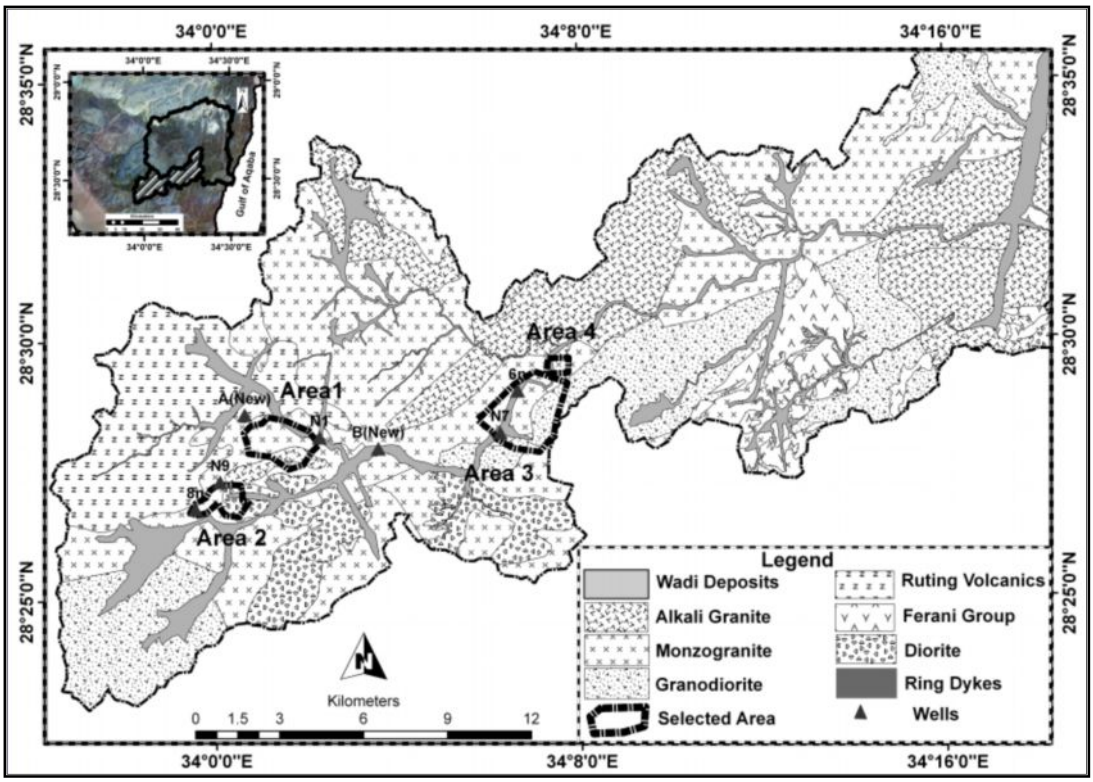

Figure 67: Location of Investigation Sites

Four different localities were selected as test sites at basement outcrops in the study area, especially at W. Nasab. These sites were selected to investigate the structural network in order to define the hydraulic conductivity of hard rocks. These localities are sited near the wells number 1, 6, 7 and 8 (fig. 67). The sites are located near hand dug wells which people use for agricultural purposes. Different rock types were exposed in selected sites as monzogranites, granodiorite, volcanic and alkali granites (fig. 67).

3.2.2.1 The Method of investigation

The proposed procedure for getting lineament traces of the study area used Landsat data (ETM+ 7) which relies mainly on the Landsat bands 1,2,3,4,5 and 7 with 30 m resolution and panchromatic band 8 with a 15 meter resolution band as in chapter 1. The fracture traces were described by the endpoint coordinates of each fracture. The generation of the fracture trace map was accomplished by combining Landsat ETM+ data (manually and automatically extracted) and adding extra data from Google Earth after a georeferencing procedure. The remote sensing data was complemented with field data measurements using a GPS device to enhance fracture data converge and accuracy. The field data included observation and measurement of structural elements. The major structures encountered joints, dykes and faults. In order to calibrate the significance of fracture arrays, the results of lineament analysis were compared with the measured field data. The proposed overall process flow for extraction of lineaments in selected sites is shown in figure 68.

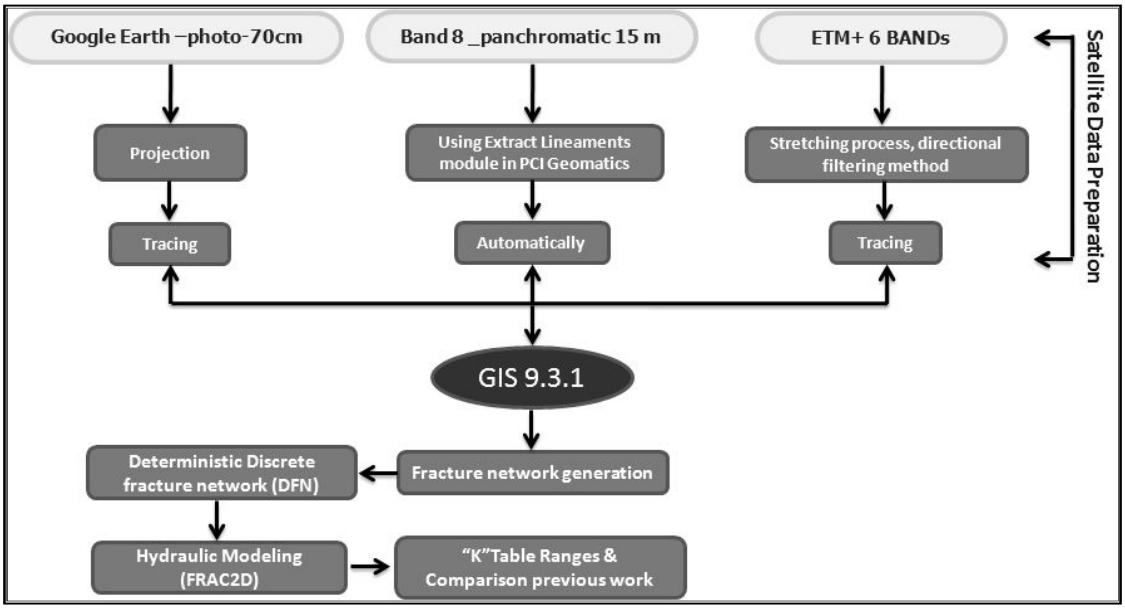

Figure 68: Flow Chart of the Used Data Layer For Lineament Extraction

The length data of the extracted lineaments from satellite images shows a truncation effect. Truncation is a typical effect caused by the limitations of techniques to detect lineaments below a certain size (length or width). When approaching the detection limit, fewer lineaments were recognized (Pickering et al., 1995; Bonnet et al., 2001). The truncation bias was accounted by

applying the chord method proposed by Pérez-Claros et al. (2002) and Roy et al. (2007) as shown in fig. 69. The summarized results of trace line map analysis are shown in table 15.The chord method was used for determining the cut-off point. This method connected the leftmost and rightmost data points on the plot with a straight line (chord); then, the perpendicular distance between each of the remaining data points on the plot and the line was calculated (fig.69). The data point that gave the largest distance was designated as the cut-off and all points to the left were discarded. It allows independent estimation of fractal dimensions of the curve for both large and small measurement scales and also ignored the points that should not be used in the calculations. The chord method was considered the best among the many possible methods of determining the cut-off point, as it was the only method that was not dependent on several tuning parameters.

Area	Well No.	Traces [-]	Min-length [m]	D [-] (1)	Density [m^{-2}] (2)
1	1N	143	150	2.30	0.03
2	8N	75	142	1.87	0.015
3	7N	279	170	2.16	0.025
4	6N	143	40	2.27	0.09

(1) **Exponent of the power-law distribution.**
(2) **Density extrapolated for a lower length cut-off measured and reported in (Oada, 1995)).**

Table 15: Results of the Trace Line Map Analysis.

Different sets of fractures were distinguished using rose diagrams (fig. 70). At each location we could distinguish four different fracture sets, the first one was directed between 5°- 60°, the second was directed between 60°-105°, the third was between 105°-165°, and the last one was between 165°-5°. These sets were consistent all over the study area, varying by 5°-10° at most. After distinguishing between the different sets, the number of fractures belonging to each set was counted to evaluate the specific fracture density of each set (fig.71).

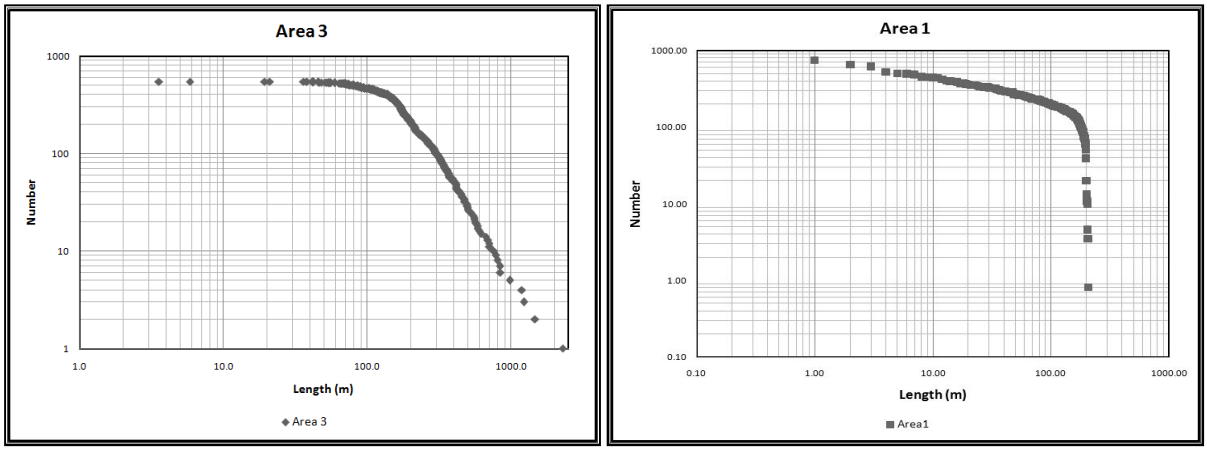

Figure 69: Results of Truncation Effect Result From Length Data of the Extracted Lineament in Area (1)and Area (3)

To develop the hydraulic conductivity model of the study area, FRAC2D model was used (Blum et al., 2005), which calculates the fracture-based fluid transport across the model boundaries. The fluid flow between two points is calculated by applying the cubic law assumption (Snow, 1965; Louis, 1967). The main fluid flow direction in the fractured aquifer can be obtained from conductivity

ellipsoid or tensor, which can be derived from principal hydraulic conductivities and their orientation (Zeeb et al. 2010).

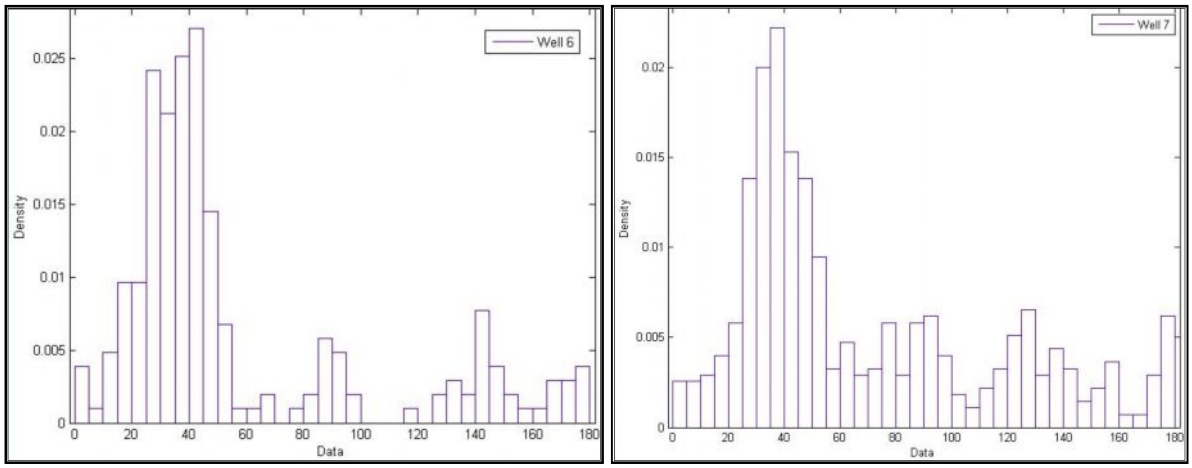

Figure 70: Orientation Rose Diagram of Fractures at Area around Well 6 & Well 7

3.2.3.2 The result and evaluation

Based on remote sensing, methods of Jackson et al. (2000) and the modified method of Blum et al. (2005), the obtained results showed that most of lineaments were directed to NE with more than 40 % while N-S and E-W directions occurred with lower percent amounts. An automatic extraction from a single band (panchromatic band 8) was applied for minor lineaments. The rose diagram of W. Nasab indicates that the main directions are NNE, NE, NNW and WNW (fig.71).

The NE and NNE directions are the most predominant directions in W. Nasab which range from 25 to 28 %. A final lineament map was constructed from the digital enhancement of individual single bands and multiband images together with their own field data and other previous work data. Four stations were setup near the area of investigation in order to study fractures' directions in the field and to evaluate extracted lineaments from the image. Through fracture traces analysis of field data and image extracted lineaments, four sets of fractures were recognized (fig. 72). Field data assured that the main trends of the fractures in basement rocks were NNE, NE, NW and NS as they were measured at four investigated areas.

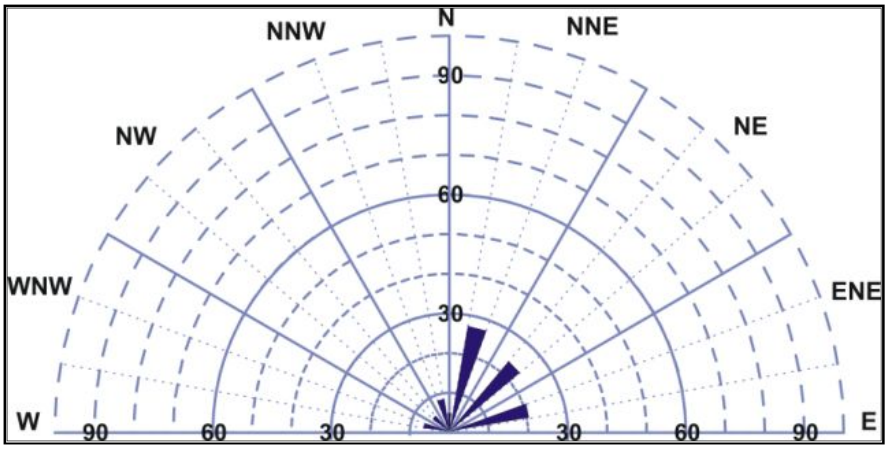

Figure 71: Trend Diagram of Minor Fracture Measurements at W. Nasab Area

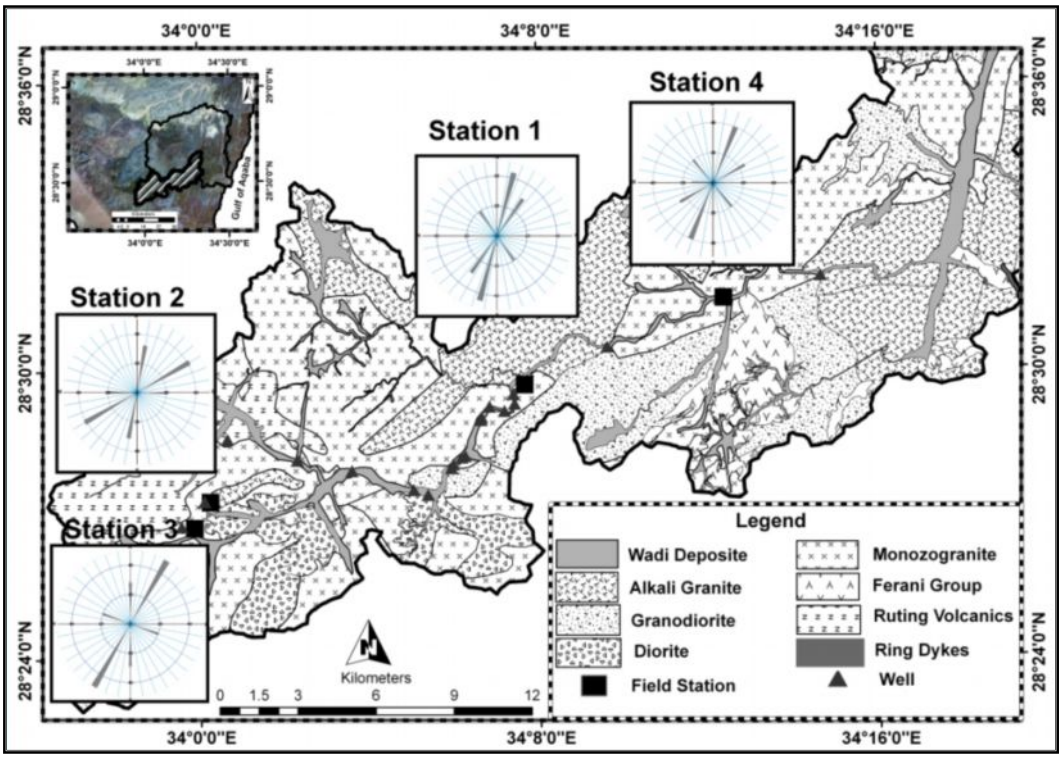

Figure 72: Field Measurements of Lineaments at W. Nasab Area

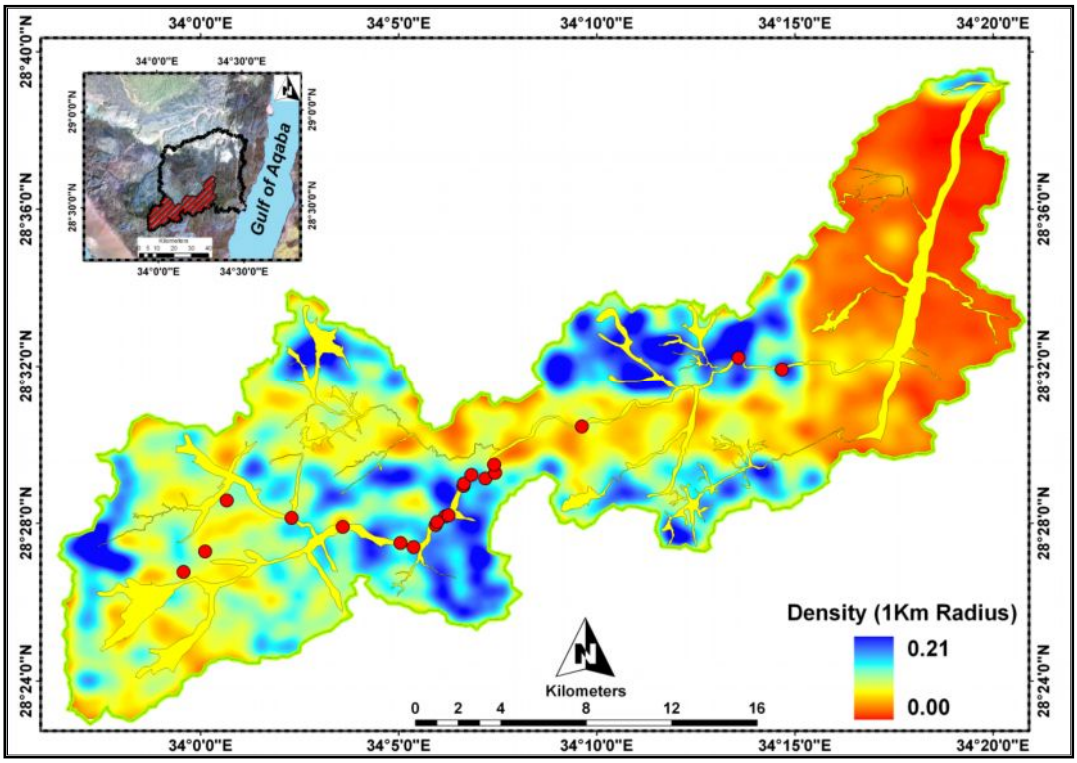

Figure 73: Lineament Intersections Density of Basement Rocks of W. Nasab Area

The density of lineaments increases in the vicinity of fault zones making them favorable for percolation and storage of rain water. The map of lineament density shows the frequency of intersections that occur in a unit cell. The purpose of using intersection density maps is to estimate the

areas of diverse lineament orientations. The density of lineament intersection was produced by counting the number of lineament intersections per unit area. The intersection of lineaments within the study area has mainly a strong effect on rainfall percolation into the basement aquifer (fig. 73). The density of lineament intersection at circle of 1km radius ranges between 0.22 to 0.001 (No./km^2). The figure shows that most of the production boreholes are located in W. Nasab, the high lineament intersection density zones.

As mentioned before, FRAC2D uses the endpoint of the fractures within DFN to calculate the flow across its boundaries. Four DFNs were setup for investigation sites as shown in figure 74. The trace map from Area 2 (Monzogranite and volcanic) and Area 4 (Alkali granite and Monzogranite) show a good connectivity between different fractured sets. The backbone of DFN proved this connectivity between the boundaries. On the other hand, Area 1 and Area 3 show that the connectivity between fractures and DFN boundaries was lower than in areas 2&4 due to the lower density of lineaments in these areas and the intersection with covered weathered material from country rocks.

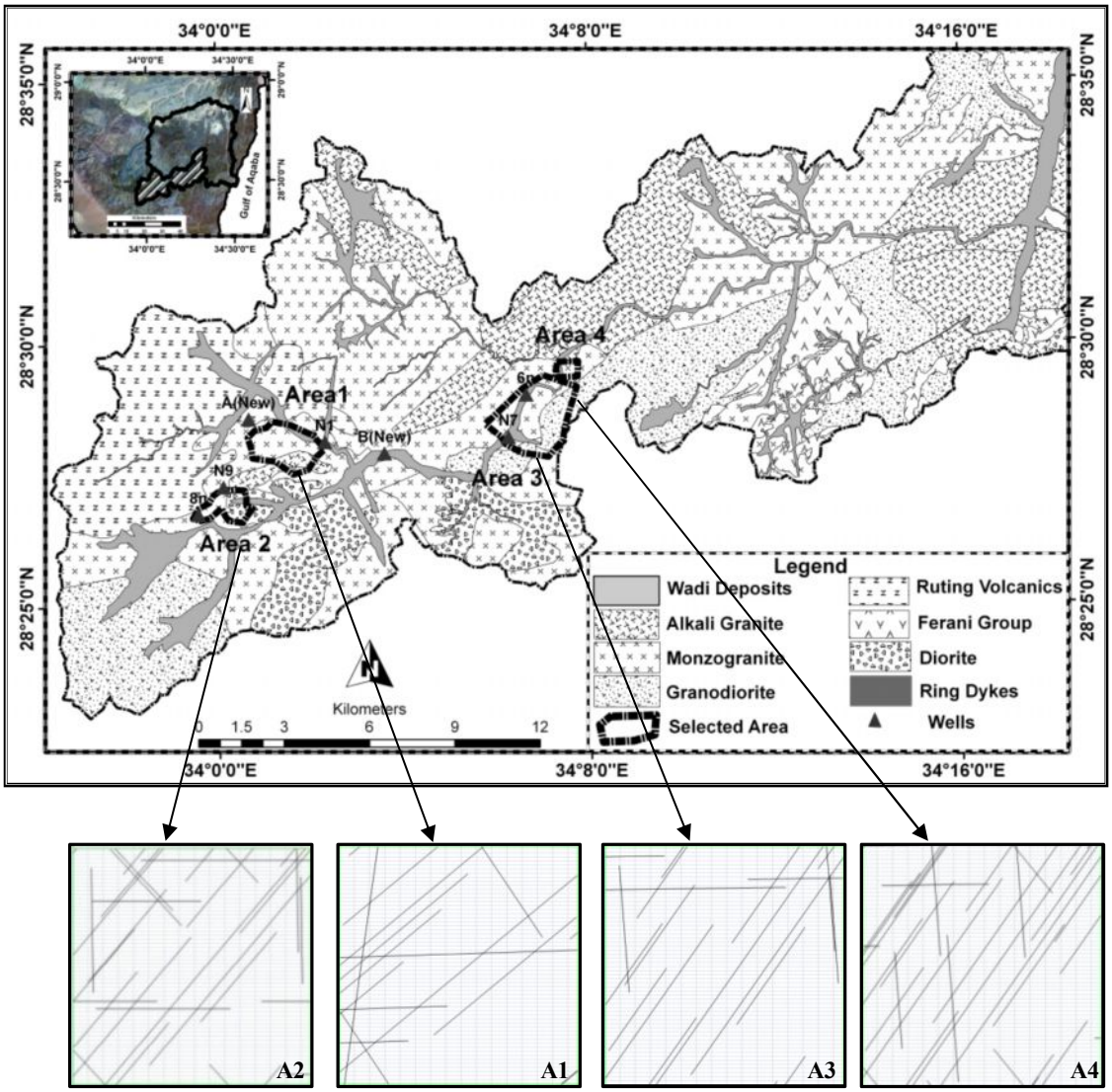

Figure 74: The DFN for Investigation Areas (A1-A4)

The hydraulic aperture was investigated in the field study and the average value (0.5mm) was taken in consideration in the model. In the hydraulic modeling of DFN for area 1 near well 1, the maximum hydraulic conductivity (K_{max}) is 3×10^{-7} m/s with evaluated flow direction of 10 ^{o} ; for area 3 near well 7, the hydraulic conductivity is 2.3×10^{-7} m/s with an evaluated flow direction 6 ^{o} ; for area 2 near well 8, the hydraulic conductivity is 4.3×10^{-7} m/s with evaluated flow direction 12 ^{o} and for area 4 around well 6, the hydraulic conductivity is 6.1×10^{-7} m/s with an evaluated flow 30 ^{o}. The average hydraulic conductivity is 4×10^{-7} m/s (2 mm/hr). The result shows that the flow of water along the fractures was strongly controlled by the main orientation of the structural lineaments of W. Nasab (NNE-SSW and NE-SW fracture set (see-fig. (75) & table (16)).

The evaluation of the hydraulic conductivities was a big issue due to the limited number of relevant field measurements, especially on fractured basement aquifers (e.g., stream flow and pumping test) in the study area. The results obtained from the FracFrac program concerning the range of hydraulic conductivity were compared with the field measurements concerning the hydraulic conductivity and the infiltration tests of previous field experiments done by Yair and Lavee (1976) and Freeze and Cherry (1979).

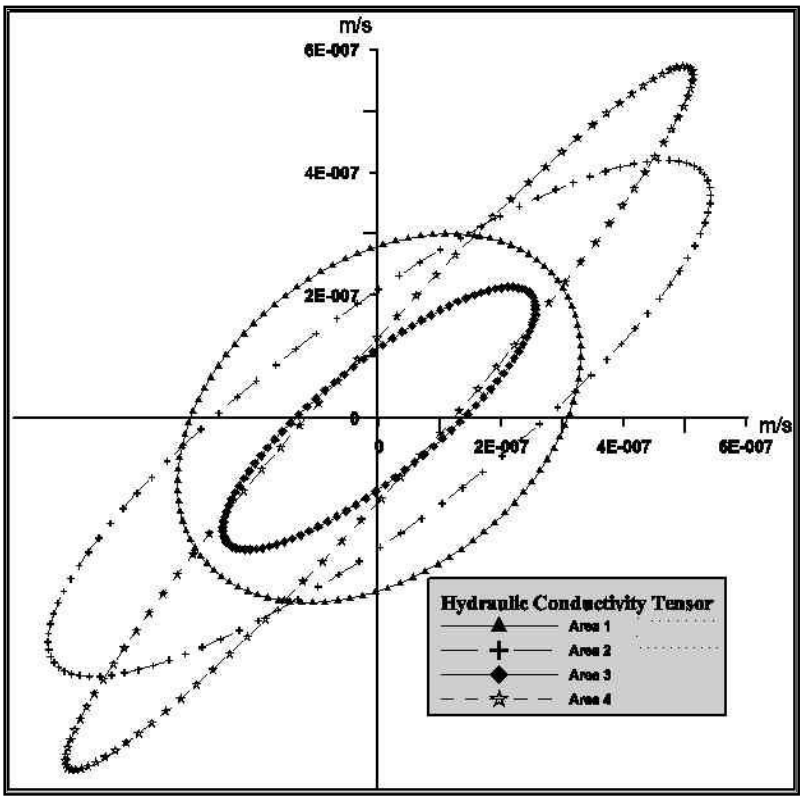

Figure 75: Hydraulic Conductivity Tensors for the Studied Discrete Fracture Networks (DFN) at Four Investigation Area at W. Nasab

The results of the experiments carried out by Yair and Lavee (1976) in the north eastern sector of Sinai were used for comparison with our evaluation due to similar geologic and hydrogeologic

settings of neighboring areas. They simulated rainstorms with different intensities on different outcrops of fractured basement and sedimentary rocks. These simulations aimed to measure the runoff yield and to calculate infiltration rates. The results for infiltration rates of fractured basement outcrops ranges between 2.6×10^{-6} m/s to 6.5×10^{-7} m/s. Freeze and Cherry (1979- p.29, table 2.3) stated that the hydraulic conductivity for fractured basement ranges from 10^{-4} m/s to10^{-8} m/s. It can show that the results of the hydraulic conductivities from DFN are located within the range of the previous evaluated values.

The fractured basement rocks cover more than 70% of the study area, especially in the western, southern and northern parts of study area. These rocks represent the main receptor of rainfall which may cause surface runoff in the study area. For the calculation of the total loss of rainfall, the average hydraulic conductivity of fracture basement rocks 4×10^{-7} m/s (37 mm/day) should be used. It means that the fractured basement of the examined W. Dahab Basin (1454 km^2) has a capability to pass a quantity of water equal to 43 million m^3/day.

The method which was used in this study can be applied in arid environments, as well as with small grass coverage as in Sinai and in the Arabian Peninsula. This remote sensing model study can help researchers to investigate areas of various sizes, in addition to reserving time and money for investigations. It is recommended to visit the site to undergo pumping tests in order to evaluate the results that were extracted from this model.

	Rock Type	Constant	FractionalDimension	Min. Length	Max. Length	Spacing				Orientation				Thickness	SR	GR	Max. K	Orientation
						set1	set2	set3	set4	set1	set2	set3	set4	Apperture			m/s	
Area 1	Monzogranite & younger granite	5.87	2.3	5	500	1.55	8.81	4.1	6.9	49.85	90.95	132.8	180	0.0005	25	100	3.00E-07	0,18 (10^{0})
Area 3	Granodiorite & Monzogranite	3.66	2.16	5	500	1.54	4.66	6.07	32.65	36.24	81.92	133.3	176.5	0.0005	25	100	2.50E-07	0,08 (4^{0})
Area 2	Monzogranite	2.08	1.87	5	500	0.77	4.4	2.06	3.47	39.6	1.8	123.8	82	0.0005	25	100	4.70E-07	0,158 (9^{0})
Area4	Monzogranite & younger granite	3.56	2.27	5	500	0.52	3.8	7.1	4.3	54.8	0.7	129.4	94.4	0.0005	25	100	6.10E-07	0,47 (27^{0})
																Avarage	4.08E-07	

Table 16: Result of Hydraulic Conductivity of Fractures Basement Rocks at Selected Areas in W. Nasab.

3.3 Hydrogeochemical Properties and Environmental Impacts

3.3.1 Introduction

Water quality is one of the most important aspects in groundwater studies. Hydrochemical investigations reveal the quality of water is suitable for drinking, agricultural and industrial purposes. Furthermore, it is possible to understand the change in quality due to rock-water interaction or any type of anthropogenic influence.

Groundwater quality can be defined as the physical, chemical and biological state of groundwater. Temperature, turbidity, color, odor, and taste make up the list of physical parameters. Naturally, groundwater contains ions. These ions slowly dissolve minerals in soils, rocks, and sediments during water flow along its flow path. Some small portion of the total dissolved solids might have originated from precipitation water that recharges the aquifer. Ions most commonly found in groundwater include: Na^{+}, Ca^{2+}, Mg^{2+}, HCO_3^{-}, Cl^{-}, and SO_4^{-2} with SiO_2 forming the major dissolved constituent. In addition, minor ions include NO_3^{-}, F^{-} ; K^{+} and heavy metal such as Zn^{2+} and Fe^{2+} that are represented with lower concentrations. The concentration of these ions gives groundwater its hydrochemical affinity and often reflects geological origin and hydrogeologic regime. In the present study, great attention was paid to investigate the physico-chemical parameters of groundwater.

Understanding factors that affect groundwater quality could help the decision maker to select water of proper quality for a particular application. The major factors that directly or indirectly affect groundwater quality include climatic influence (rainfall, temperature, evaporation etc.), permeability of rocks and the chemical properties of the sediments flown through by the groundwater. Representation of hydrochemical data in graphical form helps to understand the complexity of groundwater systems. Methods of representing water chemistry are exhibited by the proportions of ionic concentrations in individual samples. Normally, a series of diagrams are used to interpret and classify groundwater chemistry.

Water wells in W. Dahab are not well distributed over the entire basin. They are concentrated at some locations along the upstream portion of the basin (at W. Nasab, W. Rimthy and W. Saal) and along the downstream portion of the basin in the alluvial fan deposits of W. Dahab. Except the wells near Dahab city, all others are not drilled wells; they are not protected by casings and do not close by well head but are open water holes. Surface runoff can flow into holes and mix with the groundwater. Water contaminations may happen due to humans or animals; therefore, it must be considered that the measured water quality differs from pure groundwater, to a certain extent. Twenty-nine water samples were collected along two periods related to climatic condition. The first period was in April 2009, which represented the dry season while the second one was in January 2011, which represented a period of the rainy season.

Detailed chemical analyses of groundwater samples have been carried out including the determination of total dissolved solids, pH, temperature, electrical conductivity, major cations of sodium (Na^+), potassium (K^+), calcium (Ca^{2+}) and magnesium (Mg^{2+}), major anions of bicarbonate (HCO_3^-), chloride (Cl^-), Sulfate (SO_4^{-2}), and heavy metals (Hg, Cd, Pb, As, Cu, Cr, Co, Ni, Zn, Mn, Se, Ba, Ti, Zr, Fe and U). The results of the analyses of the major elements of the first period were carried out at the laboratory of Groundwater at Faculty of Science, Suez Canal University, Ismailia, Egypt, while the heavy metals and major elements of the second period samples were analyzed at the Chemical Laboratory at Hoehnheim University, Germany, and the Groundwater Lab. of the Geological Institute at Tubingen University, Germany. Chemical analyses for all major ions, as well as some minor ions (NO_3^-, F^-, Br^-), were carried out with the Dionex DX-120 ion chromatograph. The water samples for the measurement of heavy metals were filtered through 0.45µm filters, preserved with 5ml 6 N HNO_3, bottled in polyethylene bottles and then analyzed using ICP-MS.

This chapter aims to determine the chemical and physical properties of groundwater drained from the existing aquifer of W. Dahab Basin area and to study the pollution of groundwater resulting from domestic and agricultural uses of water. In addition, it also aims to assess the groundwater usability for irrigation and drinking purposes relative to the World Health Organization standards (WHO, 2006).

3.3.2 Physical and Chemical Parameters

In the following sections, the specifics of each physico-chemical parameter are discussed in detail and listed in Table 17.

3.3.2.1 Electric conductivity (Ec)

The electric conductivity (Ec) is a useful indicator of the total dissolved solids (TDS) because the conduction of the current in an electrolyte solution is primarily dependent on the concentration of ionic species. Ec of water samples is commonly used to examine the mixing of fresh water with seawater (Hiscock et al., 1996), to estimate relative contributions of precipitation and subsurface water in stream hydrograph (Kobayashi, 1986), and for the dilution gauging of stream discharge (Dingman, 2002, p. 614). The relationship between Ec and TDS depends on the chemical composition and ionic strength. The linearity relationship occurs with total dissolved salts and can be calculated approximately regarding the following equation (13) and figure (76).

$$TDS = 0.64 * Ec\ (\mu s/cm) \qquad \textbf{Equation (13)}$$

Ec values of the studied samples range from 491 to 6320 µs/cm. The average value at W. Nasab is 693 µs/cm whieh increases at the downstream area; electrical conductivity at the upstream area is 491(well N1) and increases to 1281µs/cm at the downstream (well N11). In W. Saal, the value of Ec

	No.	Name	Cation												Anions										Ion Balance	EC (µs/cm)	TDS	PH
			Si	Si	Na	Na	K	K	Mg	Mg	Ca	Ca	NH4	NH4	Cl	Cl	SO_4	SO_4	HCO_3	HCO_3	NO_3	NO_3	F	Br				
			mg/l	epm	mg/l	epm	mg/l	epm	mg/l	epm	mg/l	epm	mg/l	epm	mg/l	epm	mg/l	epm	mg/l	epm	mg/l	epm	mg/l	mg/l	%		mg/l	
Wadi Nasab	1	A	9.4	1.3	32.39	1.41	2.21	0.06	11.87	0.98	75.99	3.79	0.52	0.03	48.96	1.38	97.11	2.02	167.8	2.75	5.00	0.08	1.70	0.08	0.66	540	345.6	8.14
	2	N1	10.5	1.5	31.69	1.38	1.90	0.05	11.33	0.93	62.31	3.11			46.52	1.31	54.15	1.13	153.70	2.52	31.58	0.51	1.21	0.12	4.88	491	314.2	8.13
	3	B	10.7	1.5	39.21	1.71	2.55	0.07	12.15	1.00	72.10	3.60			70.21	1.98	83.68	1.74	131.20	2.15	32.57	0.53	1.10	0.13	4.05	573	366.7	8.3
	4	N10	10.9	1.6	41.51	1.81	2.44	0.06	12.54	1.03	76.27	3.81			74.13	2.09	79.66	1.66	145.20	2.38	30.27	0.56	1.15	0.16	4.49	560	364.2	8.22
	5	N5	10.5	1.5	41.88	1.82	2.70	0.07	13.00	1.07	71.24	3.56			75.95	2.14	78.12	1.65	156.70	2.24	31.91	0.51	1.19	0.19	4.04	592	378.9	8.3
	6	N6	11.1	1.6	39.60	1.72	2.34	0.06	12.69	1.04	75.12	3.75			72.40	2.04	78.93	1.64	144.60	2.37	32.08	0.52	1.09	0.13	4.11	579	370.6	8.21
	7	N7	10.6	1.5	40.75	1.77	2.16	0.06	11.97	0.98	70.29	3.51			74.76	2.11	81.51	1.70	120.20	1.97	33.94	0.55	1.18	0.17	4.50	587	375.7	7.3
	8	N9	10.5	1.5	45.84	1.99	2.63	0.07	11.67	0.96	70.97	3.54			72.29	2.04	92.25	1.92	119.00	1.95	40.08	0.65	1.17	0.12	5.24	606	387.8	8.4
	9	N12	11.7	1.7	59.92	2.61	4.01	0.10	27.16	2.23	169.70	8.47			185.17	5.22	205.49	4.28	147.60	2.42	92.36	1.49	1.03	0.28	5.88	1135	726.4	8.13
	10	N11	12.3	1.7	91.80	3.99	2.07	0.05	24.96	2.05	166.72	8.32			205.32	5.79	224.10	4.67	132.40	2.17	111.04	1.79	1.71	0.33	6.62	1281	819.8	8.2
Wadi Saal	11	S1	11.5	1.6	268.54	11.68	7.15	0.18	41.73	3.43	305.84	15.26			556.16	15.69	464.35	9.67	184.9	3.03	134.63	2.17	1.99	0.98	3.68	2670	1708.8	7.70
	12	S2	12.0	1.7	380.07	16.53	18.38	0.47	49.89	4.10	331.73	16.55			849.24	23.96	438.43	9.13	177.5	2.91	103.00	1.66	3.01	1.60	2.26	3240	2073.6	7.30
	13	S2/1	11.8	1.7	175.26	7.62	7.53	0.19	21.68	1.78	144.17	7.19			377.08	10.64	194.95	4.06	65.3	1.07	63.53	1.02	2.29	0.57	3.16	1547	990.1	7.30
	14	S6	13.2	1.9	120.61	5.25	6.50	0.17	16.00	1.32	68.04	3.40			138.89	3.92	145.49	3.03	153.1	2.51	41.03	0.66	1.26	0.09	3.41	904	578.6	7.70
	15	S4	13.5	1.9	122.73	5.34	5.61	0.14	15.80	1.30	68.34	3.41			140.75	3.97	145.42	3.03	155	2.54	40.58	0.65	1.30	0.09	3.31	917	586.9	7.70
	16	S7	13.6	1.9	143.62	6.25	10.60	0.27	20.35	1.67	88.67	4.42			194.57	5.49	184.48	3.84	156.8	2.57	44.80	0.72	1.23	0.12	2.93	1130	723.2	7.60
	17	S13	13.9	2.0	161.71	7.03	6.83	0.17	25.26	2.08	110.11	5.49			218.00	5.15	205.43	4.28	222.7	3.65	43.82	0.71	1.10	0.15	2.44	1330	851.2	7.80
	18	MS8	15.3	2.2	159.07	6.92	3.01	0.08	17.89	1.47	79.32	3.96			165.86	4.68	174.66	3.64	209.9	3.44	41.94	0.68	1.69	/	2.77	1119	716.2	7.80
	19	S9	17.8	2.5	247.86	10.78	3.87	0.10	23.80	1.96	95.60	4.77			269.15	7.59	272.45	5.67	216	3.54	49.89	0.80	3.03	0.21	2.33	1573	1006.7	7.70
	20	S12	18.9	2.7	538.98	23.44	11.39	0.29	49.68	4.09	188.61	9.41			617.96	17.43	677.52	14.11	279.4	4.58	69.19	1.12	3.83	0.44	1.52	3160	2022.4	7.80
	21	S10	14.9	2.1	455.12	19.80	10.66	0.27	37.72	3.10	116.67	5.82			524.01	14.78	558.58	11.63	154.4	2.53	2.71	0.04	3.86	0.31	0.09	2570	1644.8	7.80
	22	S11	6.3	0.9	511.95	22.27	21.90	0.56	176.09	14.49	303.44	15.14			1052.28	29.68	910.99	18.97	228.2	3.74	4.15	0.07	0.79	/	0.06	4180	2675.2	7.60
Wad Rimthy	23	R1	10.4	1.5	78.86	3.41	4.29	0.11	21.35	1.76	129.84	6.48			206.57	5.83	116.01	2.42	101.3	1.66	114.69	1.85	1.44	0.35	8.54	1145	732.8	7.90
	24	R2	12.0	1.7	80.81	3.51	2.41	0.06	15.04	1.24	80.78	4.03			150.81	4.25	86.27	1.80	128.1	2.10	42.46	0.68	2.16	0.24	4.07	782	500.5	8.00
	25	R4	11.9	1.7	77.33	3.36	4.95	0.13	11.47	0.94	67.76	3.38			105.91	2.99	90.44	1.88	135.4	2.22	44.73	0.72	2.72	0.16	4.86	720	460.8	8.10
	26	R5	11.9	1.7	86.30	3.75	3.10	0.08	15.03	1.24	84.08	4.20			146.06	4.12	108.32	2.26	127.5	2.09	49.84	0.80	2.48	0.19	4.51	862	551.7	8.10
D-STR.	27	D4	9.8	1.4	746.97	32.49	31.81	0.81	31.33	2.58	832.64	41.55			2148.59	60.61	288.00	6.00	531.5	10.35	29.69	0.48	1.69	24.33	0.00	6320	4044.8	7.50
	28	D11	10.7	1.5	2677.83	116.48	119.20	3.05	50.08	4.12	2465.63	123.04			8246.60	232.63	507.18	10.56	212.9	3.49			1.22	89.47	0.00	17700	11328.0	7.20

Table 17: Results of Chemical Analyses of Groundwater Samples in Dahab Basin

reaches up to 2073 µs/cm at the upper reaches (well S2) and decreases downward to 586 µs/cm in well S4 at the middle of the wadi and increases again at the downstream portion of the basin to 2675 µs/cm (well S11). At the downstream of W. Dahab, the electric conductivity amounts to 6320 µs/cm (well D4) and increases to 11328 µs/cm at well D11, while at W. Rimthy, electric conductivity ranges from 460 µs/cm at well R4 to 732 µs/cm at well R1.

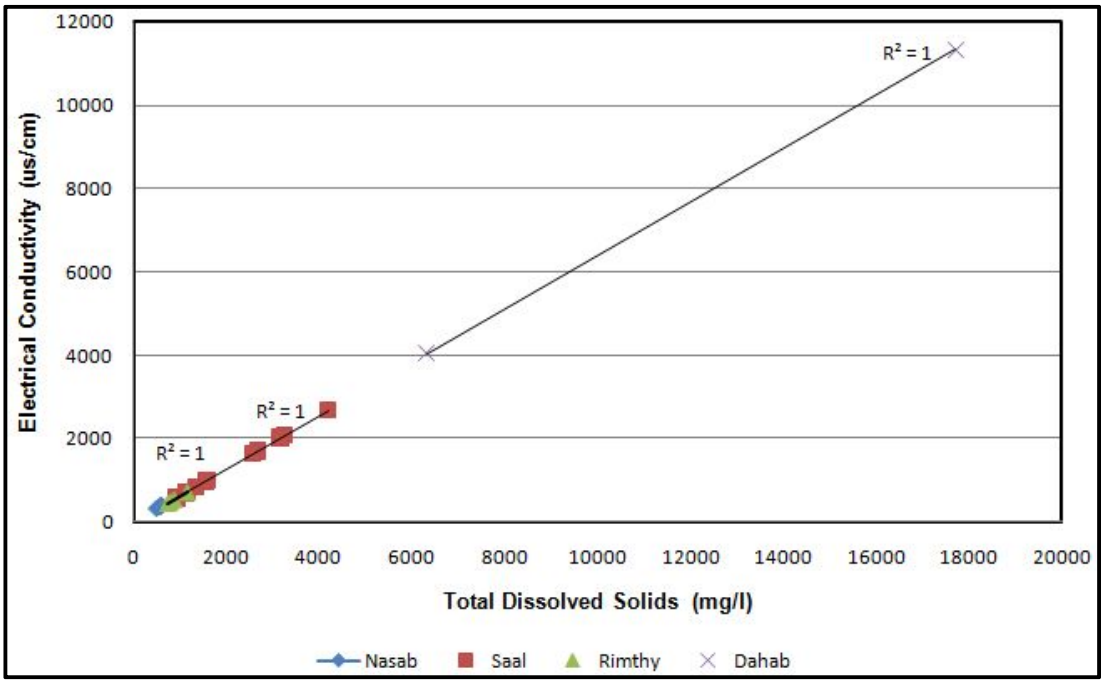

Figure 76: The Linear Relation between TDS and Electric Conductivity

It can be summarized that the electric conductivity values decrease at upstream parts of W. Nasab and W. Rimthy where these parts represent the western catchment of W. Dahab basin. These values reflect low TDS content in water of all wells in these parts of the wadi. At the downstream of W. Nasab, W. Saal and W. Dahab, Ec values increase from1250 to 11328 µs/cm. These values reflect the increase of dissolved ions in groundwater and hence, the TDS in these regions need enhancement.

3.3.2.2 Total Dissolved Salts (TDS)

TDS consist of inorganic salts and small amounts of organic matter that dissolve in water. Concentrations of TDS in water are considerably varied in different geological environs owing to the differences in mineral solubilities. The potability of water with a TDS level of less than 600 mg/l is generally considered to be good; drinking-water becomes significantly and increasingly unpotable at TDS levels greater than about 1000 mg/l (WHO, 2006).

The total salinity of the groundwater in Dahab basin increases from the upstream highland to downstream lowland areas, ranging from 314 mg/l at upstream to 4045 mg/l at the downstream of Dahab basin. In W. Nasab sub-basin, TDS increase gradually towards the downstream, ranging from

314 mg/l at the upstream to 819 at the downstream at well N11 (fig.77-A). In W. Saal, the TDS values are very high at the upstream, up to 2037 mg/l at well S2, then decrease in the middle of the stream course to 586 mg/l at well S4 and increase again toward the downstream to 2675 mg/l at well S11 (fig. 77-B).

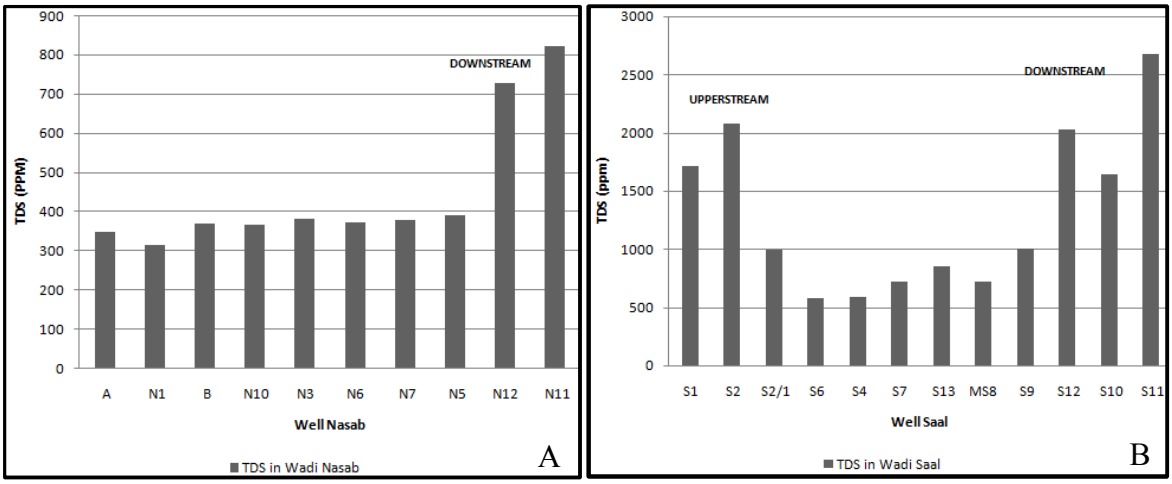

Figure 77: TDS Distribution in Dahab Basin, (A) W. Nasab and (B) W. Saal.

Generally, TDS values of most well waters of W. Dahab are lower than in the last 15 years, especially at the upstream parts of W. Nasab and W. Saal. In 1995, TDS values in water samples of W.Nasab range between 308 and 905mg/l. This range decreased to 314 - 819 mg/l in wells N5 & N11 (fig. 78). In W.Saal, TDS range from 606 to 3526 mg/l (Shendi etal. 1997), this range lowers to 586 - 2675 mg/l in wells S8 & S11 (fig. 78). The decrease in TDS may reflect a high precipitation frequency and the increasing recharge rate.

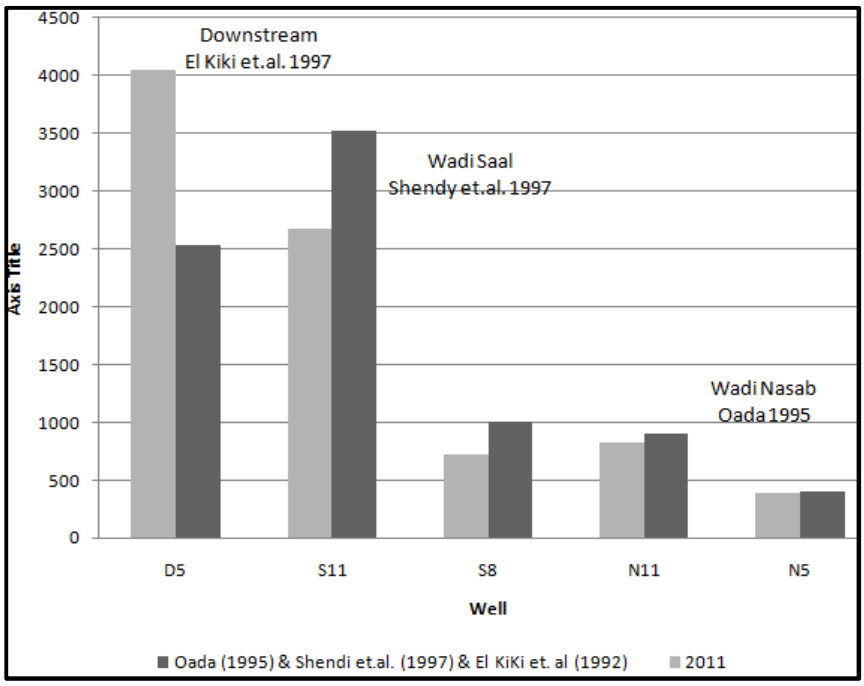

Figure 78: Comparison of TDS Values of Groundwater in W. Dahab Basin

On the other hand, the measured TDS range increases specifically at the downstream of W. Dahab where it increases to more than 4000 mg/l, compared to the previous measured values from 15 years ago that recorded 2500 mg/l (El Kiki et. al. 1992) (fig.78). The increasing of TDS may result from the impacts of a long flow path of groundwater within the alluvial aquifer, over-consuming of groundwater which led to the decline of the water table and the increase of TDS, and low amounts of precipitation at the downstream parts of W. Dahab, in contrast to the upstream parts.

Chebotarev (1955) classified groundwater into three classes based on salinity (Table 18). Most of the collected samples fall within the fresh water class, especially groundwater of upstream areas of W. Nasab and W. Rimthy within the good potable class (10 wells). Most of wells in W. Saal fall within the fairly fresh class. Wells at the downstream part of W. Dahab are definitely saline with TDS ranging from 4000 to 11000 mg/l.

The high salinity of groundwater in quaternary aquifers of the study area could be attributed to their long flow path, especially at the downstream of W. Nasab and W. Saal, while the high salinity of the basement aquifers (as in wells S1, S2 and S1/2) upstream of W. Saal could be attributed to the high content of pyrite mineralization in the bed rocks (basic rocks) and dykes of these localities (El-Rayes, 1992).

Water class	Water subclass	T.D.S (mg/l)	Sample No.
Fresh	Good Potable	<500	**A,N1,B,N10,N3,N10,N5,N6,N7, R4,**
	Fresh	500-700	**R2,R5,S6,S4,G2**
	Fairly Fresh	700-1500	**N11,N12,R1,S1/2,S7,S13,MS8,S9**
Brackish	Slightly Brackish	1500 - 2500	**S1,S2,S12,S10**
	Brackish	2500 – 3200	**S11**
	Definitely Brackish	3200 – 4000	
Saline	Slightly Saline	4000 – 6500	**D4**
	Saline	6500 – 7000	
	Very Saline	7000 – 10000	
	Extremely Saline	> 10000	**D11**

Table 18: Groundwater Classification of Dahab Basin Based on Chebotarev's Classification

3.3.2.3 pH

The pH scale ranges from 0 to 14 (very acidic to very alkaline) with 7 as the neutral condition at 77 ^{o}F and 7.5 at 32 ^{o}F. It is one of the most important parameters that describes groundwater quality,

because it controlls the amount of inorganic and organic solutes in groundwater. In most unpolluted water, pH is primarily controlled by the balance between free CO_2, CO_3^{--} and HCO_3^- ions as well as natural compounds such as humic and fulvic acids.

As formerly mentioned, rainfall is the most important source of water that feeds the existing aquifers in the study area. The pH value of the rain is about 5.6 due to the effect of carbon dioxide (Hem, 1985). The change in pH of groundwater is mainly related to interaction with lithology. World Health Organization (WHO, 2006) has established a secondary standard for pH which is between 6.5 and 9.5.The collected samples fall in the range from 7.2 to 8.4. Basic values may reveal the lithological variation and impact of mineral weathering. Most well waters of W. Nasab have a pH value that ranges between 8.1and 8.22, while in W. Saal, the pH values decrease to between 7.3 and 7.8. The pH values at W. Rimthy amount to 8.0 to 8.1. The pH decreases at the downstream of the Dahab basin where it ranges between 7.2 and 7.5. The variation of pH values is caused by mineral dissolution and impact of agricultural activities. Based on WHO standards, these waters are suitable for using as drinking water (fig.79).

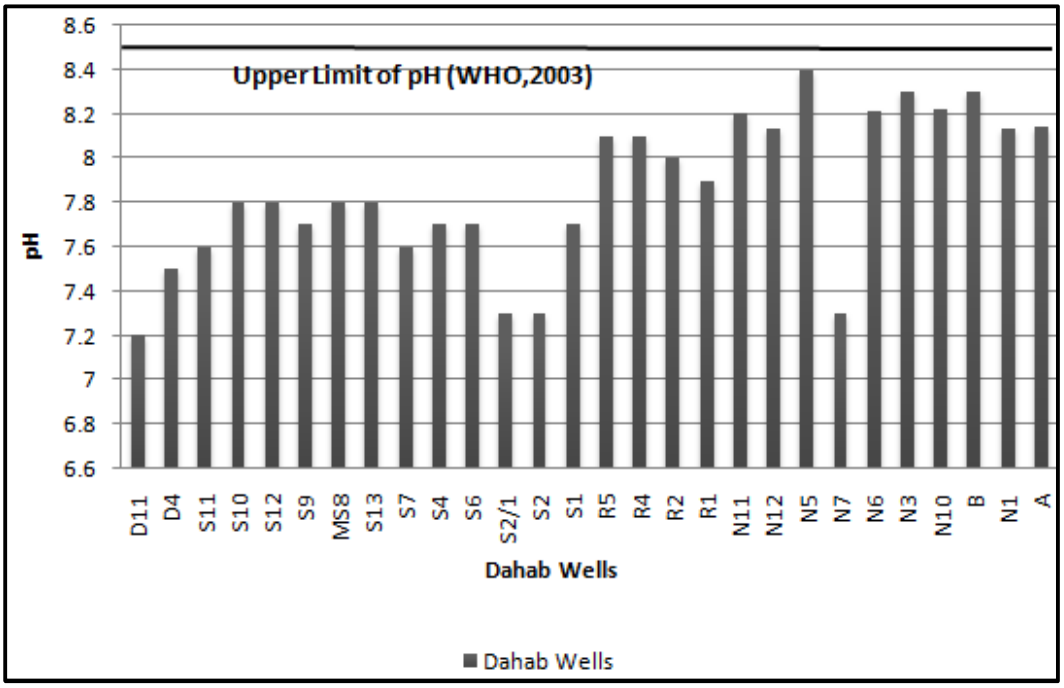

Figure 79: pH Distribution in Groundwater of Dahab Basin

3.3.2.4 Accuracy of samples analysis

A fundamental condition of electrolyte solutions, such as groundwater, is that on a macro scale, the sum of negative charges is equal to the sum of positive charges (Freeze & Cherry, 1979). The accuracy of the laboratory analysis, as well as natural or artificial influences, can be readily checked by looking at the anion-cation balance:

$$\text{Ion balance} = ((\sum C - \sum A) / (\sum C + \sum A)) * 100 \qquad \textbf{Equation (14)}$$

The total cation concentration is calculated as the sum of calcium, magnesium, sodium, and potassium; the total anion concentration is calculated as chloride, sulfate and hydrogen carbonate ions. When significant deviation from equality occurs, there must be either analytical errors in the concentration determinations or ionic species present at significant concentrations that were not included in the analysis. Normally, a charge balance error of < 10% is considered to be acceptable.

For all the water samples analyzed, the ionic balance was < 10% (see. Table 18). The highest error value occurred only at wells R1 with 8.6 % and N11 with 6.6 %. This is an indication that the data sets obtained were of good quality and all 29 samples will be used to determine the hydrochemical character of groundwater in Dahab basin.

3.3.2.5 Major elements

The concentrations of major ions in ground water depend on the hydrogeochemical processes that take place in the aquifer system. These processes occur when groundwater moves toward equilibrium in major ion concentrations. Hence, the study of concentrations of various major ions present in groundwater was used for the identification of geochemical processes.

The major dissolved components of groundwater include the anions hydrogen carbonate, chloride and sulphate, and the cations sodium, calcium, magnesium and potassium. The results of chemical analysis are listed in Table 17.The sources of major elements in water samples are discussed below:

3.3.2.5.A Chloride (Cl^-)

Chloride was found naturally in groundwater through the weathering and leaching of sedimentary rocks and soils and the dissolution of salt deposits. Chloride occurs naturally in some sedimentary bedrock layers, particularly shales. This chloride is a remnant of the seawater present at the time the rocks were formed. Chloride-bearing igneous rock minerals are few and igneous rocks in general appear to be a very minor source of chloride. Among the chloride-bearing minerals in igneous rocks is the feldspathoid sodalite, $Na_8\,[Cl_2(AlSiO_4)_6]$.

Kuroda and Sandell (1953) and Frape et al. (1984) suggested that chloride might replace the hydroxide in biotite and hornblende and might be in a solid solution in glassy rocks such as obsidian. In general, igneous rocks cannot yield very high concentrations of chloride in normally circulating natural water (Hem, 1985). Water from arid regions is often high in chloride contents (Milligan et al., 1966). It is not precipitated but is carried in solutions and attaches to sodium in the form of sodium chloride (NaCl).

Chloride concentration ranges between 46 to 8642 mg/l in Dahab basin. Low concentration occurs in W. Nasab, W. Rimthy and some wells in W. Saal (fig 80). At W. Nasab, chloride ions are low at the upstream portion (48 mg/l) and increase at the distal downstream part of the basin to 200 mg/l at

well N11 (fig.81).The average Cl content is enhanced in W. Rimthy, the concentration ranges between 105 to 264 mg/l where the maximum value is 264 mg/l at R1.

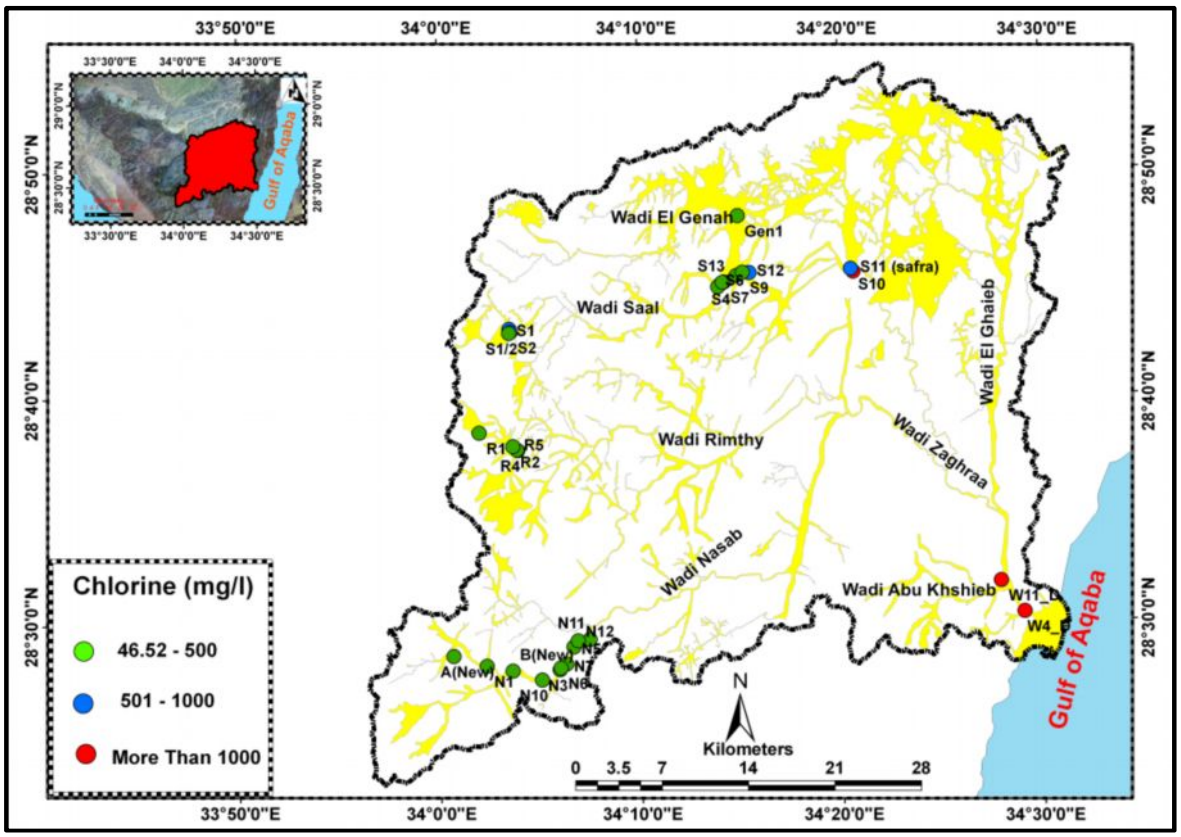

Figure 80: Distribution of Chlorine Ion in Groundwater of W. Dahab Basin

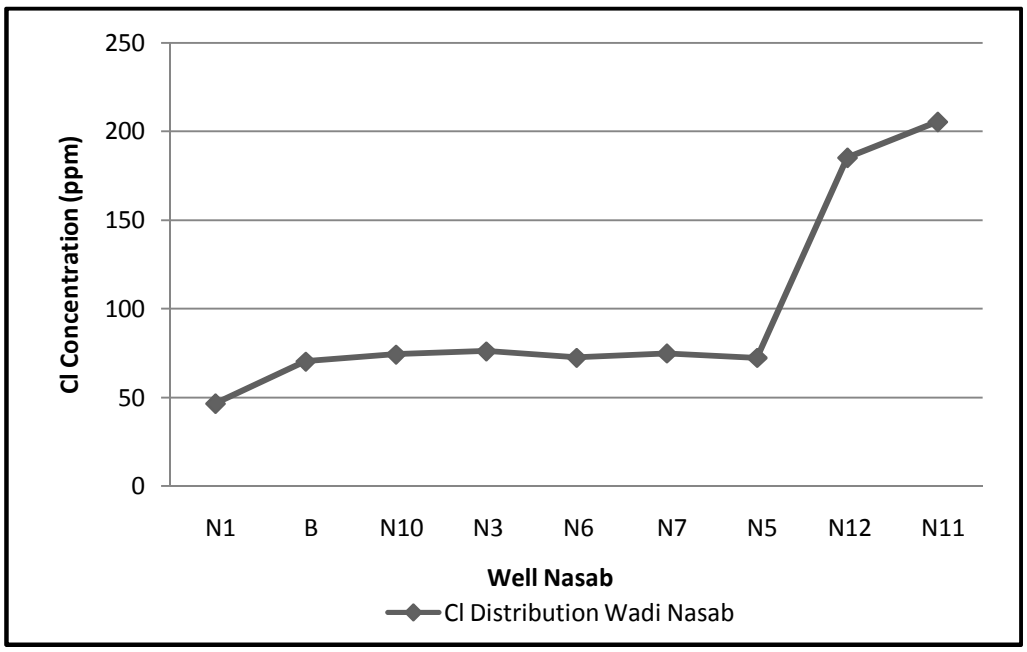

Figure 81: Distribution of Chlorine Ion in Groundwater of W. Nasab

Chloride ions increase at their recharge area of W. Saal, ranging from 556 to 849 mg/l and decrease along the downstream course, ranging from138 to 250 mg/l and increase again to 1052 mg/l (well S11) at the distal part of W. Saal. At the downstream of Dahab basin, Cl content increases to range more than 2000 mg/l (well W4,2086 mg/l) (fig 80).

3.3.2.5.B Sulphate (SO_4^{2-})

Sulphate is included in various minerals found in soils. Sulphate ions can form salts with ions of barium, calcium, magnesium and sodium. Sulphate can be leached out of soil and sedimentary rocks and is be commonly found in groundwater. Sulphate can be contained in groundwater because of the oxidation of sulphide ores, particularly pyrite which is commonly associated with many igneous rocks. It is present in rainwater and its concentrations might be as much as tens of mg/l in the study area. The rainfall in the Saint Catherine area contains sulphate between 10 to 14 mg/l and reflects a minor sulphate contribution of rain to the groundwater and surface streams (El Rayes,1992).

In agricultural areas, sulphate might come to water through ammonium fertilizer. It is quite limited and localized around a few orchards where fertilizing occurs. Plant decaying, animal actions and combustion of fuels are also important sources of sulphate in water.

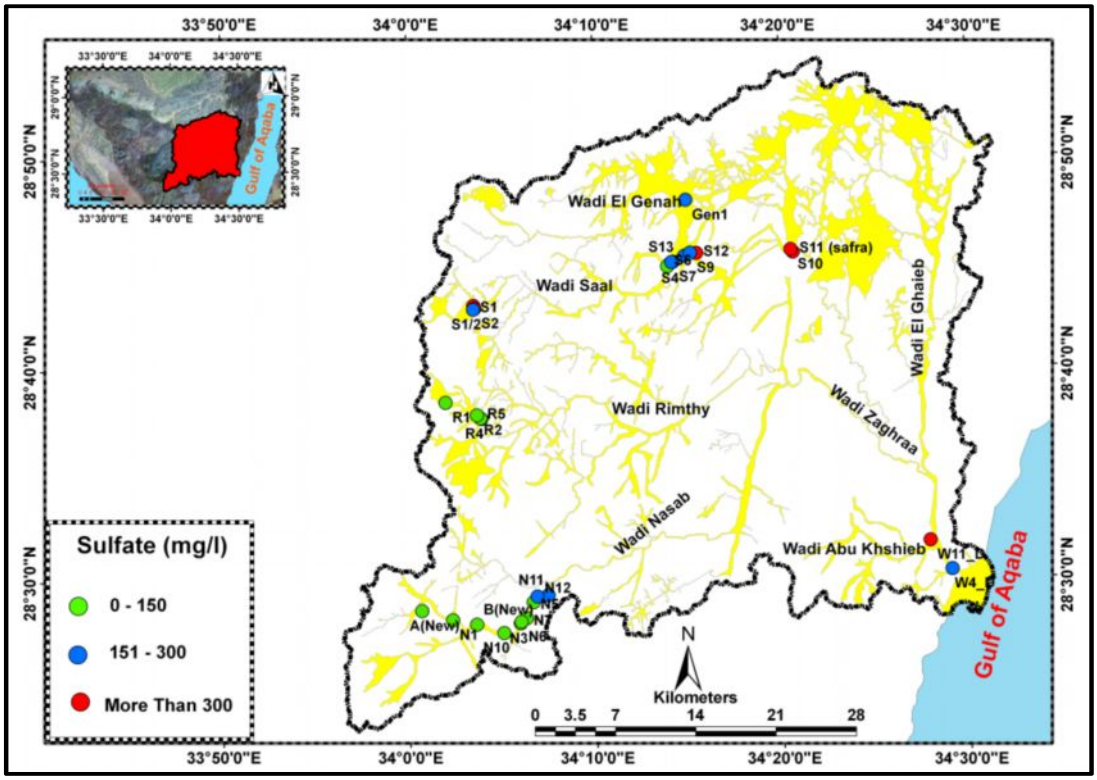

Figure 82: Sulphate Distribution in Groundwater of Dahab Basin

Sulphate concentrations in groundwater of Dahab Basin range between 54 to 559 mg/l in alluvial aquifers while it ranges between 97 to 507 mg/l in basement aquifers (fig 82). Sulphate mainly increases at the downstream of W. Nasab (wells N11&N12) and at the downstream of W. Saal (wells

S9, S10 and S12). Sulphate content of well water, mainly used for agricultural purposes, ranges between 205 to 667 mg/l. While the SO_4 content is low in alluvial aquifers at the upstream of W. Nasab and W. Rimthy, it ranges between 54 to 120 mg/l in areas without agricultural activities.

The concentration of sulphate increases in basement aquifers, especially upstream of W. Saal (wells S1, S2). It ranges between 438 and 464 mg/l and increases at well D11 downstream of Dahab to 507 mg/l, and decreases to 97 mg/l upstream of W. Nasab. The concentration of sulphate ions in groundwater at basement aquifers depends on agricultural purposes and sulphide mineralization in the study area. The SO_4 concentration increases in 2009 to 2011 in most of the wells, especially those near cultivated lands.

3.3.2.5.C Bicarbonate (HCO_3^-)

Bicarbonate is the predominant ion of groundwater in the recharge area. The main source of bicarbonate originates from rainfall. Rainwater infiltrates through fractured rock and percolates through the unsaturated zone to the groundwater table. CO_2 in unsaturated zones react with the rainwater forming carbonic acid which dissociates into bicarbonate (HCO_3) as shown in equation 15.

$$H_20 + C0_2 \rightarrow H_2CO_3 \Leftrightarrow H + HCO_3 \qquad \textbf{Equation (15)}$$

Bicarbonate results from dissolution of silicate minerals which are contained in granitic and volcanic rocks. It is known from mineralogical studies that plagioclase feldspar minerals are altered to clay and other products. Percolated rainwater begins to attack the plagioclases, bringing their constituent elements into solution and converting CO_2 into HCO_3^-.

Bicarbonate can also result from the dissolution of calcium carbonate which is a common constituent of many rocks, but dissolves fairly readily as bicarbonate in carbonic acid, and neutralizes soil water according to this reaction:

$$CaCO_3 + H_2CO_3^- \rightarrow Ca(HCO_3)_2 \Leftrightarrow Ca^{+2} + 2HC0_3^{-1} \qquad \textbf{Equation (16)}$$

Bicarbonate content in groundwater of W. Dahab basin ranges from 65 to 280 mg/l, The bicarbonate concentration increases upstream of W. Nasab (wellsN1&B) and decreases far away from the recharge area (wells N11 & N12) (fig 83). In contrast, the HCO_3 concentration at W. Saal increases downstream of the basin (wells S12, S13 and S9), reaching up to 236 mg/l. The low HCO_3 concentration in groundwater is observed at the upstream of W. Saal where the concentration ranges between 65 to 184 mg/l. This might be attributed to the impact of pyrite ore oxidation found at the upstream part of W. Saal (El-Rayes, 1992)

Bicarbonate constitutes the highest concentration of anions in upstream parts of W. Nasab and W. Rimthy (wells N1, A, N 10, B, R2 and R4) because of lack of a mineralization process. High concentration of bicarbonate might also be due to carbon dioxide uptake by surficial materials in

recharge zones (equation 15). High concentration of bicarbonate at W. Saal might result from dissolution of silicate mineral and calcite dissolution within alluvial aquifers as in wells S9, S12, and S13.

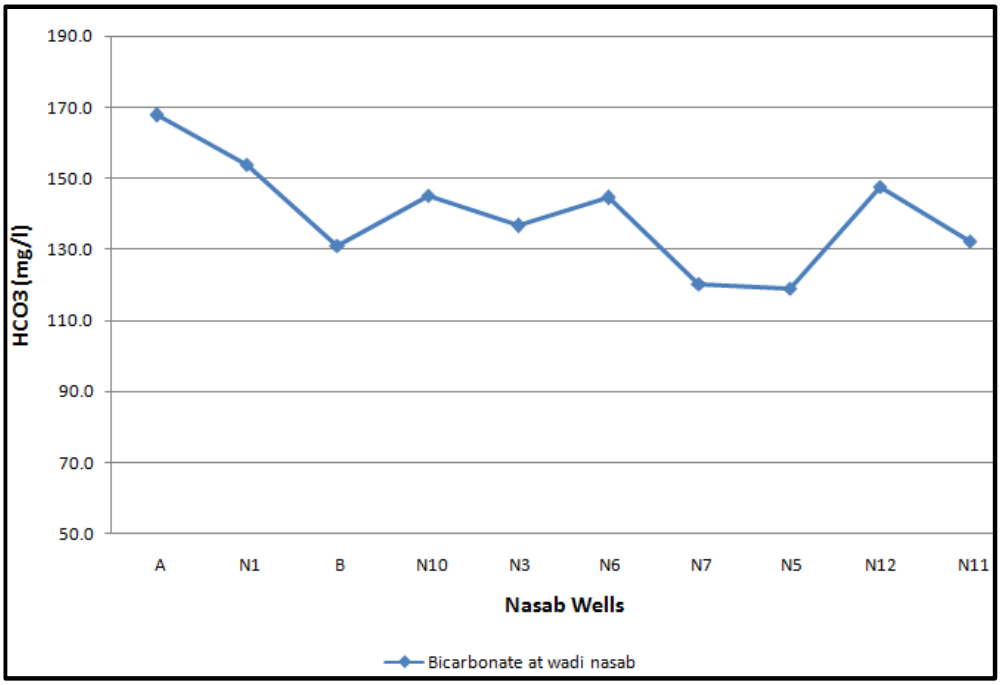

Figure 83: Bicarbonate Distribution in Groundwater of W. Nasab Basin3.3.2.5.D Sodium (Na^+)

Sodium is a non-conservative cation and interacts with minerals within soil zones and aquifers. However, it has proven to be an excellent tracer for groundwater processes taking place along flow lines within aquifers. The sodium is also an indicator for characterization of salinity. Na^+ concentration is used with reference to Cl in surface and groundwater to differentiate between different sources of salinity.

Na^+ ions are released from natural sources and by human-related activities. Natural sources include atmospheric deposition (from sea salt), water-rock (halite) interaction and silicate weathering (albite component of plagioclase with the formula $NaAlSi_3O_8$), and seawater intrusion or brine and cation exchange of Ca^{2+} with Na^+ on clay minerals. From human-related activities, Na^+ ions are released from: agricultural, wastewater, industrial wastewater, municipal landfill and road deicing and water softeners.

The main sources of sodium in water of granitic terrene are the feldspar minerals. The common feldspars in these rocks are orthoclase and microcline ($KAlSi3O_8$) and the plagioclase series (albite, $NaAlSi_3O_8$, to anorthite, $CaAl_2Si_2O_8$). Some sodium might be present, substituting for potassium in orthoclase and microcline (Hem, 1985). The decomposition of plagioclase feldspar (that could be represented by andesine minerals: $Na_{0.5}Ca_{0.5}Al_{1.5}Si_{2.5}O_8$) will generally yield considerable amounts of calcium and sodium and some soluble silica to water (Garrels, 1967).

The sodium ion content in groundwater of W. Dahab basin ranges from 32 to 2677 with an average value of 262 mg/l. Concentration of Na^+ reaches up to 32 mg/l (well N1) at the upstream areas and increases to 91.8 mg/l at well N11 downstream of W. Nasab (fig. 84).In contrast, Na^+ ions increase upstream of W. Saal (wells S1, S2 and S1/2) with values ranging from 175 to 380 mg/l and continues to increase downstream of W. Dahab along the alluvial aquifer, especially at wells S9, S10 and S12 ranging from 248 to 539 mg/l. Downstream of Dahab basin, Na^+ content in water well D4 recorded the highest value of about 746 mg/l.

The high Na^+ content in groundwater of alluvial aquifers is attributed to the long flow path and the interaction with aquifer rock materials which takes place at the downstream portion of Dahab basin. In the basement aquifer, the Na^+ concentration is high due to leaching of silicate minerals. The presence of high sodium concentration in well waters upstream of W. Rimthy refers to the closeness of these wells to granitic outcrops and hence, silicate dissolution is the dominant process producing Na^+ ions in groundwater.

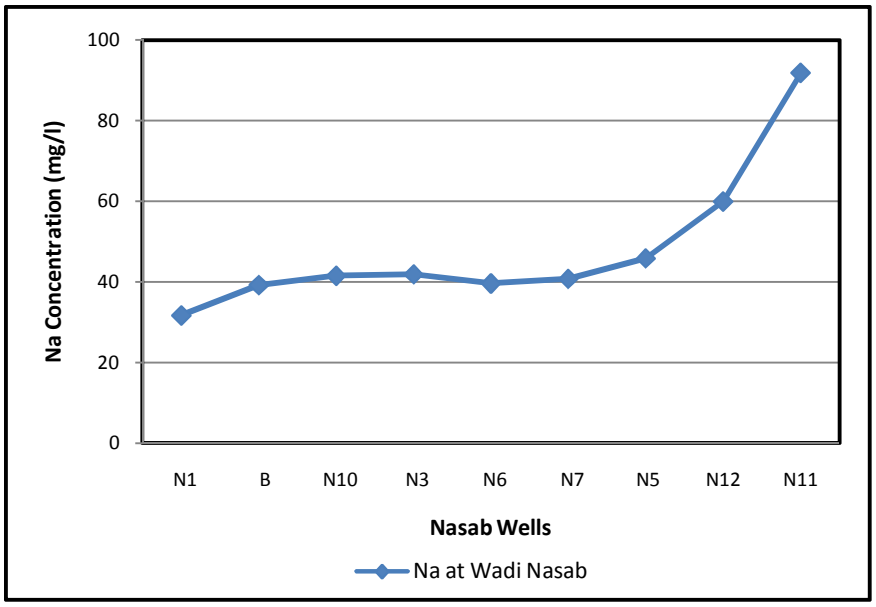

Figure 84: Sodium Distribution in Groundwater of W. Nasab

3.3.2.5.E Potassium (K^+)

In most natural waters, potassium concentration is much lower than the concentration of sodium because of the adsorption of clay materials (El Rayes, 1992). Potassium concentrations in water were low because of the high stability of the potassium-bearing silicate minerals (Hem, 1985). However, species containing sodium and calcium are somewhat more susceptible to chemical attack, yielding sodium to solution. The principal sources of potassium in waters of igneous rocks are alkali feldspars ($KAlSi_3O_8$), micas and feldspathoid leucite ($KAlSi_2O_6$). Potassium salts are widely used as fertilizers for agriculture and enter the freshwater by the returned flow water from cultivated land (UNESCO/WHO/UNEP, 1992).

Potassium has low concentrations at all wells in Dahab basin; it ranges from 1.9 to 119.2 mg/l. Low concentrations occur at W. Nasab and W. Rimthy where it ranges from 1.9 to 4.95 and increases relatively at wells N12, R1 and R4. While the Potassium ion concentration is enhanced at W. Saal, ranging between 3 to 22 mg/l, the value increases around the local agricultural area at wells S2, S10 and S12 where it ranges from 10.6 to 18.3 mg/l. High average concentration of Potassium ion in groundwater at W. Saal and downstream of Dahab basin indicates the effect of silicate minerals dissolution at the upstream parts of the basin in addition to the agricultural return flow water at the downstream portions.

3.3.2.5.F Calcium (Ca^{2+})

Calcium is present to some extent in nearly all waters because of its widespread occurrence in soils and rocks, and the high solubility of its minerals. Calcium is an essential constituent of many igneous rock-forming minerals. The plagioclase feldspar group includes mixtures of various proportions of end members of albite, $NaAlSi_3O_8$ and anorthite, $CaAl_2Si_2O_8$. Calcium also occurs in other silicate minerals that were produced in metamorphism. Some calcium is, therefore, expected to be in water that has been in contact with igneous and metamorphic rocks. Calcium is produced by the decomposition process of anorthite which is represented by the following equation:

$$CaAl_2Si_2O_8 + H_2O + 2H+ = Al_2Si_2O_5(OH)_4 + Ca^{2+} \qquad \textbf{Equation (17)}$$

Anorthite **kaolinite**

The normal composition of plagioclase feldspar lies between pure sodium and pure calcium forms, and decomposition will, therefore, generally yield considerable amounts of calcium and sodium and some soluble silica. Calcium and sodium can be added to the groundwater by the decomposition of andesine minerals (as a common constituent); this is represented by equation 18.The resultant water would contain Ca^{2+}, SiO_2 and Na^+ with the ratio 2:2:1 (Garrels, 1967).

$$Na_{0.5}Ca_{0.5}Al_{1.5}Si_{2.5}O_8 + 3/2H^+ + 11/4\ H_2O = ¾\ Al_2Si_2O_5(OH)_4 + 1/2Na^+ + Ca^{2+} + SiO_2 + H_2O$$

Equation (18)

andesine **kaolinite**

Calcium ion content in groundwater of the study area might have come from dissolution of the precipitates of $CaCO_3$ and Ca-Mg $(CO_3)_2$ during recharge. Carbonate weathering is considering to be one of the main sources of calcium ion in groundwater. In this reaction, carbonic acid (from atmospheric CO_2 and water) and calcium carbonate in soil react to form bicarbonate and calcium ion:

$$CO_2 + H_2O = H_2CO_3 \qquad \textbf{Equation (19)}$$

$$CaCO_3 + H_2CO_3 = Ca^{2+} + 2HCO_3^- \qquad \textbf{Equation (20)}$$

Calcium ion represents the highest cation concentration at the W. Dahab wells; it ranges from 62.4 to 832 mg/l (fig. 85). Calcium ion in groundwater of W. Nasab has low concentration ranging from 62 to 169 mg/l, especially at the upstream portions (well N1) and increases downstream (wells N11 & N12), ranging from 166.7 to 169.8 mg/l. Low calcium concentrations occur in W. Rimthy between 67 and 130 mg/l; Calcium concentration increases relatively at well R1 while it decreases in other wells of the same W..

At basement aquifers, Ca concentration ranges between 76 and 332 mg/l. High concentration occurs at W. Saal, ranging from 68 to 332 mg/l; it increases at the upstream part (wellsS1, S2 and S1/2) where it ranges between 95 and 188 mg/l. At well N11 the calcium content amounts to 303 mg/l. This high value may be attributed to the presence of the carbonate aquifer dominating this area and hence, the dissolution of carbonate mineral produces the obtained value. Very high concentration appears downstream of Dahab basin at well D4 where it reaches 823 mg/l.

Generally, in alluvial groundwater, calcium ion decreases at the upstream parts of both W. Nasab and W. Rimthy, ranging between 62 and 100 mg/l and it increases at the downstream parts of W. Nasab and W. Saal, ranging between 100 and 188 mg/l. Generally, Ca ion concentration increases downstream of the alluvial aquifers due to the dissolution of carbonate minerals and cation exchange processes. The difference of Ca ion concentrations occurs between well A in W. Nasab, where granitic rocks are predominant, and upstream of W. Saal. The reason for this relation is the dissolution of contained Ca-minerals in granitic rocks which is relatively lower than in basic rock.

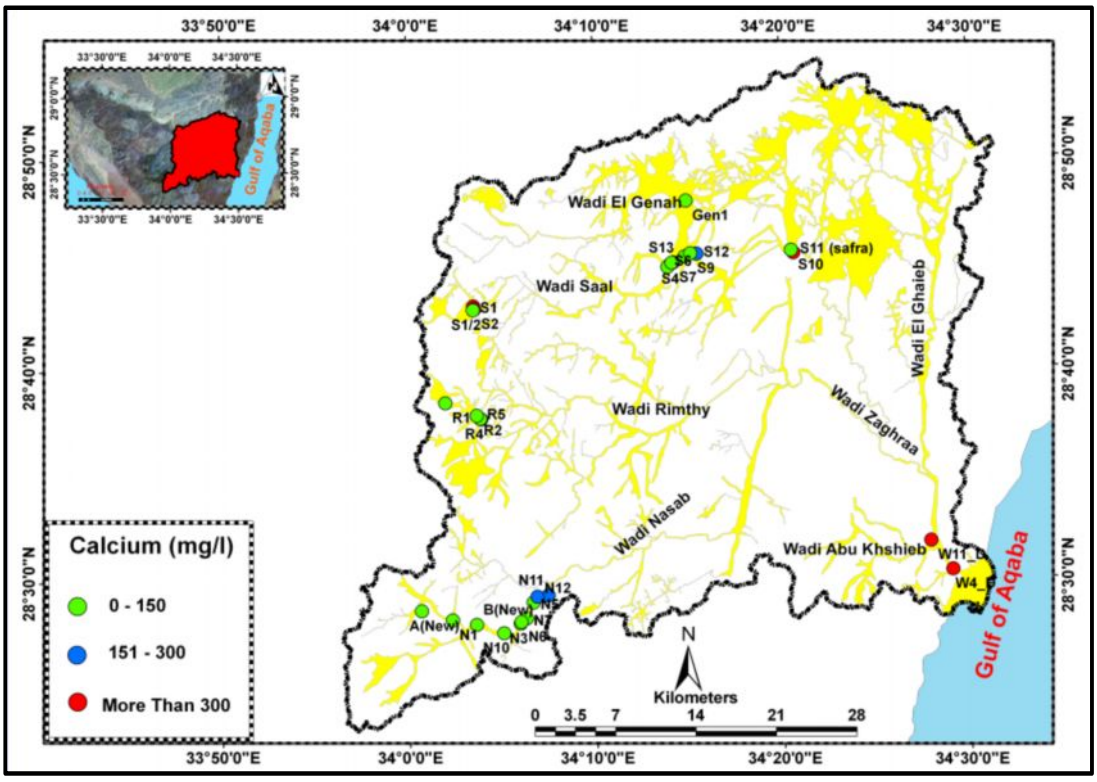

Figure 85: Calcium Distribution in Groundwater of W. Dahab Basin

3.3.2.5.G Magnesium (Mg^{2+})

Magnesium ranks eighth among the elements in order of abundance and is a common constituent of natural water. Magnesium is found in different rock types. In Igneous rocks, magnesium is a major constituent of ferromagnesian minerals including olivines, pyroxenes, amphiboles and micas. The ionic form of magnesium in water has a stronger tendency to remain in solution than calcium. It may be partly immobilized by the adsorption process (Feth et al., 1964).

A source of magnesium in groundwater of igneous rocks is the decomposition of biotite (phlogopite mineral) and/or pyroxene and magnesium olivine (forsterite). The decomposition of biotite is represented by the following equation:

$$KMg_3AlSi_3O_{10}(OH)_2 + 7H^+ + 1/2H_2O = 1/2Al_2Si_2O_5(OH)_4 + K^+ + 3Mg^{2+} + 2Si(OH)_4. \quad \textbf{Equation (21)}$$

Phlogopite **kaolinite**

A large number of minerals contain magnesium such as dolomite ($CaMg(CO_3)_2$) and magnesite ($MgCO_3$). Magnesium is released from weathered rocks and subsequently ends up in water. The concentration of magnesium ion ranges from 11.76 to 176 mg/l in Dahab basin. Lower concentrations occur in W. Nasab and W. Rimthy where, at the upstream, it ranges between 11.67 and 15 mg/l and increases via downstream to wells N11 and N12 where it ranges between 26.7 and 27,8 mg/l. The average concentration of magnesium in basement aquifers ranges between 76 and 332 mg/l. it increases at W. Saal from 21 to 49.6 mg/l at the upstream parts and it decreases at the downstream portion along alluvial aquifers where it ranges from 15.8 to 40 mg/l.

Figure 86: Outcrops of Upper Cretaceous Rocks Near W. S11 in W. Saal

Magnesium ion concentration shows a high level in groundwater of the downstream parts of W. Saal, especially at well S11 where it reaches 177 mg/l. High concentration in this area might be attributed to the dissolution of carbonate aquifers that constitute the upper cretaceous rocks downstream of W. Saal (fig. 86). Mg concentration mainly coincides with the concentration of Ca in groundwater of all wells in all aquifers (fig.87), confirming the hypotheses that Mg and Ca originate solely from both the dissolution of carbonates in the aquifer materials and the weathering of accessory pyroxene or amphibole minerals in basic rocks of W. Saal (Sami, 1992), and the governing weathering equation would be:

for pyroxene

$$CaMg(Si_2O_6) + 4CO_2 + 6H_2O = Ca + Mg + 4HCO_3 + 2Si(OH)_4$$ **Equation (22)**

and for amphiboles

$$Ca_2Mg_5Si_8O_{22}(OH)_2 + 14CO_2 + 22H_2O = 2Ca + 5Mg + 14HCO_3 + 8Si(OH)_4$$ **Equation 23)**

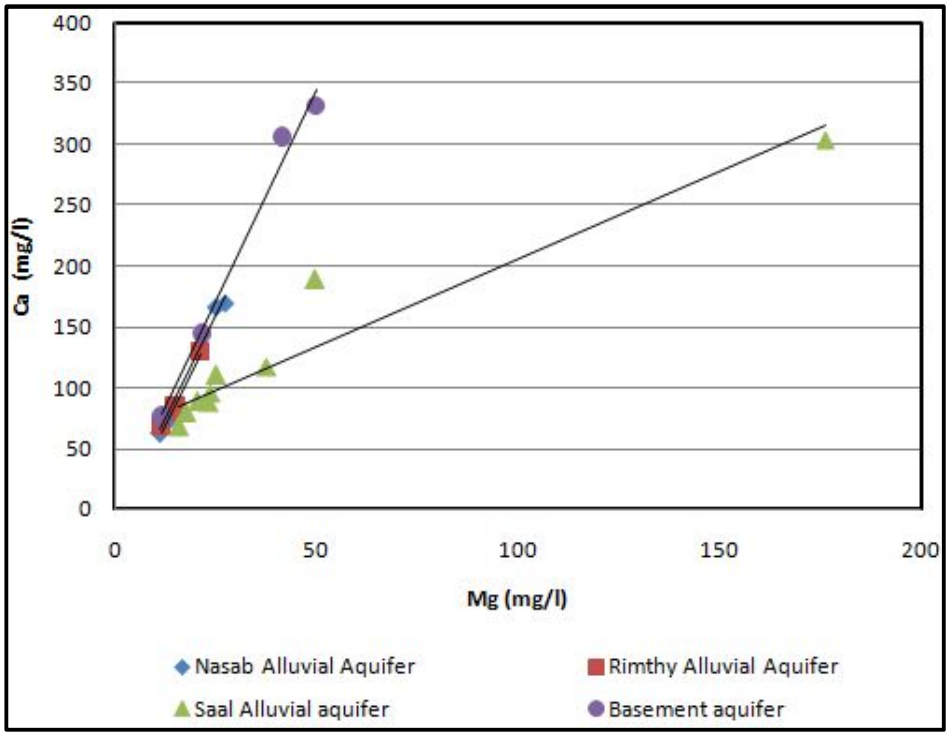

Figure 87: Relation between Ca & Mg Concentrations in Groundwater of Dahab Basin

3.3.2.5.H Silica (SiO_2)

Silica occurs in nearly all waters deriving from basement aquifers because it constitutes the main components of igneous rock-forming minerals which are small soluble. Silica is released by chemical weathering. It is acquired by circulating groundwater and therefore, the source of silica (SiO_2) in groundwater is almost exclusively a result of water– rock interaction.

The concentration of silica decreases by dilution during recharge periods. Thus, the silica concentrations are influenced by the amount of precipitation received within a drainage basin and the

residence time of groundwater within an aquifer. Silica content of groundwater increases due to an increase in the contact time span with silicate rocks and the silica content is directly proportional to the residence time of water underground (Marchand et al, 2002).

Silica concentration is low in groundwater of W. Dahab. It ranges between 6.5 and 18.2 mg/l with an average of about 12 mg/l. The high concentration occurs in W. Saal, ranging between 11.5 and 12 mg/l in basement aquifers. In alluvial aquifers, it ranges between 13.2 and 18.9 mg/l. Relatively high silica concentrations are recorded in the downstream area of W. Saal (wells S12 and S9) which ranges from 17.9 to 18.9 mg/l.

The silica concentration in groundwater of W. Nasab and W. Rimthy ranges from 9.4 to 12 mg/l. Groundwater of the upstream area of W. Nasab has low silica content ranging from 10.5 to 11 mg/l and increases at the downstream part (wells N11 and N 12) to around 12 mg/l. In Dahab basin, silica concentration in groundwater originates from decomposition of aluminum silicate and amphibole minerals such as feldspar; micas are the main source of silica in groundwater.

3.3.2.5.I Bromide (Br)

Bromide has geochemical characteristics like chlorine which tends to behaves conservatively when ionized in water. It does not occur in large concentrations in rock-forming minerals except in evaporate minerals. Bromide is commonly found in nature along with sodium chloride, owing to their similar physical and chemical properties, but in smaller quantities. Large portions of Br originate from atmospherically transported materials which fall as both wet and dry fallout and move to subsurface into groundwater. Bromide concentrations in seawater are generally in the range between 65 mg/l and 80 mg/l and in some seas surrounded by lands, it reaches 85 mg/l e.g. the Gulf of Aqaba (MMS, 1999).

Br is also released by dissolution of evaporites, extrusion of brines from compacted clay, diffusion of ions out of saline fluid inclusions and micropores, expulsion of water through recrystalization of minerals, and intrusion of seawater into coastal aquifers (Davis et al., 1997). Moreover, Br occurs in groundwater due to human activities. It has been used extensively in pesticides, gasoline additives and water purification compounds (Price et al., 1988). Bromide was once used as an anticonvulsant and sedative at doses as high as 6 g/day. Large doses of bromide caused nausea and vomiting, abdominal pain, coma and paralysis.

Bromide is distributed differently in the Dahab basin (fig. 88). This figure shows that the concentration of bromide is low at the upstream areas, especially in W. Nasab (0.12 and 0.14 mg/l) in wells N1 and B. It is low in the downstream area W. Nasab (0.28 and 0.33 mg/l) in wells N11 and N 12. In the upstream area of W. Saal, the concentration of Br ranges from 0.57 to 1.6 mg/l at wells S1, S2 and S1/2. Increasing concentration of Br at the upstream of W. Saal and downstream parts of W.

Nasab and W. Saal may be attributed to anthropogenic activities such as application of pesticides and fertilizers at local cultivated areas near these wells.

High Br concentration is recorded downstream of W. Dahab along the coastal zone of the basin at well D4 with a value up to 24 mg/l. This high value is caused by the effect of sea surface evaporation, dissolution of halite and local intrusion of seawater along the coast. High concentrations of Br and Cl along the alluvial aquifers downstream of W. Nasab and W. Saal might be attributed to rock-water interaction and the dissolution of evaporates. The concentration near the coastal zone of the basin may be caused by the local effect of seawater intrusion and dissolution of evaporate minerals as well.

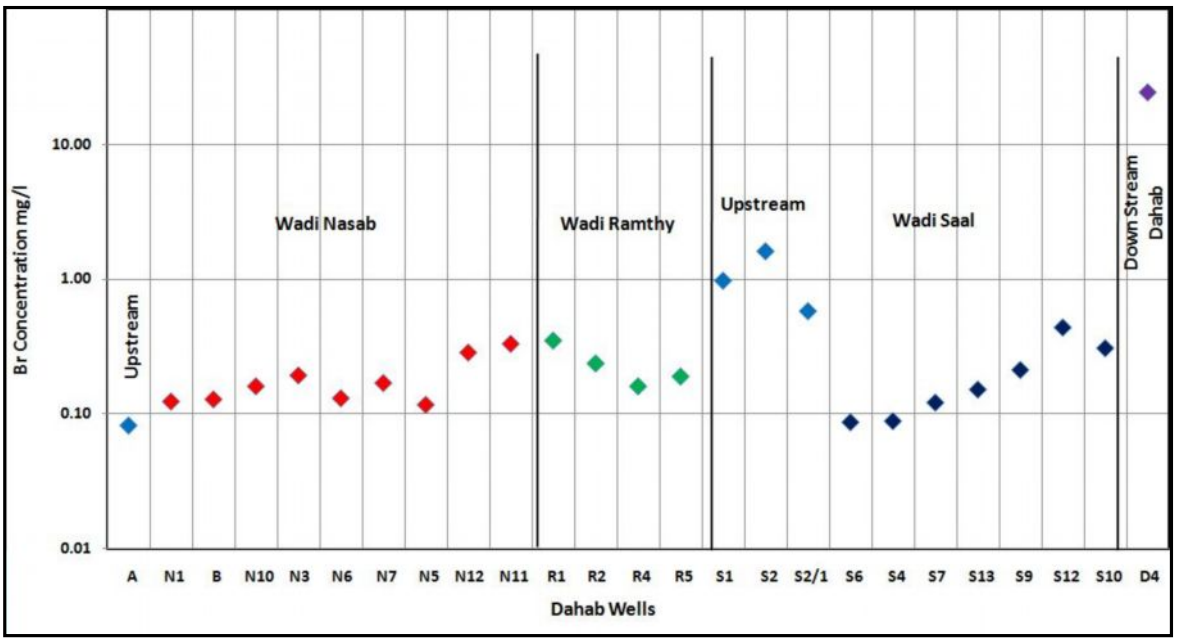

Figure 88: Bromide Distribution in Groundwater of W. Dahab Basin

3.3.2.6 Heavy metals

One of the most important environmental issues today is groundwater contamination. Among the contaminants affecting water resources, heavy metals receive particular concern because of their strong toxicity even at low concentrations (Marcovecchio et al., 2007). Heavy metals in water bodies are either of natural origin (eroded minerals within sediments, leaching of ore deposits and volcanic products) or of anthropogenic origin (solid waste disposal, industrial or domestic effluents). Some of the metals are essential to sustain life such as cobalt, copper, iron, manganese, molybdenum and zinc. They are needed at low concentrations as catalysts for enzyme activities (Adepoju-Bello et al., 2009); in higher concentrations, they are toxic to human beings and animals. In case of such risk, either the anthropogenic or geogenic origin of these concentrations needs to be assessed.

The aim of the present work is to develop a transferable decision scheme that allows risk assessment for groundwater systems affected by heavy metal contamination and to provide recommendations concerning present and further damages by heavy metals. To estimate and to

describe the damage to groundwater resources in the case of local accidents, leakages or widespread regional input, knowledge of both the groundwater flow and the transport behavior of the contaminants is required. Some of heavy metals have been detected by analysis of the water samples. Other elements are not detected in dry and wet seasons such as Ta, Nb, Hg, Ti and Be. The elements such as Mn, Pb and Fe have been detected only in the rainy season (Table 19).

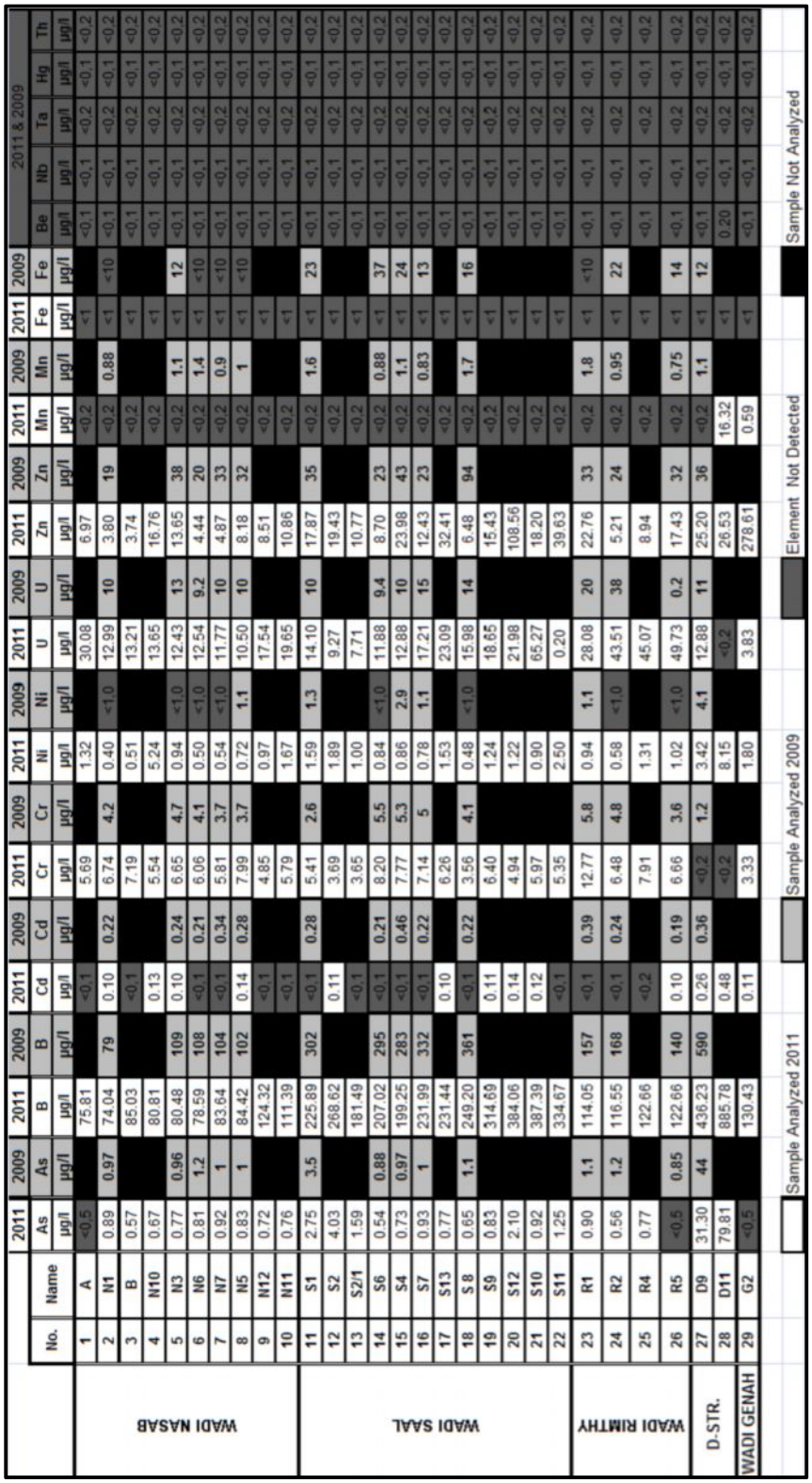

	No.	Name	2011 As µg/l	2009 As µg/l	2011 B µg/l	2009 B µg/l	2011 Cd µg/l	2009 Cd µg/l	2011 Cr µg/l	2009 Cr µg/l	2011 Ni µg/l	2009 Ni µg/l	2011 U µg/l	2009 U µg/l	2011 Zn µg/l	2009 Zn µg/l	2011 Mn µg/l	2009 Mn µg/l	2011 Fe µg/l	2009 Fe µg/l	2011 & 2009 Be µg/l	Nb µg/l	Ta µg/l	Hg µg/l	Th µg/l
WADI NASAB	1	A	<0.5		75.81		<0.1		5.69		1.32		30.08		6.97		<0.2		<1		<0.1	<0.1	<0.2	<0.1	<0.2
	2	N1	0.89	0.97	74.04	79	0.10	0.22	6.74	4.2	0.40	<1.0	12.99	10	3.80	19	<0.2	0.88	<1	<10	<0.1	<0.1	<0.2	<0.1	<0.2
	3	B	0.57		85.03		<0.1		7.19		0.51		13.21		3.74		<0.2		<1		<0.1	<0.1	<0.2	<0.1	<0.2
	4	N10	0.67		80.81		0.13		5.54		5.24		13.65		16.76		<0.2		<1		<0.1	<0.1	<0.2	<0.1	<0.2
	5	N3	0.77	0.96	80.48	109	0.10	0.24	6.65	4.7	0.94	<1.0	12.43	13	13.65	38	<0.2	1.1	<1	12	<0.1	<0.1	<0.2	<0.1	<0.2
	6	N6	0.81	1.2	78.59	108	<0.1	0.21	6.06	4.1	0.50	<1.0	12.54	9.2	4.44	20	<0.2	1.4	<1	<10	<0.1	<0.1	<0.2	<0.1	<0.2
	7	N7	0.92	1	83.64	104	<0.1	0.34	5.81	3.7	0.54	<1.0	11.77	10	4.87	33	<0.2	0.9	<1	<10	<0.1	<0.1	<0.2	<0.1	<0.2
	8	N5	0.83	1	84.42	102	0.14	0.28	7.99	3.7	0.72	1.1	10.50	10	8.18	32	<0.2	1	<1	<10	<0.1	<0.1	<0.2	<0.1	<0.2
	9	N12	0.72		124.32		<0.1		4.85		0.97		17.54		8.51		<0.2		<1		<0.1	<0.1	<0.2	<0.1	<0.2
	10	N11	0.76		111.39		<0.1		5.79		1.67		19.65		10.86		<0.2		<1		<0.1	<0.1	<0.2	<0.1	<0.2
WADI SAAL	11	S1	2.75	3.5	225.89	302	<0.1	0.28	5.41	2.6	1.59	1.3	14.10	10	17.87	35	<0.2	1.6	<1	23	<0.1	<0.1	<0.2	<0.1	<0.2
	12	S2	4.03		268.62		0.11		3.69		1.89		9.27		19.43		<0.2		<1		<0.1	<0.1	<0.2	<0.1	<0.2
	13	S2/1	1.59		181.49		<0.1		3.65		1.00		7.71		10.77		<0.2		<1		<0.1	<0.1	<0.2	<0.1	<0.2
	14	S6	0.54	0.88	207.02	295	<0.1	0.21	8.20	5.5	0.84	<1.0	11.88	9.4	8.70	23	<0.2	0.88	<1	37	<0.1	<0.1	<0.2	<0.1	<0.2
	15	S4	0.73	0.97	199.25	283	<0.1	0.46	7.77	5.3	0.86	2.9	12.88	10	23.98	43	<0.2	1.1	<1	24	<0.1	<0.1	<0.2	<0.1	<0.2
	16	S7	0.93	1	231.99	332	<0.1	0.22	7.14	5	0.78	1.1	17.21	15	12.43	23	<0.2	0.83	<1	13	<0.1	<0.1	<0.2	<0.1	<0.2
	17	S13	0.77		231.44		0.10		6.26		1.53		23.09		32.41		<0.2		<1		<0.1	<0.1	<0.2	<0.1	<0.2
	18	S 8	0.65	1.1	249.20	361	<0.1	0.22	3.56	4.1	0.48	<1.0	15.98	14	6.48	94	<0.2	1.7	<1	16	<0.1	<0.1	<0.2	<0.1	<0.2
	19	S9	0.83		314.69		0.11		6.40		1.24		18.65		15.43		<0.2		<1		<0.1	<0.1	<0.2	<0.1	<0.2
	20	S12	2.10		384.06		0.14		4.94		1.22		21.98		108.56		<0.2		<1		<0.1	<0.1	<0.2	<0.1	<0.2
	21	S10	0.92		387.39		0.12		5.97		0.90		65.27		18.20		<0.2		<1		<0.1	<0.1	<0.2	<0.1	<0.2
	22	S11	1.25		334.67		<0.1		5.35		2.50		0.20		39.63		<0.2		<1		<0.1	<0.1	<0.2	<0.1	<0.2
WADI RIMTHY	23	R1	0.90	1.1	114.05	157	<0.1	0.39	12.77	5.8	0.94	1.1	28.08	20	22.76	33	<0.2	1.8	<1	<10	<0.1	<0.1	<0.2	<0.1	<0.2
	24	R2	0.56	1.2	116.55	168	<0.1	0.24	6.48	4.8	0.58	<1.0	43.51	38	5.21	24	<0.2	0.95	<1	22	<0.1	<0.1	<0.2	<0.1	<0.2
	25	R4	0.77		122.66		<0.2		7.91		1.31		45.07		8.94		<0.2		<1		<0.1	<0.1	<0.2	<0.1	<0.2
	26	R5	<0.5	0.85	122.66	140	0.10	0.19	6.66	3.6	1.02	<1.0	49.73	0.2	17.43	32	<0.2	0.75	<1	14	<0.1	<0.1	<0.2	<0.1	<0.2
D.STR.	27	D9	31.30	44	436.23	590	0.26	0.36	<0.2	1.2	3.42	4.1	12.88	11	25.20	36	<0.2	1.1	<1	12	<0.1	<0.1	<0.2	<0.1	<0.2
	28	D11	79.81		885.78		0.48		<0.2		8.15		<0.2		26.53		16.32		<1		0.20	<0.1	<0.2	<0.1	<0.2
WADI GENAH	29	G2	<0.5		130.43		0.11		3.33		1.80		3.83		278.61		0.59		<1		<0.1	<0.1	<0.2	<0.1	<0.2

Sample Analyzed 2011 | Sample Analyzed 2009 | Element Not Detected | Sample Not Analyzed

Table 19 : Results of Heavy Metals Analysis within Groundwater Samples in Dahab Basin

3.3.2.6.A Zinc (Zn) & Cadmium (Cd)

Zn occurs in igneous and sedimentary rocks and is housed within the structure of silicates and oxides. The most abundant Zn minerals are sphalerite (ZnS), smithsonite ($ZnCO_3$), and zincite (ZnO). Zinc can also be adsorbed as clay minerals, iron oxides, organic matter, and unconsolidated sediments. Zn is especially enriched in mafics relative to felsic rocks. The principal Zn carrier in mafic rocks is magnetite, while biotite is generally the most important in granite (Ure and Berrow, 1982).

Zn has high concentrations within basic volcanic and acidic rocks. The concentration reaches 67 ppm in acidic rhyolite and rhyodacite rocks where in basaltic rocks it reaches 117 ppm (Hassan et al., 2004). The concentration of Zn increases in metagabbro and diorite rocks at the southern part of Dahab basin to 65 and 140 ppm respectively (El Gharbawi and Hassen, 2001).

Zn is dominant among the dissolved heavy metals in all groundwater samples (3.8 to 108 µg/l). High concentration (9 to 108 µg/l) occurs in groundwater of W. Saal and (9 to 22.7 µg/l) in W. Rimthy. A low Zn concentration ranges from 4.4 to 16.7 µg/l at other wells in W. Dahab.

Cadmium originates from both natural and human sources. Igneous and metamorphic rocks have a normally small range between 0.02 and 0.2 ppm (Cook and Morrow 1995). It is associated with zinc ores and may be found in volcanic emissions; it is also released from smelting of copper ores and from sewage sludge (Nicholson et.al. 1983).

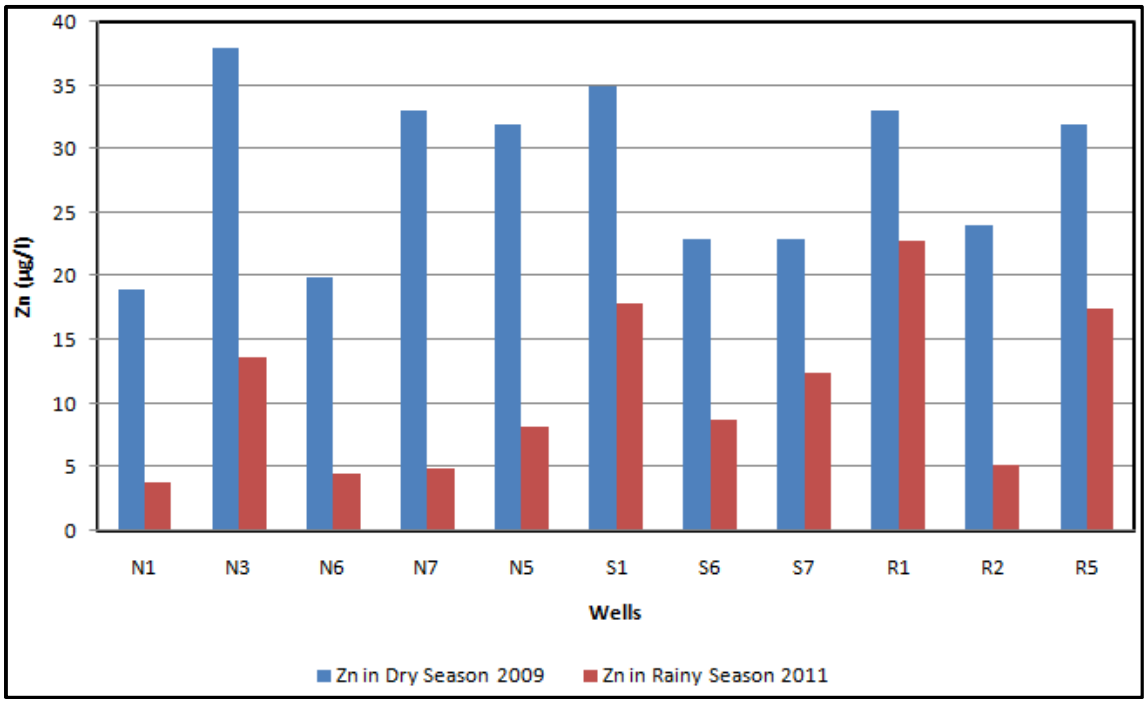

Figure 89: Zinc Distribution in Groundwater of W. Dahab Basin during Rainy and Dry seasons.

Many geochemical analyses were done by El Gharbawi and Hassen (2001) and Hassen et al. (2004) of different metamorphic and igneous rocks at different localities in W. Dahab. They confirmed that cadmium was not detected in basalts, andesits, rhyollite, diorite and metagrabbro. It

can be concluded that the source of cadmium in groundwater results mainly from anthropogenic effects. Low Cd concentration was recorded in all wells of Dahab basin ranging between 0.101 and 0.14 µg/l.

Zn concentration in groundwater is lower during the rainy season than in the dry season (fig. 89). The mobility of Zn is increased at low pH values (Reddy et al., 1995). The reason for the behavior in last figure may be by the dilution impact of rainfall. The lower concentration of Zn in the wet season comes mainly from the dilution effect of rainfall in wells (fig. 89). The low Cd level which reaches to no detection in the rainy season is also referred to for the same reason.

3.3.2.6.B Chromium (Cr) & Nickel (Ni)

Chromium is widely distributed through the earth's crust. The main source of chromium is the constituent of igneous rocks that probably occur as separate phase minerals such as chromite, chromium-bearing magnetite, and/or ilmentite. It ranges from 100 mg/kg in amphiboles, pyroxenes (where it is actually dispersed in augite), biotite, magnetite, and olivine to1.0 mg/kg in plagioclase and potassium feldspars (Bricker and Jones, 1995). Many ultramafic rock types contain significant amounts of chromium. Matzat and Shiraki (1974) reported that dunite, peridotite, pyroxentite, and serpentinite carry chromium concentrations to a maximum of 2400 mg/kg. Soils and sediments derived from these rocks also contain chromium. In high concentration, Cr is one of the most toxic elements for human beings. The limiting value for Cr concentration in drinking water is 0.05 mg/l (WHO, 2006).

There are high concentrations of Cr in basalts and metavolcanics rocks of Dahab basin, especially at W. Saal and W. Zaghraa (Hassen et al. 2004). Chromium is highly concentrated in basaltic andesite and basaltic rocks of the study area (Hassen et al. 2004), where the concentration ranges from 113 ppm in rhyolite and rhyodacite rocks to 168.5 ppm in basalt and ranges from 45 ppm to 377 ppm in gabbroic rocks of W. Nasab and southern W. Dahab.

Nickel naturally occurs in the environment at low concentrations. It is generally associated with basic and ultra basic rocks such as basalts, dunite and their serpentinite derivatives. Ni has lower concentrations than Cr but it increases more in basic rocks than in acidic rocks. Its concentration reaches 72 ppm in basaltic rocks, 8 to 14 ppm in rhyolite and rhyodacite rocks and it ranges from 25 to 244 ppm in gabbro and metadiorite rocks (Hassen et al. 2004).

The main source of nickel and chromium in groundwater aquifers is due to rock–water interaction. Oxidation processes and the pH values affect the solubility of Ni and Cr. Chromium is converted from Cr (III) to Cr (VI) in the presence of oxygen where Cr (VI) is highly mobile in most water systems and has a higher solubility than Cr (III). Cr adsorption increases with decreasing pH. The dominant species of Nickel in groundwater is a non-complex metal in the entire relevant pH range. Soluble nickel is derived mainly under oxic conditions form nickel sulphate ($NiSO_4$). The

positive relation between Ni and SO_4 in groundwater of basement and alluvial aquifers indicates that the source of nickel in groundwater results from the solubility of $NiSO_4$ (fig. 90).

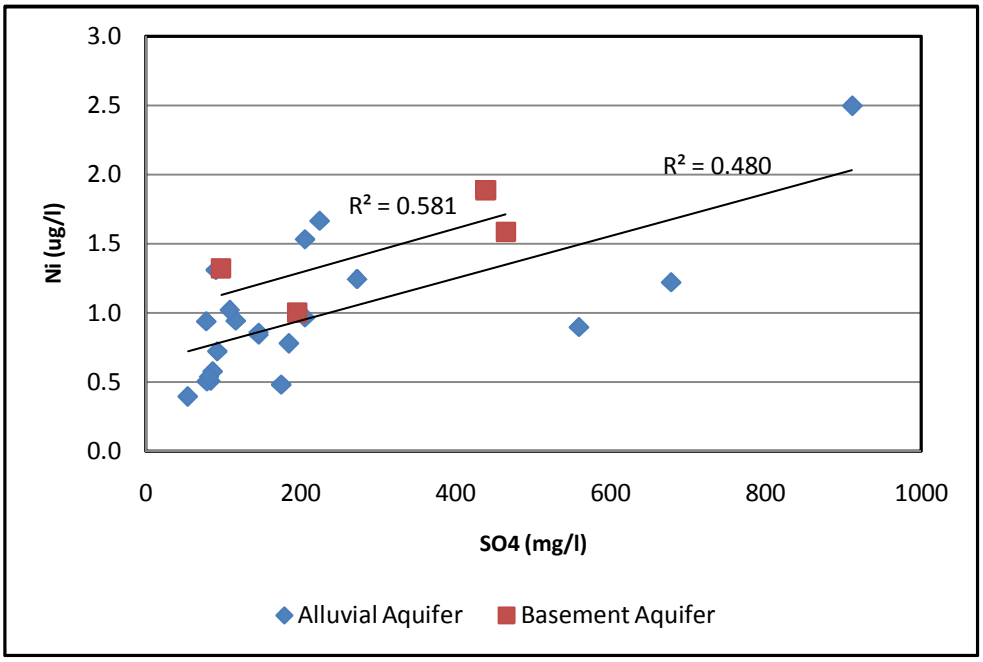

Figure 90: The Relationship between Nickel and Sulphate Contents in Groundwater of Dahab Basin

The concentration of Cr in groundwater of W. Dahab basin ranges from 3.5 to 12.6 µg/l. A high concentration range is also recorded in groundwater of W. Rimthy (6 to 12.6 µg/l) and in W. Saal (4 and 8 µg/l), while at W. Nasab it has a lower concentration range between 4 and 6.2 µg/l. The concentration of Ni ranges from 0.3 to 5.6 µg/l in groundwater of W. Dahab basin. Ni concentration in groundwater of W. Saal ranges between (0.4 to 1.8 µg/l) and is higher at the upstream area of Saal basin where the basement basic rocks are widely distributed with a range between 1 and 1.9 µg/l. Low concentration is recorded in groundwater of W. Nasab (0.3 to 1.5 µg/l) while high concentration reaches 5.2 µg/l at well N10.

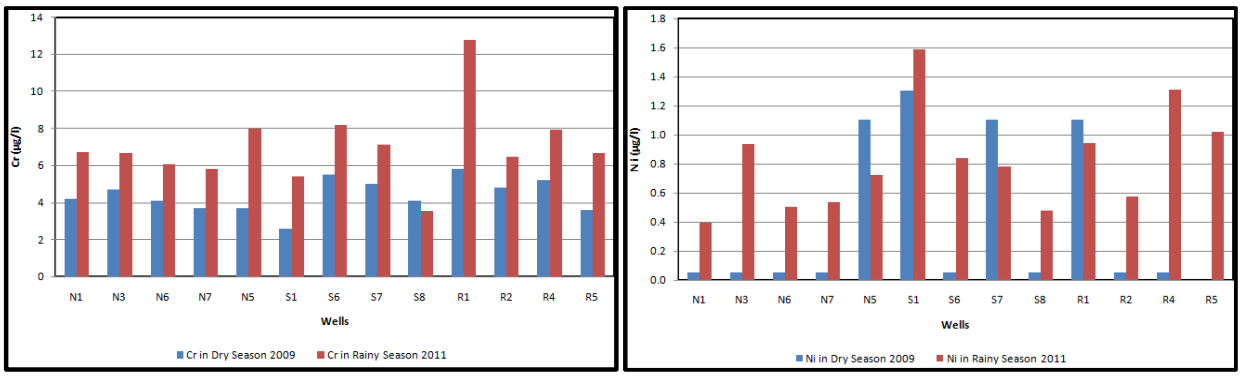

Figure 91: Comparison of Chromium and Nickel Concentrations in Dry and Rainy Seasons in Groundwater of Dahab Basin

Basic igneous and metamorphic rocks such as gabbro, basalts, metadiorite and metabasalt at W. Saal and the area around well R1 of W. Rimthy contain the main source of both Cr and Ni. The concentration values of Cr and Ni increase in the rainy season (fig 91) due to the oxidation process which affects percolation, causing the dissolution of Cr and Ni minerals in groundwater and the rising of the pH value of groundwater as in wells at W. Saal.

3.3.2.6.C Manganese (Mn) & Iron (Fe)

Manganese is one of the most abundant metals of the earth's crust and is usually associated with iron. The most common sources of manganese in groundwater are of natural origin, for example, via weathering of manganese-bearing minerals and rocks, such as amphiboles, ferromagnesian micas, iron sulphides, magnetite, oxides, carbonates, and iron clay minerals. Surour et al. (2003) stated that magnetite was the predominant oxide in Dahab stream sediments. The average range of MnO in basic and acidic rocks varies between 0.04 and 0.19 ppm. Manganese naturally occurs in many surface water and groundwater sources, particularly in anaerobic or low oxidation conditions. Under aerobic conditions typical of many shallow aquifers, manganese is stable in oxidized form, $Mn(IV)O_2$ which is highly insoluble. Hence, concentrations of manganese in aerobic water are usually low and commonly below analytical detection limits.

Iron is one of the most distributed elements of different rock types in nature. The source of iron in groundwater comes mainly from the dissolution of iron-bearing minerals which occurs in most minerals such as pyrite, magnetite, hornblende, and chlorite. The iron dissolves in groundwater with soluble form (Fe II). (Fe II) is oxidized to insoluble form (Fe III) when it contacts oxygen in air or by biochemical oxidation via iron-related bacteria.

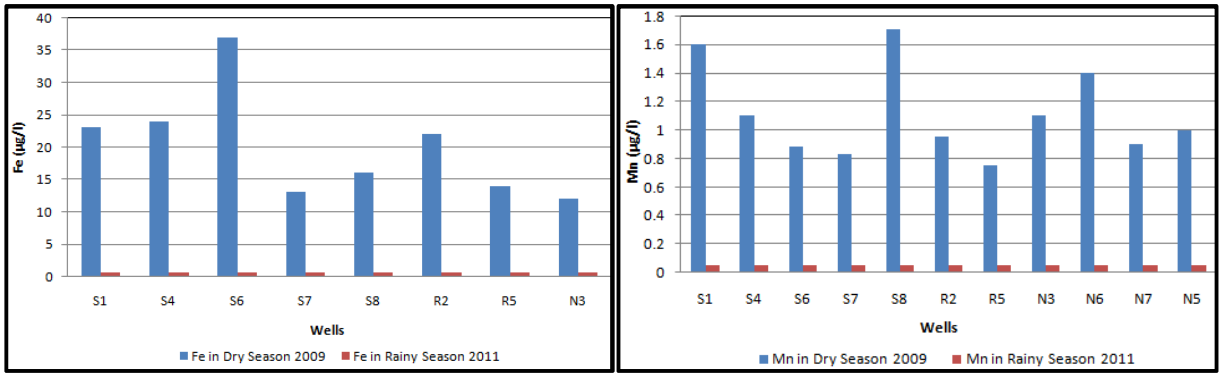

Figure 92: Availabilities of Iron and Manganese During Dry and Rainy Seasons in Groundwater of W. Dahab Basin

The richness of manganese and iron elements in basic, metabasic rocks and stream sediment in W. Dahab may be the main reason for the presence of Mn and Fe in groundwater. Low concentrations of Mn and Fe are detected in the groundwater of Dahab basin. In the dry season, Mn concentration ranges between 0.66 and 1.8 µg/l while Fe has ranges between 12 and 24 µg/l. In the

wet season, both elements are not detected in all groundwater samples of W. Dahab basin (fig.92). The main reason for this behavior comes from the shallow depth of the water table in most wells. The shallowness of the water table gives a chance for connection of groundwater with atmospheric oxygen and the inducing oxidation process. This process affects the solubility of Fe and Mn and may cause deficiency of both Fe and Mn during the rainy season.

3.3.3 Hydrogeochemical groups

Groundwater facies of the unconfined aquifers in the study area have been studied on the basis of chemical analysis of the water wells. Schoeller (1955) proposed the use of semilogarithmic graph paper to plot the concentration of anions and cations in meq/l. This type of diagram allows a visual comparison of different waters. Based on this table, the groundwater of Dahab basin are divided into four groups (Table 20).

The obtained data indicates that Ca is the dominant cation in 22 water samples,followed by Na and Mg. These samples are derived mainly from W. Nasab, W. Rimthy, with two samples from W. Saal. On the other hand, Na is a dominant cation in 10 water samples of the downstream of W. Saal.

Group	Anionic Group	Cationic Group	Samples
A	$HCO_3 > SO_4 > Cl$	Ca> Na>Mg	(A)- W. Nasab
B	$HCO_3 > Cl > SO_4$	Ca> Na>Mg	(N1-B-N10-N3-N6)-W. Nasab
C	$Cl > HCO_3 > SO_4$	Ca> Na>Mg	(N7-N5) – W. Nasab (R2-R4)-W. Rimthy (D4)-Downstream Dahab
D	$Cl > SO_4 > HCO_3$	Ca> Na>Mg	(N11-N12)-W. Nasab (R1-R5)- W. Rimthy (S1-S2)-W. Saal (D11) - Downstream Dahab
		Na> Ca> Mg	(S1/2-S4-S6-S7-MS8-S13-S9-S12-S10-S11)- W. Saal

Table 20: Hydrogeochemical Groups of The Examined Groundwater of Dahab Basin

3.3.3.1 Group A

Group A is represented by the water sample from well A at W.Nasab. This well is dug in basement rock in the upstream area of W. Nasab (fig. 93). This group is characterized by the dominance of HCO_3 (HCO_3>SO_4>Cl) (fig. 94).

Both the high bicarbonate content and low salinity (345 mg/l) of this water represent the finger print guide for groundwater of basement aquifers in recharge areas. Bicarbonate is generally dominant among anions in ground water. During infiltration of rainwater and the availability carbonate minerals along the path, the infiltrated water dissolves these minerals depending on the availability of dissolved free CO_2 and carbonic acid (Acworth, 1987).

Figure 93 : Dug waterhole in Basement Rocks at the Upstream of W. Nasab

During the recharge process, HCO_3^- and Ca^{2+} are dissolved by groundwater. Similarly, silicate weathering also increases HCO_3^- concentration in groundwater according to the following equation:

$$2NaAlSi_3O_8 + 2H_2CO_3 + 9H_2O \longrightarrow Al_2Si_2O_5(OH)4 + 2Na^+ + 4H_4SiO_4 + 2HCO_3^- \quad \textbf{Equation (24)}$$

(Albite) **(Kaolinite)**

Sulphate concentration in groundwater (97.11 mg/l) is higher than the chloride content (48.96 mg/l). The sulphate concentration is derived by oxidation of sulphide minerals such as pyrite in basic volcanics, granodiorite and monzogranite rocks at Rahabah Plain upstream area of W. Nasab (El Rayes et al., 2001).

Calcium is the dominating cation in groundwater (79 mg/l), Na (53 mg/l) is the second most abundant, with Mg (11.8 mg/l) being the third most abundant cation (Ca>Na>Mg). The

abundance of Ca in groundwater results from the chemical weathering of Ca-feldspar (Anorthite), which dominates the mineral constituents of granodiorites, gabbros and monzogranites in the upstream area of W. Nasab. This process produces clay minerals such as Ca-montmorillonite and Kaolinite (Feeze and Cherry, 1979). The dissolution of feldspar is associated with a deficiency of hydrogrn (H^+) and increasing calcium and bicarbonate ions. By this process, the pH of groundwater becomes a value from 7 to 8. This estimation is confirmed by the pH value (8.14) that is recorded at well A.

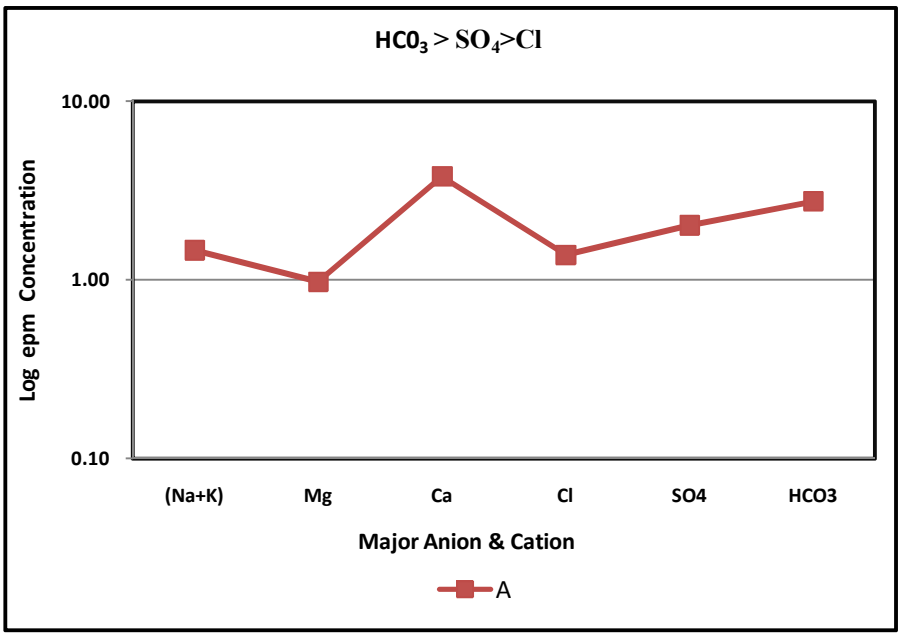

Figure 94 : Scheoller Diagram of Hydrochemical Group A

3.3.3.2 Group B

Hydrochemical group B comprises of groundwater samples derived from wells N1, B, N10, N3 and N6 at W.Nasab. They are located mainly in the upstream area of W.Nasab along its main stream. Groundwater discharges from the soil zone (B) of the alluvial aquifer located at the upper part of the underlying fractured basement. This group has a slight change in anion sequence while cations have the same sequence as in group A without any change. It is characterized by the dominance of bicarbonate ion over chloride and sulphate ions (HCO_3>Cl>SO_4) (fig.95).

Bicarbonate concentrations in all groundwater groups have the same level ranging from 131 to 153 mg/l. This resulted by dissolution of carbonate minerals available along its flowpath, based on the availability of free CO_2 and carbonic acid (equation 2), and weathering of silicate minerals.

Chloride concentration consititutes the second main anion of group B water. Chloride is the most conservative ion which is easily dissolved from the rock matrix, but is rarely precipitated (Zereini and Hötzl, 2008); therefore, the concentration of chloride increases or remains nearly constant along the flowpath. The chloride concentration in groundwater of this group ranges from 46 to 76 mg/l which is

high especially in the water wells N6- N3 at the distal part of the basin. The source of chloride in groundwater, especially at the upper wells of this group may have resulted from rainwater, which chloride ion dissolves in wind-aerosols of the surrounding sea (Gulf of Aqaba and Gulf of Suez).

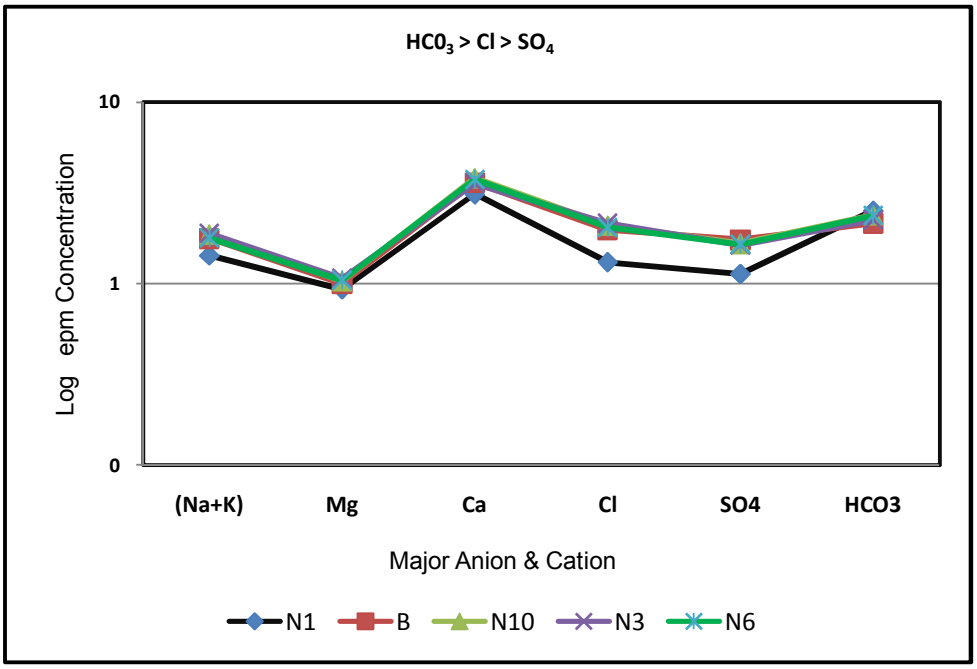

Figure 95: Scheoller Diagram Representing Group B Groundwater of Dahab Basin

Sulphate concentration in water of group B is lower than chloride in wells discharging alluvial deposits. Its concentration ranges from 50 to 74 mg/l. Sulphate is strongly correlated to chloride ion where both have the same distribution pattern along the alluvial aquifer. Sulphate in groundwater of the study area is produced by oxidation of sulphide minerals.

Bicarbonate and calcium contents have the highest ion concentrations in water of this group, reflecting the chemical characters of water exploited from the recharge area. Dominance of calcium higher than sodium and magnesium is similar to group A and indicates the characteristics of the recharge area even though sodium concentration is increases relatively in this group. Na content is produced by the dissoloution of albite mineral and has a range from 38 to 45mg/l.

3.3.3.3 Group C

Group C waters are widely distributed along different localities in Dahab basin. They are recorded at slightly distal parts from the recharge area such as wells N5 and N7 in W.Nasab and wells R2 and R4 in W.Rimthy. They occur also in the downstream area of Dahab basin at well D4.

All these wells tap groundwater of the alluvial aquifer. Due to the relative large thickness of the alluvial deposits and longer flowpath of groundwater, the chemistry of this group is developed relative to the groups (A&B) of the recharge area. Water facies of group C are characterized by the dominance of chloride over bicarbonate and followed by sulphate (fig.96).

Chloride concentrations in this group range from 72 to 74 mg/l in W.Nasab, while it ranges (105 to 150 mg/l) in W.Rimthy and finally, increases at the downstream area of Dahab (2148 mg/l). Increasing of chloride content in all wells is acquired through the long flowpath of groundwater in the alluvial aquifer relative to well waters of the groups A&B. In addition, chloride content is extremly high in the downstream area of Dahab basin (well D4) and is slightly impacted by seawater intrusion which appears in the chloride distribution map along Dahab basin (fig. 80).

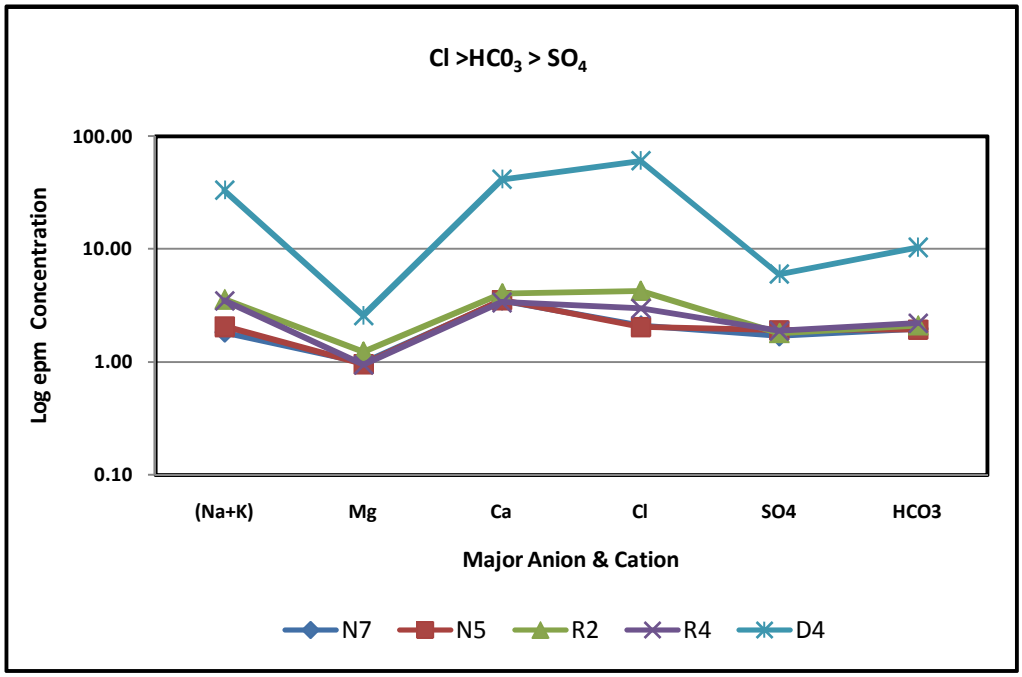

Figure 96: Scheoller Diagram of Group C Facies of Groundwater at Dahab Basin

Bicarbonate is the second dominant anion after chloride. It ranges from 120 to 147 mg/l in wells N7, N5, R2 and R4 while it has a high value (531 mg/l) at well D4 in the downstream area of W. Dahab. Bicarbonate content in groudwater of this group is lower than that of groups A&B. That is due to the long flowpath of groundwater which causes deficiency in bicarbonate and an increase in salinity.

The sulphate ion is the lowest anion in group C. It ranges from 81 to 92 mg/l at wells in W. Nasab and W. Rimthy,while the concentration increases in the downstream area of Dahab basin reaching up to 288 mg/l. The source of sulphate in water is the product of sulphide oxidation. The dissolution of gypsum may be considered the second source of sulphate and calcium ions in the downstream of Dahab basin. It may be represented by the following equation:

$$H_2O + CaSO_4.2H_2O \longrightarrow Ca^{2+} + SO^{2-}_4 + 3H_2O \qquad \textbf{Equation (25)}$$

Calcium constitutes the dominant major cation in this group. Dissolution of Ca–feldspars and gypsum are the main processes producing calcium ions in groundwater of the downstream area of

Dahab basin. Sodium ion is the second dominant cation; its concentration increases more or less in groundwater of W. Rimthy and downstream of W. Dahab due to the influence of the long flowpath.

It can be concluded that geochemical group c of groundwater at the study area has chloride and calcium ions as dominant species. The water of this group represents the chemical nature of the transitional zone between recharge and discharge zones in W. Nasab and W. Rimthy. In the downstream area, the effect of a long flowpath and sea intrusion may cause increasing chloride, calcium ions and salinity (6320 mg/l) in groundwater.

3.3.3.4 Group D

This group represents the most dominant hydrochemical group in Dahab basin (fig. 97). Some wells (N11&N 12) in this group are located at distal parts of W. Nasab and downstream of W.Dahab (D11). Some other wells are located at the recharge zone of W. Rimthy (R1, R5) and W. Saal (S1, S2). All these wells tap alluvial aquifers (soil zone c) except well D11, S1 and S2 which tap basement aquifers. High salinity is the main character of all well waters of group D. It ranges from 600 to 2000 mg/l and increases downstream of Dahab in well D11 up to 17000 mg/l D11.

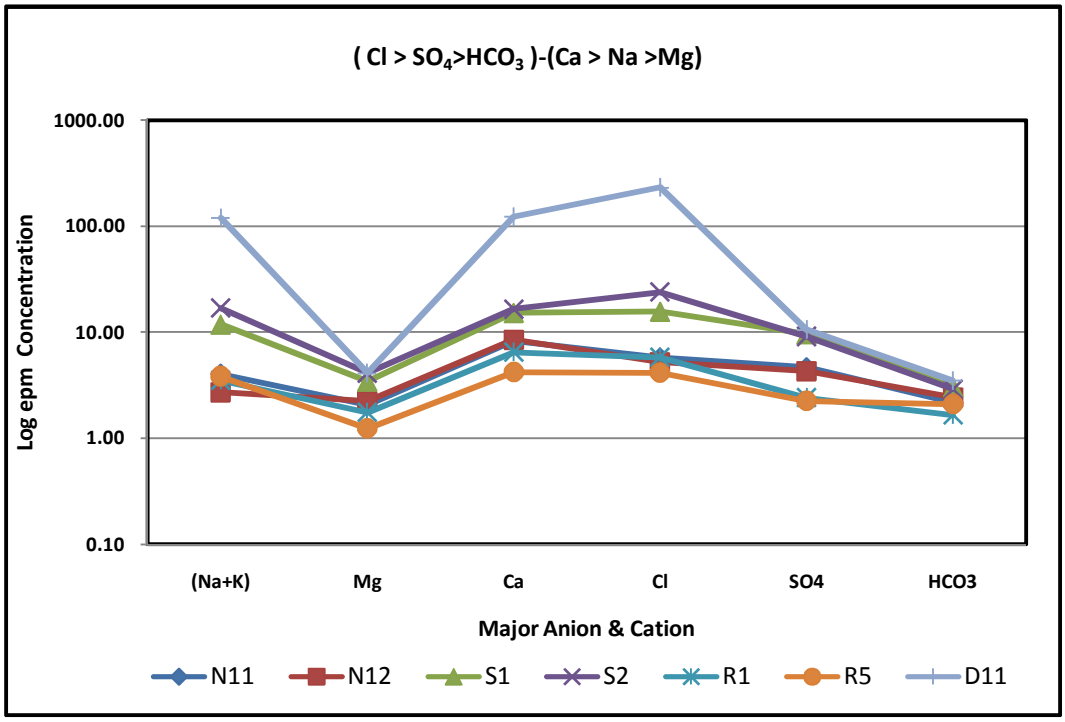

Figure 97: Scheoller Diagram of Hydrochemical Group D-Subgroup 1 at W. Dahab Basin Area

The Chloride ion is the dominant ion in this group. It is observed that there is a gradual increase of chloride content along the stream course of W. Nasab in wells N11 and N12 and W. Saal in wells S11 and S10. The gradual increases in chloride content downstream of both Wadis results from the long flowpath. Although the wells S1, S2, S2/1 and R1 located in the recharge area, they have high Cl concentrations. High chloride concentration could have be reached because of the presence of high

mineralized zones (El Rayes, 1992), especially in W. Saal. Chloride ions could have be released from microstructure and fluid inclusions through the weathering of hard rocks.

It has been proposed that some solutes, particularly chloride and portion of sulphate, originate from fluid inclusions in quartz that are opened by fractures, weathering or other processes that bring them into contact with the surface (Gascoyne and Kamineni, 1994). The total amount of extractable chloride in a particular crushed granite could be high (Stober and Bucher, 1999b). The chloride stored in the opened inclusions will be washed away with the first batch of water that wets the fresh fracture. In contrast, unstable feldspar can be exposed to water for a very long period of time and feldspar hydrolysis continuously makes its contribution to water chemistry.

Sulphate ions are the second dominant ion in this group. The concentrations range in W. Rimthy from 106 to 108 mg/l, in W. Saal from 204 to 224 mg/l, and in the downstream area of W. Dahab in Well D11 up to 525 mg/l. The shallowness of groundwater table causes an interaction between groundwater and atmosphere and leads to enhance the oxidation process in water wells as mentioned before. Moussa (1999) states that radiometric investigation detects radioactive elements associated with sulphide deposits concentrated at shallow to moderate depth in W. Rimthy. The sulphide deposits may indicate a good source of sulphate ions in the associated groundwater. Additionally, anthropologic impacts, such as the application of plant nutrient and fertilizers containing calcium sulphate, in some local areas at W. Nasab around well N11 & N12 cause an increase in the sulphate content in the well water.

Cations play an important role in understanding the chemical origin and chemistry of rock-water interaction. In group D, cations are divided into two sub-groups. The first one has a sequence of Ca>Na>Mg, the second one has a sequence of Na > Ca >Mg. The first sub-goup distributes along all recharge areas and includes some wells that tap basement rocks by wells S1and S2 in W. Saal and well D11 downstream of Dahab. This cationic sub-group includes well waters produced from alluvial deposits wells N11 and N12 in W. Nasab and wells R1 and R5 in W. Rimthy.

Although the locations of wells N11 and N12 are far from the recharge area, calcium has the highest concentration ranging from166 to 169 mg/l at these wells. A high concentration of calcium is related to the availability of calcium sources in alluvial deposits. The large thickness of the aquifer at wells N11 and N12 (fig. 98-A) gives water a good chance to dissolve calcium from basement rocks and calcium carbonate as mentioned before.The importance and significance of plagioclase dissolution for the hydrogeochemical properties of groundwater in crystalline rocks has been demonstrated by Gasconye and Kamineni (1994). The presence of plagioclase in alluvial deposit might cause an increase of calcium. Anorthite minerals are included in granitic and granodioritic rocks of the study area. The weathering of this mineral during rainy seasons in the presence of water and carbon dioxide is represented by the follwing equation:

$$H_2O + 3CO_2 + Ca\,Al_2Si_2O_8 \longrightarrow Al_2Si_2O_5(OH)_4 + Ca^{++} + 2HCO_3 \qquad \textbf{Equation (26)}$$

Anorthite **Kaolinite**

The dissolution rates of Quartz, K-Feldspar and Albite were slower than that of anorthite (Blum and Stillings, 1995). The groundwater with high Ca content could be derived by preferential weathering and dissolution of anorthite-rich rocks and dissolution of calcium carbonate (Stober and Bucher, 1999).

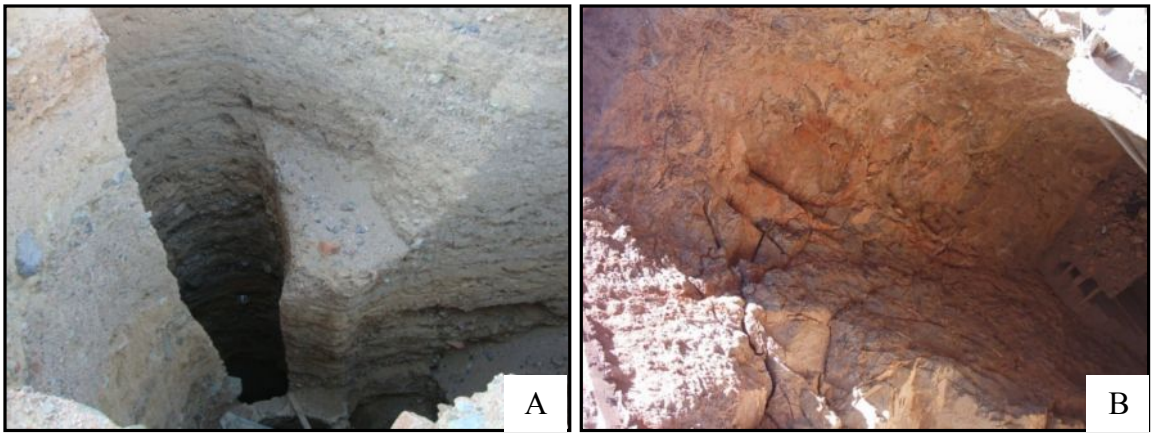

Figure 98- A: Well N11 Downstream of W. Nasab B: Well S1 in the Upstream area of W. Saal

The concentration of calcium is high in wells of basement rocks such as the wells S1, S2 and D11. It is produced by direct interaction between groundwater and basement rocks. The presence of mafic rocks and dykes causes an increase of calcium and salinity at these wells (fig.98-B).

The high concentrations of calicum and chloride characterizes the water of alluvial aquifer in discharge areas (case of wells N11 and N12). On the other hand, the presence of dykes and highly mineralized rocks causes an increase of chlorine and calcium (case of wells S1, S2 and D11).

Sodium is dominant in the second sub-group groundwater of group D (Table 22). The second sub-group includes all well waters which are located at W.Saal (fig.99). All these wells tap alluvial aquifers except well S2/1 which discharges basement rocks. The range of sodium concentration in these well is between 120 and 538 mg/l. It ranges between 455 and 511 mg/l at wells S6 and S12 and increases in the upstream area to 175 mg/l at well S1/2.

Sodium is positively correlated to TDS and tends to increase toward the downstream area of the basin at wells in W. Saal (fig.100). It is strongly influenced by lithological variation along the main channel course where it attains at 170 mg/l in the upstream area in well S2/1 and 120 mg/l in well S6 which tapped the alluvial aquifer and reaches up to 538 mg/l in well S12. Sodium content is related to the weathering process of feldspar. Dissolution of feldspars may increase sodium content of groundwater but by minor values (Fontes et al., 1991). Gradual increase of sodium along the upstream to trough area could be used as an indicator of the freshening process in alluvial aquifers (Geriesh and El Rayes, 2000). The freshening process means the control of the increasing salinity by recharge from precipitation. The process leads to increase the groundwater table and decrease salinity. This process will permit increasing salinity (by adding Na ion by ion excahnge) to high limit values causing the

unusability of groundwater. Concentration of sodium ion of subgroup 1 in upstream area of W. Saal has a high value in comparison to concentration of sodium of subgroup 2 at certain wells (e.g. S1, S2).The chemical facies changed from (Ca,Na- Cl) water to (Na,Ca-Cl) water due to cation exchange.

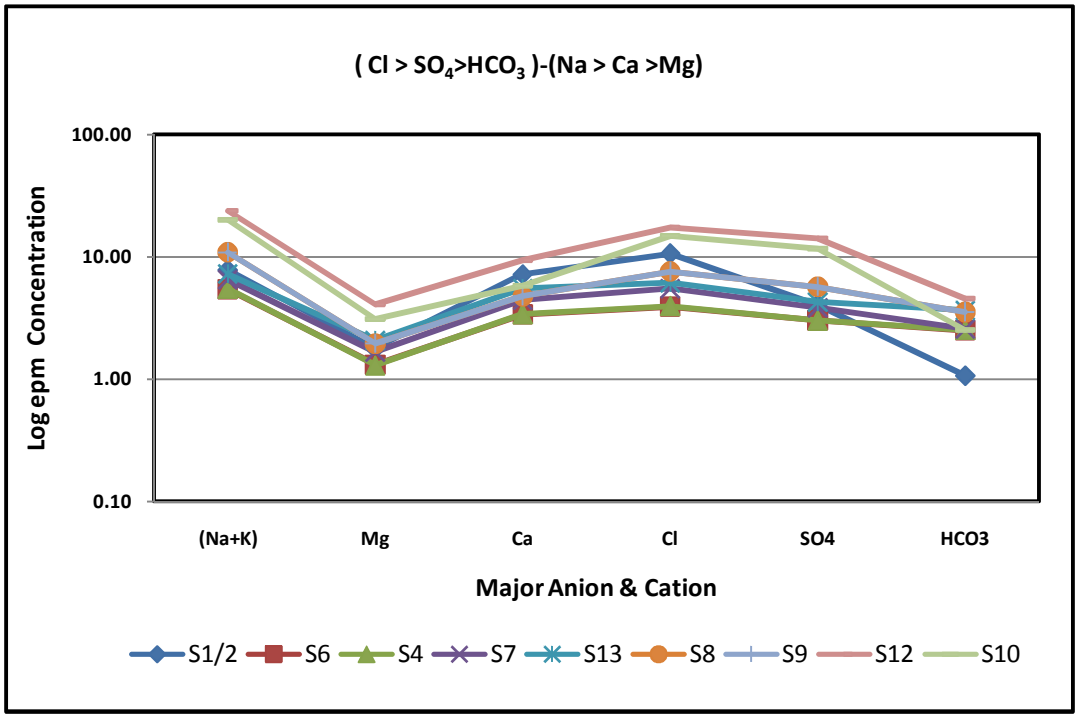

Figure 99: Scheoller Diagram of Hydrochemical Group D, Sub-group 2 of Groundwater at Dahab Basin

Magnesium is the least prominent cation of group D. The presence of ferromagneisum and clay minerals (illite and biotite) in metamorphic rocks and dolomite (Hassan et al. 2004) represent the main source of magnesium ion in alluvial aquifers. Garrels (1976) stated that magnesium is realeased from the dissolution of magnesium calcite (dolomite). Freeze and Cherry (1979) stated that sources of magnesium ions may result from reactions for incongruent dissolution of some aluminosilicate minerals as in equations 27 & 28.

$$\underset{\text{Dolomite}}{Ca\,Mg\,(CO_3)_2} + 2H_2CO_3 \longrightarrow Ca^{2+} + Mg^{2+} + 4HCO_3^- \qquad \textbf{Equation (27)}$$

$$\underset{\text{Biotite}}{KMg_3AlSi_3O_{10}(OH)_2} + 7\,H^+ + \tfrac{1}{2}\,H_2O \longrightarrow \tfrac{1}{2}\,\underset{\text{Kaolinite}}{Al_2Si_2O_5(OH)_4} + K^+ + 3Mg^{2+} + 2\,Si(OH)_4 \qquad \textbf{Equation (28)}$$

The concentration of magnisum ions along the course of alluvial aquifers increases especially downstream of W. Saal at well S11 (178 mg/l). The reason for this is the presence of dolomite rocks and Upper cretaceous clay layers in this area.

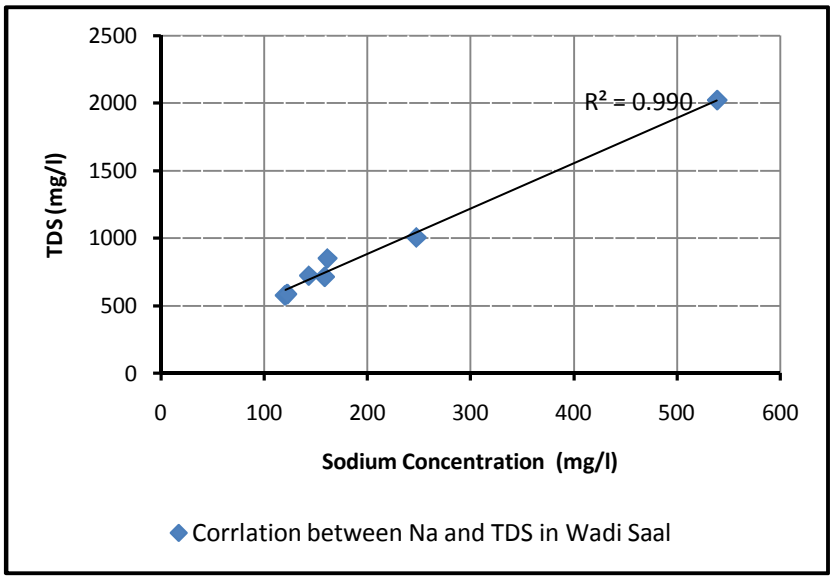

Figure 100: Relation between Sodium Concentration and TDS of Groundwater at W. Saal

Summarizing, bicarbonate ions increase in the recharge area, especially of W. Nasab with the dominant calcium ions in groups A & B. Groundwater facies change to increase the chloride ions over bicarbonate in group C. Finally, chloride-sulphate increases over bicarbonate towards the discharge area and is influenced by the local cultivated area around the wells of group D (fig. 101-A).

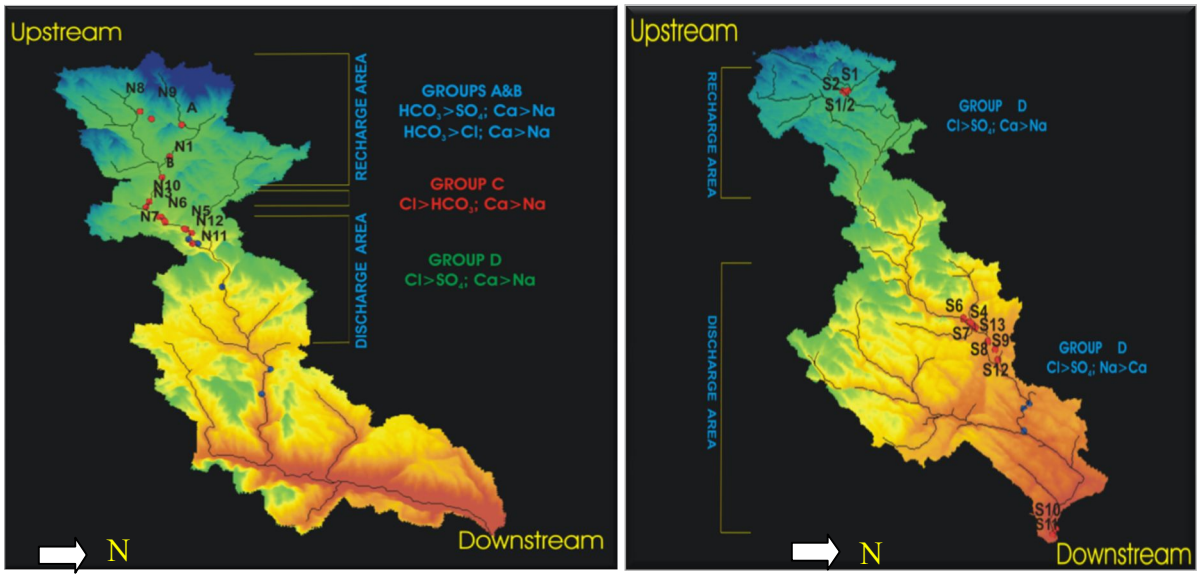

Figure 101-A: Hydrochemical Facies in W. Nasab B: Hydrochemical Facies in W. Saal

Groundwater facies at the upstream of W. Saal (Group D) represented by a sequence Cl> SO_4>HCO_3 and Ca >Na>Mg differ from those at upstream of W. Nasab (Group A). They are influenced by the presence of dykes, shallow wells and increasing evaporation. All these factors support an increase of salinty and enhance the interaction between water and rocks. Downstream of W. Saal, groundwater facies change into Na >Ca>Mg type due to the effect of long flowpath (Group D) (fig.101-B).

In the recharge area of W. Rimthy, chloride and calcium are the most dominant ions. The pattern of water chemistry is similar to that of W. Saal due to the effect of dykes and shallowness of the water table which cause high salinity. The increasing sulphate ion concentration is due to the oxidation process of sulphide minerals causing an increase in the sulphate content of groundwater (Group D) (fig.102-A).

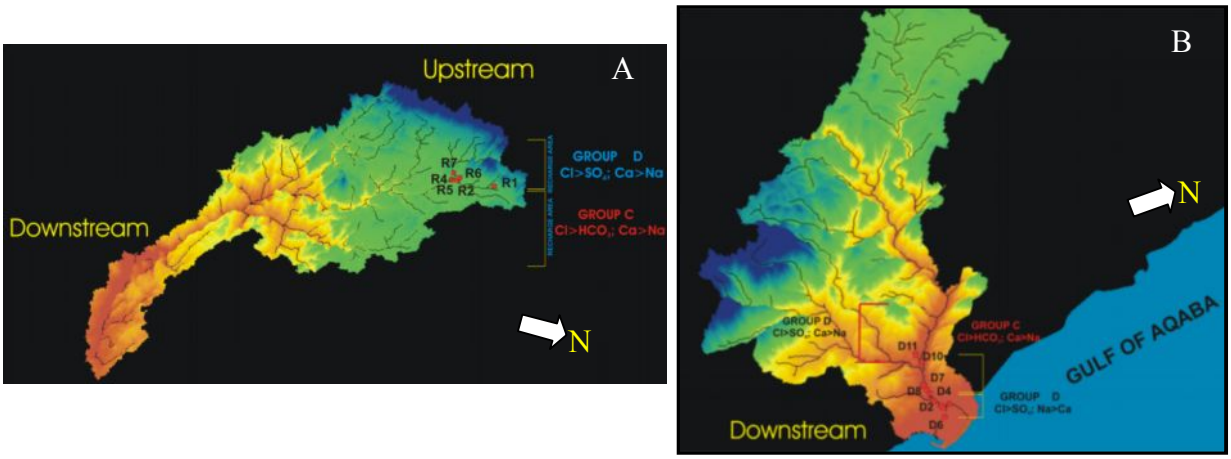

Figure 102-A: Hydrochemical Facies in W. Rimthy

Figure102-B: Hydrochemical Facies in Downstream of Dahab

Downstream of the Dahab basin, chloride, sulphate and calcium are highly dominant in the groundwater of the basement aquifer. The reasons for this, besides the low recharge, include the shallowness of the groundwater table and the high rate of evaporation (e.g. well D11,Group D). In contrast, the chloride, bicarbonate and calcium contents dominate groundwater of the alluvial aquifer. This pattern is changed to chloride – sodium facies due to the effect of long flowpath and the impact of seawater intrusion at the coastal area of the basin (fig.102-B).

3.3.4 Hydrochemical ratio

Ionic ratios are very helpful for establishing the chemical similarities among the different types of water representing a single aquifer. Values of some characterized ion ratios are listed in table 21 and compared with standard ratios of seawater afterwards (Ovichinikov, 1955). The selection of the more significant ratios to be studied should be made according to the possible sources of ions and the expected chemical processes along groundwater flow paths. The hydrochemical ratios are also useful in detecting processes affecting the water quality such as leaching, mixing and ion exchanges. The ratios are expressed as meq/l.

The hydrochemical coefficients are rNa/rCl, rMg/rCl, rSO_4/rCl, $rCl/rHCO_3$ and rBr/rCl ratios. Ovitchinikov (1955) took the hydrochemical ratios (rNa/rCl, rMg/rCl,and rSO_4/rCl) of the seawater as standard values (0.854, 0.198 and 0.103 respectively). These values are compared with the calculated values of the hydrochemical parameters of groundwater in the study area.

	No.	Name	rMg/rCl	rNa/rCl	rSO_4/rCl	rBr/rCl	$rCl/rHCO_3$	Aquifer
WADI NASAB	1	A	0.707	1.020	1.464	0.00075	0.502	Basement
	2	N1	0.710	1.050	0.859	0.00118	0.521	Alluvial
	3	B	0.505	0.861	0.880	0.00082	0.921	Alluvial
	4	N10	0.493	0.863	0.793	0.00095	0.879	Alluvial
	5	N3	0.499	0.850	0.759	0.00113	0.957	Alluvial
	6	N6	0.511	0.843	0.805	0.00080	0.862	Alluvial
	7	N7	0.467	0.840	0.805	0.00101	1.071	Alluvial
	8	N5	0.471	0.978	0.942	0.00072	1.046	Alluvial
	9	N12	0.428	0.499	0.819	0.00068	2.158	Alluvial
	10	N11	0.355	0.689	0.806	0.00072	2.669	Alluvial
WADI SAAL	11	S1	0.219	0.745	0.616	0.00078	5.178	Basement
	12	S2	0.171	0.690	0.381	0.00083	8.232	Basement
	13	S2/1	0.168	0.717	0.382	0.00068	9.941	Basement
	14	S6	0.336	1.339	0.773	0.00028	1.561	Alluvial
	15	S4	0.327	1.345	0.763	0.00028	1.563	Alluvial
	16	S7	0.305	1.138	0.700	0.00028	2.136	Alluvial
	17	S13	0.338	1.144	0.696	0.00031	1.685	Alluvial
	18	MS8	0.315	1.479	0.777	0.00000	1.360	Alluvial
	19	S9	0.258	1.420	0.747	0.00035	2.145	Alluvial
	20	S12	0.234	1.345	0.809	0.00032	3.806	Alluvial
	21	S10	0.210	1.339	0.787	0.00026	5.843	Alluvial
	22	S11	0.488	0.750	0.639	0.00000	7.937	Alluvial
WADI RIMTHY	23	R1	0.301	0.585	0.415	0.00076	3.510	Alluvial
	24	R2	0.291	0.826	0.422	0.00069	2.026	Alluvial
	25	R4	0.316	1.126	0.630	0.00067	1.346	Alluvial
	26	R5	0.300	0.911	0.547	0.00057	1.971	Alluvial
D-STR.	27	D4	0.043	0.536	0.099	0.00502	5.856	Alluvial
	28	D11	0.018	0.501	0.045	0.00481	66.655	Basement
		Refrence	0.1986	0.854	0.103	0.0035		

Table 21 : Hydrogeochemical Ratios For Groundwater Samples in Dahab Basin.

3.3.4.1 rMg/rCl ratio

The ratio helps to understand the impact of evaporation on shallow aquifers and reflects the effect of the length of pathway on the chemical characteristic of groundwater. rMg/rCl ratio ranges between 0.217 and 0.717, especially in the alluvial aquifer of W.Dahab sub-basins. At W. Nasab, the ratio ranges from 0.707 at well A to 0.33 at well N11. The ratio decreases toward downstream of W. Nasab (fig. 103-A). The gradual increasing of Cl ion in alluvial aquifers towards the downstream of W. Nasab is due to the flowpath effect that is considered the main reason for the gradual decreasing ratio (rMg/rCl) (fig. 103-A).

In W. Saal, the ratio ranges from 0.219 (wells S1&S10) to 0.338 (well S13) and reaches 0.488 (well S11). The rMg/rCl ratio varies along the Wadi Course (fig. 103-B). High Cl concentration in the upstream area of W. Saal, especially at wells S1, S2 and S2/1 (basment aquifer), is recorded due to the effect of evaporation on the shallow groundwater table in addition to the presence of a highly mineralized zone (El Rayes, 1992). A high ratio in the downstream area of W. Sall results from increasing Mg ion concentration relative to Cl ions. The gradual decrease of the ratio along the alluvial aquifer is due to an increase of Cl ion by the long flowpath process from well S6 to s 10 (fig.

103- B). The abrupt change in the ratio at well S11 in the downstream part of W. Saal is due to the dissolution of dolomite of the lower Cretaceous aquifer at this zone (fig 103-B).

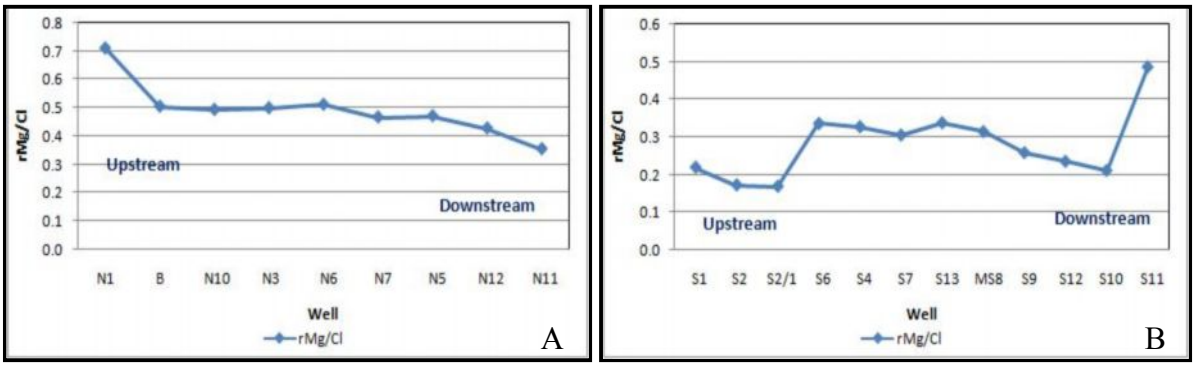

Figure 103-A: rMg/rCl Distribution along W. Nasab B: rMg/rCl Distribution along W. Saal

Generally, the long flowpath process along the alluvial aquifer tends to decrease the Mg concentration due to the cation exchange between the Ca, Na and Mg ions. Additionally, the long flow path increases groundwater salinity due to enhanced Cl ion content. Therefore, the ratio decreases gradually along alluvial aquifer e.g. from N1 to N11 in W. Nasab and from S6 to S10 in W. Saal.

Several factors cause the increase in Cl ion concentration and then the decreasing ratio in the basment aquifer (e.g. wells A in W. Nasab and wells S1,S2 and S2/1 in W. Saal). These factors include the evaporation effect due to the shallow depth of the water table, including Cl ions in wind blown aerosol and that originate from fluid inclusions in quartz that are opened by fracturing, weathering or other processes that bring them in contact with water(Gascoyne and Kamineni, 1994).

3.3.4.2 rNa/rCl ratio

This ratio expresses the dissolved amount of sodium chloride in water. The rNa/rCl ratio has a range between 0.5 and 1.4. Most samples have higher rNa/rCl values than the standard value of seawater (0.853). The high rNa/rCl ratio is mainly found at the upstream of W. Nasab at wells A,N1,B and N10 and in the downstream area of W. Saal at wells S9,S8,S10 and S12. The high ratio may result from the uptake of Na caused by the dissolution of feldspar of the basement rocks (e.g. well A) and the dissolution of evaporites as well as cation exchange processes along the stream course in the alluvial aquifer at W. Nasab andW.Saal.

Low values of the rNa/rCl are recorded in the upstream area of W. Saal (wells S1, S2 and S2/1), in the upstream area of W. Rimthy (R1, R2), along the downstream part of W. Nasab (wells N11 and N12) and in the downstream area of Dahab basin. The low rNa/rCl value relative to seawater indicates that the source of Cl ion is not directly connected to seawater. The enrichment of Cl may be attributed to the presence of a higly mineralized zone, especially at the upstream part of W. Saal, in addition to

the influence of the evaporation process during dry seasons and long flowpaths in the alluvial aquifer in the downstream areas of W. Nasab and W. Dahab.

3.3.4.3 $rCl/rHCO_3$ ratio

The $rCl/rHCO_3$ ratio is used to recognize recharge and discharge zones (Rosenthal, 1987 and Alyaamani and Hussein, 1995). Based on this ratio, Todd (1959) classified the groundwater into six classes from fresh water to seawater. The $rCl/rHCO_3$ ratio ranges from 0.5 to 9.7 and increases to 66 in the downstream area of W.Dahab (well D11) in the basement aquifer. The ratio varies between 0.5 in the upstream area and 2.6 in the downstream area of W.Nasab. The water well in W.Nasab produces fresh groundwater according to Todd's classification. The hydrochemical properties change to moderately contaminated groundwater in the downstream area of the Wadis.

The $rCl/rHCO_3$ ratio ranges from 1.5 to 9.2 in W.Saal. The ratio increase at the recharge area, while the low values are recorded in the middle part of the Wadi, and increases once again in the downstream area of W. Saal. Water is classified into slightly contaminated water in the middle area of the Wadi to seriously contaminated in both the recharge area of W.Saal (well S2, S2/1) and the discharge area (well 10, 11). The ratio increases in the downstream area of Dahab basin.

The low $rCl/rHCO_3$ value indicates the predominance of HCO_3 relative to Cl and refers to areas close to the recharge zones. This is confirmed at the upstream zone of W. Nasab, especially at wells A, N1, B and N10; on other hand, the salinity of the groundwater of these wells is low compared to the groundwater in other wells in W.Nasab. The high $rCl/rHCO_3$ ratio indicates an increase of Cl because of the long flowpath of groundwater away from the recharge area, especially within the alluvial aquifer.

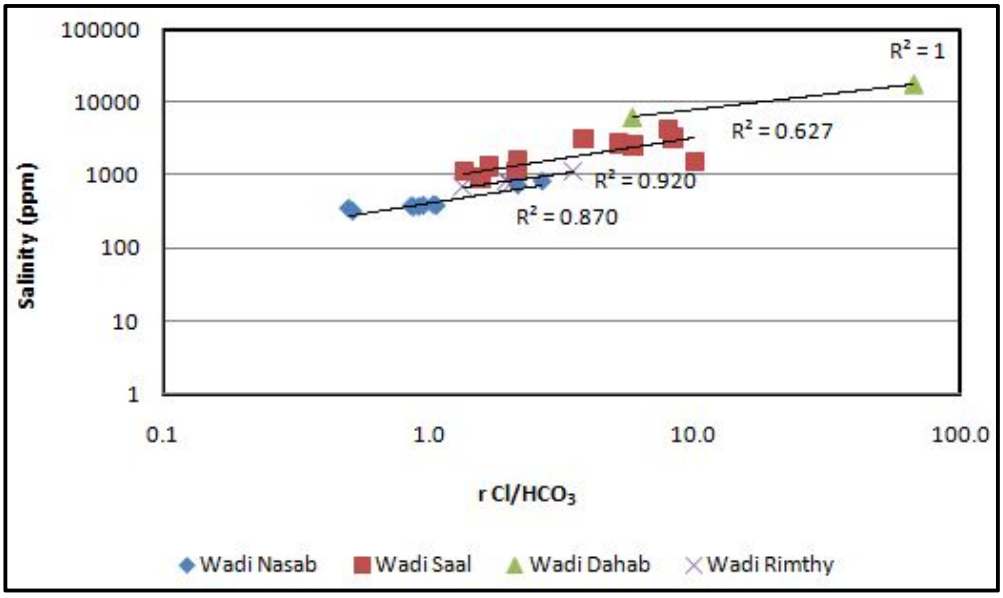

Figure 104 : Relation Between $rCl/rHCO_3$ Ratio and TDS in Groundwater of W. Saal

With the increasing distance from the recharge area, the ratio $rCl/rHCO_3$ changes (Rosenthal, 1987). The $rCl/rHCO_3$ ratio has a high value at areas close to seawater, especially at the downstream of Dahab basin (wells D4 &11). The abnormally high ratio is recorded at the upstream of W. Saal due to the presence of mineralization at this area.

Summarizing, the groundwater in the recharge zone is characterized by high contents of HCO_3 and low contents of Cl, as well as low salinity. On the other hand, groundwater in the discharge area has low concentrations of HCO_3 and high contents of Cl. The obtained results reflect the direct relation between the $rCl/rHCO_3$ ratio value and salinity (fig.104).

3.3.4.4 rSO_4/rCl ratio

The calculated rSO_4/rCl ratio for most of the collected groundwater samples from the alluvial aquifer has a higher value than that of the standard normal seawater value (0.1030), where it ranges from 0.213 to 0.982 and reaches up to 1.47 at the basement aquifer, especially well A of W. Nasab. The ratio increases due to the effect of the oxidation of sulphide minerals. The sulphate concentration increases in alluvial deposits due to the effect of fertilizer application in local cultivated areas around wells N11, N12 inW. Nasab and along alluvial streams of W. Saal. Addtionally, the dissolution of gypsum minerals delivers sulphate ion along the groundwater flowpath within the alluvial aquifer.

In the downstream area of Dahab basin, low values of rSO_4/rCl have been measured between 0.045 and 0.099 at wells D4 and D11. The low ratio is due to the impact of lithologic leaching and long flowpath in addition to the impact of seawater intrusion. At a certain distance from the recharge zone, chloride (which is the most soluble ion) became the leading anion, its concentration exceeds both SO_4 and HCO_3.

3.3.4.5 rBr /rCl ratio

The rBr/rCl ratio may help to identify sources of salinity (Kim et al., 2003; Hernández-García and Custodio, 2004). Cl concentrations largely reflect the input conditions at the time of recharge and may be modified subsequently by mixing with formation waters, seawater or dissolution of evaporites and long length flowpath from upstream to downstream. Br generally behaves conservatively and may be used to constrain the source of Cl. The rBr/rCl ratio in seawater is 0.0035 ± 0.0002 (weight ratio) and unpolluted precipitation concentrations lie close to this value. Thus, assuming no other sources of Br and Cl are present, the Br/Cl ratio should be constant when salinization of fresh water occurs by simple mixing with seawater.

The rBr/rCl ratio ranges in Dahab basin between 0.00026 and 0.0054. It is relatively low in the downstream areas of W. Nasab and W. Saal where it ranges between 0.00026 and 0.0008. The same range has been found in the upstream area of W. Saal. The low ratio in the downstream areas of W. Nasab and W. Saal is because of the increasing of the concentration of the chloride content from different sources along the wadi in comparison with a low Br concentration. The high Cl ion

concentration came from the effect of long flowpaths along the alluvial aquifer. At the upstream part of W. Nasab, the rBr/rCl ratio is relatively high, ranging from 0.0009 to 0.001, especially at wells N1, B and N3. This is due to the decreasing of the chloride conconcentration and confirms that the recharge area of W. Nasab has a low source of Cl.

A bivariate diagram of rBr/rCl ratios and Cl concentrations of the groundwater is shown in figure 105. The rBr/rCl ratios of groundwater plot below the marine value. The scattering of data indicates multiple sources of Cl, probably including the anthropogenic origin. the anthropogenic origin is confirmed by the nitrate association found in some well water samples in the downstream area of W. Nasab and upstream of W. Saal. As the Cl content of the groundwater increases, the rBr/rCl ratios approach marine levels, indicating the source of salinity was of marine origin (e.g. samples at the downstream of W. Dahab). High rBr/rCl ratios above marine levels could be attributed to the high Br contents derived from the decomposition of evaporite minerals or to the local impact of seawater-groundwater mixing (Maritin et al., 2004).

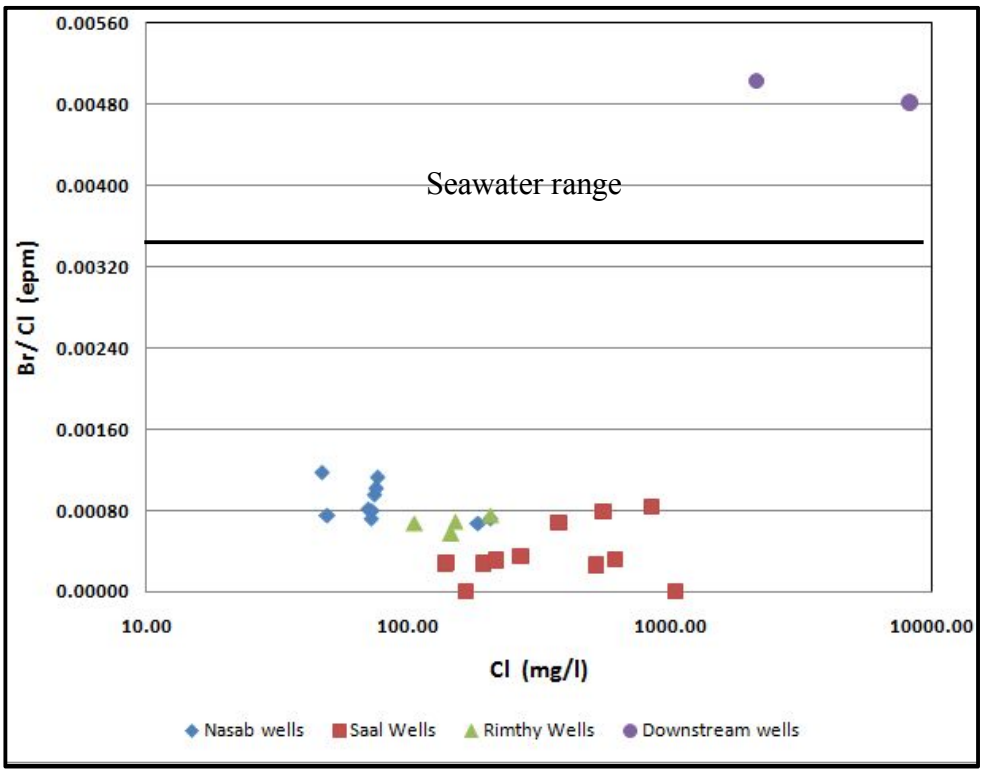

Figure 105 : Relation Between rBr/rCl ratio and Cl Concentration in Groundwater of W.Dahab

3.3.5 Hydrogeochemical processes

The hydrogeochemical processes and the hydrogeochemical condition of the groundwater vary spatially and temporally, depending on the geology and chemical characteristics of the aquifer. Major ions constitute a significant part of the total dissolved solids presented in groundwater. The

concentrations of these ions in groundwater depend on the hydrogeochemical processes that takes place in the aquifer system. These processes occur when the groundwater moves toward equilibrium in major ion concentration. Hence, the study of concentrations of various major ions present in groundwater is used in the identification of geochemical processes.

Studying chemical evolution of the groundwater that takes place in this study area is as follows:

a) Reactions of rainwater as it infilterates the surface soil zone and percolates through the unsaturated zone to the water table.
b) Dissolution reactions of evaporite and sulphate salts in soil zone throughout flushing processes due to flood events.
c) Chemical weathering of silicate minerals and sediments.

Apodaca et al. (2002) inferred that hydrogeochemical processes such as dissolution, precipitation, ion-exchange processes, and the residence time along the flo path control the chemical composition of the ground water in the shallow alluvial aquifers. In this part, factors affecting water-rock interaction processes that produce dissolved ion contents and elevate water salinity will be discussed. These processes help to identify the hydrogeochemical characters and control the chemistry of groundwater in the study area.

3.3.5.1 Origin of dissolved ions

The mechanism controlling water chemistry and the functional sources of dissolved ions can be assessed by plotting the hydrochemical data according to the variations in the ratios of Na^+: (Na^+ + Ca^{2+}) as functions of TDS (Gibbs, 1970). The plots of data on the Gibbs diagram (fig.106) suggest that chemical weathering of rock-forming minerals are the dominant factors controlling groundwater chemistry in the study area. On the other hand, the evaporation process plays an important role in wells S1, S2, S11 and S10 in W. Saal and well D11 in the downstream area of W. Dahab due to shallowness of the groundwater table.

Hard rocks in Dahab basin are widely distributed in the upstream parts of the basin; therefore, the presence of cations in groundwater may originate from dissolution of silicate minerals. The cation contribution in groundwater by silicate weathering can be estimated by the (Na + K)/total cations index (Stallard and Edmond, 1983; Sarin et al., 1989). The (Na + K) vs. total cations (TZ+) scatter diagram of the study area shows that most samples fall along and above the (Na + K) = 0.5 TZ+ line. Datta and Tyagi (1996) observed that the contribution of cations may be derived from silicate weathering when (Na + K) = 0.5 TZ+ as is the case of the alluvial aquifer of W. Saal (fig. 107).

Sodium and potassium are important cations in groundwater. Sodium may originate by dissolution of silicate minerals such as feldspar. It may result also by dissolution of halite minerals and cation exchange processes which may occur during the flowpath through aquifer. The relation between Na + K and Cl can help to investigate the source of both cations.

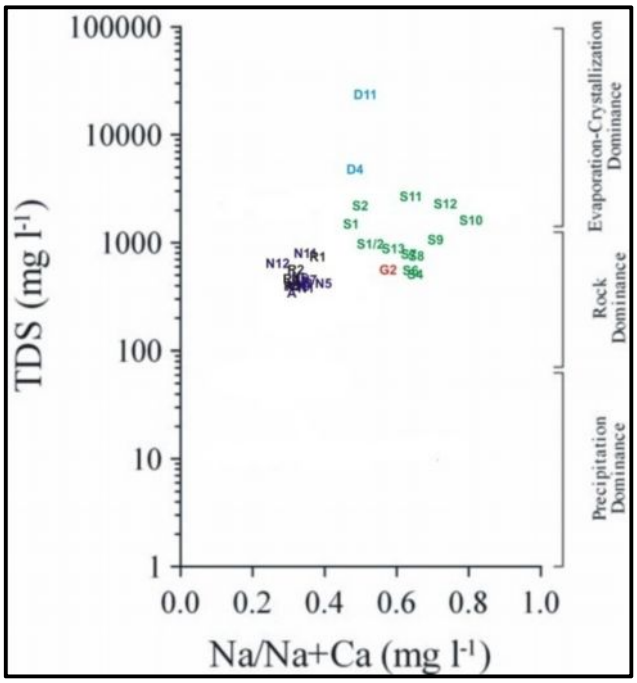

Figure 106: Gibbs Diagram of Groundwater of W. Dahab

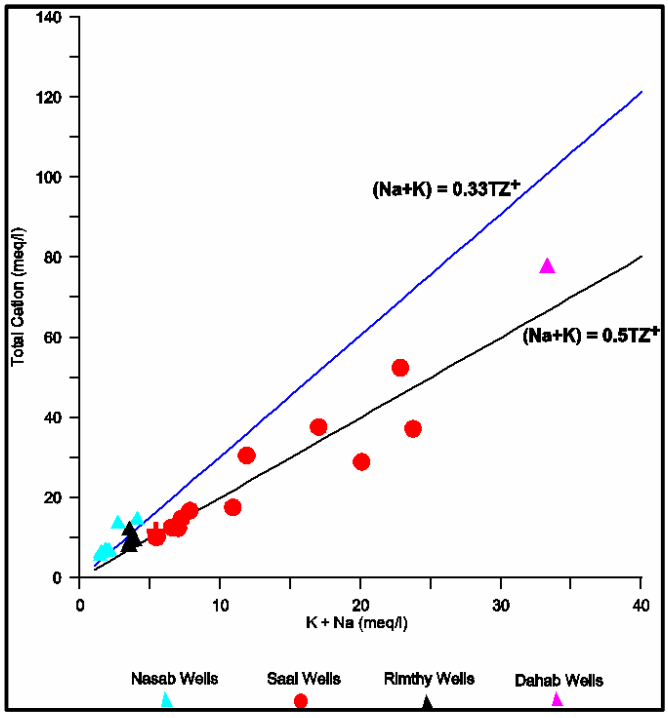

Figure 107: Relation Between Total Cation (meq/l) and K+Na (meq/l) in Groundwater of Dahab Basin

The excess of $Na^+ + K^+$ over Cl^- (fig.108) at low chloride content reflects input from the weathering of Na and K rich minerals. When halite dissolution and cation exchange is prominent, it implies a 1:1 relationship between Na +K and Cl. The diagram shows that most of the sample points fall on and above the 1:1 equiline which indicates that Na and K ions originate from cation exchange

and halite dissolution processes. These processes mainly occur along the alluvial aquifers of W. Nasab and W. Saal. Some of the sample points below the 1:1 equiline indicate the origin of Na ions from the weathering of Na and K rich minerals (silicate minerals), especially in basement aquifers as in the upstream areas of W. Saal.

Calcium and magnesium are the dominant ions in groundwater of the study area and are found in considerable amounts. The dominance of Ca, Na, and Mg is associated with silicate minerals (clay minerals) such as montmorillonite, illite, and chlorite (Garrels, 1967) besides feldspar minerals. Calcium ion present in the groundwater of the study area may come from dissolution of $CaCO_3$ and $CaMg(CO_3)_2$ during recharge; Datta and Tyagi (1996) explain this in the (Ca + Mg) vs. (HCO_3 + SO_4) scatter diagram (Fig.109). The ionic concentrations falling above the equiline result from carbonate weathering, whereas those falling along the equiline are produced by both carbonate and silicate weathering.

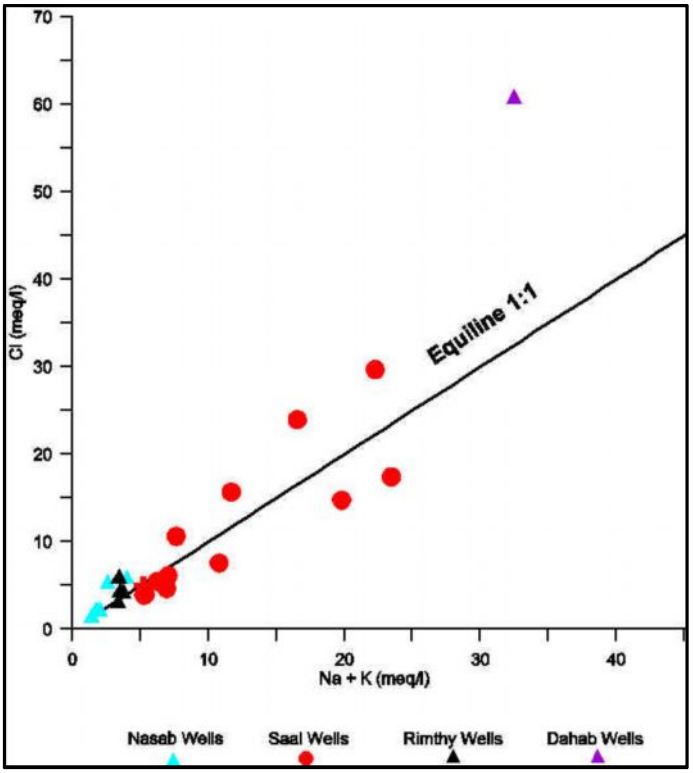

Figure 108 : Relation Between Cl (meq/l) and K+Na (meq/l) in Groundwater of Dahab Basin

The (Ca + Mg) vs. (HCO_3 + SO_4) scatter diagram of groundwater shows that few water sample points lie above the equiline, with most of samples falling along the equiline and below. This indicates that silicate weathering is the main source of calcium ion in the groundwater, whereas few points above the equiline indicate carbonate weathering and cation exchange. The figure shows that some samples in W. Nasab and W. Saal fall on the equiline. The long flowpath of groundwater along alluvial aquifesr to the downstream may enhance the cation exchange and dissoultion of carbonates in aquifer sediments.

It can be concluded that the dissolution of silicate minerals such as feldspar and mica is the main source of cations in the study area. Silicate minerals, which are distributed in basement rocks or in alluvial deposits as weathered material, are strongly influenced by the chemical and slightly aggrisive nature of rainwater caused by dissolved CO_2. When CO_2 charged waters that are low in dissolved solids react with silicate minerals, high cations and silica are leached and then released into groundwater. The residue materials which result from the previous process are mainly clay minerals such as illite, kaolinite and montomorllionite (Freeze and Cherry, 1979).

Silicate minerals like feldspars (plagioclase, orthoclase and andesine), amphiboles, micas, pyroxenes and clay minerals are the most important minerals that are included in basement rocks in the watershed and as weathered loose material in alluvial deposits. According to Garrels (1967), the weathering of the plagioclase (andesine) can be represented as in equation 29. In this reaction, andesine dissolves under the leaching action of carbonic acid (H_2CO_3) to produce HCO_3^-, SiO_2, Ca^{2+} and Na^+ as well as the clay mineral residue (kaolinite).

$$4Na_{0.5}Ca_{0.5}Al_{1.5}Si_{2.5}O_8 + 6CO_2 + 9H_2O = 3Al_2Si_2O_5(OH)_4 + 4SiO_2 + 2Na^+ + 2Ca^{2+} + 6HCO_3^-$$

Andesine Kaolinite **Equation (29)**

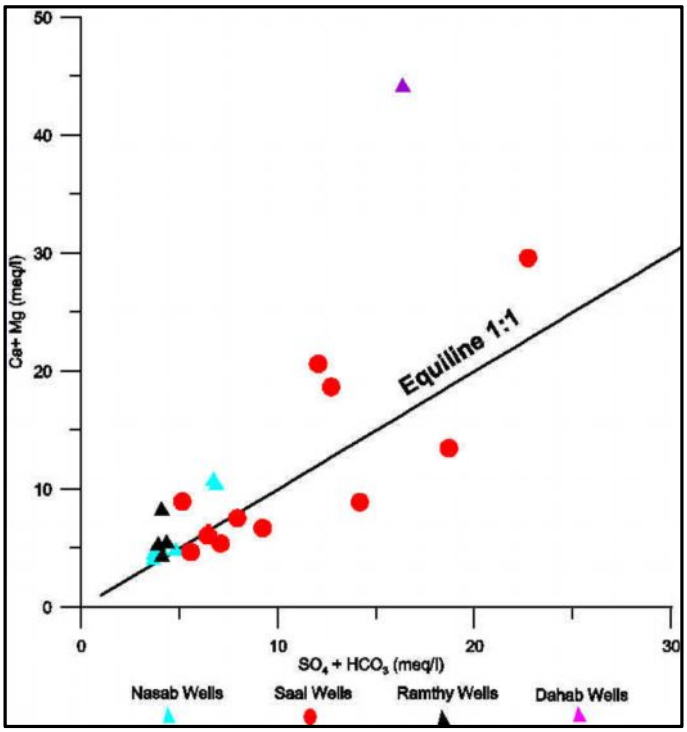

Figure 109: Relation Between Ca+Mg (meq/l) and SO_4 +HCO_3 (meq/l) in Groundwater of Dahab Basin

3.3.5.2 Origin of groundwater salinity

Several parameters help to understand the origin of groundwater salinity and explain the hydrogeochamical process responsible for the resulted chemical properties of groundwater. These parameters are discussed below.

3.3.5.2.A Rock type

The chemistry of water and its salinity from basement aquifers depend on the rock types which are flown through. Waters derived from the basic rocks are more saline than water obtained from the granitic rocks (El Rayes, 1992). The relatively high salinity in those waters is attributed to the high susceptability of basic rocks for chemical weathering compared to granites. Major ion contents in waters from volcanics and metabasic rocks in the upstream part of W. Saal (e.g. S1 and S2 have TDS 1708 and 2073 mg/l) are somewhat higher than the corresponding concentrations in waters from the granitic rocks and acid volcanic rocks in W.Nasab and W.Rimthy (e.g. Well A at W. Nasab has low TDS 345 mg/l).

3.3.5.2.B Groundwater movement

The effect of surface lithology on groundwater flow may be significant, especially in shallow alluvial aquifers. The bedrock with a set of barriers either supports or impedes the water flow system. The groundwater flow is interrupted in many parts along the wadi course due to the presence of the basement rocks at and/or near the surface. This is clear in the upstream area of W. Nasab, where several igneous outcrops are encountered across the main wadi channel. Geophysical data and field investigations show that, in the lower parts of the W. Nasab (wells N11and N12) and W. Saal (S9, S10, S13, and S12), the thickness of the alluvial aquifer reaches more than 50m and there is a low presence of rock barriers (dykes) that influence the groundwater flow. The length flow of alluvial aquifers support the dissolution of minerals, adding major ions to groundwater and causing an increase of salinity. It was observed that the salinity ranges in the lower parts between 726 and 819 mg/l in W. Nasab while it ranges between 851 to 1600 mg/l in W. Saal.

In the upper part of the W. Saal (wells S1 and S2), dykes and shallow bedrock form impediments to groundwater flow and tend to break the saturation zone into small basins, permitting more water-rock interaction to affect the water quality. Consequently, the concentration of salts increases at these localities from 990 to 2073 mg/l.

3.3.5.2.C Water-Table position

The aquifer of W. Dahab is unconfined and the watertable is not deep enough to be protected from pollution effects, especially in the upstream parts of the wadis . However, the watertable depth in the upper part of the wadi ranges between 7 and 14 m which is shallow enough to be affected by the continuous evaporation process. This process causes mineral precipitation during the period between runoff events. The evaporation process is clearly observed in the upstream part of W. Saal and W. Rimthy in wells S1, S2, R1, and R5 and also in the downstream part of W. Saal and W. Nasab at S8, S9, S12 and N11.

On the other hand, the watertable depth in different parts the same wadis (W. Nasab &W. Saal) at wells N10, B,N3,N5,N7, N12, S4,S6 and S7 is deeper, ranging between 15 and 43 m in depth and resulting in a reduction of evaporation compared to those shallow wells in W. Saal and W. Rimthy.

3.3.5.2.D Agricultural uses

The forming of salt crust results from flooding irrigation follwed by evaporation. The salt remained on the top soil rising the soil salinity which is leached by the infiltrated water during the wet seasons and moved down into the groundwater body.

In the upstream part of W. Nasab, where the groundwater is exploited from wells of the main channel at wells N1, N10, B, and N3 and has a low salinity ranging from 315 to 370 mg/l. These wells are used for domestic and livestock purposes but they are not located near cultivated areas. On the other hand, wells N11 and N12 and those along the main stream of W. Saal at S9, S12, S10 and S13 have a high salinity due to mixing with the effluent of returned flow irrigation water that results from the local cultivated areas.

3.3.6 Health and environmental impacts

One of the aims of this study is to characterize groundwater quality and assess its suitability for drinking use and irrigation purposes. The presence of human activities such as agriculture, animal breeding and farming exert anthropogenic pressure on the quality of groundwater of basement and shallow alluvial aquifers in W. Dahab. Shallow groundwater is more likely to show impacts of anthropogenic contamination from artificial activities than deep grounwater (Gillion et al., 1995).

In the study area, there are several sources of contamination of groundwater. These are the return flow of irrigation water and the leakage of sewage from the residential area, especially at W. Saal and W. Nasab where disposal of domestic waste water is carried out in unlined septic tanks and latrines. The behavior of trace metals in groundwater is complicated and is related to sources of water and the bio-geochemical processes taking place along the flow path. Some metals are needed for normal functioning of the human body, whereas others are non-essential. Most of the metals are important for the growth,development and health of living organisms.

There are several parameters which indicate quality of groundwater and measure the degree of contamination.These parameters describe the physical and chemical properties of water. There are some metals that cause health problems beyond certain concentration levels. Some of these physico-chemical parameters are discussed below.

3.3.6.1 Total Dissloved Solid distribution as a contamination indicator

The values of total dissolved solids in groundwater show a systematic control on rock-water interactionand land-use characteristics and are tended to increase in the agricultural and residential

areas downstream of W. Nasab and W. Saal. The gradual increase of TDS values towards the downstream area of W. Nasab reflects the change ion concentration in groundwater. The ion change is caused by not only water-rock interactions along the groundwater flow path in alluvial aquifer, but also the dominant land use and agricultural use around each well. The high TDS may result from impact of seawater intrusion in the coastal zone of Dahab basin. The TDS values can be effectively used as an indicator of groundwater contamination for planning suitable mangment of this groundwater resource. The TDS of groundwater samples from upstream localites at W. Dahab is variable (fig. 110).

TDS of groundwater has a strong postive correlation with the Cl content. This is due to the conservative nature of Cl in groundwater systems (fig.111). Cl in groundwater can be used as indicator for anthropogenic contamination (Al Ahmadi and El Fiky, 2009). Potential sources for Cl include domestic wastewater from local houses, agro-chemicals and manure of grazing lot. The highest Cl concentrations are recorded at the upstream area in wells R1, S1,S2, S2/1 and at the downstream area in wells N11, N12, S9, S10 and S12 where agricultural activities are common at these sites, as well as their closeness to reseidential areas.

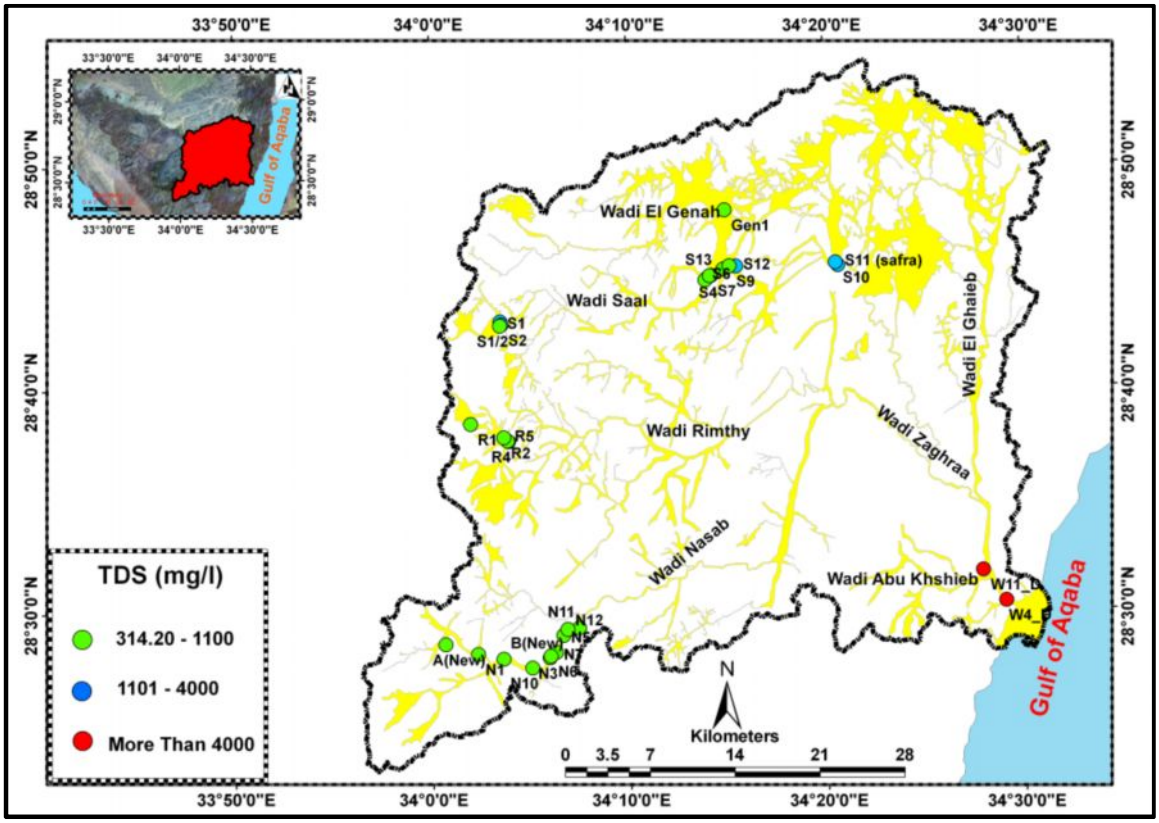

Figure 110: TDS Distribution in Groundwater of Dahab Basin

3.3.6.2 Nitrate (NO_3^-)

Nitrogen is a major constituent of the earth's atmosphere and occurs in many different gaseous forms such as nitrate (NO_3^-) and ammonia (NH_4^+). Natural reactions of atmospheric forms of nitrogen

result in the formation of nitrate and ammonium ions. While nitrate is a common nitrogenous compound due to natural processes of the nitrogen cycle, anthropogenic sources have greatly increased the nitrate concentration, particularly in rainwater.

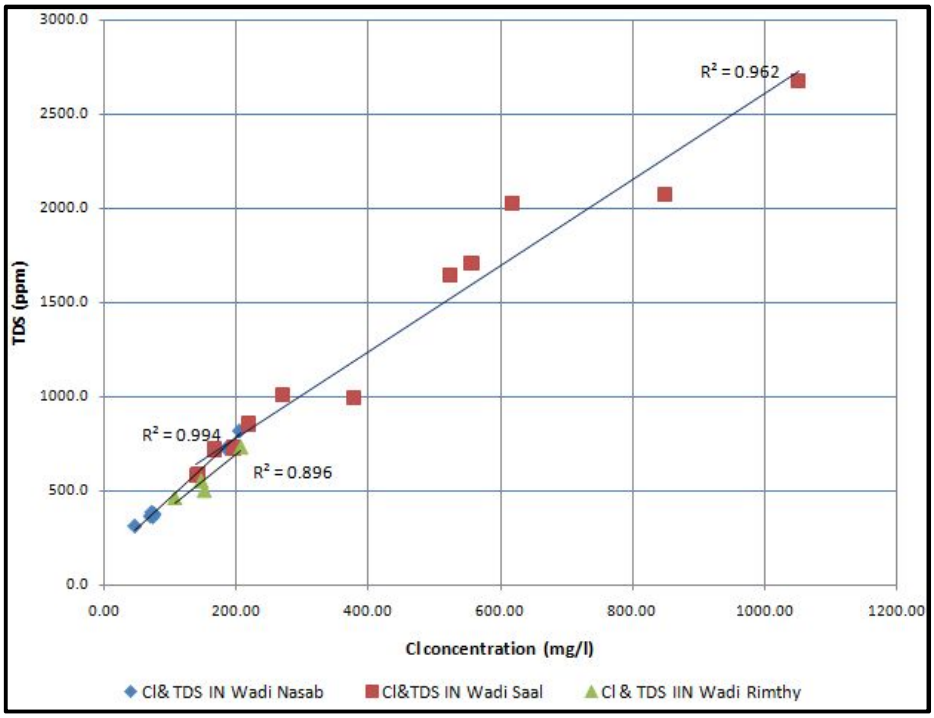

Figure 111: Relationship Between Cl and TDS in Groundwater of Dahab Basin

Possible sources of NO_3^- contamination include manure applied to land, agricultural fertilizer, industrial effluent, domestic wastewater, septic tanks, human waste lagoons, native soil organic matter as well as geologic sources (Helmut, 2000). Because NO_3^- is very mobile in most soils, it might be leached from soil and washed into groundwater (Nolean,1999). Particularly in private wells, incidence of methemoglobinemia appeared to be the result of high NO_3^- levels. In drinking water, the limit for NO_3^- is 50 mg/l (WHO, 2006) and exceeds the value that may be toxic for infants and may be responsible for the increase of stomach cancer.

Because of the fact that nitrite (NO_2^-) and ammonia (NH_4^+) were not found in all samples of W. Dahab, it can be reasoned that aerobic conditions of the shallow aquifer lead to oxidation of nitrogen compounds to NO_3. Increasing NO_3 levels in groundwater of the study area with increasing TDS confirmed the idea of groundwater contamination by anthropogenic activities (fig.112). Groundwater having high value of NO_3 concentration (more than 50 mg/l) is asscociated with high TDS level.

The NO_3 concentration in groundwater of W. Nasab ranges between 5 mg/l in well A to 111.04 mg/l in well N11 downstream of the W.Nasab (fig.113). The NO_3 value increases at sites where cultivated areas surround wells, especially at wells N11 and N12. While the NO_3 has high values ranging from 63 to 135 mg/l upstream of W. Saal at wells S1, S2 and S2/1, the value decreases along the wadi course to range from 40 to 49.8 mg/l and increases again to 70 mg/l in the downstream area

of W. Saal. The range decreases again toward the downstream to a value between 2 and 4 mg/l. No NO_3 is detected at the distal downstream of W. Dahab (well D11) and only low concentration occurs at well D4.

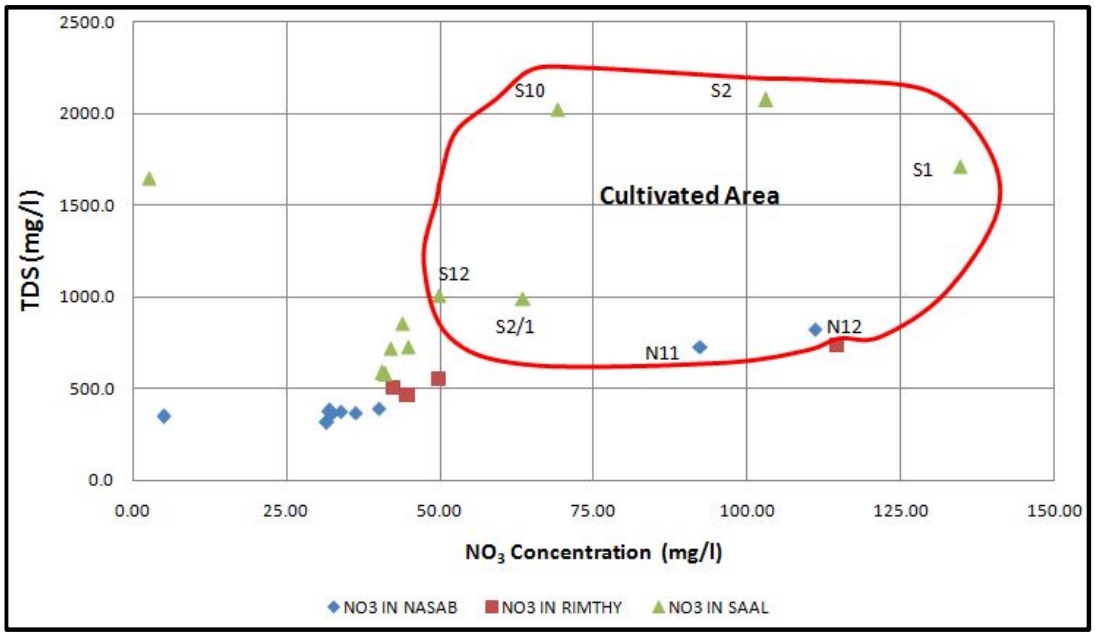

Figure 112: Relationship Between NO_3 and TDS in Groundwater of Dahab Basin

Summarizing, it is observed that the high NO_3 content in groundwater is accompanied with high TDS value and high SO_4 concentrations. This fact occurs in the upstream areas of W. Saal (S1 and S2), downstream of W. Nasab (N11 and N12) and in downstream area of W. Saal (S9 and S12). This confirms that high NO_3 concentrations originate from agricultural and anthropogenic contamination sources.

3.3.6.3 Flouride (F)

Flouride (F) in water is derived mainly from dissolution of natural minerals in rocks and soils. Macdonald et al. (2005) indicated that the most common flouride-bearing minerals are fluorite, apatite and micas. High concentration of flouride problems tens to appear to increase where these minerals are most abundant in the host rocks. Groundwaters from crystalline rocks, especially granites, are particularly susceptible to higher F concentration because they contain abundant fluoride-bearing minerals. Besides this effect, the replacement of hydroxyl by F ions in mica, hornblende and soil that mostly consists of clay minerals, are the major sources of F in circulating water (Hem, 1989). Distribution of basement rocks in the study area and the presence of weathering products of various types of igneous and metamorphic rocks in aquifer matrix or alluvial deposits could be possible sources of F in groundwater.

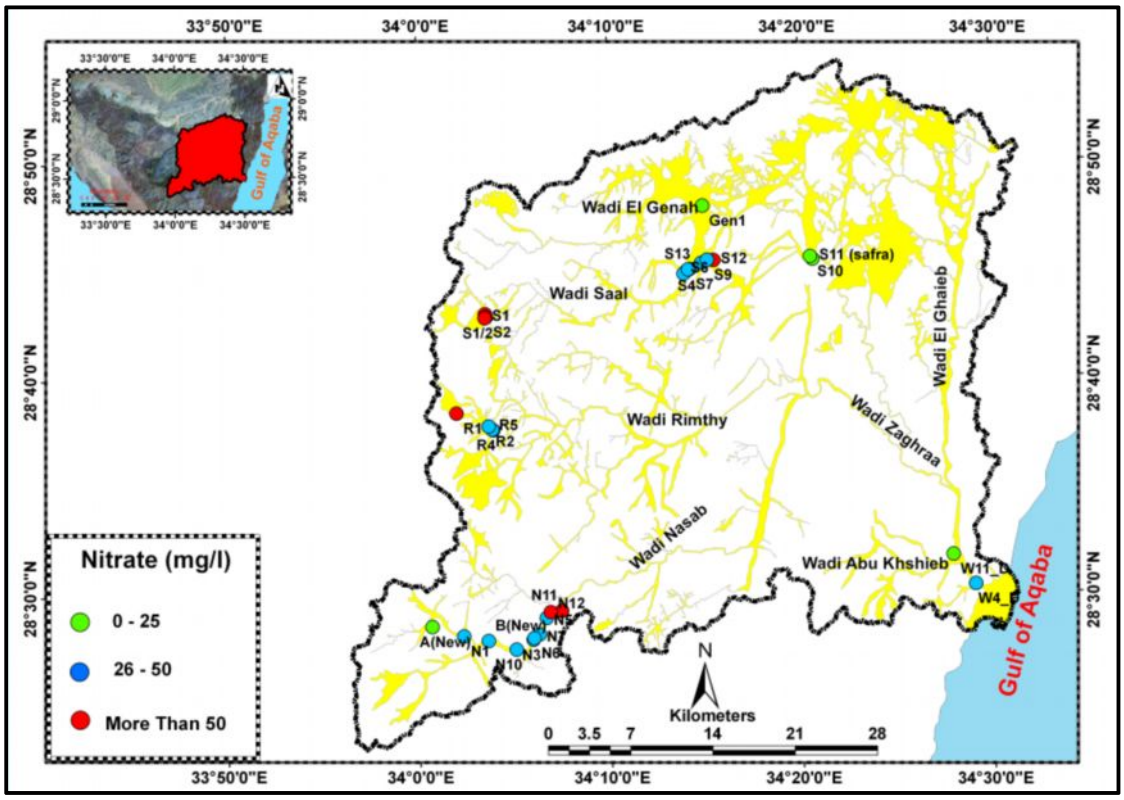

Figure 113 : NO_3 Distribution in Groundwater of Dahab Basin

The source of F may be assiociated with agricultural activities. Flouride (F) is considered one of the main component in chemical fertilizers. The relation between F content in groundwater and TDS shows a high F concentration is associated with high TDS, especially at cultivated areas in W. Dahab (fig.114). The figure emphasizes that dissolution of silicate minerals is not only the source of F ion in groundwater; the effect of fertilizer may be another source.

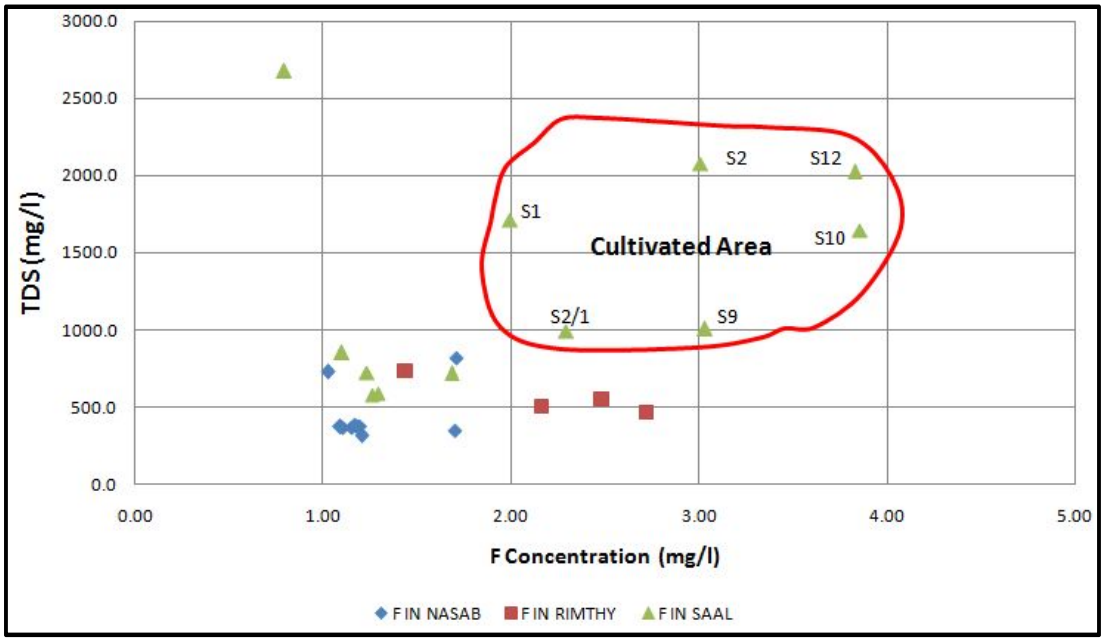

Figure 114: Relationship Between Flouride and TDS in Groundwater of Dahab Basin

Flouride (F) is essential for healthy human beings. It has been found to have a significant mitigating effect against dental caries and it is widely accepted that some flouride presence in drinking-water is important. Optimal concentrations are usually around 1 mg/l. The chronic ingestion of F concentrations much greater than the limit value from WHO (2004) of 1.5 mg/l, however, is linked with development of dental flourosis. High F concentration in drinking water has also been linked with cancer (Marshall, 1990). As several studies have shown (Jones et al., 1997), low doses of fluoride are useful for the prophylaxis of caries, and for the treatment of osteoporosis. If the doses are too high, dental and skeletalfluoroses, changes of the skeleton, and other disorders may occur .

Flouride (F) concentration has general medium to high concentrations in groundwater of W. Nasab. The concentration ranges from 1.03 to 1.71 mg/l. Groundwater of basement aquifers has a high concentration, especially in well A where the silicate minerals are predominant in these rocks.

All groundwater samples of W. Rimthy have a high F concentration. The F content ranges from 1.45 to 2.72 mg/l (fig. 115). A low TDS value and high F concentration indicate that the source of F is dissolution from silicates minerals (fig. 114).

At W. Saal, high F concentration is recorded in groundwater of basement aquifers, especially at wells S1, S2 and S1/2 in the upstream area and along alluvial aquifers in the downstream area at wells S9, S12 and S10 where alluvium deposits include weathered products from granitic outcrops. The agricultural activities may help to enhance flourine concentration in groundwater in cultivated areas in W. Saal (fig. 115).

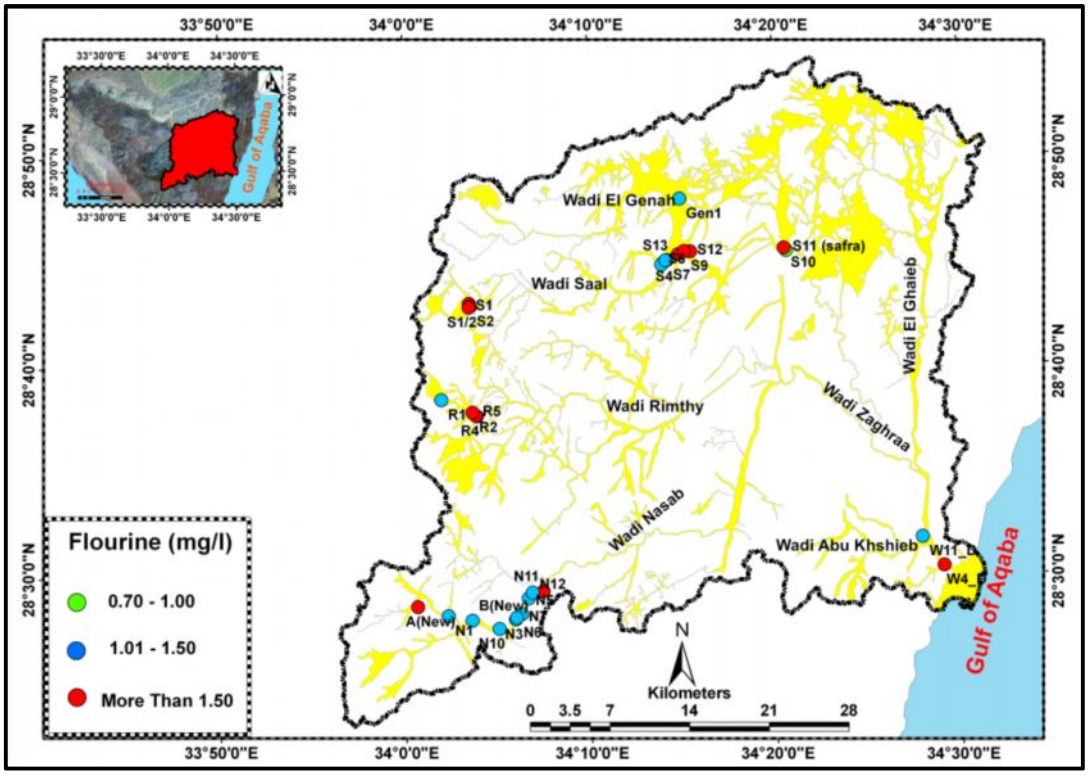

Figure 115: Flouride Distribution in Groundwater of Dahab Basin

3.3.6.4 Uranium (U)

Uranium (U) is a naturally occurring radioactive element that is present to some degree in our environment, including soil, rocks, air and water. It may be found mainly in acidic igneous rocks such as granites and other rock types such as syenites, pegmatites, rhyolites and metamorphic rocks. Uranium (U) is included within most of the basement rocks and alluvial sediments in W. Dahab basin where it is found in acidic, basic volcanic and metavolcanics in W. Saal and W. Rimthy-Zaghraa (Hassan et al., 2004). Radioactive minerals are found in stream sediments such as thorite and uranium rich zircon (Sorour et al., 2003). Geophysically, Moussa (1999) stated the presence of deep seated radioactive anomalies associated with sulphide deposits and uranium is the main cause for these anomalies due to the presence of uranium within mineralization zones. The mobility of uranium in water is controlled by a number of factors, among them especially Eh, pH, and concentrations of coexisting dissolved ions (Smedley et al., 2006; Lauria et al., 2004). Under oxidizing condition, U is highly soluble (U^{+6}) and is therefore mobile while under the reducing condition it precipitates (U^{+4}).

The actual limit value of WHO (15 µg/l) is suggested as a provisional guideline value until additional an health effect is obtained. However, Nephritis is the primary chemically induced effect of uranium in humans (Hursh and Spoor, 1973).

The concentration of U in groundwater of W. Nasab ranges between 10.5 and 30.08 µg/l. The U content has its highest value at well A in the upstream area of W. Nasab. The well taps granitic rocks of the basement aquifer. It also increases in the downstream, especially at wells N11 and N12 (fig. 116). A comparison between water analyses of both seasons (2009 and 2011) indicates an increase of the uranium concentration of most wells. Some of them reach nearly 15 µg/l in water wells A, N11 and N12.

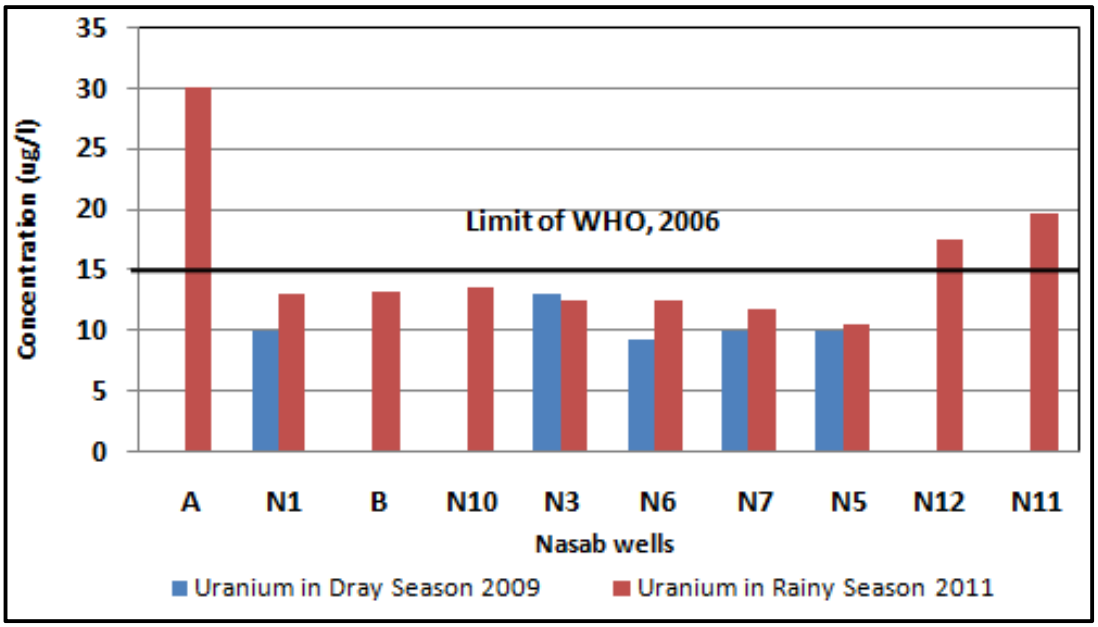

Figure 116 : Uranium Concentration in Groundwater of W. Nasab During Dry and Rainy Seasons

The highest value has been measured in W. Rimthy. It ranges from 28 µg/l to 49 µg/l (fig.117). These values have been measured in groundwater due to the contact of granitic and volcanics rocks in the area of Sanit Catherine. The increasing of U concentration between 2009 to 2011 reflects the oxdition of groundwater during the 2011 season (fig.118). All the water samples in W. Rimthy have concentrations higher than the permisible limit of WHO (2006).

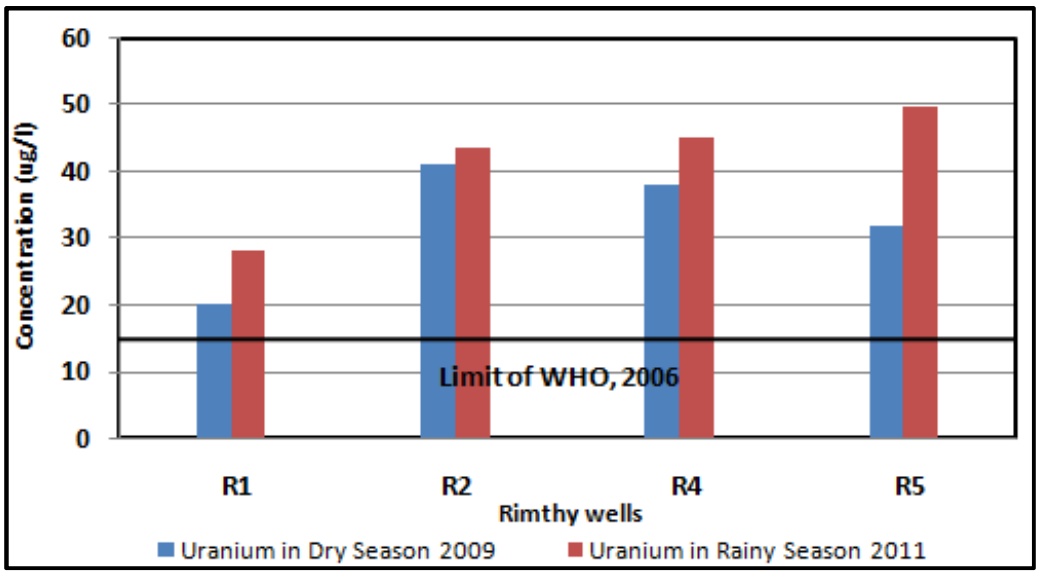

Figure 117: Uranium Concentration in Groundwater of W. Rimthy During Dry and Rainy Seasons

The concentrations of uranium in the groundwater of W. Saal are varied relative to aquifer types. It ranges between 7.4 to 14.08 µg/l in basement aquifers and increases in alluvial aquifers ranging from 11.2 to 65 µg/l in well S10 in the downstream area of W. Saal. No uranium is detected in the groundwater of carbonate aquifers which is represented by well 11 (Safra Well).

The water samples of those taken during the rainy season (January 2011) represent actively recharged water into aquifers and reflect the oxidation environment that enabled uranium to be easily soluble in groundwater. This may explain why uranium contents have higher levels during the 2011 season sampling program. The high concentration of U increases at wells that tap alluvial aquifers. The concentration reaches 65 µg/l at well S10 which is located close to uranium source rocks like basic and granitic rocks of W. Saal.

The high risk level of uranium concentration is mainly found in W. Rimthy and in the downstream area of W. Saal where the wells are located closed to granitic outcrops and sulphide deposits which are associated with radioactive elements (Mussa, 1999). In the downstream area of W. Dahab, there is low to medium concentration of uranium, whereas W. Nasab has high to medium levels of uranium concentration.

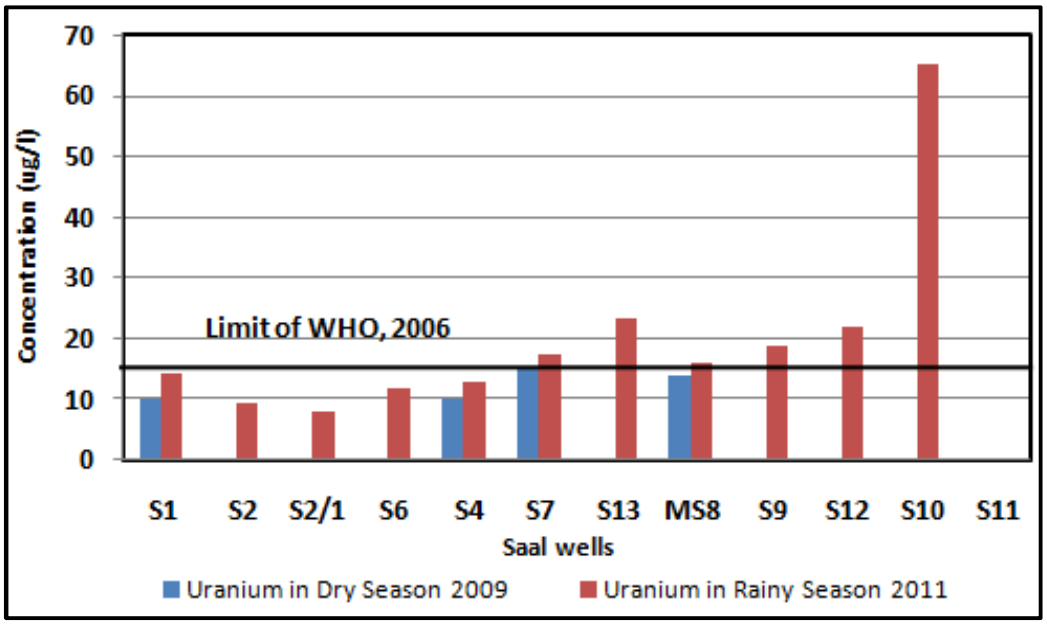

Figure 118: Uranium Concentration in Groundwater of W. Saal During Dry and Rainy Seasons

3.3.6.5 Boron (B)

Boron (B) is widely distributed in nature with an average concentration of 10 mg/l in the earth's crust. It is a minor dissolved constituent of groundwater where it is associated with flourine (Queste et al., 2001). In aqueous solutions, boron was mostly present as $B(OH)_4^-$ and dissociated as boric acid H_3BO_3 (Pennisi et al. 2006).The occurrence of these species in the environment is controlled by the pH value. B is mainly released into the groundwater through the weathering of rocks, seawater intrusion into aquifers, and volcanic activities (Hem, 1985; Pennisi et al., 2006). Therefore, the leaching of rocks and soils is responsible for most of the B dissolved in natural waters. B undergoes a number of interactions with the aquifer-forming rocks, among which the process of adsorption and desorption of boron to clay mineral surfaces plays a crucial role.

High B levels in drinking water are considered to be risky for human health. The limiting value of World Health Organization guidelines for B amounts to 0.5 mg/l. The long-term experiments with animals have shown that excessive content of B leads to reduced fertility and sterility, low weight of fetus, metabolistic disorders and acute neurological effects (WHO, 2006). However, human data is lacking, the only available data shows that acute exposure is associated with short-term irritant effects of the upper respiratory tract (Wegman et al., 1994).

There are low concentrations of B in groundwater of W. Nasab and W. Rimthy. The concentrations range between 74 and 124 µg/l. At W. Saal, the B concentration is low to moderate. It reaches 181µg/l in the upstream area and increases to 384 µg/l downstream of W. Saal. A high concentration of B occurs mainly downstream of the Dahab basin where it ranges from 436 to 885 µg/l.

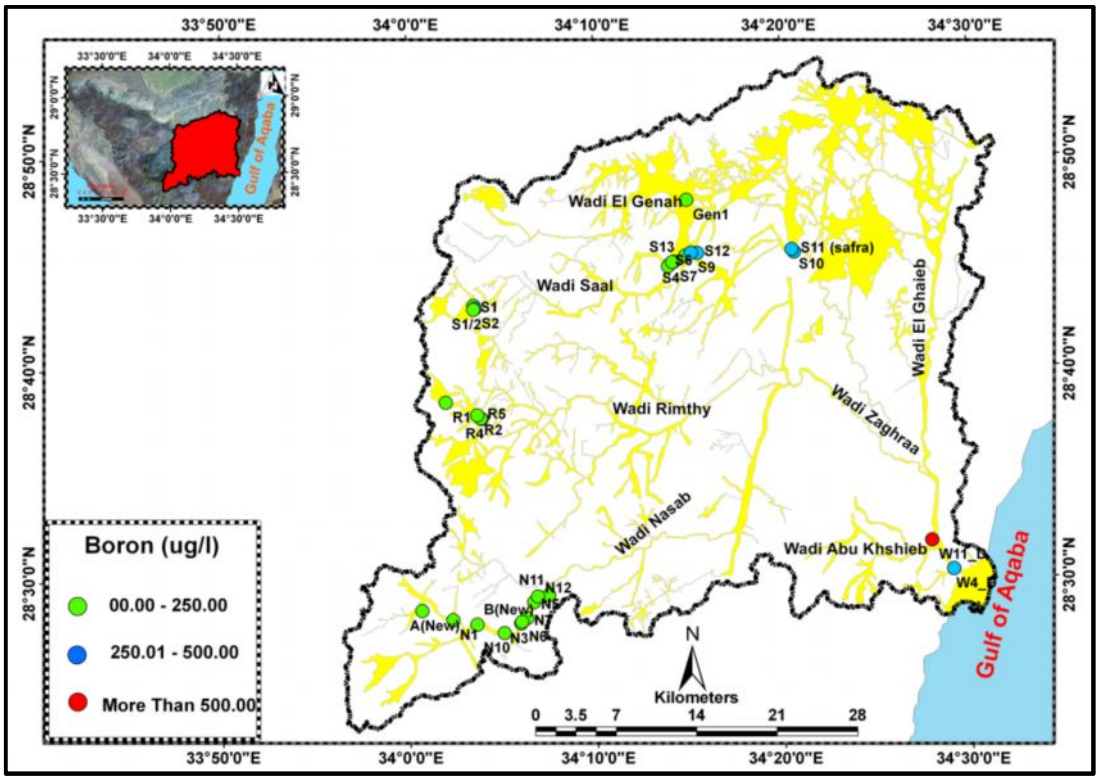

Figure 119: Boron Distribution in Groundwater of Dahab Basin

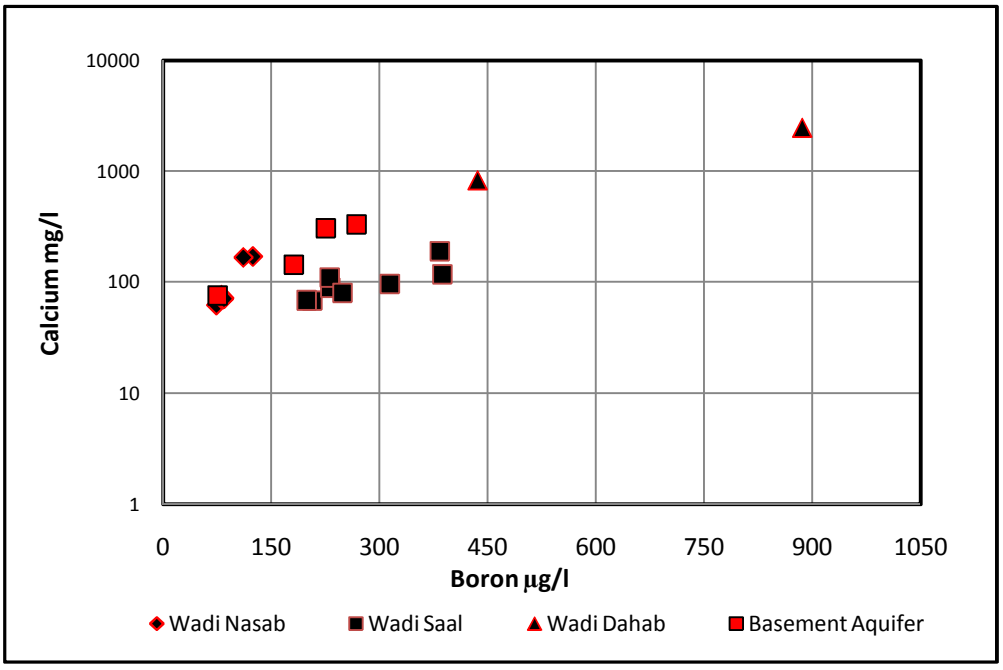

Figure 120 : Relation Between Calcium and Boron Concentrations in Groundwaters of Dahab Basin

B forms readily soluble compounds with alkali elements. The compounds with calcium and magnesium are relatively insoluble and the presence of these elements could decrease the B concentration in waters (fig.120). The figure shows that most of the groundwater samples are located in the upper left part of the figure. This means that the samples have a low B concentration with high

calcium concentration. It is mentioned that most groundwater samples have calcium dominant cations. Therefore, high presence of calcium in groundwater may control on the solubility of B. However, the solubility of B in water is dependent on the presence of calcium and magnesium chloride in water. The concentration of B and calcium show that B is obviously released mainly by water – rock interaction and is derived from silicate minerals except in the downstream areas

The increasing of sodium and chloride ions along the flow path will increase groundwater salinity and then more B ion will dissolve in groundwater. The positive relation between B concentration in groundwater and TDS emphasizes this explanation (fig.121). The presence of sodium and chlorine in the downstream area of W. Dahab confirms high salinity values and more B ions will be dissolved as in well D.4 (upper right part of fig. 121).

Generally, B concentration increases due to the cation exchange process between cations in water and B in aquifer rock materials. High B concentrations are recorded in the downstream of W. Dahab. The impact of seawater intrusion may be the cause for the presence of high concentrations of sodium and B, especially at well D4 and the presence of sodium facies which helps increase B solubility. The increasing of calcium concentrations in all groundwater facies at W. Nasab and W. Saal may assure low boron concentration compared to values measured in the downstream area of W. Dahab.

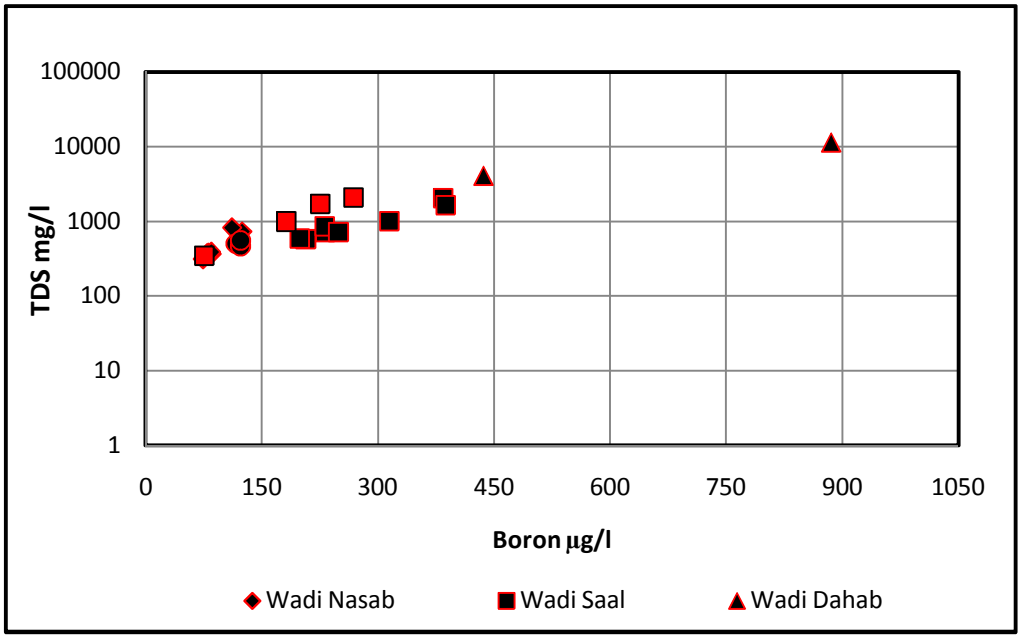

Figure 121: Relation Between TDS and Boron Concentration in Groundwater of Dahab Basin

3.3.6.6 Arsenic (As)

Arsenic (As) occurs in minerals mostly as a formal state of arsenites [As_2O_3] or arsenates [AsO_4]$^{-3}$. Arsenic appears in high concentrations in sulphide minerals. One of the most important As-bearing minerals is pyrite, which occurs in ore bodies. High arsenic can be found also in metal oxides and (oxy) hydroxides, and adsorbs to these minerals, especially at lower pH values.

The As concentrations in rocks vary. In igneous rocks, it is generally low, with little differences between basic and acidic rock types. The same is true for metamorphic rocks, which tend to resemble the concentrations in their igneous and sedimentary precursors. Unconsolidated material is not notably different from those in their indurate equivalents, but higher concentrations are found in fine sediments (e.g. clays). It commonly occurs in artificial produce substances such as insecticides, fungicides and herbicides.

As is toxic and carcinogenic. Hyper pigmentation, keratosis and peripheral vascular disorders are the most commonly reported symptoms of chronic arsenic exposure, but skin cancer and a number of internal cancers can result as well. Acute As intoxication is often associated with the ingestion of well water containing very high concentrations (21.0 mg/l) of arsenic. The WHO provisional limiting guideline value for As in drinking water is 10 µg/L.

The As concentrations are low at W. Nasab and W. Rimthy, ranging between 0.67 and 0.94 µg/l (fig.122). The As concentration decreases toward the downstream area of W. Nasab at wells N11 and N12. At W. Saal, the values of As (0.65 to 4.03 µg/l) are higher than those of the aforementioned areas. The concentration of As ranges between 3.4 and 4.03 µg/l in the upstream area of W. Saal and decreases in the downstream where it amounts to 0.83µg/l at well S9. High As concentration can be found in the downstream of W. Dahab (31 to 80 µg/l).

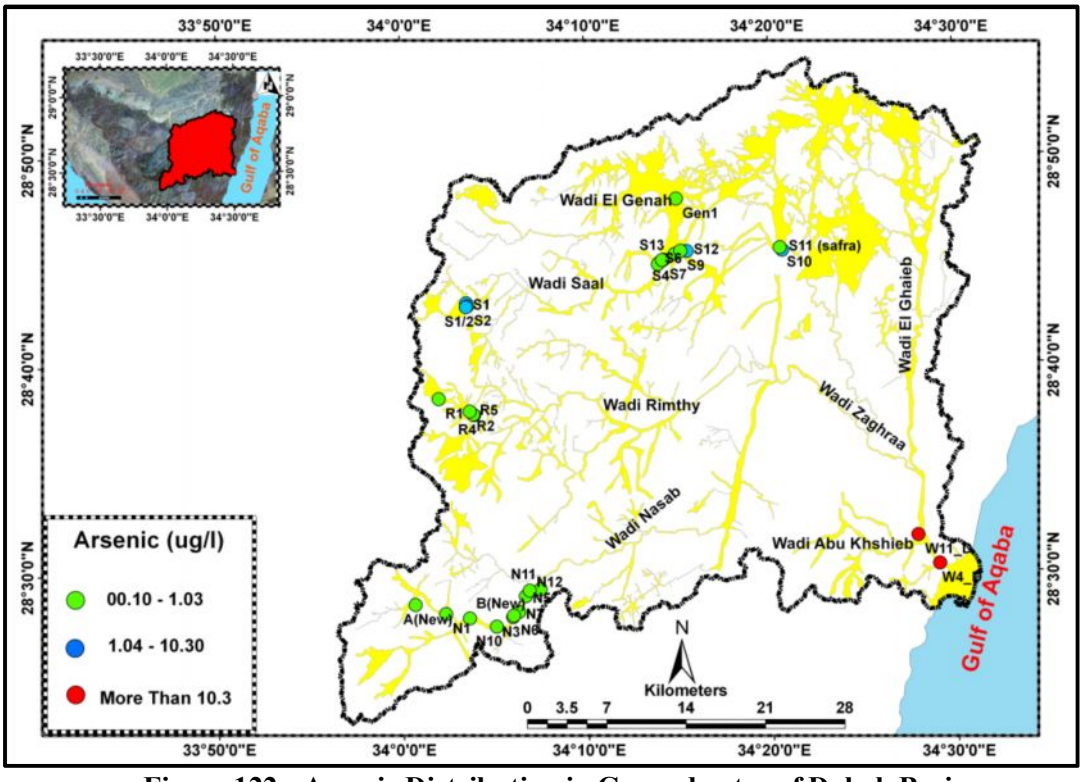

Figure 122 : Arsenic Distribution in Groundwater of Dahab Basin

It can be concluded that the low As concentrations in groundwater of W. Dahab basin may result from a low As content in basement rocks. Additionally, the oxidizing processes in shallow aquifers have a negative effect on the solubility of As in most wells in the study area. On the contrary, the

relatively deep aquifer in the downstream area of Dahab may form a reducing environment which positively affects the As solubility beside anthropogenic effects. These conditions may explain the high As concentration in the downstream of Dahab basin.

3.3.7 Water uses in drinking purposes

There are no limiting values of WHO (2006) for TDS, chloride, sodium, potassium and sulphate in drinking water. The limiting value of nitrate concentration is based on health impacts. This is valid for fluorine, uranium and arsenics. The chloride standard is primarily based on the undesirable taste appearing at a concentration higher than 250 mg/l. However, people may get used to drinking water with a chloride concentration higher than 250 mg/l.

Regarding sodium, it is believed that no health-based guideline value was proposed. However, soudium may affect the taste of drinking-water at levels above about 200 mg/l (WHO, 2006). Sodium salts are not acutely toxic because of the efficiency with which mature kidneys excreted sodium. However, acute effects and even death have been reported following accidental overdoses of sodium chloride. Acute effects may include nausea, vomiting, convulsions, muscular twitching and rigidity, and cerebral and pulmonary edema. There is no data available on the possible health effects of TDS content in the groundwater. Water containing TDS concentrations below 1000 mg/liter is usually acceptable to consumers, although acceptability may vary according to circumstances (WHO, 2006).

Sulphate is one of the least toxic anions. However, the presence of a high concentration in drinking water may lead to stomach complaints, and possibly diarrhea. The presence of sulphate in drinking water can be resulted in a noticeable taste; the lowest taste threshold concentration for sulphate is approximately 250mg/l. No health-based guideline value for sulphate in drinking water is proposed. However, there is an increasing likelihood of complaints arising from a noticeable taste as concentrations in water increase above 500 mg/l (WHO, 2006). The 50 mg/l standard for nitrate is based on health impacts. The WHO standard for fluoride of 1.5 mg/l is also based on health impacts. Arsenic is most important cancroid element which mainly affects human health. The WHO standard for arsenic guidelines is 10 µg/l while the boron standard limit is 0.5 mg/l (Table 22).

It is concluded that the groundwater wells in W. Nasab (wells N1, B, N3, N6, N10, N5 and N7), W. Saal (S4 and S6) and well G2 at W. El Genah are suitable to use as drinking water (see fig. 123). The wells S7, S8 and S13 in W. Saal and wells R2, R4 and R5 in W. Rimthy are of moderate suitablity for drinking purposes although they have high uranium contents. The wells in the downstream area of Dahab basin and wells S1, S2, S1/2, S9, S10, S11 and S12 in W. Saal, as well as well R1 in W. Rimthy, are not suitable for drinking purposes. Generally, groundwater in the downstream areas of W. Saal andW. Nasab is not suitable for drinking purposes. On the other hand, the areas in the northern part of W. Dahab and in the upstream area of W. Nasab are considered to be suitable for drinking purposes .

Wadi	SYMBOL	F	Degree_Flo	Score_F	NO_3	Degree_Nit	Score_NO3	U	Degree_Ura	Score_U	As	Degree_Ars	Score_As	B	Degree_Bor	Score_B	TDS	Degree_TDS	Score_TDS	Degree_dri	Final_dri
Wadi Nasab	A	1.70	High	1.00	5.00	Low	0.00	30.08	High	1.00	0.10	Low	0.00	75.81	Low	0.00	345.6	Low	0.00	2	moderate
	N1	1.21	Moderate	0.50	31.58	Moderate	0.50	12.99	Moderate	0.50	0.90	Low	0.00	74.04	Low	0.00	314.2	Low	0.00	1.5	Low
	B	1.10	Moderate	0.50	32.57	Moderate	0.50	13.21	Moderate	0.50	0.57	Low	0.00	85.03	Low	0.00	366.7	Low	0.00	1.5	Low
	N10	1.15	Moderate	0.50	36.27	Moderate	0.50	13.65	Moderate	0.50	0.67	Low	0.00	80.81	Low	0.00	364.2	Low	0.00	1.5	Low
	N3	1.19	Moderate	0.50	31.91	Moderate	0.50	12.43	Moderate	0.50	0.77	Low	0.00	80.48	Low	0.00	378.9	Low	0.00	1.5	Low
	N6	1.09	Moderate	0.50	32.08	Moderate	0.50	12.54	Moderate	0.50	0.81	Low	0.00	78.59	Low	0.00	370.6	Low	0.00	1.5	Low
	N5	1.17	Moderate	0.50	40.09	Moderate	0.50	10.50	Moderate	0.50	0.83	Low	0.00	84.42	Low	0.00	387.8	Low	0.00	1.5	Low
	N7	1.18	Moderate	0.50	33.94	Moderate	0.50	11.77	Moderate	0.50	0.92	Low	0.00	83.64	Low	0.00	375.7	Low	0.00	1.5	Low
	N12	1.03	Moderate	0.50	92.36	High	1.00	17.54	High	1.00	0.72	Low	0.00	124.30	Low	0.00	726.4	Low	0.00	2.5	Moderate
	N11	1.71	High	1.00	111.04	High	1.00	19.65	High	1.00	0.76	Low	0.00	111.40	Low	0.00	819.8	Low	0.00	3	Moderate
Wadi Saal	S1	1.99	High	1.00	134.63	High	1.00	14.10	Moderate	0.50	2.75	Moderate	0.50	225.90	Low	0.00	1708.0	Moderate	0.50	3.5	High
	S2	3.01	High	1.00	103.00	High	1.00	9.27	Moderate	0.50	4.03	Moderate	0.50	268.60	Moderate	0.50	2073.0	Moderate	0.50	4	High
	S1/2	2.29	High	1.00	63.53	High	1.00	7.71	Low	0.00	1.59	Moderate	0.50	181.50	Low	0.00	990.0	Low	0.00	2.5	Moderate
	S4	1.30	Moderate	0.50	40.58	Moderate	0.50	12.88	Moderate	0.50	0.73	Low	0.00	199.30	Low	0.00	586.0	Low	0.00	1.5	Low
	S6	1.26	Moderate	0.50	41.03	Moderate	0.50	11.88	Moderate	0.50	0.54	Low	0.00	207.00	Low	0.00	578.0	Low	0.00	1.5	Low
	S7	1.23	Moderate	0.50	44.80	Moderate	0.50	17.21	High	1.00	0.93	Low	0.00	232.00	Low	0.00	723.0	Low	0.00	2	Moderate
	S13	1.10	Moderate	0.50	43.82	Moderate	0.50	23.09	High	1.00	0.77	Low	0.00	231.40	Low	0.00	851.0	Low	0.00	2	Moderate
	S8	1.69	High	1.00	41.94	Moderate	0.50	15.98	High	1.00	0.65	Low	0.00	249.20	Low	0.00	716.0	Low	0.00	2.5	Moderate
	S12	3.83	High	1.00	69.19	High	1.00	21.98	High	1.00	2.10	Moderate	0.50	384.10	Moderate	0.50	2022.0	Moderate	0.50	4.5	High
	S9	3.03	High	1.00	49.89	Moderate	0.50	18.65	High	1.00	0.83	Low	0.00	314.70	Moderate	0.50	1006.0	Low	0.00	3	Moderate
	S10	3.86	High	1.00	2.17	Low	0.00	65.27	High	1.00	0.92	Low	0.00	387.40	Moderate	0.50	1644.0	Moderate	0.50	3	Moderate
	11 (safra	0.79	Low	0.00	4.15	Low	0.00	0.20	Low	0.00	1.25	Moderate	0.50	334.70	Moderate	0.50	2675.0	Moderate	0.50	1.5	Low
Wadi Rimthy	R1	1.44	High	1.00	114.69	High	1.00	28.08	High	1.00	0.90	Low	0.00	114.10	Low	0.00	732.8	Low	0.00	3	Moderate
	R4	2.72	High	1.00	44.73	Moderate	0.50	45.07	High	1.00	0.77	Low	0.00	122.70	Low	0.00	460.8	Low	0.00	2.5	Moderate
	R5	2.48	High	1.00	49.84	Moderate	0.50	49.73	High	1.00	0.10	Low	0.00	122.70	Low	0.00	551.7	Low	0.00	2.5	Moderate
	R2	2.16	High	1.00	42.46	Moderate	0.50	43.51	High	1.00	0.56	Low	0.00	116.60	Low	0.00	500.5	Low	0.00	2.5	Moderate
Wadi Genah	Gen1	1.16	Moderate	0.50	12.39	Low	0.00	3.83	Low	0.00	0.10	Low	0.00	130.40	Low	0.00	681.2	Low	0.00	0.5	Low
Downstream	W4_D	1.69	High	1.00	29.69	Moderate	0.50	12.88	Moderate	0.50	31.30	High	1.00	436.60	Moderate	0.50	4404.8	High	1.00	4.5	High
	W11_D	1.22	Moderate	0.50	0.00	Low	0.00	0.01	Low	0.00	79.80	High	1.00	885.00	High	1.00	11328.0	High	1.00	3.5	High

Table 22 : Chemical parameters affecting drinking water at Dahab Basin

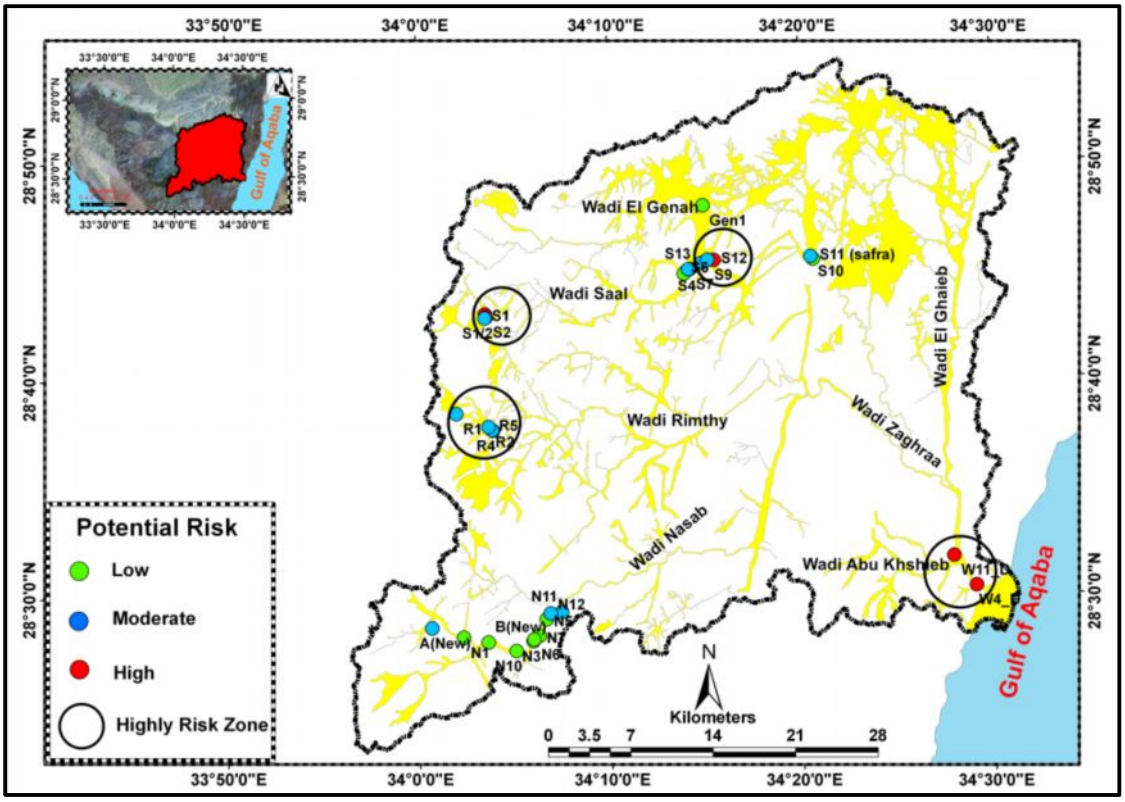

Figure 123: Potential Risk Map For Drinking Water at W. Dahab Basin

CHAPTER IV

CLIMATE-RUNOFF ANALYSIS

Chapter IV

Climate and Runoff Analysis

The climate of Egypt in general is of hyper-arid to semi arid nature. It is arid in middle and upper Egypt, while the northern shore line is hot and humid in summer and of moderate to low temperature in winter, with low to moderate rainfall intensities. Sinai is surrounded almost entirely by large bodies of saline water of the Red and Mediterranean seas, and no natural streams flow through Sinai. The only source of fresh water in Sinai is rainfall during winter months. Consequently, the hydrology of the region is mainly governed by the surface runoff through the wadis caused by the rainfall events. The climatic conditions of the Sinai Peninsula are similar to those which characterize desert areas in other parts of the world. They include extreme aridity, long hot and rainless summer months and a mild winter. During the winter months, some areas of Sinai experience brief rainfall but with high intensity that makes the Wadi beds overflow and sometimes causes severe flash floods which might damage the roadways and, sometimes, human lives.

In general terms, the climate of Sinai can be categorized in dry and wet seasons. Annual rainfall is scarce and fully concentrated in the wet season which lasts from October to May, where rainfall intensity increases especially from November to February. The wet season includes winter, spring and autumn seasons. In the summer, from June to September, there is no rainfall at all (El Rayes, 1992 and JICA, 1999).

Dahab basin is characterized by arid climatic conditions with a long period of hot rainless summers and mild winters (Danin, 1983). Considerable precipitation occurs as a result of convective clouds which have limited horizontal extent and are irregular in occurrence. In spite of the prevailed arid condition of the study area with its low rainfall intensity, relatively high temperatures, and evaporation rate, it is still frequently vulnerable to heavy rainstorms causing flash flooding.

4.1 Climate analysis

The meteorological records are collected from five stations surrounding the study area including Saint Catherine, Sharm El Sheikh, Nuweiba, El Tor and Dahab stations in different periods (Table 23 and see app. 12-16). Sharm El Sheikh station covers the southern part of the Dahab basin, Saint Catherine the western part of the study area, and Nuweiba station the northern part; El Tor station covers the south western part of the Dahab Basin and finally, Dahab station covers the downstream part of the study area (fig.124).

Some records are missing from the majority of these stations. Many stations in the study area are no longer in use because of the war during the period between 1967 and 1973; a couple was renewed after 1989 as in the case of Dahab and Nuweiba stations. The climate settings are known in Wadi Dahab area from studying the following climate elements described in the following sub-chapters.

Station	Longitude	Latitude	Elevation (m)
Nuweiba	34° 41′ 13″	28° 58′ 57″	2
Dahab	34° 30′ 28°	28° 29′ 31″	17
El Tor	33° 37′	28° 23′	14
Sharm El Sheikh	34° 23′	28° 14′	51
Saint Catherine	34° 04′	28° 41′	1354

Table 23: Location of Meteorological Stations Surrounds Dahab Basin

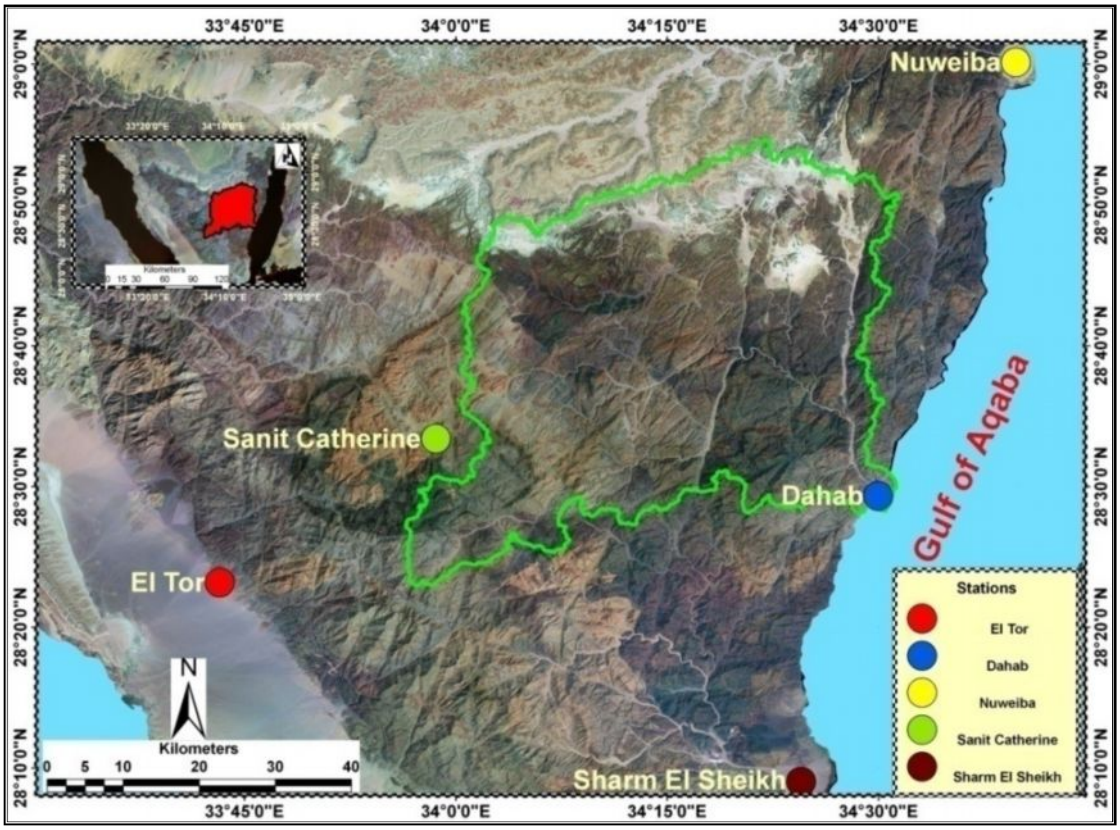

Figure 124 : Meteorological Stations Surrounding W. Dahab Basin

4.1.1 Temperature

The temperature and humidity data are collected from three stations in Saint Catherine, Sharm El Sheikh and El Tor form the period of 1961 to 2008, for Dahab and Nuweiba stations within the period 1990-2008 (app.12-16). Temperature directly influences the intensity of rainfall and the rate of evaporation and transpiration. It is a factor that has been related to the predication of the occurrence of water in the study area.

The average monthly maximum temperature ranges between 29.5 and 370C in the southern part of Dahab basin with a maximum air temperature of 37.4 0C in August, while in the western and south western parts it ranges from 30 to 38 0C during the summer period with a maximum air temperature reaching 38.4 0C at Saint Catherina station. The range of monthly maximum air temperature decreases in northern and eastern parts; it ranges from 26 to 37 0C during summer seasons and reaches 37.6 0C at Nuweiba station. During rainy months, the values of the monthly maximum

temperature decrease to between 9 and 26 0C. The monthly maximum temperature decreases at the western and southern part of Dahab basin ranging from 9 to 200C due to elevation effect.

Average monthly minimum temperatures in the southern part of the area of study ranges between 21 and 28 0C during the summer period, while during winter, average temperatures range from 12 to 20 0C. In the western part of the study area, the average monthly minimum temperature ranges between 16 and 23 0C in the summer season while averages range between -2 and 10 0C in the winter season, with a minimum temperature of – 7.2 0C on the 14/1/2008 according to General Meteorological Authority. This is due to the effect of the elevation that allows snow to cover the city of Saint Catherine many times during this period, especially during January and February (fig. 125).

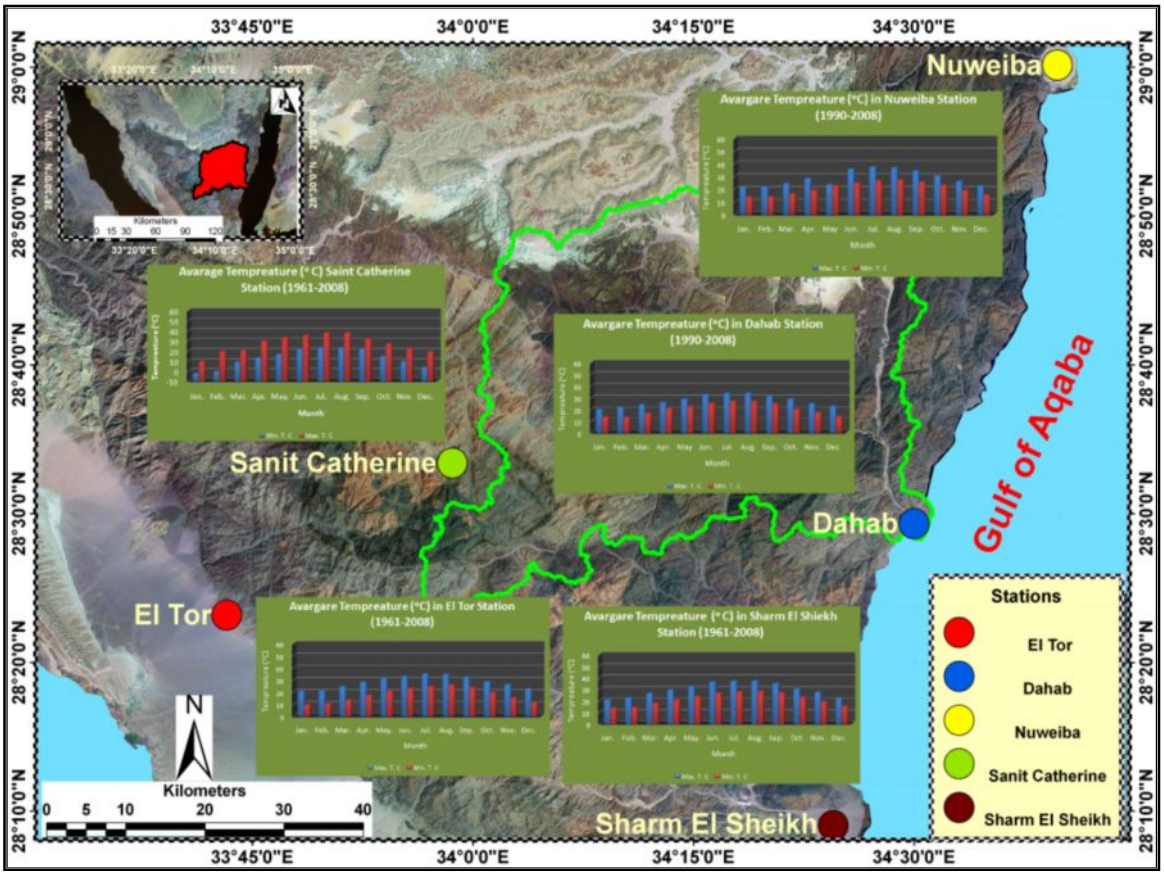

Figure 125 : Average Maximum and Minimum Temperature in Stations Surrounding W. Dahab

In general, the average of the air temperatures decreases in the western part of Dahab basin in comparison with southern, northern and eastern parts due to the elevation effect. It reaches negative values especially in January and February. The average monthly temperature decreases during the rainy months (October to February) while it increases in summer months, especially from May to August as shown in appendixes 12-16.

4.1.2 Humidity

At any given temperature, air can hold a maximum amount of moisture which is the saturation humidity that is directly proportional to the air temperature. The relative humidity for an air mass is the percent ratio of the absolute humidity to the saturation humidity for a given temperature of the air mass, whereas the absolute humidity of a given air mass is the number of grams of water per cubic meter of air. As the relative humidity approaches 100 %, evaporation ceases because of the relationship between the evaporation of the water and the relative humidity of the air mass.

In the southern part of the study area, the monthly relative humidity ranges from 34 to 37% during the summer season (April to August) with its maximum in August, recording 36.8%. While in winter, the relative humidity increases ranging between 44 and 45%. At the western part of the study area, the monthly relative humidity ranges in summer months from 21 to 25 %, while in the winter months it varies from 28 to 37% (fig. 126).

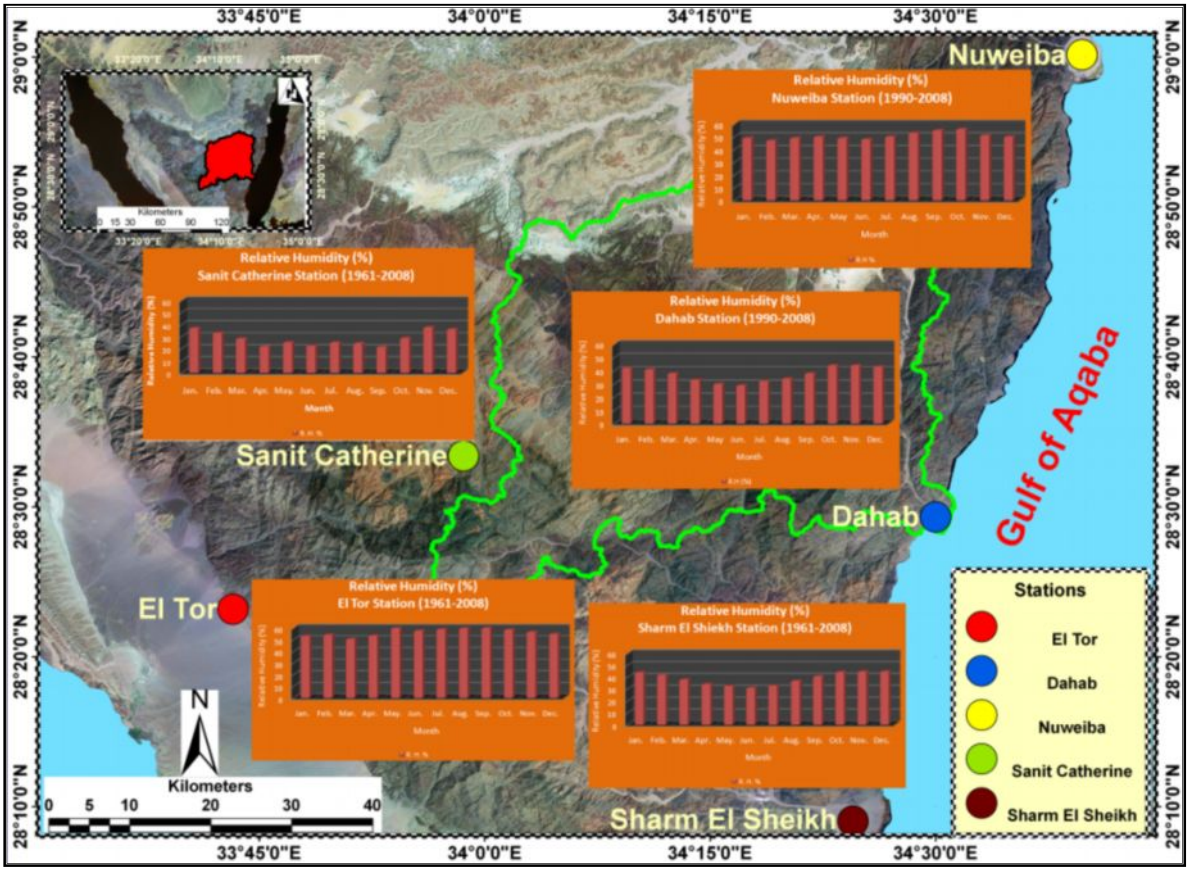

Figure 126: Average Humidity in Stations Surrounding W. Dahab

The relative humidity increases in south western and northern parts of Dahab basin. It ranges in the summer period between 53 and 60% (April to August) and decreases from 53 to 65% during the winter months (November to January). In general, the average relative humidity in south western and northern parts of the study area is higher than in the western, southern and eastern parts. The low

range of temperature in western and southern parts of Dahab basin, with its high topographic elevation, might decrease the relative humidity values.

It is observed that the relative humidity in the rainy months (October to February) in the western and southern parts is relatively high in comparison to dry months, while the relative humidity in the northern and south western parts of Dahab basin in the dry months is higher than that of the rainy months. Generally, the high topographic areas at western and southern parts of Dahab basin are characterized by low temperature, low humidity and low evaporation averages in rainy months in comparison with the northern and south western part of the study area during the same period.

4.1.3 Wind

Surface wind plays an important role for horizontal and vertical thermal exchange and dominates most of the climate elements such as evaporation, humidity and precipitation. On the other hand, wind speed is different from one area to another and from season to season depending on pressure distributions, topographic and local relief (Salem, 1990).

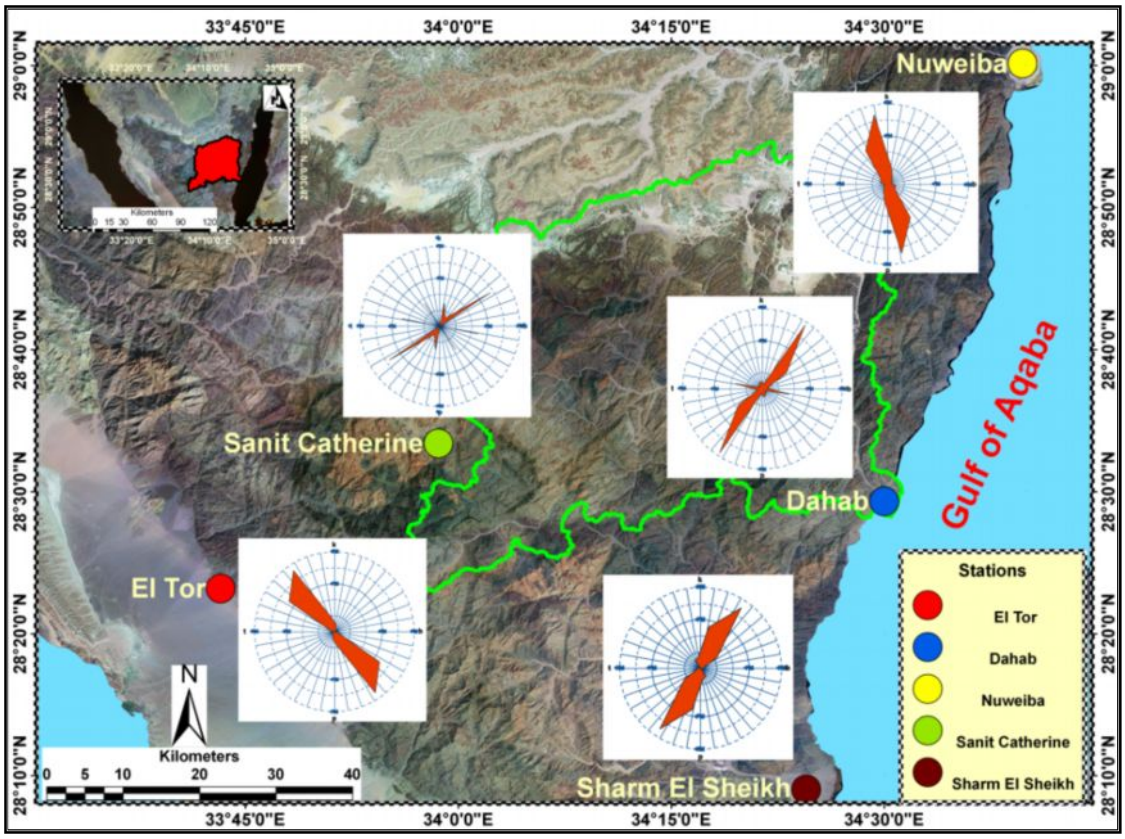

Figure 127 : Rose Diagram of Wind Direction at The Station Surrounding Dahab Basin

Wind is the movement of air. The wind has been measured by speed and direction. Wind speed is important because it can be related to water losses and precipitation events. In order for precipitation to occur, a sustained flow of moist air is required. Winds provide the forces to sustain the moist air flow. During a day, wind speed and direction might change which is called diurnal changes that result

from temperature contrasts between land and water. Winds tend to flow from cooler bodies towards warmer ones. Mountains also influence wind currents because of diurnal heating of the side of mountains, which can cause unequal heating of air mass, causing wind currents.

Dahab basin is affected by prevailing winds directed northeast at the western, southern and eastern parts of the study area and directed northwest at the southwestern and northern parts in Dahab basin. It is observed that the wind direction towards the north, northeast and northwest is recorded in all meteorological stations and that the wind blows north with lower intensity than other wind directions.

The prevailing wind direction at the southwestern and northern parts of the study area is from NW-SE and from N-S (fig.127). At the southern and eastern parts, the prevailing wind direction is generally directed from the NE-SE. At the western parts, the prevailing wind is directed from NNE-SSE direction.

The wind speed records show that the average wind speed is about 4-20 knot/h. The southwestern and southern parts of dahab basin are considered to have relatively high wind speed records. Maximum monthly speed has been recorded at El-Tor up to 20 knot/h in June and 19 knot/h in August and September. Relatively high speed was recorded in summer during June and August along the Gulf of Aqaba at Sharm El Sheikh station where the speed reaches 14 and 15 Knot/h, while the minimum speed ranges between 5.5 and 7 knot/h at Nuweiba. At the western and northern catchment, average wind speed is of relatively low value in comparison with other catchments in Dahab basin.

The high wind speed may reflect the power of storms, especially in rainy months. During this period, the wind speed records are between 4 and 18 Knot/h. The monthly maximum average is about 18 knot/h in October and November at Saint Catherine station while at Sharm El Sheikh station it is 11 knot/h (Table 24). It can be concluded that October and November have the highest records of wind speed and the possibility of a strong rainfall storm may occur during these periods.

Stations	Jan.	Feb.	Mar.	Apr.	May.	Jun.	Jul.	Aug.	Sep.	Oct.	Nov.	Dec.
Sharm El Sheikh	9	10	13	12	13	14	12	14	15	11	11	9
Nuweiba	7.8	7.6	8	7.9	6.9	6.9	5.5	5.9	7.3	6.2	7	7.5
Sanit Catherine	7	4	6	9	9	11	11	11	7	18	18	12
El Tor	13	14	17	16	18	20	18	19	19	16	14	13
Dahab	10.1	9.2	9,4	9,7	10	12	11	11	8	8	9	12

Table 24: Average Wind Velocity at Meteorological Stations (Knot/hr) (Source-General Egyptian Meteorological Authority)

4.1.4 Precipitation

The severity of flash floods at any location depends mainly on precipitation such as the maximum rainfall depth and the duration of a storm. Such parameters, in turn, depend on the type and nature of the rainy storms. The analysis of the rainfall data is used to determine runoff volumes and discharges

according to rainfall excess. The elaboration design of the rainfall events using historical data is the first step in the design of flood protection schemes.

Rainfall in arid climate regions is typically meager, irregular and highly variable (Ahrens, 2003). The spatial distribution of rainfall over the catchment is not well represented by rain-gauge networks. Rainfall events occur in huge amounts due to convective cloud mechanisms in arid and semi-arid zones, producing storms typically of short duration, relatively high intensity and limited areal extent (Cooke and Warran, 1973).

In Sinai, relatively low-intensity rainfall may represent the greater part of annual rainfall during storm periods. Precipitation occurring in Sinai Peninsula is commonly associating with small, convective cells that could produce intense, short- duration storms in conditions of atmospheric instability at the front of a belt of low-pressure (Yair and Lavee, 1985). The observations of high rainfall events are different during the year. It is concentrated in winter season, while in autumn and spring, it is rare. Furthermore, the intensity of rainfall events due to these storms is high over the southern parts of Sinai. These storms have been responsible for most of the disastrous flash flood events in the past. The hydrographical basins in Sinai have high surface water potentialities due to the fact that the western branches of their steep sloping channels drained the highlands of southern and central Sinai, where high rates of rainfall prevailed (WRRI, 2006) and the chances for infiltration are limited due to the steep rocky slopes of their Wadis.

Rainfall data for the study area is collected from five meteorological stations and from different other sources. The data is:

1- Average and total annual rainfall for all the five stations during the period from1970 to 2008.
2- Annual maximum rainfall (peaks) during 1934 to 2004 for Saint Catherine and El Tor stations.
3- Monthly maximum rainfall and dates within the period from 1919 to 2003 for stations Sharm El Sheikh, El Tor and Saint Catherine, in addition to during the period from 1992 to 2003 for Dahab and Nuweiba stations.
4- Mean monthly rainfall within the period from 1970 to 2008 at Saint Catherine, El Tor, Nuweiba and Sharm El Sheikh stations and in the period between 1992 to 2008 at Dahab station.
5- The hyetograph of the maximum storm events in Saint Catherine station (1937) has been measured 76.2mm per day.

Long term rainfall data has not been available except for Saint Catherine and El Tor. The Saint Catherine station is located at a high elevation at the catchment part of Dahab basin. It will be used as a representative for mountainous areas feeding the wadi during storm events. The available records are used for statistical methods to estimate the probability of the occurrence of the maximum rain fall depth anticipated within 10, 50, 100 or any other number of years.

Factors controlling the distribution of rainfall over the earth's surface are the belts of converging-ascending air flow, air temperature, moisture-bearing winds, inland distance from the coast, and mountain ranges. The topography plays a considerable role in increasing rainfall in some areas, such

as St. Catherine area where moisture bearing clouds are transported through deeply incised valleys. The influence of mountains or ridges on horizontal scales of 10^{th} to 100^{th} of kilometers has occurred. The reason of this effect has mostly been laid on the so-called orographic effect, i.e. the increase in rainfall caused by topography inducing cloud formation processes.

4.1.4.1 Annually and monthly rainfall distribution

The average monthly rainfall increases in November, December, March and January ranging between 4.7-23.4 mm. No records are scored during dry months. High average rainfall increases in the northern, southern and western catchments (Table 25). Saint Catherine station recorded the highest total monthly rainfall, reaching 64.2 mm in the western part of the study area where this station is located at the highest point in comparison with other stations.

Stations	Jan.	Feb.	Mar.	Apr.	Mai	Jun.	Jul.	Aug.	Sep.	Oct.	Nov.	Dec.	Sum
Sanit Catherine (1)	1.7	1.4	13.5	8.9	6.4	0	0	0	0.1	3.4	22	7.2	64.6
El Tor(1)	0.6	1.2	0.7	0.6	0.3	0	0	0	0	0.6	1.1	2.7	7.8
Sharm El Sheikh(1)	0.2	0	0	0.2	0	0	0	0	0	0	0	23.4	23.8
Nuweiba(1)	4.7	1.1	0.6	0.9	0.8	0	0	0	0	2.4	2.2	0.7	13.4
Dahab(2)	0.2	0.4	0.3	0.2	0.2	0	0	0	0	0.3	0.2	0.5	2.3
1) Data from (1970-2008) 2) Data from (1999-2008)													

Table 25: Average Monthly of Rainfall (Source -General Egyptian Meteorological Authority)

The data of annual average rainfall was collected from different sources such as Issar, A. and Gilad, D. (1982), the General Meteorological Authority (GMA) of Egypt, and the Water Resources Research Institute (WRRI). It ranges from 4mm to 30 mm (Table 26). The value increases mainly in the western and southern catchment of the study area with annual average values between 30mm/year and 8.4 mm/year as at Saint Catherine, El Tor and Sharm El Sheikh stations. The values increase in the western catchment due to the high elevation at this part in Dahab basin.

	Rainfall Data (1970-2008) mm/year				
	Sanit Catherine	El Tor	Sharm El Sheikh	Nuweiba	Dahab
Avarage Anuual rainfall	30mm	8.4mm	8.0mm	5.7mm	4.0mm
Sum of Annual rainfall	1124mm	320mm	301mm	218mm	151mm

Table 26: Average Annually of Rainfall (Source GMA and WRRI)

4.1.4.2 Average rainfall over the study area

The average depth of rainfall over a specific area of a single storm with a season or one year basis is required in many types of hydrologic problems. These problems can be partially overcome if topographic influences and the areal extension representatively are considered by the selection of meteorological station sites (Linsley, et.al, 1982). Determination of the weighted average rainfall using the isohyetal method is based on the average annual rainfall data.

The isohyetal method considers topographic effects and other information about the meteorological patterns in the region (Fetter, 1994). A rainfall-depth contour map is determined by tabulating rainfall in a map of the region and constructing lines of equal rainfall called isohyets. Average depths are obtained by measuring the areas between adjacent isohyets (zones). Each increment of an area in percent of the total basin area is multiplied by the estimated rainfall depth for that area. This product for each zone is summed up to obtain the basin average rainfall. The accuracy is largely dependent on the method used to construct the isohyets, how the analysis performs and the number of gauges is used.

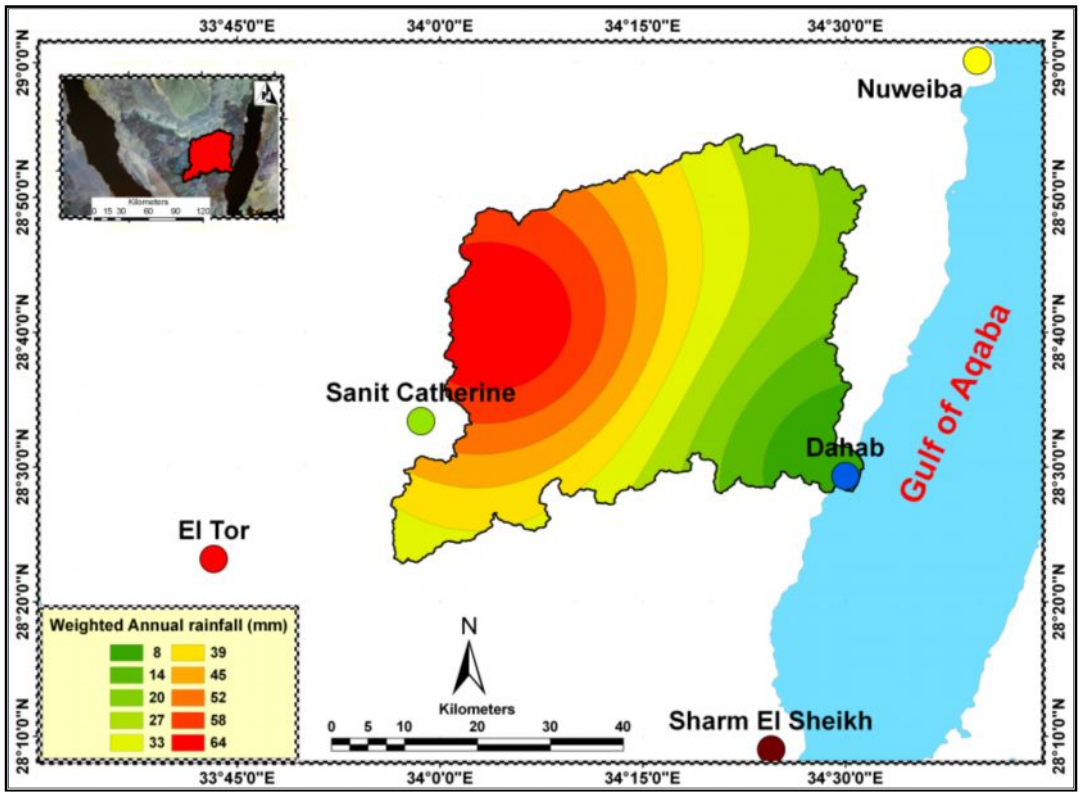

Figure 128 : Weighted Annual Rainfall in Dahab Basin

	Isohyets	Mean	Area	per_are2	Percent_ar	Weighted Rf.
	mm	mm	km²	%		mm
1	2-8	5.00	102.86	4.93	0.049	0.25
2	8-14	11.00	116.59	5.59	0.056	0.61
3	14-20	17.00	203.93	9.78	0.098	1.66
4	20-27	24.00	267.61	12.83	0.128	3.08
5	27-33	30.00	269.67	12.93	0.129	3.88
6	33-39	36.00	284.07	13.62	0.136	4.90
7	39-45	42.00	224.71	10.77	0.108	4.52
8	45-52	48.00	182.31	8.74	0.087	4.20
9	52-58	55.00	194.02	9.30	0.093	5.12
10	58-64	61.00	240.33	11.52	0.115	7.03
			2086	100		35

Table 27 : Isohyetal Method for Calculation Weighted Rainfall in Dahab Basin

The results show that the average weighted annual rainfall over Dahab basin is about 35mm/year. It can be concluded that the study area receives annually about 70 million m^3/year (fig. 128). The project JICA (1999) stated that average annual rainfall over Southern Sinai ranges between 32 and 38mm /year. The relief plays an important role to increase the amount of rainfall. The 29.5% of the total area has more than 50 mm/year which represents the western catchment area of Dahab basin as well as the Catherine area. The western catchment receives rainfall of 10 million m^3/year. This catchment part covers W. Nasab, W. Rimthy and W. Saal, while 25% of Dahab basin has between 20-33 mm and receives about 3.5 million m^3/year. This area represents the northern, southern and north eastern parts of the study area, especially the catchments of W. El Ghaieb and W. Abu Khshieb (Table 27).

4.1.4.3 The highest amounts of rainfall and their dates

The highest amount of rainfall in one day is considered to be one of the important pieces of data to study the distribution of effective rainfall in arid zones. Gereish (1998) stated that runoff in southern Sinai results from storms more than 10mm. Therefore, it is considered as a threshold value to estimate the possibility of runoff in the study area.

Saint Catherine station records the highest amount of rainfall /day with 76.2 mm on 17/11/1937 (Table 29). This amount of rainfall is considered the highest record which led to a large flash flood in southern Sinai. El Tor station has the second highest storm in one day that reaches 70.1 mm recorded on 03/09/2002 (autumn season) while the highest storm value reaches 48.3 mm on 17/11/1985 at Sharm El Sheikh station. It is observed that the highest records occurred in the autumn season (September-October) and the beginning of the winter period (November). It should be mentioned that the last two storms that blew on southern Sinai were on 1/10/2012 and 14/10/2009, affecting Dahab basin. The maximum rainfall records indicate that the month of November has the highest amount of rainfall storms at Saint Catherine, Sharm El Sheikh and El Tor stations (Table 28).

	Jan.	Feb.	Mar.	Apr.	Mai	Jun.	Jul.	Aug.	Sep.	Oct.	Nov.	Dec.
	El Tor Station (1925-2008)											
Max. Rainfall (mm/day)	9.5	10	22	3.2	5.6	0	0	0	70.1	13	37.4	22
Date	30/1938	4/2/1937	2/3/1941	7/4/1963	4/5/1963				9/3/2002	31/10/1938	8/11/1925	7/12/1955
	Sharm El Sheikh Station (1934-2008)											
Max. Rainfall (mm/day)	6	20.4	10.3	?	0	0	0	0	?	8.6	48.3	3
Date	10/1/1992	7/2/1955	9/3/1989							30/10/1996	17/11/1985	17/12/1985
	Sanit Catherine Station (1934-2008)											
Max. Rainfall (mm/day)	51.6	7.6	18.2	?	?	0	0	0	?	35.5	76.2	15.8
Date	12/1/1996	7/2/1999	20/3/1980							30/10/2002	8/11/1937	26/12/1985
	Nuweiba Station (1992-2008)											
Max. Rainfall (mm/day)	34	9.4	3.5	0	0	0	0	0	0	10.2	8.7	2.3
Date	1/1/1994	8/2/1996	30/3/1995							30/10/2002	7/11/1996	14/12/2003
	Dahab Station (1992-2008)											
Max. Rainfall (mm/day)	0	0	0	0	0	0	0	0	0	6.9	0	2.5
Date										30/10/2002		14/12/2003

Table 28 : Maximum Rainfall in (mm/day) Data in Dahab Basin (Source General Meteorological Authority)

The highest values of storms are recorded mainly at Saint Catherine station due to high land and mountainous nature, especially at the western side of Dahab basin. In spite that the average of daily rainfall is small, still it might occur intensively within one day, which might cause a huge runoff. For example, the average rainfall per day in November at Saint Catherine station is 0.7mm, whereas the maximum rainfall per one day in November is 76.2 mm. This indicates that the maximum precipitation per day might be more than 100 times the average in one day. Moreover, the highest storm value might be repeated more than once during the next period of storms. For this reason, the present study uses this value (the maximum rainfall per day) in the estimation of runoff hazards and calculation of water balance. Because of the availability of long time records of the maximum storm at Saint Catherine station from 1934 to 2004 (fig.128), it will be used to study the probability of repetition.

4.1.4.4 High storm analysis

It is necessary to know the approximate chance of exceeding a storm event. Unfortunately, the amount of data points available usually does not coincide with the length of the time interval for which prediction was necessary. In other words, if it is desired to find out the expected highest storm over the next 10,000 years for an area that only has 70 years of rainfall storm history available, this is where extreme value theory can help to predict the chance of an event occurring in a given period of time. For this purpose, only the maximum daily storm per year record for Saint Catherine station ranging seventy years (1934 to 2004) will be used (fig.129). This analysis will indicate the probabilities that these records are repeated.

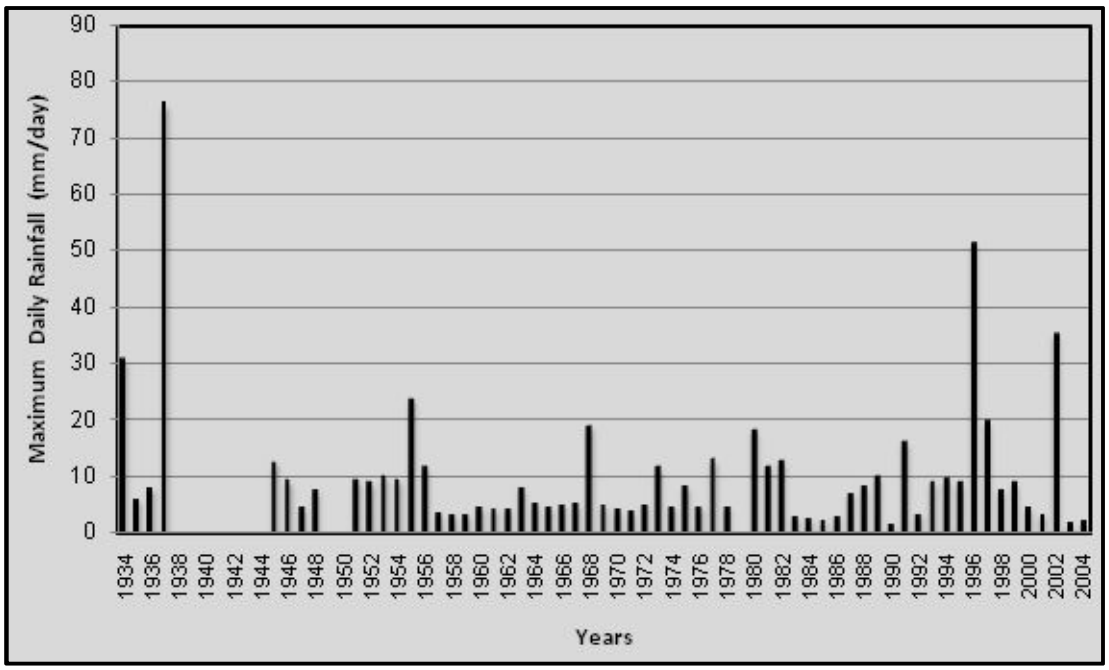

Figure 129: Maximum Daily Storm Recorded at Saint Catherine Station from (1934-2004)

The high peak of a storm is analyzed using the Gumbel distribution to expect peak values, which provides an assessment of storm events and its returned period in the future. The Gumbel distribution has been consistently used by Gumbel (1958) and Myers and Zehr (1980) for precipitation frequency analysis. The standard Gumbel distribution function is stated as follows:

$$\mathbf{G(x) = e^{-e^{\frac{-(x-\propto)}{\beta}}}} \qquad \textbf{Equation (30)}$$

Where G(X) is the cumulative distribution function; $\propto$ and β represent location and scale parameters that are determined, so that the Gumbel distribution function fits the given data.

The concept of analysis depends on the sorting of the observed {x1, x2, x3, …, xn} values from smallest to largest to form the order statistics x(1) < x(2) < x(3) <…< x(n). In order to fit the data to a particular Gumbel distribution, the two shape parameters α and β must be determined. There were several methods used to estimate these parameters. Here in this study, the Method of Moments is used to estimate these parameters (Devore, 2000). In this method, mean and variance of the data are calculated by:

$$\beta^2 = \frac{6*(s^2)}{\pi^2} \ (1) \qquad \propto = \bar{x} - (\beta.\lambda) \ (2) \qquad \textbf{Equation (31 -32)}$$

where $\bar{x}$ and s^2 were respectively, the mean and variance for the sample data and $\lambda \cong 0.577216$, which is Euler's constant.

Station	Mean	Variance	α	β
Sanit Katherine Station	**10.4**	**146.6**	**5.0326**	**9.4352**

The mean of highest storm records is 10.4 mm/day and the variance of records was 146.6; then, the parameter of α *and* β are 5.03 and 9.43 respectively. Gumbel's distribution curve G(x) is drawn using Matlab software (app. 17). By the definition of a Gumbel curve, G(x) = Probability (P(x)) when x ≤ xi (maximum value) the chance of exceeding of the maximum storm is computed to P(x) = 1-G(x). For the predication T-year (recurrency time) level for various storms, it is found that recurrency time is T = 1/ P(x) (fig. 130-B).

The recurrence time for maximum storm records is estimated. The results show that the return period of maximum rainfall (76.2 mm/day) in the study area has a probability of more than 180 years. At the moderate records (45 to 55 mm/day), the return time might occur after 25 and 50 year while the minimum record (from 10 to 20mm /day) is approximately returned between 3 to 5years. The analysis stated that the maximum is expected storm after 60 years and that the rainfall would repeat at this station about 56mm/day; this amount is similar to records in 1996 which were about 52mm. It can be concluded that the study area will heavy rainfall (more than 65 mm/day) within 50 to 150 years at

Saint Catherine station. This amount can produce destroying flash floods which have a direct impact on the human activities and infrastructure in the study area.

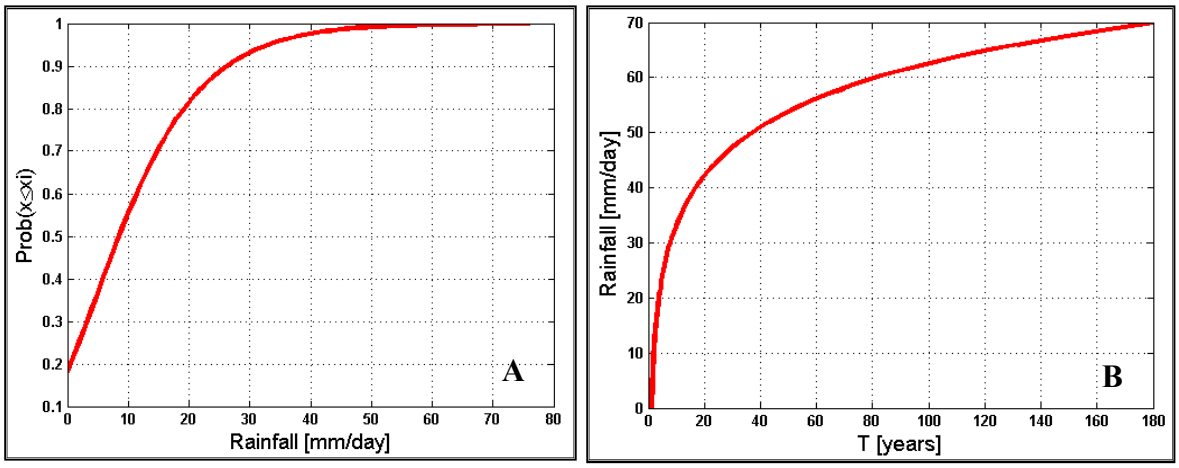

Figure 130-A: The Probability Curve For the Maximum Rainfall Event in Saint Catherine Station

Figure 130-B: Recurrence Time Curve For the Maximum Rainfall Event in Saint Catherine Station

4.1.5 Evaporation

Evaporation is considered the most important element of climate, which is used in hydrology especially to calculate the loss of precipitation during storm events. In the context of the hydrological cycle, evaporation involves the conversion of solid or liquid precipitation which reaches the earth's surface to water vapor and returns to the atmosphere. Evaporation is expressed as a rate in millimeters per day. This rate is a function of several meteorological and environmental factors. Those important factors from a hydrologic viewpoint are net solar radiation, the saturation vapor pressure, the vapor pressure of the air, air and water surface temperatures, wind velocity, atmospheric pressure and relative humidity. These factors change from one location to another according to topographic and environmental conditions; so the amount of evaporation depends upon the individual condition of the location.

Temperature mainly affects evaporation, where temperature is dependent upon solar radiation. Solar radiation as an energy source is able to change large quantities of liquid water into water vapour. The amount of radiation increases during the summer season, therefore, the evaporation rate increases in summer with high average temperature. The humidity has an indirect relation to evaporation. In hot and dry conditions, large amounts of water can be consumed and much water vapour can be stored in the air thus, the evaporation rate will increase. In humid and cold conditions, the air is close to saturation, so that less additional water can be stored and hence, the evaporation rate will be low. The rate of evaporation is influenced to some extent by air movement. Wind helps to remove the evaporated water vapour from the zone of evaporation, thereby creating greater scope for

evaporation. It can be concluded that the evaporation rate tends to increase as the temperature, sunshine and wind speed increases and as the humidity decreases.

	Jan.	Feb.	Mar	Apr	May	Jun	Jul	Aug	Sep	Oct	Nov	Dec	Avarge
Sanit Catherine	5.7	6.9	9.1	13.4	15.6	18.2	16.6	15.9	13.4	10.7	6.9	6.2	11.55
El Tor	7.2	8	9.5	11.1	12	12.5	12	11.9	11	8.2	7.5	7.3	9.85
Sharm El Sheikh	11.1	13.2	14.7	17.6	21	26.8	25	22.6	21.1	16.4	13	11.7	17.85

Table 29: Mean Daily Evaporation (mm/day) from period (1934 to 2004) (Source – GMA)

The mean daily evaporation data is collected from three stations (Table 29). The data covers the western, southern and south western parts of W. Dahab. The data presents that high mean evaporation occurs in summer months ranging from 11.1 to 26.8 mm/day while the mean decreases in winter months from 5.7 to 16.4 mm/day. The high mean value increases during summer months at Sharm El Sheikh station ranging between 17.6 and 26.8 mm/day. The effect of the topography might affect the evaporation rate, especially in rainy months. During rainy periods, the lowest mean values occur at Saint Catherine station ranging between 5.7 mm/day in January and 10.7 mm/day in October.

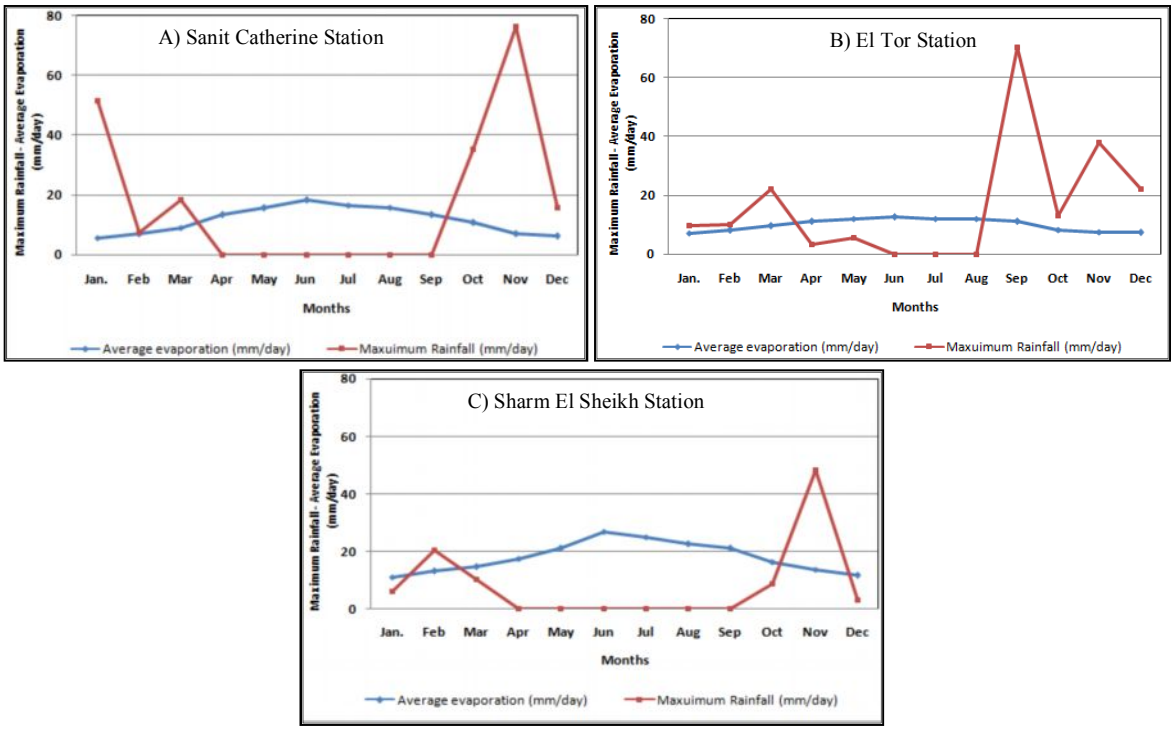

Figure 131-A-C: Water Surplus Period of the Studied Records of Different Meteorological Station Surrounding in W. Dahab

The study area has two main periods of water surplus in which the maximum precipitation in one day exceeded the evaporation. The two periods extend from January to March and from October to December, especially at Saint Catherine and El Tor station (fig. 131 A-C). The water excess during

these periods is available to recharge the existing aquifer in the study area; otherwise it would discharge into the downstream area of W. Dahab as surface runoff.

Due to the shortage of daily evaporation data within other stations in Dahab basin, it has been decided that the evaporation rate for all the stations should be calculated and the results should be compared with the collected mean evaporation data. The calculated evaporation aims to define average evaporation at each station in the study area, to estimate the lack data in Nuweiba and Dahab, especially at the rainy month and to calculate the expected average evaporation loss. Because of the different conditions of the equations used for estimating evaporation values, it was decided that the average value between the results of the equations must be taken. Generally, the daily evaporation can be calculated using many methods; the first method is the direct evaporation estimation by pan experiments, but unfortunately there is no chance to measure the evaporation during the field visits. The second method is the Thornthwaite method which depends on temperature with an adjustment being made for the number of daylight hours. The Thornthwaite method calculates potential evaporation per month. The results from the formula can be divided by 30 days to get average evaporation per day.

$$PE_m = 16 * N_m * \left[\frac{10 * \overline{T_m}}{I}\right]^a \qquad \textbf{Equation (33)}$$

Where:-(m):- Months

(N_m):- Monthly adjustment factor related to hours daylight.

($\overline{T_m}$):- Monthly mean temperature ^oC

(I):- Heat index for the year, which given by:

$$I = \sum i_m = \sum \left[\frac{\overline{T_m}}{5}\right]^{1.5} \qquad \textbf{Equation (34)}$$

$$a = (6.7 * 10^{-7}) * I^3 - (7.7 * 10^{-5}) * I^2 + (1.8 * 10^{-2}) * I + 0.49$$

The third way is the Penman method. This method depends on meteorological data like solar radiation, wind speed and vapor pressure. The Penman equations are used for depth of water (mm/day) using the principals of energy budget and mass transfer theories (chow 1964) as follows:

$$\mathbf{E} = \frac{\Delta\left[\mathbf{H_A}.(\mathbf{1}-\mathbf{r}).\left(\mathbf{0.22}+\mathbf{0.55}\frac{\mathbf{n}}{\mathbf{N}}\right)-\boldsymbol{\sigma}.\mathbf{T}.\mathbf{a}^{\mathbf{4}}(\mathbf{0.56}-\mathbf{0.09}.\mathbf{e_a}).\left(\mathbf{0.1}+\mathbf{0.9}\frac{\mathbf{n}}{\mathbf{N}}\right)\right]+\left[\frac{\boldsymbol{\gamma}(\mathbf{0.175}+\mathbf{0.002}.\mathbf{U_2}).(\mathbf{e_s}-\mathbf{e_a})}{\Delta+\boldsymbol{\gamma}}\right]}{\Delta+\mathbf{r}}$$

Equation (35)

E = Daily evaporation of free water surface.

H_A= Extraterrestrial solar radiation received on horizontal surface (mm/day).

R = Reflection coefficient. n = Duration of bright sunsh

N = Maximum possible hour of bright sunshine

σ = Stefan Boltzman constant (1.17 × 10 -7 Cal / cm^2 / K^4/ day) T_a = Mean Temperature.

ea = Vapor pressure of air (mm/Hg)

es = Saturation vapor pressure at mean temperature (mm/Hg) γ = Constant 0.49 mm Hg / 0C

Δ = Slope saturation vapor pressure – temperature curve at (T_a) U2 = Wind velocity.

Stations	Jan			Feb.			Mar			Oct.			Nov.			Dec.			Avarage
	PM	TM	CD	PM	TM	CD	PM	TM	CD	PM	TM	CD	PM	TM	CD	PM	TM	CD	
Sanit Catherine	3.84	0.5	5.7	6.72	5.76	6.9	8.6	6.7	9.1	11.5	22.08	10.7	7.2	10.5	6.9	4.6	4.8	6.2	7.68
Sharm El Sheikh	5.4	4.8	11.1	7.2	8.16	13.2	11.5	5.7	14.7	10.8	15.36	16.4	7.7	9.9	13	5.2	7.6	11.7	9.97
El Tor	6.20	6.4	7.20	8.64	7.3	8	11	14.4	9.5	9.6	26.88	8.6	8.3	14.4	7.5	6.5	9.6	7.3	9.85
Nuweiba	6.2	3.6		7.6	4.5		9.6	20.2		12.96	35.04		8.1	22.5		5.3	3.8		11.61
Dahab	5.7	5.7		7.6	9.12		9.1	13.9		10.56	28.84		7.2	14.9		8.16	10.4		10.93
Method Avarage (mm/day)	5.47	4.20	8.00	7.55	6.97	9.37	9.96	12.17	11.10	11.08	25.64	11.90	7.70	14.44	9.13	5.95	7.24	8.40	
Month Avarage (mm/day)	5.89			7.96			11.08			16.21			10.42			7.20			
Water loss Million m^3	12.2			16.5			23			33.2			21			15			
	PM	Penmann Method			TM		Thornthwaite Method				CD		Collected Data						

Table 30 : Calculated Evaporation at the Study Area

The mean daily evaporation rate is calculated for rainy months in all meteorological stations at W. Dahab (Table 30). The results show that the calculated daily evaporation values by the Penmann method match the collected evaporation data while there is little difference with Thornthwaite method results, especially in October. Therefore, the average value between the results is used in the lack data at Dahab and Nuweiba stations. The difference in results is caused by the factors in calculating the evaporation equation of the Thornthwaite method; they are monthly dependent like daylight hours. The average daily evaporation decreases at Saint Catherine station to about 7.68 mm/day while it increases at Nuweiba station to about 11.6mm/day. The average daily evaporation rate decreases in January and December between 5.8 and 7.2 mm/day while it increases in October and March between 16.2 and 11.08 mm/day.

The relation between average evaporation and altitude occurs in the results; the evaporation decreases at high elevations as at Saint Catherine station at the western side of Dahab basin while it increases at the low elevation stations of Nuweiba and El Tor at the southwest and eastern part of the study area. It can be seen from the results that evaporation might reach less than 1 mm per day as shown for the month of January at Saint Catherine station. Salem (1990) confirmed the previous result that the lowest evaporation was recorded during the winter months at less than 1 mm (0.78 mm) on 27-1-1987.

The total evaporation losses have different amounts during storm months in the study area (fig. 132). The values range from 12.2 million m^3/day in January to 33.2 million m^3/day in October. These amounts in one day often have little influence to mitigate flash floods compared with the amount of the maximum event (76.2 mm/day) that reaches about 158 million m^3/ maximum storm which might occur in one day. It can be observed that the evaporation during rain storms is lower than any other time during the year; therefore, the amount of evaporation at the time of rain is very small and its influence is limited.

The evaporation rate is considered one of the loss factors which helps to determine rainfall excess and its volume amount. The hyetograph of maximum event data represents the nature of rainfall within Dahab basin. The collected data from Saint Catherine station in November 1937 is considered the oldest and the most representative in W. Dahab because of its location and the amount of data collected. Due to the lack of evaporation rate data for storm events (mm/hr), a constant evaporation rate is used by dividing mean daily evaporation rate by 24 hours to get the amount of evaporation during a short rainy storm. The selected mean daily evaporation value is (6.9 mm/day approximately 0.2 mm/hr) at Saint Catherine station in November because it is where the maximum storm was recorded during the period.

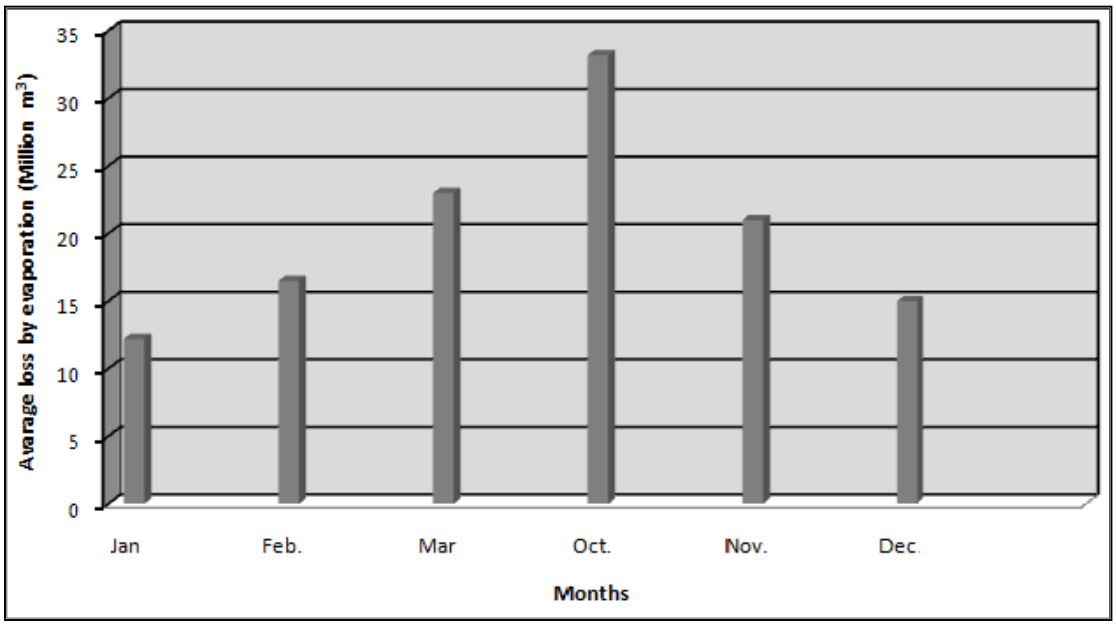

Figure 132 : Average Evaporation loss According to Calculated Evaporation and Measured values at Dahab Basin in Storm Months

4.2 Runoff analysis

The predication of quantitative runoff and its flow to the basin outlet represents one of the challenging tests in hydrology. GIS tools have opened up many opportunities for enhancing hydrologic modeling of watershed systems by using powerful capabilities to process DEM data for water management. Most of the watersheds in Egypt do not have sufficient historical climate gauged records, hydrological records (flow discharge) or detailed watershed information that are needed for hydrological models. The lack of reliable data stands as a barrier in front of developing a successful model to establish a water management system. Therefore, a simplified representation of the runoff process through the input linkage without detailed description of the process has been used. This is the basis of the linear theory of hydrologic systems.

This part describes a simplified surface water model that can be used to estimate the hydrological parameters like peak discharge, time to peak and flow velocities at sub-basin watersheds in Dahab

basin for the prevailing maximum rainfall pattern. For this purpose, two hydrological models based on GIS techniques are used to describe the catchment topography and the active hydrological processes as well as to simulate the runoff generation and to develop the hydrograph of direct runoff.

Difficulties in acquiring runoff data and the general lack of hydrometeorological data causes many problems in evaluating the models and thus it is considered a crucial issue. The evaluation of hydrological model parameters is not performed in all ungauged catchments in Southern Sinai due to the absence of hydrological data as flow discharge measurements; so the model results were calibrated either directly from field data measurements by creating station points along the main stream or indirectly through comparing the results with measurement values in surrounding areas with similar conditions. The indirect evaluation method was applied for comparing the results with measurements in the southern part of Negev area which is located in the northeastern part of Sinai Peninsula.

4.2.1 Hydrograph

The hydrograph is a graph plot of flow rate versus time resulting from a combination of physiographic and meteorological factors in a watershed. It represents the integrated effects of climate, hydrologic losses, surface runoff, and groundwater flow. Sherman (1932) originally introduced the theory of the unit hydrograph (UH), which was defined as "basin outflow resulting from “unit depth” of direct runoff generated uniformly over the drainage area at a uniform rainfall during specified period of rainfall duration".

Several assumptions inherent in the unit hydrograph tend to limit its application (Jonhnstone and Cross, 1949) for a given watershed. These assumptions include:

1) Rainfall excesses of equal duration are assumed to produce hydrographs with equivalent time bases regardless of the intensity of the rain.
2) Direct runoff ordinates for a storm of given duration is assumed directly proportional to rainfall excess volumes.
3) The time distribution of direct runoff is assumed independent of antecedent precipitation.
4) Rainfall distribution is assumed to be the same for all storms of equal duration.

The rainfall excess or effective rainfall volume are the same as the volume of runoff, i.e. the area under the runoff hydrograph. By estimating the effective rainfall and determining the watershed characteristics, a runoff hydrograph can be constructed. The average peak discharge measures the risk degree of the basins in case of lack of any hydrologic data within the study area.

The procedures for deriving hydrographs from gauged watersheds have been applied with success using available stream flow and rainfall data for relatively few watersheds. Hence, methods for driving hydrographs for ungauged basins or shortages have evolved based on the theoretical or empirical formulas relating hydrograph peak flow and basin characteristics. These are referred to as

Synthetic Unit Hydrographs. This is an attractive approach for runoff prediction in ungauged catchments (Gibbs et al., 2009).

4.2.2 Synthetic hydrograph

A synthetic hydrograph can be defined as the hydrograph of an ungauged watershed, developed using known physical characteristics of another gauged watershed, provided that the gauged watershed is identical regarding meteorological and hydrological conditions to the ungauged watershed.

A synthetic hydrograph is used in determination of flood peak and runoff volume, especially from ungauged watersheds. The qualifier 'synthetic' denotes that hydrographs are obtained without using rainfall-runoff data from watersheds. Before reviewing various synthetic hydrograph methods for estimating the hydrograph peaks and shapes without stream data, factors affecting the hydrograph according to Wanielista (1990) are listed:

1) **Basin Area (A):-** The total volume of runoff and peak discharge is proportional to the area of the watershed. As the area contributing to a point of discharge increases, the volume and peak discharge increases. Also, the hydrograph base will increase with increased area.
2) **Basin Slope (S):-** basin slope is the average vertical elevation change per horizontal distance along a watercourse bed. The steeper the channel slope, the greater the velocity of runoff and the greater peak discharge.
3) **Basin Length (L):-** basin length is the travel length associated with the longest time it takes for a particle of water to flow overland. The basin length and slope determine the watershed time of concentration, that means the time for a drop of rainwater in a intense storm takes from the furthest point on the catchment to the outlet of the catchment.
4) **Soil and Vegetation cover:** This affects the amount of rainfall excess and thus, the peak of a hydrograph. The greater the initial abstraction and infiltration, the less the rainfall excess.
5) **Stream pattern and watershed shapes:** A fan-shaped area with streams radiating from the same point suggests contributing incremental area increases with time, such that a late but high peak in the hydrograph is suggested, whereas an elongated area traversed by one major stream with some relatively uniformly spaced tributaries suggests a less pronounced rise and fall of the hydrograph.

The hydrograph is a lumped model because it directly transforms rainfall into runoff without explicitly representing the internal distribution of flow within the watershed. Lumped models have been frequently used in the description and analysis of precipitation-runoff relationships (Chow et al., 1988). The advantage of lumped models is its relative simplicity. This model is an abstraction where the watershed is considered as a unit characterized by a reduced number of variables and parameters, whose averages can be derived empirically or physically (Maidment, 1993b). Thus, a lumped model is often used in flood predication, can be applied for different catchment sizes and is successfully

applied to divide a watershed into sub watersheds (Singh & Fiorentino, 1996). It is limited by the inability to account for the internal variation of the hydrologic systems and processes.

Chow et al.(1988) categorized synthetic hydrograph procedures into: 1) hydrographs based on models of watershed storage (e.g., Nash, 1957), 2) hydrographs based on runoff characteristics as (time to peak, peak flow) with watershed topographic characteristics (e.g., Snyder, 1938; Geomorphologic Instantaneous Unit Hydrograph); and 3) synthetic hydrographs based on a dimensionless unit hydrograph (e.g., Soil Conservation Service, 1975 (SCS)).

Due to the availability of geomorphological watershed characteristics of different wadis in the study area, synthetic hydrographs based on topographic characteristic have been selected to calculate the hydrological parameters for the high risk sub-basins in the Dahab basin. There are two main approaches used to derive synthetic hydrographs from topographic information: the Geographic Instantaneous Unit Hydrograph (GIUH) method based on the work of Nash (1957) and Rodriquez – Iturbe and Valdes (1979), and the spatially distributed unit hydrograph method which is based on the time area relationship for the catchment (Maidment, 1993b). A number of approaches have been developed based on these two initial studies, but they all essentially involve using measurements of distance, velocity and time to derive to the physical characteristics of the watershed and to parameterize a unit hydrograph in absence of observed runoff and rainfall data (Cleveland et al., 2008). All approaches to derive hydrographs from topographic information require at least one parameter to describe the timing of flow across the catchment, often in the form of average velocity. The average flow velocities parameter is then used to derive the final unit hydrograph using travel distance through the catchment.

4.2.2.1 Geomorphic unit hydrograph

Geomorphology reflects the topographic and geometric properties of the watershed and its drainage channel network. It affects the hydrologic processes from rainfall to runoff and the subsequent flow routing through the drainage network. Certain characteristics of the drainage basins reflect the hydrologic behavior. Therefore, it is useful, when quantified, in evaluating the hydrologic response of the basins. These characteristics relate the physical characteristics of the drainage basin including drainage area, basin shape and ground slope as well as of the drainage network including channel order, channel length, channel slope, channel profile, and drainage density.

The GIUH approach is used for deriving a unit hydrograph using only the information obtainable from topographic maps or remote sensing possibly linked with geographic information system (GIS) and digital elevation model (Kumar et al., 2002). The GIUH technique is applicable to estimate the direct runoff component of stream flow and hence, can be used to generate the direct hydrograph runoff (DHR). The steps followed in the methodology are summarized in figure. 133. The model is particularly applicable in ungauged basins having scarce hydrologic data (Al-Wagdany and Rao, 1998). It has many advantages over the regionalization techniques. It can work without requirement of

flow data and computation for neighboring gauged catchments in the region as well as without updating parameters.

The hydrologic response is a function of climatic parameters, land use, soil parameters and topography. Therefore, physical based models require a time to time change in their parameters, due to variations encountered with respect to gradual climatic changes of the watersheds (Rodriguez-Iturbe et al., 1982a). However, the geomorphological parameters are mostly time-invariant in nature and the rainfall pattern undergoes a change due to global atmospheric change. Accordingly, a geomorphological based approach can be the most suitable technique for modeling runoff processes for ungauged catchments.

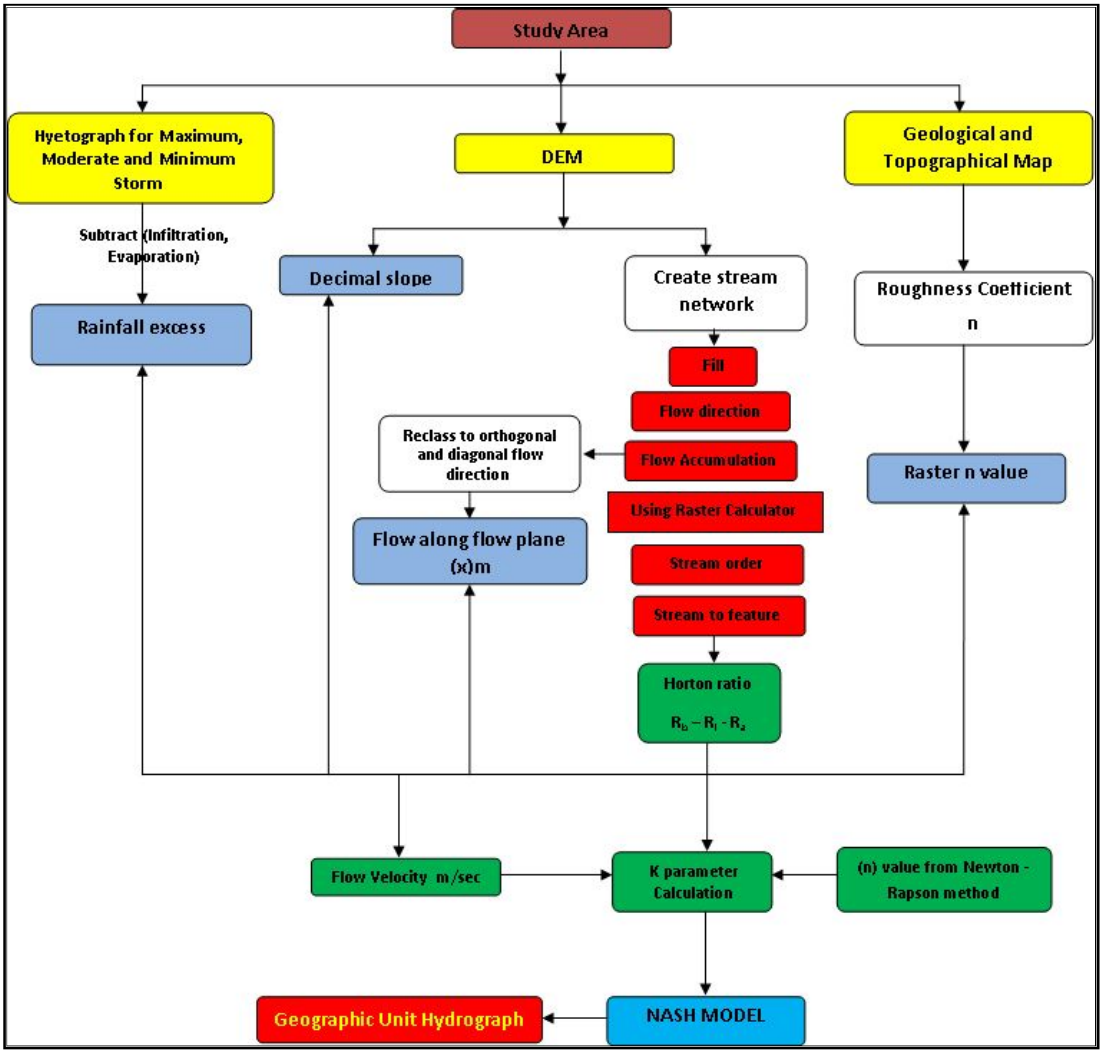

Figure 133 : Schematic Diagram of Geomorphic Unit Hydrograph Model

4.2.2.1.A The concept of geomorphic unit hydrograph based on Nash model

The Nash model (Nash, 1957) is based on the concept of routing of the instantaneous input of rainfall excess through the drainage basin of "n" identical to linear reservoirs in series with equal storage coefficient "k" to obtain the outflow from the n^{th} reservoir. The concept of the Nash model suggests that any catchment may be replaced by a series of 'n' reservoirs, when the instantaneous

inflow of volume 'V' takes place in the first reservoir, its level raises by an amount sufficient to accommodate the increased storage and the discharge rises instantaneously from zero to V/k and diminishes with time. The Nash model can be expressed as follows:

$$\mathbf{u} = \frac{\mathbf{V}}{\mathbf{k} * \Gamma(\mathbf{n})} * \boldsymbol{e}^{-\frac{\mathbf{t}}{\mathbf{k}}} * \left(\frac{\mathbf{t}}{\mathbf{k}}\right)^{\mathbf{n-1}} \qquad \textbf{Equation (36)}$$

V= Volume of hydrograph (m^3) u= the ordinate of the hydrograph (discharge m^3/s)

t= Time (hr) k= the storage constant for reservoir

n= the shape parameter denoting the number of reservoirs Γ = Gamma function

The GIUH theory introduced by Rodriguez-Iturbe and Valdes (1979) suggests that it is adequate to assume a triangular form of IUH. They obtained expressions for the time to peak t_p which is the time interval from the start of surface runoff to the peak of the resultant hydrograph, the peak discharge q_p of the IUH which are functions of geomorphology, and of the dynamic parameter represented by the velocity as follows:

$$\mathbf{q_p} = \frac{\mathbf{1.31}}{\mathbf{L_\Omega}} * \mathbf{R_l^{0.43}} * \boldsymbol{v} \qquad \textbf{Equation (37)}$$

$$\mathbf{t_p} = \frac{\mathbf{0.44 * L_\Omega}}{\boldsymbol{v}} * \left(\frac{\mathbf{R_b}}{\mathbf{R_a}}\right)^{\mathbf{0.55}} * \mathbf{R_l^{-0.38}} \qquad \textbf{Equation (38)}$$

L_Ω is the length of the highest order stream in kilometers, *v* is the dynamic velocity in m/s, R_b is bifurcation ratio, R_a is basin area ration, R_l is basin length ratio, and the units of q_p and t_p are the customary units of inverse time (h^{-1}) and time in (h), respectively.

To predict the hydrograph of storm runoff, the shape parameter (n) and the scale parameter (k) of the Nash conceptual model of (IUH) are related with Horton´s order ratio (Bifurcation ratio (R_b), Length ratio (R_l) and area ratio (R_a)). The complete shape of the GIUH can be obtained by linking the q_p and t_p of the GIUH with scale (k) and shape (n) parameters of the Nash model as follows:

The value of time to peak of this IUH could be obtained by differentiating equation 36 with respect to time and applying the condition $\frac{du(t)}{dt} = 0$, which can be mathematically represented as: $\mathbf{t = t_p = (n-1)*k}$ **Equation (39)**

The peak of the IUH, q_p, was obtained by putting the value of $t = t_p$ in equation (39) and expressed as:

$$\mathbf{q_p} = \left[\frac{\mathbf{V}}{\mathbf{k} * \Gamma(\mathbf{N})}\right] * \mathbf{e^{-(n-1)}} * \mathbf{(n-1)^{n-1}} \qquad \textbf{Equation (40)}$$

The characteristics of the IUH, time to peak t_p and peak q_p obtained from equation 39 and equation 40, respectively, were multiplied and expressed as:

$$\mathbf{q_p\, t_p} = \frac{\mathbf{(n-1)*V}}{\Gamma(\mathbf{n})} * \boldsymbol{e}^{-(\mathbf{n-1})} * \mathbf{(n-1)^{n-1}} \qquad \textbf{Equation (41)}$$

In order to relate the parameters of the Nash model and the GIUH of Rodriguez-Iturbe, equations 37 and 38 and equation 41 were compared and the resultant expression is written as:

$$\frac{(\mathbf{n-1})*\mathbf{V}}{\Gamma(\mathbf{n})} * \boldsymbol{e}^{-(\mathbf{n-1})} * (\mathbf{n-1})^{\mathbf{n-1}} = {}_{0.58} * \left(\frac{R_b}{R_a}\right)^{0.55} * \mathbf{R_l}^{0.05} \qquad \textbf{Equation (42)}$$

The Nash parameter n, can be obtained by solving eq. 42 using mathematical equations of the Newton-Rapson method. The Nash parameter k for the given velocity (v) is obtained using k and can be expressed as follows:

$$k=\frac{0.44*L_\Omega}{v} * \left(\frac{R_b}{R_a}\right)^{0.55} * \mathbf{R_l}^{-0.38} * \frac{1}{(n-1)} \qquad \textbf{Equation (43)}$$

where L_Ω is length of the highest stream order of the watershed , R_a and R_b are Horton's ratios, and v is the dynamic velocity which is taken as a constant.

The scale parameter of the model is time variant and dependant on both the catchment geomorphology and the average velocity of surface runoff along the stream network of the watershed. In this study, the uniform velocity of flow (v) of a stream is assumed to be dynamic velocity and it is determined from both the geomorphologic parameters of the network and the intensity of the effective rainfall spread uniformly over the watershed as shown below. The derived values of n and k are used to determine the complete shape of the Nash based GIUH using eq. 43 and the direct runoff hydrograph (DRH) is estimated by convoluting the excess rainfall hyetograph.

4.2.2.2.B Determination of Horton's ratio

Three of Horton's ratios, namely bifurcation ratio (R_b), stream-length ratio (R_l) and stream-area ratio (R_a), are unique representative parameters for a given watershed and fixed values for a given watershed system. The DEM of Dahab basin was processed to delineate the basin boundaries and drainage networks. The extracted stream network process is discussed in chapter 2. The geomorphological parameters in terms of Horton's ratios are determined using drainage networks of the watershed. The logarithm of number of streams (N_u), mean stream length (L_m), and mean stream area (A_m) are plotted against the order of stream (u) and are shown in appendix 18. The slope of straight lines that fit best to stream order with number of streams, mean stream length, and mean stream area gives the values of R_b, R_l, R_a respectively which are presented in appendix 19.

- **Bifurcation ratio R_b**

The number of channels of a given order in a drainage basin is a function of the nature of the surface of that drainage basin. In general, greater ratio value means the infiltration of the soil cover will increase; the lower ratio value is the number of channels required to carry the remaining runoff

water. Moreover, the larger the number of channels of a given order, the smaller the area drained by each channel order is (Strahler, 1964). This ratio is calculated in chapter 2.

- **Stream-length ratio R_l**

This refers to the length of channels of each order. The average length of channels of each higher order increases as a geometric sequence, which can be further explained as: the first order channels are the shortest of all the channels and the length increases geometrically as the order increases. The length of channels of a given order are determined mainly by the type of soil covering the drainage basin. Generally, the more pervious the soil, the longer the channel length will be of a given order. The higher the value R_l, the soil cover will be more imperviousness. Generally, it varies between 1.5 and 3.5 (Rai et al., 2009). This relation is called Horton's law of channel length and can be formulated as follows:

$$R_l = \frac{L_{m(u+1)}}{L_{m\,(u)}} \qquad \textbf{Equation (44)}$$

where L_{mi} is the mean length of channel of order I and R_l is the stream-length ratio.

The mean length of each stream order is calculated in chapter 2. The stream length ratio is calculated for more hazard risk sub-basins at dahab basin. The values vary from 1.76 at W. Zaghraa to 2.6 at W.Nasab (app. 19). The high values occur at W.Nasab , W. El Ghaieb and W. Ramithy while the low values appear at W. Saal, W. El Genah and W. Zaghraa.

- **Stream-area ratio R_a**

The Horton law of stream areas states that there exists a geometric relationship between the mean area drained by streams of a given order and the corresponding order (u). The channel area of order u, A_u is the area of the watershed that contributes to the channel segment of order u and all lower order channels. According to the previous law, stream area ratio is calculated by dividing the mean basin area of streams of one order by the mean of area basins of the next lower order. It can be quantified as:

$$R_a = \frac{A_{m(u+1)}}{A_{m(u)}} \qquad \textbf{Equation (45)}$$

where $A_{m(u)}$ is the average area of order i and R_a is the stream area ratio.

The mean stream area (A_m) for each stream order in each sub-basin is caluclated in chapter 2. There is good correlation between stream area ratio and stream length ratio (app.19).

4.2.2.2 Spatially Distributed Unit Hydrograph (SDUH)

Spatially distributed models have been used to evaluate hydrological conditions (runoff, infiltration, groundwater recharge) and climatic change in a number of geographical regions (Najjar, 1999). Distributed models can be applied to every hydrological problem, including predictions in ungauged watersheds (Refsgaard, 1996). This model is used where basins are regularly partitioned into a number of hydrological response units, sub-watersheds or representative hillslopes (Kite and Kouwen, 1992; Bergström and Graham, 1998).

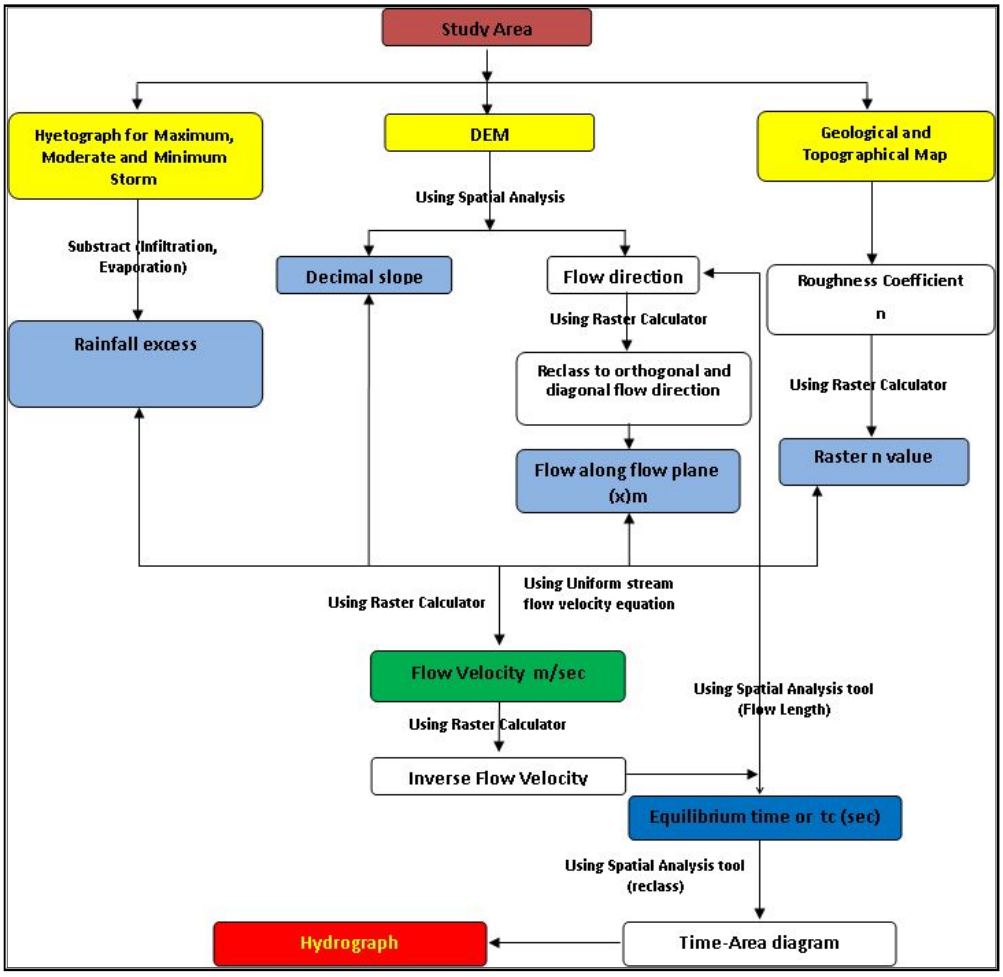

Figure 134 : Schematic Diagram of Spatially Distributed Unit Hydrograph Model

Maidment (1993) suggested the name "spatially distributed unit hydrograph" to distinguish it from the traditional unit hydrograph concept requiring a uniform spatial distribution of excess rainfall. The distributed unit hydrograph is derived from the time-area diagram compiled for a watershed by means of GIS. The GIS-based approach permits to vary the spatial pattern of excess rainfall by isochrones zones within the watershed, thus, relaxing the requirement for uniform excess rainfall over the whole watershed.

The hydrograph is compiled along the drainage network in numerous locations in Dahab basin assumed to be the outlets of theoretical sub-catchment by computing flow distances with flow

velocity. The whole procedure is carried out in a GIS environment; a grid format is used to represent the spatial distribution of values of all variables involved. The travel time through each individual cell along the flow path will be summed up to estimate the cumulative travel time from the start of each flow path to the outlet. The travel time to the outlet from each grid cell in DEM is estimated based on the runoff pathway and the travel time through each grid cell (DEM) along the path using flow length function in Arc GIS (fig. 134).

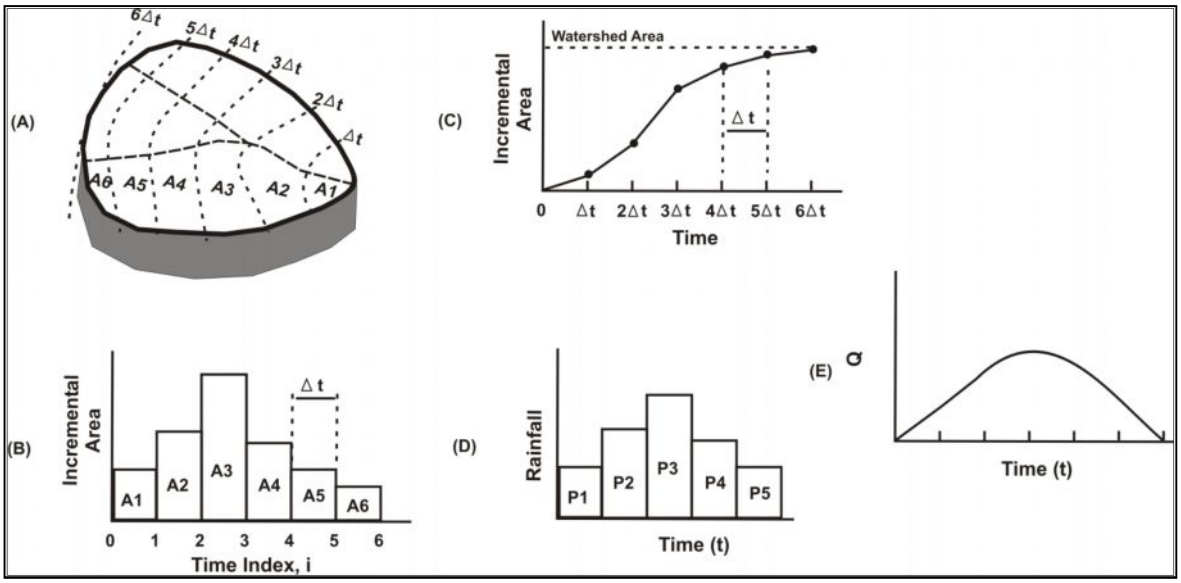

Figure 135 : The Main Concept of Spatially Distributed Unit Hydrograph Model (after Maidment;1993)

The distributed hydrograph is derived from the time-area diagram compiled for a watershed by means of GIS. The time- area analysis is widely known as hydrologic water techniques to derive the discharge hydrograph due to a given rainfall hyetograph excess. It is represented as a diagram of cumulative drainage area that water can flow through the areas to the outlet within a specified time of travel (Madiment, 1993 and Muzik, 1996). In this model, the storage effects are ignored and the watershed is divided into a number of sub-areas separated by isochrones (fig. 135). An isochrone is a contour joining those points in the watershed that are separated from the outlet by the same travel time.The isochrones cannot cross one another, cannot close, and can only originate or terminate on the watershed boundary. Maidment (1993) pointed out that an isochrone which has a maximum time of flow to the outlet is the time of concentration of the watershed, t_c, and is also sometimes called the time of equilibrium.

The unit hydrograph of a watershed can be derived from the watershed's time-area diagram. Following the derivation given by Maidment (1993), if an excess rainfall occurs at a rate I over the watershed, the runoff at the outlet is given by Q(t) = IA(t), which is an S-hydrograph of runoff tending to an equilibrium discharge of IA where A is the total area of the watershed. Lagging the S-

hydrograph by At and subtracting it from the original S hydrograph yields the Δt time unit hydrograph ordinates as:

$$\mathbf{U(t) = \frac{A*(t) - A*(t-\Delta t)}{\Delta t}} \qquad \textbf{Equation (46)}$$

Because the time-area diagram values are known only at discrete time points, t = iΔt, where i = 0, 1, 2, ..., n represents zones which are bounded by isochrones. The unit hydrograph ordinates at the corresponding time points are given by:

$$\mathbf{U(i.\Delta t) = \frac{A*(i*\Delta t) - A*[(i-1)*\Delta t]}{\Delta t}} \qquad \textbf{Equation (47)}$$

Or simply

$$\mathbf{U(i) = U(i.\Delta t) = \frac{A(i)}{\Delta t}} \qquad \textbf{Equation (48)}$$

where At = A *(i*Δt) — A*[(i— 1)* Δt] are the incremental areas. The dimension of U(i) is the area dimension $[L^2]$ divided by time $[T^{-1}]$.

The deriviation of the direct runoff hydrograph (DRH) was suggested by Maidment (1993), using excess rainfall (P) in meters or inches and their correponding discharge rate (Q) at the watershed outlet (m^3/s). The calculated direct hydrograph is computed for the first time interval as:

$$\mathbf{Q1 = \frac{P1*A1}{\Delta t}} \qquad \textbf{Equation (49)}$$

And after time 2Δt, Maidment (1993) assumes that there are two rainfall pulses to contend with, P1and P2, which includes the immediate impact at the outlet of P2 flowing from area A1 plus the delayed effect of P1 flowing from area A2 and direct runoff is computed by:

$$\mathbf{Q2 = \frac{[(P2*A1)+(P1*A2)]}{\Delta t}} \qquad \textbf{Equation (50)}$$

So the direct runoff at any time t= n*Δ t is given by summing the runoff contributions from each of the applicable isochrone zones suitably lagging in time.

$$\mathbf{Qn = \sum_{i=1}^{n} \frac{P_{ij}*A_i}{\Delta t}} \qquad \textbf{Equation (51)}$$

Where Pij is the average excess rainfall over all cells in isochrone zone i during time interval j. and j = n-i+1.

It can be summerized that the concepts of the previous models use flow velocity as a main factor to calculate the hydrological parameters (peak discharge and time to peak) from a synthetic hydrograph. In a SDUH model, the flow velocity is used with flow direction layer to calculate the

flow time required for water to cross the whole grid while, in a GIUH model, flow velocity is used to calculate storage values (k) for solving GIUH based on Nash's model and then can calculate hydrological parameters.

4.2.3 Models Development

The techniques of synthetic hydrographs can be implemented using existing GIS functionality. The basic modelling approach uses the raster GIS functions, therefore, all calculations are based on raster. The topographic data, land cover and climate data are used to develop the models for estimation the runoff parameters. The adapted layers for both models are as follows:

4.2.3.1 Topographic data

4.2.3.1.A Digital Elevation Model (DEM*)*

The main data set of the current study is a DEM. The raster digital elevation models are the most used type of model because their representation is extremely simple (a simple matrix where the topological relations between the cells is implicit) and for the ease of representing them in computer memory (Moore et al., 1991). It is considered to be important data in determining the slope of the terrain and flow direction, which are used for drainage network and delineating drainage basins as in chapter 2.

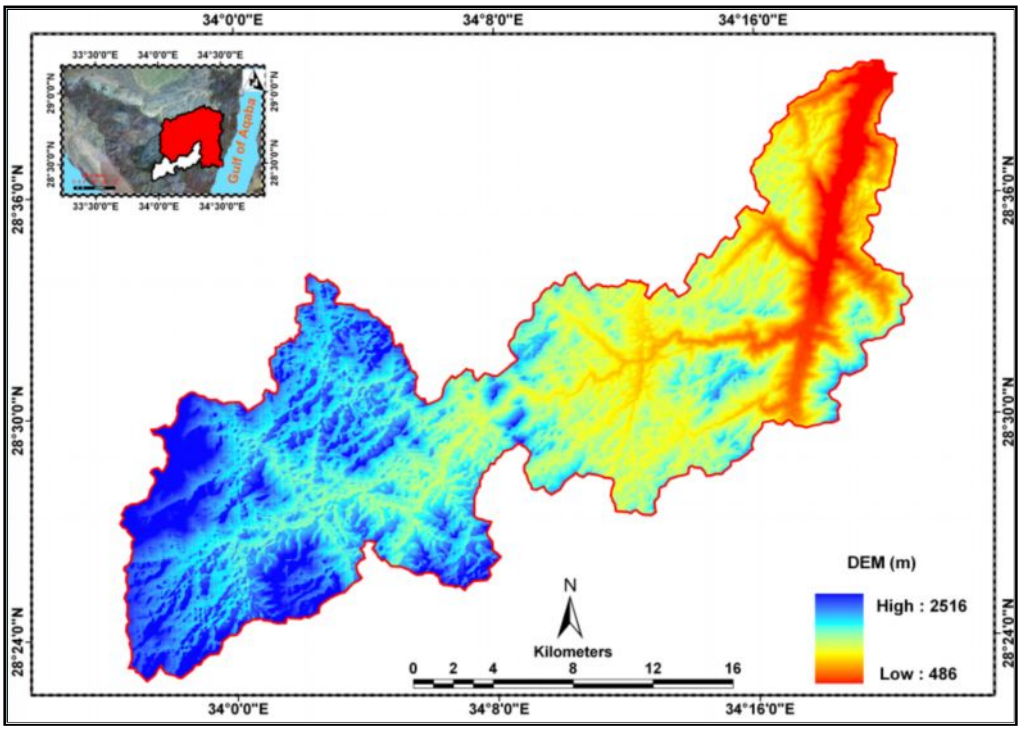

Figure 136 : Digital Elevation Model of Subbasins in W. Nasab

(ASTER) DEM data with 30m resolution is used in the study. The accuracy of the (ASTER) DEM freely available dataset is suitable for the representation of urban areas or other smaller areas,

but in larger river basins and for other purposes, data at a lower resolutions may be sufficient (Maidment, 2002). The high data resolution and no-cost availability are the most attractive reasons to utilize ASTER data.

Dahab basin was divided previously into three major sub-basins: W. El Ghaieb and W.Zaghraa and W. Abu Khshieb. W. Zaghraa was divided into four major sub-basins which are W.Nasab, W. Rimthy, W. El Genah and W. Saal. It was mentioned in chapter two that wadis Zaghraa, Nasab, Rimthy, El Ghaieb and Abu Khshieb are the high runoff risk ares from a geomorphological point of view, while W. Saal and W. El Genah are considered moderate to low risk sub-basins. Digital elevation models were prepared for the risky sub-basins in addition to low risk sub-basins to evaluate the hydrological background as runoff discharge and its volume for all different scenarios of storms as shown in fig.136 and appendix 20.

4.2.3.1.B Slope

The slope is one of the most important data layers to calculate hydrograph parameters. The algorithm of slope calculation is illustrated in chapter 2. The decimal slope will be used for estimation of surface flow velocity for each sub-basin in Dahab basin (fig.137 and appendix 21).

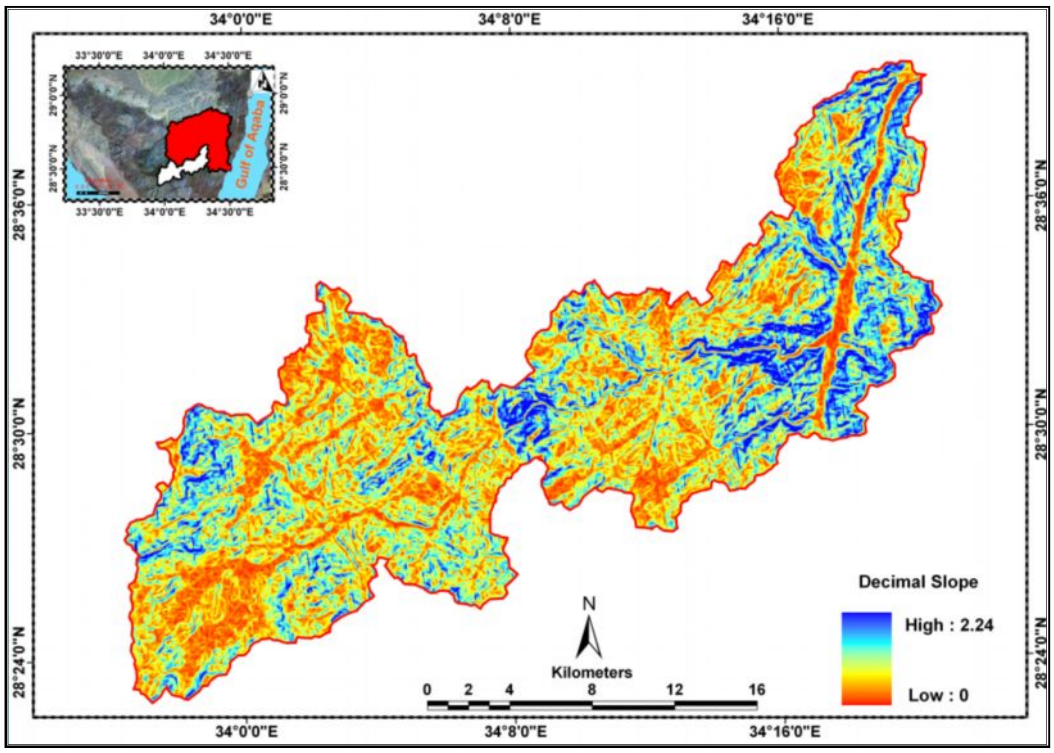

Figure 137 : Decimal Slope of Subbasins in W. Nasab

4.2.3.2 Land cover

Dahab basin is characterized by rocks only sparsly covered by desert vegetation (Omran et al., 2012). The land cover is studied easily due to sparse vegetation and low urban communties in the

study area. The Manning roughness value “n” is used to calculate flow velocity of surface runoff (Chow, 1959). The Manning value is highly variable and depends on a number of factors including surface roughness, vegetation, channel irregularities, size and shape of channel and obstructions.

Manning’s values should be calibrated whenever observed water surface profile information (gaged data, as well as high water marks) is available. When gauged data is not available, values of Manning’s value computed for similar stream condition or values obtained from experimental data should be used as guides in selecting "n" values.

Dahab basin includes three different rock types which are in the high lands of basements rocks in the southern, western and eastern part of the basin, plateaus of sedimentary rocks in the northern part and alluvial channels. These surfaces are cut by channels with different shapes and characteristics. The Manning values have been determined by the study of the channel surface through field visits. Low vegetation cover is facilitated by the study of channel characteristics from satellite images. The characteristics of channels are compared with reference tables to determine suitable values for the surface.

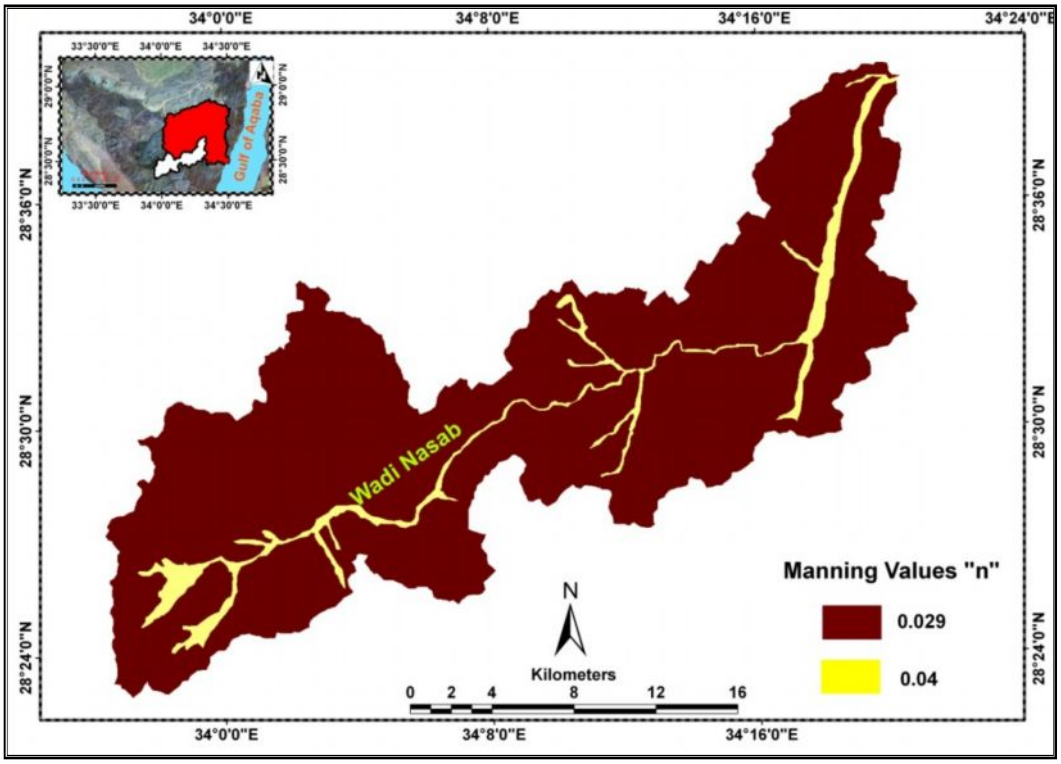

Figure 138 : Manning Value “n” of Subbasins in W. Nasab

There are several references in selecting Manning’s "n" values for typical channels. The attribute and cell grid values are assigned with Manning’s roughness coefficient according to Chow (1959); the most common types of channel are described in tables in order to determine channel roughness as shown in figure 138 and appendix 22. There are three values:

1- For alluvial channels: the channels filled with weathered material from sedimentary and basement rocks. Manning' value 0.029 can be chosen (Chow, 1959).
2- For channels in high lands of basement rocks: it has outcroping basement rocks and no vegetation within the channel and they are filled with gravels and cobbels. The channels occur at mountainous areas (mountainous streams). Manning' value (0.04) can be chosen (Chow, 1959).
3- For channels cut in sedimentary rocks: they have no vegetation with smooth shape and uniform section with coarse sediments. Manning' value (0.025) can be chosen (Chow, 1959).

4.2.3.3 Climate data

Rainfall is an important factor for the use of models. The study area is subjected to maximum rainfall storm per day (fig.129). These records might be repeated according to the probability diagram of figure 130. The previous storms were recorded at Saint Catherine station. The maximum storms were recorded in this station from 1934 to 2004 with the highest one being (76.2 mm/day) in November 1937. The elevation and location of Saint Catherine station at the western catchment of Dahab basin is the main reason that records from this station are a good representative of the rainfall amount.

The hyetograph of the highest storm (76.2 mm) was collected from WRRI (2006) (fig.139). A hyetograph is a graphical representation of the distribution of rainfall over time. Rainfall intensity progressively increases until it reached a maximum and then gradually decreases (fig. 139). The intensity of rainfall varies along the duration of the maximum storm. The hyetograph of the maximum storm shows that the intensity of a storm increases from 2.1 to 5.4 mm/hr after 7 to 9 hours from the storm starting and decreases to 1.9 mm/ hr after 19 to 21 hours (fig. 139).

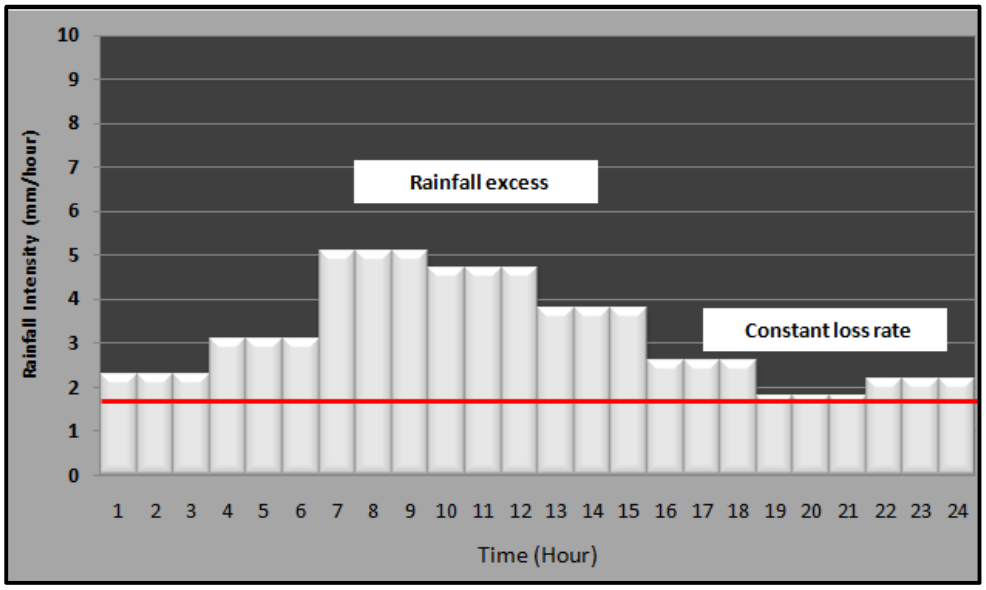

Figure 139 : Measured Hyetograph of Maximum Storm (76.2mm) in Saint Catherine Station (WRRI, 2006)

Due to the lack of historical background of rainfall in stations, the maximum storm is used as maximum scenario rainfall data. The hyetograph of the maximum storm will be used to build other scenarios of storms e.g. 65, 55, and 45 mm/day to estimate the volume and discharge of possible runoff which may result from these different scenarios. The configuration of hyetographs of other scenarios is designed depending on the maximum graph, but they have lower intensities per hour.

The excess rainfall is part of the rain in a given storm which falls at intensities exceeding the infiltration capacity of the land which represents the volume of rainfall available for direct runoff. Since there are no data records available for runoff of the study area, the average volume of runoff is calculated using available measurement of hydraulic conductivity and calculated evaporation rates to estimate the average loss. The loss rate is determined as a constant value that must be subtracted from the actual rainfall so that the resulting rainfall excess volume over the entire catchment is equal to the actual storm runoff volume (Brutsaert, 2005).

The average hydraulic conductivity of fractured basement rocks will be used as infilteration rate because the basement rocks cover about 70 % of the study area, especially at the high lands of the western, southern and north eastern parts of Dahab basin. The hydraulic conductivity of fractured basement rocks is estimated in chapter three as 4.2×10^{-7} m/s i.e (1.6 mm/hr). The average evaporation rate at Saint Catherine station in November is 6.9 mm/day (0.2mm/hr) (Table 30). It can be concluded that the average constant loss rate at Saint Catherine station is 1.82 mm/hr during rainy seasons. This value will be used for estimation of the amount of rainfall excess per hour. Based on that, the total voulme amount of runoff for each sub-basin in Dahab basin will be estimated.

4.2.3.4 Velocity of flow

Kilgore (1997) and Behera et. al. (2008) used a kinematic wave approximation in order to calculate flow velocity of runoff in every cell of the raster grid representing a catchment. In this process, they combined the depth of flow at equilibrium equation 52 (as given by Overton and Meadows, 1976) with Manning´s equation to calculate the equilibrium runoff velocity for overland flow equation 53:

$$\mathbf{y} = \left(\frac{\mathbf{n} * \mathbf{i_e} * \mathbf{x}}{\mathbf{S_o^{0.5}}}\right)^{\mathbf{0.6}} \qquad \textbf{Equation (52)}$$

x :- the distance along the flow plane (m) **So:-** decimal slope **y:-** the depth of flow at equilibrium (m)
ie:- excess rainfall (m/s) **n:-** Manning's roughness coefficient

$$\boldsymbol{v} = \left(\frac{(\mathbf{i_e} * \mathbf{x})^{\mathbf{0.4}} * \mathbf{S_o^{0.5}}}{\mathbf{n^{0.6}}}\right) \qquad \textbf{Equation (53)}$$

Where, $\boldsymbol{v}$ is the velocity of flow (m/s)

The flow velocity is calculated only for the overland flow velocity because, for the drainage channels, the complexity of the geometrical and hydraulic characteristics is too high. Moreover, the overland flow velocity has greater influence than channel flow velocity in such areas. The calculations are based on simple mathematical functions between raster grids. "The velocity grid" was used as a weight grid that indicates the time need for water passing through each cell of the grid.

The distance along the flow plane is considered as the distance between any given raster cell and the closest ridge cell. This assumption involves simplification. However, it is considered that the error can be neglected in spite of other simplifications already used in the model. The flow direction cell layer represents the distance along the flow plane. The flow direction cell is reassigned to 42m if the flow is diagonal and 30 m if the flow is orthogonal.

4.2.4 The results

Both models are applied on the main risky sub-basins in wadi Dahab. The peak discharge (Q_p) and time to peak (t_p) are estimated for each sub-basin. The obtained results are listed in table 31 and the hydrographs of both results are illustrated in appendixes 23-24. The results show that the Q_p values from both the GUH and SDUH models match in the selected sub-basins, while differences in t_p values are observed between both models. The values of t_p and Q_p in the SDUH model are higher than those in the GUH model.

The difference of t_p between the models is caused by the fact that the output hydrograph in (SDUH) time-area method depends on the effects of time varying rainfall without any contribution of the storage effect. The same remarks of storage neglecting were mentioned by Ajward (1996) who predicted hydrological parameters as t_p with the same method. On the other hand, GUH based on Nash's method has taken into consideration that the (k) value (constant storage) for solving the model depends on morphometric parameter ratios (see equations 43 and 46). The instantaneous assumption of the Nash model in GUH plays an important role for the t_p differences, and then the value of t_p in GUH will be lower than in the time-area method.

The average peak discharge of the maximum storm of 76mm ranges from 64 to 556 m^3/s for sub-basins in W. Dahab. W. Zaghraa, W. Zaghraa-nasab. W. Zaghraa-saal has high discharge values of 215.2 to 556 m^3/s; W. Nasab and W. Rimthy represent a moderate value of discharge ranging from 130 and 200 m^3/s respectively, while W. Abu Khshieb, W. Saal, W. El Ghaieb and W. El Genah have the lowest discharge values of 64 to 119 m^3/s. The values of discharge are relatively low at sub-basins of W. Dahab in the lowest storm of 45mm ranging from 10.3 to 50 m^3/s. At moderate storms of 65mm and 55 mm, the peak discharge ranges from 41.69 to 261 m^3/s and from 128 to 23 $m^3/$ sec.

It can be concluded that the peak discharge value at W. Zaghraa Nasab is higher than at Zaghraa Saal. The peak discharge values are higher in W. Rimthy, W. Zaghraa Nasab and W. Zaghraa than in W. Nasab, W. Zaghraa-Nasab and W. Zaghraa. The volume of excess rainfall, the basin area and the high mean topographic elevation are the main reasons for the high peak discharge in W.Rimthy-W.

Zaghraa area. The sedimentary cover in the northern part of the study area affects the peak discharge value, especially at W. El Ghaieb and W.El Genah, while the small basin size of W. Abu Khshieb causes low values of peak discharge as shown in table 31.

			Geomorphic Unit Hydrograph		Spatial Distrbuted Unit Hydrograph						
			Q_p	t_p	Q_p	t_p	Tc	V	v	$Q_{p\ avg}$	$t_{p\ avg}$
			m^3/s	hr	m^3/s	hr	hr	$*10^6 m^3$	m/s	m^3/s	hr
W. Zaghraa	*Storm 76mm*	*(T > 180 year)*	530	20	582.0	40.0	53.0	64.7	0.63	556.0	27.00
W. Zaghraa Nasab			315	19	320.0	32.0	49.0	38.5	0.67	317.5	27.00
W. Zaghraa Saal			212	19	219.0	35.0	45.0	27.5	0.58	215.5	25.00
W. Nasab			124	22	136.0	30.0	40.7	16.0	0.71	130.0	26.00
W. Rimthy			188	12	212.0	25.0	26.2	16.5	0.68	200.0	18.50
W. El Ghaieb			113	15	125.0	25.0	27.0	12.0	0.6	119.0	20.00
W. El Genah			110	15	111.0	30.0	39.0	11.3	0.41	110.5	22.50
W. Saal			100	12	105.0	25.0	31.1	9.9	0.5	102.5	18.50
W. Abu Khshieb			60	9	68.0	15.0	17.0	3.7	0.63	64.0	12.00
W. Zaghraa	*Storm 65mm*	*(T= 100 year)*	253	25	270.0	57.0	73.0	46.6	0.45	261.5	41.0
W. Zaghraa Nasab			160	24	163.0	47.0	69.0	27.50	0.46	161.5	35.5
W. Zaghraa Saal			107	24	124.0	45.0	63.0	19.50	0.42	115.5	34.5
W. Nasab			71	25	81.0	35.0	58.0	12.00	0.6	76.0	30.0
W. Rimthy			105	15	112.3	30.0	37.3	12.30	0.56	108.6	22.5
W. El Ghaieb			64	18	70.1	30.0	55.0	8.70	0.5	67.1	24.0
W. El Genah			62	18	65.0	35.0	39.0	8.20	0.32	63.5	26.5
W. Saal			57	16	60.9	30.0	44.1	7.30	0.37	58.9	23.0
W. Abu Khshieb			36.5	11	46.9	20.0	24.0	2.60	0.52	41.7	15.5
W. Zaghraa	*Storm 55mm*	*(T= 50 year)*	122	36	134.0	62.0	100.0	31.8	0.33	128.0	49.0
W. Zaghraa Nasab			83	33	85.0	60.0	93.0	18.50	0.35	84.0	46.5
W. Zaghraa Saal			52	34	58.0	62.0	83.0	13.50	0.3	55.0	48.0
W. Nasab			38	32	42.6	45.0	80.0	8.30	0.5	40.3	38.5
W. Rimthy			54	20	59.6	35.0	50.4	8.40	0.45	56.8	27.5
W. El Ghaieb			32	30	39.5	40.0	74.2	5.70	0.4	35.8	35.0
W. El Genah			30	21	32.2	35.0	52.0	5.40	0.26	31.1	28.0
W. Saal			29	20	30.2	35.0	60.0	4.70	0.29	29.6	27.5
W. Abu Khshieb			20	14	26.2	25.0	28.0	1.60	0.38	23.1	19.5
W. Zaghraa	*Storm 45mm*	*(T= 25 year)*	46	55	54.0	82.0	150.0	18	0.22	50.0	68.5
W. Zaghraa Nasab			30	50	34.1	80.0	138.0	10.90	0.23	32.1	65.0
W. Zaghraa Saal			18	52	24.0	82.0	127.0	8.00	0.2	21.0	67.0
W. Nasab			17	40	21.8	45.0	128.0	4.10	0.38	19.4	42.5
W. Rimthy			26	23	29.8	35.0	74.2	4.30	0.37	27.9	29.0
W. El Ghaieb			14	34	18.0	40.0	110.0	3.30	0.3	16.0	37.0
W. El Genah			13	25	17.2	40.0	77.0	2.80	0.22	15.1	32.5
W. Saal			10.5	27	12.6	35.0	88.0	2.30	0.25	11.5	31.0
W. Abu Khshieb			9.3	16	11.1	30.0	37.0	0.70	0.26	10.2	23.0

Q_p	Peak Discharge (m^3/s)
V	Runoff Volume ($*10^6 m^3$)
Tc	Time of Equilibrium (hr)
T_p	Time to peak (hr)
v	Avarage velocity (m/s)

Table 31 : Results of Hydrographs Parameters for the Main subbasins in Dahab Basin

The expected runoff volume is calculated depending on rainfall excess. At maximum storms, rainfall excess amounts to 40 mm, and the runoff volume ranges from 3.7 Mm^3 at W. Abu Khshieb to 16 Mm^3 at W. Nasab, while at storms of 55mm, rainfall excess reaches 19 mm and the expected runoff volume has a range from 1.6 Mm^3 at W. Abu Khshieb to 8.3 Mm^3 at W. Nasab. The runoff volume ranges from 0.75 to 4.1 Mm^3 at storms of 45 mm where rainfall excess is about 9 mm. It can be observed that the main sub-basins of W. Dahab receive great amounts of runoff resulting from different storm events during rainy seasons.

The average flow velocity ranges from 0.41 to 0.71 m/s during the maximum storm. The high velocities occur in W. Nasab, W. Rimthy, W. Abu Khshieb and W. El Ghaieb, ranging between 0.63 and 0.71 m/s, while low values of average flow velocity occur in W.Saal and W. El Genah, ranging from 0.41 to 0.5 m/s. It can be concluded that high velocities are affected by topographic elevations, high average slope, and length of the basin to outlet as in W. Abu Khshieb and W. Zaghraa Nasab. The values of average velocity decrease especially at the northern part of the study area because of the sedimentary rock cover and the low average slope within basins as in W. El Genah and W. Saal.

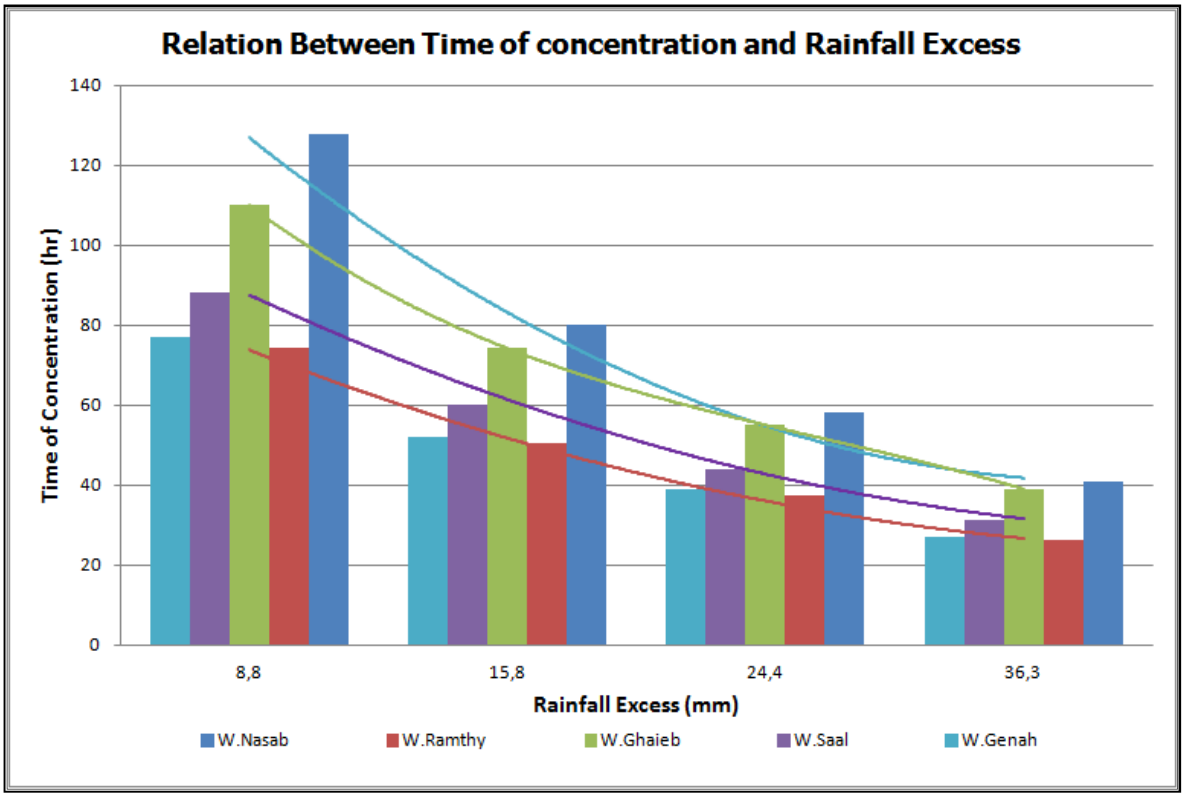

Figure 140 : Variation of Time of Concentration With Rainfall Excess

The time of concentration (t_c) is determined by using the SDUH method. The time defines the maximum time of flow to the outlet of the sub-basin. The result shows that W. Rimthy and W. Abu Khshieb have the shortest time of concentration with 17 and 26 hrs respectively during the maximum storm. The high values of t_c range between 39 and 53 hrs in W. Zaghraa, W. Nasab, W. El Ghaieb and W. Saal. The length of the basin, average velocity and the average slope of the basin are the main

factors influencing the time of concentration. W. Abu Khshieb and W. Rimthy have a short basin length of 19 and 43 km respectively whereas W. Nasab and W. El Ghaieb have long basins of 62 and 55 km respectively. The average flow velocity has a high value in W. Rimthy and in W. Abu Khshieb of 0.7 and 0.63 m/s.

It can be shown from the results that the values of the time of concentration are relatively decreasing with increasing amounts of storm and rainfall excess in all sub-basins of W. Dahab. Table 31 shows that W. Rimthy (t_c) has values from 26.2 hrs at the maximum storm of 76.2 mm and its rainfall excess of 36.3 mm to 74 hrs at a storm of 45mm and its rainfall excess of 8.8mm (fig.140). It can be concluded that when the storm value and the rainfall excess increase, then the time of concentration decrease. This result is confirmed by Saghafian et al. (2008). He stated that there is an inverse relation between time of concentration and rainfall excess.

4.2.5 Data Comparison with other location

Due to destruction of stations during wars and by vandalism, station records are not as complete as desired. A number of stations have been moved to new locations as for Dahab and Sharm El Sheikh stations. The stations were reopened in 1990, but other stations have been abandoned. Due to the difficult operating conditions and limited number of field data, no hydrologic measurements have been carried out in the Dahab basin. The results of two models have been processed by analysis of the data available from the station of Saint Catherine which has been compared with available records from similar basins in the surrounding area as in the Negev area in the northeastern part of Sinai. The calculated main hydrological parameters of peak discharge and volume of runoff are compared with observed parameters in similar basins which have the same climatological and geological conditions.

The southern part of the Negev area has similar geological and geomorphological conditions as the Dahab basin. It is located at the border of the Sinai Peninsula in Egypt. The area is generally devoid of vegetation (Ben Zvi and Shentsis, 2000). Geologically, the southern part of Negev area is covered by three main rock unit outcrops 'Quaternary alluvium, Cretaceous Sandstone and Precambrian rocks'. The area located within an arid region where average precipitation ranges between 20 and 30 mm/year. The runoff events are infrequent and intense and occur from late September to mid May; the number of runoff events reach to one event/year (Ben Zvi and Shentsis, 2000).

The observed peak discharges are collected by Meirovich et al. (1998) from different basins in Sinai and the Negev area within the period from 1980 to 1998. The authors established an envelope curve originating from a relation between peak discharges and appropriate catchment areas (fig.141). The figure shows that the watershed areas between 100 km^2 and 1000 km^2 have a range of peak discharges between 70 and 800 m^3/ sec. These observations depend on the amount of the rainfall intensity which is recorded for different storms.

W. Ramon at Elat Rd and W. Arod at Canyon are located in the south Negev area and they are similar concerning the geological and geomorphological conditions with W. Abu Khshieb and W. Saal in W. Dahab. The maximum observed discharge at W. Ramon at Elat Rd is about 72 m^3/s while it is at W. Abu Khshieb 64 m^3/s and the maximum discharge observed in W. Arod at Canyon is about 90 m^3/s while maximum peak discharge at W. Saal is about 100 m^3/s. It can be concluded that there are similarities between the calculated average maximum peak discharges at sub-basins in W.Dahab and those observed at the southern part of Negev areas.

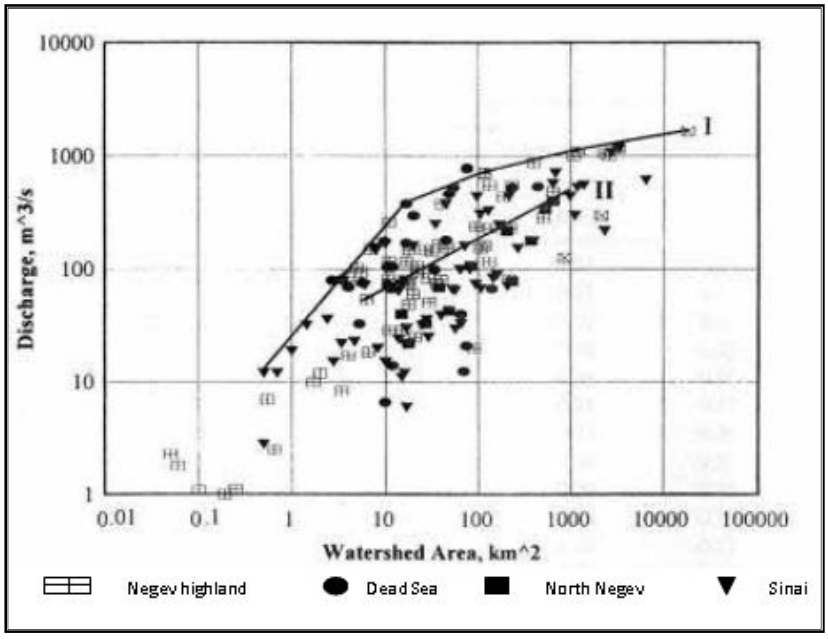

Figure 141 : Maximum Observed Discharges Versus Watershed Area According to (Ben Zvi & Shentsis, 2000)

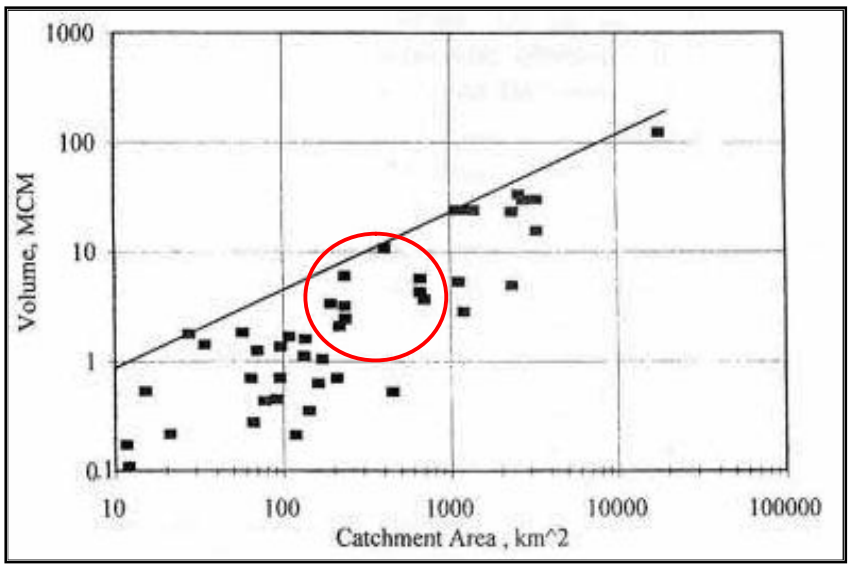

Figure 142 : Maximum Observed Runoff Volumes Versus Watershed Area After (Ben Zvi & Shentsis, 2000)

Meirovich et al. (1998) estimated a relation between the maximum observed runoff volume and the area of watershed within Sinai and Negev (fig. 142). This kind of relation follows the same logic as that for maximum observed discharges. The fit line is decided depending on statistical analysis of values at high events. The curve for entire Negev can be described by:

$$V_m = 0.17 * A^{0.71} \qquad \textbf{Equation (54)}$$

V_m is the maximum observed volume of event (10^6 m^3) and A is the catchment area (km^2)

It is noted that there is a convergence in the results between the caluclated volume of the maximum runoff in sub-basins in W. dahab and the maximum volume from the previous equation. The calculated volumes of maximum storm values in sub-basins of W. Dahab range between 16 million m^3 at W.Nasab and 3.7 million m^3 at W. Abu Khshieb. On the other hand, values from the previous relation range between 13 million m^3 at W. Nasab and 4.2 million m^3 at W. Abu khshieb as shown in table 31.

Basin Name	Maximum volume by relation ($10^6 m^3$) Meirovich et al., 1998	Calculated Maximum volume ($10^6 m^3$)
Wadi Nasab	*13*	*16*
Wadi Ramthy	*12.2*	*15*
Wadi Saal	*8.4*	*9.9*
Wadi El Ghaieb	*9.7*	*12*
Wadi Genah	*9.4*	*11.2*
Wadi Abu Khshieb	*4.2*	*3.7*

Table 32 : Comparison Between Calculated Runoff Volume and Calculated Runoff Volume by Equation's Meirovich et al., 1998

4.2.6 Integrated hydrologic parameter

Basins of high peak discharge, short time to peak and high runoff volume are considered risky basins. The shape of the hydrograph reflects the size of the basin and the rate of discharge that flows out of the basin in addition to the parameters which governs the risk rank of the basin.

The calculated hydrograph parameters reflect runoff conditions across the drainage of Dahab basin. The integrated hazard map (see fig. 143) is used to define high risk areas based on runoff parameters as peak discharge, time to peak and volume of runoff. The map is categorized in four classes. Each parameter is classified into four classes based on the statistical parameters as mean and standard deviation for each parameter. The statistical calculation is used because of the high

difference between the maximum and minimum values, like the peak discharge range of 64 to 560 m^3/s (Table 33). To generate a final runoff risk map, different scores on a scale according to the importance of the parameters were assigned. An overlay operation will evaluate the intersected regions by a sum of the scores, so that each sub-basin is characterized by a one score measure. The result is scored on a 1 to 4 scale in ascending order of risk significance. Red color is assigned to areas with the highest values, whereas pale green is assigned to the lowest ones. The hydrologic parameters corresponding to hazard zonation are shown in table 33.

Hydrological Parameters	Statistical Parameters	Values	Ranges	Score
Maximum Volume (Mm^3)	Maximum	64 Mm^3	3.7 – 13.1 Mm^3	1
	Minimum	3.7 Mm^3	13.2 - 30.03 Mm^3	2
	Mean	22 Mm^3	30.04 - 46.09 Mm^3	3
	Standard deviation	18 Mm^3	46.1 - 64 Mm^3	4
Peak Discharge (m^3/s)	Maximum	560 m^3/s	64 - 129.15 m^3/s	1
	Minimum	64 m^3/s	129.16 - 273.95 m^3/s	2
	Mean	200 m^3/s	273.96 - 418.75 m^3/s	3
	Standard deviation	140 m^3/s	418.76 - 560 m^3/s	4
Time to peak (hr)	Maximum	27 hr	12 - 14.53 hr	4
	Minimum	12 hr	14.54 - 19.32 hr	3
	Mean	22 hr	19.33 - 24.11 hr	2
	Standard deviation	4.8 hr	24.12 - 27 hr	1

Table 33 : Hydrological Paramters for the design of Runoff Risk Map in Dahab Basin

The integrated hazard map shows that W. Rimthy tends to be a high risk sub-basin in W. Zaghraa due to the moderate average peak discharge of 200 m^3/s, short time to peak of 18 hrs and moderate runoff volume of 16 Mm^3 in a maximum storm (fig. 145). W. Nasab is considered a moderate risk basin due to a moderate average peak discharge of 130 m^3/s, moderate volume amount of runoff of 16.8 Mm^3 and relative long time to peak range of about 26 hrs at maximum storm. W. Saal is considered a moderate risk sub-basin because it has a relatively low value of average peak discharge, moderate to low time to peak of about 18 hrs and low runoff volume of about 9.8 Mm^3 at a maximum storm. W. El Genah has the lowest risk level because it has a value of low average peak discharge 110

m^3/s, relative long time to peak of about 23 hrs and relative low volume of runoff of about 11.3 Mm^3 at a maximum storm (76.2mm).

It can be concluded that W. Zaghraa is the highest risk main sub-basin in W. Dahab, with the highest volume of about 64 Mm^3, a high peak discharge of about 556 m^3/s and a long average time to peak of about 27 hr. Although W. Abu Khshieb is the lowest main sub-basin in Dahab basin, it is considered a moderate risk sub-basin because it has a relative moderate value of peak discharge, low time to peak of 12 hrs and a low runoff volume at maximum storm of about 3.7 Mm^3. W. El Ghaieb sub-basin is considered a low risk basin due to its moderate peak discharge of 119 m^3/s at high storms and the relative long duration to peak of about 20 hrs (high storm) with moderate to low volume of about 12 Mm^3 (fig. 143).

The results show that W. Zaghraa Nasab sub-basin has higher risks than W. Zaghraa Saal sub-basin. The sedimentary rock cover, relatively low slope value and lowest average velocity are the main factors decreasing the runoff risk in the northern part of the basin, compared with wadis in the southern part of Dahab basin. According to previous conclusion, the northern area has good conditions for groundwater occurrence at W. El Genah, W. Saal and Northern part of W. El Ghaieb. The southern catchment of W. Zaghraa is the main cause of high runoff risk at W. Rimthy and W. Nasab. The basement cover, relative high average slope and high average velocity are the main conditions for increasing the runoff risk, especially at the outlet of sub-basins near the main road to Dahab city (fig. 143).

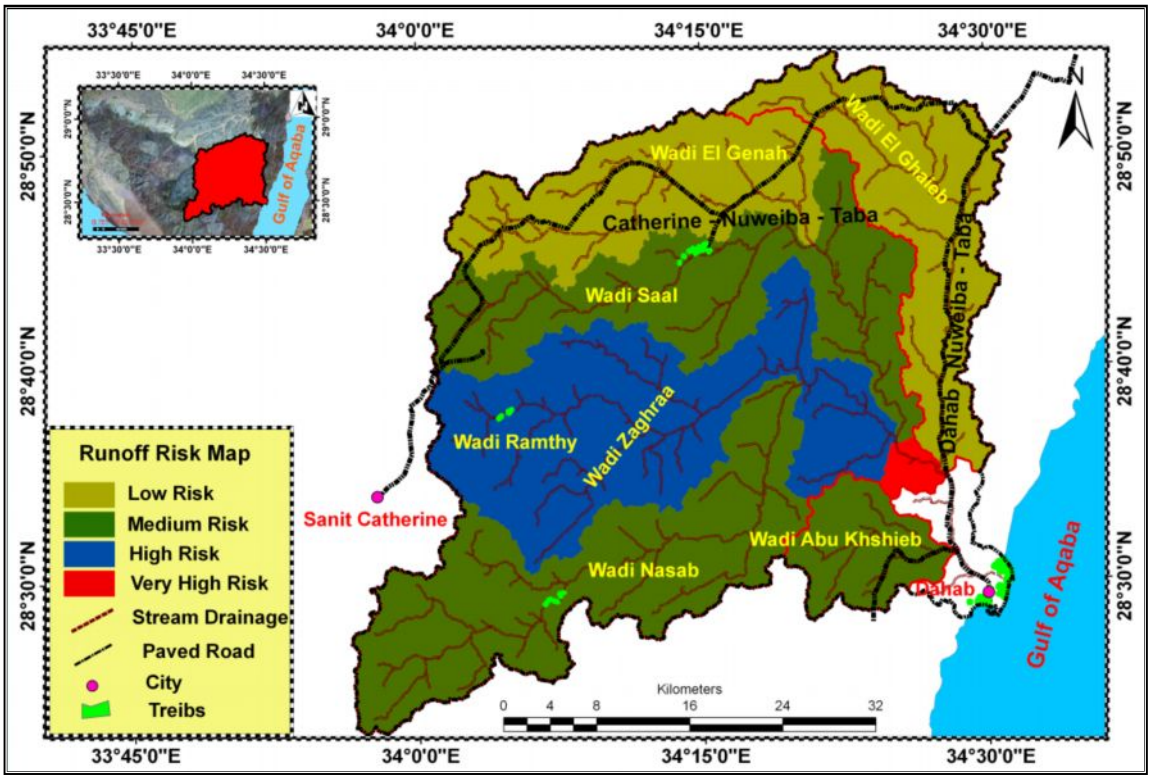

Figure 143 : Integrated Runoff Risk Map Depending on Hydrologic Parameters

Housing communities and the main roads are plotted on the maps and show good correlation with the distribution of flood hazard values. The contact sites between outlets of high and moderate risk sub-basins and the Dahab – Nuweiba road are considered dangerous locations. These sites can be damaged by tremendous storms, especially at the outlet of W. Zaghraa and W. Abu Khshieb. Many of the houses are located on the main streams of high and moderate risk sub-basins as in W. Nasab, W. Saal and W. Rimthy. Generally, high and moderate risk areas should be protected against runoff risk, especially in areas related to residential communities and major roads as in W. Nasab, W. Rimthy, Saal and W. Zaghraa, while the areas of low risk have a high possibility for groundwater recharge as in W. El Genah and the northern part of W. El Ghaieb.

For verification purposes, past flood damage locations in W. Dahab are correlated with a hazard map. Last damage occured in a storm on 1/10/2012 which was monitored by witnesses living in the area. Heavy rain and floods blocked the main highways leading to Nuweiba and Sanit Catherine and Wadi El-Nasb dam and several nearby houses were destroyed by heavy flood waters. The floods have also led to power cuts. (http://english.ahram.org.eg/NewsContent/1/2/54440/Egypt/Society/Alert-Floods-block-roads-to-Sinais-Nuweiba,-St-Cat.aspx).

CHAPTER V

WATER MANAGEMENT

Chapter V

Water Management

Water management and flood risks are important issues in Wadi hydrology. The relationship between water management and its impacts on the environment is also of special concern. The selection of suitable water management alternatives needs a detailed analysis for all factors involved. These factors include the political, environmental, ecological, hydrological, and socio-economical attributes. The damage effect is one of the negative impacts of Wadi flooding, which includes destruction of infra-structure such as buildings, roads, transportation and communication facilities in addition to erosion of cultivated lands. The effect may also cause the dangering of the nation's socio-economic condition (Farid and Allam, 1996).

The present chapter is divided into two parts: the first one discusses the protection techniques applied against runoff in Dahab basin. Surface water which generates from runoff events in southern Sinai highly threats people's lives, their lands, and their livestock. The evaluation of the present situation of flood management in Dahab is an important step to investigate surface water management. This evaluation tells us how to develop the system aiming to protect people and their infrastructure against flood events.

The second part deals with the possibility of locating new wells to overcome the shortage in water needs of the local inhabitants. This will be achieved based on several factors estimated in previous chapters such as lithology, structure, stream density, topography and slope. The proposed wells are located within basement and alluvial aquifers. The final map of the new locations will help people to select the best sites to find groundwater.

5.1 Surface water management

Flood risk management, in a narrow sense, is the process of managing an existing flood risk situation. In a wider sense, it includes the planning of a system, which will reduce the flood risk that is a flood protection system to prevent flood disaster and to minimize its impacts.

Floods can be handled in two ways, structural and non-structural. A structural solution looks towards measures such as dams, culverts and retaining walls. Non-structural measures depend upon social welfare and human development. Social welfare comes through governmental subsides or insurance programs, while human development is usually built upon public training and awareness systems.

5.1.1 Evaluation of existing dams

The Water Resources Research Institute (WRRI-Egypt) has developed a protection project of the southeastern Sinai regions. This project includes protection of the main roads against flooding hazards

at W. Dahab and W. Watir which are known as to be hydrologically active and have steep topographic features.

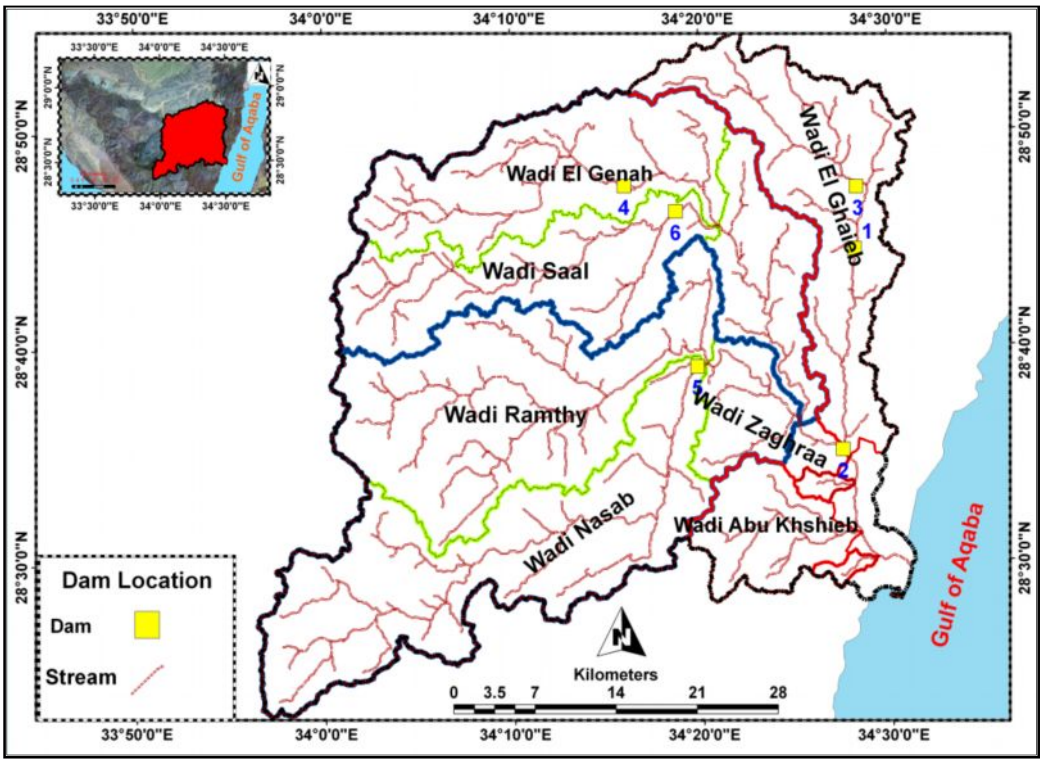

Figure 144: Dam Locations in W. Dahab Basin

Six dams (protection dams) are constructed by the WRRI in the study area (fig.144). An analysis using GIS bases on the available data, besides field surveying, is carried out to estimate the storage capacity of these dams in order to determine their efficiency for runoff harvesting and to come up with some suggestions for better water management within the study area. Therefore, the Institute has completed a number of works for protection of the downstream part of W. Dahab along W. El Ghaieb, especially at Saint Catherine-Dahab road, and at the downstream of W. Saal, W. Nasab and W. El Genah. The constructed dams are investigated through the field survey in the area of study. All the sites are located precisely by GPS measurements. Surveying work took place using measuring taps for defining heights and widths of dams. The measurements have been evaluated through the internal reports of WRRI (2006) (Table.34).

Retention dams that have been constructed in W. El Ghaieb and W. El Genah are sited in valleys based on their natural geomorphological and topographical nature, in addition to being of low hydrological energy (figs. 145 &146). Obstacle barriers are constructed in order to block the passages of flood water to decrease surface water velocity and increase the time needed for joining water coming from other run off paths. Therefore, two sites of obstacle barriers have been constructed in both W. El Ghaieb (dams 3 and 1) and W. El Genah (4).

Dam No.	Name	Lat.	Long.	Height (m)	Length (m)
1	Up W. El Ghaieb	28^0 44\ 30\\	34^0 28\ 17\\	6	180
2	Down W. El Ghaieb	28^0 35\ 14\\	34^0 27\ 30\\	5.2	300
3	W. El Gieby	28^0 47\ 24\\	34^0 28\ 25\\	6	600
4	W.Genah	28^0 47\ 30\\	34^0 16\ 06\\	6	220
5	W. Nasab	28^0 39\ 00\\	34^0 19\ 48\\	5	170
6	W.Saal	28^0 46\ 14.5\\	34^0 18\ 44\\	6	135

Table 34: Dams Specifications of Dahab Basin

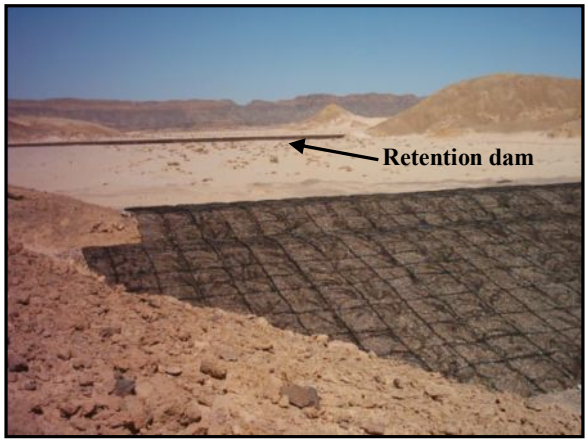

Figure 145: Retention dam of Dam No. 4

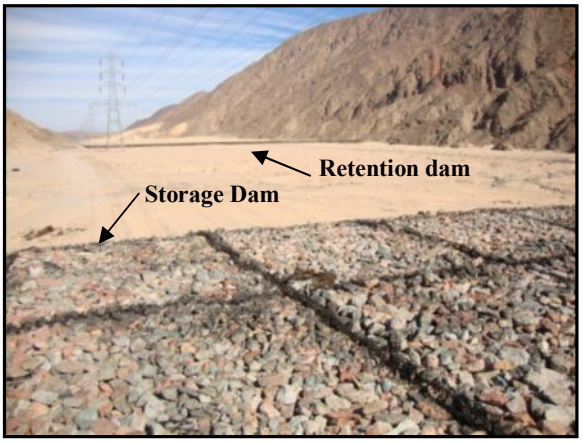

Figure 146 : Retention dam of Dam No. 3

Storage reservoirs are established in front of protective dams as in dam 2 at W. El Ghaieb and dam 6 at the downstream of W. Saal (fig. 147). These constructions aim to collect sufficient amount of surface runoff (about 250 m^3 each) before reaching the protective dams. These reservoirs consist of three components including **impluvium,** which represent an inclined paved runoff way, the **settling basin,** which allowed sedimentation of runoff loads and the **storage compartment,** which consists of a hole dug in the ground coated with concrete that leads to a large size tank (figs 147&148).

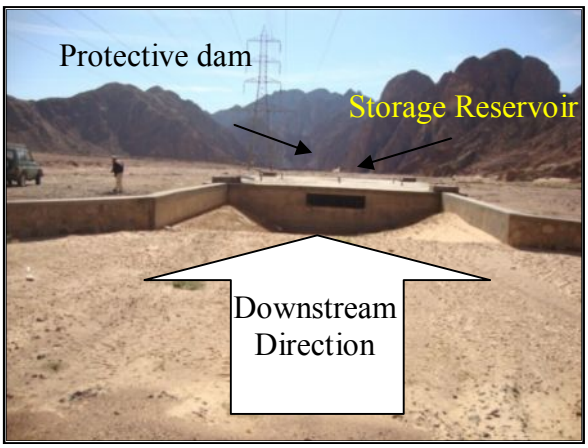

Figure 147: Storage reservoir at W. El Ghaieb

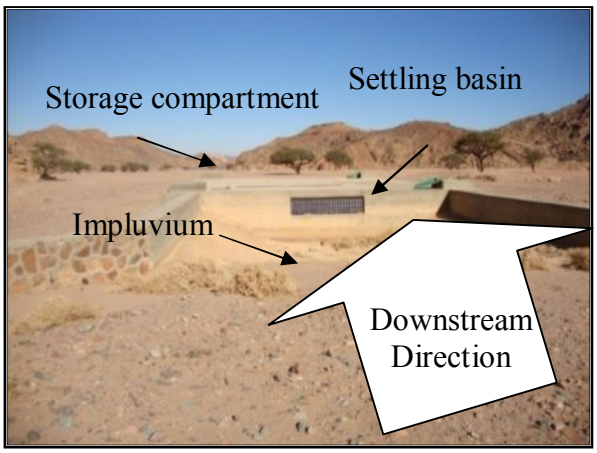

Figure 148: Storage reservoir at W. Saal

To get the storage capacity of the constructed dams in the study area, topographic maps of scale 1:50,000 are used to digitize ground elevation above sea level and the top surfaces of the dams (fig. 149). The digitized contour lines, point elevation data and streams are used to create an interpolated surface (elevation model) with 15 m resolution using Topo to Raster tool. This tool is used to create a raster surface dataset for the area in front of the constructed dam by interpolation of elevation values from contour data and digitized elevation points. The natural area contains high land and low land (sink) which results from the drainage pattern. The sink (low land) area will be neglected by the interpolation method in this tool; therefore, the stream line should be added as input data to produce an accepted raster surface. So the corrected data from contour lines and stream network should be digitized accurately from topographic maps. For more reading about this tool see the website below. (http://webhelp.esri.com/arcgisdesktop/9.2/index.cfm?TopicName=Hydrologically_correct_surfaces%3A_Topo_to_Raster).

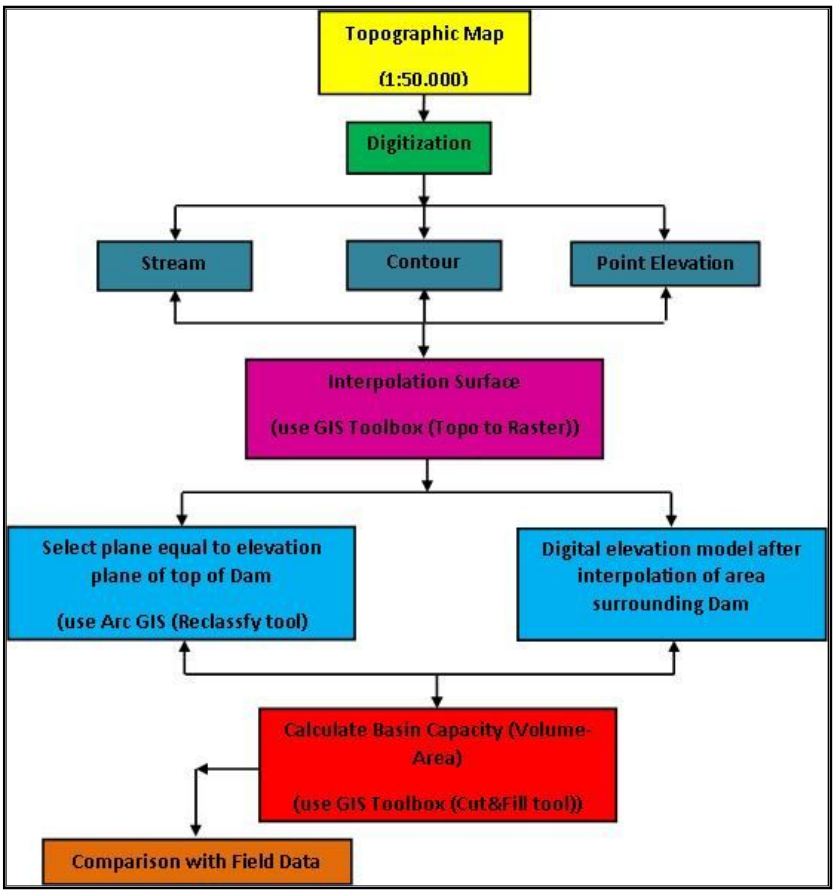

Figure 149: Chart of Methodology for Measuring Storage Capacity of Dams using GIS

The volume and area of storage space in front of a dam is calculated using "Cut and Fill tool" in GIS software. The "Cut and Fill tool" is used to calculate the volumes and surface areas (area in front of the dam) to be filled to the level of dam height and areas to be removed (rest of the ground level) (fig. 150). The tool is used to produce a raster for areas where surfaces are removed or added by the action of weathering. The resulted raster is accompanied by calculated volume and area of each of the

surfaces listed in the attribute table. In the attribute table, in areas where surface is removed, the volume value is positive. In areas where surface is built with sediment, the volume is negative.

In our case study, it is suggested that the surface of the maximum elevation of the dam (Raster before weathering) is removed by weathering effects which are caused by the existing surface in front of the dam (Raster after weathering) (fig.150). The volume is calculated for each cell in raster data according to following equation:

Volume of the removed area = (Cell Area) . ($Z_{before} - Z_{after}$)

Z_{before}:- Elevation in cell at maximum elevation surface of dam (suggested before weathering)- (Raster data)

$Z_{after:-}$ Elevation in cell at DEM was created by Topo to raster tool (suggested after weathering) – (Raster data)

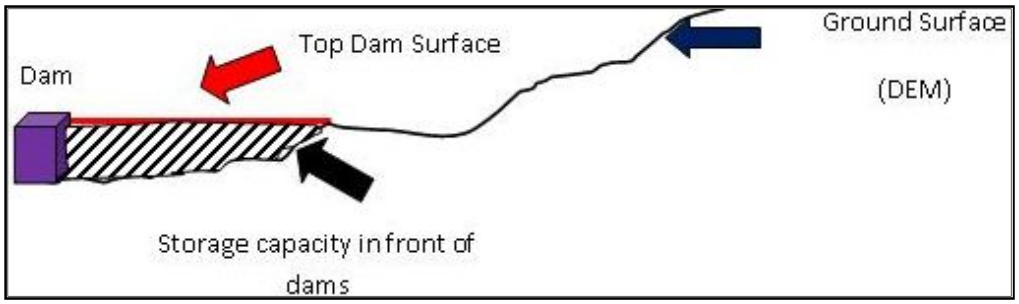

Figure 150: The Main concept for Cut and Fill Tool working for calculating Storage Capacity of Dams using GIS

The storage capacity of the existing dams ranges between 70000 and 800000 m^3 (Table 35). The highest volume is recorded for the dam at the upper part of W. El Ghaieb. It has a storage capacity of about 800×10^3 m^3. The lowest volume is recorded for the dams downstream of W. Saal and W. Nasab which range from 70 to 90 $\times$ 10^3 m^3. The result shows that the highest storage capacity is recorded for the dam that protects the Saint Catherine – Dahab road. The dam locations are focused on the downstream portion without applying any protection or retardation tools for the oncoming runoff from the upstream area. It can be noticed from the obtained data and field survey that the main purpose of these dams is for protection of the main road using additional cisterns as local reservoirs of runoff water with limited capacity.

5.1.2 Specifications of the existing major protective dams

5.1.2.1 Dam 1

This dam lays at W. El Ghaieb sub-basin next to Saint Catherine- Dahab road at a distance of about 1 km away from the road and is located at the middle of W. El Ghaieb near the economic area at a distance of about 0.5 km. It is surrounded by a number of hills of basement rocks. It is a moderatly high dam reaching 6 m in height and 180 m in width. This dam is designed with a suitable slope from the front side, while the back side is built with a number of steps to protect the dam's body

against disintegration (fig. 151). The storage basin in front of the dam has a capacity of 151 $\times 10^3$ m^3 with an area of about 55 $\times$ 10^3 m^2. The dam has another obstacle dam of 2 m in height, 200 m in width and the distance between the obstacle dam and the protective dam is 200 m .

Dam No.	Name	Dam Height (m)	Dam Width (m)	Storage Capacity (*10^3 m^3)	Area of Basin (*$10^3 m^2$)
1	Upper W. El Ghaieb	6	180	151	55
3	W. El Gieby	6	550	800	250
2	Lower W. El Ghaieb	5.2	250	240	50
5	Lower W.NASAB	5	170	90	58
4	W. El Genah	6	200	220	90
6	W.Saal	6	150	70	30

Table 35: Specification of Constructed Dams in Dahab basin

5.1.2.2 Dam 2

It lays down to Dam 1 at the junction of W. Zaghraa with W. El Ghaieb, near the road Saint Catherine – Dahab and is located 0.5 km away from the road. The dam is designed with a number of steps at both sides. It has a lower height than of dam 1 at 5.2 m high with 250 m in width and has a storage capacity of about 240 $\times 10^3$ m^3. A cistern is located 300 m from the upstream side with a capacity of about 450 m^3. The dam is surrounded by heights of basement rocks (fig.152).

Figure 151: Protective Dam 1 at W. El Ghaieb Figure 152: Protective Dam 2 at W. El Ghaieb

5.1.2.3 Dam 3

Dam 3 lays at the junction of W. El Geeby with W. El Ghaieb. It is located at the northern part of W. El Ghaieb 1 km away from the road. It is designed with the same specifications as dam 1 which is a moderately high dam with a height of 6m and a width of 550 m. The storage capacity of this dam is about 800 $\times 10^3$ m^3 and it covers an area of 250 $\times 10^3$ m^2. There is an obstacle dam located 200 m

upstream of the dam with 2 m built up by gabions. The dam is surrounded by several hills made of basement rocks (fig.153).

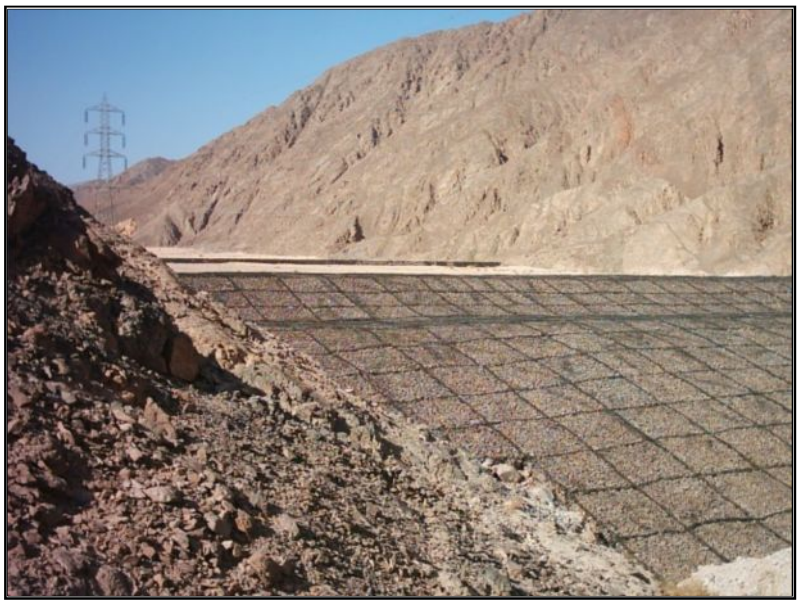

Figure 153: Protective Dam 3 at W. El Ghaieb

5.1.2.4 Dam 4

The dam lays downstream of W. Genah near the road of Saint Catherine – Dahab. It is designed with the same specifications as dam 1. The height of the dam reaches up to 5m, with a width of 200 m and a storage capacity of about 220 $\times 10^3$ m^3 and has an area of 90 $\times 10^3$ m^2. Its obstacle dam is located 200 m toward the upstream side from Dam 4 with a height of 2m. The dam is surrounded by lower cretaceous rocks (fig. 154).

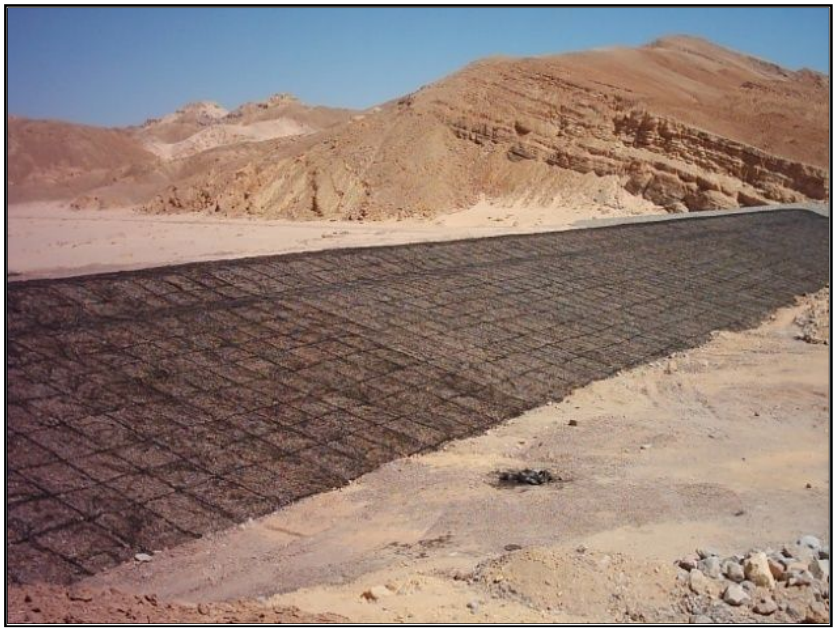

Figure 154: Protective Dam 4 at W. El Genah

5.1.2.5 Dam 5

The dam is located downstream of W. Nasab at the connection with W. Zaghraa. It is built up with gabions. The height of dam reaches to 6 m, its width is 170 m with a storage capacity about 90 ×103 m3 and its area is 58 ×103 m2. The dam is surrounded by hilly surfaces from basement rocks.

5.1.2.6 Dam (6)

This dam lays downstream of W. Saal. It is designed with the same specifications as dam 1. The height of the dam reaches up to 6m, its width is 150 m with a storage capacity of about 70 $\times 10^3 m^3$ and an area of 300 $\times 10^3 m^2$. The storage reservoir is located 200 m upstream of the dam with a storage capacity of 250m^3. The dam is surrounded by several hills of basement and Paleozoic rocks. The dam is designed with slopes at both sides. Mud accumulations are recorded at the front side slope of the dam revealing damming of previous flooding (fig. 155).

Figure 155 : Protective Dam (6) at W. El Saal

5.1.3 Factors affecting surface water management

Some morphologic, meteorological and hydrogeological analyses are required in order to suggest measures for the utilization of possible sources of water and hence, for augmentation, the precious groundwater in the study area and avoiding the catastrophic flooding behavior that causes environmental hazards. Some factors are required to make a water balance as discussed herein below.

5.1.3.1 Climatic conditions and rainfall analysis

The meteorological data indicates that the study area is characterized by low avarge rainfall, high temperature and high evaporation in summer seasons to mild dominated rain storms, low temperature and evaporation rates in winter seasons. The average maximum temperature varies between30 and 36

^{o}C in summer and from 0 to 5 ^{o}C during storm or rainy seasons. A typical rainfall event can be characterized by thunderstorms with heavy showers and short duration.

Annual precipitation on the study area reaches up to about 35 mm in W. Dahab basin as revealed from the constructed isohyetal map of the study area. The maximum recorded rainfall reaches up to 76.2 mm in November 1937 at Saint Catherine station which is equivalent to 33 million cubic meters/ rainy storm in W. Nasab basin, about 32 million cubic meters/storm in W. Ramthy basin and about 18 million cubic meters/storm in W. Saal basin. The maximum rainfall storm must be considered in flood management planning.

The average potential evaporation (PE) in rainy seasons varies between 5.8 and 16.2 mm/day during January to March and from October to December (see chapter 4). The selected average evaporation value is related to a maxiumum storm of about 6.9 mm/day in November. W. Zaghraa is subjected to water losses by evaporation of about 9 million cubic meters in a rainy storm that represents 7 % of the total maximum rainfall amount. The losses of W. Rimthy basin are of about 2.8 million cubic meters, W. Nasab basin is of 2.6 million cubic metesr in a rainy storm representing 7.8% of the total maximum storm quantity, W. Saal is of 1.3 million cubic meters in a maximum rainy storm representing 7% of the total rainy storm quantity and W. Abu Khshieb is about 0.6 million cubic meters in a rainy storm about 7.4% of the total rainy storm quantity.

5.1.3.2 Runoff volume

Hydrograph calculations and morphometeric analysis point to risky basins where flash floods result from heavy rainfall in short durations. Geriesh (1998) stated that floods in Southern Sinai could be produced by a rainstorm exceeding 10mm in depth. This depth does not refer to time peroid. According to our study area, the minimum storm amount of 35 mm/day should produce runoff floods. This rainfall intensity might happen once per 8 years (fig.131- see chapter 4), while the maximum storm record of 76.2 mm/day may be repeated each 180 years or more with probability of occurrences less than 1% each year.

Maximum rainstorms lead to produce large volume quantities of runoff, which in turn could affect the study area. The maximum runoff volumes are different in the main risky sub-basins in the study area. The maximum volume is 3.7 Mm^3 at W. Abu Khshieb while it reaches 64 Mm^3 in W. Zaghraa. The maximum runoff volume at the high risk W. Rimthy sub-basin reaches 16 Mm^3 whilst at moderat risk sub-basins W.Nasab and W. Saal, the volume is 16.8 and 9.9 Mm^3 respectively. Runoff quantities decrease at storm events of 45mm/day. It amounts to 18 Mm^3 in W. Zaghraa basin and at W. Abu Khshieb it is 0.7 Mm^3. In W. Rimthy basin, the minimum quantity of runoff is 4.3 Mm^3 while it is 4 Mm^3 at W. Nasab basin.

5.1.3.3 Mean groundwater recharge

The top soil layer and the unsaturated zones are dry during the non storm period which cause large amounts of rainfall absorption through them during storm periods that consequently increase groundwater storage. The hydraulic conductivity (K) is measured in the field along the main stream in alluvial deposits at each sub-basin and the same parameter is estimated in fractured basement rocks at some locations of W. Nasab. The estimated avarage hydraulic conductivity of basement rock is 1.6 mm/hr which is used for calculation of groundwater recharge. The maximum infiltration, from which the aquifers and the soil zone are recharged, is about 50.5% in W. Zaghraa and about 50 % at each Rimthy sub-basin, W. Nasab and W. Saal. It reaches 49% at W. El Genah and W. El Ghaieb.

The geological, geomorpholgical and hydrogeological investigations in the study area confirm that W. El Ghaieb and W. El Genah basin areas have the lowest rank of flooding risk owing to their gentle gradient ranging from 14 to 18.8 m/km along the main streams, the low elevations of the catchment areas ranging from 500 to 660 m, and the sedimentary cover of the northern part of Dahab basin. The obtained results confirm that the constructed dams (WRRI, 2006) in these basins do not aim to manage the flood water but have been constructed to protect the main road of Saint Catherine – Dahab and Nuweibae-Dahab .

W. Rimthy, W. Nasab and W. Saal sub-basin of W. Zaghraa basin and W. Abu Khshieb are ranked as moderate to high risk basins, owing to their high elevation of basement terrain at the catchment areas as at G. Saint Catherine and G. Shiekh Al Arab of Nasab sub-basin, G. Um Louz, G. Hamami and G.Um Alawi of Rimthy sub-basin, and G. Ferani G. Abu Khshieb of Abu Khshieb sub-basin. Also, the gradient of the main stream in W. Rimthy sub-basin reaches 25 m/km and in W. Nasab gradient reaches 24 m/km in the upstream area and decreases to 15 m/km in the downstream area. Gradient values are 22 m/km in W. Saal basin and W. Abu Khshieb. About 80% of these basins are covered with basement rocks which have very low conductivity; in addition to the low hydraulic conductivity values of soils at W. Nasab, W.Rimthy and W.Saal basins range from 0.15 to 8.7 m/day.

It should be mentioned that there are no management plans of flood water protection at W. Rimthy and W. Abu Khshieb. Moreover, only two dams have been constructed in the downstream area of W. Nasab and W. Saal. The studies confirm that these constructions are not sufficient to protect the area against runoff and one of them was damaged during the last storm (October 2012). Therefore, the flood control system should be applied to protect the study area and to use the flood water in recharging and augmenting the groundwater resources.

5.1.4 Delineating areas of possibly high flooding risk

Runoff processes are expected to affect the load of water in streams, although possibly in different ways due to different flow paths. The identification of potential runoff-contributing areas in a basin can provide guidance for the targeting of best management practices to reduce runoff (Kyle, 2000). In

order to demarcate sites with the highest potential for flood risk on road networks, as well as those that may be used for recharging groundwater, a DEM-based Wetness index (WI) and relative stream power (RSP) index are derived. These indices are assumed to affect soil characteristics, distribution and abundance of soil water, susceptibility of landscapes to erosion by water, and the distribution and abundance of flora and fauna (Moore et al., 1991; Wilson and Gallant, 2000).

5.1.4.1 Wetness Index (WI)

The wetness index (WI) is a function of the natural logarithm of the ratio of the local upslope contributing area and the slope. The index describes the tendancy for a site to be saturated. The wetness index has been used to study spatial scale effects on hydrological processes (Sivapalan et al., 1987; Beven et al., 1988; Famiglietti and Wood, 1991) and to identify hydrological flow paths for geochemical modeling (Robison et al., 1999). The wetness index is used to identify potential zones of saturation at the base of concave slopes (a decrease in the slope) (Moore et al., 1991). A simple threshold technique is used on the wetness index to map topographic depressions and the areas of potential groundwater discharge. Bevan & Kirkby (1979) proposed that a wetness index map could be made using the formula:

$$\text{Wetness index} = \ln \frac{A_S}{\tan \beta} \qquad \textbf{Equation (55)}$$

Where A_S is the contributing catchment area in m^2 (in a DEM the number of upstream elements multiplied by their area) and β is the slope measured in degrees.

Wetness Index is considered as a raster which DEM uses to produce it. It serves to identify areas which are relatively flat, and where locations of saturation-excess of overland flow would occur. Generally, long, flat areas of land or areas at the bottom of valleys with a flat slope may contribute to high wetness indices. According to the previous concept, it can be concluded that the higher the value of wetness index, the higher the possibility of a land unit remaining wet after a flood. This is one possible measure that can be recommended in order to recharge groundwater. The locations of high wetness index may help to suggested dam locations to increase groundwater recharge.

The results show that the high index values increase at the downstream of basins while the index at the upstream part is low.The high value of the wetness index is found in W. Nasab sub-basin, in the downstream area of W. Rasies, Abu Khashab, W. Nabaa, W. Meer, W. El Shalal, and W. Nasab. The value increases in these locations ranging from 13.5 to 19, while the index is low at upstream parts ranging from 0 - 4 (fig. 156-A).

At W. Rimthy, the wetness value increases downstream of W. Rakita, W. Mekafa, W. Merkh, W. Um Saial, W. Um Retm, W. Sanad, W. Maaran and downstream of W. Rimthy. The value of the index in these wadis ranges between 13.5 and 19. The results indicate that there are similarities of index values at both wadis Nasab and Rimthy due to geological and topographical conditions. In W.

Saal, downstream of W. Saal El Atshaan, W. Mwyilha, W. Mytorah, W. Tyniah and downstream of W. Saal there are high index values (fig. 155-C), as well as at W. Um Shawky, W. Um Harq, W. Um Ataqa, W. Maeen and W. Abu Khshieeb (fig. 156-D).

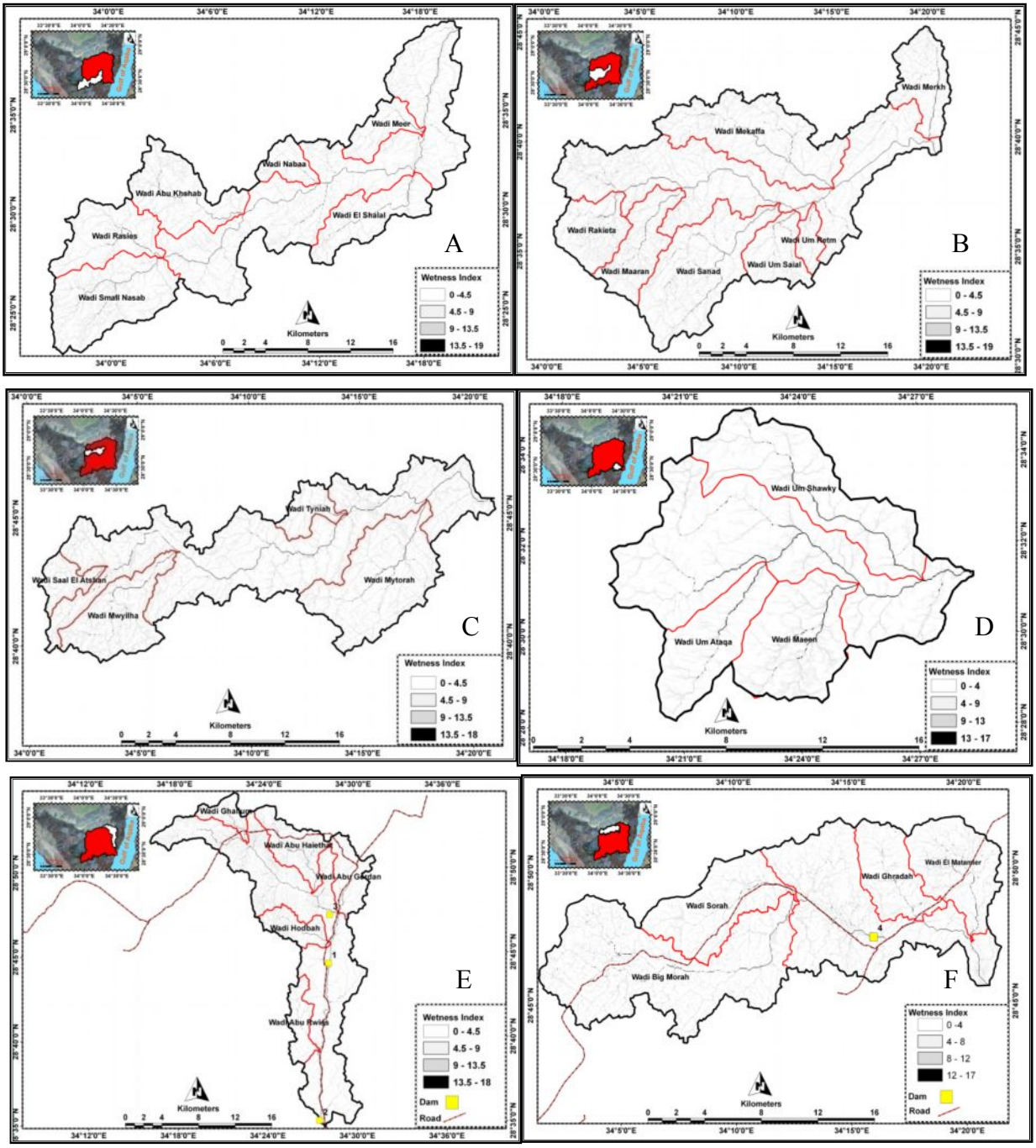

Figure 156: Wetness Index distribution in subbasins of W. Dahab

A large area with high WI value is recorded at W. Genah. It is located downstream of W. Sorah, W. Morah (main), W. Matamier, W. Ghoradah and downstream of W. Genah. These basins have wide wet areas with gentle slopes (fig.156-F). At W. El Ghaieb, the high value of WI increases at the upstream area, especially at W. Ghalium, W. Bathier, W. Abu Haiethat, W. El Marwah and W. Abu

Gerdan. High wetness index values are found along the main stream of W. Hodbah, W. Abu Rwies and at the downstream of W. Ghaieb ranging between 13.5 and 18 (fig.156-E).

The comparison between calculates WI values and sites of the existing dams proves the validity of wetness index calculation. It is observed that the sites of constructed dams are well matched with the high wetness index values. Dams No. 1, 2 and 3 at W. El Ghaieb sub-basin are built in the downstream area of W. South Um Mertha and W. El Ghaieb where dam No. 3 is built to protect the main road, while in W. Genah sub-basin, dam No. 4 is sited at the downstream of W. El Morah to protect Saint Catherine – Dahab road (fig.156-E&F).

5.1.4.2 Relative Stream Power Index (RSP)

The Relative Stream Power Index (RSP) is the time rate of energy expenditure and has been used extensively in studies of erosion, sediment transport and geomorphology as a measure of potential erosive power of the overland flows (Moore et al., 1991). It is usually computed as:

$$RSP = A_s * \tan \beta \qquad \textbf{Equation (56)}$$

Where As: is the specific catchment area β: is the slope in degrees.

The Relative stream power index is calculated as a raster using DEM to identify highly erosive power areas depending on slope (degree) and flow accumulation. Relative stream power predictes net erosion in areas of profile convexity and net deposition in area of profile concavity. As the gradient of a specific catchment area increases, the amount of water contributed by the upslope areas and the velocity of the water flow increase, hence, stream power index and erosion risk increase too.

The areas with high relative stream power values and high wetness index values are those at the down slope of the valley. These have high specific catchment areas and low slopes, making both of the parameters high. The potential for erosion and surface runoff are both quite high at the down slope of these valleys. The areas along the valley slopes have high RSP but low WI since their slopes are somewhat high.In order to reduce the sediment loss, it is optimum to put a dam along the slope, since the low wetness index results in some absorption of water along the slope, reducing the strength requirement for the dam, since it needs to retain less water flow. At halfway down the slope, though, it catches all the sediment eroded from the slope (indicated by high RSP values).

The stream power index mainly coincides with the area which has a high value of slope (i.e. steep slope). The amount of erosion increases relatively with increasing slope value, so the stream power index should increase as well. At W. Nasab, the stream power index value of the upstream of W. Rasies, W. Abu Khshab, W. Ferani, W. El Shalal and W. Nabaa sub-basins range between 12 and 16.6. These localities have steep slopes ranging from 44 to 65 degree. The SP index has a high value at W. Mekaffa, W. Rakietta, W. Maaran and W. Sanad sub-basins of W. Rimthy basin where it ranges

between 12 and 15.5. These areas have high erosive power due to their steep slope at the upstreams of these sub-basins (fig. 157-A&B).

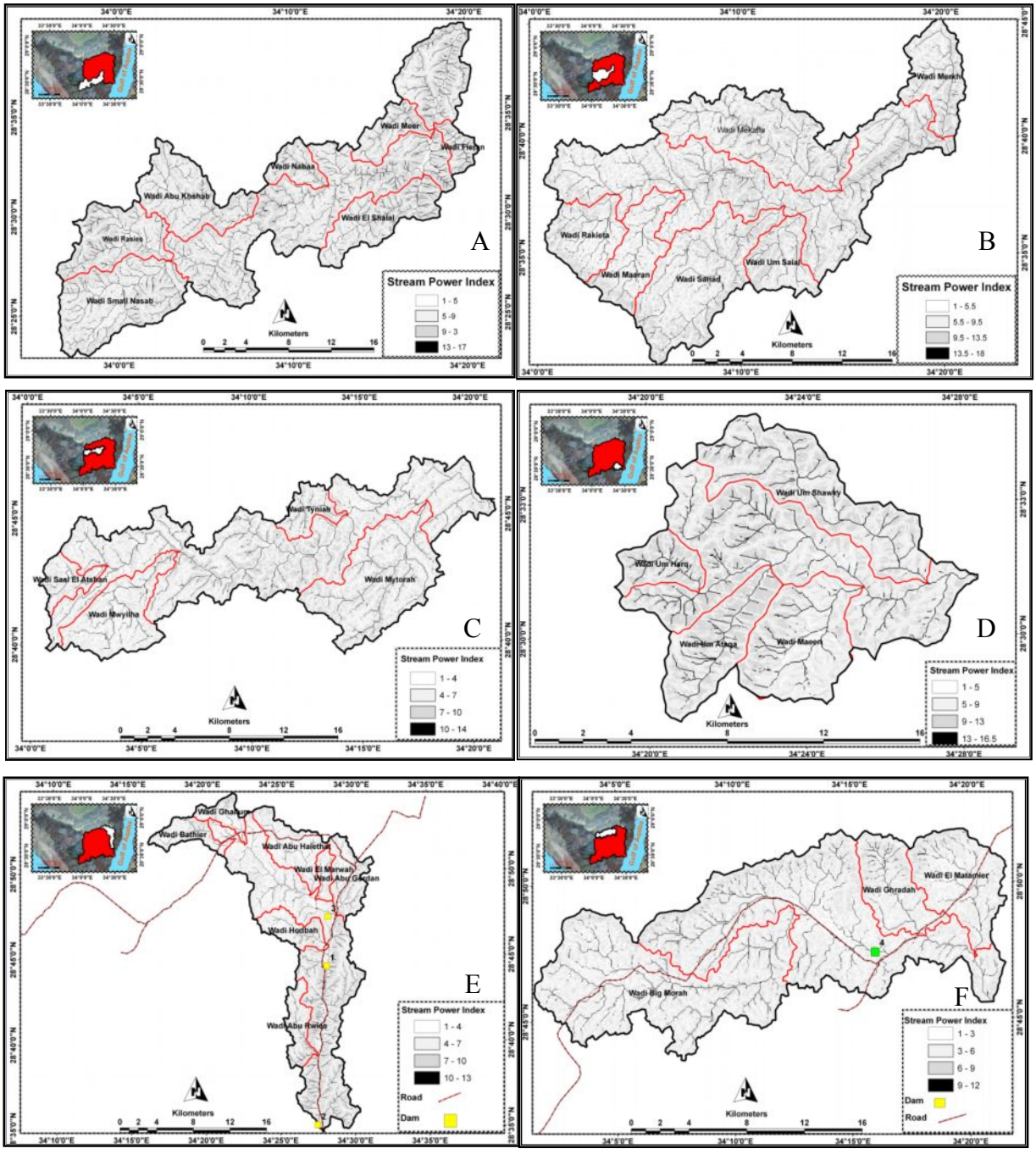

Figure 157: Stream Power Index of subbasins at W. Dahab Basin

At W. Saal, the value of the SP index ranges from 0-14. The highest values are recorded at the upstream part of W. Tyniah, W. Mytorah, W. Saal El Atshan and W. Mwyilha, ranging between 10 and 14 where they have high slope values. Morphometrically, these locations have high to moderate risk ranks, high erosive power and high storm events which may cause catastrophic impacts on the downstream of W. Saal. High SP index values are recorded at W. Um Ataqa, W. Um Harqa, W.

Maeen and W. Um Shawki, ranging between 13 and 16.5. Slope values at W. Maeen and W. Um Ataqa vary from 40 to 55^{o} and morphometrically, these wadis have high risk rank which may produce catastrophic effects downstream of Dahab basin during high storm events (fig. 157-C&D).

The value of the SP index ranges from 1-13.5 in W. Ghaieb. The highest values are found in the upstream part of W. Ghalium, W. Bathier, W. Hodbah, W. Abu Gerdan and Abu Rweis where they are associated with high slope (Fig. 157-E). It is observed that a high value of stream power can be found near Dahab road, giving good evidence that dams were already constructed mainly to protect the road as in W. Abu Gerdan and W. Abu Rwies. The low value of slope degree at W. El Genah reflects the low SP index value ranging between 1 and 12; the high value is found at the upstream part of W. Morah (main) and W. Ghradah, ranging from 10- 13 (fig. 157-F). The density of streams which have a high SP index is very low at W. Genah due to the low slope value and sedimentary rocks that cover the area of W. Genah.

5.1.5 Runoff management

Different watershed management trials are applied on upstream and downstream parts of the investigated hydrographic basin to mitigate floods, prevent soil erosion and to increase the yield of water supply for limited agricultural activities. Some of these trials are served by the local inhabitants who manage the vegetation and land use. These trials include cisterns, detention and storage dams.

Although water among all sectors has the least cost recovery, it is still of high concern. The sustainable flood water utilization provides the necessity of saving this water for longer periods and wider uses. Flood hazard protection trials can be achieved using flood peak discharge and velocity (Farid and Allam, 1996). The different trials inhibit many environmental impacts.

5.1.5.1 Cisterns

A new type of cistern is proposed to serve as water reservoirs and collectors for both surface runoff and groundwater wells; therefore, it is called a well-like cistern (Geriesh, 1998) and is dug into shallow alluvial deposits screened along the upstream side with gravel back to collect the runoff and underflow. This cistern could be used as a well for recharging the groundwater. The presence of the screen along its front, together with earlier constructed upstream retention dams, serves as a sediment top to prevent silting. This cistern type is designed to restore up to 400 m^3 of water (fig.158).

5.1.2.2 Storage and detention dams

Detention and storage dams are applied to ensure a sustainable water resource for domestic and agricultural purposes. These dams reduce the energy of flood water and increase the travel time. The benefits of these dams can be summarized as:

1- They can store a big amount of surface water to act as a protection tool of urban areas against damage risk.
2- They allow the collection of big quantities of appropriate water quality for domestic and industrial purposes.
3- They decrease the flow velocity and momentum at the main structure, controlling the flow depth.
4- They decrease the sediment loads in front of the main structure (Detention Dams).

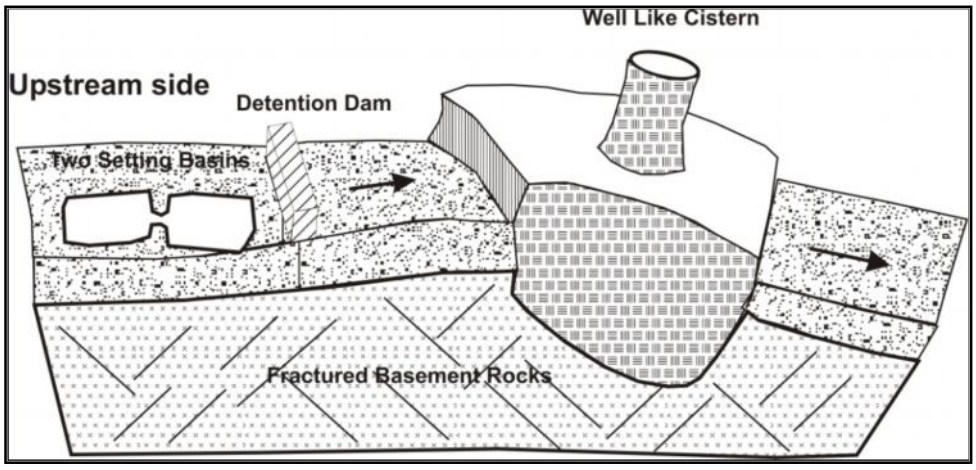

Figure 158: Proposed Design of Cistern (after Geriesh, 1998)

Elongation of the flood water travel time encourages water to infiltrate into the subsurface layers, and gives a higher chance for seepage. The system at the downstream encourages collecting more water quantity to recharge groundwater.

The selected dam sites are characterized by the following maintains:

- The soil should be sufficiently permeable to yield acceptable infiltration potential; this character is clear at a hydraulic conductivity of alluvial deposits (2.4 m/day).
- There are no impermeable layers in the vadose zone that could form a perched aquifer and restrict excess infiltration into soil.
- The water table is sufficiently deep to keep groundwater mound below the bottom of the recharge basin.
- The aquifer is unconfined and has sufficient hydraulic properties to allow lateral movement without building a groundwater mound.

5.1.5.3 Storage and recharge pits

The field conditions of the investigated area show that the topmost soil surface is hard and compact, which reduces the infiltration capacity of the top soil layer to a great extent. Therefore, a pit excavated into the permeable formation serves as an ideal facility for groundwater recharge. The

storage pit is proposed to control floods of risky basins, especially in W. Nasab and W. Saal. Both wadis have geophysical and hydrogeological data at the upstream and downstream to determine water level along the main stream. The pit is aimed to collect the excess water quantity over the dams constructed at downstream sites, enhancing the recharge of aquifer.

The proposed pits are designed with a trapezoidal shape (fig. 159) trench with steep sides to provide a high silt tolerance, where silt usually settles on the bottom of the pit, leaving the walls relatively unclogged. To minimize silt accumulation, it is recommended to fill the pit with gravel or rock fragments to a few centimeters above the bottom (fig.160). The geometry of the proposed pit is longitudinally excavated to regulate the rising of the water mounds and deep enough to reach the wet zone above the water table. The selected dimensions are 1.5 to 2 km long at the upstream to 6.5 km long at the downstream, with 10 to 15 m in depth and 40 m average in width. The surface capacity of storage pit is about 0.8 to 2.6 million m^3 in W. Nasab and 0.6 to 0.9 million m^3 in W. Saal, where the maximum rate of recharge from canal sides into alluvial aquifers can be approximately determined using the same equations of dewatering process from an open trench with reverse drawdown into a cone of recharge as in the following equation:

$$\frac{Q}{x} = \frac{K*(H^2-h^2)}{2*L} \qquad \textbf{(Driscoll, 2003)} \qquad \textbf{Equation 57}$$

Where

H: - is the height of the formed water mound above the aquifer bottom

h: - is the aquifer thickness in

L: - is the influence radius (distance to end of the pit – no recharge)

X: - is the trench length

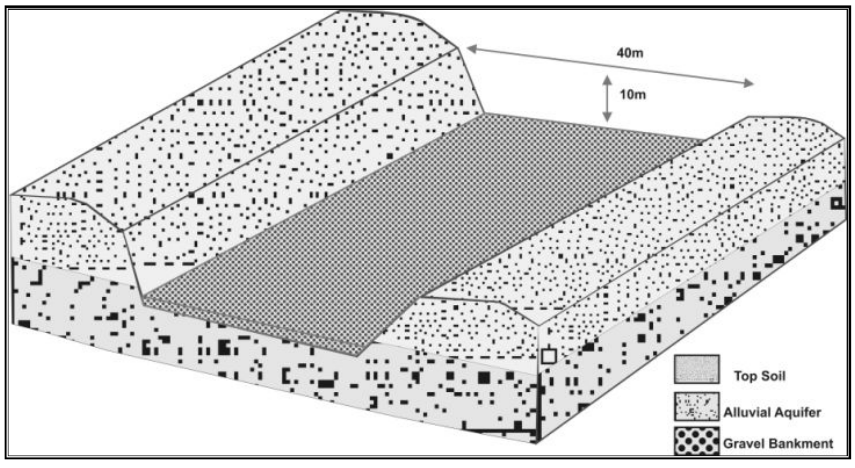

Figure 159: Dimensions of the Proposed Mitigation Canal

Based on this estimation, the maximum recharge rate from pit to alluvial aquifer ranges from 2080 to 69266 m^3 /day where the total capacity is about 5 million m^3 in W. Nasab; while in W. Saal,

the maximum recharge rate ranges from 73000 m^3 /day to 146000 m^3 /day where the total capacity is about 1.7 million m^3 (Table 38&40).

5.1.5.4 Retardation system

This system aims to decrease runoff water flow and helps for enhancement of groundwater recharge at upstream sides of the basins. There are many types of retardation systems and they can be established with simple materials as follows:

5.1.5.4.A Sand and rock barriers

The prevailing geological condition in Dahab basin is suitable for stone barrier design where the weathering product of basement rocks is available at wadis. The boulder materials are supposed to be the rock boulders existing along the wadi floor. This system is very suitable along stream tracks, but at upstream sites. The same system is suggested by El Shamy (1992) with successive water barriers in the form of incomplete low rocky dams attached only to one wadi side (fig.160).

This simple mean orients the runoff flow to pass through a zigzag like path, enhancing the downward infiltration. Geriesh (1998) discussed the problems facing these types of protection systems. Silting and clogging may form the main problems facing this type of dam. For repairing this problem, bulldozers or normal tractors can be used, especially where the area is almost dry during summer seasons.

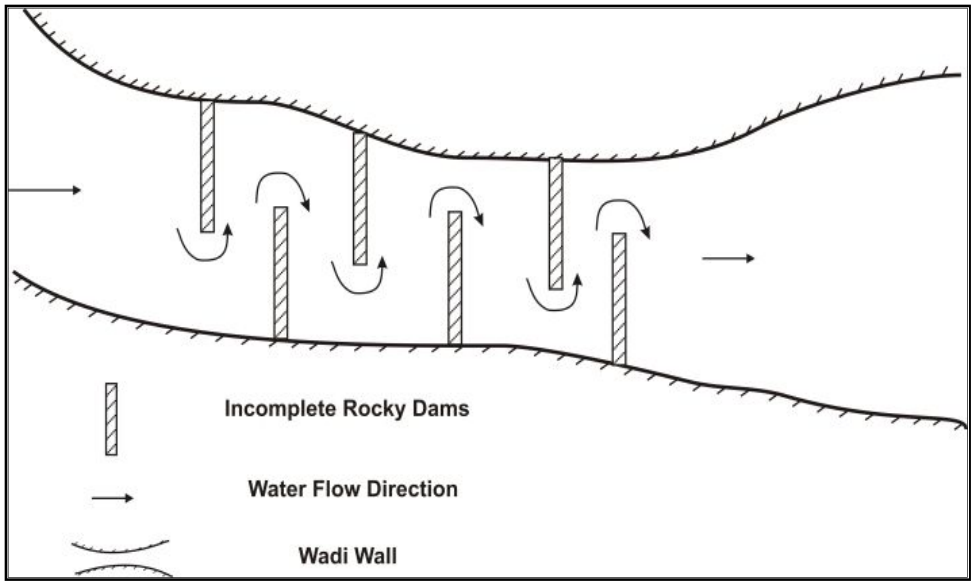

Figure 160: Proposed Zigzag rock barriers in wadis

5.1.5.4.B Terracing

Terracing helps to provide silt free water for storage. The system is more suitable for wide areas with geographical extension of soil (fig.161). Terraces can be used as temporary water storages to

reduce flow velocities of surface water and prevent erosion. The slow flowing water may be directed into a storage facility. It is recommended to use this system in the northern part of the study area where the sedimentary cover is outcropping. The wide area, low average slope and elevation help to establish terracing easily in this area.

Figure 161: Proposed Terracing method at wide area within basin

5.1.5.4.C Rainwater Collection

This tool is used mainly for roof water collection in countries where conventional water resources are extremely scarce and each drop of rain has a real value. The ready availability of some form of roof sheeting and innovative ideas for water storage have made roof water a serious water resource consideration. Storage containers (jars) are used by householders from concrete to hold volumes 100 to 3000 L and measures could be applied in order to keep away insects. This is mainly for domestic uses. This system is applied in very small locations in the study area, especially at the downstream of W. Zaghraa (fig.162). It is recommended to use these systems in other locations in Dahab basin near housing communities at W. Saal, W. Nasab and W. Zaghraa.

Figure 162: Proposed rainfall storage (collector) method in W. Zaghraa.

5.1.6 Proposed design and flood control efficiency

A lot of runoff water is needed to saturate the thick alluvial cover along the main streams of the sub-basins in the study area. Several methods have been proposed for sub-basins of W. Dahab to store water for using in irrigation and for domestic purposes.

5.1.6.1 Flood control in W. Nasab and its efficiency

Nasab basin has one protection dam which was constructed by WRRI (2006). A lot of water at a maximum storm could threat the residential and small agricultural areas. Huge parts of water may be lost due to evaporation, in addition to the disadvantages in dam location downstream of W.Nasab. Additionally, there are no management practices in the upstream areas of the basin. The proposed design should support the old constructed one; this is of prime importance. The highest potential for flooding risk concentrates at sub-basins of W. Nasab as in W. Nabaa, W. Meer, W. El Shalal, W. Rasies, W. Abu Khashab, W. Ferani and W. Small Nasab. Several numbers of flood control systems are proposed along the main streams of these wadis (fig.163).

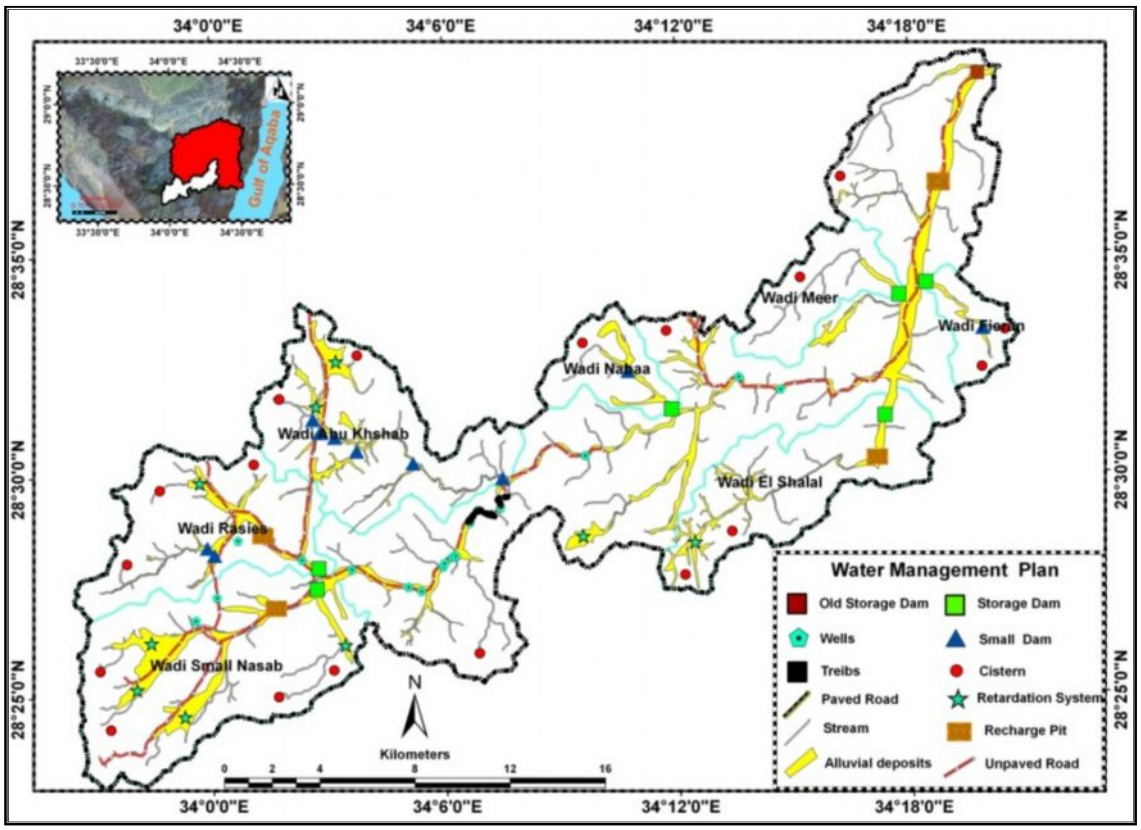

Figure 163: Proposed Water Management plan in W. Nasab

The proposed design includes six storage dams in the downstream area of high erosive potential sub-basins in W. Nasab. It is aimed to protect the tribe area against floods during high storm season. The proposed plan includes six small detention dams along W. Abu Khshab main sub-basin, two dams at W. El Rasies sub-basin, one at W. Ferani sub-basin and one at W. Nabaa sub-basin. The sites

of the proposed dams are controlled by the suitable geomorphological and geological conditions. The main specifications of the proposed dams are listed in table 36.

Seventeen cisterns are proposed to be constructed in the upstream areas of W.Nasab basin, especially at sub-basins of W. Rasies, W. Small Nasab, W. Abu Khshab and W. El Shalal due to their high elevations, steep slopes and hard accessibility. These cisterns are suitable to reduce the energy of runoff and to store an amount of water that reaches up to 400 cubic meters. The total capacity of these cisterns is about 6800 cubic meters. Also, the rocks of the catchment area are highly fractured permitting a good chance to recharge the existing aquifer.

The proposed recharge and storage pits in the downstream area of W. Rasies, W. El Shalal, W. Small Nasab and W. Nasab basin are designed to reduce the runoff velocity and to recharge the groundwater of the alluvial deposits. The pits have a storage capacity ranging from 0.8 to 2.6 million cubic meters. The soil has a hydraulic conductivity ranging from 0.15 to 0.31 m/day and can recharge the aquifers by additional quantities ranging from 2080 to 69266 cubic meters. So the total capacity reaches up to 5 million cubic meters (Table 36).

		Dam Name	Height of dam (m)	Width of dam (m)	Area of basin (* $10^3 m^2$)	Max. Storage Capacity (m^3)	
Present Plan		Downstream Nasab	5	170	50	90	
Proposed Plan	Storage Dam	W. Meer	5	150	21.6	151000	1.9 million m^3
		W. Fieran	5	220	54	517000	
		W. Rasies	5	200	51	300000	
		W.Small Nasab	5	200	58	240000	
		W. Nabaa	4	100	3	8600	
		W. El Shalal	5	280	60	600000	
	Cistern		17			6800	
	Small Dam	W. Abu Khashab	2	50	1	7000	
			1.5	50	0.5	4000	
			1.5	50	0.5	4000	
			1.5	50	0.5	4000	
			1	40	0.4	3000	
			1	35	0.3	2000	
		W.Rasies	2	45	1	5500	
			2	45	1	5500	
		W. Fieran	1.5	55	1	5000	
		W.Nabaa	2	50	1.5	6000	
			Depth of pit (m)	Width of pit (m)	Length of pit (m)	Max. Storage Capacity (m^3)	
	Recharge Pit	W.Rasies	10	40	2000	800000	5 million m^3
					K=0.15 m/day	10640	
					H=30m, h=15m		
		W. El Shalal	10	40	2000	800000	
					K=0.31 m/day	4000	
					H=25m, h=10m		
		W.Small Nasab	10	40	2000	800000	
					K=0.15 m/day	2080	
					H=20m, h=16.3m		
		Downstream Nasab	10	40	6500	2600000	
					K=0.31 m/day	69266	
					H=40m, h=15m		

Table 36: Storage Capacities and Efficiency of the Proposed Management Design at W. Nasab basin

The total storage capacity of the old design within W. Nasab basin is about 90000 m^3 with a storage efficiency of about 0.5 % at maximum storm. The total storage capacity of the proposed design is about 6.9 million m^3 with efficiency of storage being compared with the volume of runoff at maximum storm of about 43.3 %. The increasing of storage capacity helps to increase infiltration about 40 % and hence, increases the recharge of the underlying aquifers.

The efficiency of storage capacity of the proposed management plan in W. Nasab is about 43 % at a maximum storm of 76mm, 53.9% at a storm of 65mm, 83 % at a moderate storm of 55mm and finally about 100% at a low storm of 45mm (fig. 164). So the proposed design helps to protect mainly residential areas at W. Nasab, the area at downstream of Dahab basin and also helps to use the excess runoff water to recharge the aquifer which could provide large amounts of water for bedouins who lived in this basin.

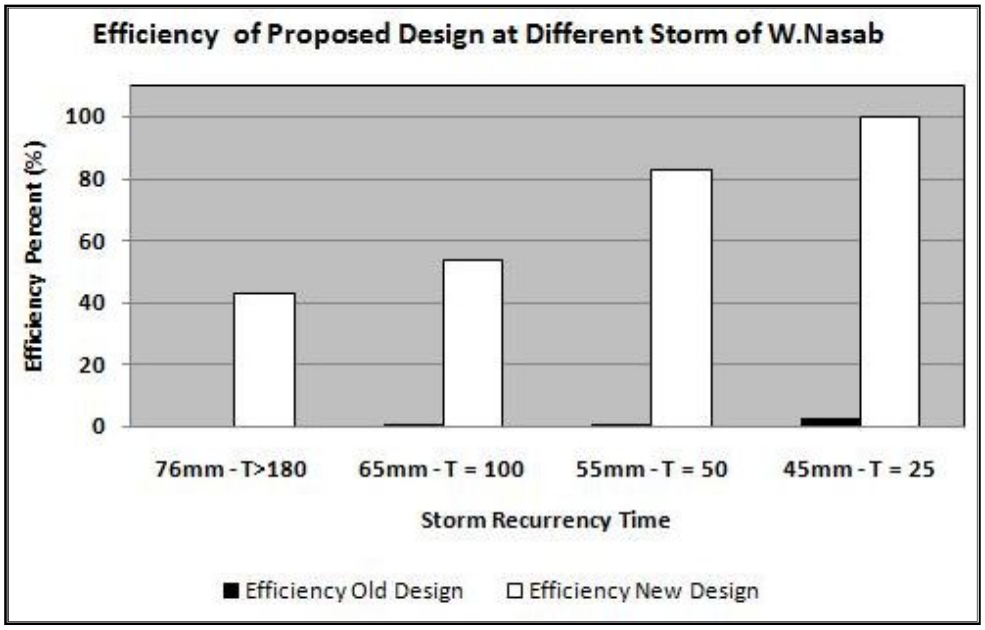

Figure 164: Efficiency of Proposed Design at Different Storms in W. Nasab Basin

5.1.6.2 Flood control in W. Rimthy and its efficiency

W. Rimthy is considered the highest risk sub-basin in W. Zaghraa. The basin has different geological, geomorphological and hydrological parameters qualifying it as a high risk basin caused by the relatively short distance from upstream to downstream, relatively high gradient, high elevation, especially in the upstream area, and it is mostly covered by basement rocks. Despite the dangerous effects of runoff in W. Rimthy and W. Zaghra basin areas, runoff controlling tools are not built within these basins.

A management plan is proposed for areas which have a high flood risk potential in the upstream parts and along the main stream of W. Rimthy. This plan aims firstly to protect Bedouins against runoff hazards and to save water for their uses. The second aim is protection in the downstream area of W. Zaghraa which debouches directly in the downstream area of Dahab basin. The highest

potential areas are located at W. Merkh, W. Mekaffa, W. Sanad, W. Um Saial, W. Maaran, W. Rakieta, W. Um Retm and W. Small Ramthy (fig.165).

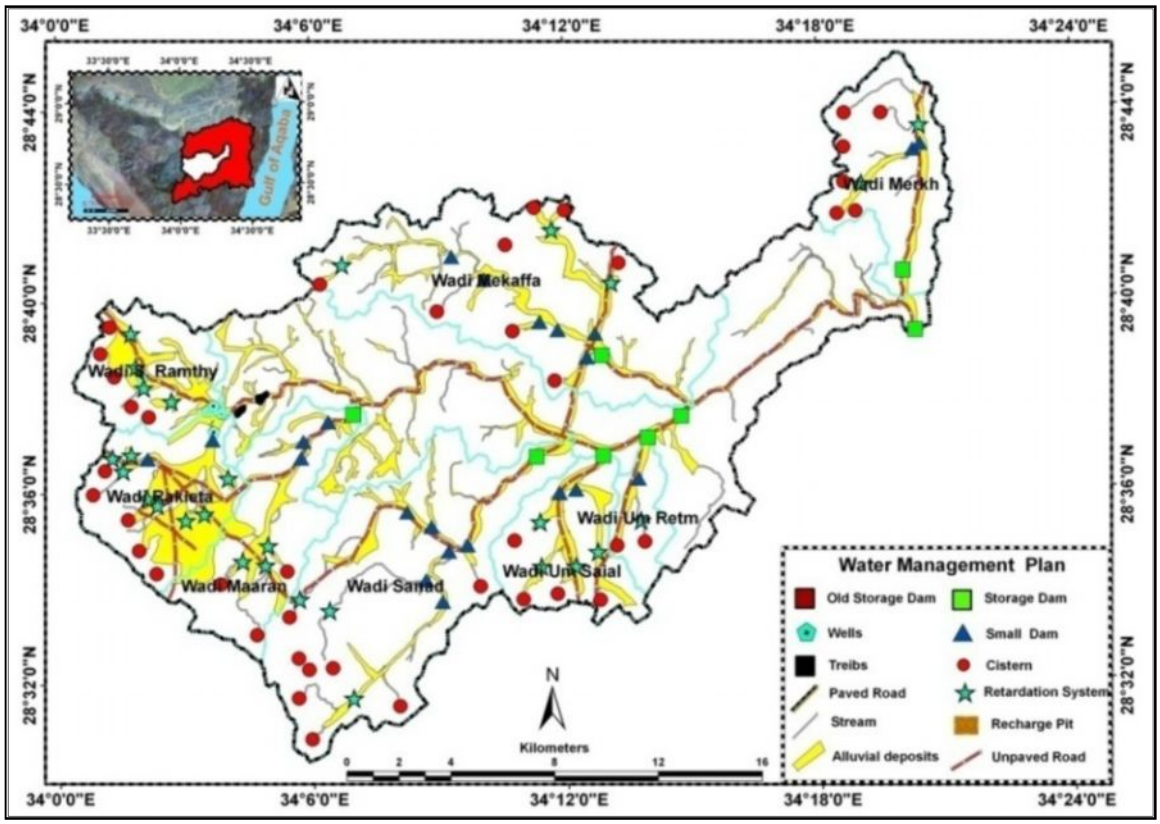

Figure 165: Proposed Water Management plan in W. Rimthy

The proposed design includes 8 storage dams, 20 small dams and 41 cisterns (Table 37). Two storage dams are suggested along the main stream of W. Rimthy and the others on the outputs of the high risk potential wadis. The small dentention dams are located in order to support the storage dams, especially in W. Sanad and W. Mekkafa. Because of a low gradient value of 14 m/km and wide areas of loose sediments at the upstream part of the basin, a retardation system is proposed there. The system helps to increase the infiltration and hence, to increase the recharge of the underlying aquifer. On the other hand, the system reduces the quantity of runoff to protect the local inhabitants in these areas. Recharge pits are not suggested in this basin because geophysical data is not available and groundwater wells are not well distributed along W. Rimthy.

The efficiency of storage capacity of the proposed management plan in W. Rimthy is of about 10.8 % at a maximum storm of 76mm, 15% at a storm of 65mm, 25 % at a storm of 55mm, and finally about 53% at a storm of 45mm. The proposed design helps to protect mainly the residential areas downstream of Dahab basin and assists in using the excess runoff water to recharge the aquifer.

		Dam Name	Height of dam (m)	Width of dam (m)	Area of basin (* $10^3 m^2$)	Max. Storage Capacity (m^3)	
Proposed Plan	Storage Dam	W. Merkh	5	180	31.7	227234.23	1.6 million m^3
		Downstream Ramthy	5	250	29.25	61114	
		Main Stream	5	250	44.32	227276	
		W. Um Retm	4	170	36.9	84630	
		W. Um Saial	5	150	50.85	283146.73	
		W. Sanad	5	230	112.725	105000.9	
		W. Maraan	4	130	113.17	401593	
		W. Mekaffa	5	200	73.8	147597.9	
	Cistern	41				16400	
	Small Dam	Wadi Merkh	2	60	1.5	3000	
			3	120	1.2	5000	
		W. Um Retm	2.5	140	1	3000	
		W. Sanad	2	70	1	2500	
			2.5	120	1.5	3000	
			2.5	120	1.5	3000	
			1	50	0.5	2000	
			2	70	1	2500	
			2.5	120	1	3000	
		W. Mekaffa	1	50	0.5	2000	
			2	70	1	2500	
			2.5	150	1.5	3000	
			2	130	1.2	3000	
			2	130	1.2	3000	
			1	50	0.5	2000	
		W. Maraan	2.5	80	1.2	2500	
			2	70	1	2500	
			2	70	1	2500	
		W. Rekita	2.5	120	1	3000	
			2.5	120	1	2500	

Table 37: Storage Capacities and Efficiency of the Proposed Management Design in W. Rimthy basin

5.1.6.3 Flood control in W. Saal and its efficiency

Although W. Saal basin has an elongated shape, it is considered as a basin with moderate risk potential due to relative high elevations in the upstream area, especially at the southern and western parts of the basin, a short distance between the upstream and the downstream area and a relatively high gradient of the basin along the main stream of W. Saal which affects the downstream area of W. Zaghraa and hence, downstream of W. Dahab.

According to the aforementioned conditions, WRRI (2006) constructed a storage dam in the area downstream of W. Saal with a storage capacity of about 70000 m^3, in addition to a sand dam at the upstream parts for retardation purposes (fig.166). The high potential risk areas include W.Tyinah and W. Murad in the northern part of basin, W. Saal al Atshan and W. Mwyilha at the western part of basin and W. Mytorah at the southern part of basin.

Due to the high risk level of W. Saal basin on the downstream of Dahab basin, the management plan suggests to support the existing old design. The proposed new design aids to provide excessive protection and to use the runoff water to recharge the existing aquifer. The proposed new design includes five storage dams at the downstreams of W. Murad, W. El Tyinah and W. Mytorah with two

dams along the main stream, eleven small dams to support storage dams and twenty-one cisterns at the upstream of the basin to reduce the energy of the runoff and to help to recharge the underlying aquifer, with a total capacity of 8400 cubic meters.

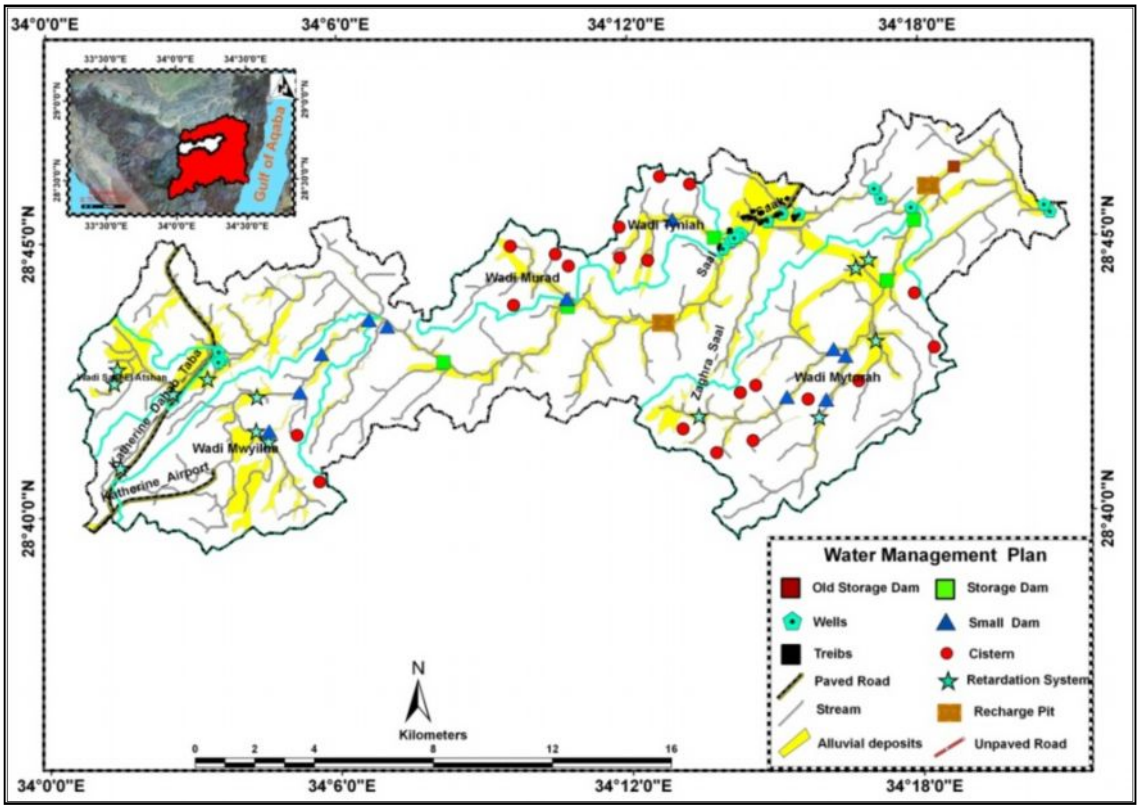

Figure 166: Proposed Water Management Plan of W.Saal

Two recharge pits along the main stream and at the downstream area of W. Saal basin are also proposed to collect the overflow runoff from the constructed dam, and to recharge this water into the underlying aquifer. The storage capacities of the pits range from 0.6 to 0.9 million cubic meters; the surface soil has a hydraulic conductivity ranging from 7.4 to 8.7 m/day. So the aquifer can be recharged by about 73000 to 146000 m^3 of running water. The total storage capacity of the proposed management plan reaches up to 1.7 million cubic meters (Table 38).

The total storage capacity of the old design within W. Saal is about 70000 m^3 with a storage efficiency of 0.7 % at maximum storm rate. The total storage capacity of the proposed design is 2.2 million m^3 with an efficiency to store runoff volume at maximum storm rate of about 24 %. The increasing of the efficiency causes an increase in infiltration to about 23% and hence, increases the recharge of the underlaying aquifers.

The efficiency of the proposed design in W. Saal basin is 24% of the maximum storm rate, for a storm of 65mm; the efficiency increases up to 34% , for a storm of 55mm; the efficiency is 57%, and finally get to 100% in a storm of 45mm. The design fully protectes the area at minimum storms and it helps to protect the residential area and the downstream area of W. Dahab where the proposed design

reaches 100 % efficiency. Moreover, the design suggests that more than 80 % of the runoff water should be used enhance groundwater storage (fig.167).

		Dam Name	Height of dam (m)	Width of dam (m)	Area of basin (* $10^3 m^2$)	Max. Storage Capacity (m^3)	
Present Plan	Storage Dam	Downstream Saal	6	150	30	70000	0.534 million m^3
Proposed Plan	Storage Dam	W. Saal (Main Stream) 1	5	250	34.4	111700	
		W. Saal (Main Stream) 2	5	170	7.8	20250	
		W. Abu Tyinah	5	240	22.7	73810	
		W. Mytorah 1	5	170	52.2	188700	
		W. Mytorah 2	5	170	14.8	32390	
	Cistern		21			8400	
	Small Dam	W. Mwyilha	2.5	80	1.2	2500	
			2	50	1	2000	
			2	100	1.2	2500	
			2	100	1.2	2500	
		W. Mytorah	2.5	185	2	2500	
			2.5	175	2	2500	
			2	150	2	2500	
			2	150	2	2500	
		W. Saal (Main Stream)	2.5	100	1.5	3000	
		W. Murad	2.5	120	1.5	3000	
		W. Abu Tyinah	3	250	3	3500	
			Depth of pit (m)	Width of pit (m)	Length of pit (m)	Max. Storage Capacity (m^3)	
	Recharge Pit	Downstream Saal	15	40	1500	900000	1.7 million m^3
					K=7.4 m/day	146000	
					H=50m, h=55m		
		W. Saal (Main Stream)	10	40	1500	600000	
					K=8.7 m/day	73000	
					H=25m, h=20m		

Table 38: Storage Capacities and Efficiency of the Proposed Management Design in W. Saal basin

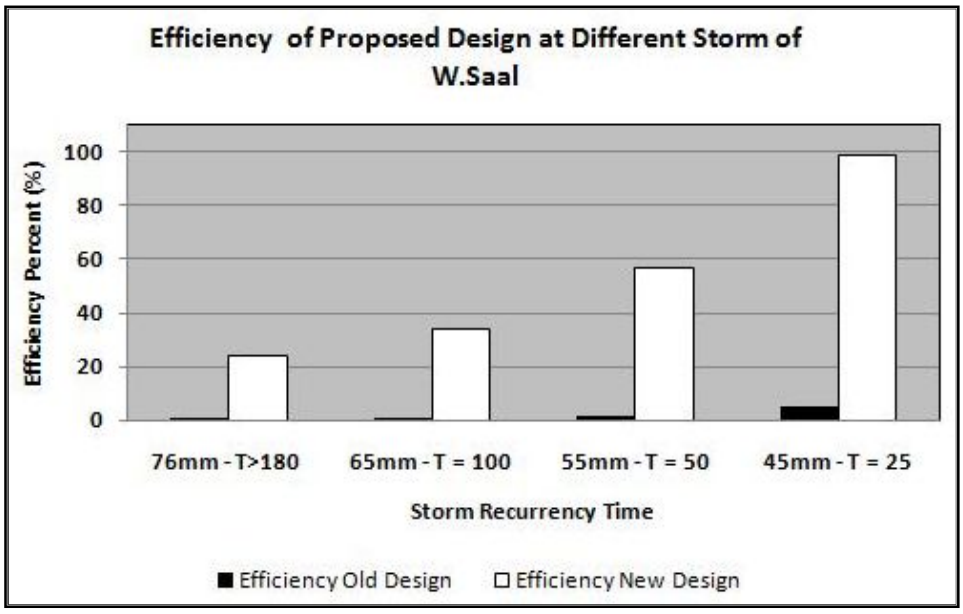

Figure 167: Efficiency of Proposed Design at Different Storms in W. Saal Basin

5.1.6.4 Flood control in W. Abu Khshieb and its efficiency

Geological, geomorphological and hydrological studies confirm that Abu Khshieb basin has a moderate flooding risk rank. The basin is drained directly into the downstream of Dahab basin and it causes a catastrophic effect on the main road to the cities of Dahab and Sharm El Sheikh. Abu Khshieb basin has some characteristics which favor it to be a moderate risk basin, such as the coverage of the entire basin with basement rocks of low conductivity, the circular shape of the basin, the short distance from the upstream to the outlet of the basin of about 11 km, and the relative steep gradient of 22 m/km, especially at the upstream parts of the basin. All these factors help to produce dangerous floods during thunder storms.

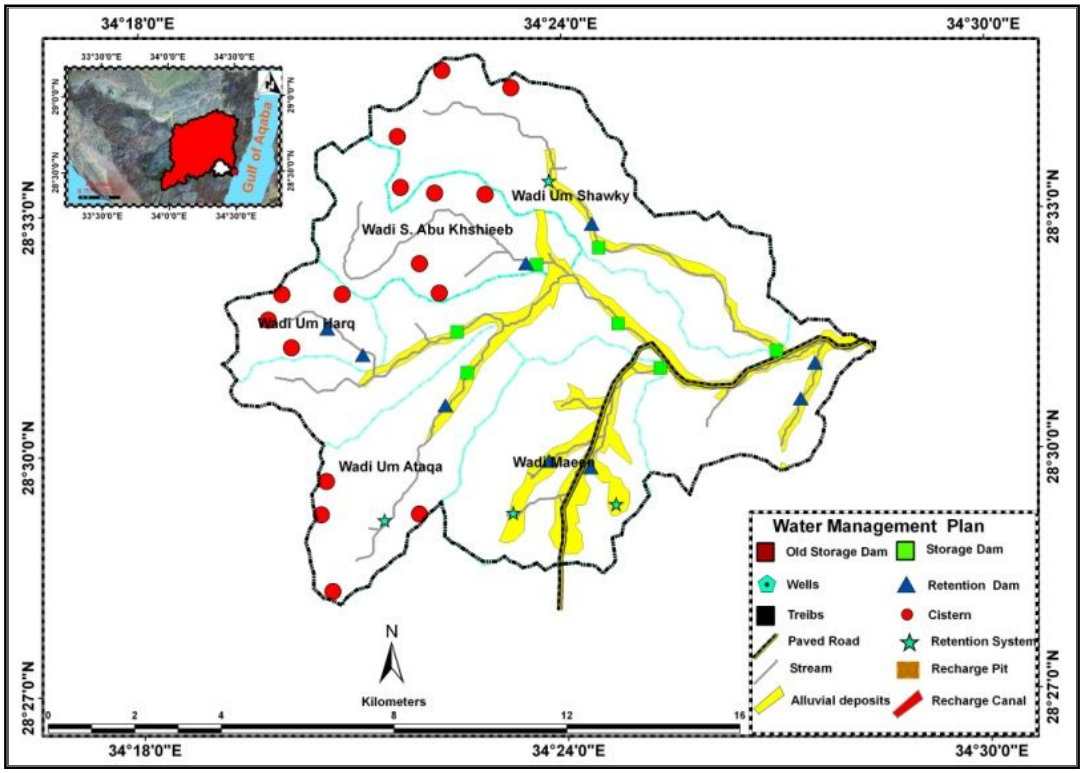

Figure 168: Proposed Water Management plan at W. Abu Khshieb

The management plan advises to protect flood hazards during storm periods in the basin. Four storage dams are suggested at the downstream of W. Um Shawky, Maaen, W. Um Ataqa and two storage dams are proposed along the main stream just before the highway to Sharm El Sheikh. Sixteen cisterns are planned at the upstream of basin to reduce the energy of the runoff and aid to recharge about 6400 cubic meters of runoff to be stored. Nine small dams are proposed to support the storage dams in order to reduce water and sediment loads before storage dams (Table 39).

The maximum storage capacity of this design is 460000 m^3. The efficiency of the plan is about 12.8 % at a maximum storm of 76mm, for a storm of 65mm it is 17%, while for a storm of 55mm, it is 27 %, and finally, about 49% at a storm of 45mm. In spite of the dangerous situation of this basin and the presence of an important road through it, no management plan is established within Abu Khshieb

basin. The proposed design assists to protect mainly the highway to Sharm El Sheikh and the downstream area of Dahab basin (fig. 168).

		Dam Name	Height of dam (m)	Width of dam (m)	Area of basin (* $10^3 m^2$)	Max. Storage Capacity (m^3)	
Proposed Plan	Storage Dam	Main stream 1	5	270	41.10	150096.00	460000 m^3
		Main stream 2	5	200	6.7	13868.00	
		W. Maaen	5	115	9.50	18372.00	
		W. Um Ataqa	5	210	27.6	120128.00	
		W. S. Abu Khshieeb	4	150	24	67169.00	
		W. Um Shawky 1	5	155	14.6	32600.00	
		W. Um Shawky 2	4	115	16.2	31193.00	
	Cistern		16			6400	
	Small Dam	Downstream	2	185	2.00	2500	
			1.5	150	1.00	2000	
		W. S. Abu Khshieeb	1.5	100	1.00	1000	
		W. Um Harqa	1.5	80	0.70	1500	
			2	80	1.00	2000	
		W. Um Ataqa	1	50	0.5	2000	
		W. Maaen	2.5	150	1.5	3000	
			2.5	150	1.5	3000	
		W. Um Shawky	2.5	120	1	3000	

Table 39: Storage Capacities and Efficiency of the Proposed Management Design at W. Abu Khshieb basin

5.2 Potential map for groundwater exploration

5.2.1 Introduction

Groundwater exploration in the study area has many problems such as the scarcity of available data, the high cost of data gathering, and the relatively remote target aquifer. Therefore, remote sensing and GIS techniques are the most appropriate alternative tools for groundwater exploration (Moore, 1982). Upgrading the living standards of Sinai's population in the last few decades has caused an increase in water demand (Elwa and El Qaddah, 2011). Drinking water is distributed by tanker-lorries in the absence of a piped distribution network. In some parts of Sinai, the local inhabitants have to use salty groundwater as potable water to face the water crisis.

Occurrence of groundwater has been studied for many decades using aerial photo interpretation and geophysical techniques, but computer-based analysis of GIS has rarely been used for groundwater exploration in Egypt. Hence, there is a need for this work, which mainly concentrates on locating water wells in the study area. The main advantages of using remote sensing and GIS techniques for groundwater exploration are the reduction of costs and time needed for the selection of promising exploration areas.

Groundwater potential maps are studied using GIS techniques by many researchers such as Musa et al. (2000), Sener et al. (2004) and El Naqa et al. (2009). The same techniques have been conducted by several researchers in some parts of Sinai, among them: El-Shazly et al. (1983 & 1985), Masoud and Koike (2005) and Elwa and El Qaddah (2011). El-Shazly et al. (1983) used the geomorphologic

features, land cover, vegetation, and geologic units as effective parameters in the groundwater investigations of the W. Araba area in the Eastern Desert of Egypt.

Smith et al. (1997) used a method which incorporates satellite images and GIS to detect areas of likely groundwater accumulation in the northern Sinai Peninsula. The technique involves integration of bifurcation ratio, drainage density, stream frequency, slope, and precipitation. El-Baz (1992) used the lineaments, topography and drainage system as effective parameters for preliminary assessment of potential environmental damage to groundwater systems due to the Gulf War (1990, 1991).

5.2.2 The model

Most of the previous works have used a limited number of GIS layers and gained somewhat reasonable results. The higher the number of significant GIS data layers used in groundwater potentiality mapping, the higher the accuracy gained. The main objective is identifying prospective areas for groundwater exploration based on topographic, geological, structural, and climatic data. These controlling parameters help to find groundwater occurrence in W. Dahab watershed. However, drilling boreholes are required to confirm the existence of groundwater potential zones.

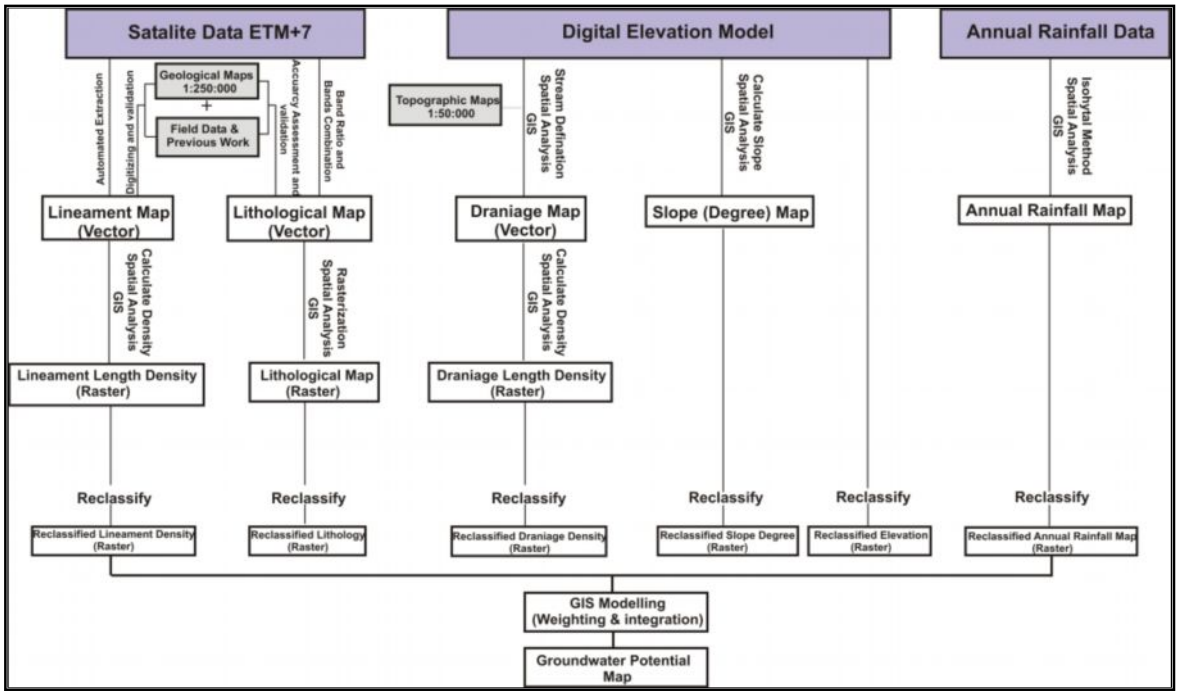

Figure 169: Flow Chart for Groundwater Potential Model

This model approach to model groundwater potential is summarized in the flow chart (fig. 169). This chart shows the different factors of inputs and outputs used to generate the final groundwater potential map. The final result will help to find proposed areas for groundwater accumulation.

The method used in this model is a modification of the DRASTIC model, which is used to assess groundwater pollution vulnerability by the Environmental Protection Agency of United States of

America (Aller et al., 1985). The equation of groundwater potentiality model is implemented as below:

Groundwater Potential = Rf + Lt + Ld + Te + S + Dd **Equation 58**

Where Rf: (annual rainfall weight), Lt: (Lithology weight), Ld: (Lineament density weight), Te: (Topography weight), S:(Slope weight), and Dd: (Drainage density weight).

The grid cells in each thematic layer are categorized depending on their contribution to groundwater potential. A description of these parameters is given in the following section.

5.2.2.1 Annual rainfall factor

The main source of groundwater in the study area comes mainly from rainfall. The long term mean annual precipitation reaches about 35mm/year at W. Dahab. This precipitation value is weighted to reflect the influence of precipitation on the groundwater. As the precipitation value increases, more water will be available for surface runoff and infiltration. Sener et al (2005) and El Naqa et al. (2009) agreed that in the areas which receive high rainfall, the groundwater potentiality should be high. These areas should take a high score rank and a high grade for the model

An annual rainfall map is prepared using the isohyetal method for creating the isohyetes that cover the study area using the average annual rainfall data of the meteorological stations at South Sinai. The map is converted to a raster grid (30 × 30 meter). The resulting map exhibits five major classes discriminated into the ranges < 11, 11–30, 31–44, 45–60 and > 60 mm/year. The map shows that the elevated areas received much more water than the lowland areas. Areas surrounding Saint Catherine station aquire more than 60 mm/year water while the area surrounding Dahab station at lowland received less amount than 11mm/year. Figure 170.A shows that the area which receives high rainfall should take a high grade for groundwater occurrence posibility while very a low grade is obtained for low rainfall sites. Due the importance of the rainfall paramter for groundwater recharge, it should take a high weight value of 30.

5.2.2.2 Lithology factor

The lithologic character of the exposed rocks is significant in governing recharge. The knowledge of the litho-stratigraphy of a region is essential to understand the nature and distribution of their water bearing properties (Fetter, 1994). The litho-stratigraphic units of the area are generated from the EGSMA (1992) geological map of Southern Sinai with a scale of 1:250,000. Further modifications of this map are performed using remote sensing data (Omran et al., 2012) and used in this model. More certainly, the use of ASTER (pixel size 15 m) and Landsat 7 ETM + satellite images (pixel size 30 m) are helpful in this regard; thus, boundaries of many exposed rock formations are precisely corrected.

Some studies neglecte lithology factors once they use only lineament and drainage (El shazly et al., 1985 and Edet et al., 1998). The reason of neglection is considered that the lineaments and drainage characters are a primary and secondary porosity, thus, providing information about lithology;

however, others like El Baz et al. (1995) incorporated the lithology factor due to its strong influence on water percolation. The rocks become aquifers through development of weathering and fracturing as secondary porosity.

Dahab basin is considered to be one of the major basins in Sinai; therefore. its lithologic cover can be classified into four classes:

1- Basement rocks (Granitic and metamorphic rocks).
2- Volcanic rocks and metasedmentary rocks
3- Cretaceous rocks (Limestone, dolomite and calcareous sandstone).
4- Alluvial deposits (Quaternary rocks) and Cambrian rocks (Sandstone and clay).

The influence of hydraulic properties such as permeability in the lithological units cause different rates of discharge at each unit. Sherief (2008) investigated the permeability range for different lithological units at El Qaa plain area in the western part of Southern Sinai (Table 40). The values show that alluvial deposits have a high ability to infilterate rainfall through them while granitic rocks have a low permeability value. El Naqa et al. (2009) and Baharuddin et al. (2006) put a high weight value on alluvial deposits as an indication of a high significant value for the groundwater recharge condition, while basement rocks get a low weight score and low significant value for recharge. An empirical classification of the lithologic formations according to their infiltration capabilities is carried out in Sinai Peninsula (Elewa and Qaddah, 2011). They classified Sinai into four major classes to reveal rock formations of similar infiltration properties or lithologic groups A, B, C and D depending on intensive previous investigations.

Lithology	Permeability ranges 1000 $m^3/day/km^2$ Sherief (2008)	Score value Baharuddin et al., 2006	Infilteration Rate(mm/hr) and Soil Group Elewa and Qaddah, 2011	Groundwater Potentiality Rank
Alluvium (sand , gravel) + Cambrian Rocks	15140	55	>7.62 , A	Very high
Sedimentary rocks include (Upper and Lower Cretaceous rocks)	1514	36	3.81–7.62 , B	High
Volcanics rocks, Metasediments and Phyllite	37.9	21	1.27–3.81, C	Moderate
Basement rocks (Granites and Metamorphic rocks)	3.79	17	<1.27, D	Low

Table 40: Different Permeabilties, Weighted Values for Lithological Units in Dahab Basin.

Alluvial deposits consist of loosely cemented gravel, sand and clay. The hydraulic conductivity may reach 2.9 m/day. The basement rocks are described as impermeable units. The tectonic effect causes fracturing of most rocks which may absorb the rain water and percolate it to an aquifer. The estimated hydraulic conductivity for fractured basement rocks is very low compared to that of the other rock units. According to previous investigations, alluvial deposits should take a very high rank for groundwater potentiality while a very low rank should be given to basment rocks as an indication of groundwater recharge (Table 40 and fig. 170- B). The lithology layer is assigned as weight 25 for the model because of its importance for groundwater occurrence.

5.2.2.3 Lineament density

Lineaments give a clue to the movement and storage of groundwater (Subba et al., 2001) Lineament analysis for groundwater exploration is of considerable importance, where the joints and fractures serve as conduits for movement of groundwater and have a high water-holding capacity (El-Rayes, 2004). Fractures in rocks increase their secondary permeability and porosity, and thus, accelerate vertical water percolation to recharge the aquifers. For this reason, identifying fractures in rocks are considered as a major factor characterizing groundwater potential areas.

Lineaments are extracted from satellite images using lineament filters and visual enhancements of Landsat (ETM+7 band 8) and automated extraction techniques to enhance the existing data of the available structural map (see chapter 1). The density of linear features in the neighborhood of each output raster cell is calculated in units of length per unit of area. The lineament density is expressed by classifying the area into specific frames (1 km × 1 km), and thus, the length in (km) of lineaments in each grid cell is automatically counted, and the resulted value is plotted in the mid-point of each cell, producing a grid map with attribute values.

Sener et al. (2005) stated that groundwater potentiality should increase when the lineament density for lithological units increase. According to the previous conclusion, the high weighted value for a groundwater potential area should be taken for the areas that have high linement density. The resulting density map at Dahab basin is divided into five classes with each class referring to a range of lineament density, which represents the length of lineaments per unit area. The five classes in this study are < 1.5, 1.5–3, 3.1–5.5, 5.6–7 and > 7 km/km^2 (fig.170-C).

The high density value appears in basment rocks more than 7 km/km^2 where borehole and spring are investigated during field visits at wells A1, N8 and N9 in W. Nasab. The low density values occur in the downstream of W. Dahab where alluvial fan deposits and urban landuse are the main features in this area. The northern part of Dahab basin has a high to moderate range for the lineament density due to the effect of the geologic conditions of lithology and tectonics, in addition to the scarce landuse of this area. As a conclusion of the previous investigation, the highly lineament density areas should take very high rank while low lineament density should take low rank as is significant for groundwater occurrence in Dahab basin. Due to the importance of lineament density for the groundwater occurrence, it should be taken as third factor and it would be assigned 15 as weight value.

5.2.2.4 Drainage density

Drainage pattern is one of the most important indicators of hydrogeological features, because drainage pattern, texture, and density are controlled in a fundamental way by the underlaying lithology (Sener et al., 2005). The rate of surface-water recharge by runoff to groundwater is governed by the characterization of the drainage systems. Therefore, the drainage density has often been a part of similar studies, and is almost embedded with lineaments, as they control the drainage lines in some

parts of the watersheds, to propose groundwater potential areas (Edet et al., 1998 and Robinson et al., 1999). Omran et al. (2011) used drainage density as one of the main parameters for runoff hazard indication.

Drainage density, which is defined as the unit length of stream channel per unit area, has been shown to vary between regions due to different climatic regimes, natural landscape characteristics, and land-use impacts (Tucker and Bras, 1998). A surface drainage map has been prepared from the DEM of 30 m resolution, toposheets at 1:50,000 scale and satellite ETM + image. The drainage map for Dahab basin is created using hydrology tools in GIS based on the digital elevation model.

The shape of the stream network reflects the possibility of precipitation to permeate and its density could help to increase groundwater storage, or to make overland flow and then surface runoff occur. When comparing two terrain types, the one that contains the greater drainage density usually has a less permeable top soil layer. It is well known that the denser the drainage network is, the less the recharge rate is and vice versa (Edet et al., 1998). Musa et. al and El Naqa et al. agreed to put high weighted value for the areas that have a low drainage density while the areas that have a high drainage density are assigned low weighted values.

Drainage Density (km/km^2)	Score value Musa et al., 2006 Sener et al.,2004	Groundwater Potentiality Rank
<1	50	Very High
1 - 2	40	High
2.1-3	30	Moderate
3.1-4	20	Low
>4	10	Very Low

Table 41: Weight Values and Rank of Drainage Density of Dahab Basin

The resulting drainage map is also assigned to five classes by following the same approach used in preparation of the lineament density map. Therefore, each class represents a range in the length of drainage segments per unit area of (km^2). These classes are ordered as: < 1, 1–2, 2.1–3, 3.1–4 and > 4 km/ km^2. Each class gets a rank according to the weight value (Musa et .al., 2005) and its contribution for groundwater occurrence. The high density class takes a very low rank while the low density area gets a very high rank grade (Table 41 and fig. 170-D). Drainage density factor is desginated a weight of 10 in the model.

5.2.2.5 Topography factor (Elevation and Slope)

Topographic data is one of the important elements in determining the water table elevations (Sener et al., 2005). The combination of fractures with topographically low ground can also serve as the best aquifer horizon. Generally, flat and gently sloping areas promote infiltration and groundwater recharge, while steeply sloping grounds encourage runoff resulting in little or no infiltration.

In mountainous regions, there is a high flow of energy where water is often diverted into channels (i.e. runoff), maximizing the overland flow. This in turn will minimize the degree of groundwater recharge (Doll et al., 2002), because water flow will be restricted to streams, feeding groundwater only from the interflow process. While in relatively gentle sloping terrains, the overland flow distributes over a large area and the degree of recharge would be much more. Therefore, groundwater potentiality is expected to be greater in the flat and gently sloping area (Solomon, 2003). Flatter topography will then give more of chance for groundwater accumulation.

In this study, a digital elevation model with spatial resolution of 30 m (ASTER version) is used to generate the topographic elevation and slope degree layers. Values of slope angle are calculated as first derivatives from the DEM. The slope classification map is comprised of five classes for Dahab basin, which are less than 2°, 2-8 °, 8-15 °, 15-30 ° and 30-68 ° (fig. 170-E). The maximum slope terrain is 68%. Van Engelen and Wen (1995) classified slopes into five classes. Musa et al. (2006) put weight values on slope depending on their contribution in groundwater occurrence. Typically, a steep area points to increase the energy of water flow within a stream and the possibility of groundwater recharge should be low. On the other hand, the gentle slope area signifies to decrease the water flow and the degree of recharge will be much more. According to the previous conclusion, the steep slope area in Dahab basin will take high rank and flat slope will take very low rank as shown in Table 42.

Slope (Degree)	Score value Musa et al., 2006	Description Van Engelen and Wen, (1995)	Groundwater Potentiality Rank
<2	50	Flat	Very High
2-8	40	Undulating	High
8-15	30	Rolling	Moderate
15-30	20	Moderately Steep	Low
30-68	10	Steep	Very Low

Table 42: Weight Values and Rank of Slope (Degree) of Dahab Basin

The elevation layer influences the occurrence for groundwater in Dahab basin. At elevated land, the loose sediments within stream are rare and their thickness will be very small due to the slope influence. Therefore, the occurrence of groundwater at high land should be small. At the low land, the thickness of alluvial loose sediments will be high and due to slope effect, the possibility of groundwater occurrence is high. It can be seen that 15 wells are dug at the downstream of Dahab basin while about 22 wells are dug at its catchment parts. Due to previous observations, the high elevated land should take low rank for groundwater potentiality while the low land will get high rank for groundwater occurrence (fig. 170-F). For the model, both slope layer and elevation layer are assigned 10 as a weight value.

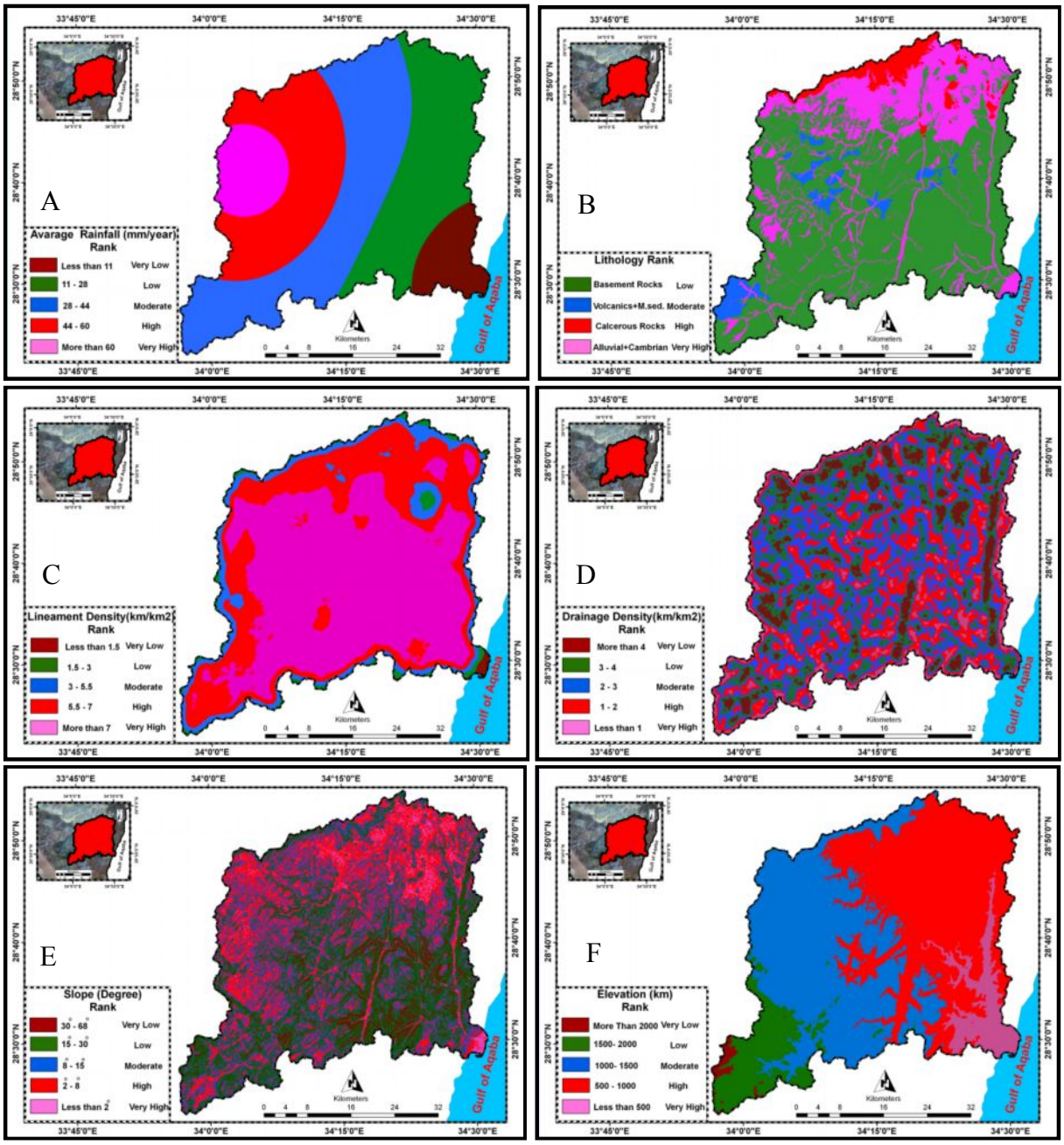

Figure 170 A, B: Average rainfall and Lithology Classification Classes of Dahab basin. C, D: Lineament Density and Drainage Density Classification Classes of Dahab basin. E, F: Slope (Degree) and Elevation Classification Classes of Dahab basin.

5.2.2.6 Method of weighting factors

The five Weighted Spatial Probability Model (WSPM) classes, each including the determining factors discussed in the previous sections, are ranked according to their magnitude of contribution to groundwater entrapment; thus, they are categorized from very high to very low contribution, and the same classes are used in groundwater potentiality mapping (Table 43). The philosophy of data manipulation implies integrating all factors as thematic layers. Accordingly, an output map contains a

number of classes indicating the categories of groundwater potentiality e.g. very high, high, moderate, etc.

Data Layer (Factor)	*Rank*	*Average Rank (R)*	*Weight (W)*	*Degree of effectiveness*
Rainfall	very high	90	30 (0.3)	27
	High	70		21
	Moderate	50		15
	Low	30		9
	very low	10		3
Lithology	very high	90	25 (0.25)	22.5
	high and moderate	60		15
	Low	30		7.5
	very low	10		2.5
Lineament density	very high	90	15 (0.15)	13.5
	High	70		10.5
	Moderate	50		7.5
	Low	30		4.5
	very low	10		1.5
Drainage density	very high	90	10 (0.1)	9
	High	70		7
	Moderate	50		5
	Low	30		3
	very low	10		1
Slope	very high	90	10 (0.1)	9
	High	70		7
	Moderate	50		5
	Low	30		3
	very low	10		1
Elevation	very high	90	10 (0.1)	9
	High	70		7
	Moderate	50		5
	Low	30		3
	very low	10		1

Table 43: Ranks and Weights for Factors and Their Influencing Classes Used for Groundwater Potentiality Mapping in Dahab Basin

.

The previously discussed factors do not have the same magnitude of contribution on groundwater potentiality. For example, the factors of rainfall amount are much more effective than lineament density. From this point, the slope and drainage factors, which have two different degrees of influence on groundwater recharge (Horton, 1938), are given the least level of contribution and thus, each factor is assigned a specific weight of effect on groundwater potentiality.

The weights and rates are adopted by the extracted factors from the results of experience of the author with the study area and the knowledge of experts in the previous similar works on groundwater

potentiality mapping e.g.. Edet et al. (1998) and Robinson et al. (1999). The weights and rates are modified based on the magnitude of relations between each layer range of the WSPM classified layers. Therefore, the integrated factors in this study are given the following weights: rainfall (30%), lithology (25%), lineament density (15%), drainage density (10%), terrain slope (10%) and elevation (10%) . In addition to the proposed weighting, categorization is applied to each of the five classes among each factor. For this purpose, the classes range from I (very high potential) up to V (very low potential) in terms of their importance with respect to groundwater occurrence or potentiality (Table 43).

It is considered that the maximum value for the rank is 100% ; thus, for the five classes, ranks will be categorized as 100–80, 80–60, 60–40, 40–20 and 20–0%, respectively. Therefore, the average of ranking for each class will be 90, 70, 50, 30 and 10% for classes from I to V, respectively (Table 43). In order to calculate the degree of effectiveness (E) for each factor (input data layer) from the factor weight (W) and factor rank (R), the weight is multiplied by the rank (W * R). Following this procedure of data manipulation enables evaluation of the effectiveness of each factor; it also provides a comparative analysis between different input data layers.

5.2.3 Result and discussion

The resulting map with five major classes of groundwater potentiality is ascribed from very low to very high potentiality. This is attributed as: < 20% (very low), 20–40% (low), 40–60% (moderate), 60–80% (high) and >80% (very high) for groundwater potentiality (fig. 171).

The produced groundwater potentiality map points to the promising localities for groundwater accumulations which are almost always located at areas where rainfall is relatively high and the surficial outcropped rocks are highly permeable, which are found in the elevated region at the western parts of Dahab basin, especially at W. Saal and W. Rimthy (fig. 171). Regions having very high groundwater potentiality rank cover an area of 55 km^2 representing 2.6% of W. Dahab's total area, whereas regions characterized by very low groundwater potentiality rank cover about 10.3 km^2 area representing 0.5% of W. Dahab's total area. However, the moderate groundwater potentiality rank occupies 43.7% of the mapped area, while the low potentiality rank covers of about 35.5% of Dahab basin area, indicating that the moderate groundwater potentialities dominate Dahab basin (fig.172).

The high groundwater potentiality areas are located mainly at the northern part of Dahab basin. They are found at W. Genah, especially in alluvial deposits and Cambrian rocks. High potentiality areas appears along the main streams of W. Nasab, W. Rimthy and W. Saal where rainfall is high. The moderate potential areas appear mainly in basement rocks upstream of W. Rimthy, W. Saal and some localities of W. Nasab. They are also found downstream of W. Dahab, where the area is characterized by low rainfall and hence, the aquifer recharge mainly depends on the inflow of groundwater from the upstream area.

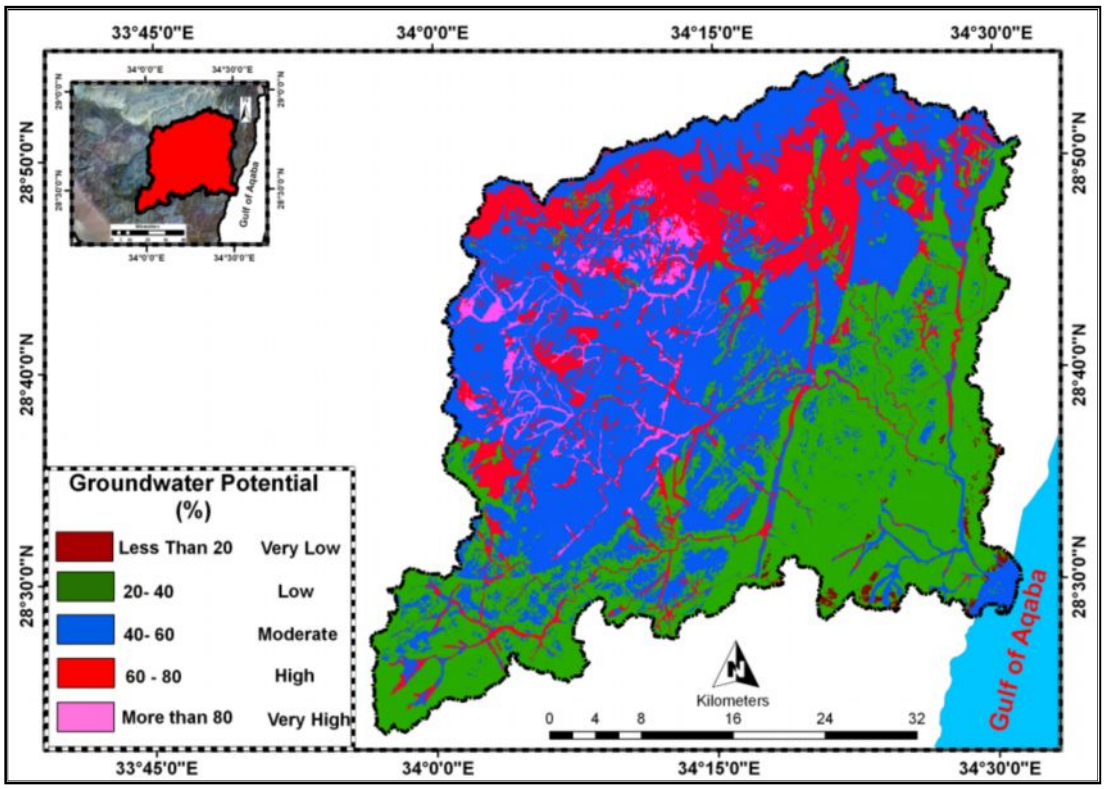

Figure 171: Groundwater Potentiality Map of W.Dahab

The low potentiality areas are found mainly in the basement rocks, especially in the downstream areas of W. Zaghraa, W. Abu Khshieb, W. El Ghaieb and upstream part of W. Nasab. The low fracture density, relatively low amount of rainfall and high drainage density cause low groundwater potentiality of these areas. It is concluded that W. Genah has the most groundwater potentiality which results in low risk of flooding danger. Although W. Rimthy and W. Nasab have moderate to high risk for runoff as shown in fig.171, there are many localities, especially in alluvial deposits at upstream and downstream areas. Some localities in basement rocks have high chance for groundwater accumulations (fig.173).

The evaluation of the groundwater potentiality map is checked against the borehole productivity in the study area, which reflects the overview of groundwater potential. Figure (173) shows that the groundwater potential zones match with the actual working boreholes. This data is obtained during field surveys and some other sources (WRRI, 2006 and El KiKi et al., 1992). Most of the working boreholes are located at zones of high to very high groundwater potentialities. W. Rimthy's wells are located at a zone which ranks high to very high. These boreholes are produced mainly from alluvial aquifers with fractured basement zones. The location near to the upstream sites helps to have good recharge from the rainfall in rainy seasons and hence, good productivity. It is observed on the map that the main stream of W. Rimthy represents an excellent area for groundwater exploration.

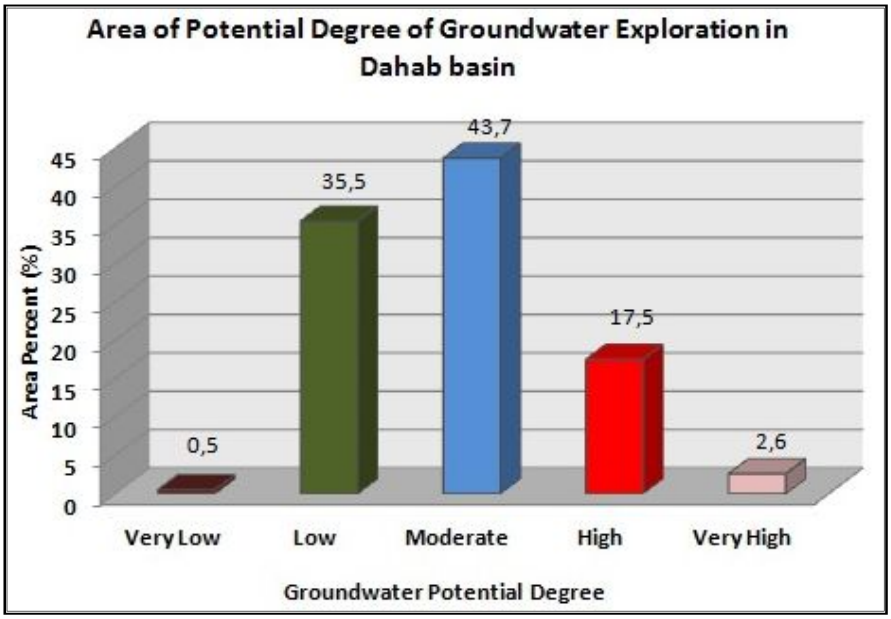

Figure 172: Ratios of Groundwater Potentiality Rank Areas in W. Dahab

Wadi	Well No.	Degree of Effectivness	Potential Degree
Well Nasab	A	46	Moderate
	N8	37	Low
	N9	45	Low
	N1	66	High
	B	64	High
	N10	70	High
	N7	63	High
	N5	66	High
	N11	60	Moderate
	E	68	High
	D	66	High
Well Ramthy	R1	74	Very High
	R2	69	Very High
	R4	75	Very High
	R5	75	Very High
	R6	72	High
Well Saal	S1	74	Very High
	S2	80	Very High
	S6	73	High
	S8	69	High
	S12	68	High
	S9	65	High
	S10	63	High
	S11	58	Moderate
Wadi Genah	Gen1	63	High
Wadi Dahab	D7	62	High
	D11	34	Low
	D5	53	Moderate
	D6	46	Moderate
	D9	55	Moderate

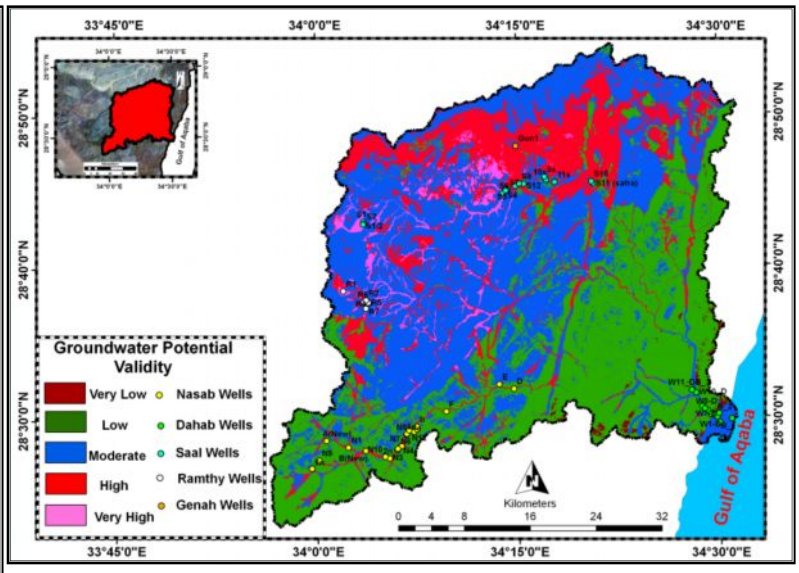

Figure 173: Comparison between Model Results and productive wells in Dahab Basin

At W. Saal, all boreholes are located within the very high to high zone except well S11-safra which is located in the moderately elevated zone and taps a carbonate aquifer. Saal's boreholes along the main stream tap mainly alluvial aquifers while boreholes of the upstreams (S1 & S2) tap basement aquifers. The location of boreholes at the highly elevated upstreams near zones of dense rainfall enhances the recharge of aquifer and reflects the good productivity of these wells. Highly fractured basic rocks in W. Saal with gentle slope in addition to its moderate risk of runoff enhance recharging

of rainwater into the existing aquifer. All these factors nominate W. Saal area as a good area for groundwater accumulation, especially during the rainy seasons.

The northern part of the study area is considered the most promising area for groundwater exploration. Only one well (Gen1) was drilled in this zone during the beginning of field work, but it was noticed that at the last field visit, three wells were drilled near the old one. Gentle slope, low to moderate drainage density and widely spread sedimentary rocks and alluvial deposits help recharge an aquifer. In the future, more wells might be dug in this area.

At W. Nasab, more than 60 % of wells are located at the elevated zone and tap alluvial aquifers. Wells at the upstream area are located in moderately elevated to low elevation zones where they tap fractured basement aquifers. The high elevation zones occur mainly at the main stream of the wadi and at some parts along the upstream area in the Rahabh Plain. The distribution of granitic rocks with low fractured, high drainage density and steep slope, especially at upstream area, cease the recharge of aquifers and increase the runoff and overflow during rainy seasons. It can be concluded that W. Nasab needs a management system for groundwater recharge and protection against flooding risk.

Most of the wells in the downstream area of W. Dahab are found in moderately elevated zones. These wells tap alluvial aquifers. Low lineament density and low rainfall density classify this zone as having low groundwater potential, while low elevation, low drainage density and gentle slope nominate it for good groundwater potentiality, so this area is ranked as a zone of moderate groundwater potentiality. More than 90 % of the wells in this zone are out of work because of the low productivity and lowered water level; some of them are affected by sea water intrusion, especially those at the coastal zone. It can be concluded that this area needs the proposal of a management system to enhance the groundwater recharge in order to increase the groundwater potentiality.

The produced groundwater potentiality map is checked by matching it with the published groundwater potentiality map of Sinai (Elwa and Qaddah, 2011). It is observed that the map has a high degree of confidence. The high potential groundwater zones of the present work are equivalent to the local and high productive wells subjected to occasional surface recharge from rainfall at W. Saal and W. El Genah in the northern part of W. Dahab and some parts along W. Rimthy. The produced map shows that most of Dahab basin falls within moderate to high groundwater potentiality. Thus, the generated map can be used in the future as a preliminary confidential reference map to select sites of promising wells and in land-use planning for groundwater protection.

CHAPTER VI

CONCLUSIONS AND RECOMMENDATIONS

Chapter VI

CONCLUSIONS AND RECOMMENDATIONS

6.1 Conclusion

The Wadi Dahab area is located at the south eastern part of the Sinai Peninsula. It includes five main hydrographic subbasins. The largest one is W. Zaghraa and the smallest is W. South Zaghraa. The main stream of W. Dahab is drained into the Gulf of Aqaba. Stratigraphically, the study area includes basement rocks and phanerozoic rocks. W. Dahab catchments are covered mainly with Precambrian to Cretaceous rocks. Sedimentary rocks of Cambrian to Cretaceous ages are located in the north of the basin, while the rest of the basin is covered by Precambrian rocks (igneous and metamorphic rocks), in addition to recent wadi deposits which cover the valley floors of the main streams.

The satellite image data (ASTER) was used for updating the lithological map of the Dahab basin; maximum likelihood classification (MLC) and band ratio stackings approaches for improving the existing geologic map in the Dahab basin. These methods can be used to improve the geological maps of the southern Sinai Peninsula. The study shows how the approaches of MLC and band ratios succeed through differentiation of the different types of granitoid rocks, metamorphic rocks and Phanerozoic rocks. For checking the quality of the classification map an accuracy assessment was carried out. For this purpose an error matrix was determined which compared the classification map with existing geologic maps. The final geological map of the Dahab basin comprises 19 classes of phanerozoic, metamorphic and igneous rocks. Ring-dykes at W. El Ghaieb, acidic metavolcanics, basic metavolcanics and metasediments at the Wadis Saal, Zaghraa and Rimthy and metasediments at W. Rimthy and Alluvial wadi deposits units are the main rock units which are added in the final lithological map.

Structurally, the area of study is influenced by tectonical processes of Gulf of Aqaba. Mapping of major fault was done by visual interpretation of various digitally enhanced multi band satellite images. More than 350 faults were manually extracted using processed images with different bands. The fault lengths range between 0.6 to 36 km. There are two well-known main trends in the study area including the Gulf of Aqaba fault trend NE-SW strike (54%) and NW-SE direction (33%). The longest fault is recorded along W. Ghaieb with 35 km length while the fault of W. Nasab reaches up to 22 km. The main fault trends are directed to NS, NE-SW and NNE-SSW.

The aim of the analysis of lineaments is to understand the relationship between the lineament trends as the main structural trends and the zones of the high recharge to aquifers. Therefore an automated work flow was used for lineament extraction. Landsat panchromatic image (15m) resolution was prepared to conduct this test under the user defined parameters of Line module of PCI software. The results show that there are six dominating trends in the study area including NNE-SSW,

NE-SW, NW-SE, ENE-WSE, NNW-SSE and N-S. The prominent directions of these lineaments coincide with major structural trends. The density lineament map shows that the high density area is recorded at the basement area (5.5 to 7 km/km^2) especially in the eastern and southern parts of Dahab basin, while the low density area (0.2 to 1.5 km/km^2) is recorded in the northern part of the study area.

Geomorphologically, the study area is subdivided into five geomorphic units including mountainous basement terrain, flat-topped limestone plateau, alluvial fans, coastal plain and drainage network. The denderitic drainage pattern dominates the northern part of the study area at W. El Genah and it occurs in local parts of W. Nasab and in the western part of Dahab basin. The rectangular drainage pattern reflects the faults pattern which is distributed in different subbasins within the Dahab basin as in W. Saal subbasin and some tributaries of W. Nasab. The trellis pattern reflects the homogeneity of rock types and dominates in the watersheds of W. Nasab, W. Rimthy and W. Saal.

GIS techniques were used to extract stream network parameters, with emphasis on ordering and measuring the length of each stream segment using an automated workflow, basin delineation and also to produce a flood hazard risk map based on the results of the morphometric analysis. A code of Visual Basic code was implemented to solve the numbering of stream orders based on the Strahler theory, whereas the Python model was applied to build attribute table including morphometric data for each subbasins.

174 sub-basins in Wadi Dahab were delineated based on their nested hierarchy. Quantitatively, six morphometric maps showing the distribution of stream frequency, stream density, bifurcation ratio, elongation ratio, circularity ratio and overland flow were constructed for the studied basin. The high risk basins having high stream frequency and high stream density values tend to collect more runoff water, which increases the rate of flow discharge out of the basin. In high risk basins, the bifurcation ratio will also be low and they have high circularity and elongation ratios (Rc and Re). Circular basins are also more susceptible to flash floods. By an overlaying of the above mentioned morphometric maps, the risk zones were recognized.

The flood hazard risk map shows that 34% of the total sub-basins in the Dahab basin have a high flooding risk level. 60% of all sub-basins have medium flooding risk level, which includes the Dahab mega-basin. Only a few of the sub-basins have low flooding risk susceptibility. The high risk zones are concentrated in three zones. The first zone is W. Zaghraa-Nasab which has two main subbasins (Wadi Nasab and W. Rimthy). The second zone belongs to the headwater parts of W. Abu Khshieb and the last zone includes different subbasins at the headwater part of W. El Ghaieb. W. El Genah and W. Saal are ranked as moderate to low levels of flooding risk.

Hydrogeological cross sections were drawn along the main streams of W. Nasab, W. Saal and in the downstream area of W. Dahab. The cross-section shows that the unconfined aquifer is the main water-bearing formation of Dahab basin. The unconfined aquifer is differentiated into an alluvial aquifer and a fractured basement aquifer. The unconfined aquifer is divided into three main zones: the first one is the dry top zone which consists of sand, silt and gravels and has thicknesses ranging from 1

to 17m at the catchment zones, while it reaches up to 22m in the downstream area of the Dahab basin. The second one represents the water-bearing zone; it is composed of alluvial sands and gravels in addition to the underlined weathered basement rocks. This zone also includes the highly fractured basement rocks whose thickness ranges between 17 and 30 m. It has about 60 m thickness in the downstream area of W. Dahab. The third zone represents a dry zone at the headwater of W. Dahab basin composed of slightly fractured granitic and volcanic rocks. At the downstream of Dahab basin, the third zone is not fully penetrated by wells, it is composed of alluvial sand with weathered rocks and it produces saline water as found in some wells.

At upstream boreholes, the water level is affected by topographic and structural parameters of the basement rocks where the depth to water ranges between 6 to 35m from the ground surface. Many boreholes have been located at the contact zone between the dykes and basement rocks. At the downstream areas, water depth has a range between 35 to 60m from the ground surface. A low rate of the groundwater recharge in these wells and increasing water pumping are the main reasons for the lowering of the water table and they increase the water salinity in all of downstream wells.

The hydraulic conductivity of the Quaternary deposits was determined by infiltration tests at seven locations within Dahab basin. The results show that the hydraulic conductivities vary between 0.011 cm/ min to 0.25 cm/min. The hydraulic conductivity is increased at the headwaters of W. Rimthy and W. El-Ghaieb, where it ranges between 0.18 to 0.25 cm/min or about 2.5 to 3.6 m/day while at W. Nasab, the hydraulic conductivity decreases to 0.02 cm/min or about 0.2 m/day. The values of the hydraulic conductivities decrease in the downstream areas where they range from 0.011 to 0.4 cm/min (0.15 to 5 m/day) due to the fine sediments in the soil.

The basement rocks cover about 70% of the total area of the Dahab basin which represent the main receptor of the rainfall. Due to their low hydraulic conductivity, there is a high possibility of runoff. Then, the determination of the hydraulic conductivity of the basement rocks is an important factor for the groundwater recharge especially in the areas of high flooding risks.

The hydraulic conductivity of fractured basement rocks was estimated using the deterministic district fractured network (DFN) method (Zeeb et al. 2010). Four selected areas were used as reference sites at the headwater of W. Nasab. The results of the hydraulic modeling of DFN show that the hydraulic conductivities range between 2.3×10^{-7} to 6.1×10^{-7} m/s. The estimated average hydraulic conductivity values at the four reference sites amount to 4×10^{-7} m/s (2 mm/hr). The water flow through the fractures is strongly controlled by the main orientation of the structural lineament of W. Nasab (NNE-SSW and NE-SW). The average hydraulic conductivity of fracture basement rocks governs, besides other factors, the calculation of the total loss of rainfall. It can be concluded that the fractured basement of W. Dahab Basin has a capability to recharge of about 43 million m^3/day.

Hydrochemically, the analyses of the water samples showed that most of the water out of wells located within the fresh water range represents good potable to fairly fresh groundwater. Some of

water samples out of wells consist of brackish to slightly brackish groundwater. Two wells at the downstream of Dahab basins deliver saline water.

Wells of the study area are grouped into four groups based on their hydrochemical patterns.

1- A group "A" which is represented by $HCO_3 > SO_4 > Cl$ pattern.

2- A group "B" which is represented by $HCO_3 > Cl > SO_4$ pattern.

3- A group "C" which is represented by $Cl > HCO_3 > SO_4$ pattern.

4- A group "D" which is represented by $Cl > SO_4 > HCO_3$ pattern.

At W. Nasab, bicarbonate ions increase in the recharge areas with dominant calcium ion in groups A & B. Groundwater facies change to increase the chloride ion over bicarbonate in group C, and finally facies change to chloride-sulphate over bicarbonate toward the discharge area and are impacted by the local cultivated area around wells of group D. At the upstream of W. Saal and W. Rimthy, the anion pattern is mainly $Cl > SO_4 > HCO_3$ while the cation pattern is Ca >Na>Mg which referred to group D. It is characterized by the presence of dykes, shallow wells and increased evaporation rates. The increase of the concentration of sulphate ion is due to the presence of sulphide minerals in the wadi, while the groundwater facies changes into Na >Ca>Mg type due to the impact of the long flow path (Group D) in the downstream area of W. Saal,

At the downstream area of Dahab basin, chloride, sulphate and calcium are highly dominant ions in the groundwater of the basement aquifer. In contrast, chloride, bicarbonate and calcium concentrations are dominating ions in the groundwater of alluvial aquifers in the same area. The pattern of the groundwater facies is changed from chloride – calcium in upstream areas of the Dahab basin to chloride – sodium facies due to the impacts of the long flow path and sea water intrusion at the coastal zone of the basin.

The chemical analyses show that most of the dissolved ions in groundwater originate mainly from weathering of rocks forming minerals (Gibbs, 1970). The dissolution of silicate minerals such as feldspar and mica are the main sources of cations in the groundwater of the study area. Silicate minerals, which are distributed in the basement rocks or in alluvial deposits as weathered material are strongly influenced by dissolution processes.

Heavy metals were investigated in 29 wells in both rainy and dry seasons. The concentration of heavy metals changed with different seasons. Ni, Cr, Zn and Cd increase in concentration while Fe , Mn are not detected during the rainy season. During the dry season, the concentrations of Fe and Mn increase and other elements decrease. The reason of changes in the concentration is the different hydrogeochemical behavior of heavy metals dissolved in groundwater depending on the oxidation state of the medium.

The analysis shows that some substances such as NO_3, F, U, B and As affect human health if they have concentrations beyond certain levels. The concentrations of such elements are compared with the standard concentration for drinking water (WHO, 2006). Due to the dangerous effect of these substances in human and animal health, the wells delineations for safe drinking water in the study area

were specified. It can be concluded that W. Nasab wells N1, B, N3, N6, N10, N5 and N7, W. Saal wells S4 and S6 and well (G2) at W. El Genah are suitable for drinking purposes, while wells S7, S8 and S13 at W. Saal and wells R2, R4 and R5 at W. Rimthy are of moderate suitability for drinking although they have a high uranium content. Wells in the downstream area of Dahab basin, wells S1, S2, S1/2, S9, S10, S11 and S12 in W. Saal and the well R1 at W. Rimthy are unsuitable for drinking purposes.

Dahab basin is vulnerable to occasional heavy rainstorms causing dangerous flash floods. It was observed that the highest records occur in the autumn period during September- November. The availability of long time records of the maximum storm at Saint Catherine station from 1934 to 2004, made it possible to study the probability of the repetition of a maximum storm using the Gumbel method. The results show that the maximum rainstorm of 76.2 mm/day may be repeated within a period of more than 180 years. The lowest rainstorm of 10mm may be repeated within a period of 3 years with a probability of 50%. The moderate rainstorm of 45 - 55 mm/day may be repeated within a period of 25 to 50 years with a probability of 1 to 2%.

The evaporation rate constitutes one of the loss factors which determine rainfall excess. The mean daily evaporation rate was calculated for rainy months at W. Dahab. The average daily evaporation decreases at Saint Catherine for about 7.68 mm/day, while it increases at Nuweiba to about 11.6 mm/day. The average daily evaporation rate ranges between 5.8 and 7.2 mm/day in January and December and between 16.2 and 11.08 mm/day in October and March.

The Synthetic unit hydrograph is the most important tool to measure the degree of the flooding risk of the ungaged basins. Two main approaches were used to derive synthetic hydrograph from topographic information. The results show that W. Zaghraa has the highest risk in W. Dahab because it has the highest volume, highest peak discharge and moderate time to peak. W. Abu Khshieb is considered as a moderate risk subbasin due to a moderate value of peak discharge, a low time to peak of 12 hr and a low runoff volume at maximum storm. The W. El Ghaieb subbasin is assessed as a low risk subbasin due to its moderate peak discharge, its relative long duration to peak with moderate to low volume of about 12 Mm^3.

W. Rimthy is considered the highest risk sub catchment in W. Zaghraa because it has an average peak discharge of 200 m^3/s, a short time to peak is of 18 hr and a moderate runoff volume in maximum storm, while at W. Nasab it is assessed as moderately risk due to its moderate average peak discharge of 130 m^3/s, moderate runoff volume and relative long time to peak of 26 hr at maximum storm. W. Saal is a moderately risk subbasin because it has a relatively low value of average peak discharge, relative long time to peak and low runoff volume of about 9.8 Mm^3 at maximum storm. It can be concluded that the wadi path W. Rimthy-W. Zaghraa Nasab – W. Zaghraa is the highest risk route because it directly affects directly the downstream part of Dahab basin.

The sedimentary rock cover area has a relatively low slope value and the smallest average flow velocity in the area under investigation. These factors are the main reasons for decreasing the runoff

risk in the northern part of Dahab basin compared with the southern part. Accordingly, the northern part of the basin area has good groundwater potentiality especially at W. El Genah, W. Saal and the Northern part of W. El Ghaieb areas.

The existing dams in the study area were investigated to test their efficiencies using GIS Tools and field visits. Six constructed dams have a total capacity of 1.5 Mm3. These dams were constructed by WRRI (2006) in W. El Ghaieb, W. Saal and W. El Genah in order to protect the main road between Dahab city and Nuweiba. Some of these dams have been subjected to little damage and some of them are subjected to water overflow during storm events. This is due to the improper dam sitting and the weakness of the dam body.

A new protection system is proposed to upgrade the current protection level and increase its storage efficiency in order to protect the local inhabitance (Bedouins) and main infrastructures in Dahab basin against floods and to enhance groundwater recharge into the alluvial aquifer along the main streams. This system is suggested at the risky subbasins such as W. Rimthy, W. Nasab, W. Saal and W. Abu Khshieb.

At W. Nasab, water management design was applied to mitigate floods, prevent soil erosion and to increase the yield of water sources. Three management tools were proposed, the first tool is represented by seventeen cisterns to be constructed at the upstream area of the basin, especially in the southern catchments to control and store flood water of up to 400 m^3 for each one, so the total capacity of these cisterns amount to about 6800 m^3. The second tool is represented by six storage dams which are proposed to be constructed along the main stream of W. Meer, W. Fierani, W.Rasies, W. Nabaa, W. El Shalal and W. Small Nasab, so the total capacity of these dams is about 1.8 Mm^3. The third tool is represented by mitigation canals at the downstreams of W. Rasies, W. El Shalal, W. Small Nasab and the main stream of W. Nasab to absorb the excessive runoff water and to recharge the unsaturated zone of the alluvial deposits along the main stream of W. Nasab. The surface storage capacity of these canals is about 4.8 Mm^3, and it will recharge the aquifer by about 85000 m^3, so the total capacity reaches about 5 Mm^3.

The same design is proposed at W. Saal basin; twenty one cisterns should be constructed at the upstream with a total capacity of about 8400 m^3. Five storage dams are proposed with total storage capacity of 426500 m^3 at the main stream of W. Saal, W. Mytorah and W. Tyinah. Two mitigation canals are suggested along the main stream of W. Saal and downstream of the same wadi with a total storage of about 1.7 Mm^3.

A different protection system was suggested at W. Rimthy and W. Abu Khshieb. The plan depends on small storage dams and cisterns while the construction of a mitigation canal is not considered due to the shortage of aquifer characteristics data in both wadis. At W. Rimthy, eight storage dams were proposed along the main stream of wadis Merkh, Um Retm, Um Saial, Sanad, Maraan, Mekaffa and downstream of W. Rimthy with total storage capacities of 1.5 Mm^3. It is proposed to build 41 cisterns with a total storage capacity of about 16400 m^3. Additionally, 20 small

dams should be constructed to support the storage dam with a total storage of 56000 m^3. Seven storage dams, 9 small dams and 16 cisterns have been suggested to be built up for the protection in W. Abu Khshieb with total storage capacities of about 460000 m^3.

At W. Nasab, the total capacity of the old design (existing dam) is 90000 m^3 which represents an efficiency of about 0.5% of the maximum rainstorm (76.2 mm - >180 year). The present proposed design will increase the storage capacity up to 6.9 Mm^3, so the total capacity of the proposed design and the old design together is about 7 Mm^3 with an efficiency of 43% of the maximum rain storm. At W. Saal, the total capacity of the old design is 70000 m^3 with an efficiency of about 0.7% of the maximum rainstorm. The present additional design will increase the storage capacity up to 2.2 Mm^3 with protection efficiency of 24% of the maximum storm. No protection plan is proposed at W. El Ghaieb and W. El Genah due to low flood risk. The existing dams at W. El Ghaieb are designed for the protection of the main road with a storage capacity are about 1.2Mm^3 and an efficiency of about 10 % regarding the maximum storm.

An integrated approach using GIS and remote sensing was adopted to find new potential sites for groundwater exploration in Dahab basin. A weighted overlay was implemented using six different effective weighted parameters including; annual rainfall, lithology, lineament density, topography, slope and drainage density. The final map of groundwater potential shows that about 19.5% of W. Dahab is classified as high potential areas. These areas are concentrated at the northern part of the study area at W. El Genah, W. Saal and W. Rimthy and some parts along the main stream of W. Nasab and W. Zaghraa. Furthermore, about 40% of the study area has only a low potential for groundwater exploration. These areas are located in the southern and eastern part of W. Dahab, where the basement rocks are outcropping.

Most of wells in use are located in zones of high to very high groundwater potentialities. Groundwater wells in W. Saal and some in W. Nasab are located within the very high to high zone and tapping alluvial aquifers. Most of the wells at the downstream of W. Dahab are found in moderately potential zones. These wells are out of work because of the low productivity and the drop of the groundwater level. Some of them are affected by sea water intrusion especially those at the coastal zone. The northern part of the study area is assessed as the most promising area for groundwater exploration.

6.2 Recommendations

To protect the area of W. Dahab from flash floods and to enhance aquifer recharge, the following recommendations should be taken into consideration:

1- Remote sensing is a very helpful technique to update the geological maps and extract structure lineaments. This technique is useful in areas which are sparsely covered by desert vegetation and where rock dominates the appearance of landscape. It is recommended to use remote sensing data in similar regions in Egypt's Eastern desert, Southern Sinai and the western part of Saudi Arabia.

2- Protection measures for the W. Dahab Delta should be applied at the headwater area of the wadi. Hence the study concentrated on locating the effective sites at the headwater area which contribute to the main channel of the wadi.

3- The shortage of historical climate data in the study area limits the use of hydrological models. It is recommended to establish new meteorological stations within Dahab basin along a grid where each station should serve an area of about 50 km^2. In addition, should be setup a regional data base for wadi hydrometeorology from the historical available data sets in Arab and neighboring countries.

4- The estimation of hydraulic conductivity of fractured basement rocks through satellite data is considered a new method to investigate the recharge rate of the rainfall receptor rocks in the study area. Pumping tests should be conducted to evaluate the extracted results. This method is very promising in areas which have scarce grass coverage as in the Sinai and Arabian Peninsula.

5- One of the important problems facing the study is the inability to validate the results of the hydrological modeling. This is due to the lack of monitoring stations for measuring the discharge of surface water flow along the course of the wadis. Therefore, it is recommended to establish extra monitoring stations for measuring the hydrological parameters, especially along the path of the risky wadis such as W. Rimthy, W. Nasab, W. Abu Khshieb and W. Saal.

6- The high salinity of groundwater at downstream of Dahab basin may result from the impact of sea water intrusion. Groundwater modeling techniques should be applied and a monitoring system should be set up to provide a quantitative evaluation of the water budget of the aquifer as well as to test various hypotheses about recharge and discharge rates. The model can be used to find a solution to the increasing salinity in all wells in this province.

7- A monitoring system should be established to detect the possible natural contaminants such as Boron, Arsenic, Fluorine, Uranium and the agricultural contaminants which may be leached from the soil of the agricultural areas such as nitrate and pesticides. In addition, biological examination of the groundwater should be used to monitor the possible contamination from the wastewater disposal system.

8- The map of groundwater exploration could be used in the future as a preliminary reference in selecting well sites and in land-use planning. It is recommended to drill new groundwater wells in the northern part of Dahab basin, at the headwater zones of W. Nasab and W. Rimthy.

9- Implementing commonly used structures such as cistern, small dams and mitigation canals are highly necessary in order to store surface water. The use of these structures, to augment the floodwater is of prime importance in the sustainable development strategy of Sinai.

REFERENCES

Reference

Abdallah, A. M. and Adindani, A. (1963): Stratigraphy of Upper Paleozoic rocks, western side of Gulf of Suez. Geol. Surv. Egypt, Pap. v.25,18p.

Abdeen, M. M., Allison, T. K., Abdelsalam, M. G. and Stern, R. J. (2001): Application of ASTER band-ratio images for geological mapping in arid regions; the Neoproterozoic Allaqi Suture, Egypt. Geological Society of America, v. 3(3), p.289.

Abu El Leil, I., Hassan, M. M., Abdel Tawab, M. M. and Abdel Rahman, H. B. (1990): Geological and Geochemical studies of the Feirani Group; The proposed late Proterozoic younger volcanic rocks, Sinai, Egypt. Mineral, v. 2, p.61-80.

Acworth, R. I. (1987): The development of crystalline basement aquifers in a tropical environment. Q. J. Eng. Geol. London. v. 20, p. 265-272.

Adepoju-Bello, A. A., Ojomolade, O. O, Ayoola, G. A and Coker, A. A. B. (2009): Quantitative analysis of some toxic metals in domestic water obtained from Lagos metropolis. The Nig. J. Pharm., v.42 (1), p.57-60.

Ahrens, C.D., (2003): Meteorology Today: An Introduction to Weather, Climate, and the Environment. Brooks/Cole, Thomson Learning.

Ajward, M. H. (1996): A spatially distributed unit hydrograph model using a geographical information system. Ph.D. diss. Civil Engineering Dept., University of Calgary, Calgary.

Akaad, M. K. and El Ramly, M. F. (1960): Geological history and classification of the basement rocks of the Central Eastern Desert of Egypt. Geol. Surv. Egypt, p. 9-24.

Akaad, M. K and Noweir, A. M. (1980): Geology and lithostragraphy of the Arabian Desert orogenic belt of Egypt between latitudes 25o 35′ and 26o 30′ N, Institute of Applied Geology Bulletin, Jeddah 3, p. 127–136.

Akl, M. T. (1994): An approach to the morphometric analysis of wadi Tayyibah drainage basin through using geographic information systems (GIS), Menoufia University, Faculty of Arts. Journal, v.19, p.91-146.

Al Saud, M. (2008): Using ASTER images to analyze geologic linear features in Wadi Aurnah basin, Western Saudi Arabia. Submitted to the Open Remote Sensing Journal. v.74, p.1089–1100.

Al Ahmadi, M. E and El Fiky, A.A. (2009): Hydrogeochemical evaluation of shallow aquifer of wadi Marwani, western Saudi Arabia. Journal of King Saud University, v.21, p.179-190.

Aller, L., Bennett, T., Lehr, J. H. and Petty, R. J. (1985): DRASTIC: A standard system for evaluating groundwater pollution potential using hydrogeologic settings. EPA/600/2-85/018, R.S. Kerr Environmental Research Laboratory, U.S. Environmental Protection Agency, Ada, Oklahoma.

Al-Wagdany, A. S., and Rao, A. R. (1998): Correlation of the velocity parameter of three geomorphological instantaneous unit hydrograph models. Hydrol. Process., v.12, p.651-659.

Alyaamani, M. S., and Hussein, M. T. (1995): Hydrochemical study of groundwater in recharge area, Wadi Fatimah basin, Saudi Arabia. Geo Journal, v.37.1, p.81-89.

Apodaca, L. E., Jeffrey, B. B., and Michelle, C. S. (2002): Water quality in shallow alluvial aquifers, UpperColorado River Basin, Colorodo. Journal of the American Water Resources Association, v.38, p.133–143.

Ashmaway, M. H, Swedan H. A. and AbdelFattah, T. (2000): Flash flood hazards of drainage basins of Sinai Peninsula, Egypt. Ann Geol Sur Egypt. v.23, p.467-489.

Ashour, M. (2002): Flash flood in Egypt- A case study of Durunka village – upper Egypt, Soc., geog. Egypt, vol. 75.

Awad, A (1952): A new type of desert cuesta in Central Sinai, Proc. 27th intl. Geographical Congress, Washington. p. 126-131.

Baharuddin, T. M., Tjahjanto, D., Othman, A. R., Ab. Latiff, A. A., Masiri, K. and Wong, W. C. (2006): Application of geographic information system (GIS) in demarcation groundwater potential zones, National Conference – Water for Sustainable Development Towards a Developed Nation by 2020, 13-14 July 2006, Guoman Resort Port Dickson.

Baker, V. R. (1977): Stream-channel response to floods, with examples from Central Texas. Geological Society of Amerika, Bulletin., v.88, p.1057-1071.

Bartov, T. and Steintiz, G. (1977): The Judea and Mount Scopus Group in the Negev and Sinai with trend surface analysis of the thickness data. - Israel J. Earth Sci. v.26, p.119-148.

Bayer, H., El-Isa, Z., Ringle, K. and Saffarini, Gh. (1988): Tensional and strike slip tectonics in the Karak area (SE Dead Sea region)- results from tectonics and photogrammetric investigations, N. Jb. Palaont. Mh., H. v.4, p. 223-232.

Bedell, R.L. (2001): Geological mapping with ASTER satellite: new global satellite data that is a significant leap in remote sensing geologic and alteration mapping. Special Publication, Geo. Soc. of Nevada. v. 33, p.329–334.

Behera, R., Kumar, A. and Singh, J. K. (2008): GIUH Model for Runoff Estimation from a Small Hilly Watershed. IE(I) Journal–AG. v. 89, p. 17-21.

Ben Zvi, A and Shentsis, 1 (2000): Runoff events in the Negev, Israel. Proceedings of the Jerusalem Conference. IAHS Publ. no. 261

Bentor, Y. K. (1985): The crustal evolution of the Arabo-Nubian Massive with special reference to the Sinai Peninsula. – Precambrian Research, v.28, p.1–74.

Bentor, Y. K. and Eyal, M. (1987): The Geology of Southern Sinai, Its Implication for the Evolution of the Arabo-Nubian Massif. Israeli Academy of Sciences and Humanities, Jerusalem. 484 p.

Bentor, Y.K. and M. Eyal (1979): History of Precambrian massif of Sinai Peninsula, Egypt. – Geol. Soc. Am. Abstr. Progr., v.2, 387 p.

Bergström, S. and, Graham, L. P. (1998): On the scale problem in hydrological modeling. Journal of Hydrology, v.211, p.235–65.

Beven, K. J. and Kirkby, M. J. (1979): A physically based, variable contributing area model of basin hydrology, Hydrolological Sciences Bulletin, v.24, p.43–69.

Beven, K. J., Wood, E. F., and Sivapalan, M. (1988): On hydrological heterogeneity – catchment morphology and catchment response, J. Hydrol., v.100, p.353–375.

Blum, A. E. and Stillings, L. L. (1995): Feldspar dissolution kinetics, in A.F.White & S.L.Brantley (eds.) Chemical Weathering Rates of Silicate Minerals: 291-346 Washington, D.C.:Mineralogical Society of America.

Blum, P., Mackay, R., Riley, M. S. and Knight, J. L. (2005): Performance assessment of a nuclear waste repository: upscaling coupled hydro-mechanical properties for far-field transport analysis. Int J Rock Mech Min Sci, v.42 (5-6), p.781-792.

Bonnet, E. O., Bour, N. E., Odling, P., Davy, I., Main, P. and Cowie, B. Berkowitz (2001): Scaling of fracture systems in geological media: Reviews of Geophysics, v. 39, p. 347-383. doi:10.1029/1999RG000074

Bricker, O. P. and Jones, B. F., (1995): Main factors affecting the composition of natural waters. In: Salbu, B., Steinnes, E. (Eds.), Trace Elements in Natural Waters. CRC Press, Boca Raton, FL, 1-5.

Brutsaert, W. (2005): Hydrology : An Introduction. Cambridge, Cambridge University Press.

CEOS. (2003): The use of earth observing satellites for hazard support: assessments and scenarios, final report of the CEOS Disaster Management Support Group (DMSG). Helen M. Wood, Chair. National Oceanic and Atmospheric Administration (NOAA) United States Department of Commerce

Chebotarev, I. (1955): Metamorphism of natural waters in the crust of earth. Geochem. Cosmochem. Acta, v. 8, p. 137-179.

Chow, V. T., (1959): Open-channel hydraulics: New York, McGraw- Hill Book Co., 680 p.

Chow, V. T., Maidment, D. R. and Mays, L. W. (1988): Applied hydrology. New York: McGraw- Hill.

Clark, R. N., Swayze, G. A., Wise, R., Livo, K. E., Hoefen, T. M., Kokaly, R. F. and Sutley, J. S. (2007): USGS Digital Spectral Library splib06a, U.S. Geological Survey, Data Series 231

Clarke, J. I (1966): Morphometry from Maps. Essays in Geomorphology. Elsevier Publ. Co., New York, p. 235-274.

Cleveland, T. G., Thompson, D. B., Fang, X. and He, X. (2008): Synthesis of unit hydrographs from a digital elevation model. Journal of Irrigation and Drainage Engineering v.134 (2), p. 212–221.

Congalton, R. G., (1991): A review of Assessing the Accuracy of Classification of Remotely Sensed Data. Remote Sens. Environ. v.46. p. 35-46.

Cook, M. E. and Morrow, H. (1995): Anthropogenic sources of cadmium in Canada. In National workshop on cadmium transport into plants, Canadian Network of Toxicology Centres, June 20-21, 1995. Ottawa, Ontario, Canada.

Cooke, G., Warran, A. (1973): Geomorphology in deserts, Batsford, London, 394 p.

Cunderlik, J. M. and Burn, D. H. (2002): Analysis of the linkage between rain and flood regime and its application to regional flood frequency estimation. J Hydrol. v.261(1–4), p.115–131.

Dames and Moore (1983): Sinai development study, phase I, water supply and costs. Final report, Vol.V, submitted to the advisory committee for reconstruction. Ministry of Development, A.R.E. L

Danin, A., (1983): Desert Vegetation of Israel and Sinai. Cana Publishing House, Canada.

Datta, P. S. and Tyagi, S. K. (1996): Major ion chemistry of groundwater in Delhi area: Chemical weathering processes and groundwater flow regime. J. Geol. Soc. of India, v.47, p.179-188.

Davis, N. S., Whittemore, D. O. and Martin, J. F. (1997): Uses of Chloride/Bromide Ratios in studies of Potable Water. Groundwater, v. 36, No. 2, p.338-350.

Devore, J. L. (2000): Probability and Statistics for Engineering and the Sciences, Duxbury, Pacific Grove, CA.

Dingman, S. L. (2002): Physical Hydrology, 2nd ed., Prentice-Hall, 646p.

Doll, P., Lehner, B. and Kaspar, F. (2002): Global modeling of groundwater recharge. 399 Proceedings of 3rd International Conference on Water Resources and the Environment Research, vol 1. Technical University of Dresden, Germany, p. 27–33.

Driscoll, F. G. (2003): Groundwater and wells. Johnson Screens, St. Paul, Minnesota, 1089p.

Drury, S. A., (1987): Remote sensing of geologic structures in temperate agriculture terrains. Geological Magazine. v.123, p.113–121**.**

Eastman, J. R. (1995): Eastman, IDRIS for Windows, User's Guide, Clark University, Worcester, MA, USA, 405p.

Edet, A., Okereke, S., Teme, C. and Esu, O. (1998): Application of remote sensing data to groundwater exploration: a case study of the Cross River State, southeastern Nigeria. Hydrogeol J., v. 6(3), p.394–404.

EGSMA (1994): Egyptian Geological Survey and Mining Authority. Geologic map of Sinai, Arab Republic of Egypt. Sheet No.1, Scale 1:250.000.

El Asmar, H. M. (1997): Quaternary isotope stratigraphy and paleoclimate of coral reef Terraces Gulf of Aqaba, South Sinai, Egypt. Quat. Sci. Rev. London,UK., v.16, p. 911-924.

El Gaby, S. (1975): Petrochemistry and chemistry of some granites from Egypt: Neues Jahrbuch fur Mineralogie-Monatshefte, v. 124, p. 147–189.

El Gharabawi, R. I. and Hassen, I. S. (2001): The Late Precambrian Metagabbro-Diorite Complex, Wadi Melheg Area, Southeastern Sinai, Egypt: An Active Continental Margin Setting. Annals Geol. Surv. Egypt, v. xxiv, p. 131- 158.

El KiKi, M. F., Eweida, A. E., El Refeai, A. A. (1992): Hydrogeology of the Aqaba Rift Border Province, Proc. 3rd Conf. Geol. Sinai Develop, Ismailia, p. 91-100.

El Masry, N. N. (1991): Geological studies of paleovolcanics and volcanoclastics of Saint Catherine mountain area, South Sinai, Egypt, M.Sc. Thesis. Faculty of Science. Suez Canal Univ., Ismailia. 128 p.

El Masry, N .N. (1998): Geology of Extrusive and Intrusive rocks of Ferani area, Southern Sinai, Egypt. PhD. Thesis, Suez Canal University, Ismailia, 206p.

El Masry, N. N., Hassen, I. S. and Hegazi, A. M. (2003): A Newly recognized example of a Late Precambrian subsurface cauldron subsidence intrusion in Southern Sinai: Jabal Laiq ring dyke. 5th International Conference on the Geology of the Middle East, p.549-558.

El Morsy, M. M. (1988): Geological studies of paleovolcanics and volcaniclastics of Saint Catherine mountain area. South Sinai, Egypt. M.Sc. Thesis, Faculty of Science, Suez Canal University, Ismailia, 128 p.

El Ramly, M .F. (1972): A new geological map for the basement rocks in the Eastern and south-western Desert of Egypt, 1:1000,000. Ann. Geol. Surv. Egypt, v.II, p. 1-15.

El Shafei, M. K., Khawasik, S. M. and El Ghawaby, M. A. (1992): Deformational styles in the tectonites of Wadi Sa`al area, south Sinai. Proc. 3rd Conf. Geol. Sinai Develop., Ismailia, Egypt, p.1–8.

El Baz, F. (1992): Preliminary observations of environmental damage due to the Gulf War. Nat Resour Forum. V.16(1), p.71–75.

El Baz, F., Himida, I., Kusky, T. and Fielding, L. (1995): Research project. Groundwater potential of the Sinai Peninsula, Egypt. United States Agency for International Development, Cairo, Egypt.

El Naqa, A., Hammouri, N., Ibrahim, K. and El-Taj, M. (2009): Integrated Approach for Groundwater Exploration in Wadi Araba Using Remote Sensing and GIS. Jordan Journal of Civil Engineering, v.3, No. 3.

El Rayes, A. (1992): Hydrogeological studies of Saint Katherine area, South Sinai, Egypt. M.Sc. thesis, Suez Canal Univ., Ismailia Egypt, 95p.

El-Rayes, A. (2004): Use of lineament analysis and joint measurements as guides for drilling high yield water wells in the basement aquifer of South Sinai. J. Petroleum Min. Eng., v.7, No. 1.

El-Rayes, A. E., Soliman, F. A., Kehew, A. E. and El-Shamy, I. Z. (2001): Hydrogeochemical exploration for sulphide mineralization: Application in the Arabo-Nubian Shield, Sinai, Egypt. New Approaches Characterizing Groundwater Flow, Seiler & Wohnlich (eds), © 2001 Swets & Zeitlinger Lisse, ISBN 902651 848 x

El Shamy, I. Z. (1992): Towards the water management in Sinai Peninsula. Proc. 3rd Conf. Geol. Sinai develop., Suez Canal Univ., Ismalia, p. 63-70.

El Shazly, E. M. (1964): On the classification of the Precambrian and other rocks of magmatic affiliation in Egypt. Int. Geol. Congr. India, v.10, p.1-19.

El-Shazly, E. M., Mohamed, S. S., Abd Alatif, T. A., Misak, R. and Mabrouk, M. A. (1985): Groundwater potential of St Catherine Monastery Environs, Sinai, Egypt. J Geol., v.11, p.89–100

El-Shazly, M., El Rakaiby, M. and El Kassas, M. (1983): Groundwater investigation of Wadi Araba area, Eastern Desert of Egypt, Using Landsat Imagery. Proc. 17th Symp. on Remote Sensing of the Environment. Ann Arbor, MI, 9–13 May 1983, p.1003–1113

Elwa, H. H. and El Qaddah, A. A. (2011): Groundwater potentiality mapping in the Sinai Peninsula, Egypt, using remote sensing and GIS-watershed-based modeling. Hydrogeology Journal, v. 19, p.613–628.

ESRI (2008): ArcGIS® 9.3 Enterprise Deployment "Technical Paper". New York Street, Redlands.USA. pp.1-28.

Eyal, M., Eyal, Y., Bartov., and Steinitz., G. (1981): The Tectonic development of the western margin of Gulf of Elat (Aqaba) rift. Tectonophysics, v.80, p. 39-66.

Famiglietti, J. S. and Wood, E. F. (1991): Evapotranspiration and runoff from large land areas – land surface hydrology for atmospheric general-circulation models, Surv. Geophys., v.12, p.179–204.

Farid, S. M. and Allam, I. G. (1996): Flood risks and water management in wadi system. Proc. UNESCO/NWRC/ACSAD. "Workshop on wadi Hydrology and groundwater protection". UNESCO Cairo Office, No. 1, p. 14-20.
Feth, J. H., Roberson, C. E. and Polzer, W. L. (1964):-Sources of mineral constituents in water from granitic rocks, Sierra Nevada, California and Nevada. U.S. Geol. Surv. Water Supply Paper 1535-I.
Fetter, C. W. (1994): Applied hydrogeology, 3rd edn. Prentice Hall, Upper Saddle River, NJ, 691p.
Fontes, J. C., Andrews, J. N., Edmunds, W. M., Guerre, A. and Travi, Y. (1991): Palaeorecharge by the Niger River (Mali) deduced from groundwater geochemistry. Water Resources Research, v.27, p.199-214.
Frape, S. K., Fritz, P. and McNutt, R. H. (1984): Water-rock interaction and chemistry of groundwaters from the Canadian Shield. Geochim. Cosmochim. Acta, v.48, p.1617-1627.
Freeze, R. A. and Cherry, J. A. (1979): Groundwater. Englewood Cliffs, NJ, Prentice-Hall, Inc., 604p.
Freund, R., Garfunkel, Z., Zak, I., Goldberg, M., Weissbrod, T., and Derin, B., (1970): The shear along the Dead Sea Rift: Royal Society of London Philosophical Transactions, ser. A, v. 267, p. 107–130.
Gad, S. and Kusky, T. M. (2007): ASTER spectral ratioing for lithological mapping in the Arabian-Nubian shield, the Neoproterozoic Wadi Kid area, Sinai, Egypt. Gondwana Research. v. 11 (3), p.326–335.
Garfunkel, Z. and Bartov, Y. (1977): The tectonics of the Suez rift. - G.S.L Bull. v.71, p.1-44.
Garrels, R. M. (1967): Genesis of some ground water from igneous rocks. In: Abelson, P. H (ed.): Researches in geochemistry, John Wiley & Sons Inc., v.2, p.405-420.
Gascoyne, M. and Kamineni, D. C. (1994): The hydrogeochemistry of fractured plutonic rocks in the candian shield. Applied Hydrogeology, v.2, p.43-49.
Geriesh, M. H. (1998): Artificial recharge as an effective tool for augmenting the natural groundwater resourses in Saint Katherine area, South Sinai, Egypt. Proc. 5th conf. Geol. Sinai develop., Suez Canal Univ., Ismailia, p. 47-64.
Geriesh, M. H. and El Rayes, A. E. (2000): Water Quality Assessment of Wadi Ferani catchment area, South Sinai, Egypt. Proceed. 5th international Water Technology Conference (IWTC), Alexandria, Egypt, p.139-157.
Gibbs, M. S., Maier, H. R. and Dandy, G. C. (2009): The use of GIS to derive distributed unit hydrographs for stream flow prediction. 18th World IMACS / MODSIM Congress Cairns, Australia. p.3704-3710
Gibbs, R. J. (1970): Mechanisms controlling world waterchemistry. Science Journal, v.170 , p.795–840.
Gillion, R. J., Alley, W. M., Gurtz, M. E., (1995): Design of the National Water-Quality Assessment Program: Occurrence and Distribution of Water-Quality Conditions. US Geol. Surv. Circ. v.1112, 33p.
Gomez, C., Delacourt,C., Allemand, P., Ledru, P. and Wackerle, R. (2005): Using ASTER remote sensing data set for geological mapping, in Namibia. Physics and Chemistry of the Earth. v.30, p.97–108.
Gumbel, E. J. (1958): Statistics of Extremes, Columbia University Press, New York, NY p.245.
Haeng Heo, J., Salas, J. D. and Boes, D. C. (2001): Regional flood frequency analysis based on a Weibull model, part 2 Simulations and applications. J Hydrol. v. 242(3–4), p.171–182.
Hassan, A. A. (1967): New Carboniferous occurrence in Abu Durbah Sinai, Egypt. 6th Arab Petrol. Congr., Mar. v. 2, No.39 (B-30), 18 p.
Hassan, O. A., Ahmed, M. H. and Arafat, S. M. (2005): Environmental land use/landcover use change detection in coastal zones of the Gulf of Aqaba, Egypt, using multi-temporal Landsat imagery. Egypt. J. Remote Sensing & Space Sci. v.8, p. 21-38.
Hassen, I. S., El Shafei, M. K. and Stüwe, K. (2007): Late Proterozoic crustal evolution in the Arbian-Nubian Shield of Wadi Zaghra tectonites, South Sinai, Egypt. Annal Geol. Surv. Egypt. v.XXIX, p.77-93.
Hassen, I. S., Ibrahim, S. K. and El Emer, P. M. (2004): Evolution and origin of the metavolcanics at Wadi Saâl area, south Sinai, Egypt. – Annals Geol. Surv. Egypt. v. 27, p.61–78.
Hegazi, A. M. (2006): Tectonic evolution of the polydeformed Sa'al Belt, South Sinai, Egypt. Acta Geologica Hungarica, v. 49/3, p.1-14.
Helmut, K. (2000): Soil and groundwater contamination and remediation technology in Europe. In: Sato, K. (Ed.), Groundwater Updates. Springer, Best-set Typesetter Ltd., Hong Kong, p. 3–8.
Hem, J. D. (1985): Study and interpretation of the chemical characteristics of natural water (3rd ed.). U.S. Geolog-ical Survey Water-Supply Paper, v.2254, 263p.
Hem, J. D. (1989): Study and Interpretation of the Chemical Characteristics of Natural Water, third ed. US Geological Survey Water- Supply Paper 2254, Washington, United States Government Printing Office, 263p.
Hernández-García M. E. and Custodio E. (2004): Natural baseline quality of Madrid Tertiary Detrital Aquifer groundwater (Spain): a basis for aquifer management. Environmental Geology, v. 46, p.173-188.
Hess, L. L., Melack, J., Filoso, S. and Wang, Y. (1995): Delineation of inundated area and vegetation along the Amazon floodplain with the SIR-C Synthetic Aperture Radar. IEEE T Geosci Remote. v.33, p.896–903.
Hewson, R. D., Cudahy, T. J. and Huntington, J. F. (2001): Geologic and alteration mapping at MtFitton, South Australia, using ASTER satellite-borne data. International Geosciences and Remote Sensing Symposium v.2,p.724–726.

Hiscock, K. M., Dennis, P. F., Saynor, P. R. and Thomas, M. O. (1996): 'Hydrochemical and stable isotope evidence for the extent and nature of the effective Chalk aquifer of north Norfolk, U.K.', J. Hydrology, v.180, p. 79−107.
Horritt, M. S. and Bates, P. D. (2002): Evaluation of 1D and 2D numerical models for predicting river flood inundation. J Hydrol. v.268, p.87-99.
Horton, R. E. (1945): Erosional development of streams and their drainage basins: hydrophysical approach to quantitative morphology. Bull. Geol. Soc. Amer., v.5, p.275-370.
Hume, W. F. (1935): The Geology of Egypt; Vol. (II): The fundamental Precambrian rocks of Egypt and the Sudan. Part (II) the later plutonic and minor intrusive rocks. Egypt. Survey Dept., Cairo. p.301- 688
Hume, W. F. (1906): The Topography and Geology of the Peninsula of Sinai (south-eastern portion).Egypt.Survey Dept. Cairo, 280p.
Hursh J. B. and Spoor N. L. (1973): Data on man in: Handbook of experimental pharmacology. Uranium, Plutonium, transplutonic elements. H.C. Hodge et al. (eds.). Springer- Verlag, Berlin, v. 36. p,197-240.
Ignacio, R. and Luis, A. (1982): The dependence of drainage density on climate and geomorphology, Hydrological Sciences – Journal. des Sciences Hydrologiques, v.27.
Issar, A. and Gilad, D. (1982): Groundwater flow systems in the arid crystalline province of Southern Sinai. Journal Hydrological Sciences, v.27, p.309-325.
Issawi, B., El Hinnawi, M., Francis, M. and Mazhar, A. (1998): Contribution to the geology of East Sinai.- Ann. Geol. Surv, v.21, p.55-88.
Jackson, C. P., Hoch, A. R. and Todman, S. (2000): Self-consistency of a heterogeneous continuum porous medium representation of fractured media. Water Resour. Res. v.36(1), p.189-202.
Japan International Cooperation Agency, (JICA) (1999): South Sinai groundwater resources study in the Arab Republic of Egypt, main report, pacific consultations international, Tokyo in association with sandy consultation. Tokyo.
Jarrar, G., Wachendorf, H. and Saffarini, G. (1992): A late Proterozoic Bimodal volcanic/subvolcanic suite from Wadi Araba, Southwest Jordan. Precambrian Res. v.56, p.51–72.
Jones, C. M., Taylor, G. O., Whittle, J. G., Evans, D. and Trotter, D. P. (1997): Water fluoridation, tooth decay in 5year olds, and social deprivation measured by the Jarman score: analysis of data from British dental surveys. British Medical Journal (b); v.315, p. 514-517
Jonhstone, D. and Cross, W. P. (1949): Elements of applied hydrology, Ronald Press Company, New York.
Junge, C. E. (1960):- Sulphur in the atmosphere. J. Geophys. Res., v.65, p.227-237.
Khalil, E. M. (1990): Petrological and geochemical studies on basements rocks of Wadi Nasab area, south eastern Sinai, Egypt.PhD. Thesis, Zagazig University, Zagazig, Egypt.
Kilgore J. L., (1997): Development and evaluation of a GIS-based spatially distributed unit hydrograph model. Dissertation, Faculty of Virginia Polytechnic Institute, State University.
Kim, Y., Lee, K. S., Koh, D. C., Lee, D. H., Lee, S. G., Park, W. B., Koh, G. W. and Woo, N. C. (2003): Hydrogeochemical and isotopic evidence of groundwater salinization in a coastal aquifer: a case study in Jeju volcanic island, Korea. J Hydrol., v. 270, p.282–294.
Kite, G. W. and Kouwen, N. (1992): Watershed modeling using land classification. Water Resources Research, v.28(12), p.3193–200.
Kocal, A., Duzgun, H. S., and Karpuz, C. (2004): Discontinuity mapping with automatic lineament extraction from high resolution satellite imagery. XXth ISPRS Congress, Istanbul, Vol. XXXV, partB7–ThS 20: Application of High Resolution Data.
Kora, M. and Genedi, A. (1995): Lithostratigraphy and facies development of Upper Cretaceous carbonates in East Central Sinai, Egypt. Facies, v.32, p.223-236.
Kora, M. and Hamama, H. (1988): Biostratigraphy of the Cenomanian - Turonian of Gabal Gunna, southeastern Sinai. - Mans. Sci. Bull. v.14, p.289-301.
Kumar, R., Chatterjee, C., Lohani, A. K., Kumar, S., and Singh, R. D. (2002): Sensitivity analysis of the GIUH based Clark model for a catchment. Water Resour. Manage., v.16, p.263-278.
Kumar, R., Kumar, S., Lohani, A. K., Nema, R. K. and Singh, R. D. (2000): Evaluation of geomorphological characteristics of a catchment using GIS. GIS India. v. 9(3), p.13–17.
Kuroda, P. K. and Sandell, E. B. (1953): Chlorine in igneous rocks. Geol. Soc. Am. Bull., v.64, p.879-896.
Kyle. E. (2000): Estimation of potential runoff – contributing areas. USGS Information Services, iv, 55 p.
Lauria, D. C., Almeida, R. M. R. and Sracek, O. (2004): Behavior of radium, thorium and uranium in groundwater near the Buena Lagoon in the Coastal Zone of the State of Rio de Janeiro, Brazil. Environ Geol., v. 47(1), p.11–19
Le Toan, T., Ribbes, F., Wange, L.F., Floury, N., Ding, N. and Kong, K. H. (1997): Rice crop mapping and monitoring using ERS-1 data based on experiment and modeling results. IEEE T Geosci Remote. v.35, p.41–56.

Linsley, R. K., Kohler, M. A. and Paulhus, J. L. H. (1982): Hydrology for Engineers, 3rd Edition, McGraw-Hill, New York, 508 p.
Louis, C. (1967): Stömungsvorgänge in klüftigen Medien und ihre Wirkung auf die Standsicherheit von Bauwerken und Böschungen im Fels (Flow phenomena in fractured systems and their contribution to structural integrity of buildings and slopes at rock). PhD Thesis, Technical University Karlsruhe, Germany.
Macdonald, A., Davies, J., Calow, R. and Chilton, J. (2005): Developing groundwater: a guide for rural water supply. ITDG Publishing, Rugby, UK, 358 p.
Macka, Z. (2001): Determination of texture of topography from large scale contour maps. Geografski Vestnik v.73(2), p.53–62
Madani, A. A. and Emam, A. A. (2009): SWIR ASTER band ratios for lithological mapping and mineral exploration: A case study from El Hudi area, southeastern desert, Egypt. Arabian Journal of Geosciences. v.4, p.45-52.
Madani, A. A. (2009): Utilization of Landsat ETM+ Data for Mapping Gossans and Iron Rich Zones Exposed at Bahrah Area, Western Arabian Shield, Saudi Arabia. Earth Sci., v. 20 No. 1, p. 35-49.
Maidment, D. R (1993): Developing a spatially distributed unit hydrograph by using GIS. Proceedings of the Vienna conference, IAHS publ., no. 211, p. 181- 192.
Maidment, D. R., (1993b): GIS and hydrologic modeling. In Goodchild, M.F., Parks, B.O. and Steyaert, L.T., editors, Environmental modeling with GIS. New York: Oxford University Press.
Maidment, D. R., (2002),: Arc Hydro: GIS for Water Resources, ESRI Press, Redlands CA, 2002, 220 p.
Marchand, A. M. E., Smalley, P. C., Haszeldine, R. S., Fallick, A. E. (2002): Note on the importance of hydrocarbon-fill for reservoir quality prediction in sandstones. AAPG Bull. v.86, p.1561-1571.
Marcovecchio, J. E, Botte, S. E and Freije, R. H. (2007): Heavy Metals, Major Metals, Trace Elements. In: Handbook of Water Analysis. L.M. Nollet, (Ed.). 2nd Edn. London: CRC Press; p.275-311.
Maritin, C., Aquilina, L., Gascuel-Odoux, C., Molénat J., Faucheux M. and Ruiz L. (2004): Seasonal and interannual variations of nitrate and chloride in stream waters related to spatial and temporal patterns of groundwater concentrations in agricultural catchments. Hydrological Processes, v. 18, p.1237-1254.
Marshall, E. (1990): The fluoride Debate: one more time. Science, v.247, p.276-277.
Matzat E. and Shiraki K. (1974): Chromium. Handbook of Geochemistry, v.11(3), p.24(A). Middle East and North Africa. Berlin: Springer.
Mechie, J. and El-Isa, Z. (1988): Upper lithospheric deformations in the Jordan Dead Sea transform regim, Tectonophysics. v.153, p.153-159.
Meirovich, L., Ben-Zvi, A., Shentsis, I. and Yanovich, E. (1998): Frequency and magnitude of runoff events in the arid Negev of Israel. J. Hydrol. v.207, p.204-219.
Melton, M. A. (1958b): Correlation structure of morphometric properties of drainage systems and their controlling agents, Journal of Geology. v. 66, p.442–60.
Miller, V. C. (1953): A quantitative geomorphic study of drainage basin characteristics in the Clinch Mountain area, Varginia and Tennessee. Project NR 389042, Tech. Rept. 3.,Columbia University, Department of Geology, ONR, Geography Branch, New York.
Milligan, J. H., Marsell, R. E. and Bagley, J. M. (1966): Mineralized springs in Utah and their effect on manageable water supplies. Report WG23-6, Utah Water Research Laboratory, Utah State University, 50p.
Mohana, A. M. (1989): Geological and radioactivity investigation on some minerals in Sinai. Master thesis. Suez Canal University, Ismailia, Egypt, 211p.
Moore, G. (1982): Groundwater applications of remote sensing. Open file report 82 – 240. U.S. Department of Interior Geological Survey. EROS Data Center, Sioux Falls, South Dakota.
Moore, I. D., Grayson, R. B. and Ladson. A. R. (1991): Digital Terrain Modelling: A Review of Hydrological, Geomorphological and Biological Applications. Hydrological Processes, v.5(1), p.3-30.
Morsy, E. A.; Gamal, M. A.; Dahroug, S.M (2007): Geohazard Analysis for land use planning in Dahab area, Gulf of Aqaba. (http://ipac.kacst.edu.sa/eDoc/2007/165203_1.pdf).
Moussa, H. E. (2003): Geologic setting, petrography and geochemistry of the volcano-sedimentary succession at Gebel Ferani area, southeastern Sinai, Egypt. Egyptian Journal of Geology. v. 47, p.153-173.
Moussa, M. M. (1999): Application of the Turam-EM Technique in Radiometric Investigation: Acase study From Wadi Remthi Copper Prospect, South Sinai, Egypt. Proc. 5th Conf. Geol. Siani Develop., Saint Catherine, p. 151-159.
MSS (1999): Environmental appraisal of the Jordanian coast of the Gulf of Aqaba,unpublished report. Marine Science Station, Aqaba, Jordan, 88p.
Musa, K. A., Juhari Mat, A., and Abdullah, I. (2000): Groundwater prediction potential zone in Langat basin using the integration of remote sensing and GIS. The 21st Asian Conf. on Remote Sensing, Taipei (Taiwan).
Muzik, A. (1996): GIS-derived distributed unit hydrograph. In: Application of geographic information systems in hydrology and water resources (ed. by K. Kovar & H.P. Nachtnebel), IAHS Publ. no. 235, p.453-460.

Myers, V. A. and Zehr, R. M. (1980): A Methodology for point to area rainfall frequency ratios. NOAA Technical Rpt. NWS 24, National Weather Services, NOAA, US, Dept. of Commerce, Washington, D.C.
Najjar, R. G. (1999): The water balance of the Susquehanna River Basin and its response to climate change. Journal of Hydrology, v.219, p.7–19.
Nash, J. E. (1957): The Form of Instantaneous Unit Hydrograph'. International Association of Scientific Hydrology Publication, v.45, No 3, p 114.
Nicholson, R. V., Cherry, J. A. and Reardon, E. J. (1983): Migration of contaminants in groundwater at a landfill: a case study, 6. Hydrogeochemistry. J. Hydrol., v.63, p. 131-176.
Nolan, B. T. (1999): Nitrate behavior in groundwater of southeastern USA. J. Environ. Qual., v.28, p.1518–1527.
Oada, K. (1995): Hydrogeological studies on East Saint Katherine environ, South Central Sinai, Egypt. M.Sc. thesis, Suez Canal Univ., Ismailia, Egypt, 130p.
Omara, S. (1972): An Early Cambrian outcrop in southwestern Sinai, Egypt. N. Jb. Geol. Paleontol, Mh., v.5 , p. 306-314.
Omran, A., Hahn M., Hochschild, V., El Rayes, A. and Geriesh, M. (2012): Lithological Mapping of Dahab Basin, South Sinai, Egypt, using ASTER Data.PFG. Schweizerbrat Science Publishers, Heft6, p. 711-726.
Omran, A., Schröder, D., El Rayes, A. and Geriesh, M. (2011): Flood Hazard Assessment in Wadi Dahab Based on Basin Morphometry using GIS Techniques, Egypt. GI_Forum Symposium and Exhibit applied Geoinformatics. Salzburg, Austria, Wichman, p. 1-11.
Overton, D. E. and Meadows M. E. (1976): Stormwater modeling. Academic press, New York.
Ovichinikov, A. M. (1955): General hydrology. Gosgeolitchizdat, Moscow, U.S.S.R. 375p. (In Russian).
Patton, T.L. (1988): Drainage basin morphometry and floods. In: Baker VR, Kochel RC, Patton PC (eds) Flood geomorphology. Wiley, USA, p.51–65.
Penman, H. L. (1948): Natural evaporation from open water, bare soil, and grass. Proc. Roy. Soc. London A193:120-146.
Pennisi, M., Gonfiantini, R., Grassi, S. and Squarci, P. (2006): The utilization of boron and strontium isotopes for the assessment of boron contamination of the Cecina River alluvial aquifer (central-western Tuscany, Italy). Appl. Geochem. v.21, p.643–655.
Pérez-Claros, J. A., Palmqvist, P. and Olóriz, F. (2002): First and second orders of suture complexity in ammonites: A new methodological approach using fractal analysis: Mathematical Geology, v. 34, p. 323-343. doi:10.1023/A:1014847007351
Philip, J.R. (1957a): The theory of infiltration. 1. The infiltration equation and its solution, Soil Science, v.83, p.345-357.
Pickering, G., Bull, J. M. and Sanderson, D. J. (1995): Sampling power-law distributions: Tectonophysics, v. 248, p. 1-20. doi:10.1016/0040-1951(95)00030-Q
Pike, R. J. (2002): A Bibliography of Terrain Modeling (Geomorphometry), the Quantitative Representation of Topography-Supplement 4.0.Open-File Report 02-465, U.S. Geological Survey.
Ponce, V. M. (1989): Engineering Hydrology, Principles and Practices. Prentice-Hall, Englewood Cliffs, New Jersey.
Pradhan, B. (2010b): Flood susceptible mapping and risk area estimation using logistic regression, GIS and remote sensing. J Spatial Hydrol. v. 9(2), p.1–18.
Price, D., Iddon, B. and Wakefield, B. J. (1988): Bromine compounds: chemistry and applications. New York: Elsevier, 422p.
Qari, M. H. T., Madani, A. A., Matsah, M. I. M. and Hamimi, Z. (2008): Utilization of ASTER and Landsat data in geologic mapping of basement rocks of Arafat Area, Saudi Arabia. Arabian Journal for Science and Engineering. v.33, p.99–116.
Queste, A., Lacomb, M., Hellmeier, F., Bortulussi, B., Kaup, M., Ott, K. and Werner, M. (2001): High concentrations of fluoride and boron in drinking water wells in the Münster region – results of a preliminary investigation, Int. Jour. of Hygiene and Env. Health, v.203, p.221-224.
Rai, R. K., Upadhyay, A., Sarkar, S., Upadhyay, A. M. and Singh, V. P. (2009): GIUH Based Transfer Function for Gomti River Basin of India. Journal of Spatial Hydrology, v.9, No.2, p.29-50.
Reda, A., Kusky, T. and Ghulam, A. (2010): Lithological mapping in the Central Eastern Desert of Egypt using ASTER data. Journal of African Earth Science. v.56, p.75-82.
Reddy, K. J., Wang, L., Gloss, S. P. (1995): Solubility and Mobility of Copper, Zinc and Lead in Acidic Environments. Planr and Soil Kluwer Academic Publishers Printed in the Netherlands, v.171, p.53-58.
Refsgaard, J. C. (1996): Terminology, modeling protocol and classification of hydrological model codes. In Abbott, M.B. and Refsgaard, J.C., editors, Distributed hydrological modeling. Dordrecht: Kluwer Academic, p.17–39.

Robinson, C., El-Baz, F. and Singhory, V. (1999): Subsurface imaging by RADARSAT: comparison with Landsat TM data and implications for groundwater in the Selima area, northwestern Sudan. Rem Sens Abst, v.25(3), p.45–76.
Rodriguez-Iturbe, I. and Valdes. J. B. (1979): The Geomorphologic Structure of Hydrologic Response. Water Resources Research, v 15, No 6, p. 1409.
Rodriguez-Iturbe, I., Gonzalez-Sanabria, M. and Bras, R. L. (1982a): A geomorphoclimatic theory of the instantaneous unit hydrograph, Water Resources Research, v. 18, No. 4, p. 877-886.
Rosenthal, E. (1987): Chemical composition of Rainfall and groundwater in recharge areas of the Bet Shean-Harod multiple aquifer system. Jour. Hydrology, v.89, No.3/4, p.329-352.
Rowan, L.C. and Mars, J.C., (2003): Lithologic mapping in the Mountain Pass, California area using Advanced Spaceborne Thermal Emission and Reflection Radiometer (ASTER) data. Remote Sensing of Environment. v.84, p.350–366.
Roy, A., Perfect, E., Dunne, W. M. and Mckay, L. D. (2007): Fractal characterization of fracture networks: an improved box-counting technique: Journal of Geophysical Research, v. 112, B12201. doi:10.1029/2006JB004582
Saad, K. F., EL Shamy, I. Z. and Sweedan, A. S. (1980): Quantitative analysis of the geomorphology and hydrology of Sinai Peninsula. Ann. Geol. Surv. Egypt. v. 10, p.818-836.
Saghafian, B., Farazjoo, H., Bozorgy, B. and Yazdandoost, F. (2008): Flood intensification due to changes in land use. Water Resour Manag, v. 22, p.1051–1067
Said, R. (1962): The Geology of Egypt. Elsevier, Amsterdam, 377 p**.**
Said, R. (1971): Explanatory notes to accompany the geological map of Egypt . Geol. Surv. Egypt, Pap. v.56, 123 p.
Salem, A (1990): report on southern Sinai field trip for risk evaluation of flash floods, institute for water resources development- South Sinai office.
Sami, K., (1992): Recharge mechanisms and geochemical processes in semi arid area sedimentary basin, eastern cape, South Africa, Jour. Hydrology, v.20, no.3, p. 27-48.
Sanyal, J. and Lu, X.X. (2005): Remote sensing and GIS-based flood vulnerability assessment of human settlements: a case study of Gangetic West Bengal, India. Hydrol Process. v.19, p.3699–3716
Sarin, M. M., Krishnaswami, S., Dilli, K., Somayajulu, B. L. K. and Moore, W. S. (1989): Major ion chemistry of the Ganga-Brahmaputra river system: Weathering processes and fluxes to the Bay of Bengal. Geochim. Cosmochim. Acta, v.53, p.997–1009.
Schoeller, H. (1955): Geochemie des eaux souterraines. Revue de L'Institute Francais du Petrole. v.10, p. 230-344.
Schumm, S. A. (1956): Evaluation of drainage systems and slopes in badlands at Perth Amboy, New Jersy. Bull. Geol. Soc. Amer, v.67, p. 597-646.
Schumm, S. A. (1963): Sinuosity of alluvial rivers on the Great Plains. Geol. Soc. Am. Bull. Geol. Soc. Am. Bull. v.74, p.1089–1100
Sener, A., Davraz, A. and Ozcelik, M. (2005): An integration of GIS and remote sensing in groundwater investigations: a case study in Burdur, Turkey. Hydrogeol. J., v.13, p.826-834.
Shendi, E. H. and Oada, K. (1999): Groundwater Possibilities of Wadi El-Nasab Basin, southeastern Sinai. Annals. Geol. Surv. Egypt, v.XXII, p.403-418.
Shendi, E. H.; Geriesh, M. H. and Mousa, M. M. (1997): Geophysical and Hydrogeological studies on Wadi Saal Basin, Southern Sinai, Egypt. Egyptian Journal of Geology, v.41/2B, p.871-908.
Shendi, E. H. and El Rayes, A. E. (1992): Geophysical prospecting for ground water in Wadi Sibaiya-Wadi El Shiekh area, south Sinai, M.E.R.C . Ain Shams Univ., Earth Sci. Ser., v. 6, p.55-61.
Sherief, Y. (2008): Flash floods and their effects on the development in El Qaa Plain area in south Sinai, Egypt. A Study in applied geomorphology using GIS and Remote sensing. Johannes Gutenberg- Universität Mainz. 255p.
Sherman, L. K. (1932): Stream from rainfall by the unit graph. Method. Eng. News-Rec., v. 108, p. 501 – 505.
Shimron, A. (1984): Evolution of the Kid Group, southeast Sinai Peninsula: thrusts, mé-langes, and implications for accretionary tectonics during the late Proterozoic of the Arabian–Nubian Shield. Geology, v.12, p. 242–247.
Shimron, A. E., Bogoch, R., Harold, F. and David, P. (1993): The Sa`al Group: an ensialic island arc sequence in Sinai. – In: Thorweihe, ?., ?. Schandelmeler (Eds): Scientific Research in Northeast Africa. Balkema, Rotterdam, p. 90–95.
Singh, V. P., and Fiorentino, M. (1996): Geographical information systems in hydrology. Dordrecht, Netherlands: Kluwer Academic Publishers.
Sivapalan, M. and Wood, E. F. (1987): A multidimensional model of nonstationary space-time rainfall at the catchment scale, Water Resour. Res., v.23, p.1289–1299.

Smedley, P. L., Smith, B., Abesser, C. and Lapworth, D. (2006): Uranium occurrence and behaviour in British groundwater. Report CR/06/050 N. British Geological Survey, Keyworth.
Smith, S. E., El-Shamy, I. and Abd-El Monsef, H. (1997): Locating regions of high probability for groundwater in the Wadi EI-Arish Basin, Sinai, Egypt. J Afr Earth Sci., v.25(2), p.253–262.
Snow, D. T. (1965): A parallel plate model of fractured permeable media. PhD Thesis, University of California, Berkeley, USA.
Snyder, F. F. (1938): Synthetic unit graphs. Trans. AGU. v. 19, p. 447 - 454.
Soil Conversation Service (1975): (USDA-SCS). National Engineering Handbook, Section 4 , USA Department of Agriculture, Washington, D.C.
Soliman, F. A. (1986): Geology of Wadi Sa'al area with special emphasis of metamorphism and tectonics, Central Sinai of Egypt. Ph. D. Thesis, Faculty of Science, Suez Canal Univ., Ismailia, Egypt, 240 p.
Soliman, S. M. and El Fetouh, M. A. (1970): Carboniferous of Egypt, isopach and lithofacies maps. Bull. Amer. Assoc. Petrol. Geol., v.54, p. 1918-1930.
Solomon, S. (2003): Groundwater study using remote sensing and geographic information systems (GIS) in the central highlands of Eritrea, Doctoral Dissertation, Environmental and Natural Resources Information Systems, Royal Institute of Technology, SE-100 44 Stockholm, Sweden.
South Sinai Governorate Environmental Action Plan (2003): South Sinai Development Profile. Egyptian Environmental Affairs Agenc . SEAM Programme. Internal Report - Egypt.
Stallard, R. F., and Edmond, J. M. (1983): Geochemistry of the Amazon 2. The influence of geology and weathering environment on the dissolved load: Journal of Geophysical Research, v. 88, p. 9671–9688.
Stern, R. J. (1985): The Najid Fault system, Saudi Arabia and Egypt: A Late Precambrian rift-related transform system. Tectonics, v.4, p.497-511.
Stober, I., Bucher, K. (1999b): Origin of salinity of deep groundwater in crystalline rocks. Terra Nova, v.11, p.181-185.
Strahler, A. N. (1952): Hypsometric (area-altitude) analysis of erosional topography, Geological Society American Bulletin, v.63, p.1117-1142.
Strahler, A. N. (1964): Quantitative geomorphology of drainage basins and channel networks. In. Handbook of Applied Hydrology, McGraw Hill Book Company, New York, p. 4–76.
Subba Rao, N., Chakradhar, G. K. J. and Srinivas, V. (2001): Identification of Groundwater potential zones using remote sensing techniques in around Guntur Town. Andhra Pradesh, India, v.29(1&2), p.69-78.
Suror, A. A., El Kammar, A. A.; Arafa, E. H and Kornay, H. M. (2003): Dahab Stream Sediments, southeastern Sinai, Egypt: a potential source of gold, magnetite and zircon. Journal of Geochemical Exploration, v.77, p. 25-43.
Süzen, M. L., and Toprak, V. (1998): Filtering of satellite images in geological lineament analyses: An application to a fault zone in Central Turquey. International Journal of Remote Sensing, v.19(6), p.1101−1114.
Todd, D. K. (1959): Groundwater hydrology. 2nd ed., John Willy and Sons Inc., New York, 336p.
Tucker, G. E. and Bras, R. L. (1998): Hill slope processes, drainage density, and landscape morphology. Water Resour Res., v. 34, p.2751–2764.
Tylor, G. G. and Schwarz, E. (1952): Unit hydrograph lag and peak flow related to basin characteristics. Transactions of the American Geophysical Union, p. 235-246.
United Nation Environmental Programm, (UNEP) (2007): An Overview of the State of the World's Fresh and Marine Waters - 2nd Edition http://www.unep.org/dewa/vitalwater/article182.html.
Ure, A. M. and Berrow, M. L.(1982): The chemical constituents of soils. In: H.J.M. Bowen (Editor), Environmental Chemistry. R. Soc. Chem., Burlington House, London, p. 94-202.
Verstappen, H. (1983): the applied geomorphology, International Institute for Aerial Survey and Earth Science (I.T.C), Enschede, Netherlands, Amsterdam, Oxford, New York.
Wang, J. and Philip. J. (1990): Use of the hough transform in automated lineament detection, IEEE Transactions on Geoscience and remote sensing. v.28(4), p. 561-566.
Wanielista, P. H. (1990): Hydrology and water quantity control. John Wiley & Sons, New York, USA. Pub. in Canada. p. 207 – 240.
Water Resources Researches Institute (WRRI) (2006): Architectural and Engineering Services For The Flood Protection of the city of Dahab in South Sinai, Arab Republic of Egypt. Report , EuropeAid/122288/D/SV/EG.
Wegman, D. H., Eisen, E. A., Hu, X., Woskie, S. R., Smith, R. S. and Garabrandt, D. (1994): Acute and chronic respiratory effects of sodium borate particulate exposures. Environmental Health Perspectives v.102, p. 119–128.
Wilson, J. P. and Gallant, J. C. (2000): Secondary Topographic Attributes. In: Wilson, J. P. and Gallant, J. C. (Hrsg.): Terrain Analysis: Principles and Applications, NewYork: John Wiley and Sons, Inc., p.87-131.
World Health Organization (2006): Guidelines for drinking-water quality, first addendum to third edition, v. 1, recommendations. ISBN 92 4 154696 4 (NLM classification : WA 675). 515P.

Yamaguchi, Y. and Naito, C., (2003): Spectral indices for lithologic discrimination and mapping by using the ASTER SWIR bands. – International Journal of Remote Sensing. v. 24 (22), p.4311–4323.
Yair, A. and Lavee, H. (1976): Runoff generative process and runoff yield from arid talus mantled slopes. Earth Surf. Process., v.1, p. 235-247.
Youssef, M. A., Pradhan, B. and Hassan, M. A, (2010): Flash flood risk estimation along the St. Katherine road, southern Sinai, Egypt using GIS based morphometry and satellite imagery. Environ Earth Sci., v. 62, p.611–623
Zalata, A. A., El Metwally, A. A., El Aassy, I. E. and El Sayed, A. A. (1997): Evolution and Geochemistry of the Basement rocks of west Dahab area, Southeastern Sinai Third Conference on Geochemistry, Alexandria University, p.1-15.
Zeeb, C., Göckus, D., Bons, P., Al Ajmi, H., Rausch, R. & Blum P. (2010): Fracture flow modeling based on satellite images of the Wajid Sandstone, Saudi Arabia. Hydrogeology Journal, v.18, p.1699-1712.
Zereini, F. and Hötzl, H. (Eds.) (2008): Climatic Changes and Water resources in the Middle East and North Africa. Springer-Verlag, 552 p. ISBN 078-3-540-85046-5.
Zerger, A. (2002): Examining GIS decision utility for natural hazard risk modeling. Environ Modell Softw. v.17(3), p.287–294.
Zernit, E. R. (1932): Drainage patterns and their significance, Columbia University, Jour. Geol. v.40, p. 498-521.
Ziko, A., Darwish, M. and Eweda, S. (1993): late Cretaceous-Early Tertiary stratigraphy of the Themed area, East Central Sinai,Egypt. - N. Jb. Geol. Paläont. Mh. Stuttgart. v.3, p.135-149.

Internet sites

1. http://webhelp.esri.com/arcgisdesktop/9.2/index.cfm?TopicName=Hydrologically_correct_surfaces%3A_Topo_to_Raster
2. http://english.ahram.org.eg/NewsContent/1/2/54440/Egypt/Society/Alert-Floods-block-roads-to-Sinais-Nuweiba,-St-Cat.aspx

APPENDIX

Appendix

```
arc = read all arcs

for order = 1 to maximal order loop

   start_arcs = select all starting arcs of actual order

   for all a in start_arcs loop

       c = a

       do while b = select arc where c.to_node = arc. from_node

          If c.order = b.order Then

              c.dissolve = dissolve_counter

              c = b

          else

              dissolve_counter = dissolve_counter + 1

              exit do

          end If

   next a

next order

dissolve all segments with same dissolve_counter
```

App. 1: Pseudo-code for dissolving stream segments according to Strahler ordering System

```
# Create the Geoprocessor object
gp = arcgisscripting.create()

# get parameters
Stream_Network_ori= gp.GetParameterAsText(0)
maxorder = int(gp.GetParameterAsText(1))
Input_Feature_Class=gp.GetParameterAsText(2)
temp_folder = gp.GetParameterAsText(3)

# define intermediate files
Output_Feature_Class = temp_folder + "\\sp_join.shp"
Iterate_Feature_Class=temp_folder + "\\sp_join_1.shp"
Stream_Network= temp_folder + "\\str_network.shp"

# delete intermediate files if existing
if (fFileExist(Iterate_Feature_Class) != 0):
   gp.Delete_management(Iterate_Feature_Class)
if (fFileExist(Output_Feature_Class) != 0):
   gp.Delete_management(Output_Feature_Class)
if (fFileExist(Stream_Network) != 0):
   gp.Delete_management(Stream_Network)

gp.copy_management(Input_Feature_Class, Iterate_Feature_Class, "")
i=1
for i in range(1,maxorder):
   # Process: Select Layer By Attribute...
   str_sql= "\"order_\" ="+str(i) #+"\""
   gp.Select_analysis(Stream_Network_ori, Stream_Network,str_sql )
   # Process: Spatial Join...
   gp.SpatialJoin_analysis(Iterate_Feature_Class,Stream_Network,
Output_Feature_Class,"#","#","#","CONTAINS")
   # Process: Add Field...
   gp.AddField_management(Output_Feature_Class, "cnt_ord_"+str(i), "LONG", "", "", "", "",
"NON_NULLABLE", "NON_REQUIRED", "")
   # Process: Calculate Field...
   gp.CalculateField_management(Output_Feature_Class, "cnt_ord_"+str(i), "[Join_Count]", "VB", "")
   # Process: Delete Field...
   gp.DeleteField_management(Output_Feature_Class, "Join_Count")
   # Process: Rename...
   gp.Delete_management(Iterate_Feature_Class)
   gp.Rename_management(Output_Feature_Class, Iterate_Feature_Class, "")
   gp.Delete_Management(Stream_Network)
```

App. 2: Python code snippet for counting stream segments of each Strahler order

NAME	Basin No.	Code No.	Au	1st order		2nd order		3rd order		4th order		5th order		6th order		7th order		8th order		Total No.	Total Length
			Km²	No.	Length	No.	Length	No.	Length	No.	Length	No.	Length	No.	Length	No.	Length	No.	Length	No.	km
Wadi Mega Dahab	1	D	2088.00	8083.00	2429.33	1846.00	1295.10	427.00	644.87	94.00	285.65	24.00	174.00	6.00	160.79	2.00	38.49	1.00	19.81	10483.00	5048.04
Wadi South Zaghraa	2	SZ	8.25	37.00	17.73	6.00	4.28	2.00	2.16	1.00	3.35	0.00	0.00	0.00	0.00	0.00	0.00	0.00	0.00	46.00	27.53
Wadi Um Asaam	3	UA	7.04	31.00	7.53	7.00	4.59	2.00	1.70	1.00	2.87	0.00	0.00	0.00	0.00	0.00	0.00	0.00	0.00	41.00	16.69
Wadi Abu Khshieeb	4	Ak	107.00	433.00	122.69	94.00	54.29	20.00	29.21	6.00	23.84	2.00	8.38	1.00	5.70	0.00	0.00	0.00	0.00	556.00	244.11
Wadi El Ghaieb	5	Gh	298.80	1535.00	741.00	275.00	183.88	61.00	87.01	14.00	43.99	3.00	20.40	1.00	31.25	0.00	0.00	0.00	0.00	1889.00	1107.54
Wadi Zaghraa	6	ZA	1617.00	8072.00	3897.41	1423.00	1007.86	335.00	517.91	71.00	210.47	19.00	145.22	4.00	123.75	2.00	38.49	1.00	6.11	9927.00	5947.22
Wadi Zaghraa Nasab	7	ZA1	936.00	3691.00	1043.66	836.00	548.76	190.00	303.50	40.00	116.03	11.00	84.41	2.00	83.27	1.00	13.26	0.00	0.00	4771.00	2192.88
Wadi Zaghraa Saal	8	ZA2	662.70	2452.00	783.85	573.00	449.86	142.00	208.67	31.00	94.45	8.00	60.81	2.00	40.48	1.00	25.12	0.00	0.00	3209.00	1663.25
Wadi Abu Rwies	9	Gh1	19.59	70.00	21.28	14.00	10.61	3.00	7.06	1.00	4.72	0.00	0.00	0.00	0.00	0.00	0.00	0.00	0.00	88.00	43.67
Wadi Kharza	10	Gh2	11.17	33.00	13.07	6.00	4.77	1.00	4.93	0.00	0.00	0.00	0.00	0.00	0.00	0.00	0.00	0.00	0.00	40.00	22.76
Wadi Hamarah Ghai	11	Gh3	11	38	9.4	6.0	6.3	2.0	4.1	1.0	1.6	0.0	0.0	0.0	0.0	0.0	0.0	0.0	0.0	47.00	21.43
Wadi South Um Marha	12	Gh4	7.45	27	6.6	4.0	4.7	1.0	3.6	0.0	0.0	0.0	0.0	0.0	0.0	0.0	0.0	0.0	0.0	32.00	14.91
Wadi Hodbah	13	Gh5	20.18	72.00	23.75	18.00	16.54	4.00	2.66	1.00	6.73	0.00	0.00	0.00	0.00	0.00	0.00	0.00	0.00	95.00	49.69
Wadi Abu Gerdan	14	Gh6	26.94	104.00	29.17	26.00	15.28	6.00	11.82	2.00	6.00	1.00	1.49	0.00	0.00	0.00	0.00	0.00	0.00	139.00	63.77
Wadi El Geeby	15	Gh7	134.40	553.00	171.17	141.00	82.35	34.00	46.10	9.00	24.81	2.00	18.63	1.00	4.33	0.00	0.00	0.00	0.00	740.00	347.39
Wadi Um Shawky	16	Ak1	24.62	121.00	52.19	21.00	14.69	4.00	5.30	1.00	8.24	0.00	0.00	0.00	0.00	0.00	0.00	0.00	0.00	147.00	80.42
Wadi Maeen	17	Ak2	18.68	113.00	48.97	20.00	13.64	5.00	4.22	2.00	3.83	1.00	2.86	0.00	0.00	0.00	0.00	0.00	0.00	141.00	73.52
Wadi Small Abu Khshieb	18	Ak3	51.00	274	116.5	46.0	21.1	9.0	15.8	3.0	11.7	1.0	5.5	0.0	0.0	0.0	0.0	0.0	0.0	333.00	170.51
Wadi Rimthy	19	ZA3	413.30	1590.00	460.44	369.00	250.09	84.00	150.59	18.00	46.23	5.00	47.79	1.00	28.94	0.00	0.00	0.00	0.00	2067.00	984.09
Wadi El Genah	20	ZA4	284.60	1076.00	346.93	267.00	203.00	70.00	99.64	15.00	44.69	4.00	14.27	1.00	33.13	0.00	0.00	0.00	0.00	1433.00	741.66
Wadi Mega Saal	21	ZA5	245.80	892.00	287.97	188.00	158.37	44.00	62.45	10.00	40.61	2.00	39.61	1.00	7.18	0.00	0.00	0.00	0.00	1137.00	596.19
Wadi Nasab	22	ZA6	444.90	1812.00	506.21	401.00	260.40	93.00	133.90	19.00	58.28	5.00	31.37	1.00	53.92	0.00	0.00	0.00	0.00	2331.00	1044.08
Wadi Korna	23	ZA7	32.68	126.00	34.23	31.00	18.96	6.00	7.81	2.00	5.45	1.00	5.24	0.00	0.00	0.00	0.00	0.00	0.00	166.00	71.68
Wadi Small El Hamam	24	ZA8	6.00	19.00	6.12	4.00	4.81	1.00	2.29	0.00	0.00	0.00	0.00	0.00	0.00	0.00	0.00	0.00	0.00	24.00	13.22
Wadi Mega Barka	25	ZA9	29.04	107.00	36.76	25.00	26.45	6.00	11.96	2.00	2.25	1.00	3.58	0.00	0.00	0.00	0.00	0.00	0.00	141.00	81.01
Wadi Naghmishy	26	ZA10	6.00	20.00	5.68	7.00	4.01	2.00	1.90	1.00	1.21	0.00	0.00	0.00	0.00	0.00	0.00	0.00	0.00	30.00	12.81
Wadi South Um Athan	27	ZA11	5.00	15.00	4.80	4.00	3.29	1.00	3.10	0.00	0.00	0.00	0.00	0.00	0.00	0.00	0.00	0.00	0.00	20.00	11.20
Wadi Remty	28	ZA12	9.00	35.00	10.34	9.00	6.39	1.00	4.69	0.00	0.00	0.00	0.00	0.00	0.00	0.00	0.00	0.00	0.00	45.00	21.42
Wadi South Akry	29	ZA13	9.00	36.00	11.52	10.00	7.79	3.00	3.85	1.00	1.63	0.00	0.00	0.00	0.00	0.00	0.00	0.00	0.00	50.00	24.79
Wadi Mega North Akry	30	ZA14	26.00	94.00	32.38	22.00	16.53	7.00	9.03	2.00	4.00	1.00	3.32	0.00	0.00	0.00	0.00	0.00	0.00	126.00	65.26
Wadi Small Hodbah	31	Gh8	8.00	27.00	9.61	6.00	6.53	2.00	0.89	1.00	2.02	0.00	0.00	0.00	0.00	0.00	0.00	0.00	0.00	36.00	19.04
Wadi South Small Hodbah	32	Gh9	3.00	12.00	3.19	3.00	2.65	1.00	0.98	0.00	0.00	0.00	0.00	0.00	0.00	0.00	0.00	0.00	0.00	16.00	6.82
Wadi Khalal	33	Gh10	6.00	21.00	6.52	6.00	4.62	2.00	1.52	1.00	0.96	0.00	0.00	0.00	0.00	0.00	0.00	0.00	0.00	30.00	13.62
Wadi Geb Um Reglah	34	Gh11	19.00	73.00	21.14	20.00	10.01	4.00	10.30	1.00	5.04	0.00	0.00	0.00	0.00	0.00	0.00	0.00	0.00	98.00	46.50
Wadi El Marwah	35	Gh12	8.00	41.00	12.42	8.00	4.03	3.00	3.17	1.00	3.15	0.00	0.00	0.00	0.00	0.00	0.00	0.00	0.00	53.00	22.77
Wadi Abu Haiethat	36	Gh13	33.00	138.00	42.44	38.00	23.97	9.00	9.07	2.00	5.13	1.00	7.32	0.00	0.00	0.00	0.00	0.00	0.00	188.00	87.93
Wadi South Small El Geeby	37	Gh14	3.00	13.00	4.95	3.00	3.05	1.00	0.69	0.00	0.00	0.00	0.00	0.00	0.00	0.00	0.00	0.00	0.00	17.00	8.69
Wadi Small El Geeby	38	Gh15	82.00	335.00	103.83	83.00	46.31	20.00	32.32	6.00	16.52	1.00	11.23	0.00	0.00	0.00	0.00	0.00	0.00	445.00	210.20
Wadi Um Ataqa	39	Ak4	13.92	60.00	21.09	9.00	4.80	2.00	1.32	1.00	6.04	0.00	0.00	0.00	0.00	0.00	0.00	0.00	0.00	72.00	33.25
Wadi S.Abu Khshieeb	40	Ak5	14.00	60.00	14.95	14.00	5.99	3.00	8.38	1.00	1.60	0.00	0.00	0.00	0.00	0.00	0.00	0.00	0.00	78.00	30.93
Wadi Um Harq	41	Ak6	6.00	24.00	8.19	7.00	2.16	1.00	2.98	0.00	0.00	0.00	0.00	0.00	0.00	0.00	0.00	0.00	0.00	32.00	13.34
Wadi South Um Harq	42	Ak7	4.00	20.00	5.55	5.00	2.80	2.00	2.48	1.00	0.26	0.00	0.00	0.00	0.00	0.00	0.00	0.00	0.00	28.00	11.08

App. 3: Stream Order and Stream Length for Subbasins in W. Dahab

NAME	Basin No.	Code No.	Au	1 st order		2nd order		3rd order		4th order		5th order		6th order		7th order		8th order		Total No.	Total Length
			Km²	No.	Length	No.	Length	No.	Length	No.	Length	No.	Length	No.	Length	No.	Length	No.	Length	No.	km
Wadi El Shalal	43	ZA15	42.00	160.00	40.25	39.00	20.20	9.00	9.05	2.00	3.35	1.00	10.31	0.00	0.00	0.00	0.00	0.00	0.00	219.00	99.17
Wadi Fieran	44	ZA16	10.55	46.00	12.61	10.00	5.29	2.00	1.62	1.00	4.10	0.00	0.00	0.00	0.00	0.00	0.00	0.00	0.00	59.00	23.63
Wadi Meer	45	ZA17	20.57	80.00	23.20	15.00	9.38	4.00	4.23	1.00	7.02	0.00	0.00	0.00	0.00	0.00	0.00	0.00	0.00	100.00	44.82
Wadi Tieeha	46	ZA18	10.79	37.00	9.78	7.00	5.96	1.00	7.08	0.00	0.00	0.00	0.00	0.00	0.00	0.00	0.00	0.00	0.00	45.00	22.81
Wadi Hamam	47	ZA19	8.32	34.00	10.17	6.00	5.88	1.00	3.88	0.00	0.00	0.00	0.00	0.00	0.00	0.00	0.00	0.00	0.00	41.00	19.94
Wadi Agnid	48	ZA20	20.87	89.00	27.25	17.00	8.55	4.00	9.18	1.00	5.79	0.00	0.00	0.00	0.00	0.00	0.00	0.00	0.00	111.00	50.76
Wadi Sudud	49	ZA21	9.70	38.00	11.81	7.00	9.08	2.00	0.79	1.00	2.54	0.00	0.00	0.00	0.00	0.00	0.00	0.00	0.00	48.00	24.22
Wadi Nabaa	50	ZA22	15.57	59.00	16.50	15.00	7.65	3.00	6.75	1.00	3.44	0.00	0.00	0.00	0.00	0.00	0.00	0.00	0.00	78.00	34.34
Wadi Abu Khshab	51	ZA23	52.45	224.00	55.17	44.00	33.28	11.00	16.75	2.00	2.87	1.00	10.73	0.00	0.00	0.00	0.00	0.00	0.00	282.00	118.81
Wadi Nasab Main	52	ZA24	165.10	692.00	185.90	158.00	103.74	39.00	49.84	9.00	27.71	3.00	10.22	1.00	17.74	0.00	0.00	0.00	0.00	902.00	395.15
Wadi Merkh	53	ZA25	30.31	119.00	34.16	35.00	15.02	5.00	11.35	2.00	2.99	1.00	6.15	0.00	0.00	0.00	0.00	0.00	0.00	162.00	69.66
Wadi El Faraa	54	ZA26	13.26	47.00	11.66	11.00	9.34	3.00	6.25	1.00	2.67	0.00	0.00	0.00	0.00	0.00	0.00	0.00	0.00	62.00	29.92
Wadi Meer Zaghraa	55	ZA27	10.99	46.00	14.25	10.00	5.00	2.00	5.34	1.00	1.74	0.00	0.00	0.00	0.00	0.00	0.00	0.00	0.00	59.00	26.33
Wadi Mekaffa	56	ZA28	73.02	265.00	84.67	63.00	41.03	18.00	22.86	4.00	6.27	1.00	15.03	0.00	0.00	0.00	0.00	0.00	0.00	351.00	170.76
Wadi Um Retm	57	ZA29	8.86	39.00	9.07	7.00	6.34	1.00	4.39	0.00	0.00	0.00	0.00	0.00	0.00	0.00	0.00	0.00	0.00	47.00	19.80
Wadi Um Saial	58	ZA30	23.94	90.00	28.56	18.00	10.31	4.00	12.74	1.00	4.55	0.00	0.00	0.00	0.00	0.00	0.00	0.00	0.00	122.00	56.15
Wadi Sanad	59	ZA31	72.01	290.00	74.51	60.00	41.05	14.00	23.31	3.00	16.32	1.00	9.31	0.00	0.00	0.00	0.00	0.00	0.00	368.00	164.50
Wadi Zaghraa Main	60	ZA32	148.90	577.00	173.03	138.00	108.39	31.00	57.97	6.00	11.65	2.00	16.38	1.00	11.03	0.00	0.00	0.00	0.00	755.00	378.45
Wadi Um Athan	61	ZA33	9.26	34.00	11.24	8.00	9.04	2.00	3.82	1.00	0.26	0.00	0.00	0.00	0.00	0.00	0.00	0.00	0.00	45.00	24.37
Wadi North Um Athan	62	ZA34	3.62	14.00	4.45	3.00	4.52	1.00	1.36	0.00	0.00	0.00	0.00	0.00	0.00	0.00	0.00	0.00	0.00	18.00	10.33
Wadi Small Barka1	63	ZA35	7.36	24.00	10.50	8.00	5.27	4.00	0.35	1.00	0.09	0.00	0.00	0.00	0.00	0.00	0.00	0.00	0.00	37.00	22.28
Wadi Small Barka 2	64	ZA36	3.14	14.00	4.11	3.00	4.32	1.00	0.50	0.00	0.00	0.00	0.00	0.00	0.00	0.00	0.00	0.00	0.00	18.00	8.94
Wadi Small North Akry	65	ZA37	5.07	10.00	0.12	5.00	4.46	1.00	0.95	0.00	0.00	0.00	0.00	0.00	0.00	0.00	0.00	0.00	0.00	24.00	13.53
Wadi Maryowat	66	ZA38	12.73	48.00	14.97	11.00	6.03	4.00	5.51	1.00	3.79	0.00	0.00	0.00	0.00	0.00	0.00	0.00	0.00	62.00	30.29
Wadi El Kurry	67	ZA39	5.22	20.00	4.00	5.00	5.04	2.00	2.55	1.00	0.21	0.00	0.00	0.00	0.00	0.00	0.00	0.00	0.00	28.00	12.08
Wadi El Matamier	68	ZA40	34.99	132.00	43.51	30.00	22.58	7.00	14.57	1.00	10.01	0.00	0.00	0.00	0.00	0.00	0.00	0.00	0.00	170.00	90.67
Wadi Ghradah	69	ZA41	25.50	107.00	30.11	27.00	22.85	7.00	8.02	1.00	6.70	0.00	0.00	0.00	0.00	0.00	0.00	0.00	0.00	142.00	67.70
Wadi Hablhah	70	ZA42	5.93	22.00	6.07	4.00	5.56	2.00	1.38	1.00	0.70	0.00	0.00	0.00	0.00	0.00	0.00	0.00	0.00	29.00	13.70
Wadi Mabad	71	ZA43	7.03	26.00	8.96	5.00	5.69	1.00	3.20	0.00	0.00	0.00	0.00	0.00	0.00	0.00	0.00	0.00	0.00	32.00	17.85
Wadi El Hoo	72	ZA44	5.31	19.00	7.95	6.00	4.40	2.00	2.68	1.00	0.08	0.00	0.00	0.00	0.00	0.00	0.00	0.00	0.00	28.00	15.11
Wadi Naqab Um Rdeom	73	ZA45	21.80	82.00	26.99	22.00	14.80	5.00	11.21	2.00	5.18	1.00	0.34	0.00	0.00	0.00	0.00	0.00	0.00	112.00	58.52
Wadi Surah	74	ZA46	39.73	153.00	51.49	35.00	29.81	12.00	11.85	3.00	7.40	1.00	0.74	0.00	0.00	0.00	0.00	0.00	0.00	204.00	107.28
Wadi Big Morah	75	ZA47	103.20	408.00	123.82	105.00	71.16	25.00	37.84	6.00	13.21	5.00	13.96	1.00	14.48	0.00	0.00	0.00	0.00	550.00	274.48
Wadi Mytorah	76	ZA48	55.65	210.00	64.71	39.00	30.23	12.00	14.03	4.00	11.06	1.00	6.56	0.00	0.00	0.00	0.00	0.00	0.00	266.00	131.19
Wadi Tyniah	77	ZA49	10.51	38.00	11.00	9.00	7.01	3.00	3.33	1.00	3.58	1.00	0.14	0.00	0.00	0.00	0.00	0.00	0.00	52.00	25.06
Wadi Murad	78	ZA50	10.06	30.00	10.09	0.00	7.95	1.00	3.04	0.00	0.00	0.00	0.00	0.00	0.00	0.00	0.00	0.00	0.00	47.00	25.09
Wadi Um Maksour	79	ZA51	7.19	26.00	6.70	4.00	6.21	1.00	3.73	0.00	0.00	0.00	0.00	0.00	0.00	0.00	0.00	0.00	0.00	31.00	16.63
Wadi El Thmilah	80	ZA52	6.43	26.00	7.00	6.00	4.08	1.00	2.04	0.00	0.00	0.00	0.00	0.00	0.00	0.00	0.00	0.00	0.00	33.00	15.01
Wadi El Halall	81	ZA53	5.88	17.00	4.49	4.00	4.82	1.00	3.24	0.00	0.00	0.00	0.00	0.00	0.00	0.00	0.00	0.00	0.00	22.00	12.56
Wadi Mwyilha	82	ZA54	31.46	116.00	43.07	27.00	21.56	5.00	0.08	1.00	10.80	0.00	0.00	0.00	0.00	0.00	0.00	0.00	0.00	149.00	85.50
Wadi Saal El Rayan	83	ZA55	44.73	166.00	54.66	37.00	29.96	9.00	7.19	4.00	14.23	1.00	8.13	0.00	0.00	0.00	0.00	0.00	0.00	217.00	114.17
Wadi Hagag	84	Gh16	11.43	49.00	14.58	13.00	8.34	3.00	2.77	1.00	4.07	0.00	0.00	0.00	0.00	0.00	0.00	0.00	0.00	66.00	29.75
Wadi South Hagag	85	Gh17	3.87	18.00	4.01	5.00	4.03	2.00	1.29	1.00	1.05	0.00	0.00	0.00	0.00	0.00	0.00	0.00	0.00	26.00	10.98
Wadi Abu Arshy	86	Gh18	5.97	24.00	8.84	6.00	5.65	1.00	1.89	0.00	0.00	0.00	0.00	0.00	0.00	0.00	0.00	0.00	0.00	31.00	16.38
Wadi Ghalium	87	Gh19	12.03	54.00	15.65	14.00	7.02	2.00	3.52	1.00	5.32	0.00	0.00	0.00	0.00	0.00	0.00	0.00	0.00	71.00	32.11
Wadi Bathier	88	Gh20	17.62	73.00	21.79	19.00	8.47	2.00	8.07	1.00	6.02	0.00	0.00	0.00	0.00	0.00	0.00	0.00	0.00	95.00	44.36
Wadi North Bathier	89	Gh21	4.60	16.00	4.71	6.00	4.32	2.00	2.73	1.00	0.52	0.00	0.00	0.00	0.00	0.00	0.00	0.00	0.00	25.00	12.29
Wadi Mezirah	90	Gh22	9.64	45.00	15.78	12.00	5.43	3.00	3.33	1.00	3.05	0.00	0.00	0.00	0.00	0.00	0.00	0.00	0.00	61.00	27.59

App. 4: Stream Order and Stream Length for Subbasins in W. Dahab

NAME	Basin No.	Code No.	Au	1 st order		2nd order		3rd order		4th order		5th order		6th order		7th order		8th order		Total No.	Total Length
			Km²	No.	Length	No.	Length	No.	Length	No.	Length	No.	Length	No.	Length	No.	Length	No.	Length	No.	km
Wadi Um Shietan	91	ZA56	11.30	42.00	14.13	10.00	6.36	3.00	3.33	1.00	3.09	0	0.00	0.00	0.00	0.00	0.00	0.00	0.00	56.00	26.90
Wadi Masharaah	92	ZA57	5.65	24.00	4.93	6.00	4.99	2.00	2.85	1.00	0.22	0	0.00	0.00	0.00	0.00	0.00	0.00	0.00	33.00	12.98
Wadi Main Abu Khshab	93	ZA58	52.00	149.00	36.86	32.00	23.63	9.00	11.79	2.00	2.87	1	5.47	0.00	0.00	0.00	0.00	0.00	0.00	193.00	80.64
Wadi Haziema	94	ZA59	5.78	23.00	6.19	3.00	3.66	1.00	2.86	0.00	0.00	0	0.00	0.00	0.00	0.00	0.00	0.00	0.00	27.00	12.71
Wadi Wedah	95	ZA60	10.81	46.00	12.78	14.00	4.86	2.00	4.14	1.00	3.59	0	0.00	0.00	0.00	0.00	0.00	0.00	0.00	63.00	25.38
Wadi Um Ariefat	96	ZA61	8.02	35.00	9.98	7.00	4.67	3.00	2.79	1.00	1.59	0	0.00	0.00	0.00	0.00	0.00	0.00	0.00	46.00	19.02
Wadi Small Nasab	97	ZA62	72.43	287.00	77.49	66.00	51.60	17.00	22.76	5.00	12.56	2	4.93	1.00	0.00	0.00	0.00	0.00	0.00	378.00	169.33
Wadi Rasies	98	ZA63	45.22	206.00	57.26	44.00	23.42	11.00	13.60	2.00	9.96	1	5.29	0.00	0.00	0.00	0.00	0.00	0.00	264.00	109.52
Wadi Baryiga	99	ZA64	10.10	40.00	11.40	12.00	4.78	2.00	6.56	1.00	1.06	0	0.00	0.00	0.00	0.00	0.00	0.00	0.00	55.00	23.81
Wadi Small Merkh	100	ZA65	7.98	26.00	7.63	8.00	3.78	2.00	3.26	1.00	1.76	0	0.00	0.00	0.00	0.00	0.00	0.00	0.00	37.00	16.43
Wadi Naieema	101	ZA66	6.97	26.00	8.19	4.00	4.34	1.00	2.96	0.00	0.00	0	0.00	0.00	0.00	0.00	0.00	0.00	0.00	31.00	15.48
Wadi Main Mekaffa	102	ZA67	37.37	130.00	43.52	35.00	19.59	10.00	11.80	3.00	2.35	1	10.98	0.00	0.00	0.00	0.00	0.00	0.00	179.00	88.24
Wadi Small Mekaffa	103	ZA68	16.26	65.00	21.29	12.00	10.23	3.00	3.99	1.00	3.90	0	0.00	0.00	0.00	0.00	0.00	0.00	0.00	81.00	39.40
Wadi El Kasied	104	ZA69	8.75	39.00	11.07	7.00	4.31	1.00	5.14	0.00	0.00	0	0.00	0.00	0.00	0.00	0.00	0.00	0.00	47.00	20.53
Wadi Small Um Saial	105	ZA70	13.64	54.00	16.21	10.00	5.82	3.00	7.41	1.00	2.94	0	0.00	0.00	0.00	0.00	0.00	0.00	0.00	68.00	32.39
Wadi Gabr	106	ZA71	35.72	143.00	37.16	31.00	19.42	9.00	9.17	2.00	15.10	1	1.51	0.00	0.00	0.00	0.00	0.00	0.00	186.00	82.37
Wadi Small Sanad	107	ZA72	21.63	82.00	22.99	16.00	13.44	3.00	12.04	1.00	1.18	0	0.00	0.00	0.00	0.00	0.00	0.00	0.00	102.00	49.65
Wadi El Maha El Olia	108	ZA73	8.24	24.00	9.18	6.00	6.94	1.00	3.33	0.00	0.00	0	0.00	0.00	0.00	0.00	0.00	0.00	0.00	31.00	19.44
Wadi Dakek	109	ZA74	3.78	16.00	3.32	5.00	2.24	1.00	3.30	0.00	0.00	0	0.00	0.00	0.00	0.00	0.00	0.00	0.00	22.00	8.86
Wadi Maaran	110	ZA75	32.28	125.00	41.27	29.00	23.48	9.00	10.87	2.00	2.68	1	7.79	0.00	0.00	0.00	0.00	0.00	0.00	166.00	86.09
Wadi Mokhzenah	111	ZA76	9.53	38.00	10.05	10.00	7.51	2.00	5.16	1.00	0.44	0	0.00	0.00	0.00	0.00	0.00	0.00	0.00	51.00	23.17
Wadi El Mokhtar	112	ZA77	7.76	28.00	10.09	8.00	6.71	1.00	2.57	0.00	0.00	0	0.00	0.00	0.00	0.00	0.00	0.00	0.00	37.00	19.37
Wadi S. Ramthy	113	ZA78	20.92	89.00	24.79	22.00	14.20	4.00	11.12	1.00	3.40	0	0.00	0.00	0.00	0.00	0.00	0.00	0.00	116.00	53.50
Wadi Rakieta	114	ZA79	29.05	112.00	38.88	27.00	20.06	8.00	13.89	2.00	5.09	1	2.67	0.00	0.00	0.00	0.00	0.00	0.00	150.00	80.58
Wadi Aska	115	ZA80	5.37	18.00	8.33	5.00	4.72	1.00	1.86	0.00	0.00	0	0.00	0.00	0.00	0.00	0.00	0.00	0.00	24.00	14.91
Wadi Small Matamier	116	ZA81	11.79	44.00	17.61	10.00	5.45	3.00	6.68	1.00	2.56	0	0.00	0.00	0.00	0.00	0.00	0.00	0.00	58.00	32.30
Wadi Defdeef	117	ZA82	15.08	59.00	20.47	15.00	8.67	3.00	8.44	1.00	3.03	0	0.00	0.00	0.00	0.00	0.00	0.00	0.00	78.00	40.61
Wadi West Deef	118	ZA83	6.55	26.00	6.34	7.00	6.13	2.00	2.77	1.00	1.98	0	0.00	0.00	0.00	0.00	0.00	0.00	0.00	36.00	17.22
Wadi Big Sorah	119	ZA84	26.50	101.00	35.25	23.00	19.46	9.00	8.01	3.00	5.69	1	3.72	0.00	0.00	0.00	0.00	0.00	0.00	137.00	72.13
Wadi Samll Sorah	120	ZA85	9.41	43.00	13.29	9.00	8.51	3.00	2.60	1.00	1.71	0	0.00	0.00	0.00	0.00	0.00	0.00	0.00	56.00	26.11
Wadi West Borady	121	ZA86	3.74	15.00	4.81	4.00	2.77	1.00	2.10	0.00	0.00	0	0.00	0.00	0.00	0.00	0.00	0.00	0.00	20.00	9.69
Wadi Borady	122	ZA87	11.04	40.00	12.16	11.00	6.86	2.00	4.51	1.00	3.56	0	0.00	0.00	0.00	0.00	0.00	0.00	0.00	54.00	27.08
Wadi El Tabieh	123	ZA88	21.47	90.00	27.43	23.00	15.24	7.00	7.05	2.00	3.32	1	4.57	0.00	0.00	0.00	0.00	0.00	0.00	123.00	57.62
Wadi Meksan	124	ZA89	3.95	19.00	4.04	4.00	4.07	1.00	1.95	0.00	0.00	0	0.00	0.00	0.00	0.00	0.00	0.00	0.00	24.00	10.06
Wadi Tabaiek	125	ZA90	28.47	110.00	31.76	27.00	19.15	6.00	15.52	2.00	4.78	1	2.64	0.00	0.00	0.00	0.00	0.00	0.00	146.00	73.84
Wadi Um Asaam	126	ZA91	10.62	41.00	10.84	8.00	5.72	2.00	1.33	1.00	6.04	0	0.00	0.00	0.00	0.00	0.00	0.00	0.00	52.00	23.93
Wadi Thmilah	127	ZA92	6.78	23.00	8.50	5.00	4.58	2.00	1.67	1.00	1.28	0	0.00	0.00	0.00	0.00	0.00	0.00	0.00	31.00	16.04
Wadi Small Mytorah	128	ZA93	14.23	61.00	16.23	12.00	7.90	3.00	4.08	1.00	4.35	0	0.00	0.00	0.00	0.00	0.00	0.00	0.00	77.00	32.55
Wadi Abu Dalal	129	ZA94	9.44	37.00	13.15	6.00	7.60	1.00	4.02	0.00	0.00	0	0.00	0.00	0.00	0.00	0.00	0.00	0.00	44.00	24.77
Wadi Small Mywilha	130	ZA95	11.76	45.00	15.79	10.00	6.61	2.00	4.75	1.00	3.80	0	0.00	0.00	0.00	0.00	0.00	0.00	0.00	58.00	30.95
Wadi Small Saal	131	ZA96	8.63	31.00	8.84	7.00	3.66	2.00	2.19	1.00	5.73	0	0.00	0.00	0.00	0.00	0.00	0.00	0.00	41.00	20.42
Wadi Saal El Atshan	132	ZA97	9.94	34.00	10.84	6.00	10.28	2.00	0.56	1.00	4.20	0	0.00	0.00	0.00	0.00	0.00	0.00	0.00	43.00	25.89
Wadi Manader	133	ZA98	3.17	11.00	5.04	3.00	1.80	1.00	1.30	0.00	0.00	0	0.00	0.00	0.00	0.00	0.00	0.00	0.00	15.00	8.14
Wadi Small Saal El Rayan	134	ZA99	1.78	9.00	3.07	3.00	1.55	1.00	0.24	0.00	0.00	0	0.00	0.00	0.00	0.00	0.00	0.00	0.00	13.00	4.86

App. 5: Stream Order and Stream Length for Subbasins in W. Dahab

NAME	Basin No.	Code No.	Au	1st order		2nd order		3rd order		4th order		5th order		6th order		7th order		8th order		Total No.	Total Length
			Km²	No.	Length	No.	Length	No.	Length	No.	Length	No.	Length	No.	Length	No.	Length	No.	Length	No.	km
Wadi Small Abu Khashab	135	ZA100	13.00	56.00	13.43	11.00	9.93	3.00	4.41	1.00	2.08	0.00	0.00	0.00	0.00	0.00	0.00	0.00	0.00	71.00	29.86
Wadi Hassa	136	ZA101	5.63	26.00	6.06	7.00	3.80	2.00	3.51	1.00	0.79	0.00	0.00	0.00	0.00	0.00	0.00	0.00	0.00	36.00	14.16
Wadi El Waraa	137	ZA102	10.87	46.00	9.96	8.00	5.27	3.00	5.36	1.00	3.75	0.00	0.00	0.00	0.00	0.00	0.00	0.00	0.00	58.00	24.34
Wadi Small Nasab	138	ZA103	57.20	215.00	65.20	52.00	39.50	14.00	17.30	4.00	8.70	2.00	4.90	1.00	4.90	0.00	0.00	0.00	0.00	288.00	140.50
Wadi Myenat	139	ZA104	14.57	67.00	18.17	13.00	7.55	4.00	6.90	1.00	2.36	0.00	0.00	0.00	0.00	0.00	0.00	0.00	0.00	85.00	34.98
Wadi Roting	140	ZA105	18.77	84.00	24.80	20.00	10.21	5.00	3.80	1.00	7.47	0.00	0.00	0.00	0.00	0.00	0.00	0.00	0.00	110.00	46.27
Wadi Haialah	141	ZA106	4.23	11.00	3.44	4.00	2.15	1.00	2.44	0.00	0.00	0.00	0.00	0.00	0.00	0.00	0.00	0.00	0.00	16.00	8.03
Wadi Small Haialah	142	ZA107	2.50	9.00	3.36	3.00	1.43	1.00	0.76	0.00	0.00	0.00	0.00	0.00	0.00	0.00	0.00	0.00	0.00	13.00	5.55
Wadi Um Harhal	143	ZA108	4.40	17.00	6.83	5.00	1.33	2.00	2.71	1.00	0.56	0.00	0.00	0.00	0.00	0.00	0.00	0.00	0.00	25.00	11.43
Wadi Small El Faraa	144	ZA109	5.02	19.00	5.45	5.00	2.68	2.00	3.15	1.00	0.69	0.00	0.00	0.00	0.00	0.00	0.00	0.00	0.00	27.00	11.97
Wadi Homrah	145	ZA110	8.93	31.00	9.46	6.00	5.10	2.00	2.82	1.00	1.65	0.00	0.00	0.00	0.00	0.00	0.00	0.00	0.00	40.00	19.02
Wadi Small Homrah	146	ZA111	3.86	15.00	4.51	4.00	3.37	1.00	1.13	0.00	0.00	0.00	0.00	0.00	0.00	0.00	0.00	0.00	0.00	20.00	9.00
Wadi Goo	147	ZA112	20.09	85.00	21.59	19.00	9.09	5.00	6.65	1.00	7.63	0.00	0.00	0.00	0.00	0.00	0.00	0.00	0.00	110.00	44.96
Wadi Abu Tabak	148	ZA113	14.60	53.00	15.13	12.00	10.33	4.00	2.52	1.00	7.37	0.00	0.00	0.00	0.00	0.00	0.00	0.00	0.00	70.00	35.34
Wadi Abu Sahsieh	149	ZA114	13.24	53.00	14.86	10.00	8.44	1.00	8.44	0.00	0.00	0.00	0.00	0.00	0.00	0.00	0.00	0.00	0.00	64.00	31.75
Wadi Khadrah	150	ZA115	2.27	6.00	2.64	3.00	0.92	1.00	0.97	0.00	0.00	0.00	0.00	0.00	0.00	0.00	0.00	0.00	0.00	10.00	4.53
Wadi Small Maraan	151	ZA116	5.28	26.00	8.10	5.00	5.52	2.00	0.94	1.00	1.87	0.00	0.00	0.00	0.00	0.00	0.00	0.00	0.00	34.00	16.44
Wadi East Small Maraan	152	ZA117	6.02	27.00	8.44	7.00	3.55	2.00	4.39	1.00	0.74	0.00	0.00	0.00	0.00	0.00	0.00	0.00	0.00	37.00	17.13
Wadi Small Ramthy	153	ZA118	9.55	44.00	9.38	11.00	5.73	4.00	6.38	1.00	2.15	0.00	0.00	0.00	0.00	0.00	0.00	0.00	0.00	60.00	23.64
Wadi Small Zaghraa	154	ZA119	10.23	44.00	13.71	11.00	8.46	1.00	4.74	0.00	0.00	0.00	0.00	0.00	0.00	0.00	0.00	0.00	0.00	56.00	26.91
Wadi Hamami	155	ZA120	15.62	65.00	20.86	17.00	7.60	5.00	10.23	1.00	3.47	0.00	0.00	0.00	0.00	0.00	0.00	0.00	0.00	88.00	42.16
Wadi El Aranyia	156	ZA121	8.06	26.00	11.27	6.00	8.80	2.00	3.26	1.00	1.59	0.00	0.00	0.00	0.00	0.00	0.00	0.00	0.00	35.00	24.91
Wadi Abu Tehimah	157	ZA122	5.94	22.00	9.70	5.00	3.57	2.00	2.58	1.00	0.52	0.00	0.00	0.00	0.00	0.00	0.00	0.00	0.00	30.00	16.37
Wadi South Abu Tehimah	158	ZA123	2.38	10.00	4.13	3.00	2.42	1.00	0.38	0.00	0.00	0.00	0.00	0.00	0.00	0.00	0.00	0.00	0.00	14.00	6.93
Wadi El Saraah	159	ZA124	6.42	24.00	6.30	5.00	4.71	2.00	3.50	1.00	1.32	0.00	0.00	0.00	0.00	0.00	0.00	0.00	0.00	32.00	15.82
Wadi Small Tabieh	160	ZA125	7.73	29.00	9.64	7.00	6.36	2.00	1.40	1.00	2.44	0.00	0.00	0.00	0.00	0.00	0.00	0.00	0.00	39.00	19.83
Wadi South Small Tabaieh	161	ZA126	3.95	19.00	4.58	3.00	2.87	1.00	2.65	0.00	0.00	0.00	0.00	0.00	0.00	0.00	0.00	0.00	0.00	23.00	10.10
Wadi North Small Tabaieh	162	ZA127	4.67	24.00	6.24	8.00	3.29	3.00	2.80	1.00	0.87	0.00	0.00	0.00	0.00	0.00	0.00	0.00	0.00	36.00	13.19
Wadi Retem	163	ZA128	5.79	23.00	6.55	6.00	3.43	2.00	5.15	1.00	0.22	0.00	0.00	0.00	0.00	0.00	0.00	0.00	0.00	32.00	15.35
Wadi North Retem	164	ZA129	4.90	15.00	6.33	4.00	3.86	1.00	3.53	0.00	0.00	0.00	0.00	0.00	0.00	0.00	0.00	0.00	0.00	20.00	13.72
Wadi Small Tabaiek	165	ZA130	5.99	27.00	6.07	7.00	4.45	1.00	4.36	0.00	0.00	0.00	0.00	0.00	0.00	0.00	0.00	0.00	0.00	35.00	14.88
Wadi South Small Tabaiek	166	ZA131	7.03	27.00	6.73	7.00	5.43	2.00	2.43	1.00	2.78	0.00	0.00	0.00	0.00	0.00	0.00	0.00	0.00	37.00	17.38
Wadi Zaraa	167	ZA132	22.86	85.00	26.51	25.00	15.61	6.00	7.00	2.00	3.30	1.00	3.53	0.00	0.00	0.00	0.00	0.00	0.00	119.00	55.95
Wadi Rahabah	168	ZA133	22.00	94.00	26.39	25.00	15.32	5.00	7.85	2.00	5.46	1.00	1.18	0.00	0.00	0.00	0.00	0.00	0.00	127.00	56.20
Wadi North Zaraa	169	ZA134	6.25	24.00	2.24	7.00	4.69	2.00	2.24	1.00	1.71	0.00	0.00	0.00	0.00	0.00	0.00	0.00	0.00	34.00	10.87
Wadi South Zaraa	170	ZA135	8.33	27.00	2.75	7.00	6.29	2.00	2.75	1.00	1.58	0.00	0.00	0.00	0.00	0.00	0.00	0.00	0.00	37.00	13.36
Wadi Small Nasab	171	ZA136	8.99	41.00	4.05	10.00	6.02	3.00	4.05	1.00	1.05	0.00	0.00	0.00	0.00	0.00	0.00	0.00	0.00	55.00	15.16
Wadi Small Rahabah	172	ZA137	11.15	44.00	3.80	9.00	7.30	2.00	3.80	1.00	4.22	0.00	0.00	0.00	0.00	0.00	0.00	0.00	0.00	56.00	19.12
Wadi East Maeen	173	Ak8	8.96	41.00	13.10	9.00	5.71	2.00	2.47	1.00	1.87	0.00	0.00	0.00	0.00	0.00	0.00	0.00	0.00	53.00	23.15
Wadi West Maeen	174	Ak9	4.75	23.00	6.98	7.00	4.64	2.00	0.33	1.00	2.00	0.00	0.00	0.00	0.00	0.00	0.00	0.00	0.00	33.00	13.95

App. 6: Stream Order and Stream Length for Subbasins in W. Dahab

NAME	basin_or u	A_U km^2	P km	L km	W km	D km^{-1}	F km^{-2}	OIF	R_c	R_e	R_{ba}	R_{bw}
Wadi Mega Dahab	8 th	2088	288.00	57.79	74.47	2.42	5.02	0.21	0.32	0.50	3.74	4.37
Wadi South Zaghraa	4 th	8	14.24	4.93	1.92	3.34	5.57	0.15	0.51	0.37	3.72	5.44
Wadi Um Asaam	4 th	7	15.64	5.88	1.30	2.31	5.68	0.22	0.37	0.29	3.31	4.04
Wadi Abu Khshieeb	6 th	107	53.72	15.09	11.78	2.28	5.20	0.22	0.47	0.44	3.50	4.54
Wadi El Ghaieb	6 th	299	140.90	32.67	10.57	3.71	6.32	0.13	0.19	0.34	4.42	4.10
Wadi Zaghraa	8 th	1617	242.80	47.38	65.21	3.68	6.14	0.14	0.34	0.54	3.88	3.72
Wadi Zaghraa Nasab	7 th	936	211.20	37.72	26.60	2.60	5.79	0.19	0.26	0.52	4.12	4.42
Wadi Zaghraa Saal	7 th	663	186.30	51.71	22.95	2.87	5.49	0.17	0.24	0.32	3.80	4.24
Wadi Abu Rwies	4 th	20	29.18	5.91	3.69	2.41	5.05	0.21	0.29	0.48	4.22	4.82
Wadi Kharza	3 rd	11	18.19	5.47	2.27	2.02	4.03	0.25	0.42	0.39	5.75	5.44
Wadi Hamarah Ghai	4 th	11	16.92	3.72	4.49	2.17	4.70	0.23	0.48	0.56	3.78	5.59
Wadi South Um Marha	3 rd	7	13.49	3.11	3.34	2.16	4.70	0.23	0.51	0.56	5.38	6.20
Wadi Hodbah	4 th	20	25.68	8.61	3.03	3.15	5.40	0.16	0.38	0.33	4.17	4.05
Wadi Abu Gerdan	5 th	27	30.06	6.40	4.14	2.50	5.90	0.20	0.37	0.52	3.33	3.96
Wadi El Geeby	6 th	134	72.19	20.69	10.96	2.85	6.30	0.18	0.32	0.36	3.67	3.95
Wadi Um Shawky	4 th	25	31.04	10.45	3.04	3.27	5.97	0.15	0.32	0.30	5.00	5.60
Wadi Maeen	5 th	19	18.89	6.50	4.07	3.94	7.55	0.13	0.66	0.42	3.54	5.21
Wadi Small Abu Khshieb	5 th	51	40.31	10.74	10.03	3.32	6.48	0.15	0.40	0.42	4.27	5.72
Wadi Rimthy	6 th	413	137.20	34.91	18.74	2.38	5.00	0.21	0.28	0.37	4.39	4.22
Wadi El Genah	6 th	285	117.60	31.26	11.13	2.61	5.04	0.19	0.26	0.34	4.05	4.10
Wadi Mega Saal	6 th	246	128.40	33.73	10.72	2.43	4.63	0.21	0.19	0.30	4.08	4.00
Wadi Nasab	6 th	445	169.80	47.97	12.53	2.35	5.24	0.21	0.19	0.28	4.51	4.49
Wadi Korna	5 th	33	30.85	9.96	4.55	2.19	5.08	0.23	0.43	0.37	3.56	4.18
Wadi Small El Hamam	3 th	6	12.14	2.92	3.05	2.34	4.24	0.21	0.48	0.52	4.38	4.43
Wadi Mega Barka	5 th	29	26.40	7.86	4.86	2.79	4.86	0.18	0.52	0.44	3.36	4.14
Wadi Naghmishy	4 th	6	10.84	2.04	3.47	2.33	5.45	0.21	0.59	0.73	2.79	2.85
Wadi South Um Athan	3 rd	5	12.05	3.79	2.39	2.06	3.68	0.24	0.47	0.39	3.88	3.61
Wadi Remty	3 rd	9	16.40	4.91	2.70	2.34	4.92	0.21	0.43	0.39	6.44	4.82
Wadi South Akry	4 th	9	13.49	3.81	4.27	2.76	5.56	0.18	0.62	0.50	3.31	3.44
Wadi Mega North Akry	5 th	26	28.58	8.91	4.10	2.49	4.81	0.20	0.40	0.37	3.23	3.96
Wadi Small Hodbah	4 th	8	15.76	3.77	1.88	2.43	4.60	0.21	0.40	0.47	3.17	3.99
Wadi South Small Hodbah	3 rd	3	7.88	2.26	2.38	2.50	5.86	0.20	0.55	0.46	3.50	3.56
Wadi Khalal	4 th	6	12.16	3.60	2.48	2.23	4.91	0.22	0.52	0.44	2.83	3.18
Wadi Geb Um Reglah	4 th	19	25.60	7.63	4.11	2.42	5.09	0.21	0.37	0.37	4.22	3.90
Wadi El Marwah	4 th	8	16.28	5.91	2.06	2.74	6.39	0.18	0.39	0.31	3.60	4.54
Wadi Abu Haiethat	5 th	33	32.70	10.87	5.53	2.66	5.69	0.19	0.39	0.34	3.59	3.76
Wadi South Small El Geeby	3 th	3	9.74	2.29	1.48	2.74	5.36	0.18	0.42	0.49	3.67	3.84
Wadi Small El Geeby	5 th	82	60.68	15.37	5.36	2.55	5.40	0.20	0.28	0.38	4.38	4.04
Wadi Um Ataqa	4 th	14	17.94	7.49	2.94	2.64	5.68	0.19	0.54	0.32	4.39	6.17
Wadi S.Abu Khshieeb	4 th	14	19.84	5.80	3.09	2.05	6.38	0.24	0.45	0.41	3.24	4.26
Wadi Um Harq	3 rd	6	11.78	3.75	2.41	1.99	6.04	0.25	0.57	0.43	5.21	4.10
Wadi South Um Harq	4 th	4	9.13	3.26	2.21	2.58	7.00	0.19	0.67	0.41	2.83	3.45

A_U	Basin Area (km^2)	D	Drainage Density (km^{-1})	R_e	Elongation ratio	
P	Basin Permieter (km)	F	Drainage Frequency (km^{-2})	R_{ba}	Bifurcation ratio	
L	Basin Length (km)	OIF	Overland Flow	R_{bw}	Weighted Bifurcation ratio	
W	Basin Width (km)	R_c	Circulatory ratio			

App. 7: Results of Morphometric Analysis in Subbasins of W. Dahab

NAME	basin_or u	A_U km^2	P km	L km	W km	D km^{-1}	F km^{-2}	OIF	R_c	R_e	R_{ba}	R_{bw}
Wadi El Shalal	5 th	42	38.61	12.74	4.86	2.13	5.19	0.23	0.36	0.32	3.79	4.28
Wadi Fieran	4 th	11	16.20	5.42	2.08	2.24	5.59	0.22	0.51	0.38	3.87	4.50
Wadi Meer	4 th	21	26.05	5.53	6.72	2.18	4.86	0.23	0.38	0.52	4.36	4.99
Wadi Tieeba	3 rd	11	21.47	8.00	1.95	2.11	4.17	0.24	0.29	0.26	6.14	5.43
Wadi Hamam	3 rd	8	12.55	4.06	3.44	2.40	4.92	0.21	0.66	0.45	5.83	5.58
Wadi Agnid	4 th	21	26.47	8.18	2.93	2.43	5.32	0.21	0.37	0.36	4.50	4.99
Wadi Sudud	4 th	10	15.21	3.93	3.70	2.50	4.95	0.20	0.53	0.50	3.64	4.89
Wadi Nabaa	4 th	16	19.29	5.62	3.23	2.21	5.01	0.23	0.53	0.45	3.98	4.05
Wadi Abu Khshab	5 th	52	43.30	11.02	6.19	2.27	5.38	0.22	0.35	0.42	5.53	4.90
Wadi Nasab Main	6 th	307	132.10	35.49	17.71	2.39	5.46	0.21	0.35	0.38	4.69	4.30
Wadi Merkh	5 th	30	30.84	9.55	4.52	2.13	5.34	0.23	0.40	0.37	3.73	4.11
Wadi El Faraa	4 th	13	21.03	3.46	6.98	2.26	4.68	0.22	0.38	0.67	3.65	4.03
Wadi Meer Zaghraa	4 th	11	17.91	4.79	3.47	2.40	5.37	0.21	0.43	0.44	3.87	4.50
Wadi Mekaffa	5 th	73	56.14	15.38	6.51	2.13	4.81	0.23	0.29	0.35	4.05	4.08
Wadi Um Retm	3 rd	9	15.70	6.14	2.30	2.23	5.30	0.22	0.45	0.31	6.29	5.67
Wadi Um Saial	4 th	24	24.49	6.71	4.90	2.35	5.10	0.21	0.50	0.46	4.67	5.26
Wadi Sanad	5 th	72	47.96	14.97	6.98	2.17	5.11	0.23	0.39	0.36	4.20	4.71
Wadi Zaghraa Main	6 th	149	72.01	19.48	9.31	2.38	5.07	0.21	0.36	0.40	3.76	4.25
Wadi Um Athan	4 th	9	14.35	3.94	3.19	2.63	4.97	0.19	0.57	0.49	3.42	4.01
Wadi North Um Athan	3 rd	4	9.71	3.39	1.82	2.85	4.97	0.18	0.48	0.36	3.83	4.13
Wadi Small Barka1	4 th	7	17.19	3.21	5.38	3.03	5.02	0.17	0.31	0.54	3.00	2.81
Wadi Small Barka 2	3 rd	3	8.70	3.00	1.54	3.71	6.70	0.13	0.52	0.38	3.83	4.13
Wadi Small North Akry	3 rd	5	9.56	2.53	3.19	2.67	4.74	0.19	0.70	0.57	4.30	3.74
Wadi Maryowat	4 th	13	21.79	6.13	2.21	2.38	4.87	0.21	0.34	0.37	3.64	3.85
Wadi El Kurry	4 th	5	12.43	3.81	1.09	2.43	5.36	0.21	0.43	0.38	2.83	3.45
Wadi El Matamier	4 th	35	29.39	8.82	5.53	2.59	4.86	0.19	0.51	0.43	5.23	4.46
Wadi Ghradah	4 th	26	27.16	8.23	3.71	2.65	5.55	0.19	0.44	0.39	4.94	4.06
Wadi Habibah	4 th	6	11.69	3.31	2.05	2.31	4.89	0.22	0.55	0.47	2.63	4.62
Wadi Mabad	3 rd	7	14.74	4.65	1.71	2.54	4.55	0.20	0.41	0.36	5.10	5.01
Wadi El Hoo	4 th	5	9.61	2.49	2.56	2.83	5.08	0.18	0.72	0.59	2.72	2.93
Wadi Naqab Um Rdeem	5 th	22	22.92	4.56	7.31	2.71	5.14	0.18	0.52	0.65	3.16	3.74
Wadi Sorah	5 th	40	35.95	11.27	3.52	2.61	5.18	0.19	0.39	0.36	3.57	4.06
Wadi Big Morah	6 th	103	72.65	17.49	7.50	2.44	5.33	0.20	0.25	0.37	3.69	3.93
Wadi Mytorah	5 th	56	42.87	12.61	6.62	2.26	4.78	0.22	0.38	0.38	3.91	4.92
Wadi Tyniah	5 th	11	19.27	4.34	2.01	2.47	4.95	0.20	0.36	0.48	2.81	3.80
Wadi Murad	3 rd	10	18.21	3.46	3.36	2.55	4.67	0.20	0.38	0.58	6.38	5.20
Wadi Um Maksour	3 rd	7	14.25	5.43	2.35	2.31	4.31	0.22	0.44	0.31	5.25	5.97
Wadi El Thmilah	3 rd	6	12.79	3.88	2.73	2.33	5.13	0.21	0.49	0.42	5.17	4.51
Wadi El Halall	3 rd	6	12.41	4.39	1.63	2.14	3.74	0.23	0.48	0.35	4.13	4.01
Wadi Mwyilha	4 th	31	32.83	10.71	5.79	2.72	4.74	0.18	0.37	0.33	4.90	4.49
Wadi Saal El Rayan	5 th	45	44.83	8.68	5.84	2.39	4.85	0.21	0.28	0.49	3.71	4.30
Wadi Hagag	4 th	11	17.79	5.77	2.53	2.60	5.77	0.19	0.45	0.37	3.70	3.79
Wadi South Hagag	4 th	4	10.63	2.02	3.67	2.84	6.72	0.18	0.43	0.62	2.70	3.13
Wadi Abu Arshy	3 rd	6	12.07	3.59	2.53	2.74	5.19	0.18	0.52	0.43	5.00	4.26
Wadi Ghalium	4 th	13	21.29	5.29	1.98	2.54	5.62	0.20	0.35	0.43	4.29	4.37
Wadi Bathier	4 th	18	27.02	9.37	2.42	2.52	5.39	0.20	0.30	0.29	5.11	4.89
Wadi North Bathier	4 th	5	10.35	3.57	1.80	2.67	5.44	0.19	0.54	0.38	2.56	2.59
Wadi Mezirah	4 th	10	14.22	4.13	3.64	2.86	6.33	0.17	0.60	0.48	3.58	3.70

A_U	Basin Area (km^2)	D	Drainage Density (km^{-1})	R_e	Elongation ratio
P	Basin Permieter (km)	F	Drainage Frequency (km^{-2})	R_{ba}	Bifurcation ratio
L	Basin Length (km)	OIF	Overland Flow	R_{bw}	Weighted Bifurcation ratio
W	Basin Width (km)	R_c	Circulatory ratio		

App. 8: Results of Morphometric Analysis in Subbasins of W. Dahab

NAME	basin_or	A_U	P	L	W	D	F	OIF	R_c	R_e	R_{ba}	R_{bw}
	u	km^2	km	km	km	km^{-1}	km^{-2}					
Wadi Um Shietan	4 th	11	15.34	4.87	2.64	2.38	4.96	0.21	0.60	0.44	3.51	3.91
Wadi Masharaah	4 th	6	10.73	2.43	3.73	2.30	5.84	0.22	0.62	0.62	3.00	3.58
Wadi Main Abu Khshab	5 th	36	31.08	6.71	5.98	2.26	5.40	0.22	0.47	0.57	3.68	4.41
Wadi Haziema	3 rd	6	11.03	4.01	1.87	2.20	4.67	0.23	0.60	0.38	5.33	6.86
Wadi Wedah	4 th	11	17.01	5.35	2.04	2.35	5.83	0.21	0.47	0.39	4.10	4.02
Wadi Um Ariefat	4 th	8	11.98	3.07	2.94	2.37	5.74	0.21	0.70	0.59	3.44	4.36
Wadi Small Nasab	6 th	72	40.35	12.72	5.82	2.42	5.22	0.21	0.56	0.43	3.23	4.18
Wadi Rasies	5 th	45	38.61	9.33	7.32	2.42	5.84	0.21	0.38	0.46	4.05	4.56
Wadi Baryiga	4 th	10	15.27	3.60	3.99	2.36	5.45	0.21	0.54	0.56	3.78	3.81
Wadi Small Merkh	4 th	8	16.18	4.90	2.84	2.06	4.76	0.24	0.38	0.37	3.08	3.26
Wadi Naieema	3 rd	7	12.20	3.85	2.41	2.22	4.45	0.23	0.59	0.44	5.25	5.97
Wadi Main Mekaffa	5 th	37	37.47	11.07	4.76	2.36	4.79	0.21	0.33	0.35	4.52	3.62
Wadi Small Mekaffa	4 th	16	21.71	6.13	6.35	2.42	4.98	0.21	0.43	0.42	4.14	5.05
Wadi El Kasied	3 rd	9	19.03	5.40	1.21	2.35	5.37	0.21	0.30	0.35	6.29	5.67
Wadi Small Um Saial	4 th	14	17.55	5.67	3.72	2.37	4.99	0.21	0.56	0.41	3.91	4.91
Wadi Gabr	5 th	36	30.38	9.08	5.08	2.31	5.21	0.22	0.49	0.42	4.85	4.36
Wadi Small Sanad	4 th	22	31.56	4.47	11.73	2.30	4.72	0.22	0.27	0.66	4.49	5.04
Wadi El Maha El Olia	3 rd	8	13.00	3.44	2.96	2.36	3.76	0.21	0.61	0.53	5.00	4.26
Wadi Dakek	3 rd	4	11.18	3.90	1.22	2.34	5.82	0.21	0.38	0.32	4.10	3.46
Wadi Maaran	5 th	32	34.29	10.88	3.24	2.67	5.14	0.19	0.35	0.33	4.68	4.08
Wadi Mokhzenah	4 th	10	15.94	4.80	2.61	2.43	5.35	0.21	0.47	0.41	3.60	3.89
Wadi El Mokhtar	3 rd	8	12.98	3.52	2.73	2.50	4.77	0.20	0.58	0.50	5.75	4.38
Wadi S. Ramthy	4 th	21	22.58	5.68	5.38	2.56	5.54	0.20	0.52	0.51	4.52	4.28
Wadi Rakieta	5 th	29	24.55	6.94	6.01	2.77	5.16	0.18	0.61	0.49	4.51	3.94
Wadi Aska	3 rd	5	10.64	3.53	2.30	2.78	4.47	0.18	0.60	0.42	4.30	3.74
Wadi Small Matamier	4 th	12	16.91	3.39	4.80	2.74	4.92	0.18	0.52	0.65	3.58	4.07
Wadi Defdeef	4 th	15	18.85	5.85	4.76	2.69	5.17	0.19	0.53	0.42	3.98	4.05
Wadi West Deef	4 th	7	13.00	4.55	2.28	2.63	5.50	0.19	0.49	0.36	3.07	3.47
Wadi Big Sorah	5 th	27	28.39	9.55	4.68	2.72	5.17	0.18	0.41	0.34	4.32	3.93
Wadi Samll Sorah	4 th	9	15.56	4.08	3.11	2.78	5.95	0.18	0.49	0.48	3.59	4.31
Wadi West Borady	3 rd	4	9.87	3.20	1.71	2.59	5.35	0.19	0.48	0.38	3.88	3.61
Wadi Borady	4 th	11	21.27	6.54	2.41	2.45	4.89	0.20	0.31	0.32	3.71	3.89
Wadi El Tabieh	5 th	21	22.98	7.88	4.23	2.68	5.73	0.19	0.51	0.37	4.23	3.71
Wadi Meksan	3 rd	4	10.36	3.45	1.74	2.54	6.07	0.20	0.46	0.37	4.38	4.43
Wadi Tabaiek	5 th	28	31.29	6.61	7.11	2.59	5.13	0.19	0.37	0.51	4.52	4.05
Wadi Um Asaam	4 th	11	20.35	7.30	2.15	2.25	4.90	0.22	0.32	0.28	3.71	4.73
Wadi Thmilah	4 th	7	14.49	3.02	4.49	2.37	4.57	0.21	0.41	0.55	3.03	3.95
Wadi Small Mytorah	4 th	14	19.40	5.70	3.32	2.29	5.41	0.22	0.48	0.42	4.03	4.77
Wadi Abu Dalal	3 rd	9	14.42	4.64	2.04	2.62	4.66	0.19	0.57	0.42	6.08	6.00
Wadi Small Mywilha	4 th	12	18.03	4.59	3.37	2.63	4.93	0.19	0.45	0.48	3.83	4.42
Wadi Small Saal	4 th	9	20.73	7.04	1.75	2.37	4.75	0.21	0.25	0.27	3.31	4.04
Wadi Saal El Atshan	4 th	10	19.28	4.91	3.58	2.61	4.33	0.19	0.34	0.41	3.56	4.99
Wadi Manader	3 rd	3	8.16	2.24	1.98	2.56	4.73	0.19	0.60	0.51	3.33	3.29
Wadi Small Saal El Rayan	3 rd	2	6.35	1.29	1.48	2.74	7.32	0.18	0.55	0.65	3.00	2.77

A_U	Basin Area (km^2)	D	Drainage Density (km^{-1})	R_e	Elongation ratio	
P	Basin Permieter (km)	F	Drainage Frequency (km^{-2})	R_{ba}	Bifurcation ratio	
L	Basin Length (km)	OIF	Overland Flow	R_{bw}	Weighted Bifurcation ratio	
W	Basin Width (km)	R_c	Circulatory ratio			

App. 9: Results of Morphometric Analysis in Subbasins of W. Dahab

NAME	basin_or u	A_U km^2	P km	L km	W km	D km^{-1}	F km^{-2}	OIF	R_c	R_e	R_{ba}	R_{bw}
Wadi Small Abu Khashab	4 th	13	19.01	3.58	4.62	2.23	5.29	0.22	0.47	0.65	3.92	4.71
Wadi Hassa	4 th	6	10.24	2.87	3.15	2.51	6.39	0.20	0.68	0.53	3.07	3.47
Wadi El Waraa	4 th	11	16.22	4.31	4.79	2.24	5.34	0.22	0.52	0.49	3.81	5.08
Wadi Small Nasab	6th	57	36.80	11.50	7.20	2.42	5.22	0.21	0.56	0.43	3.23	4.18
Wadi Myenat	4 th	15	19.68	4.54	6.41	2.40	5.83	0.21	0.47	0.53	4.13	4.75
Wadi Roting	4 th	19	21.72	7.85	3.98	2.47	5.86	0.20	0.50	0.35	4.40	4.16
Wadi Haialah	3 rd	4	10.89	3.60	1.89	1.90	3.78	0.26	0.45	0.36	3.38	2.89
Wadi Small Haialah	3 rd	2	6.94	2.12	2.04	2.22	5.21	0.22	0.65	0.47	3.00	2.77
Wadi Um Harhal	4 th	4	10.32	3.48	2.01	2.60	5.69	0.19	0.52	0.38	2.63	2.97
Wadi Small El Faraa	4 th	5	10.84	3.77	1.89	2.38	5.38	0.21	0.54	0.38	2.77	3.29
Wadi Homrah	4 th	9	15.95	4.56	2.63	2.13	4.48	0.23	0.44	0.42	3.39	4.55
Wadi Small Homrah	3 rd	4	8.43	1.90	3.08	2.33	5.18	0.21	0.68	0.66	3.88	3.61
Wadi Goo	4th	20	26.99	6.43	3.99	2.24	5.48	0.22	0.35	0.44	4.43	4.34
Wadi Abu Tabak	4 th	15	21.18	7.54	2.60	2.42	4.79	0.21	0.41	0.32	3.81	4.09
Wadi Abu Sahsieh	3 rd	13	24.15	3.20	9.21	2.40	4.83	0.21	0.29	0.72	7.65	5.95
Wadi Khadrah	3 rd	2	6.79	1.65	2.31	2.00	4.41	0.25	0.62	0.58	2.50	2.10
Wadi Small Maraan	4 th	5	12.54	3.60	1.54	3.11	6.44	0.16	0.42	0.41	3.23	4.46
Wadi East Small Maraan	4 th	6	11.86	3.86	2.21	2.85	6.15	0.18	0.54	0.40	3.12	3.58
Wadi Small Ramthy	4 th	10	14.87	4.88	2.94	2.48	6.28	0.20	0.54	0.40	3.58	3.70
Wadi Small Zaghraa	3 rd	10	17.30	5.00	2.12	2.63	5.47	0.19	0.43	0.41	7.50	5.30
Wadi Hamami	4 th	16	18.65	5.09	5.15	2.70	5.63	0.19	0.56	0.49	4.08	3.77
Wadi El Aranyia	4 th	8	14.11	5.42	2.33	3.09	4.34	0.16	0.51	0.33	3.11	3.85
Wadi Abu Tehimah	4 th	6	11.11	2.75	3.85	2.75	5.05	0.18	0.61	0.56	2.97	3.78
Wadi South Abu Tehimah	3 rd	2	8.03	2.16	2.22	2.91	5.88	0.17	0.46	0.46	3.17	3.02
Wadi El Saraah	4 th	6	13.95	4.65	1.75	2.46	4.98	0.20	0.41	0.35	3.10	4.12
Wadi Small Tabieh	4 th	8	14.91	4.06	2.48	2.56	5.17	0.20	0.44	0.44	3.21	3.81
Wadi South Small Tabaieh	3 rd	4	12.25	3.96	1.07	2.56	5.82	0.20	0.33	0.32	4.67	5.62
Wadi North Small Tabaieh	4 th	5	10.12	3.00	2.34	2.82	7.92	0.18	0.57	0.46	2.89	2.84
Wadi Retem	4 th	6	12.25	4.27	2.45	2.65	5.70	0.19	0.48	0.36	2.94	3.44
Wadi North Retem	3 rd	5	12.38	4.29	1.43	2.80	4.08	0.18	0.40	0.33	3.88	3.61
Wadi Small Tabaiek	3 rd	6	13.86	4.52	1.91	2.49	6.01	0.20	0.39	0.34	5.43	4.38
Wadi South Small Tabaiek	4 th	7	14.99	4.44	2.47	2.47	5.26	0.20	0.39	0.38	3.12	3.58
Wadi Zaraa	5 th	23	22.90	6.35	4.72	2.45	5.21	0.20	0.55	0.48	3.14	3.49
Wadi Rahabah	5 th	22	25.07	7.25	5.71	2.55	5.77	0.20	0.44	0.41	3.32	3.90
Wadi North Zaraa	4 th	6	11.38	3.16	4.16	2.43	5.44	0.21	0.61	0.50	2.98	3.26
Wadi South Zaraa	4 th	8	12.97	4.52	2.02	2.55	4.44	0.20	0.62	0.41	3.12	3.58
Wadi Small Nasab	4 th	9	16.65	2.35	5.03	2.63	6.12	0.19	0.41	0.81	3.48	3.83
Wadi Small Rahabah	4 th	11	20.19	7.26	1.28	2.30	5.02	0.22	0.34	0.29	3.80	4.64
Wadi East Maeen	4 th	9	15.40	3.28	3.98	3.20	7.59	0.16	0.47	0.58	3.69	4.36
Wadi West Maeen	4 th	5	9.78	3.67	2.09	4.29	9.68	0.12	0.62	0.38	2.93	3.15

A_U	Basin Area (km^2)	D	Drainage Density (km^{-1})	R_e	Elongation ratio
P	Basin Permieter (km)	F	Drainage Frequency (km^{-2})	R_{ba}	Bifurcation ratio
L	Basin Length (km)	OIF	Overland Flow	R_{bw}	Weighted Bifurcation ratio
W	Basin Width (km)	R_c	Circulatory ratio		

App. 10: Results of Morphometric Analysis in Subbasins of W. Dahab

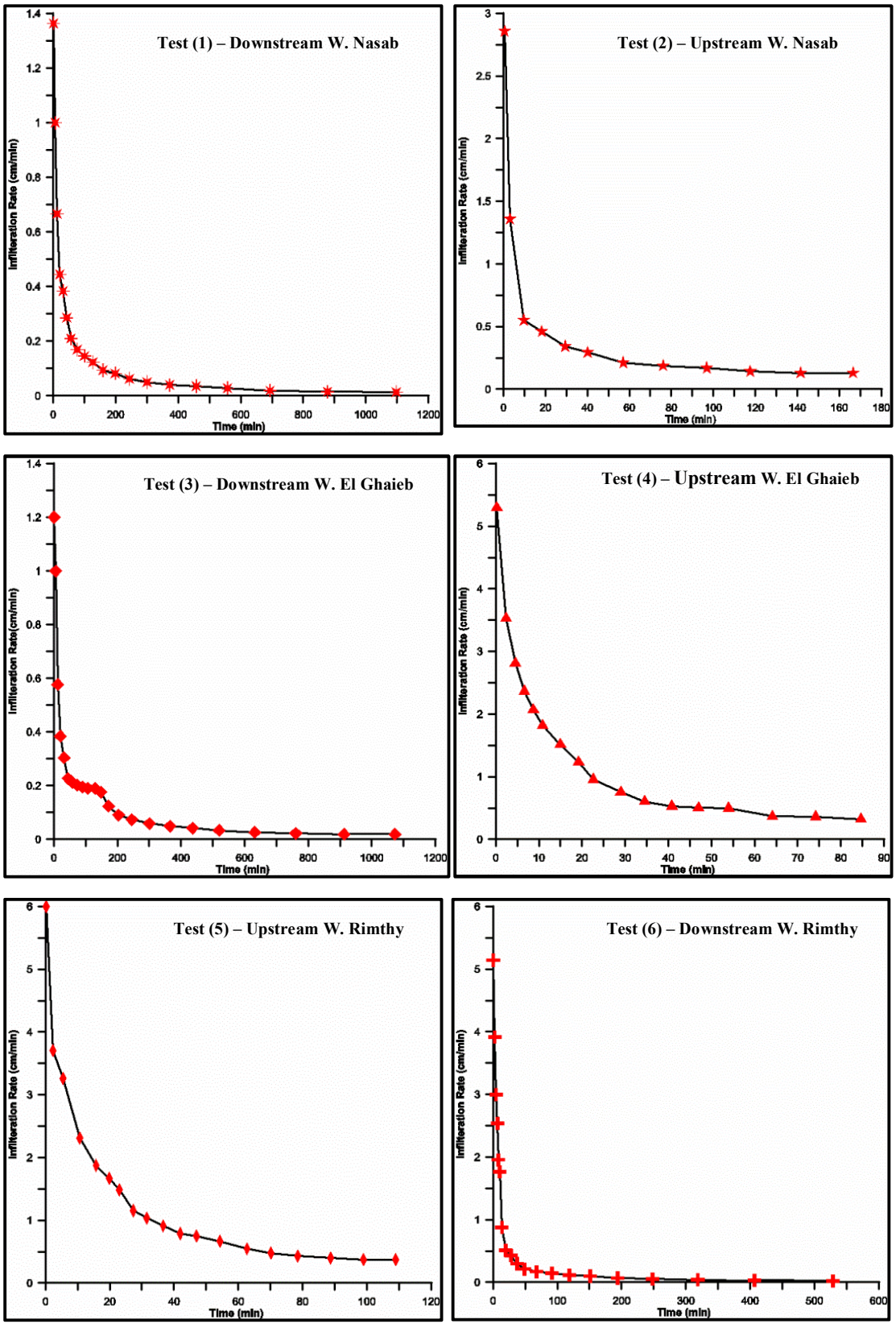

App. 11: Relation Between Infiltration Rate and Time of Infiltration of Alluvial Deposits in Each Sub basins of W. Dahab

	MMx. Temp.	MMn. Temp.	Ava. Temp.	Humidity	MMR	Mx. Prc.	Date
	^{o}C	**^{o}C**	**^{o}C**	**%**	**mm/month**	**mm**	**year/day**
Jan.	9.98	-2.14	3.92	37.1	2.4	51.6	1996/12
Feb.	19.76	-0.23	9.76	33.2	2.3	7.6	1999/02
Mar.	20.34	9.49	14.91	28.4	5.8	18.2	1980/20
Apr.	30.16	13.14	21.65	21.8	5.6	?	/
May	33.7	16.75	25.22	25.3	3.2	?	/
Jun.	35.67	21.34	28.80	22.4	0	0	0
Jul.	38.21	23.33	30.77	25.2	0	0	0
Aug.	38.22	23.4	30.81	24.6	0	0	0
Sep.	32.15	21.93	27.04	21.4	1.5	?	/
Oct.	27.22	14.61	20.91	28.8	2.1	35.5	2002/30
Nov.	23.27	9.75	16.51	37.8	11.7	76.2	1937/08
Dec.	19.24	3.86	11.55	36.2	33.6	15.8	1985/26
			Annul mean		68.2		

App. 12: Meteorological Records of Saint Catherine Station during the Period from 1961 to 2008

	MMx. Temp.	MMn. Temp.	Ava. Temp.	Humidity	MMR	Mx. Prc.	Date
	^{o}C	**^{o}C**	**^{o}C**	**%**	**mm/month**	**mm**	**year/day**
Jan.	20.87	9.78	15.32	53.18	1.3	9.5	1938/30
Feb.	21.26	10.6	15.93	54.17	1.1	10	1937/04
Mar.	24.52	13.86	19.19	50.56	1.1	22	1941/02
Apr.	28.37	17.69	23.03	53.42	0.8	3.2	1963/07
May	31.28	21.37	26.32	59.84	0.6	5.6	1963/04
Jun.	33.2	23.42	28.31	57.66	0	0	0
Jul.	35.15	24.66	29.09	59.01	0	0	0
Aug.	34.68	26.13	30.40	59.76	0	0	0
Sep.	32.68	24.04	28.36	61.49	0.8	70.1	2002/03
Oct.	28.58	19.9	24.24	58.61	0.9	13	1938/31
Nov.	26.46	15.43	20.94	56.6	2.1	37.8	1925/08
Dec.	23	11.59	17.29	54.59	10.2	22	1955/07
			Annul mean		18.9		

App. 13: Meteorological Records of El Tor Station during the Period from 1961 to 2008

	MMx. Temp.	MMn. Temp.	Ava. Temp.	Humidity	MMR	Mx. Prc.	Date
	^{O}C	**^{O}C**	**^{O}C**	**%**	**mm/month**	**mm**	**year/day**
Jan.	20.68	13.46	17.28	44	0.3	6	1992/01
Feb.	22.72	14.46	18.59	41.84	0.5	20.4	1955/02
Mar.	26.49	18.01	22.25	38.03	0.6	10.3	1989/09
Apr.	29.51	20.6	25.05	34.17	0.4	?	/
May	32.86	23.93	28.39	32.58	0	0	0
Jun.	36.55	26.98	31.76	30.97	0	0	0
Jul.	37.28	28.24	32.76	32.84	0	0	0
Aug.	37.34	28.41	32.87	36.83	0	0	0
Sep.	34.91	27.13	31.02	40.74	0.6	?	0
Oct.	30.3	23.26	26.78	44.32	0.4	8.6	1996/30
Nov.	27.55	19.59	23.57	44.73	2.3	48.3	1985/17
Dec.	22.6	15.44	19.02	44.81	11.2	3	1985/17
				Annul mean	16.3		

App. 14 : Meteorological Records of Sharm El-Shiekh during the Period from 1961 to 2008

	MMx. Temp.	MMn. Temp.	Ava. Temp.	Humidity	MMR	Mx. Prc.	Date
	^{O}C	**^{O}C**	**^{O}C**	**%**	**mm/month**	**mm**	**year/day**
Jan.	20	13.9	16.95	42	0.5	0	0
Feb.	22	13.5	17.75	41	0.2	37.3	1975/20
Mar.	24	16.8	20.4	38	0.1	0	0
Apr.	26	20.8	23.4	33	0.1	0	0
May	29	22.9	25.95	30	0	0	0
Jun.	33	25.3	29.15	29	0	0	0
Jul.	34	26.9	30.45	32	0	0	0
Aug.	34	27	30.5	34	0	0	0
Sep.	31	24.8	27.9	38	0	0	0
Oct.	29	20.1	24.55	44	0.3	6.9	2002/14
Nov.	25	17.5	21.25	44	0.8	0	0
Dec.	23	14.1	18.55	43	1.2	2.3	1973/20
				Annul mean	3.2		

App. 15: Meteorological Records of Dahab Station during the Period from 1990 to 2008

	MMx. Temp.	MMn. Temp.	Ava. Temp.	Humidity	MMRF	Mx. Prc.	Date
	^{o}C	**^{o}C**	**^{o}C**	**%**	**mm/month**	**mm**	**year/day**
Jan.	21.2	13.8	16.95	49	4.7	34.7	1994/01
Feb.	21.8	14	17.75	47	1.1	9.4	1996/08
Mar.	24.6	16.3	20.4	49	0.6	3.5	1995/30
Apr.	28.4	19.3	23.4	50	0.9	10	1990/20
May	23.7	22.8	25.95	49	0.8	?	0
Jun.	35.7	24.9	29.15	48	0	0	0
Jul.	37.6	26.8	30.45	50	0	0	0
Aug.	37	27.2	30.5	53	0	0	0
Sep.	34.4	25.6	27.9	55	0	0	0
Oct.	30.5	23.2	24.55	56	2.4	10.2	2002/30
Nov.	26.2	19.1	21.25	51	2.2	8.7	1996/07
Dec.	22.6	15.4	18.55	50	0.7	2.3	2003/14
			Annul mean		13.4		

App. 16: Meteorological Records of Nuweiba Station during the Period from 1990 to 2008

MMx. Temp.	Mean Monthly Maximum Temperature in 24 year
MMn. Temp.	Mean Monthly Minimum Temperature in 24 year
Ava. Temp.	Avarage Temperature
MMRF	Mean Monthly Rainfall
Mx. Prc.	Maximum Rainfall in one day

```
function [alpha,beta,xi,T]=gumbel()
clear;
clc;
xi=load('Sanit_Catherine.out');
%xi=load('Sanit_Catherine');
meanxi=mean(xi);
varxi=var(xi);
opt=optimset('MaxFunEvals',1000,'TolFun',1e-6,'MaxIter',100, ...
    'FunValCheck','on','Display','on');  %Define solver options
x0 = [5; 5];
lambda1=0.577216;
var1=[lambda1;meanxi;varxi];            % Make a starting guess at the solution
x =fsolve(@(x) myfun(x,var1),x0,opt);    % Call solver
beta=x(1);
alpha=x(2);
%Plot probabilities
hf=figure(1);
X=0:max(xi);
G=exp(-exp(-(X-alpha)./beta)); % P(x<=xi)
plot(X,G,'k-','linewidth',2.0);
xlabel('Rainfall [mm/day]', 'fontsize',14)
ylabel('Prob(x\leqxi)', 'fontsize',14)
grid on;
box on;
print(hf,'-dpng','I:\result of work_1\RAINFALL\rainfall_matlab\Adel\New Folder\Adel.png')
%Exceeding probabilities
hf1=figure(2);
G1=1-G; % P(x>xi)
T=1./G1; %Per
plot(T,X,'k-','linewidth',2.0);
xlabel('T [years]', 'fontsize',14)
ylabel('Rainfall [mm/day]', 'fontsize',14)
grid on;
box on;
axis([0 180 0 max(X)]);
print(hf1,'-dpng','I:\result of work_1\RAINFALL\rainfall_matlab\Adel\New Folder\Adel.png')
end
```

App. 17: Gumbel Distribution for Rainfall analysis using Matlab Software

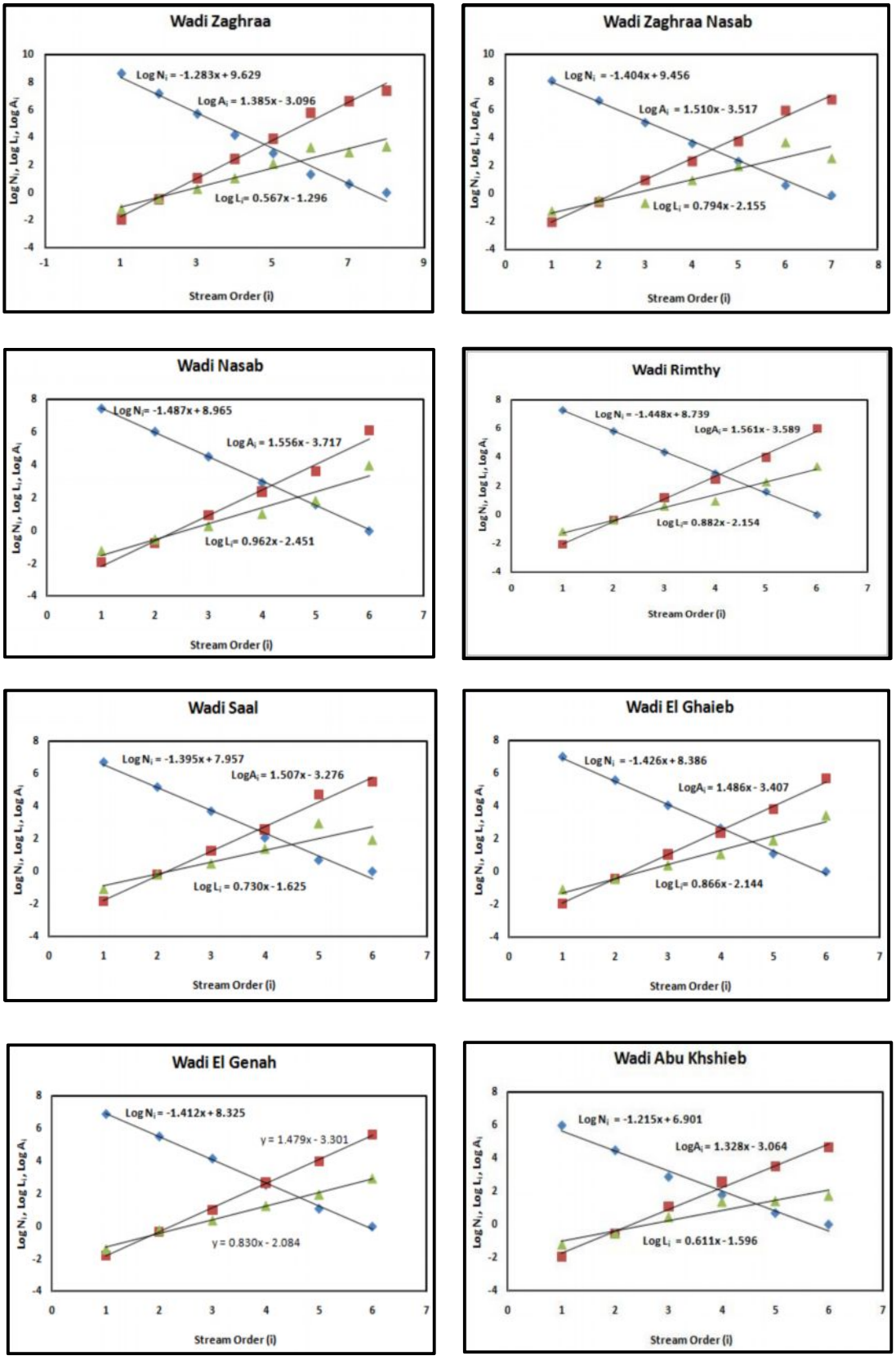

App. 18: Relationship between stream order i, stream number (Ni), stream length (Li) and stream area (Ai) for subbasins in Wadi Dahab.

	U	N_u	A_u	L_u	A_m	L_m	Ln (N_u)	Ln(A_m)	Ln(L_m)	R_b	R_l	R_a
Wadi Zaghraa	1	5804	888	1778.6	0.15	0.31	8.67	-1.90	-1.18	3.95	1.76	3.99
	2	1382	890	923.35	0.64	0.67	7.23	-0.45	-0.40			
	3	318	948.6	444.0	3.0	1.40	5.76	1.09	0.33			
	4	67	802.0	201.2	12.0	3.00	4.20	2.48	1.10			
	5	18	937.8	152.0	52.1	8.44	2.89	3.95	2.13			
	6	4	1387.0	109.0	346.8	27.25	1.39	5.85	3.31			
	7	2	1591	38.48	795.5	19.24	0.69	6.68	2.96			
	8	1	1617	25	1617	25.00	0.00	7.39	3.22			
Wadi Zaghraa Nasab	1	3479	490	1071	0.14	0.31	8.15	-1.96	-1.18	4.07	2.21	4.52
	2	830	502	549	0.60	0.66	6.72	-0.50	-0.41			
	3	183	512.0	97.2	2.80	0.53	5.21	1.03	-0.63			
	4	40	445.0	112.0	11.13	2.80	3.69	2.41	1.03			
	5	11	494.0	84.4	44.91	7.67	2.40	3.80	2.04			
	6	2	856.3	82.8	428.15	41.39	0.69	6.06	3.72			
	7	1	936	13.28	936.00	13.28	0.00	6.84	2.59			
Wadi Zaghraa Saal	1	2170	450	650.00	0.21	0.30	7.68	-1.57	-1.21	3.75	2.12	4.00
	2	516	410	426.00	0.79	0.83	6.25	-0.23	-0.19			
	3	127	393	198.00	3.09	1.56	4.84	1.13	0.44			
	4	27	305.0	89.00	11.30	3.30	3.30	2.42	1.19			
	5	7	444.0	86.00	63.43	12.29	1.95	4.15	2.51			
	6	2	530.4	30.00	265.20	15.00	0.69	5.58	2.71			
	7	1	663.0	25.21	663.00	25.21	0.00	6.50	3.23			
WadiNasab	1	1706	255	516.3	0.15	0.3	7.44	-1.9	-1.2	4.40	2.60	4.70
	2	421	201	257.15	0.48	0.61	6.04	-0.74	-0.49			
	3	93	235.2	125.2	2.56	1.4	4.52	0.94	0.31			
	4	19	206.3	54.6	10.86	2.9	2.94	2.38	1.05			
	5	5	184	31.4	36.8	6.3	1.61	3.61	1.84			
	6	1	444	53.9	444	53.9	0	6.1	3.99			
Wadi Rimthy	1	1492	205	477.7	0.13	0.31	7.31	-2.04	-1.17	4.22	2.40	4.76
	2	343	240	240	0.7	0.69	5.84	-0.36	-0.37			
	3	79	260	143.0	3.3	1.81	4.37	1.19	0.59			
	4	18	206	46.2	11.4	2.56	2.89	2.44	0.94			
	5	5	277	47.7	55.4	9.54	1.61	4.01	2.26			
	6	1	412.3	28.9	413.3	28.86	0.00	6.02	3.36			
Wadi Saal	1	844	139.3	294.3	0.16	0.34	6.74	-1.83	-1.08	4.01	2.07	4.48
	2	182	150.9	153.5	0.82	0.84	5.20	-0.20	-0.17			
	3	41	142.1	67.07	3.46	1.63	3.71	1.24	0.49			
	4	8	103.1	33.33	12.88	4.1	2.08	2.56	1.41			
	5	2	225.6	39.53	112.8	19.7	0.69	4.73	2.98			
	6	1	245.8	7.12	245.8	7.12	0.00	5.50	1.96			
Wadi Genah	1	1000	170.3	248.13	0.17	0.25	6.91	-1.77	-1.39	4.10	2.29	4.34
	2	253	182.09	203.1	0.71	0.8	5.53	-0.33	-0.22			
	3	65	179.3	94.6	2.75	1.45	4.17	1.01	0.38			
	4	13	193.6	46.5	14.89	3.57	2.56	2.70	1.27			
	5	3	163.31	21.3	54.4	7.1	1.10	4.00	1.96			
	6	1	284.6	19	285	19	0.00	5.65	2.94			
Wadi El Ghaieb	1	1108	170	380.8	0.15	0.34	7.01	-1.90	-1.08	4.13	2.42	4.39
	2	266	183.3	175	0.68	0.65	5.58	-0.39	-0.43			
	3	57	170.1	85.4	2.98	1.49	4.04	1.09	0.40			
	4	14	155.3	41.2	11.09	2.94	2.64	2.41	1.08			
	5	3	141.8	20.4	47.2	6.8	1.10	3.85	1.92			
	6	1	298.8	31.2	298.8	31.2	0.00	5.70	3.44			
Wadi Abu Khshieb	1	406	61	122.3	0.15	0.3	6.01	-1.90	-1.20	4.22	2.40	4.76
	2	90	54.22	54	0.6	0.6	4.50	-0.51	-0.51			
	3	18	54.67	28.31	3.04	1.57	2.89	1.11	0.45			
	4	6	80.15	23.79	13.36	3.97	1.79	2.59	1.38			
	5	2	69.22	8.23	34.61	4.12	0.69	3.54	1.42			
	6	1	107	5.67	107	5.67	0.00	4.67	1.74			

U	Stream Order	L_m	Mean basin Length
N_u	Number of Stream Order	R_b	Bifurcation ratio
A_u	Area of basin order (km^2)	R_l	Length ratio
L_u	Length of Stream order (km)	R_a	Area ratio
A_m	Mean basin area		

App. 19: Results of Hortonian Ratio of Subbasins in Wadi Dahab

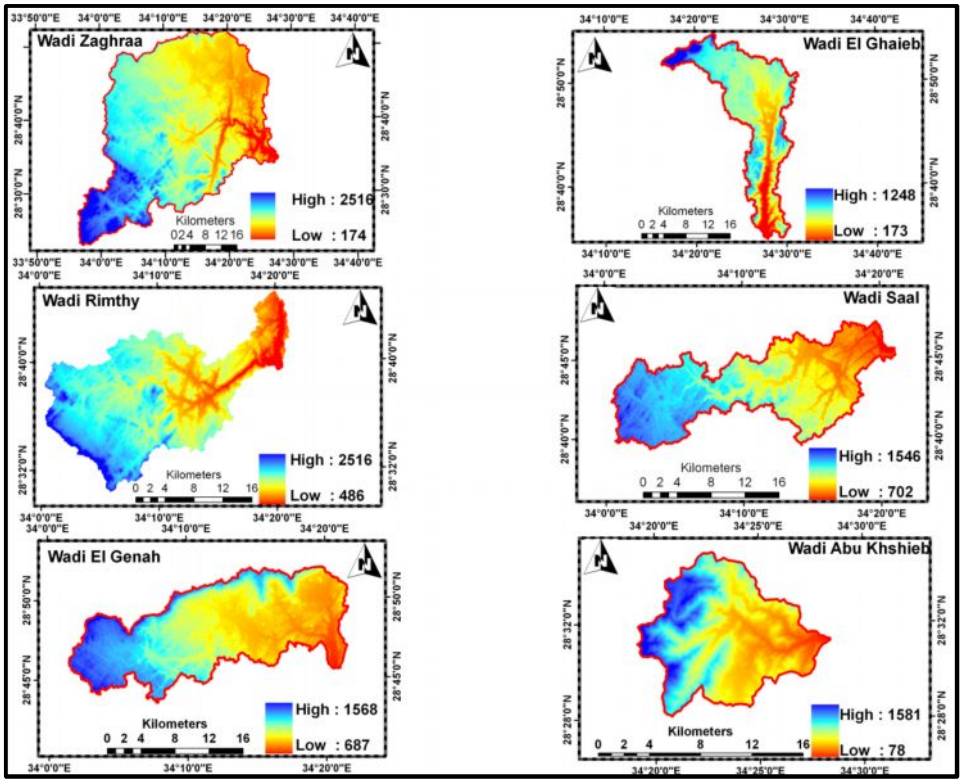

App. 20: Digital Elevation Model of Subbasins in Wadi Dahab

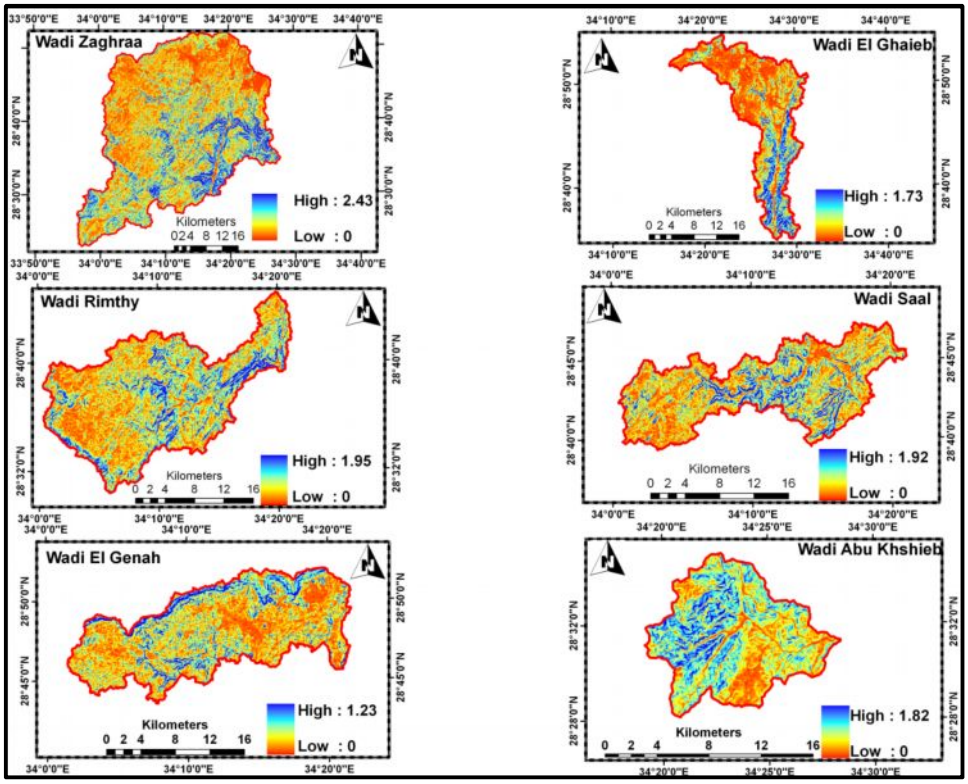

App. 21: Decimal Slope of Subbasins in Wadi Dahab

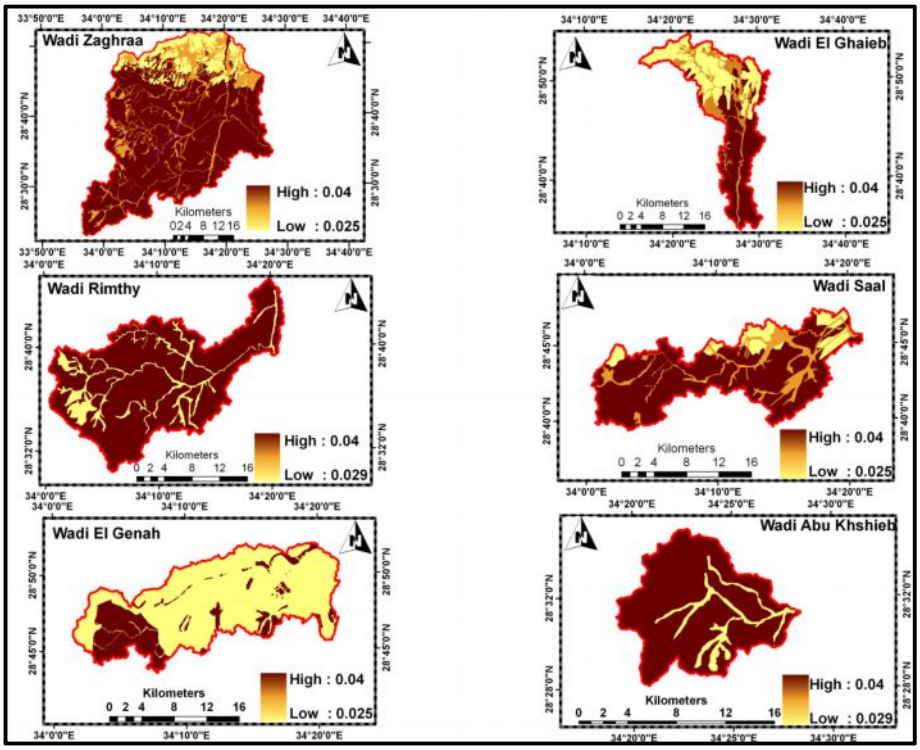

App. 22: Manning Value "n" of Subbasins in Wadi Dahab

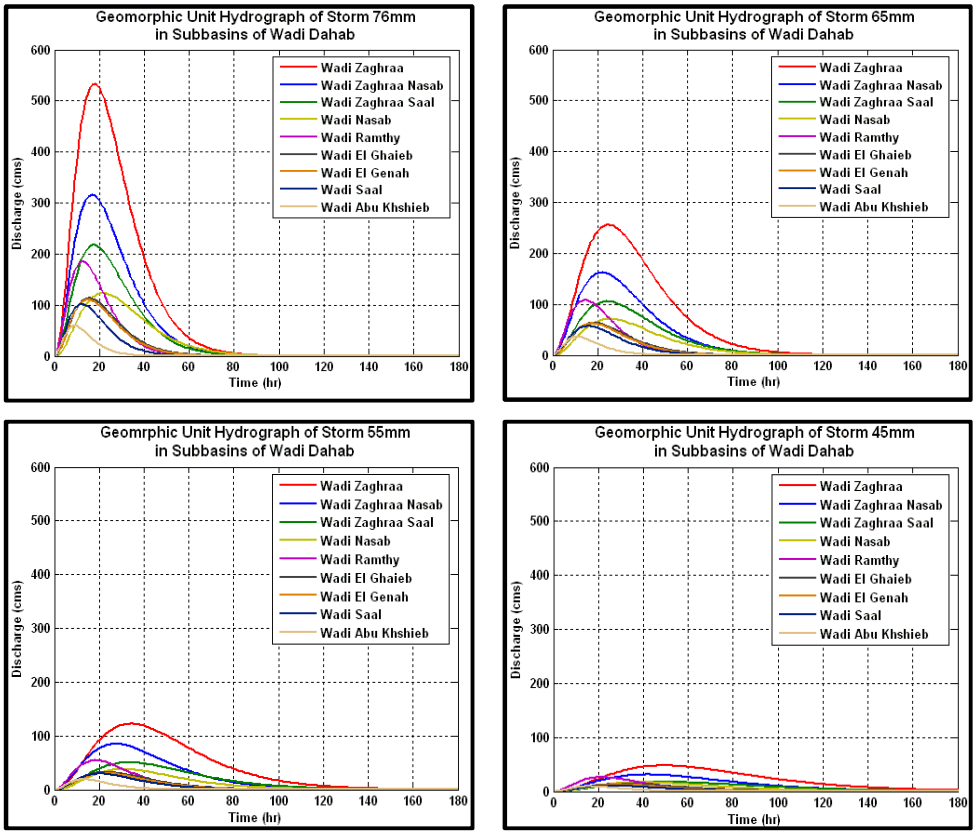

App. 23: Geomorphic Hydrograph for subbasins in Wadi Dahab

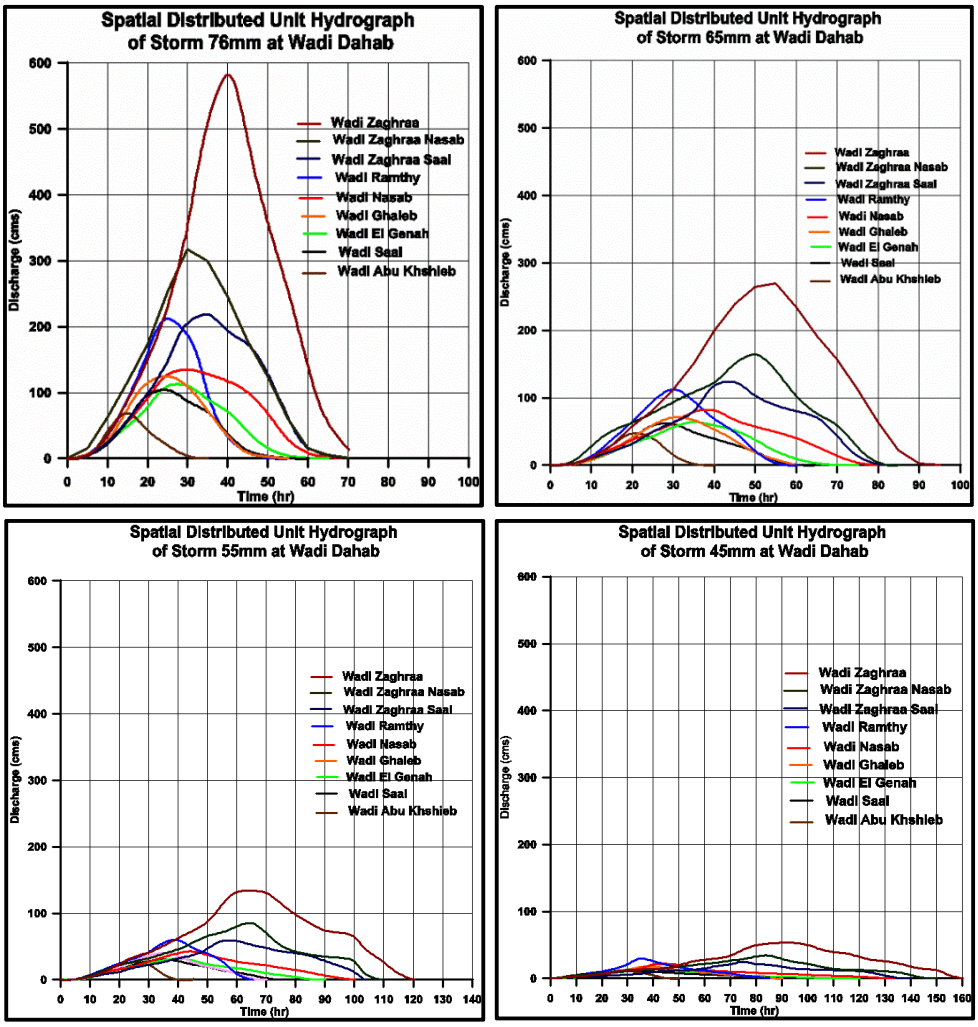

App. 24: Spatial Distributed Hydrograph for subbasins in Wadi Dahab